Development of Performance Assessment Methodologies

GRS - 259

Gesellschaft für Anlagen-
und Reaktorsicherheit
(GRS) mbH

Development of Performance Assessment Methodologies

André Rübel
Dirk-Alexander Becker
Eckard Fein
Alice Ionescu
Thomas Lauke
Jörg Mönig
Ulrich Noseck
Anke Schneider
Sabine Spießl
Jens Wolf

October 2010

Remark:

This report was prepared under contract no. 02 E 10276 with the Federal Ministry of Economics and Technology (BMWi).

The work was conducted by the Gesellschaft für Anlagen- und Reaktorsicherheit (GRS) mbH.

The authors are responsible for the content of this report.

GRS - 259
ISBN 978-3-939355-34-2

Keywords:
Long-term safety, Performance assessment, Radionuclide transport, Repository, Safety case, Safety indicator, Uncertainty

Abstract

The project PAMINA (Performance Assessment methodologies in application to guide the development of the safety case) was conducted from 2007 to 2009 on the European level to improve and harmonise integrated performance assessment methodologies and tools for various disposal concepts of long-lived radioactive waste and spent nuclear fuel in different deep geological environments. The following report presents the contributions of the GRS Braunschweig to the PAMINA project comprising the following topics:

- Overview of methodologies, tools and experiences:
  A comprehensive review is presented from the point of view of the implementer to assess the state of the art of the methodologies and approaches needed for the safety assessment of geological repositories for the German national programme, and to distil the lessons learned from the rich experience accumulated in their development and application.

- Treatment of uncertainty in integrated performance assessment:
  A protocol is presented that helps to determine adequate probability density function for parameter values to deal with parameter uncertainties in probabilistic safety analyses.
  Different sensitivity analysis methods have been tested for a performance assessment model for a high-level waste repository in rock salt. These methods include variance based FAST and EFAST methods.

- Use of safety indicators and performance indicators:
  Different safety and performance indicators have been tested for high level waste repositories in rock salt and clay formations. For the repository in clay sensitivity analysis methods have been tested to gain deeper insight into the performance of subsystems.

- Relevance of sophisticated approaches in practical cases:
  The performance assessment approach to three selected near-field processes in a repository in salt have been tested for their suitability. The three processes are convergence of salt, brine intrusion into a backfilled drift and convective driven transport. Additionally, the relevance of the complexity of modelling for the far field of a repository in salt has been assessed.

Table of contents

1 Introduction

A comprehensive set of arguments and analyses – represented in a safety case – is needed to justify that geological disposal of long-lived radioactive waste and spent nuclear fuel is safe. One pillar of the safety case is the integrated performance assessment of the repository by numerical methods. This Performance Assessment requires a powerful and qualified instrument. The approach used for the performance assessment must meet national regulations on the one hand and should be internationally accepted on the other hand. Further it must be continuously adapted to the state of the art of science and technology. Computer codes used for the assessments must be tested and verified and be designed for the prerequisites of a real waste repository system.

On the European level the project PAMINA (Performance Assessment methodologies in application to guide the development of the safety case) was conducted from 2007 to 2009 to improve and harmonise integrated performance assessment methodologies and tools for various disposal concepts of long-lived radioactive waste and spent nuclear fuel in different deep geological environments. PAMINA aimed at providing a sound methodological and scientific basis for demonstrating the safety of deep geological disposal of such wastes, that will be of value to all national radioactive waste management programmes, regardless of waste type, repository design, and stage, that has been reached in PA and safety case development.

The following report presents the different contributions of the GRS Braunschweig to the different tasks of the PAMINA project. On a national level, this work was co-funded by the Federal Ministry of Economics and Technology (BMWi). Some of the work described in the following is presented in a similar way in public PAMINA reports given at the according sections.

The following chapter gives for selected topics an overview of PA methodologies, tools and experiences for the German national programme from the point of view of the implementer. The other chapters (3 to 5) present methodological advancements achieved in different areas, which are

- the treatment and management of uncertainty during PA and safety case development (chapter 3),
- the use of safety and performance indicators for repositories in salt and clay (chapter 4) and finally,

- the improvement of methods and tools regarding process understanding and conceptualization and the determination of needs for implementing more sophisticated modelling approaches in PA (chapter 5).

2 Overview of methodologies, tools and experiences

During the last decades a very large body of experience regarding safety assessment of geological repositories of radioactive waste has been generated, both in European countries and outside of Europe. This experience provides a firm basis for future steps in national development programmes. In parallel with development activities, a growing number of formal evaluation processes, including regulatory processes, have been and are being carried out, generating important guidance for future work. A significant part of these efforts has been realised under the auspices, and in the framework, of the programmes of international organisations. A comprehensive review was performed in the project PAMINA with the objective to assess the state of the art of the methodologies and approaches needed for the safety assessment of geological repositories, and to distil the lessons learned from the rich experience accumulated in their development and application. The following issues have been addressed:

1. Safety indicators and performance/function indicators
2. Safety functions
3. Definition and assessment of scenarios
4. Uncertainty management and uncertainty analysis
5. Assessment strategy - Safety Approach
6. Evolution of the repository system
7. Modelling strategy
8. Sensitivity analysis
9. Biosphere
10. Human intrusion
11. Criteria for input and data selection

The following nine sections of this chapter give the review work of the GRS Braunschweig addressing the German radioactive waste disposal programme from the viewpoint of the implementer. The overall results of the PAMINA review are presented in the RTDC1 deliverables /PAM 06, PAM 09, PAM 10/. All the topics share a common structure including the following areas:

- Background/Introduction
- Regulatory requirements
- Key terms and concepts
- Treatment in the safety case
  - Methodology
  - Related topics
  - Databases and tools
  - Application and experience
  - On-going work and future evolution
- Lessons learnt

Not all areas are addressed in each of the topic. The statements towards the regulatory requirements are similar for all the topics and are summarised in the following. Additional comments in each of the topics chapters towards the regulatory requirements are only given if deviant or supplementary comments have been given to that specific topic.

The German Atomic Energy Act merely requires the safe disposal of radioactive waste. There is an old German guideline ("safety criteria for the final disposal of radioactive wastes in a mine"), originating from 1983, which is formally still valid /BMI 83/. Concerning long-term safety, it simply requires that "even after decommissioning radionuclides that could reach the biosphere in consequence of non-excludable transport processes from a sealed repository must not lead to individual doses exceeding the value given in the Radiation Protection Ordinance". This value is 0.3 mSv/yr and is valid for all nuclear facilities. A supplementary regulation from 1988 defines the time frame for which the individual dose rate should be evaluated as 10 000 years. The consideration of other safety indicators is not required, nor are probabilistic criteria defined. There is, however, a consensus in Germany that the mentioned guideline is outdated and should be revised soon. A first draft for a new version, proposed by GRS, is currently under intense discussion. It requires the consideration of six indicators with fixed reference values as well as a probabilistic analysis. This paper is, however, a controversial matter and will be essentially changed before being accepted by the authorities. Therefore, it

is not presented here. Nevertheless, it can be said that the future guideline is very likely to contain the following regulations:

- the calculated individual effective dose rate must not exceed the reference value of 0.1 mSv/yr,
- several additional safety indicators have to be calculated,
- the time frame for which safety has to be proven is 1 million years or more.

Besides the review performed within the PAMINA project the GRS also followed the German network for research on the actinide migration in natural claystone from the long-term safety assessment point of view. This view is given in the final section 2.10 of this chapter.

2.1 Current status of the German national context regarding repository projects

According to the Atomic Energy Act /ATG 85/ the German Federal Government has to ensure the safe disposal of radioactive waste by providing repositories. The legal basis for licensing of federal installations for the safekeeping and final disposal of radioactive waste is the "Plan Approval Procedure" required by the Atomic Energy Act. Radioactive waste disposal policy in Germany is based on the decision that all types of radioactive waste are to be disposed of in deep geological formations. The currently valid safety criteria for the final disposal of radioactive waste in a mine dates from 1983 /BMI 83/. Since then, regulatory expectations have advanced, now reflecting the international standards set out by ICRP /ICRP 98/, NEA /NEA 04/ and IAEA /IAEA 06/. On this account, GRS proposed “Safety requirements for the disposal of high active wastes in deep geological formations” /BAL 07/ on behalf of BMU (Federal Ministry for the Environment, Nature Conservation and Nuclear Safety), which is expected to serve as a sound basis for a new regulation. The BMU is presently elaborating the final version of the Safety Requirements. A draft version of the Safety Requirements was presented in November 2008 to the public /BMU 08/.

Prior to 1980 the former iron ore mine Konrad was selected as a site for disposal of short-lived and long-lived radioactive waste with negligible heat generation and the salt dome at Gorleben as a site for the disposal of all types of radioactive waste. In the for-

mer German Democratic Republic short-lived low- and intermediate-level radioactive waste was disposed of in the Morsleben repository, a former rock salt and potash mine.

The **Konrad** repository had been licensed in May 2002. All suits that were filed against it were rejected by the competent court in 2006. Complaints against the courts decision were definitely rejected by the Federal Administrative Court in April 2007. Following necessary planning adjustments the former iron ore mine will be converted into a repository for all kinds of radioactive waste with negligible heat generation by the end of 2013.

The disused salt and potash mine Morsleben (ERAM), located in the Federal State of Saxony-Anhalt, has been in operation since 1971 as a repository for short-lived low- and intermediate-level radioactive waste. Disposal was terminated in 1998. A waste volume of about 37 000 m^3 has been disposed of with a total activity of approx. $4.5 \cdot 10^{14}$ Bq. Since 1990, the Morsleben facility has the status of a federal repository. The license for operating the repository originates from the former German Democratic Republic and do not include the license for the closure of the repository. Therefore, according to the German Atomic Energy Act /ATG 85/ a license application for the closure of the repository is being prepared by BfS (Federal Office for Radiation Protection).

The Gorleben salt dome in the north-east of Lower Saxony has been investigated for its suitability to host a repository for all types of solid and solidified radioactive waste for several decades. However, after the licensing of the Konrad repository the focus is mainly on heat generating radioactive waste originating from reprocessing and spent fuel elements. The exploration of the Gorleben salt dome was interrupted on 1st October 2000 according to a moratorium of up to 10 years.

The German radioactive waste management and disposal concept as well as the site selection process are still under discussion. In terms of the site selection process, a respective concept from BMU was suggested in 2006. This concept includes the examination whether site alternatives exist in addition to Gorleben, which let expect or possess a higher level of safety /GAB 08/.

The current R&D concept focuses on all types of host rocks, prioritised in the following order: rock salt, argillaceous rock, crystalline rock. Concerning rock salt, which has been the preferred option in Germany for several decades, the technical and engineering know how as well as the scientific expertise are considered well advanced and are

now available for the conceptual design of a high level waste repository. During the last 10 to 15 years suitable analytical tools have been continuously developed according to the world wide advancing state-of-the-art. They are ready to be tested and applied at appropriate and concrete cases. For repositories in argillaceous and crystalline rock R&D work focussing mainly on mechanical and hydraulic properties of the engineered and the geological barriers has been performed during the last decade. System models for an integrated safety assessment are available for both formations.

2.2 Safety indicators and performance/function indicators

2.2.1 Background/Introduction

Although, of course, measures for quantifying the results of performance assessment calculations, mainly dose and risk, were always in use, it is a relatively new concept to improve the understanding of the system and to support the safety case by using complementary indicators. Such indicators are calculable quantities resulting from a PA calculation. While safety indicators aim at providing a quantitative criterion for the overall safety of a repository system, other indicators are calculated and presented to show the functioning of the system or specific components. They are sometimes called ‘performance indicators’ or ‘function indicators’, but they differ, with respect to goals and intention, from what SKB calls ‘safety function indicators’. It is therefore suggested, in order to avoid confusion, to use the term ‘function indicator’ only in the latter sense as a short form. In this paper, the term ‘performance indicator’ is used.

In former German safety assessment studies, the only safety indicator used was the individual ingestion dose per year, compared to a regulatory limit. The SPIN project /BEC 03/ was initiated by a new way of thinking, based on the awareness that the robustness of the safety case could be improved by using more than one safety indicator, as well as performance indicators. Several safety and performance indicators were tested in SPIN, using four national granite studies as examples.

In 2004, a detailed performance assessment for the Morsleben LAW repository (ERAM), which is installed in a former salt mine, was performed. The safety indicators defined in SPIN, as well as some performance indicators, were successfully applied to support the safety statement. It has become clear in this exercise that a rock salt repository requires performance indicators that differ from those used for granite, while

safety indicators, though possibly depending on local reference values, are independent of the site and formation type.

The concepts and understanding of safety and performance indicators have further evolved since the end of SPIN. Presently, a new study for a HLW/SF repository in salt, called ISIBEL, is being made. Several safety and performance indicators were or will be calculated and compared with one another. This is done in parallel to PAMINA and the new concepts and ideas developed.

2.2.2 Key terms and concepts

In the following, the concept of safety and performance indicators as it is understood by GRS (Braunschweig) is described. Since the subject is under intense discussion in Germany at present, the following should neither be seen as 'the German standpoint', nor should it be regarded as final.

Safety indicators

Repositories for radioactive waste must be proven to be safe in the long-term. But what does that mean? A very general definition of repository safety can be given in the following way:

A repository is safe if it does not significantly change or disturb the natural evolution of the environment outside a narrowly limited area of influence.

Safety, in this sense, cannot be reduced to one single aspect like human health, but comprises a nearly unlimited variety of protection goals like water quality, air quality, protection of species, etc. There can, of course, be overlap between such protection goals, or one goal can completely include another one, but the often-heard statement that protection of man comprises all other protection goals cannot be proven.

A numerical calculation of the dissemination of radionuclides from a repository yields, in general, radionuclide fluxes. These results are per se not suitable for assessing the long-term safety of the repository, as they give no information about whether or not the repository can be considered 'safe' as defined above. It is necessary to convert the results into some safety-related measure, or safety measure. 'Safety-related' means that the safety measure should quantify a specific aspect of repository safety.

The word ‘significantly’ in the definition above does allow a certain influence of the repository on the environment if it is very small and negligible in comparison with natural influences. If safety with respect to some specific aspect is to be assessed using a safety measure, it is necessary to quantify a reference value as the limit of acceptability with respect to the safety aspect under consideration. Reference values should be proven to maintain the protection goal.

It is possible that different safety aspects (or protection goals) can be quantified with the same safety measure, using different reference values. Therefore, only the combination of a safety measure and a suitable, safety related reference value, both related to the same protection goal, is appropriate to give an indication of safety of the repository and is called a safety indicator. A safety indicator should always take account of the effects of all radionuclides in the repository.

There are two kinds of safety indicators. Those of the first kind are calculated for specific scenarios and the results can be compared in order to assess the consequences of different scenarios. Safety indicators of the second kind, however, are summed up over all relevant scenarios, each weighted by its probability. Such indicators are preferably calculated in terms of risk. They can be compared with risks from daily life or from natural sources like earthquakes, meteorite impacts, etc. The main problem with risk indicators is that scenario probabilities can, in most cases, only be roughly estimated.

For performing a safety assessment it is always necessary to use at least one safety indicator. The technique mostly applied in the past is to calculate the time-evolution of the annual ingestion dose to an individual or a group and to compare it with a regulatory limit. The protection goal underlying this safety indicator is human health and the reference value was, though fixed by a regulatory rule, originally derived from the demand to be negligible compared to the natural background. In Germany, a value of 0.3 mSv/yr has been used so far. This safety indicator is widely used and refers to a rather universal protection goal, but it depends on more or less uncertain assumptions about the geosphere and biosphere. Moreover, it could suggest covering all aspects of safety, while actually it does not. Therefore, it is regarded increasingly necessary to consider additional safety indicators.

Performance indicators

Safety indicators are a good means to assess the overall safety of a repository system, but they do not yield detailed information about the functioning of the system. Such information, however, can be very helpful or even necessary in the process of concept development. It can be gained by using performance indicators.

A performance indicator is a calculable measure for the performance of parts of the system. These parts, which are called compartments, can be things like single barriers, groups of barriers, emplacement fields, the complete near field, or even the total system. Compartments can include others. The compartment structure to be used for a specific repository system should be a sensibly simplified image of the real system structure and depends on the type of the repository.

Performance indicators should illustrate how the repository works. Radionuclide fluxes between or concentrations in the compartments, e. g., show how and where the radionuclides are retained during the transport through the system. The time-evolution of a performance indicator should be calculated and compared for different locations, but a comparison with an absolute value is normally not necessary.

Whereas a safety indicator always requires considering of all relevant radionuclides in order to derive a safety statement, a performance indicator can be calculated for a single radionuclide, a group of radionuclides or the total radionuclide spectrum, depending on what is to be demonstrated. In this way it is possible, e. g., to compare the system performance for sorbing and non-sorbing species, or for the uranium and the thorium chain.

2.2.3 Treatment in the safety case

This section describes which indicators have been used by GRS in the past, and why. It is pointed out how the indicators have been calculated and interpreted and which reference values were used.

2.2.3.1 Methodology

Safety indicators

According to the regulations mentioned above, in all German studies made before 2000, only the individual effective dose rate was calculated and compared with the limit of 0.3 mSv/yr, normally for different concepts or different scenarios. Additional numerical investigations were, in some cases, performed in order to explain the results, but not to derive independent safety statements. In contrast to what the valid guidelines require, however, the calculations were always executed over a model time of at least 1 million years.

The SPIN project (2000 – 2002) has triggered a new view of the problem. The three safety indicators identified in SPIN to be useful have been applied in two recent studies for real sites:

- ERAM: The long-term safety assessment study for the LAW repository in rock salt near Morsleben,
- Asse: The long-term safety assessment study for the experimental LAW/MAW repository Asse in rock salt near Wolfenbüttel.

Moreover, five of the six indicators defined in the GRS proposal for a new guideline have recently been calculated in the ISIBEL study which considers a generic HAW repository in rock salt. This, however, is a running project, and the indicators themselves are still under discussion at GRS. Therefore, the results and findings of this exercise are not presented here.

In the following, the application of the SPIN safety indicators in the ERAM study is explained more detailed.

The primary safety indicator evaluated in the study is, according to the regulations mentioned above, still the effective dose rate to an adult human individual, in combination with the regulatory reference value of 0.3 mSv/yr. It has been calculated as a function of time over 1 million years, using standardised biosphere dose conversion factors.

These dose conversion factors have been defined by GSF considering a number of typical exposure paths, which comprise:

- ingestion of drinking water,
- ingestion of plants,
- ingestion of meat,
- ingestion of fish,
- inhalation of contaminated particles,
- exposure by external radiation.

Since these paths refer to the present human population, the dose conversions factors are increasingly uncertain for longer time frames.

There was no freedom about the reference value, but since it is about 10 % of the natural radiation exposure, the repository is considered to be safe if the additional radiation exposure originating from it remains below this limit. For the ERAM reference scenario, the maximum dose rate is more than three orders of magnitude below the reference value.

Two more safety indicators have been considered. The radiotoxicity concentration in the aquifer has been calculated using the ingestion dose coefficients by ICRP. This measure is more robust than the dose rate because it is independent of the biosphere, though it is still based on the radiosensitivity of present-day humans. There is no “official” reference value for this measure, but it is rather easy to determine one. Waters that have been drunk by humans for hundreds of years without causing harm can be considered radiologically safe. There are a lot of data about concentrations of radionuclides in German drinking waters, and a typical radiotoxicity concentration of 7.7 µSv/m³ could be derived. With this reference value the radiotoxicity concentration becomes a proper safety indicator. It has been found that for the ERAM reference scenario the maximum radioxicity concentration in the aquifer is a little more than three orders of magnitude below this reference value.

The third safety indicator considered is based on the radiotoxicity flux from the repository. This is an even more robust measure than the aquifer concentration because it is independent of the geosphere, which could be influenced by ice ages etc. The problem

with this measure is to find a clearly safety-related reference value. Two different possibilities were discussed. One is the natural radiotoxicity flux in a river near the repository, which is likely to finally collect all radionuclides released from there. The other possibility is the natural flux of raditoxicity in the groundwater near the repository. It was found that the second value was about three orders of magnitude lower than the first one. This is an example for the argument that one single safety measure can yield different and independent safety indicators if compared with different reference values. If the first value is used, the safety statement will be, “there is no significant influence on the river”, which could be relevant for the river fauna and is clearly a safety aspect. If, however, the groundwater flux is used as reference value, the safety statement will be, “there is no significant influence on the groundwater”, which is a different and probably more relevant safety aspect. By this reason, and because the value is lower, it was decided only to consider the natural radiotoxicity flux in groundwater as reference value, though it was harder to determine and is considered less robust. It was found to be 0.2 Sv/yr. For the ERAM reference scenario the maximum radiotoxicity flux from the repository is a bit more than three orders of magnitude below this reference value.

Performance indicators

In order to investigate the functioning of the repository system in detail, several performance indicators have been calculated for the ERAM reference scenario. The compartment structure used for this purpose is based on the model structure which is a strong simplification of the real mine structure. There are three sealed emplacement areas, two non-sealed emplacement areas and a number of voids that have not been used for emplacement purposes and are called ‘residual mine’. Depending on the specific requirements of the investigations, the performance indicators have been calculated for slightly different compartment structures, sometimes merging the non-sealed emplacement fields together with the residual mine, sometimes not. It has become clear that, unlike a granite repository as considered in SPIN, a rock salt repository, especially if erected in an abandoned production mine, does not allow a unique and hierarchical compartment structure.

In order to show the dissemination of radionuclides within the mine, the concentration of radiotoxicity in the different compartments has been calculated as a function of time. To distinguish between the influences of the different emplacement fields, three different investigations were performed, one considering the total inventory, one considering only the inventory of the sealed emplacement areas, and one considering only the in-

ventory of the non-sealed emplacement areas. It could be showed that the sealed emplacement areas, though the seals are assumed to lose their effectiveness after about 20 000 years, still contain 90 % of that part of their inventory that has not decayed after 1 million years. Even the non-sealed emplacement areas hold the main part of their inventory for about 100 000 years.

As an additional performance indicator the integrated radiotoxicity flux from the compartments was calculated as a function of time, each normalised to the initial inventory of the appropriate compartment. As already detected in SPIN, this is a very illustrative indicator since the time curves reach asymptotic values and the comparison of these shows how much of the inventory is finally retained in each compartment. The results show that a part of less than 0.1 % of the inventory of the sealed emplacement areas leaves these and even from the worst of the non-sealed emplacement areas only 10 % of its inventory can escape. A part of 10^{-5} of the total inventory leaves the repository system and reaches the biosphere.

2.2.3.2 Related topics

The issue of safety and performance indicators is related to a number of other topics:

- assessment strategy,
- safety approach,
- safety functions,
- analysis of the evolution of the repository system,
- biosphere,
- uncertainty management and uncertainty analysis,
- sensitivity analysis.

2.2.3.3 Databases and tools

Reference data are of high importance for safety indicators and should be taken from environmental measurements, biological investigations, etc. Some of the available data

needed for determination of reference values are rather incomplete and uncertain. This problem might make it hard to apply or even test some promising indicators.

The tools needed for calculating safety and performance indicators are the same that are being used for conventional performance assessment calculations, with a few slight modifications or add-ons.

2.2.3.4 Application and experience

In the ERAM study three safety indicators were applied as described in section 4.1. The time-curves are similar in shape because they have been derived from the same calculations, but nevertheless yield independent safety statements since the reference values have been determined completely independently and with totally different assumptions. It is interesting to see that even so all three safety indicators yield nearly exactly the same gap of about three orders of magnitude between the maximum and the reference value. This is clearly a coincidence but it shows a certain robustness of the safety assessment. For the ERAM reference case, the results are shown in figure 2.1 in units relative to the respective reference value. In this representation the three curves are very close to each other.

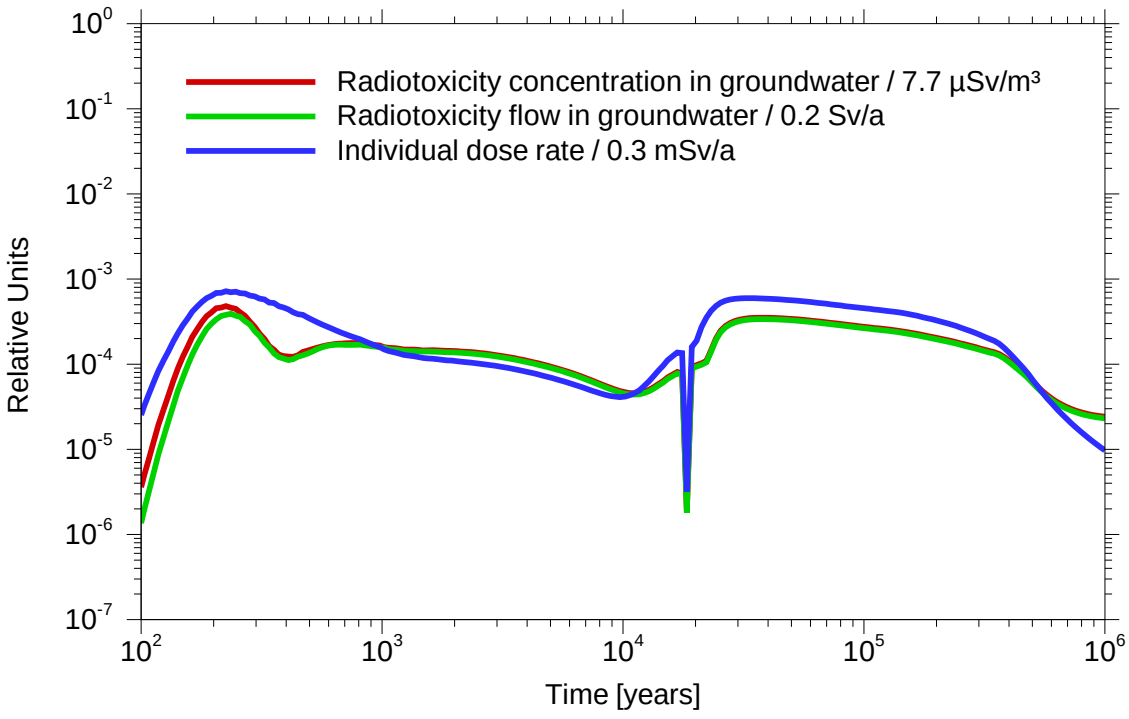

Fig. 2.1 Three safety indicators, calculated for the ERAM reference case

A very illustrative performance indicator is the time-integrated radiotoxicity flow from different compartments of the repository, related to the initial inventory of the compartment. The curves finally reach stationary values which show how much of the initial inventory leaves the compartment. For the ERAM case, this indicator has been calculated for five compartments, three of them being separated emplacement areas plus the complete mine and the total system including the geosphere. The results are shown in figure 2.2. It can bee seen that even the worst (and non-sealed) emplacement area, which is not designed to retain anything at all, nevertheless retains nearly 90 % of its inventory and the total system releases only about ten millionths of the initial radiotoxicity.

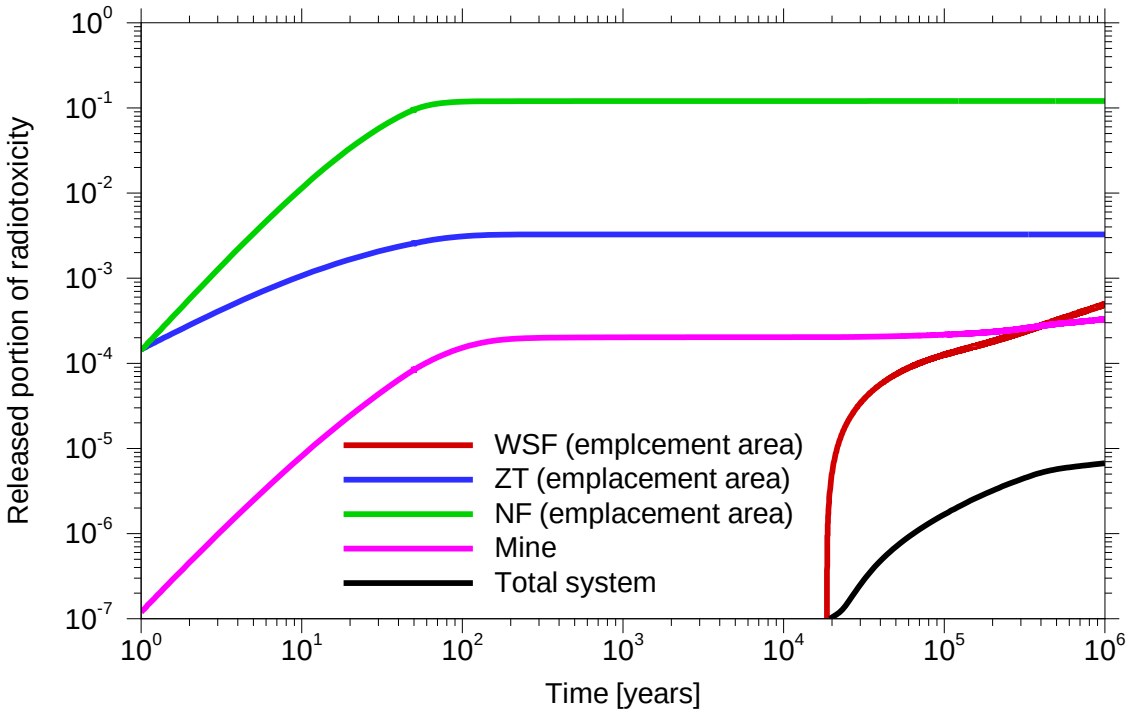

Fig. 2.2 Time-integrated radiotoxicity fluxes from different compartments of the ERAM repository (reference case; each curve is related to the initial inventory of the respective compartment)

2.2.3.5 On-going work and future evolution

Currently, different safety and performance indicators are being calculated within the new ISIBEL study for a HLW/SF repository in rock salt. Within PAMINA a wider variety of indicators including those of the risk type is tested. It is also planned to perform

probabilistic analyses in order to identify the specific sensitivities of different safety and performance indicators.

2.2.4 Lessons learnt

The application of different safety indicators does only make sense if they aim at different safety aspects and provide different and independent safety statements. A safety statement depends not only on the safety measure but also on the reference value. For a safety indicator to be robust it is necessary that neither the safety measure nor the reference value depend on uncertain data or assumptions. Therefore, the radiotoxicity flux from the repository can only be considered robust and adequate for long timeframes if combined with a robust and safety-related reference value, which is not easy to find. Establishing of reference values is a very important and sometimes difficult task. A good reference value should be provably safe and valid for a long or at least well-known time frame. Reference values can be global or site-specific. A safety indicator can never be better than its reference value.

So far, only safety indicators that aim at human health have been considered in actual studies in Germany. Other protection goals like protection of non-human biota or even the inanimate environment should be taken into account. Some of the indicators considered in ISIBEL are of a more general character and could be adequate for such a concept.

Since the number of possible protection goals is nearly unlimited, a classification of such goals with a hierarchical structure could be a sensible task. It should be tried to find a limited number of protection goals that cover large ranges of others, ideally the total field of ‘safety’. This could help defining a limited but comprehensive set of safety indicators.

Safety indicators of the risk type have not been considered so far in German studies. The reason might be that scenario probabilities are hard to determine. This kind of indicators can, however, be very illustrative and helpful in communicating with the public and should therefore be tested.

Performance indicators are always helpful to better understand the functioning of the system. They should be defined specifically for each study. As already seen in SPIN, it

is hard to give a general recommendation for the use of performance indicators. It can, however, be said that integrated fluxes from different compartments, if interpreted correctly, in many cases provide very illustrative and useful information.

2.3 Uncertainty management and uncertainty analysis

2.3.1 Background/Introduction

There are two basically different ways to handle uncertainties. One is using conservative models and parameter values instead of realistic ones, making sure that the reality cannot be worse than the calculated results. The other possibility is to establish probability distributions for all uncertain parameters and to perform a probabilistic analysis with a big number of separate runs. The first approach can cause some problems as conservativity is sometimes hard to prove. Moreover, too much conservativity can result in a failure of the proof of safety. Probabilistic analysis is always to be preferred, as it allows for an assessment of the probability of a failure, as long as the uncertainties of models and input parameter can be properly quantified. This, however, is not always possible. Therefore, normally, both approaches are combined by using conservative models and parameters only where the uncertainty is hard to quantify, and then performing a probabilistic analysis.

Probabilistic uncertainty analysis, though not required by valid regulations, is a common means for assessing the outcome of a repository model and has been in use in Germany for more than twenty years. The procedure was performed already in 1988 in the PAGIS study for a HLW/SF repository in rock salt and is described in the report /STO 88/. In later studies it was applied in the same form and using the same tools up to now, recently for the LAW repository near Morsleben (ERAM) and the experimental LAW/MAW repository in the salt mine Asse near Wolfenbüttel. The methodology for uncertainty assessment is approved. The main problems lie in identifying the essential uncertainties, finding the adequate probability distribution functions and correct interpretation of the results.

2.3.2 Key terms and concepts

In the following, the general problem of uncertainties in long-term safety assessments is described as it is seen by GRS (Braunschweig).

Aleatory and epistemic uncertainties

Basically, it can be distinguished between two different kinds of uncertainties which require their specific handling: Uncertainties that are due to physical imponderabilities or principally unforeseeable processes are called aleatory; uncertainties, however, that originate from our lack of knowledge about the nature are called epistemic. Epistemic uncertainties are those of physical parameters that are only insufficiently known. Such uncertainties can be principally reduced by additional measurements, improvement of measurement techniques or other investigations. Aleatory uncertainties, however, can neither be avoided nor reduced and have simply to be accepted as they are. An example for an aleatory uncertainty is the time of failure of a single canister. This depends on things like pitting corrosion due to the existence of microscopic fissures in the container material from the fabrication process or from mechanical impacts during the emplacement. Of course, one can argue that it is possible to reduce this uncertainty by optimising the canister fabrication and handling processes, but such measures would change the system itself and not simply the knowledge about it.

The adequate handling of uncertainties depends on their type. Aleatory uncertainties should be quantified as exactly as possible and their influence on the uncertainty of the results should be analysed. This uncertainty has to be accepted and taken into account in the safety case. A sensitivity analysis normally makes little sense for parameters that are subject to aleatory uncertainties. In contrast to this, if applied to epistemically uncertain parameters, sensitivity analysis can identify those parameters that should be analysed or measured more thoroughly in order to reduce their uncertainty.

In the practice of long-term safety assessments for final repositories, there are very few, if any at all, purely aleatory uncertainties. Most uncertainties are a mixture of both types, since there are random influences as well as lack of knowledge. The epistemic character, however, is dominant in most cases, and if it is not, like in the mentioned example of the canister failure time, it can nevertheless make sense to treat the uncertainty as if it were epistemic. The reason has been indicated above: Normally, there are possibilities to reduce even aleatory uncertainties by technical or constructional

measures, and it might be helpful to identify influential parameters by sensitivity analysis. Therefore, GRS decided not to distinguish between aleatory and epistemic uncertainties and to treat all uncertainties as epistemic ones.

Kinds of uncertainties

The most important uncertainties in long-term safety assessment are parameter uncertainties. As explained above, it is always assumed that these uncertainties are epistemic, i. e. due to insufficient knowledge about the actual natural conditions. Parameter uncertainties can origin from poorly known properties of the host rock, unclear flow conditions inside the mine, lack of knowledge about chemical conditions, etc. Parameter uncertainties are relatively easy to handle because they correspond directly with quantifiable numerical uncertainties. In many cases, a conservative value can be given, but this is only possible if the influence of the parameter to the result is monotonic.

Another kind of uncertainties is model uncertainties. In some cases, it is not clear which model has to be applied to describe a specific effect. Such uncertainties can be due to improper physical knowledge of the process, insufficient accuracy of the available models, or the inability to predict the correct physical situation. Model uncertainties are also always assumed to be epistemic. They are more difficult to handle than parameter uncertainties as they are hard to quantify. Where it is possible to specify a conservative model, this is the most convenient approach. If, however, there is no model that can be proved to be conservative, the model uncertainty can be mapped to an artificial parameter with discrete values, each representing one of the possible models. This parameter can be treated like a normal uncertain parameter in a probabilistic analysis.

Scenario uncertainties are the third kind of important uncertainties in long-term safety assessments. Normally, a number of different scenarios are developed which are considered more or less probable. Scenarios are derived from a FEP (features, events, processes) analysis and comprise things like the temporal evolution of the near field, transport through the far field and exposition paths in the biosphere. Since the probabilities of many FEPs can only roughly be estimated, scenario probabilities are very uncertain. The usual method to handle these uncertainties is investigating several scenarios independently, including a worst-case scenario and a scenario that is assumed to represent the intended evolution. Another possibility is to calculate risks which include contributions from all scenarios, but this requires a proper knowledge of the scenario probabilities.

2.3.3 Treatment in the safety case

2.3.3.1 Methodology

This section describes how uncertainties have been handled within the long-term safety assessment studies of GRS (Braunschweig). The general procedure has been basically the same for more than 20 years. The examples in the following are taken from the ERAM study for the LAW repository in an abandoned salt production mine near Morsleben. This is one of the most recent and most detailed studies by GRS.

Scenario uncertainties have been treated, as mentioned above, by investigating a normal evolution scenario, a worst-case scenario, and a limited number of additional scenarios that appear interesting by some reason. A quantification of scenario probabilities and calculation of risks has never been performed so far. Model uncertainties have mainly been handled by using conservative models. In some cases, however, model alternatives have been switched by use of artificial parameters as described above. In such cases, the model uncertainty is mapped to a parameter uncertainty and can be treated in the same way. Therefore, in the following only parameter uncertainties are considered.

Identification of uncertain parameters

Not all parameters in a safety assessment are uncertain. Geometrical dimensions of containers, distances in the mine building or well-known material constants like the mass density belong to the parameters that are more or less exactly known. Others may be less well-known, but are likely to have little influence on the results and can also be considered certain. In cases of doubt the value is chosen conservatively. In the ERAM study examples of such parameters are the void volumes in the different levels of the mine, or the radionuclide inventories, which have been collected over decades and can in some cases only be estimated.

The number of parameters that are really treated as uncertain should be kept limited, in order to allow a manageable uncertainty analysis. If for parameter a clearly conservative value can be given that is not too far away from the most probable value, are preferably simply assumed to be certain. Particularly those parameters that are suspected to have a nonlinear or unclear influence on the calculation results are selected for an

uncertainty analysis. In the ERAM study, these are 43 parameters, comprising things like global and local convergence rates, reference porosity, corrosion rates, gas entry pressure, initial permeabilities of seals, distribution coefficients and diffusion constants.

Bandwidths and probability distribution functions

Each uncertain parameter has to be assigned a bandwidth interval. This can be a difficult task, as, if chosen too small, the bandwidth does not come up to the real uncertainty and, if chosen too big, it could jeopardise the proof of safety. Therefore, the interval boundaries have to be fixed carefully and with as much expertise as possible.

The next step is defining a probability distribution function (pdf) for each uncertain parameter. There is no unique procedure for this task. So far, mainly three types of distributions have been used:

- Uniform distribution: If a parameter is known (or suspected) to lie anywhere between the boundaries with no preferred value, a uniform distribution is applied. In some cases the interval is divided into sub-intervals with different but constant probabilities. This is sometimes called a histogram distribution.
- Triangular distribution: If the parameter has a clearly preferred value within its interval but no other information is available, a triangular distribution should be chosen. It can be symmetric or asymmetric.
- Normal distribution: If a preferred value and a typical deviation is known, a normal distribution should be chosen. From a mathematical point of view, a normal distribution extends to infinity on both sides, which is physically doubtful and numerically problematic. Therefore, an interval is defined also for these parameters and the distribution must be cut at the boundaries. Sometimes, it seems plausible to choose a normal distribution within a given interval around some mean value but the standard deviation is unknown. In this case, the standard deviation has to be calculated from the interval boundaries. It is common practice to take the boundaries as the 0.001- and 0.999- quantiles of the distribution, which corresponds to a bandwidth of 3.09 times the standard deviation to both sides of the mean. This is unchangeably fixed in the EMOS code package, which has been used for all GRS studies. Therefore, it is neither possible to choose an asymmetric normal distribution nor to define the interval boundaries and the standard deviation independently.

All distribution types, except the triangular distribution, can be applied either on a linear or on a logarithmic scale. If the interval spans more than one order of magnitude, a logarithmical distribution is preferred. This pertains to parameters like diffusion constants, distribution coefficients or permeabilities. If the interval is smaller than one order of magnitude, normally a linear distribution is adequate.

Deterministic parameter variations

In the normal procedure of a safety assessment study a reference case is defined for each scenario under consideration. Every parameter is assigned a reference value within its bandwidth interval, which is either considered the most probable value or a slightly conservative one. The first exercise to investigate the influence of the uncertainty of a parameter is a deterministic parameter variation. The parameter is varied between several discrete values within its bandwidth interval, normally the boundaries possibly a few additional values, while all other parameters are kept on their reference value. Comparing the results with those of the reference case and interpreting the differences in detail often yields valuable information about the influence of the parameter. This information, however, has a qualitative character und must not be misinterpreted. If the results hardly change under variation of a specific parameter, this does not necessarily mean that the parameter generally has little influence. The observed behaviour can be due to the specific situation that results from the reference values of the other parameters and can be totally different for another combination of values.

The variation of a single parameter, keeping all others constant, is called a local parameter variation. The word ‘local’ does not mean that the variation is very small but refers to the fact that only one of the parameters is considered.

Probabilistic uncertainty analysis

For a quantitative determination of the uncertainty of the result of a model calculation, a probabilistic uncertainty analysis must be performed, varying all parameters within their bandwidths and regarding their pdfs at the same time. The model is run for a number of times, each with a new set of parameter values. A complete set of n parameter value sets is called a sample of size n.

The necessary sample size can be derived from accuracy requirements. In Germany, there is no official regulation so far, but criteria of 90/90, 95/95 or 99/90 are discussed.

The first of these numbers specifies the minimum percentage of adherence to some safety criterion normally given in form of a limit; the second number is the statistical reliability of this statement in percent. A criterion of this type specifies the admissible number of limit exceedings, but does not say anything about the acceptable amount by which the limit is exceeded. It can be shown that, if the sample is randomly chosen and all calculated results remain below the limit, a sample size of 22, 59, or 230 is sufficient to prove the 90/90, 95/95 or 99/90 criterion, respectively. This does not depend on the number of parameters. The actual number of runs, however, has been essentially higher in most studies.

There are different sampling strategies. GRS has most often used a random sampling strategy because it guarantees a statistical independence of the parameter values, which is often required by the mathematics. Intended parameter correlations can be taken into account as well in the sampling as in the evaluation. In some older studies Latin Hypercube Sampling (LHS) was applied, which allows a better covering of the total bandwidth of each parameter.

For evaluating the results and assessing the uncertainty of a model calculation, several statistical measures like mean, median or maximum are calculated. This can either be done for the absolute maxima of all runs or a specifically interesting point in time. If calculated in small steps for the total model time, the statistical values can be plotted as time curves. Another curve that is valuable for the uncertainty analysis and has always been plotted in GRS studies is the Complementary Cumulative Distribution Function (CCDF). It represents the relative frequency of runs with absolute maxima above some value versus this value. Typically, this curve has an s-shape, starting at 1 with a relatively steep decrease in the middle region and a flat tail at the end, finally reaching 0. It allows a much better assessment of the adherence to some limit than a simple statistical criterion like those mentioned above. Very useful information can also be gained from scatterplots with one dot for every run, each showing the maximum value and the time of its occurrence. These plots show, on the first sight, the highest maxima as well as the most critical time intervals. Additional interesting information can be extracted if the dots are coloured according to some properties of interest. In the ERAM study, the dots have been coloured after the radionuclide responsible for the absolute maximum. The plots show very clearly which radionuclides are responsible for the earliest, the latest, the highest, and the most maxima for each scenario.

Probabilistic sensitivity analysis

Sensitivity analysis is an own topic, but since probabilistic sensitivity analysis is closely related with uncertainty analysis it is briefly addressed here.

On the basis of a probabilistic set of calculations a global sensitivity analysis can be performed, meaning that the sensitivity of the calculation result to individual parameters under consideration of the influences of all others is investigated. A sensitivity analysis requires a much higher sample size than an uncertainty analysis. On the other hand, the sample size is limited by the computing time. By this reason, in older studies the sample size was typically a few hundred, while in the ERAM study it was chosen to be 2 000. Generally spoken, the sensitivity analysis is the more accurate, the bigger the sample is.

There are a number of different methods for probabilistic sensitivity analysis. One simple approach, named after Pearson, is to calculate the correlation coefficients between the output of the model and each individual input parameter. The higher the absolute value of the correlation coefficient is, the higher is the sensitivity to the respective parameter. A positive coefficient means that the result increases if the parameter does so, a negative value indicates an inverse correlation. Another technique is performing a linear regression and determining regression coefficients for each parameter. A high regression coefficient means a high influence of the parameter to the result. There are some more similar, but more sophisticated, methods. All these methods are linear, which means that they work best for linear systems. Since, however, the models for final repositories are typically very complex and non-linear, the use of these methods is limited. A possibility of improving their significance is to perform a rank transformation. This means that each parameter value as well as the output value is replaced by its rank in the ordered list of all values in the sample. The rank transformation makes many models, at least monotonic ones, closer to linear, but at the cost of losing the quantitative relevance of the results. So far, GRS (Braunschweig) has always performed a rank transformation in sensitivity analysis studies.

A somewhat different approach to sensitivity analysis is two-sample tests like the Smirnov test. The sample values of the parameter under consideration are divided in two groups, one containing the upper 10 %, the other the rest. If there is a significant difference between the results obtained with the two groups, the parameter is considered important.

During the last years, variance-based sensitivity analysis methods have increasingly attracted attention. Such methods use the statistical variance for calculating sensitivity measures that do not require linearity or monotonicity of the model and can be quantitatively interpreted, but need high sample sizes. The most general theory was given by Sobol, but the technique proposed by him is complicated and computational expensive. A more practical approach is the Fourier Amplitude Sensitivity Test (FAST), which is based on the idea to scan the parameter space periodically with individual frequencies for each parameter, and to recover the frequencies in the model output value by means of a Fourier analysis. It can be shown that the sensitivity measures calculated with FAST are the same as those proposed by Smirnov. The FAST method has not yet been applied by GRS in practical studies, but it has been tested for demonstration purposes. It could be shown that the FAST technique works and can yield valuable additional information, compared with a linear sensitivity analysis.

Linear as well as variance-based sensitivity analysis can be performed with the software tool SIMLAB which is planned to replace the statistical components of the EMOS package in future.

2.3.3.2 Related topics

The issue of uncertainty management is related to a number of other topics:

- the assessment strategy,
- the safety approach,
- analysis of the evolution of the repository system,
- definition and assessment of scenarios,
- safety indicators and performance/function indicators,
- sensitivity analysis,
- modelling strategy,
- criteria for input and data selection.

2.3.3.3 Databases and tools

The EMOS code package used for the GRS studies automatically calculates three linear sensitivity measures on a rank basis (Spearman rank correlation, partial rank correlation, standardised rank regression), and the Smirnov test. The methods are applied to the maximum value as well as to a number of points in time that may appear interesting. The parameters are ranked after the calculated significance for each method, and then an average ranking is calculated.

Linear as well as variance-based sensitivity analysis can be performed with the software tool SIMLAB which is planned to replace the statistical components of the EMOS package in future.

2.3.3.4 Application and experience

The results of uncertainty analysis are usually presented in different forms. In all German studies performed in the past, the complementary cumulated density function (CCDF) for the maximum was plotted. That means that the maximum output values of all runs, regardless of their time of occurrence, are evaluated together. The cumulated frequency of maxima above some value is plotted against this value. This results typically in an s-shaped curve starting at 1 for very low output values and ending at 0 for very high ones. Another method of presentation is a histogram plot directly showing the frequencies of maxima lying in specific intervals. Both diagrams are shown together exemplarily for the ERAM study in figure 2.3. It can be seen that two of 2 000 runs yield maxima slightly above the limit.

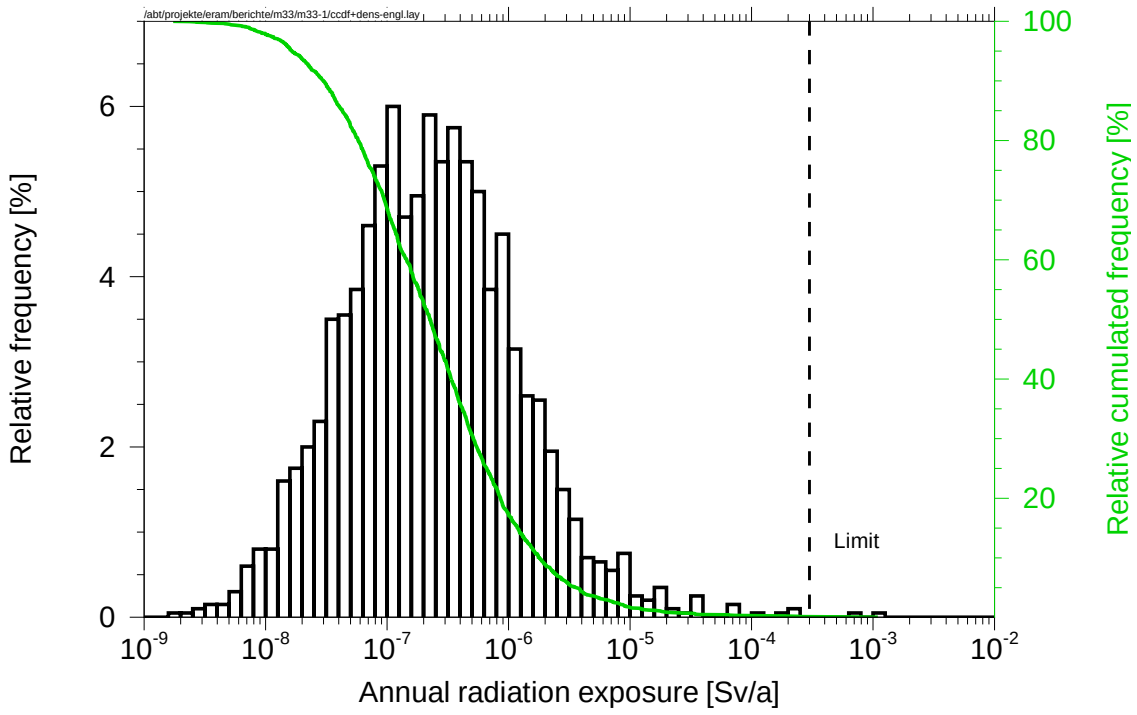

Fig. 2.3 Complementary cumulative density function (CCDF) and frequency density for the ERAM study (2 000 runs)

A very illustrative way of presenting the results of a probabilistic analysis is shown in figure 2.4 for the ERAM study. The absolute maxima of all runs are plotted in a scatter diagram versus the time of their occurrence. Additional information is provided by colour-coding the radionuclides that are responsible for the respective maxima. Only five different radionuclides appear in the diagram. The earliest maxima occur after a few hundred years and are caused by ^{90}Sr or ^{137}Cs, which are relatively short-lived. These maxima are due to the extremely pessimistic assumption that the whole mine is flooded instantaneously after repository closure. The most maxima are caused by ^{126}Sn and remain well below the limit of $3 \cdot 10^{-4}$ Sv/yr. At medium times there are some maxima caused by ^{14}C, at very late times ^{226}Ra as a decay product of ^{238}U becomes dominant. A few maxima at medium times are caused by ^{226}Ra from the inventory.

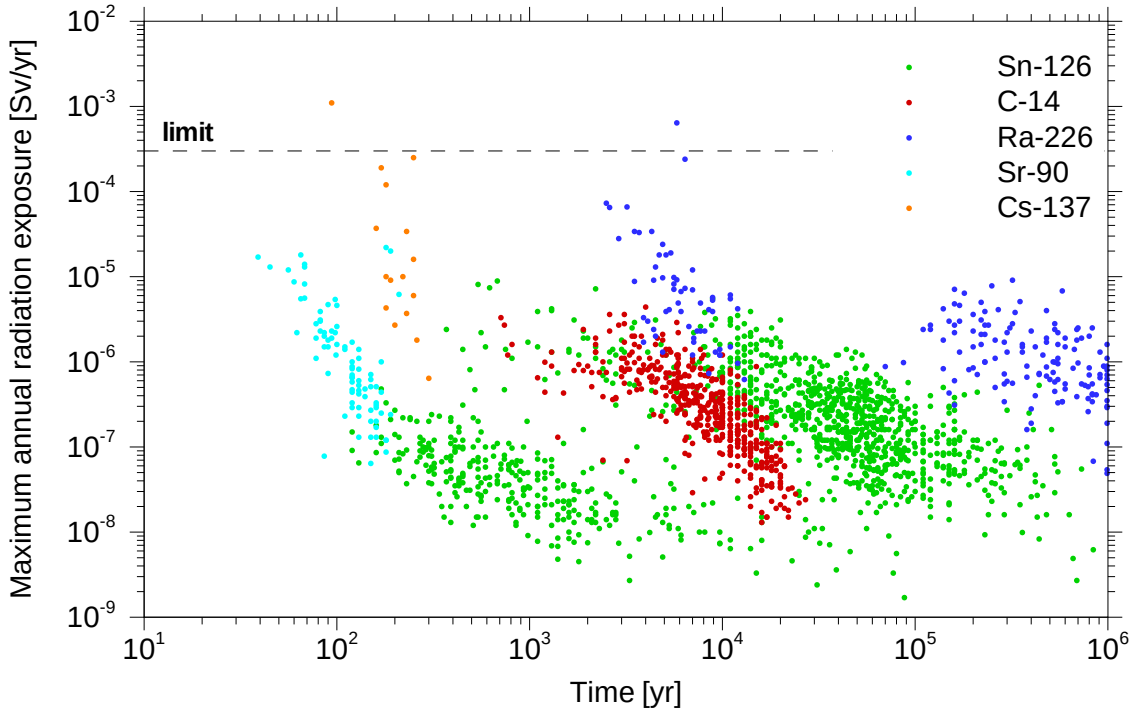

Fig. 2.4 Times and values of maximum radiation exposures

2.3.3.5 On-going work and future evolution

It is planned to create a basis for a more systematic uncertainty management. This comprises unique rules for establishing appropriate probability distribution functions according to the degree of knowledge, as well as applying standardised criteria for evaluation of the results.

2.3.4 Lessons learnt

Uncertainties can be managed by using conservative models or values or by probabilistic methods. Both approaches should be applied as they complement one another. A probabilistic uncertainty analysis should always be performed since it is the only possibility to provide quantitative measures that can be checked against formal criteria. The sample size has to be oriented at the formal criteria to be held, as well as the requirements of the methods to be applied.

A sensitivity analysis is a very useful supplement to a pure uncertainty analysis and should always be performed. Deterministic parameter variations help understanding the system behaviour and provide a qualitative local sensitivity analysis. A global sensi-

tivity analysis requires probabilistic techniques and should be performed in combination with the uncertainty analysis.

The methods for defining bandwidths and pdfs are not very systematic so far. Often they are defined by a quick expert guess. This is not satisfying. There should be a clear and transparent procedure which leads to a unique bandwidth and pdf under consideration of all available knowledge. The development and testing of such a procedure is a task of the next years.

The linear methods of sensitivity analysis, which have been applied exclusively so far, seem to be insufficient to analyse the system behaviour correctly. It is possible that they yield even misleading results. Therefore, variance-based methods should be tested in detail, the more as the computational powers of modern hardware allow increasingly big sample sizes. It has been showed that such methods can yield some added value. There is, however, no experience so far about necessary sample sizes or specific problems like the considering of statistical parameter correlations.

2.4 Evolution of the repository system

2.4.1 Background

This document describes the approaches applied by GRS-B for analysing and implementing the evolution of the repository system in performance assessment (PA) modelling for the disposal of high level waste (HLW) and spent fuel in salt rock formations in Northern Germany. This document deals neither with the evolution of repositories for intermediate level waste (ILW) nor repositories for other host rock types such as clay or granite.

In Germany salt domes are one of the favoured options for the disposal of waste in deep geological formations. The large number of more than 200 existing salt domes in Northern Germany shows, that salt masses can be exposed to deformation and halokinesis without being significantly dissolved, even during times where glacial and interglacial periods occurred and periodically covered the area. During some glacial periods the salt formations were covered by ice sheets of several 100 m thickness (figure 2.5) exposing the formations to high mechanical stress and causing inflow of a high amount of freshwater into the overburden.

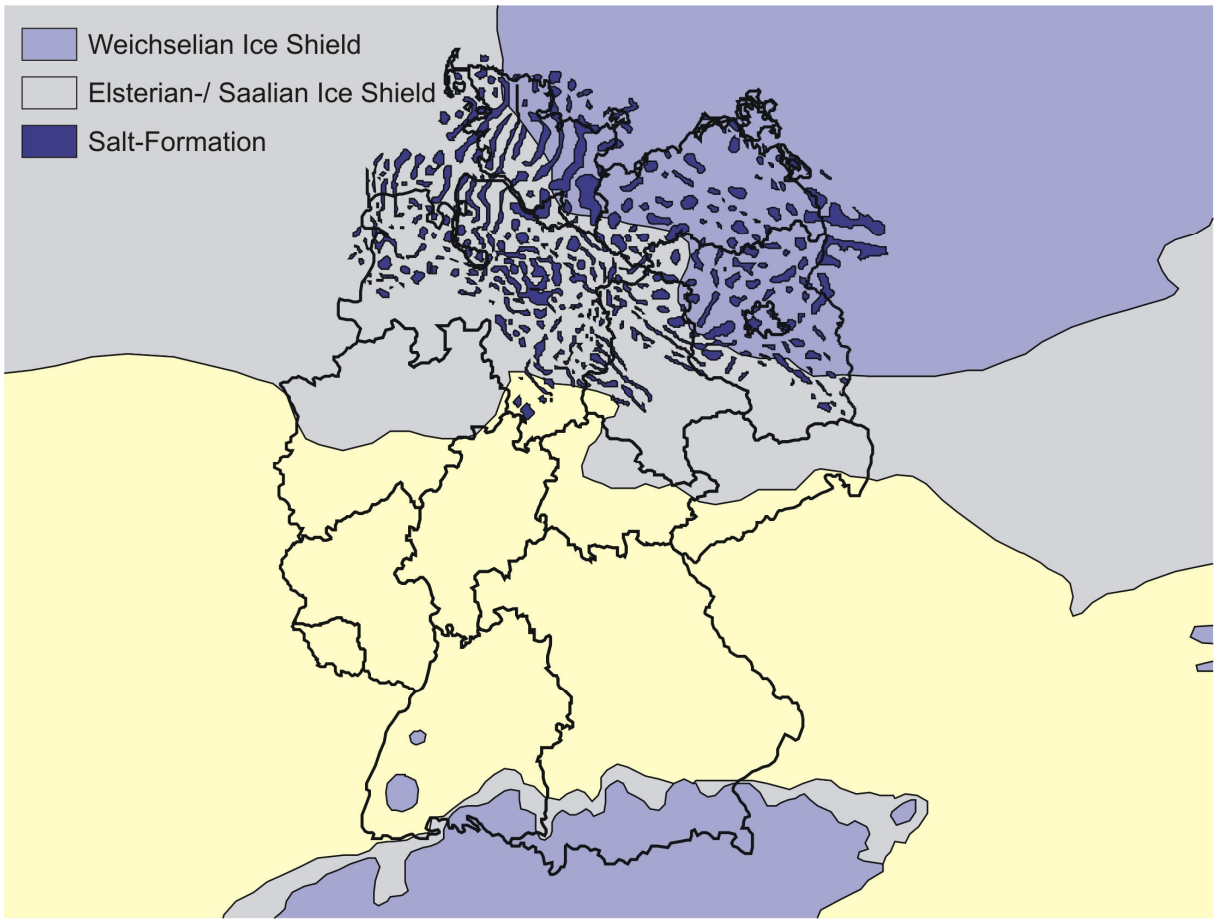

Fig. 2.5 Location of salt domes in Germany and the extension of ice covers during the last glacials /NOS 08/

This high persistency to mechanical stresses and other exogenic and endogenic geological processes in the past gives a good indication that the salt domes in Northern Germany can provide stable conditions for deep geological repositories (DGR) in the future.

2.4.2 Regulatory requirements

As said above, there are no regulatory requirements or guidelines how to deal with the evolution of the repository system up to now. However, PA must be performed according to the state of the art. For a detailed description of these criteria see the contribution of GRS-K. The safety criteria undergo currently a thorough revision. The new regulations have not been fixed yet, but it becomes apparent, that they will contain some requirements and statements that have a direct impact on the assessment of the evolution of a repository system. The following issues have to be taken into account:

- the main aspect of the safety concept is the proof of the safe enclosure of the emplaced waste; the most important component of this concept is the proof of the integrity of the isolating rock zone,
- the assessment period is one million years,
- possible evolutions of the repository system have to be distinguished according to their probability; the probability defines the way how to deal with an evolution of the repository system and its consequences,
- the assessment of a human intrusion to the repository can not be carried out by defining probabilities; these evolutions must be analysed in a special set of scenarios,
- events with direct consequences on human health that outreach the consequences of the repository system influenced by this event are not to be regarded (e. g. impact of a large meteorite),
- the nature of the biosphere and the diet of future generations can not be predicted for the whole assessment period; the evolution of the biosphere has to be presented in standardised or simplified way based on today's conditions.

2.4.3 Key terms and concepts

2.4.3.1 Safety concept

As stated in the regulatory requirements, the safety concept is based on the proof of the safe enclosure of the emplaced waste and its isolation from the environment. The proof of safety is based on numerical analyses and a collection of plausible arguments that support the concept for a defined safety level. The safety level and the required grade of isolation have not been defined yet. The main barrier is provided by the tight and long-term stable rock salt formation. The safety concept is thus focussed on the proof of the integrity of the salt formation, which is supposed to guarantee the isolation of the waste.

The function of the engineered barriers is to reseal the disturbed salt rock formation after the closure of the repository and to prevent the inflow of significant volumes of brines into the repository until the convergence of the rock salt seals the man-made voids and cavities and the safe enclosure of the waste is ensured.

2.4.3.2 Repository design

Since a site has not been selected yet in Germany, all design studies have a preliminary character. However, based on the defined safety concept the following features must be considered for a repository in rock salt:

- sealing of shafts and access drifts,
- backfilling of voids and cavities with crushed salt,
- minimisation of the water content within the repository (e. g. backfilling moisture) in order to minimise container corrosion and gas production,
- limiting the maximum temperature in the rock salt formation to 200 °C in order to avoid mineralogical or crystallographical changes of the rock salt,
- thorough exploration of the salt formation in order to minimise the possibility of the occurrence of undetected brine inclusions,
- sufficient distance to brittle (e. g. anhydrite) and thermally unstable (for temperatures < 200 °C, e. g. carnallitite) salt layers as well as adjacent rock formations,
- sufficient thickness of the salt formation above the emplaced waste in order to minimise the effect of subrosion on the integrity of the geological barrier.

2.4.4 Treatment in PA modelling

There is a high uncertainty in predicting the future development of a repository system over long time periods. One method to deal with this inevitable uncertainty is the selection of a set of scenarios, which describes several possible evolutions of the repository system. In this method, called scenario development, a single scenario specifies one possible set of features, events and processes (FEP) and provides a description of their characteristics and sequencing /NEA 01/. In a scenario development a set of such scenarios must be defined and discussed that contains a complete coverage of all relevant possible future evolutions of the repository system.

The main objective of the scenario development is the identification of relevant FEPs that affect the future behaviour of the repository system and the synthesis of these FEPs to an appropriate set of scenarios (i. e. calculation cases for PA models). Beside its importance for the scope of the PA modelling procedure scenario development is

essential for the communication of the modelling results and its underlying assumptions to the public. For this reason the scenario development has to be as systematically and transparently as possible.

In the past two basic approaches have been applied in Germany:

- the identification of all FEPs that can have an influence on the repository system and the emplaced waste and development of scenarios by combining these FEPs to plausible scenarios (bottom-up approach).
- the determination of initiating FEPs for scenarios, in which barrier functions in the repository system are affected in such a way that a contact between brine and waste is possible, and identification of FEPs that are relevant for these scenarios (top-down approach).

The first approach has the advantage to be more objective and traceable, but the step from a complete FEP-list to a set of scenarios has not been accomplished yet without using elements of the top-down approach. For the salt domes in Northern Germany a FEP-list for spent fuel and HLW was generated exemplarily for a reference site taking into account both approaches /DBE 08/. The FEP-database developed by OECD/NEA /NEA 00/ provided the starting point for this FEP-list.

Currently this list is used for the definition of a complete set of scenarios. This work has not been completed yet, but it is commonly accepted (see WP1.1 ‘scenario development’), that such a definition of scenarios must contain a definition of the expected development of the repository system, the normal evolution scenario. All other probable and less probable developments must be defined in altered evolution scenarios. The distinction between probable and less probable evolutions must be carried out according to the regulatory requirements.

2.4.4.1 Normal evolution scenario

The safety concept discussed in chapter 3.1 requires a new definition of the normal evolution scenario for a salt dome in Northern Germany. This definition has not been carried out yet, but it should be based on the following assumptions:

- there are no transport pathways in the host rock (the integrity of the host rock has been proven),

- no relevant fluid inclusions can occur within the repository,
- all geotechnical barriers fulfil their functions during their designed lifetime,
- the material for the backfill and the seal can be compacted in a way, that its remaining permeability is low enough to ensure the isolation of the waste from the groundwater,
- accumulated gas can penetrate the host rock without impairing its integrity,
- the maximum rock temperature will not exceed 200 °C.

In order to make the scenario approach more structured the evidence period of the normal evolution scenario is generally divided in several sub-periods. Normally two main phases are distinguished.

Thermal phase

The thermal phase is defined as the time period where the heat generated by the emplaced waste has a relevant impact on the temperature in the salt formation. Dependent on the definition of a relevant thermal impact this period ends between 10^3 and 10^4 years after the closure of the repository. According to the assumptions given above the convergence of the salt will produce a complete consolidation of the backfill material within several centuries in the normal evolution scenario. As a consequence the emplaced waste will be isolated within the rock salt formation and no radionuclide release from the repository will occur. An excerpt of FEPs from the existing FEP-list /DBE 08/, which play an important role during this phase, is listed in table 2.1.

Tab. 2.1 Important FEPs during the thermal phase of the normal evolution scenario

FEP-Nr.	FEP-Name
2.1.07.01	Convergence
2.1.07.04	Consolidation of backfill material
2.1.09.03	Corrosion of metals
2.1.11.01	Heat production
2.1.12.01	Gas production
2.1.12.07	Release of gas from repository compartment
2.2.01.01	Excavation damage zone
2.2.07.01	Fluids in host rock
3.1.01.01	Radioactive decay

Geological and climatic phase

After the isolation of the waste within the corresponding salt formation three main geological and climatic FEPs must be considered for the proof of the integrity of the geological barrier for salt formations in Northern Germany:

- subrosion,
- halokinesis (diapirism),
- glacials.

Since Northern Germany has been tectonically a very stable region for several millions of years and no indications exist for a fundamental change of the tectonic system in Northern Europe, magmatism and tectonic activities need not considered for the analysis of the evolution of the repository system /BGR 07/.

Subrosion and halokinesis

In the geological phase the isolated waste within the salt formation is continuously raised due to the halokinetic uplift of the salt dome. The salt domes in Northern Germany have generally uplift rates of less than one millimetre per year. Similar rates are determined for the dissolution of the rock salt from the top of the salt dome by groundwater (subrosion). The combination of subrosion and halokinetic uplift causes a 'migration' of the waste to the top of the salt dome over a long time period.

For the Gorleben salt dome the long-term subrosion rate and uplift rate are 0.02 mm/a /BGR 07/. For a repository that is built in the Gorleben salt dome with at least 500 m overlying rock salt, it will take the waste 25 million years to reach the surface of the salt dome. For these conditions subrosion does not affect the integrity of the geological barrier within the evidence period of one million years.

Glacials

During the Quaternary cycles the time frame of glacials has exceeded those of interglacials by far. The last interglacials covered time frames of app. 10 000 years, whereas glacials occurred over time periods of 60 000 to 100 000 years /NOS 08/.

The Elsterian and the Saalian glacials caused a several 100 m thick ice cover above most of the salt domes in Northern Germany (figure 2.5) for a time period of about 10 000 years, whereas the glaciers of the last glacial (Weichselian) did not extend that far and left most of the salt domes without an ice cover. During such glacial time periods without ice cover, periglacial conditions with permafrost down to a depth of 40 m to 140 m have prevailed for several ten thousand years. The formation of glaciers led to a strong subsidence of the sea-level, which caused values about 110 m to 140 m lower than today at the past glacial maxima.

There appeared also strong differences between the last interglacials. Whereas during the warmest period of the Holsteinian interglacial a transgression of the North Sea occurred at the investigation area, this was not the case during the Eemian Interglacial. Whether a future climate optimum will lead to a transgression of the site mainly depends on the amount of deglaciation of currently existing glaciers. A retreat of all glaciers existing today, which may not be expected according to the actual state of knowledge but occurred in earlier times, would result in a sea level rise of about 70 m. Due to the low elevation of the region this might cause a sea-level of about 50 m above today's ground /NOS 08/.

It is not possible to predict the exact characteristics of the future cycle of glacials and interglacials, but it is evident from the past, that the hydrogeological system will undergo fundamental changes. For the integrity of the geological barrier the effect of the glacials can be neglected as long as the barrier above the emplaced waste is sufficiently thick. Higher uplift or subrosion rates due to the change between glacials and interglacials are not expected for a longer period.

Table 2.2 summarizes the FEPs from the existing FEP-list /DBE 08/, which play an important role during the geological phase.

Tab. 2.2 Important FEPs during the geological phase of the normal evolution scenario

FEP-Nr.	FEP-Name
1.2.09.01	Diapirism
1.2.09.02	Subrosion
1.3.01.01	Global climatic changes
1.3.03.01	Transgression / regression
1.3.04.01	Permafrost
1.3.05.01	Ice age (type Weichselian)
1.3.05.02	Ice age (type Elsterian/Saalian)

2.4.4.2 Altered evolution scenarios

Dependent on the chosen salt formation different altered evolution scenarios can be defined. In the past, GRS-B used mainly three types of scenarios for the description of alternative evolutions of the repository system (e. g. /BUH 08/, /CAD 88/). These altered evolution scenarios are focussed on the development of the repository system during the thermal phase.

Anhydrite scenario

A possible natural pathway between the repository and the aquifers of the overlying rock is a vein of the brittle and often fractured salt mineral anhydrite, which is a typical component of evaporite sequences. The repository must be designed and its position in the rock mass must be selected in such a way, that the development of such a pathway is avoided. For the Gorleben salt dome this scenario can be excluded from the list of possible altered evolution scenarios, since the brittle anhydrite layers in the vicinity of the repository has been broken up into isolated blocks during the uplift of the salt dome and thus no continuous path between the repository and the aquifers exists.

Brine inclusion

Brine inclusions of a few cubic meters in volume are known to exist in salt domes /BGR 07/. In anhydrite layers brine inclusions up to 1 000 m^3 were detected. If such inclusions remain undetected during the exploration they can get in contact with the emplaced waste canisters causing corrosion, gas production and potentially a release of radionuclides.

Failure of a geotechnical barrier

Due to the construction of the repository the integrity of the geological barrier is impaired for a certain time period. The geotechnical barriers' function is to prevent any relevant brine inflow through the man-made excavations. If one of these barriers, in particular the shaft seals and the drift seals, do not work in the way they are designed for, a contact between waste and groundwater is a potential consequence. The combined failure of several geotechnical barriers can be excluded from the list of altered evolution scenarios as long as it is ensured that they are independent events and that

each of them has a fairly low probability of occurrence. In this case the combined probability of these events is extremely low.

Table 2.3 contains some important FEPs, which can play an important role in altered scenarios (additional to the FEPs listed in table 2.1).

Tab. 2.3 Possible additional important FEPs for altered evolution scenarios

FEP-Nr.	FEP-Name
2.1.07.07	Mechanical failure of sealing construction
2.1.09.02	Dissolution and precipitation
2.1.09.04	Corrosion of waste matrix
3.2.01.02	Mobilisation of radionuclides
3.2.07.01	Radionuclide transport in the liquid phase
3.2.09.01	Radionuclide transport in the gaseous phase

2.4.5 Lessons learnt and outlook

Considering the requirements of the new German “Safety Criteria” rock salt is still a favourable option for waste disposal in deep geological formations. In the past a lot of arguments have been collected for this option /NOS 07/.

The outcome of the compilation of relevant FEPs in a FEP-list for spent fuel and HLW for a reference site of a salt dome in Northern Germany supports this conclusion /DBE 08/. For the compilation of this list a combination of elements of the top-down and the bottom-up approach was used. This turned out to be a useful approach to gain a complete list of relevant FEPs for the evolution of the repository system.

The crucial point in this approach is to create a comprehensive and comprehensible record of all decisions made during the compilation of the FEP-list. The traceability of these decisions is an essential part for the definition of a set of scenarios that encompass all relevant possible future states of the disposal system (i. e. the definition of a normal evolution scenario plus several altered evolution scenarios).

2.5 Modelling strategy

2.5.1 Introduction and background

In Germany three formations have been under discussion for final disposal of heat-generating and high level radioactive waste, namely rock salt, claystone and granite. Integrated performance assessment models for long-term safety assessment have been developed for all three formations. The description here is restricted on safety assessments for disposal in rock salt, which has been the preferred option for several decades.

There is no recent safety case for a repository with heat-generating and high level radioactive waste. The information presented is based on the study SAM for a repository with HLW, SF and ILW from 1991 /BUH 91/ and the safety case for the repository for LLW and ILW in Morsleben, ERAM /STO 04/.

2.5.2 Regulatory requirements and provisions

The guideline ‘safety criteria for the final disposal of radioactive wastes in a mine’ from 1983 requires that the effective dose to a single human individual is below the acceptance level of 0.3 mSv/a given in the German Radiation Protection Ordinance. This has to be shown by consequence analyses with integrated models for relevant scenarios. Currently, revised safety criteria are under development.

In order to take credit of the inherent uncertainties it is the expectation of the regulator that the calculated dose rates are significantly below the acceptance level. Data uncertainties have to be addressed in the long-term safety assessment, e. g. in probabilistic calculations.

Programs have to be used, which comply with the state of the scientific and technical knowledge. These codes and the underlying models have to be verified and qualified (cf. section 4.1.8).

The application of the biosphere model in long-term safety assessment is mandatory under the German government regulations.

2.5.3 Key terms and concepts

An overall definition for a model is given by the ICRP: A model is a conceptual description of the disposal system or parts of this system, a mathematical description of the concept, and the implementation of the mathematical description in a computer program, and modelling is the process of generating a model and applying it to a specific problem /ICRP 98/.

Usually it is distinguished between a conceptual, a mathematical and a numerical model. A conceptual model is a description of a repository system or subsystem and its behaviour in the form of qualitative assumptions regarding aspects such as the geometry of the system, boundary conditions, time dependence, and the nature of any relevant physical, chemical and biological processes that operate, whereas a mathematical model is a set of mathematical equations designed to represent a conceptual model. A numerical model is a computer code designed to solve the problem defined by the mathematical model.

2.5.4 Treatment in the Safety Case

2.5.4.1 Methodology

Models used in the safety case can be classified mainly into two groups:

- detailed models to characterise the evolution of sub-systems, or the impact of specific processes, or to generate input data for the integrated models,
- integrated models to perform consequence analysis for selected scenarios of the whole repository system.

Detailed models

These type of models is used to simulate model and laboratory experiments and to better understand specific processes or the performance of subsystems as a whole. In some cases such modelling approaches are directly implemented into integrated models for consequence analyses. However in most cases, when identified as relevant, the respective process is implemented in a simplified form. Some of the detailed models are only used to generate input data for integrated models.

Examples for detailed models used for the near field in rock salt are:

- Rock mechanical model for calculation of convergence of residual volumes: Convergence is one of the most important processes for a repository in rock salt. Detailed rock-mechanical calculations are performed to describe this process under in particular the impact of important parameters, e. g. fluid pressure, backfill, or humidity.

- Model for corrosion induced processes in the near field (coupled): A model has been developed, which describes the coupled processes connected with container corrosion in the case of water intrusion into the emplacement area. The processes, which are considered, are volume increase, water consumption, precipitation of salt, gas generation, pressure balance, and the impact on convergence.

- Model for source term, geochemical evolution in the near field, precipitation/sorption processes of radionuclides and dissolution/precipitation of different salt minerals: Models are developed to claculate the mobilisation of radionuclides from the waste matrix observed in laboratory experiments. Geochemical codes are used to describe the development of the geochemical conditions in the near field and to calculate element-specific solubility limits. The same codes are used to calculate dissolution/precipitation processes and their impact on changes in porosity/void volumes.

- Model for the long-term behaviour of an excavation disturbed zone (EDZ) around a sealing or backfilled drift: Modelling of compaction processes considering creep and viscoplasticity of the rock salt, which lead to a sealing of the EDZ after return to a normal stress state.

- Model for gas generation and pressure build-up: A specific programme can be used to perform calculations on gas generation in detail including corrosion, radiolyses and different microbial reactions.

Examples for other detailed models are:

- Model for burn-up and activation calculations of the radionuclide inventory in the spent fuel elements and in the vitrified glass matrix: These models are only used to generate input data for the radionuclide inventory and for the distribution of radionuclides in the different fractions of the spent fuel elements: the spent fuel matrix, the zircaloy cladding and the other metal parts.

- Model for calculations of temperature distributions: These calculations are also performed to derive input data for the integrated model, i. e. the temperature distributions and its temporal changes in the repository.

By the biosphere model dose conversion factors (DCFs) for each radionuclide are calculated assuming today climatic conditions. These DCFs provide the annual dose (Sv/a) to a member of a critical group assuming a unit concentration in the near-surface water (1 Bq/m^3). The dose rates are calculated by the integrated model by multiplication of the radionuclide concentration in the near-surface aquifer and the respective DCFs.

Detailed modelling of the far field

Far field modelling is only of relevance for altered evolution scenarios, where waste forms get into contact with brine and a radionuclide release from the near field occurs. In current long-term safety analyses for repositories in rock salt only the overburden of the salt dome is considered as the far field. Far field modelling is done in three phases:

- modelling of the density-driven water flow (2D, 3D),
- transport modelling (2D, 3D, particle tracking) to identify the transport pathways from the top of the salt dome to the biosphere,
- abstraction of the results from the 2D/3D transport model to a 1D model for performance assessment.

Integrated models for consequence analysis

When modelling the disposal system it is advantageous to divide the global system into different parts that can be treated separately, as long as the interfaces between compartments are properly considered. For a repository in salt formations these compartments are near field (with emplacement boreholes / drifts and infrastructure), far field (overburden) and biosphere.

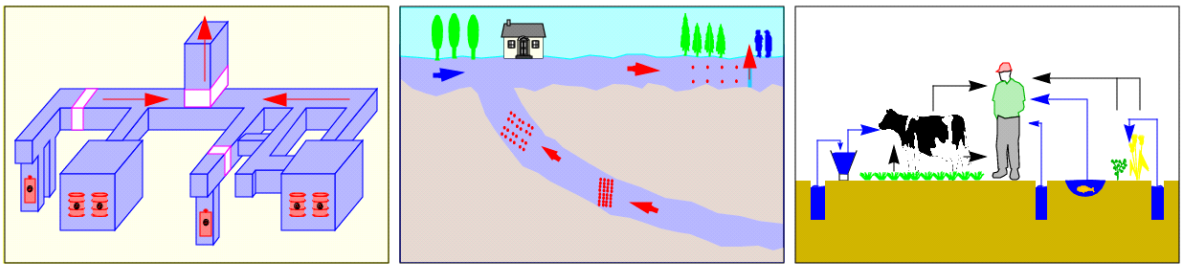

near field **far field** **biosphere**

Fig. 2.6 Schematic representation of the different compartments of the repository system considered for integrated modelling

However, for a repository in rock salt scenarios for normal evolution and altered evolution need to be distinguished. In case of a normal evolution all open voids in the salt dome will be closed after distinct time by convergence. Thereby all potential water pathways will be shut and no radionuclide realease from the salt dome occurs, i. e. the waste is completely confined in the host rock formation. The calculation of this scenario includes the convergence of void volumes, the permeability change of backfill and sealings back to values of undisturbed rock salt and the impact of gas built up by corrosion/radiolysis due to residual water content of the salt formation. All calculations are performed with the near-field model only.

In case of an altered evolution scenario at some point in time water will get into contact with the waste and radionuclide mobilisation and release will occur. For modelling of altered evolution scenarios the water-pathway and the gas-pathway are currently distinguished. Processes considered for the water pathway are:

- temperature distribution and temporal change,
- flooding of the mine by groundwater and water from brine inclusions,
- convergence including spatial heterogeneity and impact of fluid pressure, backfill and humidity of backfill,
- brine displacement by convergence,
- pressure build-up by gas production,
- gas release after increase above external pressure,
- brine displacement by gas storage,
- porosity-dependent flow resistance,

- container failure,
- radionuclide release from waste matrix,
- radionuclide retardation by precipitation (solubility limits) and sorption,
- radionuclide transport by advection and diffusion,
- instantaneous mixing in each model segment,
- transport through the overburden (geosphere),
- exposition in the biosphere.

Probabilistic versus deterministic approaches

Deterministic parameter variations are performed for basic safety demonstration, to examine the influence of a single parameter and to improve system understanding. Since the impact of a parameter can be completely different under different conditions (non-linearity of the system), deterministic variation of single parameters is, however, not sufficient.

Probabilistic Monte Carlo simulations (simultaneous variation of a certain set of parameters) are carried out to calculate the variability of the calculated dose due to parameter uncertainty and to identify the sensitive parameters according to the correlation between parameter value and calculated dose. This approach is preferred to the practice of a deterministic calculation with a “conservative” parameter set because

- different processes may compete and compensate each other, so that for many parameters it is not evident which choice is “conservative”,
- combinations of conservative values for several parameters are weighted with their low probability of occurrence,
- sensitive parameters can be identified by their degree of correlation between the parameter value and the calculated dose.

Model calculations are also performed to demonstrate the robustness of the repository system, i. e. when it can be shown that even for pessimistic assumptions for initial states and for the evolution of the repository system the acceptance level for the radiation exposure is not exceeded. However, a systematic investigation on the robustness

of the applied models itself has not been performed so far. This issue is currently treated in a national project.

Simplification / abstraction to PA

In some cases complex models are included into the integrated PA models. An example is the coupled model for corrosion in the near field (c.f. section 4.1.1). But in most cases models used on process level are simplified for application in integrated codes. The motivation for simplification is either

- very long computing times due to high complexity or large domains are regarded,
- enough data for complex models are not available, or
- the complexity is not needed for description of the process, which, of course, has to be shown.

A special case is that the model is prescribed by legislation. Examples for each of these simplifications are given in the following.

Geosphere modelling: The detailed modelling of the transport in the far field is briefly described in section 0. It is necessary to use a simple 1D model for the integrated PA calculations. The main reason for this simplification is the extremely long computing time needed for a 2D calculation of large and complex regions. For the PA calculations however many parameter variations and hundreds of runs for Monte-Carlo simulations are needed to assess the influence of the data uncertainties on the result of the calculation and the significance of certain parameters. The model and the input parameters needed to set up a simulation with a 1D code have to be determined by abstraction from the 2D/3D simulations. This can be achieved in different ways. So far particle tracking has been used in the 2D/3D model to determine the main transport pathway and to set up the 1D pathway accordingly. The hydrological units are represented by a small number of different transport sections in the 1D model. This approach can lead to notable differences compared to the 2D/3D model due to the different transport pathways of the different radionuclides. An alternative approach would be the use of a multi 1D model to account for different transport pathways for the different fission products and decay chains.

Mechanistic sorption models: Currently, a lot of studies are performed to develop thermodynamic sorption models. The advantage of these models is that they are able to describe the dependence of sorption coefficients from the geochemical conditions. The direct application of surface complexation models instead of constant Kd-values in the transport codes is only necessary, if changes of geochemical conditions occur and are coupled to the transport, i. e. their application is not necessary for scenarios without temporal changes of geochemical conditions.

However, also for scenarios with temporal changes in geochemical conditions by far not enough data for all radioelements and potential substrates in the overburden of the salt host rock are available. Therefore, these models are only used to back-up Kd-values for important elements for different geochemical conditions and to derive band-with for these values.

Biosphere model: In Germany, the biosphere model is prescribed by legislation and is specified in the rules for the assessment of the radiological impact of nuclear facilities. This approach is kind of a stylised approach, since only one biosphere model – reflecting today´s situation and standardised German exposure pathways – is applied and no uncertainties or future changes of the biosphere are taken into account.

Time scales

Usually the same integrated model is used for the calculation of the normal evolution and altered evolutions of the repository over the time scale of 1 million years. However, in case of the normal evolution of the repository at very late time scales beyond 1 million years it is a question to what extent the process of subrosion (the process of salt dissolution from the top of the salt surface connected to the uplift of the salt dome) might lead to a mobilisation of radionuclides when the rock salt is dissolved down to the repository area and cause consequences to exposed individuals. For this hypothetical, very unlikely scenario a different, highly simplified, conceptual model is used, where the activity inventory is distributed homogeneously over the volume of the disposal mine. Thus, the release rates of activity are proportional to the subrosion rate. This simplified approach seems to be justified due to the long period of time (release starts much later than 1 million years), where the detailed information about the geometry of the mine is questionable.

Validation / verification

Due to IAEA the model verification is the process of determining whether a computational model correctly implements the intended conceptual model or mathematical model /IAEA 03/. Codes are usually verified by comparison with other qualified codes of similar type or if available for the respective test cases with analytical solutions.

For radioactive waste management IAEA defines validation as the process of building confidence that a model adequately represents a real system for a specific purpose /IAEA 03/. Therefore, confidence in the codes is increased by application to as many test cases as possible. Typical test cases for model validation are

- simulation of laboratory experiments and field tests,
- simulation of paleo-systems / natural or anthropogenic analogues,
- comparison with process level models (which is only possible for subsystem models).

2.5.4.2 Databases and tools

For deterministic and probabilistic integrated performance assessment calculations the programme package EMOS is used. It consists of different modules for the compartments near field, far field and biosphere (s. figure 2.7). The interfaces of all modules are identical. Thus it is possible to directly connect each of the models with each other, e. g. to investigate the barrier effect of the far-field by one integrated calculation with and one without a far-field module.

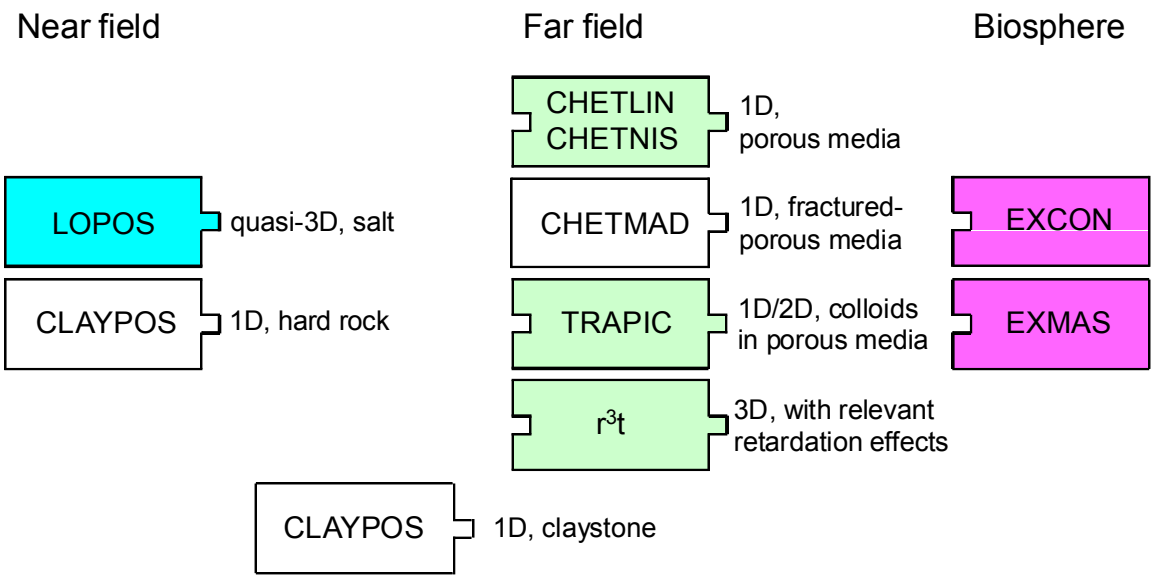

Fig. 2.7 Programme package EMOS with modules for the different compartments (the coloured modules are used for consequence analysis of a repository in rock salt)

For detailed modelling several other codes are used like

- the codes OREST and GRS-AKTIV for burn-up and activation calculations,
- the codes TOUGH and Code Bright for two phase flow: Currently Code Bright is further developed to describe the sealing processes in the excavation disturbed zone,
- the codes Chemapp, EQ3/6, PHREEQC and GWB for geochemical calculations,
- the code d^3f for density-driven flow and the code r^3t for transport calculations in the overburden of the salt dome.

2.5.4.3 Application and experience

The modelling approaches described in section 4.1 have been applied in the long-term safety assessment for a generic repository with all kind of wastes in rock salt /BUH 91/ and are currently applied in the frame of licensing applications for real repositories with intermediate and low-level waste in Morsleben /STO 04, NOS 05/ and in the Asse mine.

2.5.4.4 On-going work and future evolution

The following topics are currently under development:

- improvement of source term models based on actual R&D results, e. g. to include the Si release from the waste matrix, the impact of the Si concentration on the radionuclide mobilisation rates and its transport out of the disposal areas,
- development of a consistent and quality-assured German thermodynamic database,
- investigation of the impact of climate changes on flow and transport in the overburden and on biosphere processes,
- adaption of codes to calculate additional indicators, which are currently discussed within the revision of the German safety criteria, to demonstrate the isolation of the waste.

Furthermore GRS work performed in PAMINA to develop methods to transfer geosphere information from detailed codes to PA transport models is documented in chapter 5.2.

2.5.5 Lessons learned

The application of the models in current implementation processes for the repository for low and intermediate level waste in Morsleben and in the Asse Mine has shown that the basic structure of the integrated model is suitable. During the application the necessity to further improve models in order to simulate specific processes, which might have not been identified by analyses of a generic repository. Examples are implementation of gas storage processes and brine flow through an EDZ.

Another lesson learned is that a quality assurance and consequent documentation of the codes is vital, in particular for longer lasting repository projects, in which knowledge might get lost by experts leaving before finalisation of the project.

The participation in international projects dealing with performance assessment modelling is also very valuable. It represents a good platform for code intercomparisons

which is usually not possible on national level, due to a limited accessibility of suitable codes.

2.6 Sensitivity analysis

2.6.1 Background/Introduction

Sensitivity analysis is an important means in numerical performance assessment for radioactive waste repositories. There is always a high degree of uncertainty about input data and models. Whereas an uncertainty analysis shows how uncertain the calculation results are, it does not give any information about which parameters are mainly responsible for the uncertainty. Such knowledge, however, is essential, because it allows concentrating research specifically on reducing the (epistemic) uncertainty of highly sensitive parameters, e. g., by performing additional measurements or by improving technical procedures.

Sensitivity analysis can be performed using a deterministic or a probabilistic approach. Deterministic sensitivity analysis is done by varying one parameter between a few discrete values while keeping all others constant. The results show directly, how the parameter under investigation affects the model output. Such an approach is often helpful for system understanding. It is also called a local sensitivity analysis because the model sensitivity to one specific parameter at one specific point in the parameter space is analysed.

A probabilistic sensitivity analysis is most often performed as a global sensitivity analysis. This means that a big number of calculations are performed varying all parameters together within their respective bandwidths, as it is also done for uncertainty analysis. For evaluating the calculations a number of different methods are available, such as regression and correlation methods, statistical tests, screening methods, differential methods, variance-based methods, graphical methods and many more. Interpretation of the results has to be done with care because not all methods are equally adequate for all kinds of problems, depending, e. g., on their linearity or monotonicity.

2.6.2 Key terms and concepts

Sensitivity analysis is closely related to uncertainty analysis. Since this is an own topic, the terms and concepts referring to uncertainties are not repeated here.

Deterministic sensitivity analysis is considered an indispensable part of the safety case. Normally, one or several basic cases are defined that describe the evolution of the repository under specific scenarios with specific parameter sets. These parameters are chosen either more or less realistic, or, if possible, from the conservative end of their bandwidths. It is always of interest, how the model system reacts if a parameter that is not exactly known is changed a bit. This is analysed by performing a few deterministic model runs that are evaluated in comparison with each other. Such an analysis can show, for example, that the model output increases with the parameter during one time period but decreases during another one, so that there is no unique monotonic behaviour. A detailed system understanding can only be achieved by performing such investigations. This kind of sensitivity analysis is called local because the system behaviour at one specific point in the parameter space is investigated.

By contrast, **global sensitivity analysis** is the investigation of the model behaviour with a higher number of runs under variation of all parameters together, so that every point in the parameter space is covered by a sufficiently close combination of values. The sensitivity of the model to each individual parameter under consideration of the influences of all others is then analysed by means of appropriate statistical methods. Global sensitivity analysis is normally, though not necessarily, **probabilistic**. While some methods require specific sample generation techniques, others allow re-using of random samples that have already been generated and used for uncertainty analysis. However, a sensitivity analysis requires a much higher sample size than an uncertainty analysis. Generally spoken, the sensitivity analysis is the more accurate, the bigger the sample is.

Three types of probabilistic sensitivity analysis methods have been applied or tested by GRS:

- **Correlation and regression methods.** These techniques determine the influences of individual parameters to the model output by calculating correlation or linear regression coefficients. They are referred to in this paper as **linear methods**. The methods are related to each other and yield similar results. Such methods work

best on systems with a close-to-linear behaviour. The coefficient of model determination, R^2, provides a measure for the performance of the linear methods. It should be above 0.5. If the system is non-linear, but at least monotonic, a **rank transformation** can be performed by replacing each output or input parameter value by its rank in an ordered list. The rank transformation normally improves the performance of correlation and regression methods by increasing R^2 for the price of losing quantitative meaning. Only parameter ranking lists can be put up using rank-based linear methods. In former studies GRS applied correlation and regression methods exclusively in their rank-based version.

- **Statistical tests.** Such tests typically work with two sub-samples, separated by the model output, and compare the parameter distributions. If they differ significantly, the parameter is identified as sensitive. GRS has only applied the **Smirnov-test**.

- **Variance-based techniques.** The total variance of the model output can be decomposed into contributions from the different parameters. This results in quantitative sensitivity measures, called sensitivity indices. While the first-order indices describe the influence of one parameter alone, higher-order indices take account of interactions with other parameters. Especially, the total-order indices are a measure for the influence of one parameter in combination with all others. Different methods (SOBOL, FAST) are available for calculating the sensitivity indices.

2.6.3 Treatment in the safety case

2.6.3.1 Methodology

In the following the methods for sensitivity analysis used or tested by GRS Braunschweig are described in more detail with their specific advantages and disadvantages /BUH 04, SAL 00/.

Correlation coefficients

Calculating the linear correlation coefficients between the model output Y and any input parameter X_j yields a measure for the sensitivity of the model to variations of the respective parameter. These coefficients are named after Pearson (PEAR).

$$R_{\mathrm{PEAR}}(X_j, Y) = \frac{\sum_{i=1}^{n}(x_{ji} - \bar{x}_j)(y_i - \bar{y})}{\sqrt{\sum_{i=1}^{n}(x_{ji} - \bar{x}_j)^2} \cdot \sqrt{\sum_{i=1}^{n}(y_i - \bar{y})^2}} \tag{2.1}$$

A positive coefficient means that the result increases if the parameter does so, a negative value indicates an inverse correlation. A correlation coefficient of 1 or -1 means a strong linear direct or inverse relationship between input and output. If the coefficient is 0 the parameters are uncorrelated, which means that the output is insensitive to the parameter.

Linearity is an essential requirement for the correlation coefficient to be a meaningful measure. A strong but non-linear correlation yields a small correlation coefficient. Since repository models are often not at all linear, the Pearson's correlation coefficients do not make much sense for assessing their sensitivity. Therefore, GRS has exclusively used the rank-transformed version for PA studies.

To perform a rank transformation, the output values y_i as well as parameters x_i are arranged in ordered lists. The highest value is assigned the rank 1, the lowest value the rank n. If several values happen to be equal, they are assigned the same rank number, which is calculated as the mean of the ranks they share. A rank transformation makes a linear relationship out of a monotonic one, which improves the relevance of the correlation coefficients. If calculated on a rank basis, the correlation coefficients are named after Spearman (SPEA). It can be shown that – as long as all ranks are different – the formula simplifies to

$$R_{\mathrm{SPEA}}(X_j, Y) = 1 - \frac{6\sum_{i=1}^{n}(\mathrm{rk}(x_{ji}) - \mathrm{rk}(y_i))^2}{n(n^2 - 1)} \tag{2.2}$$

The rank correlation coefficients are a good means to assess the sensitivity of parameters, but it has to be kept in mind that the rank transformation destroys all quantitative meaning of the calculated measures. The higher the absolute value is, the stronger is the relationship between input parameter and model output, but no statement about the slope of this relationship can be made.

Standardised regression coefficients

Linear regression is based on the attempt to represent the model under analysis, as well as possible, by a linear estimator:

$$y_i = b_0 + \sum_{j=1}^{k} b_j x_{ji} + \varepsilon_i \tag{2.3}$$

with error terms ε_i, which have to be minimised using least squares method. Then the coefficients b_j are a measure for the sensitivity of the model output against variations of the parameters x_j. To allow a unified assessment of these values, the parameters are transformed such that they get the expectation 0 and the standard deviation 1. Then the coefficients are called standardised regression coefficients (SRC). Like the correlation coefficients they are always in the range between -1 and 1, where the absolute value 1 is only reached in case of a strong linear relationship. The numerical values, however, are somewhat different from the correlation coefficients.

The same concept applied on basis of ranks leads to the standardised rank regression coefficients (SRRC). The advantages and disadvantages of this procedure are the same as in the case of correlation coefficients.

The coefficient of model determination, R^2, is defined as the correlation coefficient of the estimated values (without the error correction term) and the real values. If it is close to 0, the estimation is rather bad, whereas a value near 1 indicates a close-to linear behaviour of the model and for this reason a good performance of linear sensitivity analysis methods.

Partial correlation coefficients

If the input parameters are correlated among themselves, accidentally or on purpose, their influences to the model output are coupled. The methods described so far are unable to resolve this coupling and describe the total influence of the input parameters including that resulting from couplings with other parameters. To separate these influences, two regression ansatzes can be made for the parameter under investigation and for the model output:

$$y_i = b_0 + \sum_{p=1, p\neq j}^{k} b_p x_{pi} + \varepsilon_i \qquad x_{ji} = c_{j0} + \sum_{j=1}^{k} c_{jp} x_{pi} + \delta_i \tag{2.4}$$

The partial correlation coefficient (PCC) is the correlation coefficient between the errors ε_i and δ_i. It is a measure for the model sensitivity to the parameter reduced by external influences. It can be shown that in case of uncorrelated parameters these values are identical to the SRCs. If applied on rank basis this concept yields the partial rank correlation coefficients (PRCC), which, of course, are mathematically equal to the SRRCs in case of uncorrelated parameters.

Smirnov test

The Smirnov test checks whether there is a significant influence of an input parameter on the model output. In contrast to the methods described so far, there is no need for a linear or close-to-linear relationship.

The total of all parameter sets of the sample is separated into two subsamples according to the 90%-quantile of the output. That means that the 10 percent of input parameter sets that lead to the highest output values are separated from the others. The distributions of the parameter under investigation in both subsets are compared with each other. If there is no significant difference, the model can be assumed to be rather insensitive to the parameter. The test is performed by calculating the maximum absolute difference between the empirical distributions of the parameter in both subsamples. The hypothesis of equal distributions is rejected with significance α if this difference exceeds the 1-α quantile of the Kolmogorov distribution.

It was observed that the Smirnov test can yield parameter rankings that differ essentially from those derived from correlation or regression coefficients.

Variance-based sensitivity indices

If the model under consideration is neither linear nor monotonic, which is often the case when dealing with complex repository structures, the linear methods perform rather poorly. Moreover, at least the rank-based sensitivity measures have nearly no quantitative meaning.

Variance-based methods /SAL 00/ follow a different approach and do not require linearity of the model. The variance of a statistically distributed parameter is the mean squared deviation from its mean value. To assess the influence of a parameter X_j to the model output Y the expectance of Y is calculated under the condition that X_j remains constant. The variance of this value under variation of X_j is then calculated and divided by the total variance of Y:

$$\frac{\mathrm{Var}_{X_j}[\mathrm{E}(Y|X_j)]}{\mathrm{Var}(Y)} \tag{2.5}$$

This value is a quantitative measure for the sensitivity of the output to the parameter X_j. It is called the first-order sensitivity index. There are different methods to calculate them. The most elegant way is given by Sobol's theory of decomposition of the total variance into terms of increasing dimensionality, which yields not only the first-order indices but also all higher orders, describing the influence of a parameter to the output in coactions with other parameters. Of specific interest are the total-order indices, which take account of all possible parameter interactions.

Another method for calculating the sensitivity indices is the Fourier Amplitude Sensitivity Test (FAST) /SAL 97, SAL 00/. The idea is to scan the parameter space by means of periodical functions with interference-free frequencies and to recover these frequencies in the model output by performing a Fourier analysis. A random element can be introduced by inserting random phase shift at specific points. The frequencies have to be chosen with care, especially if higher numbers of parameters are considered. Whereas the classical FAST yields only the first-order indices, the extended FAST method also calculates the total-order indices within the same evaluation. This is achieved by varying groups of parameters with the same frequency or harmonics for some periods so that they show up together in the Fourier analysis.

In comparison with the linear methods the variance-based methods have some specific advantages. In particular, they allow quantitative assessment and comparison of the parameter sensitivities, even with highly non-linear and non-monotonic models. A drawback, however, is the high number of model runs that is necessary to get reliable results. Moreover, there seem to be some limitations of these methods in practical application. FAST performs rather poorly if applied to problems that depend on discrete or quasi-discrete parameters. A second drawback of the variance-based methods in general is that, though they do not require linearity of the model, the variance is calculated

on a linear scale, and if the output varies over several orders of magnitude, high values are much overvalued. This results in a low robustness of the calculated results.

2.6.3.2 Related topics

Sensitivity analysis is closely related to uncertainty analysis, which has been considered in detail as an own topic. Other related topics are modelling strategy and criteria for input data selection.

2.6.3.3 Databases and tools

GRS uses the EMOS package for executing probabilistic calculations /BUH 04/. The integrated statistical pre- and post-processor is able to perform random or LHS sampling and to calculate linear rank-based sensitivity measures (SPEA, SRRC, PRCC) as well as the Smirnov test. Other methods have been applied using SIMLAB software, which provides a lot of sampling and evaluation methods, including all methods described here /SIM/.

2.6.3.4 Application and experience

Two newer applications of the sensitivity analysis techniques described here are presented in the following. The first is the sensitivity analysis for the Morsleben repository for low- and intermediate-level waste (ERAM), and the second is an exercise of a variance-based sensitivity analysis for a generic repository for vitrified high-level waste and spent fuel in a rock salt formation.

Linear sensitivity analysis

Within the ERAM study a probabilistic uncertainty and sensitivity analysis was performed with 2 000 model runs and a random sample. 43 parameters were selected to be varied within their uncertainty intervals according to appropriate distribution functions, mostly uniform, log-uniform or log-normal distributions /STO 04/.

Several linear methods of sensitivity analysis were applied to the results. Because of the high degree of non-linearity the evaluations were done exclusively on a rank basis. Spearman's rank correlation coefficients (SRCC), partial rank correlation coefficients

(PRCC) and standardised rank regression coefficients (SRRC) were calculated. Additionally, the Smirnov test (SMIR) was performed. Since two of the parameters are statistically correlated the PRCC and SRRC results slightly differ. Generally, however, if applied to the total maximum all methods yield the same parameter ranking for the four most important parameters. These are:

- the initial permeability of the seals,
- the reference convergence rate,
- the cross-section area of the far field transport path,
- the common variation factor for the distribution coefficients in the far field.

On the following ranks the results of the four methods begin to differ, but they are more or less in consent about the first, say, twelve parameters. If calculated not for the maximum but for fixed points in time, the results show that at times below 1 000 years the initial permeability plays no role, but the parameters that govern the gas production, such as the iron corrosion rate, are the most important. This is understandable because in the first few hundred years the release is dominated by gas effects and the seals are very unlikely to fail that early.

These results give some valuable information about the system, but are unsatisfying with respect to some questions:

- How significant is the dominance of the most important parameters?
- How reliable are the rankings of the further parameters?
- Which parameters do not play a practical role at all?

Variance-based sensitivity analysis

In order to find answers to the mentioned questions, some extensive experiments were performed with variance-based sensitivity analysis. The FAST method was chosen since it seemed promising to yield meaningful results at reasonable computational costs, though it is not yet clear whether this was the best choice /BEC 08/.

Two independent FAST evaluations for the ERAM model with all 43 parameters were performed with 10 019 model runs each. They differ only in the seed used for random number generation. The results, however, are unsatisfying, as in figure 2.8. There are

essential discrepancies between both evaluations. All what can be deduced in view of the two sets of results is that the initial seal permeability is clearly dominant over a long model period, and that the importance of the far field parameters (the cross-section area of the transport path and the variation factor for the K_d values in the caprock) increases at late times. These results are in accordance with the rank regression and rank correlation analysis. Other parameters show a non-robust behaviour, such as the reference convergence rate, which seems to have a high importance at times around 10 000 years in one set, but a very low importance at the same time in the second set.

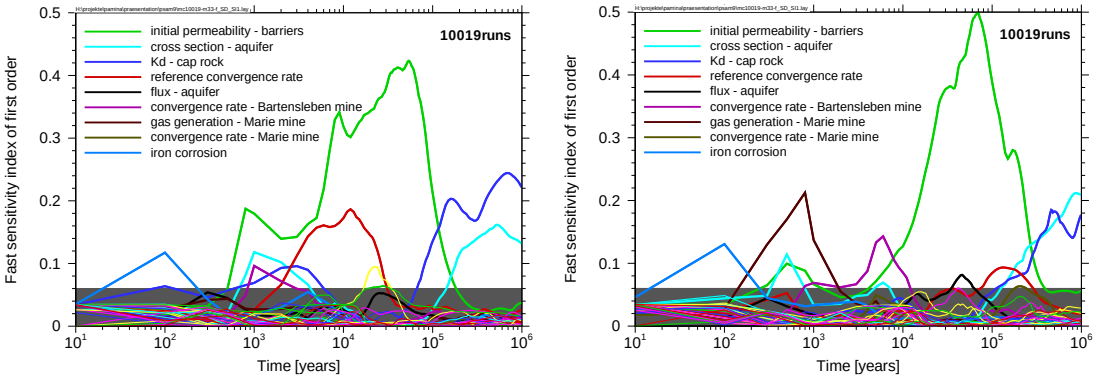

Fig. 2.8 Two FAST evaluations for the ERAM model differing in the seed used for random number generation

Two more sets of 19 995 model runs each were performed, as well as additional investigations with a reduced set of only 14 parameters, without getting more convincing results. This leads to the conclusion that there is some general problem with application of FAST to the ERAM model.

FAST is known to perform poorly on systems with a high influence of discrete parameters. There are two parameters that switch between different options and one parameter that acts a bit like a switch. Deterministic investigations as well as the rank-based regression and correlation analysis have shown, however, that the influence of these parameters is relatively low and they seem unlikely to cause discrepancies of this magnitude. For a time-dependent evaluation, however, the clearly most important parameter, the initial permeability of seals, might also show a switch-like behaviour. Due to a specific corrosion mechanism, the seals of the emplacement areas fail nearly suddenly after some time. At every point in time, the seal of the main emplacement area has either already failed or not, which can make a difference of up to two orders of magnitude in the output. The time of seal failure is directly related to the initial permeability, so that variation of this parameter will, for each point in time, cause a sudden in-

crease of the output at some specific value. It seems plausible that this effect might be the main reason for the unsatisfying performance of FAST. To check this hypothesis two sets of 1 011 runs with only three parameters and a constant value for the initial permeability were performed and evaluated, one with the classical FAST and one with the Extended FAST method. The figure below shows that the results are much more consistent with each other.

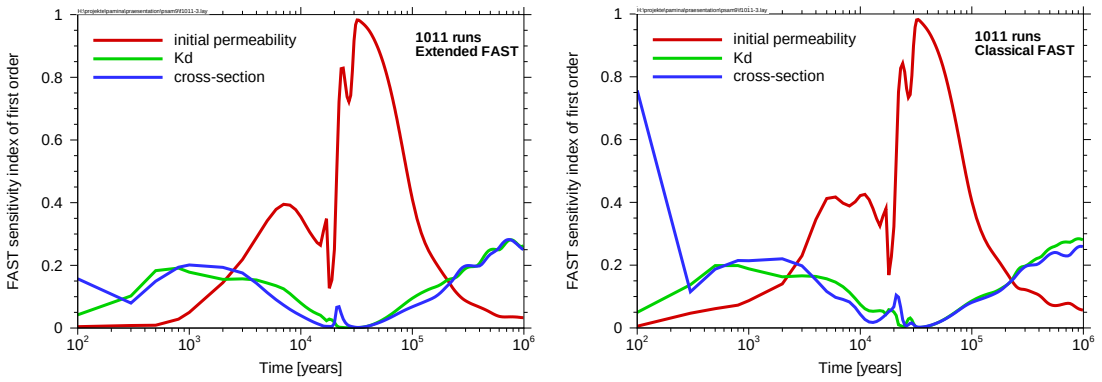

Fig. 2.9 FAST and EFAST evaluations for the ERAM model performed with a reduce parameter set

For the generic SF/HLW repository model one set of 3 030 and one set of 6 054 model runs were performed. A specific scenario was considered assuming a shaft and seal failure, because the normal evolution does not lead to any radionuclide release, and even for this altered evolution, most model runs yield a zero output.

Since the number of parameters was only 6, a lower number of runs than in the ERAM case seemed justifiable. The results, however, are as little convincing as those for the ERAM model. It is apparent that the shaft permeability is the most important parameter, though it does not reach a sensitivity index of more than 0.15. The other parameters have very low sensitivity indices and show no unique behaviour. This cannot be explained with the influence of discrete parameters because none of the parameters has a switch-like influence to the results. There is, however, the phenomenon of zero-output runs. Only 493 out of 3 030 or 885 out of 6 054 runs, yield a non-zero output at all, that means a 15 % probability. It is plausible that FAST does not perform too well on such data sets because a Fourier analysis will not produce sensible results if applied to a zero line. Parameters of low influence could completely vanish in that line. This can be seen at the curves of figure 2.10 below 1 000 years, where obviously none of the parameters is able to break through and all sensitivity indices are calculated as zero. One possibility to get around this problem would be to reduce the parameter

bandwidths such that zero-output runs are avoided as far as possible. This, however, means to change the given distributions and should not be done in a real safety assessment.

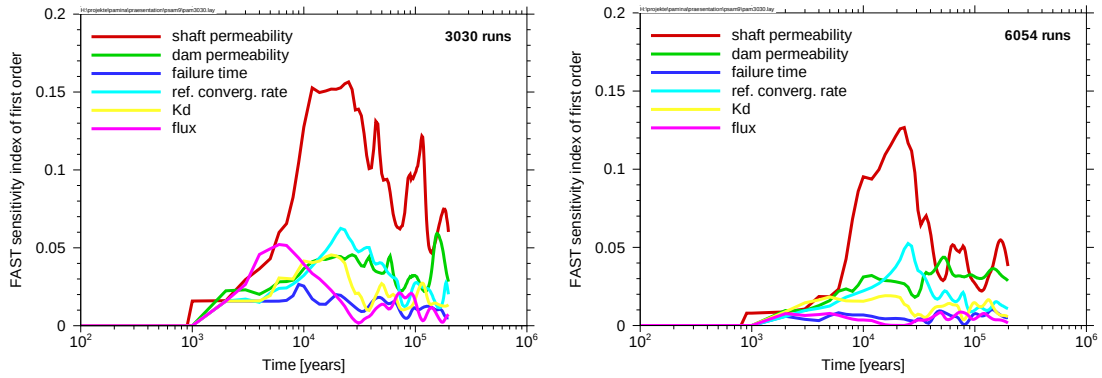

Fig. 2.10 FAST sensitivity indices for the ERAM model

There is, however, a possibility to increase the robustness and significance of the evaluations. This applies not only to FAST but to all kinds of variance-based techniques. The variance of a sample of data is the mean squared deviance from the mean value. The output of performance assessment calculations typically varies over several orders of magnitude and is best presented on a logarithmical scale. The variance, however, is calculated on a linear scale, which leads to a strong overvaluation of high values. One can calculate that in the set of output values from 6 054 runs the highest maximum value alone contributes nearly 10 % to the total variance of all maxima and the 12 highest values are responsible for more than 50 % of the variance. On the other hand, the 5 169 zero-output runs altogether make less than 2 % of the variance. It seems plausible that a variance-based evaluation of such a sample is not very robust.

The idea to handle this problem is to apply the method not directly to the model output *y* itself but to do the following transformation:

$$y^* = \log_2(y/a + 1) \tag{2.6}$$

with some adequate value *a*. In contrast to simply taking the logarithm this transformation does not overvalue extremely small values and allows even zero. It maps 0 to 0, *a* to 1 and big values practically to their logarithm. The problem is to find a proper value for *a*. It indicates the transition from “low” to “high” values. One possibility would be to choose some fixed value that is subjectively considered to mark this transition, discriminating “near-zero” output values from interesting ones. In order to avoid subjec-

tivity, a different approach was followed, calculating *a* individually for each point in time such that the expectation of the transformed distribution gets equal to 1:

$$\mathrm{E}(y^*) = 1 \tag{2.7}$$

This gives equal statistical weights to “low” and “high” values. With this transformation, applied to the set of maximum outputs of each run, the contribution of the highest value to the total variance reduces to 0.7 % and that of the zero-output runs increases to 5 %. In the following figure the time-dependent first order sensitivity indices for the transformed output of both sets of runs are shown. They look, though not identical, much more similar to each other than the curves for the untransformed output and, most notably, give a clearer impression of the real importance of the parameters.

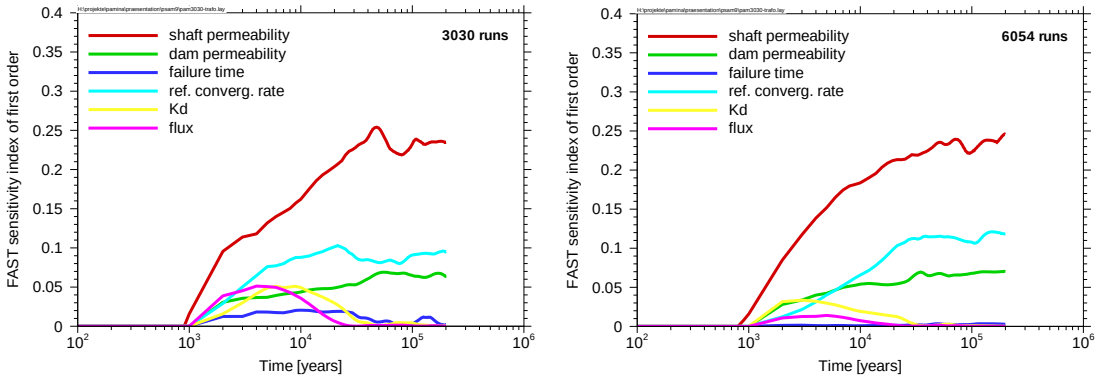

Fig. 2.11 FAST sensitivity indices for the ERAM model after application of the transformation

2.6.3.5 On-going work and future evolution

Presently, more detailed investigations using variance-based methods of sensitivity analysis, including Sobol’s method, are being tested at GRS within PAMINA and other projects. It will be investigated, which methods perform best and yield the most meaningful results under which conditions.

2.6.4 Lessons learnt

In general, sensitivity analysis is an indispensable tool for numerical performance assessment of radioactive waste repositories and should always be applied in a safety case. The linear methods are easy to apply and yield helpful results, but leave some

open questions. Variance-based methods seem promising to provide answers, but need a lot of runs.

When applied to final repository models with a very complex behaviour, as it is typical for rock salt, the FAST method does not seem to perform too well. In the two model systems under consideration two different reasons have been identified to be responsible for this. In the ERAM system, a parameter that often causes a sudden change in the model response at some value seems to disturb the Fourier analysis. Nevertheless, the results confirm and refine those of the rank regression and rank correlation analysis.

In the generic SF/HLW repository system the high number of zero-output runs is likely to cause the evaluation problems. Since in such cases the variance is strongly influenced by relatively few high values, it is expected that other variance-based methods will not perform much better. It could be shown, however, that an adequate output transformation can improve both the robustness and the significance of the evaluation. In view of the high proportion of zero-output runs of 85 % the FAST evaluation of the transformed output is surprisingly good.

Generally, variance-based sensitivity analysis, if applied and interpreted carefully, seems promising to support the safety case better than regression or correlation methods.

2.7 Biosphere

2.7.1 Introduction and background

This document describes the treatment of the biosphere in performance assessment studies performed by GRS. In recent safety analyses the biosphere was treated with a stylised model based on current consumption habits and modelling approaches and parameters prescribed by legislation (cf. section 2). This biosphere model was applied in generic safety assessments /BUH 91/ as well as for site-specific safety cases, namely for the repository for LLW and ILW in Morsleben, ERAM /STO 04/.

However, in the context of the development of new safety requirements, the treatment of the biosphere is under discussion in Germany. Therefore, currently research projects

are performed, which investigate the impact of environmental changes on the biosphere processes. Results from these investigations are also referred to in this document /NOS 09/.

2.7.2 Regulatory requirements and provisions

According to a draft version of the new German Safety Requirements Governing the Final Disposal of Heat-Generating Radioactive Waste (BMU 08), long-term predictions of the potential radiological consequences shall be performed on the basis of representative scenarios and reference biosphere models. However, lifestyles and sensitivities to ionising radiation of future generations are impossible to predict. Therefore, stylised ecosystems should be applied for assessment of radiation exposures. These models should consider the relevant present-day exposition pathways. Additionally, the models should be flexible enough to consider environmental changes in order to provide a reasonable assessment for a range of environmental and climatic conditions.

2.7.3 Key terms and concepts

The biosphere is the surface and near-surface environment that is usually inhabited by living organisms and where human beings live. In the framework of the long-term safety assessment, the biosphere is considered to be part of the entire repository system. The biosphere is not considered to fulfil any safety function but its properties have an impact on the distribution of contaminated groundwater in the environment.

The role of the biosphere models is to assess from predicted radionuclide concentrations or radionuclide fluxes individual doses to members of reference persons, which can be compared to the predefined dose limit. The reference persons are assumed to be members of a small self-sustaining community.

According to the current radiation protection ordinance, dose calculations have to be performed for six different age groups to ensure compliance for all population groups. Furthermore, organ doses have to be calculated and compliance has to be shown with organ-specific dose limits. For radionuclides, which accumulate preferably in specific organs, the organ dose might be the limiting value.

2.7.4 Treatment in the Safety Case

2.7.4.1 Methodology

The evolution of human societies, future living conditions and food consumption habits and the interaction with and impacts on evolving ecosystems in the far future is highly uncertain. Therefore, assumptions for assessing long-term radiological impacts need to build upon stylised biospheres as recommended for long-term impact assessments of nuclear waste repositories /ICRP 98/.

Biosphere model based on today's conditions

In Germany, the common approach of using radionuclide-specific dose conversion factors (Sv a^{-1} per Bq m^{-3}) to include the biosphere in the consequence analysis is applied. The key indicator for safety assessment is the average annual individual dose. Therefore, the main task of the biosphere models of the integrated code EMOS is to calculate dose rates from concentrations or radionuclide fluxes in near-surface aquifers.

It is assumed that the radionuclides enter the biosphere via a well in a near surface groundwater aquifer. Basis for the calculation is a self supplying person, who receives his entire foodstuff from the area, where the contaminated well water is used. Additionally it is assumed that the water is used for different applications without any further dilution. The model is based on the living habits of the present population in a typical area of northern Germany. Since changes of living habits in the far future cannot be predicted accurately, no changes are presupposed for the future. The following exposition pathways are considered:

- ingestion of contaminated drinking water,
- irrigation of pasture and arable land with contaminated water,
- consumption of contaminated plants,
- intake of contaminated water by cattle via watering place,
- feed of cattle with contaminated crops,
- consumption of contaminated meat and milk,
- consumption of fish from contaminated ponds,

– external exposition by occupation on contaminated areas.

Furthermore, the following exposure pathways are usually been considered, which are not explicitly mentioned in /BfS 02/:

– ingestion of contaminated soil particles,

– inhalation of contaminated soil particles,

– ingestion of contaminated soil particles by cattle,

– external exposition by occupation on contaminated areas and

– exposition by occupation in houses built by contaminated material.

A sketch summarising the considered pathways is given in figure 2.12.

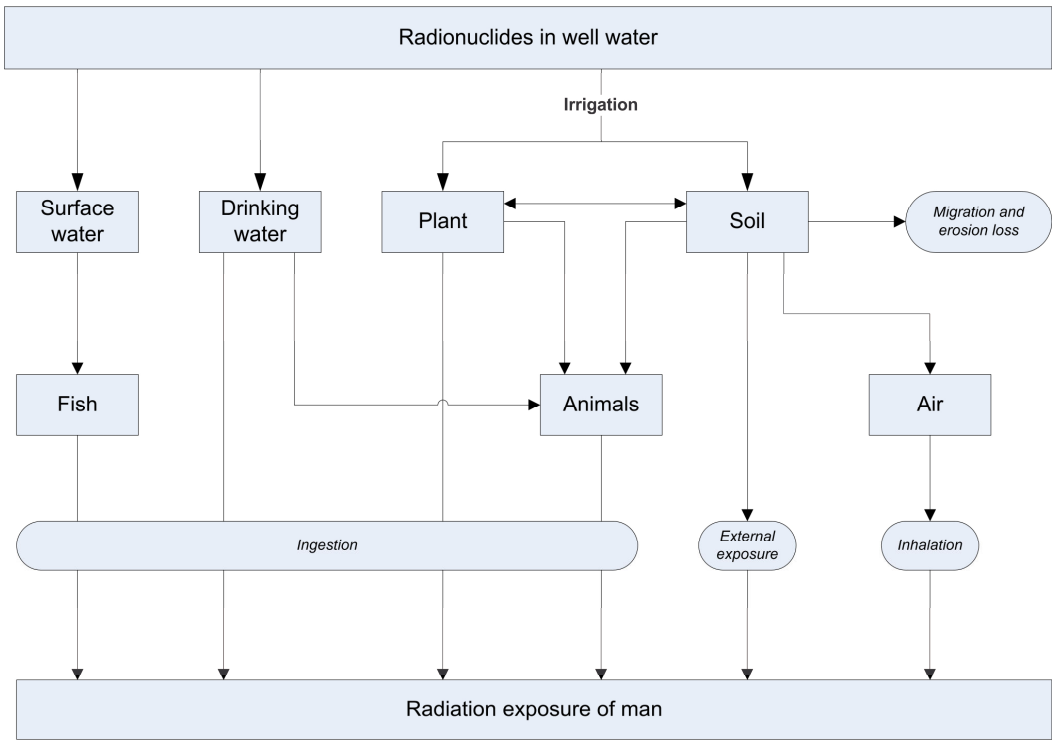

Fig. 2.12 Conceptual model for estimating the radiation exposure to man, if radionuclides enter the biosphere via well water

Currently used dose conversion factors have been calculated in /PRO 02/ on the basis of the general administrative regulation /BfS 02/ using ingestion dose coefficients from /BMU 01/.

Impact of climate changes

Within an R&D project the impact of climate changes on the evolution of the biosphere is assessed. Concerning potential repository sites in Northern Germany a variety of climates may be expected in the long-term future. In order to assess the impact of such different future climatic conditions the potential impact on the base of “what if?” considerations is studied.

In total, six different climate states, which might occur in the far future in the potential repository area, i. e., steppe (Bs), Mediterranean (Cs), temperate (Cfb), boreal (Dfa/Dfb), and tundra (Et) have been considered, respectively. Data for temperature, precipitation, and humidity were taken from so-called analogue sites, which are characterised by these climates today: Marrakesh, Rome, Magdeburg, Rostow, Turku and Vardo, respectively.

Two geosphere-biosphere interfaces (GBIs) have been considered:

- radionuclides enter the biosphere via withdrawal of contaminated groundwater (“well”),
- radionuclides enter the biosphere directly (in case of a high water table) and cause contaminations of soils (“rising groundwater”).

For all climates, dose conversion factors were calculated by a set of biosphere models. The impact of the climate state on the biosphere modelling was considered by differences in the consumption habits, in the required irrigation amounts, in the considered exposure pathways and GBIs, by adapting parameters for radionuclide behaviour in soils (migration and transfer to the plant), in parameters for erosion and resuspension, and in feeding rations for animals.

The results show that the variations among all climates are relatively small for actinides; mostly the differences are less than a factor of 5 with a tendency for increased dose conversion factors with increased aridity. In general, the transfer for these radionuclides through food chains is relatively low, and the mobility within the plant subsequent to foliar deposition is low as well. Consequently, the intake of radionuclides with drinking water dominates over the other ingestion pathways.

Furthermore, the results demonstrate that the dose conversions factors for other radionuclides vary considerably for the different climate states. This variation is strongly dependent on the different geosphere-biosphere interfaces. For the temperate and the boreal climates, the interface “well” causes higher dose conversion factors, whereas in case of the tundra climate, dose conversion factors are higher for the interface “rising groundwater”. The highest variations between the different climates are found for ^{14}C, ^{36}Cl, ^{94}Nb, ^{135}Cs and for the redox-sensitive radionuclides ^{79}Se, ^{99}Tc, and ^{129}I.

With regard to the geosphere biosphere interface, the results from flow and transport calculations in the sedimentary layers above the host rock showed a strong impact on radionuclide pathways, radionuclide transport times and locations of highest radionuclide concentrations.

The model assumptions made for the different climate states require the existence of sufficient groundwater resources. Therefore, the necessary water supply was estimated for an area that is large enough to enable sustainable food production for a small community. It was assumed that this critical group consumes plant food products and has a herd of 30 dairy cows for breeding, meat and milk production that is fed only by locally produced crops. The considerations showed that even for hot and dry climate stages the required well capacities are relatively low. It is not a problem to withdraw such amounts of water even from small aquifers.

2.7.4.2 Related topics

The topic biosphere is closely related to the topics safety indicators and modelling strategy.

2.7.4.3 Databases and tools

There is no specific database for biosphere processes available in Germany. The biosphere calculations are performed by the Helmholtz Zentrum Munich (HMGU), e. g. /PRO 02/. Within the programme package EMOS for integrated safety assessment the modules EXCON and EXMAS are available to calculate radiation exposures from radionuclide concentrations, or radionuclide fluxes, respectively /BUH 99/.

For the study on impact of climate changes the treatment of ^{14}C is different to the other radionuclides. The estimation of ^{14}C in food subsequent to application of irrigation water that contains ^{14}C requires special considerations. It is assumed that ^{14}C occurs as $^{14}CO_2$, $H^{14}CO_3^-$ or $^{14}CO_3^{2-}$. The key process for the fate of carbon dioxide is the photosynthesis, during which CO_2 is converted to carbohydrates. The photosynthesis depends on the environmental conditions as day time, insolation, temperature, water supply and plant species. Part of the carbohydrates is lost in the short-term by respiration, which maintains the metabolism of the plant. Part of it is stored in specific parts of the plant as e. g. tubers or grain.

Carbon dioxide is metabolised by the photosynthesis of the plant and enters via this pathway the human food chain and causes ingestion exposures due to the intake of contaminated food. The use of ^{14}C contaminated water for irrigation of crops is modelled assuming a conceptual model as shown in figure 2.13.

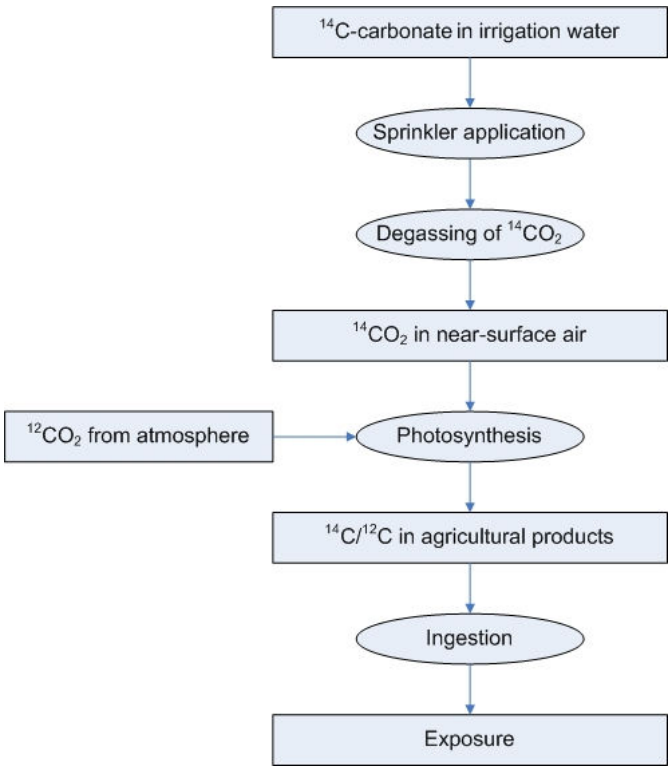

Fig. 2.13 Flowchart of the model to assess exposures due to use of water containing ^{14}C for irrigation of agricultural crops

2.7.4.4 Application and experience

The biosphere model described in section 2.7.4.1 have been applied in the long-term safety assessments for a generic repository with all kind of waste in rock salt, e. g. /BUH 91/ and are currently applied in the frame of licensing applications for real repositories with intermediate and low level waste, e. g. in Morsleben /STO 04/.

2.7.4.5 On-going work and future evolution

Further R&D work on the uncertainties of dose conversion factors and on the impact of climate changes on flow and transport in sedimentary rock overlying the host rock and on biosphere processes is under way. The next step concerns the analysis of transitions between different climate states and the evaluation of potential consequences. These will be compared to the results for the discrete climate states. It is of interest, whether radionuclide accumulation and release processes exist, which might lead to increased dose rates during transitions stages. Additionally, more work is planned on geosphere/biosphere interfaces, focussing on the interrelation between biosphere and geosphere modelling.

This work might build the basis for the development of reference biosphere models to be used in future safety assessment studies.

2.7.5 Lessons learnt

The continuous participation of HMGU in international projects like BIOMOSA or BIOCLIM is of value for the further development of biosphere models; in particular it contributed to the development of models and selection of suitable parameters for the investigation of the impact of future climate changes.

The experience gained so far from these investigations showed the need to adapt the general administrative regulation to the requirements of disposal facilities, especially to consider potential environmental changes at a specific site. Furthermore it showed the need to look in more detail in processes in the geosphere / biosphere transition zone, which are also strongly affected by climate changes.

2.8 Human intrusion

2.8.1 Introduction and background

In Germany three formations have been under discussion for final disposal of heat-generating and high level radioactive waste, namely rock salt, claystone and granite. Integrated performance assessment models for long-term safety assessment have been developed for all three formations. However, concerning human intrusion, scenarios have primarily been addressed in safety assessment for repositories in rock salt so far. Therefore, the description here is mainly focussed on safety assessments for disposal in rock salt, which has been the preferred disposal option for several decades.

There is no recent safety case for a repository with heat-generating and high level radioactive waste. The information presented is based on the studies PAGIS /STO 88/ for a generic repository with HLW and Everest /GOM 97/ for a generic repository with HLW and ILW, and the safety case for the repository for LLW and ILW in Morsleben, ERAM /STO 04/. Additionally, this topic was evaluated on behalf of BfS (Federal Office for Radiation Protection) as one single issue in the report on conceptual and safety related issues regarding the disposal of radioactive wastes /BfS 05/.

2.8.2 Key terms and concepts

Human intrusion scenarios comprise those future human actions that lead to a direct penetration of a repository and damage the barriers within the backfilled and sealed repository area and the host rock. These may either cause direct releases into the biosphere or impair the barrier system of the repository or its safety functions. Human actions with no direct penetration of the repository or the waste canisters form a different type of human action scenarios. These scenarios comprise e. g. those human actions which disturb the groundwater flow regime in the repository system leading to an increase of radiation exposures in the biosphere.

2.8.3 Treatment in the Safety Case

2.8.3.1 Methodology

There is agreement that the development of the mode of live and the behaviour of mankind, or social communities can only be assessed over a short time frame of few generations. Therefore, a systematic development of the scenario group human actions is not possible. However since human intrusion scenarios, after loss of the information about the repository, cannot be ruled out, they have to be assessed within the overall safety case. For the evaluation of human intrusion scenarios in the safety case scenarios should be consulted that are based on today's social conditions and state of the art in science and technology. Such scenarios need in particular be considered during planning and designing of the repository in order to identify appropriate counter measures.

Within the discussion of the new safety requirements in Germany, there is a tendency that the spectrum of human intrusion scenarios to be considered in a safety case should be confined and that the regulator should establish the boundary conditions for the development of such scenarios.

From the human intrusion scenarios, usually those initiated by an intentional intrusion are not included as they are in the responsibility of the respective society and the intruder is in charge of the radiological implications /NEA 95/. In case of inadvertent human actions the knowledge of the repository has to be lost at the time of occurrence. Thus, such kinds of scenarios are assumed to occur not before several 100 years after repository closure. Within the ERAM study human intrusion after 500 years has been assumed and in PAGIS and EVEREST 1 000 years have been regarded as reference values including an analysis of the impact of the occurrence time by sensitivity analyses.

Inadvertent human intrusion scenarios are mainly possible in the scope of exploration or mining activities of future generations. In PAGIS three categories of human activities have been identified, which can lead to an unintentional contact between radioactive waste disposed of in a salt dome and the population /STO 88/. These are borehole drilling, constructions of a mine, and cavern leaching.

Borehole drilling: During drilling of a borehole, which is usually done for exploration, waste containers might be struck. Radioactive material as drilling core or fines can be lifted up to the surface. It appears that very high exposures can occur to a small group of some individuals. The probability of this exposure is, however, extremely low, and during the accident very few people will come into contact with the waste fragments. If the borehole will be abandoned, water intrudes into the borehole and leaches the waste. However, the exposed surface of the waste matrix is very small. The scenario with water intrusion is similar to the cavern leaching scenario, which is discussed below. However, the consequences are expected to be smaller due to the smaller volume of the drilling borehole.

Mining: A mine can be constructed for the purpose of exploitation of salt, for storage or for final isolation of hazardous chemical or radioactive wastes. In the case that newly mined drifts should contact the already existing disposal areas, it is assumed that it will be recognized that a repository for radioactive waste is already present. For further human actions the people living at that time would have to take the responsibility. If the mine is given up and sealed, the old situation will be re-established. During the accident very few people will come into contact with wastes. The doses they receive have shown to be comparable to those for the borehole drilling scenario. On the other hand, newly mined drifts may pass very near to the waste, but in a distance that the containers cannot be recognized. In this case, miners may obtain direct radiation from the waste.

Cavern leaching: A cavern can be created in a salt dome by means of the solution mining technique. The cavern can be used for the storage of oil or gas as well as for exploitation of salt.

Storage cavern: Mining of a storage cavern is a fast process, lasting a couple of months. If the cavern is mined in the area of a repository for radioactive waste, a part of waste packages might be laid open and fall into the sump and can be transported to the biosphere. The highest impact is expected after the operational phase of the storage cavern, when the cavern will be abandoned. The storage medium will be replaced by brine or water. Radionuclides can be transported out of the sump by diffusion and by advection with the brine squeezed out of the sump due to the convergence process.

Salt production cavern: Mining a cavern for salt production can last some decades. Containers are laid open for a much longer time. A considerable amount of radioactivity

may contaminate the brine, which is brought to the surface. Since this brine is used for salt production, a not negligible health hazard to the people consuming contaminated salt is to be expected in this case. After solution mining is completed, the scenario is the same as that of a storage cavern after replacement of the stored medium.

Beside these scenarios, which have been addressed in several safety assessment studies for repositories in rock salt, a general evaluation of the issue human intrusion has been performed on behalf of the Federal radiation protection office BfS. Following the agreement between the German Federal Government and the energy supply companies in the year 2000 a total of 12 fundamental and safety-related issues relevant to all potential host rocks for a radioactive waste repository in Germany had to be investigated by different expert organisations. One of these issues was related to the possible influences of human intrusions into a repository and the consequences for the demonstration of its long-term safety. The results of this study were published in detail /COL 05/ and in short within the Synthesis Report of the BfS /BfS 05/.

The investigations focused at different generic repository types with salt, clay, granite host rock and for a repository where the main geological barrier is formed by an overlying clay capping. For these cases, a set of six covering human intrusion scenarios which lead to an exposure of the public had been identified. Scenarios with intended intrusion or exposures of the intruder were ruled out from the outset. These reference scenarios are:

Mining into the contaminated host rock region: Mining taking place in the surroundings of the repository and host rock material already contaminated is conveyed and deposited at a stockpile. The radionuclides are eluted by the rain and enter into near-surface groundwater, which is used by the population.

Drilling into a waste container: An exploration drilling directly hits the waste and perforates a container. The groundwater flow through the borehole (which is assumed to be backfilled in the meantime) releases the radionuclides adhering at the borehole wall into the groundwater of a hydraulically coupled near-surface aquifer that is directly used by the population.

Drilling into the repository without hitting any waste: An exploration drilling in the vicinity of the repository taps groundwater or brine in the repository region. Flow through the borehole (which is assumed to be backfilled in the meantime) releases contaminated

groundwater or brine from the nearby regions of the borehole, which is transported along the borehole into the biosphere where it is used by the population.

Opening up of an underlying groundwater reservoir under overpressure by drilling: An exploration drilling passes through the repository without hitting any waste and enters into an underlying groundwater reservoir under overpressure. The groundwater raised by the overpressure entrains some contaminated brine from the repository region, seeps away at the surface and enters into a near-surface aquifer, from which water is extracted which is used by the population.

Opening up of a contaminated aquifer by drilling: An exploration drilling for drinking water is put down to an aquifer located next to the repository into which radionuclides from the repository had entered. The contaminated drinking water is raised und is used by the population.

Solution mining of evaporite rocks: In the repository region salt is produced by means of solution mining. Waste containers enter into the brine sump. After corrosion of the containers the radionuclides will be raised with the brine. Table salt will be produced from the contaminated brine which is eaten by the population.

In a semi-quantitative approach the probabilities of occurrence of the scenarios and their radiological consequences had been classified for each generic repository. For evaluation, the probabilities and the consequences were combined to a criterion defined as “relevance” which is a parameter which is similar, but not identical to the “radiological risk”. The results of the study are condensed in table 2.4.

Comparing the relevance of the scenarios and the host rock types it can be stated that the relevance of the scenarios for repositories in salt and clay can be ranked into the categories “moderate” to “low” taking into account the assumed input data and boundary conditions (complete inclusion of the waste forms, repository design, etc.). Notwithstanding a relevance ranking from “moderate” to “high” was obtained for the scenario “Solution mining of evaporite rocks” for salt but only for the wastes with negligible heat generation, because of the long lifetime of the containers with heat generating waste.

For the permeable host rocks (granite and other host rocks under clay capping) relevancies in the range from “moderate” to “very high” were determined for the six scenarios considered. As a result, the relevance of human action scenarios is generally higher

for the permeable host rocks. From the low permeable host rocks (salt and clay) the salt overall showed slightly lower relevancies (except for the solution mining scenario), which mainly results from the comparatively lower probabilities of occurrence.

Tab. 2.4 Comparative rating of the relevance of different human intrusion scenarios and geosystems (from /BfS 05/)

Geosystem	Salt Diapir	Salt bedded 800 m	Salt bedded 1.300 m	Clay-stone	Granite	Other Rocks with Clay Capping
Scenario 1. Mining within contaminated host rock						
total consequence	- (+++)	- (+++)	- (+++)	- (+)	+++	+++
probability of occurrence	- (+)	- (+)	- (+)	+	+	+
relevance	- (++)	- (++)	- (++)	- (+)	++	++
Scenario 2. Drilling into a waste container						
total consequence	++	++	++	++	++	++
probability of occurrence	+	+	+	++	++	+++
relevance	+/++	+/++	+/++	++	++	++/+++
Scenario 3. Drilling into the repository without hitting waste						
total consequence	++	++	++	++	++	++
probability of occurrence	+	+	+	++	++	+++
relevance	+/++	+/++	+/++	++	++	++/+++
Scenario 4. Drilling into a reservoir with overpressure						
total consequence	++	++	++	++	+++	++
probability of occurrence	+	+	+	++	++	+++
relevance	+/++	+/++	+/++	++	++	++/+++
Scenario 5. Drilling into contaminated aquifer						
total consequence	-	- (++)	- (++)	-	++++	++++
probability of occurrence	-	- (+)	- (+)	++	+++	+++
relevance	-	- (+/++)	- (+/++)	-	+++/+++	+++/++++
Scenario 6. Solution Mining of evaporites						
total consequence	+++	+++	+++			
probability of occurrence	++	+++	+++	-	-	-
relevance	++/+++	+++	+++	-	-	-

Categories in brackets apply for the case that pressurized gas is stored in the host rock after creation of secondary porosity

relevance: ++++ very high, +++ high, ++ moderate, + low, - no consequence(s)

caused by: blue – waste with negligible heat generation, red – all waste categories

2.8.3.2 Related topics

The topic human intrusion is related to the topics evolution of the repository system and modelling strategy.

2.8.3.3 Databases and tools

No explicit databases with regard to human intrusion scenarios are available. A new German FEP catalogue based on the classification of the NEA FEP catalogue was recently developed /BUH 08a/. In this catalogue relevant FEPs for human intrusion scenarios are included.

In several cases simple models are used to estimate the impact of human intrusion scenarios. For calculations of the solution mined cavern the near-field code LOPOS (REPOS) /BUH 99/ with modified segment models is (was) used (cf. section 4.4).

2.8.3.4 Application and experience

Human intrusion scenarios have been applied in the safety assessment studies for high-level waste PAGIS and EVEREST and in the frame of licensing applications for real repositories with intermediate and low level waste in Morsleben.

Within PAGIS three activities, which can lead to radioactive waste release from the salt dome, have been analysed: mining, borehole drilling, and leakage of an abandoned storage cavern, which was constructed by solution mining /STO 88/. Valuations showed that the latter scenario is the one, which leads to a maximum release of radioactivity. The assumptions for this scenario were: A storage cavern is created by solution mining technique. The waste canisters of an old HLW borehole, which are laid open during mining of the cavern, are buried in the sump of insolubles. After the storage cavern falls into disuse, it becomes filled with water. The waste form is dissolved and contaminated brine is squeezed out through the entrance shaft. A maximum dose of about $3 \cdot 10^{-5}$ Sv/a has been calculated mainly caused by Np-237 during a time frame from 500 000 to 1 million years. Although the probability of this scenario is difficult to estimate its consequences appear still acceptable.

Within EVEREST the scenario of mining a salt exploitation cavern has been treated in a detailed deterministic and probabilistic computer simulation /GOM 97/. The uncertainty analysis yields a mean dose rate of $8.1 \cdot 10^{-5}$ Sv/year and a standard deviation of $8.7 \cdot 10^{-5}$ Sv/year. The results are spreading over three orders of magnitude and 3.2 % of the runs yield a dose rate above $3 \cdot 10^{-4}$ Sv/year. A sensitivity analysis gives in the order of importance the parameters, (1) time span between waste disposal and cavern mining, (2) reduction factors describing the salt cleaning process, (3) number of caverns mined at the same time, and (4) the freshwater injection rate, as the most sensitive ones, concerning the maximum dose rates. The time span between waste disposal and solution mining of a cavern is, of course, the most sensitive one, since the leading nuclide in most of the simulations is the short-lived Am-241. It can be generally concluded that solution mining followed by salt consumption remains the scenario with the most severe consequences for waste disposal in rock salt. It is therefore recommended to search for design alternatives, which may limit the consequences in terms of probability and exposure of the solution mining scenario.

Within ERAM only those human intrusion scenarios have been considered, which might cause radiation exposures to a larger group of people /STO 04/. The exposure of single persons, as it is the case for workers directly involved in drilling or mining has not been regarded. The three scenarios construction of a cavern, construction of a new mine for raw materials production and an exploration drilling have been considered. The first two scenarios could be ruled out for the respective site, mainly because of the strong folding and high heterogeneity of the salt structure Morsleben, with frequent interstratifications of potassium and rock salt, which would not allow an economic operation of a cavern or mine. Model calculations for the scenario exploration drilling have shown that the water inflow through a backfilled exploration borehole is very low and none of the disposal areas can become flooded within one million years. Hence, no release of radionuclides via the exploration borehole will occur.

2.9 Criteria for input and data selection

The following contribution for the review on “Criteria for input and data selection” has been a joint effort by GRS, BGR and DBE-Tec. The collaboration with J. Weber and J. Orzechowski from BGR and N. Müller-Hoeppe from DBE-Tec is kindly acknowledged.

2.9.1 Background

The long-term performance assessment of deep underground repositories for radioactive waste is based on numerical calculations. These calculations are performed using more or less simplified models that describe the behaviour of the total system, including engineered and natural sections of the near field, the far field with its specific geological properties and the biosphere. Such models can only work properly if adequate and validated input data are used. The quality of the calculations stands and falls with that of the data used. Therefore, data selection is an important topic within PA that requires a thorough proceeding. While, in some cases, it may be relatively easy to determine the input data – either because there is a comprehensive and reliable database, or the model is insensitive to the parameters – in other cases it can become necessary to establish extensive measurement and work programmes aiming at the determination of one specific input value.

Different kinds of data are typically needed in PA calculations. In this paper we use the following categorisation:

- Geological data: data referring to the natural geological environment of the repository,
- Geotechnical data: data referring to the engineered barrier system,
- Other data: everything else, especially including inventory data and chemical data.

In Germany, the geological data are mainly provided by BGR, which is the governmental research organisation dealing with geological issues. Geotechnical data are closely related to the preparation of the repository site and the construction of the EBS. Therefore, DBE-Tec as one of the main contractors of a final repository for high-level waste in Germany is most qualified to provide such data. Finally, all other data that are needed for a PA have to be established by the performance assessor himself, evaluating the available sources. Therefore, this paper has been made in co-operation between GRS, DBE-Tec and BGR.

2.9.2 Regulatory requirements

As a radioactive waste repository in a deep geological formation is located in a mine, the mining regulations must be regarded, e. g. in Germany the federal mining law and

the UVP-V Bergbau /UVP 90/. In addition the repository mine is in fact a geotechnical structure. For this reason the technical guidelines Eurocode 1 “Basis of structural design” /DIN 02/ and Eurocode 7 “Geotechnical Design” /DIN 08/ and the associated national application documents should be applied. Particularly, the European standards provide important information on data selection, e. g. when designing a geotechnical structure. Further on, the method of partial factor design and reliability analysis is exemplified, a semiprobabilistic method permitting the coupling of deterministic approaches and probabilistic approaches in order to design highly reliable structures in practice. However, it has to be noted that for the design of special constructions works, e. g. nuclear installations, dams etc. other provisions than in the Eurocodes might be necessary. The Eurocodes rely on state-of-the-art technology. Nevertheless they serve as a basis for the licensing procedure.

2.9.3 Key terms and concepts

Regarding the European standards, terms and definitions commonly used in the Eurocodes (EN 1990 to EN 1999) are given in chapter 1.5 of the Eurocode “Basis on structural design” (EN 1990:2002).

In section 2 of EN 1990:2002 requirements on structural design are established, subdivided in

- basic requirements,
- reliability management,
- design working life,
- durability (= the technical expression for long-term stability),
- quality management.

Quality management measures comprise the definition of reliability requirements, organisational measures and controls at the stages of design, execution, use and maintenance. The quality management includes internal control as well as external control, e. g. by the experts of the licensing authority or certified testing laboratories.

2.9.4 Treatment in the safety case

2.9.4.1 Methodology

Establishing of input data is an important task within the safety case. First the data needs have to be identified. That means that all model input is checked with regard to the reliability of the values. Data that are clear and well-established can be excluded from the further process. For all other input traceable procedures should be applied and documented that can considerably differ depending on the type of data. In all cases there should be a quality assurance procedure, which includes a checking of the procedures and values by independent experts.

Sensitivity analysis is a good means for discriminating data with a high relevance for the model from those which, though possibly rather uncertain, have low effects to the PA results. If the latter can be proven there is no need to put a high effort in determining such values. Sensitivity analysis is an important tool in PA and is therefore dedicated a specific topic.

2.9.4.1.1 Geological Data

Based on the German waste management concept, radioactive wastes should be concentrated and isolated in deep geological formations. The long-term safe entombment of wastes in a repository and the isolation against the biosphere will be provided by a barrier system, which consists of geological and technical barriers. In this context the geology is vitally important.

A precondition for a qualified repository site is primarily a favourable geological situation as a whole with a suitable geological barrier. Several layers in overlying and underlying strata of the repository, each with individual different facies, represent the system of the geological barrier. They are individually and at large analysed and evaluated. To ensure the effectiveness of the geological barrier in future a series of minimum requirements have to be met /AKE 02/. The effective properties of a barrier are defined by geological, geochemical, mineralogical, physical, hydraulic and strength-related variables. The effective properties of a barrier consist of several single properties as components of the overall effect. No geological component is meaningful describable without the components mineralogy, geochemistry, geomechanics, hydraulic or physic. In

fact, if a question deals only with some of the components the other components take a back seat, but basically, they are always relevant.

Beside these properties of a geological barrier also the conditions of repository location, that means geographic and geological condition in the vicinity the repository site, play an important role.

Approach and Database

Before the geological investigations of a site for a repository start, suitable rock types for the geological barrier are identified according to constraints which arise from the type of waste, the repository concept or legal requirements /NAG 02/. After this a qualified site is chosen on the basis of exclusion criteria and minimum standards by means of geological methods.

There are different methods of data acquisition, data processing and data analysing. Which method is used depends on the considered variables/criteria, the considered kind of rock, or the task of research. Basically the process of site characterisation consists of five steps: data review, data acquisition, interpretation, data matching, and the prediction for future variability.

Data Review

Data bases are technical and lab reports as well as maps which are stored in archives of the BGR (Federal Institute for Geoscience and Natural Resources), the Geological State Offices, the Federal Office for Cartography and Geodesy, and the LIAG (Leibniz Institute for Applied Geophysics). These documentations were mostly established in the context of repository- or disposal projects as well as exploration programs. Furthermore scientific relevant result from other scientific institutes and universities and industry are involved.

Data Acquisition

In addition to data, reports and maps which are already known, extensive field investigations are carried out. There are indirect and direct methods. Direct methods are exploration excavation and field mapping, sounding, drilling as well as geotechnical measurements, e. g. dislocation measurements on ground surface and in boreholes.

Indirect methods are geophysical explorations methods like seismic exploration methods, seismo-stratigraphy by stratigraphic levels, geoelectric, etc.

Further data originate from laboratory tests, calculations and modelling. This data deliver insight into currently conditions and changes in future. Several important criteria are based on laboratory tests, e. g. strengths, dilatancy boundary, stress, permissible strains, permeabilities, composition of groundwater and rocks, etc. The results of numerical modelling, e. g. stresses, strains, deformations, groundwater flow (currently and in future) etc., are basic values to evaluate the stability of the components of the repository and the integrity of the host rock barrier.

Interpretation/Data Matching/Prediction of Future Variability

Proper data documentation allows an interpretation of the geological overall situation and the barrier properties. On basis of the collected data and individual aspects the current geological suitability to dispose radioactive waste in host rock will be assessed and if it necessary further required information are specified.

In this context also the future development of a potential repository site plays an important role. For the assessment of future behaviour of geological structures and formations the consideration of past geological processes are an important aid in addition to modelling. The reference to natural analoga can support the scientific line of argumentation for disposal of radioactive wastes in deep geological formations.

Data for the conditions of repository site

Not suitable to host a repository are areas with intensive seismicity and tectonic, increased trend of uplift, recently volcanism and unfavourable hydrogeological conditions.

Vertical movement

The basis for classification of areas with vertical movements in Germany is provided by maps from the Federal Office of Cartography and Geodesy, maps from geological the State Offices as well as scientific publications on special areas. Additionally, the consideration should also include, that a vertical movement within an area is linked with

the occurrence of geodynamic activities and, therefore, should be interpreted in connection with earthquakes and arrangements of fault zones.

Tectonic stability (active fault zones)

In the emplacement zone, active fault zones (movements within the neotectonic period) must not exist. A general definition describes faults as tectonic or atectonic processes, which modify the primary stratification form of rocks. Therefore, the term comprises both ductile and brittle strain. Dislocation with an explicit off-set can be detected and documented by normal field mapping or seismic exploration methods. For localisation of damaged zones more special methods have to be used, e. g. remote sensing or geoelectricity which registers humidity anomalies, or other geophysical methods.

Seismic activity

The general basis for the indication of earthquake-jeopardised areas in Germany is provided by the German earthquake-catalogue (where all earthquakes in Germany are listed since the year 800), the map of seismotectonic areas in Germany, and the distribution of realised damage quakes in Germany.

Volcanic activity

The assessment whether a region is susceptible to volcanic activity is based on expert poll which assess recent and former volcanic activities, the probability of revivals, and the locations of eruption centres and extensions. Although an intrusion of magma into a repository is very improbably, but nevertheless the consequences of volcanic activities like temperature stress, volcanic quakes and induced fault movements have to be assessed.

Hydrogeological conditions

The hydrogeological conditions mainly consist of surface hydrography (river arrangement, water stage determinations, leakage effects, lakes, water divide, drainage areas, etc.) and the groundwater flow. The hydrography is investigated by means of hydrogeological analysing methods. A minor groundwater flow and therefore an old groundwater age points to a favourable geological situation. The groundwater age can be de-

termined from the concentration and concentration ratios of particular environment-isotopes, e. g. tritium- and C-14-values give an indication for young groundwater.

Data about Effective Barrier Properties

For the acquisition of data about the effective barrier properties surface explorations and subsurface investigations have to be conducted. This exploration work yield knowledge about geological conditions, hydrogeological conditions and geomechanics. Geological descriptions also involve geographic information of the location as well as geometric data, coordinates and the depth of the layers.

Geological Conditions

The general theme of “geology” includes subcategorisations like lithology, stratigraphy, facies, disposal area, structural conditions (macro-fabric like bedding and faulting), thickness, sedimentology, grain size, fabric, rock structure and tectonics. These parameters provide information about evolutionary history and further development of the barrier rocks. Additionally it has to find out, whether a sufficient thickness and extension of homogeneous host rock are available.

In general most of the data rest upon drilling, results of physical measurements, field mapping and laboratory tests.

Drilling and borehole-measurements

In addition to the lithological descriptions of deep drillings the correlation of geophysical borehole-measurements are used for the geological processing of the stratification investigated by drilling. Predominantly used are methods which allow conclusions about petrographic properties of intersected rocks and conclusions about the hydrogeological situation. These also include e. g. the measurement of natural gamma-radiation, self-potential log, focussed resistance measurement, density-measurements /KOE 07/. Different methods of borehole-measurements e. g. electric-electromagnetic-, acoustic- and gravimetric methods, methods regarding the determination of geometrical values, or regarding the property-state variable-movement of borehole-fluids /AKE 02/ provide information about important rock parameters used for the realisation of the final disposal of radioactive waste. Geophysical and geological analyses in connection with drilling give evidences about the borehole and its surrounding rocks. This means that

borehole measurements only provide one-dimensional information with respect to the elected parameter.

Geophysical exploration programs

In order to extrapolate the results of borehole-measurements into plane or space it is necessary to conduct two-dimensional section-measurements or three-dimensional measurements. The choice of measuring methods depends on the parameters to be determined. A possibility for correlation is the interpretation of results from seismic measurements (reflection-, refraction- and surface wave seismicity, as well as high frequency absorption measurement). Seismic measurements are electro-magnetic wave methods and detect impedance differences. Therefore they indicate lithostratigraphic boundaries and other petrophysical heterogeneities (e. g. moist zones). Seismic measurements are done on surface and in deep drillings. By means of the application of high-resolution seismicity the bedding properties of tertiary and quaternary layers are more precisely determined. Results of geophone-immersion in boreholes serve to the interpretation of high-resolution seismicity /KOE 07/.

Results of geophysical exploration programs allow the processing of a rim syncline analysis, the identification of potential migration paths of fluids within the overburden, and allow inferences on lithological bedding, stratification and fault zones. Furthermore the more exact position and shape of the salt dome, the relief of the top salt and the basement of the salt dome as well as the contour lines of the salt dome boundary can be assessed by the geophysical exploration.

Geological Field mapping

Within the framework of data collection geological field mapping can be conducted. Field mapping provides information about lithology, thickness, bedding and structure of rocks and sediments on the surface and in outcrops.

Laboratory tests

Rock samples can be obtained by drilling or during field mapping. In laboratories this samples are analysed with respect to sedimentary, lithostratigraphical, biostratigraphical features and palaeomagnetic age determination of rocks.

Sedimentary analyses involve e. g. grain size determination, carbonate content determination, determination of organic carbon content, heavy metal analyses, mineralogical-geochemical composition, etc. These analyses provide a detailed acquisition of lithological/petrographical sediment properties and resolve genetic-facial questions. The method of analysis is orientated on the main issue of analysing.

The grain size determination is carried out by means of the sieving method. This analysis exemplify the acquisition of the grain spectrum and amongst other things also the investigation of the Kf-value, a parameter for hydogeological modelling. The genesis and the maturity stage of hydrocarbons can be deduced from the mineral content as well as the type and portion of organic material. The mineralogical composition affects considerably the hydraulic and strength-mechanical properties of the analysed rock. The qualitative mineral identification is conducted by X-ray diffractometer analyses, X-ray fluorescence analyses, petrological microscopy and geochemical methods. Bromine content analyses are an important tool for the genetic interpretation of brines or stratigraphic characterisation of the salt formations. The determination of the qualitative content of minerals is carried out by computations.

Results of biostratigraphic and palaeomagnetic analyses give information about the relative age of the rocks and sediments.

In addition to the geological analyses mentioned above, the continuous monitoring of local earthquake occurrences by an installed seismic observational network and the geothermic analyses relevant for interpretation of the natural temperature field belongs to the exploration work.

Hydrogeological Conditions

Hydrogeology is primarily concerned with exploration of groundwater and the groundwater balance. Interactions between water and rock, the dependency on structures or bedding as well as changes of properties are considered. The hydrogeological structure, the hydraulic properties and the groundwater are analysed hydrogeologically.

Hydrogeological Structure

Basis of the hydrogeological structure is the knowledge about the structure of the geological layers in the underground provided by geological maps, results from drilling and

three-dimensional models. Therefore aquifers and aquitards are identifiable. Beside the geological structure the groundwater-morphology has a significant relevance. In that involved parameters reflect the state of equilibrium of the geohydraulical dynamic. For this the groundwater table is measured based on distributed control points, and water table contour maps are constructed.

Hydraulic Properties

The hydraulic properties describe important features of the geological barrier conditions. Parameters of barrier rock properties are necessary for long-term safety considerations with respect to surface and subsurface disposals. The parameters can describe the diffusion of hazardous fluids into the biosphere. The theoretical migration paths and migration mechanism are supposed as known. If they apply for the barriers of the considered site must be analysed and evaluated individually. The permeability coefficient (Kf-value) is in the centre of hydrogeological interest. It is used for the classification of the quantitative permeability of rocks. Other parameters can be derived from the Kf-value which are important for hydrogeological considerations: transmissivity, seepage velocity and transported volume of water. Grain size distributions, tracer tests, long and short pumping tests as well as laboratory tests give information about parameters like porosity, geometry of pores, permeabilities for fluids and diffusion. By means of numeric groundwater modelling e. g. hydraulic arrangements or effects of environmental damages can be calculated in advance.

Groundwater

In this area of activity data of groundwater composition, water density, groundwater recharge and groundwater movement are primarily collected. For characterisation of groundwater composition and water density water probes are mainly analysed chemically in laboratory. Furthermore geoelectric field measurements for the exploration of brine and accordingly water and electromagnetic field measurements for exploration of near-surface groundwater salinisation are made. Within the framework of extensive monitoring of the groundwater recharge rate pedologic field mapping is conducted. This mapping involves bearing tube drilling and test hole exploration and is supplemented by soil-physically field measurements and laboratory tests. Regional investigation of groundwater recharge can be made by several methods, e. g. lysimeter, from moisture balance, by groundwater models, by discharge and water level measurements, etc. Data for groundwater movements mostly originate from technical measurements, e. g.

soil-moisture tension measurement. When the movement of water is to slow (deep-groundwater) technical measurements are not suitable and the data are calculated by hydraulic models.

Geomechanics

Geomechanical data provide information about the strength and the mechanical behaviour of rocks. The main categories of parameters are: density-values, strength-values, water content and swelling behaviour.

The geomechanical in-situ conditions are evaluated by mining experiences and model calculations with the aid of data from rock-mechanical, geodetical and geophysical monitoring measurements (stress, strain, temperature, etc.). Geomechanical data originate from laboratory measurements and in-situ-measurements (deformation measurements in shafts and galleries), as well as calculations of stresses and strains by model calculation.

2.9.4.1.2 Geotechnical data

Basically, the geotechnical data are needed to perform the safety assessment, the long-term safety assessment as well as the operational safety and regarding radiological as well as conventional safety aspects. Geotechnical data must be sufficiently known to support this task. The data necessary to design a radioactive waste repository in salt rock are given below.

Repository mine

Based on the site characterisation and the geologic information the repository mine is planned, the geometric structure of the repository mine is adapted to the geologic structure. The geometry of the repository mine is an important input parameter, affecting repository performance significantly. The geometric data of the repository mine inclusive of boreholes are collected in the mine surveyors documentation. In this documentation some more important information repository specific information is available. The date of excavation of individual sections of the mine as well as the date of backfilling. In the case of a repository mine the position of the the waste respectively the waste container is also documented.

As a by-product of the site characterisation and the planning of the repository mine the primary stress state is determined as well as the initial temperature state depending on depth.

Host rock

Considering the host rock geotechnical data must be available covering the following aspects:

It has to be regarded that anhydrite layers or blocks are inherent parts of salt rock. However, in contrast to salt, anhydrite shows elastic/brittle behaviour. Thus, in the following, those geotechnical data respectively engineering properties of salt and anhydrite are summarized that are essential to the design of a radioactive waste repository in salt rock. Knowledge must be present on

- stress strain relations – to describe the deformation behaviour,
- the dilatancy boundary – to guarantee an undisturbed, effective rock salt barrier,
- the failure boundary – to guarantee the stability of mining excavations,
- thermal properties as well as quantities describing thermo-mechanical coupling – if heat-generating radioactive waste is to be disposed.

Remark: Permeability and porosity of intact rock salt are determined, however, they are extremely low forming a tight barrier if the dilatancy boundary is not exceeded. Anhydrite is assumed to be a porous medium containing joints. If anhydrite layers are connected to water-bearing overburden they are not regarded as a barrier as a rule. Anhydrite is tight in combination with salt when forming isolated blocks inside the salt structure.

Deformation behaviour

Basically, salt rock shows viscoplastic or creep deformation mechanisms. Generally, three phases of creep are distinguished, i. e. primary, secondary and tertiary creep. To describe creep behaviour of salt mathematically, several approaches for stress-strain relations have been developed.

All these models are based on an additive split of strains (small strains) or strain rates (large strains) in elastic parts ε_e, viscous parts ε_v, and plastic parts ε_p, basically, i. e.

$$\varepsilon = \varepsilon_e + \varepsilon_v + \varepsilon_p \tag{2.8}$$

All these constitutive models comprise at least the elastic and the viscous part. Often primary creep can be neglected due to its short duration while tertiary creep should be reduced to be negligible in a well-designed repository because it is coupled with cracking. To conserve the salt rock barrier, tertiary creep should be restricted to the contour of mining excavations where it is unavoidable. Thus, it can be controlled by classical mining safety measures, e. g. re-ripping.

If emplacement of heat-generating waste is considered the constitutive model must be able to reproduce thermally activated creep. In the WIPP and BGR models, the thermal influence on creep rate is covered by an additional Arrhenius function.

Depending on the salt structure and its age, the creep rate of natural rock salt differs even under identical load conditions. For classification purposes, so-called creep classes were introduced. The creep classes are defined with respect to the BGR reference creep laws. Different creep classes are coupled to the reference creep laws by a multiplicative prefactor. The creep classes cover a range of –1 to 9 subsequently doubling or halving the prefactor. The reference creep laws are equivalent to creep class 5. In general, intergranular/bound water leads to increased creep rates. For practical purposes, this effect is included in the creep class when regarding intact rock salt.

The deformation behaviour of anhydrite is described as purely elastic before failure and elastoplastic beyond the failure boundary. In a well-designed repository conditions beyond the anhydrite failure boundary should also be restricted to small zones close to the contour of mining excavations.

Dilatancy and micro-cracking

To prove the integrity of the salt rock barrier, the dilatancy criterion on the micro-cracking limit is applied. Barrier integrity is checked by comparing the existing octahedral shear stress state to the tolerable octahedral shear stress state on the dilatancy boundary. Thus, the dilatancy criterion is related to the stress. As the dilatancy boundary depends on the method of experimental evaluation, the dilatancy criterion on the mi-

cro-cracking boundary is applied in order to check the intact salt rock barrier at present. The micro-cracking boundary is the most conservative dilatancy criterion. It is based on acoustic emission measurements as a significant increase of acoustic emissions characterizes the beginning of micro-cracking.

A complementary criterion relying on the strain state is the so-called Aversin criterion. It states that the barrier integrity of protective salt rock layers is lost if the accumulated inelastic principal strain limit is exceeded. Alternatively, an equivalent strain limit may be used if the direction of principle strain is changing.

Recent research results indicate that both the aforementioned criteria must be revised if very low principal stress amounts are acting especially with regard to tensile stress amounts. For this reason tensile stresses are evaluated additionally.

As anhydrite is assumed to be a porous medium containing joints, the micro-cracking boundary of anhydrite is not of interest.

Failure

The failure boundary of rock salt and anhydrite is given by the Mohr-Coulomb failure criterion with tension-cut-off or by its Drucker-Prager approximation. As a main difference, anhydrite has a failure boundary which is independent of time whereas the failure boundary of rock salt shows time-dependent behaviour due to increasing damage as a consequence of creep beyond the dilatancy boundary.

The failure boundary is of interest when rating the load bearing capability of structural elements, e. g. pillars and stopes or contour zones close to mining excavations, which are not part of the salt rock barrier. The failure boundary represents the upper limit of short-term strength. In practice, pillars and stopes often bear uniaxial loads. For this reason the uniaxial compression strength and the tensile strength determined by the Brazilian test method are also included when evaluating the stability of mining excavations. The time-dependent stability of pillars, stopes, and contour zones exceeding the dilatancy boundary or the uniaxial compression or the above mentioned tensile strength is monitored by geotechnical measurements. If a structural element approaches its stability limit, state-of the-art engineering actions are taken, e. g. backfilling, re-ripping, rock bolting etc.

Thermal behaviour and thermo-mechanical coupling

When disposing heat-generating radioactive waste in salt rock thermal behaviour has to be taken into consideration. The influence of a rising temperature on deformation and thus acceleration of the creep rate was already mentioned. Additionally, the time-dependent temperature field has to be evaluated to check the thermal impact on the salt rock barrier. When calculating the evolution of the temperature field, heat capacity and heat conductivity of salt rock are relevant salt-specific input parameters. While the heat capacity can be assumed to be constant for practical issues, the heat conductivity is a nonlinear function depending on temperature. Heat conductivity decreases as temperature increases. This nonlinearity has to be taken into account when rating the results of temperature calculations against the permissible temperature limit. In the case of thermal loads, the stress state is indirectly affected by thermo-mechanical coupling and has to be included when rating barrier integrity and structural stability. The thermal expansion coefficient acts as a coupling parameter. It can be assumed to be constant in the range of practical application when designing a final repository for heat-generating waste in salt rock.

Backfill

For a well-designed radioactive waste repository in salt rock dry crushed salt is provided as backfill material because of its favourite sealing capabilities in the long-term, when it is highly compacted. According to rock salt for the backfill the following constitutive relations must be available:

- stress strain relations – to describe the deformation/compaction behaviour,
- thermal properties as well as quantities describing thermo-mechanical coupling – if heat-generating radioactive waste is to be disposed.

Because of its potential barrier function the permeability of the backfill is regarded depending on the compaction state of the backfill. The compaction state is related to the current porosity. As a consequence the following relationship is available:

- permeability porosity relations – to describe the increasing barrier function of the crushed salt backfill depending on its decreasing porosity.

Deformation behaviour

Basically, crushed rock salt shows viscoplastic or creep deformation mechanisms similar to rock salt. To describe creep behaviour of crushed salt mathematically, several approaches for stress-strain relations have also been developed. All these models are based on an additive split of strains (small strains) or strain rates (large strains) in elastic parts ε_e and viscous parts ε_v, basically, i. e.

$$\varepsilon = \varepsilon_e + \varepsilon_v \tag{2.9}$$

In contrast to rock salt, however, the volumetric deformation/compaction is the predominant deformation process at high porosities. For this reason some models are restricted to volumetric creep. With decreasing porosity deviatoric creep becomes more and more important.

If emplacement of heat-generating waste is considered the constitutive model crushed salt must be able to reproduce thermally activated creep as well as rock salt.

Thermal behaviour and thermo-mechanical coupling

When disposing heat-generating radioactive waste thermal behaviour of crushed salt has also to be taken into consideration. The influence of a rising temperature on deformation and thus acceleration of the creep rate was already mentioned. Additionally, the time-dependent temperature field has to be evaluated to check the thermal impact. When calculating the evolution of the temperature field, heat capacity and heat conductivity of crushed salt are relevant backfill-specific input parameters. While the heat capacity increases with decreasing porosity, the heat conductivity is a nonlinear function depending on temperature and porosity. Heat conductivity decreases as temperature increases and increases as porosity decreases. This nonlinearity has to be taken into account when rating the results of temperature calculations against the permissible temperature limit. In the case of thermal loads, the stress state is indirectly affected by thermo-mechanical coupling and has to be included. The thermal expansion coefficient acts as a coupling parameter.

Permeability porosity relationship

The permeability of the backfill depends on its compaction state. In a wide range down to $k = 10^{-16}$ m² the permeability of crushed rock salt can be described as a nonlinear function of porosity in agreement with classical approaches, which couple permeability and effective porosity. Beyond that limit a relationship of permeability and porosity is not evident.

Shaft and drift seals

Shaft and drift seals are designed individually depending on the repository structure as well as the geologic conditions and the scenarios affecting the integrity of the seals. In salt rock shaft and drift seals are designed using the following building materials as main components

- bentonite,
- salt concrete,
- magnesium oxide concrete.

The seals are designed according to national and European guidelines in civil engineering. Additionally, special attention must be paid to the durability respectively long-term stability of the seals because their working life exceeds working lives typically regarded in the guidelines significantly.

Often the EDZ of the salt rock is assigned to be part of the seal. Thus, some geotechnical data must be available for the EDZ, i. e. permeability, porosity and stress state. The stress state is of importance because in the EDZ damaged rock salt must be assumed. In damaged rock salt, however, permeability is a function of the least principal stress respectively the effective least principal stress.

2.9.4.1.3 Other data

Though the geological and geotechnical data are the most substantial part of the data acquisition process for a PA exercise, there are other groups of data that have to be established with equal accurateness. In the following, the typical selection procedures are described for the most important types of data.

Waste data

The radionuclide inventories of the repository are essential for the results of dose calculations. Since in Germany there is still no final concept for a repository for heat-generating waste, it is not clear how much waste it will contain. For estimation, three main sources of waste have to be taken into account:

- Spent Fuel (SF) Elements that are to be directly disposed of. Direct disposal is foreseen for a number of existing SF elements, especially from old Russian-type reactors. According to the valid German legislation, it is also the only option for the future. As the remaining quantities of electricity to be produced by each nuclear power plant have been prescribed, one can calculate the amounts of waste of this kind that will occur until the projected end of the use of nuclear power. This requires precise knowledge of the types of individual SF elements, their initial compositions, their burn-ups and the dates of their removal from the reactor. Some of these data can only be estimated today. The radionuclide activities and heat power are calculated for a given reference date, which is assumed to be the end of the operational phase of the repository.

- Vitrified waste from reprocessing. German Spent Fuel used to be reprocessed in France or in the UK. Since this is no longer admissible, the final amounts of waste originating from this source are in principle known. The inventories and the thermal data can be derived from the specifications of the reprocessing facility. By decay calculations they have to be projected to the reference date for the repository.

- Intermediate-level wastes (ILW), originating from the reprocessing or directly from the power plants. They comprise vitrified reprocessing water, compacted fuel element casings, structural parts and technological wastes. It is difficult to determine the radionuclide activities of these wastes exactly, the more as it is not yet known which amounts of them will accumulate until the reference date for the repository. Moreover, it is not quite clear which of these wastes will at all be disposed of in the repository, because an independent repository will be available for low- (LLW) and intermediate-level waste.

A completely different situation is given for the existing German LLW/ILW repositories ERAM and Asse. Their inventories cannot be calculated but have to be derived from the files of the waste deliverers, which stem from different decades and are sometimes

inaccurate or incomplete. Therefore, there is some uncertainty about the real inventories and the values for use in PA calculations have to be chosen conservatively.

Physical data

Some of the physical data needed for PA calculations, such as brine or rock densities, viscosities, or the coefficients of their temperature dependence, can be taken from widely available and well-established databases. This results in well-founded parameter values with low uncertainties. Others, such as diffusion constants or dispersion lengths, are poorly known under the relevant in-situ conditions and can only be estimated. Some physical parameters, however, are rather specific to the applied models and cannot be easily derived from values documented in the literature. This may relate, for example, to the parameters of the phenomenological laws used for describing bentonite resaturation, rock salt compaction, or the relation between permeability and porosity of a porous medium. For cases like the latter one, a number of investigations exist, but they lead to widely spread results. In other cases, few or no experimental investigations are available, and one is urged to derive parameter values from analogue situations or to make an estimation. Physical parameters determined in this way are subject to a high degree of uncertainty, which should be adequately considered in an uncertainty analysis.

Chemical/geochemical data

Geochemical data of relevance for PA are, above all, sorption data and solubilities. Sorption is normally sufficiently well-described by a linear model using fixed distribution coefficients. These values are element-specific and depend on the sorbing material as well as on the geochemical conditions. In general, they have to be measured under in-situ conditions. If no measured data are available, one has to use estimated values, which can be derived, for example, from known values for chemically similar elements or from other analogies. Since sorption is always an advantageous effect in PA, uncertain distribution coefficients should principally be rather under- than overestimated.

Although, in many cases, fixed element-specific solubility limits are assumed in PA models, this is a rough simplification, which is often inadmissible. The maximum element concentrations in the brine depend, to a large extent, on each other, and it is a challenging task to determine the real equilibrium composition of the brine in a specific part of the repository system. Geochemical equilibria can be calculated with the code

EQ3/6, which itself needs a comprehensive thermodynamical data basis. While some of the coefficients can be found in the literature, others have to be determined by means of extensive investigation programmes. A comprehensive thermodynamical reference data basis (THEREDA) is currently being elaborated in collaboration between five organisations from Germany and Switzerland, including GRS. The data in this database are verified and quality-assured [www.thereda.de].

Model-specific data

Some models used for PA need specific data that can neither be derived from general databases nor be provided by the operator. Where the performance assessor applies such models, it is his or her own responsibility to use adequate data. For example, in the ERAM repository seals are used, which can be disintegrated by magnesium-containing brine. For this process, a specific model has been developed, which needs to know the dissolution capacity of the brine as well as the maximum relative increase of permeability through this process. While the dissolution capacity can, with some uncertainty, be estimated by theoretical considerations, the maximum relative increase of permeability is a model parameter with no realistic meaning, as in reality, the process will most probably not stop after the permeability has increased by a given factor. Parameters like this one have to be chosen with care, and it has to be made sure that their choice does not lead to an underestimation of consequences.

Probability density functions (pdf)

Uncertainty analysis and sensitivity analysis are important parts of the safety case and are normally performed by applying probabilistic methods. These require appropriate pdfs for each uncertain parameter. To determine the pdf, the uncertainty of the parameter itself has to be estimated properly, which is not an easy task. Some simple rules for determination of pdfs are given in the GRS contribution on the topic “uncertainty analysis”.

2.9.4.2 Related topics

As already mentioned, the topic of criteria for input and data selection is related to the topics “uncertainty analysis” and “sensitivity analysis”. A sensitivity analysis can trigger the process of data selection by identifying input parameters that have a high influence

on the model results and therefore have to be determined with specific care. On the other hand, it can prevent putting too much effort in data that are more or less irrelevant for the model results.

Another related topic is “biosphere”. A proper calculation of the dissemination of radionuclides in the biosphere requires a sophisticated data generation process, which is described in the relevant topic paper.

2.9.4.3 Databases and tools

There are no specific databases or tools in use for PA data selection in Germany.

2.9.4.4 On-going work and future evolution

At the German repository sites Morsleben and Konrad, where abandoned mines are used for repository purposes, a lot of knowledge about the site’s geology already exists from the operational phase of the mines. In the other existing repository project in Germany, the Gorleben project, most of the geological exploration and data collection work was done in an early phase of the project. In all repository projects it was aspired to firstly achieve a largely comprehensive data set to have the basis available for a site specific safety assessment. The recent development appears to tend towards a partly interchange in the sequence of data collection and safety assessment. Instead of firstly trying to collect a data set which should be as comprehensive as possible, a safety assessment is already required in an early project phase regardless of the current grade of completeness of the collected geological data set. Those data, which are needed to be fed into the safety assessment but which are still to be determined, have to be soundly estimated for the safety assessment and reasonably varied. The benefit from the earlier safety assessment before exploration is completed is to be aware of the significance of the different geological data for the safety and furthermore the knowledge, with which degree of exactness the geological data have to be explored.

2.9.5 Lessons learnt

Input and data selection for PA calculations is a very important part of the process of long-term safety assessment for repositories. It will be critically checked by the licens-

ing authorities as well as by the public. Experiences have shown that questionable data used in PA studies will be identified by critical checkers and can lead to a challenge of the total investigation. Therefore, it is essential to maintain the following rules:

- All relevant data should be determined carefully and according to the state-of-the-art.
- Less relevant data that might be chosen with less care should be justified by means of a sensitivity analysis.
- It has to be made sure that uncertainties are covered either by choosing pessimistic values or by performing a qualified uncertainty analysis.
- The data determination process has to be traceably documented.
- It should never be tried to hide databases or parts of them from the public.

2.10 German network for research on actinide migration in natural claystone

The German Federal Ministry of Economics and Technology (BMWi) is funding a research network on actinide migration in natural claystone[1] to improve the knowledge on actinide clay interaction and the actinide migration in the clay on a process-level. The research network involved the following institutions:

- Forschungszentrum Rossendorf, Institut für Radiochemie
- Karlsruhe Institute of Technology, Institut für Nukleare Entsorgung
- Universität Mainz, Institut für Kernchemie
- Technische Universität München, Institut für Theoretische Chemie
- Universität Leipzig, Institut für Interdisziplinäre Isotopenforschung e.V.
- Universität des Saarlandes, Institut für Anorganische und Analytische Chemie und Radiochemie
- Universität Heidelberg

[1] German name: „Verbundvorhaben Actinidenmigration im natürlichen Tongestein“

- Universität Potsdam, Institut für Physikalische Chemie
- Technische Universität Dresden, Sachgebiet für Strahlenschutz
- Universität Hannover, Zentrum für Strahlenschutz und Radioökologie

The GRS followed the work performed by the participating organisations with two objectives. One objective was to inform the participants of the research network about the methodological approaches used in long term safety assessments and the resulting needs with respect to process understanding and model data. The second objective was to try to evaluate the potential to apply the research results in long-term performance assessments.

Several presentations were provided by GRS staff at the yearly workshops of the research network with particular emphasis on safety assessment reuirements concerning a repository in argicalleous formations. The topics covered the experience from geochemical repository research performed at GRS, the consideration of retardation processes in long-term safety assessments, and the data base for transport parameters used in long-term safety assessment model calculations.

A signicant portion of the work in the research network consists of fundamental investigations into the sorption of actinides like Neptunium, Uranium or Americium or lanthanides like Europium or Terbium on clay particles and humic substances in binary as well as in tertiary systems. The used methods include experimental studies like batch or column experiments to study sorption processes, spectroscopic methods (XPS, XANES und EXAFS) to identify radionuclide complexes and theoretical work like the quantum mechanical modeling of the complexation process on the molecular level. The work included also the development of sophicated analytical techniques to improve the determination of radionulides at very low concentrations. The experimental work has mainly been performed using either selected clay minerals or rock material from the Mont Terri rock laboratory.

From the perspective of the long-term safety of a repository for high-level waste in clay, the sorption of the actinides is one of the most important processes to provide the protection of the environment. However, the influence of the uncertainty in actual sorption parameter values on the result of a performance assessment is low; in fact, all performance assessment results confirm that the sorption parameter values have a low sen-

sitivity. At first glance, these two observations seem to contradict each other and therefore this issue will be illustrated on an example in the following.

The radionuclides that account for the calculated radionuclide fluxes from a clay formation usually are little-sorbing or non-sorbing activation products or fission products. This can be seen from figure 2.14 where the dose rate resulting from the release of radionuclides from a generic repository in clay is given. The details for this calculations can be found in /RUE 07/. The most important radionuclides contributing to the dose rate are C-14 for early times, Se-79 and Cl-36 for intermediate times and I-129 for very late times. No actinides are contributing significantly to the dose rate. This is because they are retained completely in the clay host rock by sorption. If no radionuclides sorbed at all, the actinides would be the main contributors to the dose rate. In this case, the dose rate would be increased by several orders of magnitude as can be seen in figure 2.15. This illustrate clearly that the sorption of actinides is one of the most important features affecting the safety of a repository in a clay formation.

However, on the other hand a small variation of the k_d-values within the range of the expected uncertainty - which is one order of magnitude to the maximum - the actinides still do not contribute significantly to the dose rate as can be seen in figure 2.16. A decrease of the k_d-values for all radionuclides by one order of magnitude (dashed lines in figure 2.16) results in this case in an increase in the dose rate by one order of magnitude, but this increase is only resulting from an increased contribution by I-129. Therefore, in this range of uncertainty there is no significant influence of the actual sorption parameter values of the actinides on the calculated dose rate. It needs at least a decrease in the sorption parameter values by two orders of magnitude until actinides start to become relevant for the dose rate – but still not for the peak value.

Over and above, this is only true if all sorption values are decreased at the same time. If only one radionuclide within a decay chain is sorbing less than expected, this has an even lower significance on the result if all other actinides within the same decay chain sorb as expected. This fact is exemplarily shown in figure 2.17 for Neptunium which is often mentioned as an actinide with a high uncertainty for its sorption parameter value. In this case, even a decrease in the sorption parameter value of Neptunium by four orders of magnitude does not significantly change the sum dose rate.

As a result from these findings, three general points ensue for future research on actinide sorption on clay material and one specific suggestion for the situation in Germany from the long-term safety assessment perspective:

- For the safety case it has to be shown in general that actinides are well retained by the clay host rock. This is a rather soft request that might be proven easily for every clay host rock and there is already a consensus on this statement for all clay host rocks that are currently investigated.

- Sorption parameter values have to be provided for the integrated performance assessment calculations with a limited uncertainty (e. g. less than one order of magnitude). The maximum permissible uncertainty which does not affect the long-term safety assessment results is site and concept specific. For example, it depends strongly on the thickness of the clay formation, i. e. the length of the diffusion pathway for the radionuclides.

- For the safety case, it has to be shown that the process understanding of the sorption process is sufficiently sophisticated to be sure to comply with the request for the uncertainty bandwidth of the sorption parameters.

- Since no site for a repository in clay in Germany is yet envisaged, the research work on sorption in the network on actinide migration mainly focused on Opalinus Clay from the rock laboratory at Mont Terri or on selected clay minerals. In Germany also other clay formations have been identified as potential repository host rocks like the lower cretaceous clays, where only little information exists until now. Therefore, it is suggested to focus future work more on these potential host rocks in Germany.

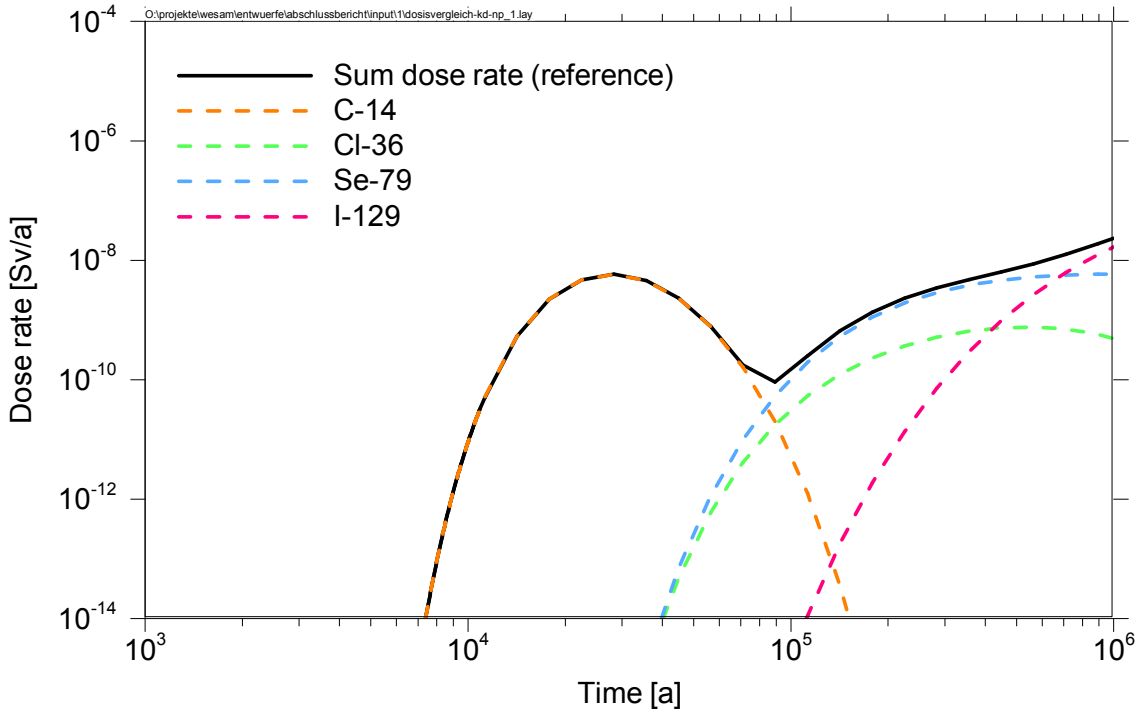

Fig. 2.14 Radionuclide flux emerging from a generic repository in clay in the reference case and the main contributing radionuclides

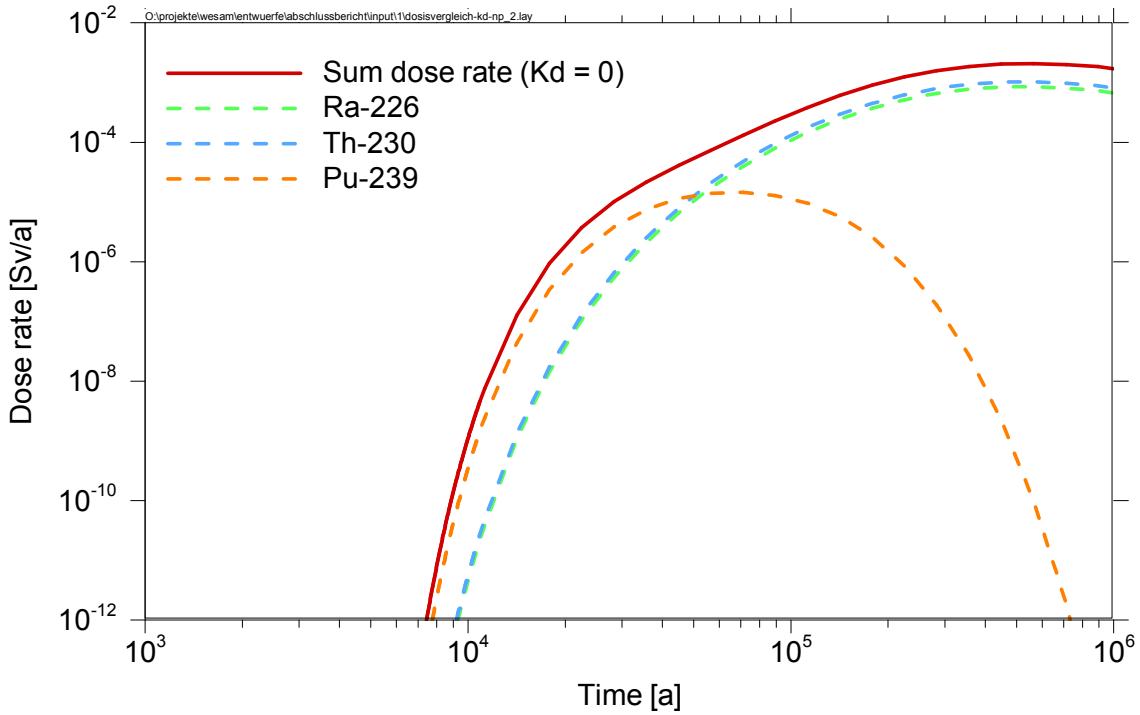

Fig. 2.15 Radionuclide flux emerging from a generic repository in clay in case of no sorption in the clay and the main contributing radionuclides

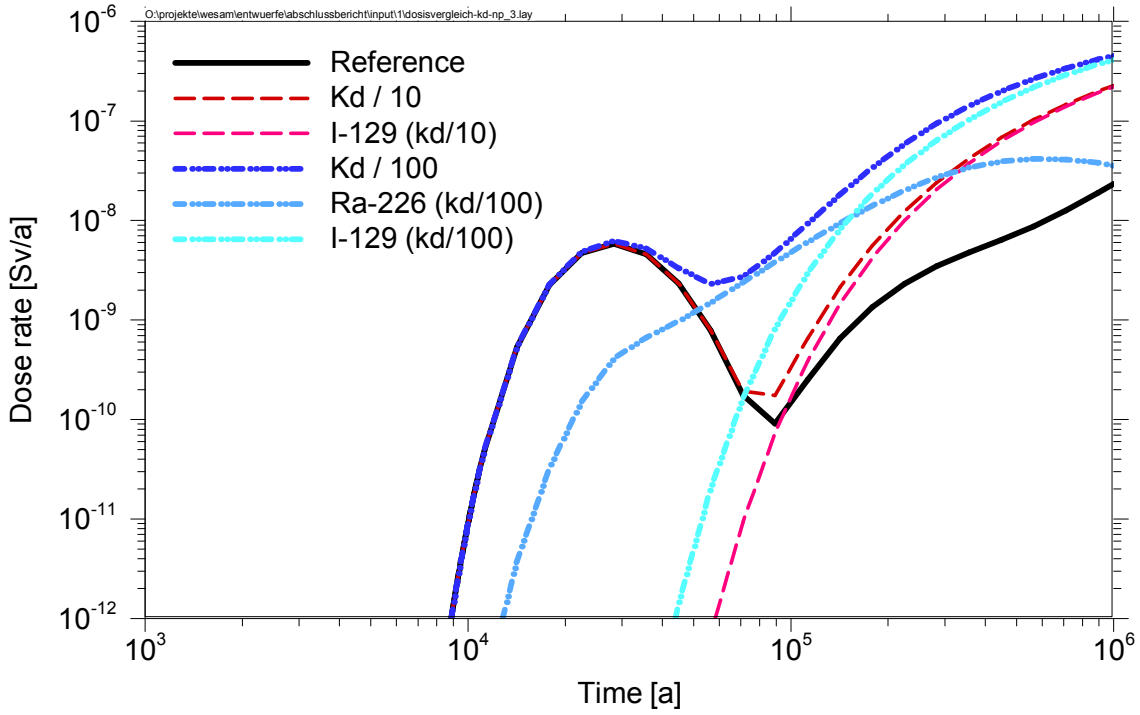

Fig. 2.16 Radionuclide flux emerging from a generic repository in clay in case of sorption in the clay reduced by one or two orders of magnitude

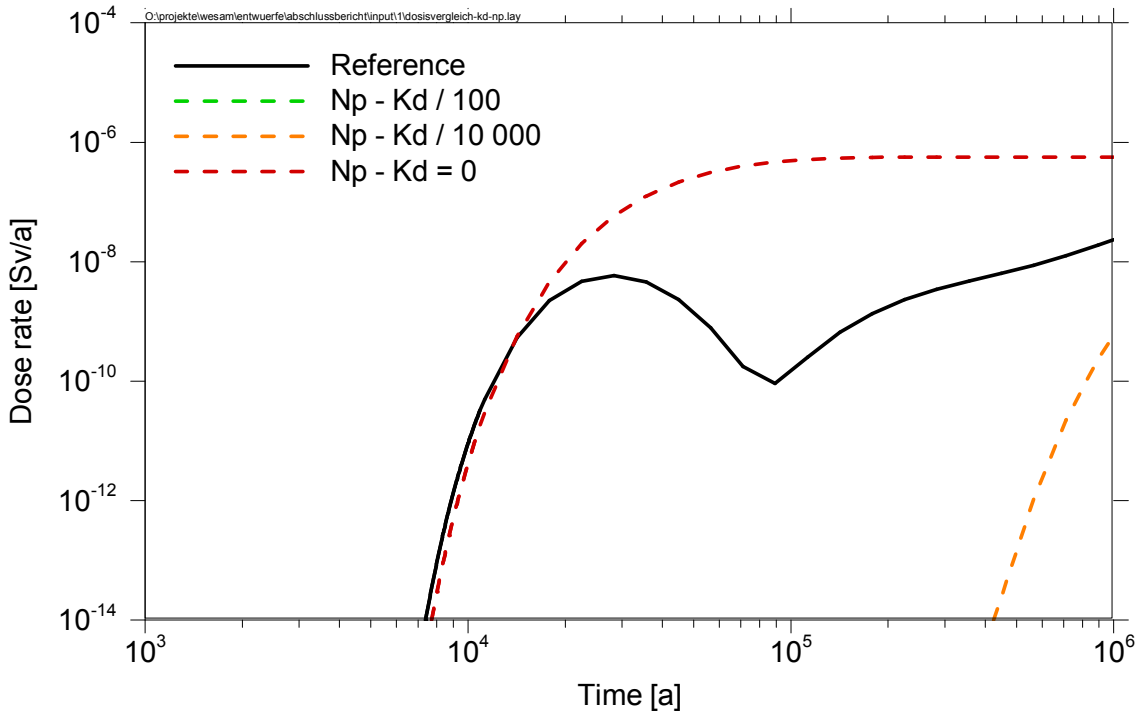

Fig. 2.17 Radionuclide flux emerging from a generic repository in clay in case of sorption of Neptunium in the clay reduced

Apart from providing data values concerning the actinide sorption on clay material or specific minerals, the investigations of several partners in the research network focused on the understanding of geochemical reactions that take place at the mineral surfaces or that affect sorption processes at these materials, respectively. This includes speciation studies concerning specific actinides like Cm, the interaction of humic substances with actinides, partly determined in an indirect way by using suitable model species like, for example, Eu (III) and polyacrylic acid, and the determinatrion of complex binding constants. These studies advance the fundamental understanding concerning sorption processes at clayeous material and in the presence of humic substances. Whether the results need to be taken into account in future safety assessments for a repository in argicalleous formations is difficult to answer at the moment. This question has to be revisited when future safety assessments are prepared on the basis of the final reports.

Other research work was directed towards improving analytical capabilities or developing new experimental techniques. In general, these investigations are of a very fundamental nature and they have no direct relevance for future safety analytical model calculations. The University of Mainz, for example, improved significantly the determination of Pu at very low concentrations with a detection limit in the ppt-range for Pu and in the ppb-range for individual Pu-species. Even though this represent a considerable progress, it is not yet sufficient for typical environmental conditions. However, this work is useful since it may allow measuring accurately the existing Pu-background concentrations in future site investigations. Also, the lower detection limits may enable to study sorption processes and to determine sorption parameters in the laboratory at Pu concentrations which are probably more representative for real repository conditions.

Using positron emission spectroscopy, the Institute für Isotopenforschung Leipzig developed a new and potentially fast detection technique to study transport processes in argillaceous material. This technique provides the tracer concentration in samples with a spatial resolution of 1 mm, provided that suitable tracers are employed. The applicability of this technique is limited, for example, it can be used for iodine but not for actinides. It may be of use for colloid transport investigations, since some types of colloids can be marked.

A general observation regarding the research network is that the training of young scientists in the field of radioactive waste disposal is fostered, since much of the work is

carried out at universities by Master or Ph.D. students. This enhances the number of possible applicants with specific knowledge in the field when vacant positions are advertised.

3 Treatment of uncertainty during safety case development

3.1 Protocol for assessing parameter uncertainty

Internationally there is a high degree of consensus on both the nature of uncertainties and how they should be classified in PA /PAM 07/. Uncertainties arise either from incomplete knowledge (epistemic uncertainties) and are, therefore, reducible by nature, or are random in nature (aleatory uncertainties) and are irreducible.

Owing to the way PA is implemented, often three classes of uncertainties are distinguished. Uncertainties arising from an incomplete knowledge or lack of understanding of the behaviour of engineered systems, physical processes, site characteristics and their representation using simplified models are called model uncertainty. Uncertainties associated with the values of parameters that are used in the implemented models are termed parameter uncertainties. Uncertainties associated with significant changes that may occur within the engineered system, physical processes and site characteristics over time are referred to as scenario uncertainties. All three classes of uncertainties are related to each other and contain elements that are epistemic and aleatory. However, model and parameter uncertainties contain a larger element of epistemic uncertainties than scenario uncertainties. In PA studies, often model uncertainties are dealt with by increasing the range of values of associated model parameters.

Parameter uncertainties result in uncertainties in the endpoint of the model calculation, e. g. the individual exposure, which need to be considered in a safety case. Appropriate mathematical methods are available

- to assess quantitatively the influence of the uncertainties of the various parameters on the uncertainty of the modelling result (uncertainty analysis) and
- to identify the sensitive parameters that affect most strongly the uncertainty of the modelling result (sensitivity analysis).

Parameter uncertainties therefore have to be mathematically quantified in order to allow for such an uncertainty and sensitivity analysis of the model results. Each uncertain parameter has to be assigned an adequate probability density function (PDF), which is used in the random sampling process for a probabilistic uncertainty/sensitivity analysis.

The quantification of uncertainties, however, is not a simple task. Protocols for systematically deriving PDFs are not yet established internationally. PDFs and their characteristics have been sometimes established in the past by modellers rating the general shape of the PDF and its characteristics, such as bandwidth or standard deviation. This approach is highly subjective and unsatisfying since in most cases it is neither traceable nor reproducible, which can be a serious problem in a licensing procedure.

The purpose of this paper is to propose a protocol for assessing the uncertainty of parameters on the basis of available data. The intention is twofold:

- to urge the modeller to think carefully about the uncertainty of parameters instead of simply defining a PDF out of a rough feeling,
- to reduce the subjectivity of the uncertainty quantification process and, in particular, to create a traceable scheme that allows a reviewer to follow and to understand the individual steps leading to the PDFs used in a probabilistic safety assessment.

3.1.1 General procedure and practical considerations

The general procedure for describing the parameter uncertainties via PDFs in a PA study is based on three steps:

- identification of the parameters that need to be considered,
- selection of a suitable data base to be used for deriving a PDF for each parameter to be considered,
- derivation of the PDF for each parameter to be considered following the general scheme that is proposed in sections 3.1.3 and 3.1.4.

Almost all parameters in a model calculation exhibit uncertainties. However, in order to be able to perform probabilistic model calculations, especially sensitivity studies, at reasonable computational costs, it is necessary to limit the number of parameters that are varied. Otherwise the number of model runs that are necessary to obtain results with the required statistical significance can become excessively high.

There are always parameters for which the values are sufficiently well-known so that their associated uncertainty can be disregarded in the probabilistic model calculations.

This applies to physical constants, but may also be valid for material parameters, geometrical dimensions or other properties that can be determined with high accuracy.

All parameters for which the uncertainty is disregarded in probabilistic model calculations should be clearly identified. No parameter should implicitly be assumed as fix. The reasons for the decisions should be justified. This will allow the reviewers of a PA study to follow the line of arguments and make their own decisions.

3.1.2 Selection and assessment of a knowledge base

For each parameter the associated uncertainty of its value has to be derived from some appropriate knowledge base. The knowledge about a parameter may sometimes be rather limited, which means a high degree of uncertainty. But even if there is comprehensive knowledge, it does not mean automatically that the uncertainty is low.

It is essential for a traceable process of uncertainty quantification that the knowledge base considered is clearly defined. That does not imply that all available knowledge has to be taken into account, there may be good reasons to exclude specific data sources from the process. It should, however, be clearly stated, on which sources the considerations are based and for which reasons particular sources have been excluded. Data sources can, for example, be publications or reports, which, ideally, should be publicly available. In some cases, however, adequate reports may not exist or have not been published for some reasons. If no reference can be given for data to be used, it should be explicitly explained how the data or information were obtained.

3.1.2.1 Assessment of the quality level of information

Each individual set of information about a parameter value is categorised first in one of the four quality levels below:

Level 3: Direct measurements. This means the parameter has been measured in situ or in the laboratory with appropriate measurement techniques and under conditions that are comparable to the real ones, and there is no reason to assume that in the real situation the parameter value could significantly differ from the measurements. A measured data set for a specific parameter can comprise lots of individual values as

well as very few values or even only one. This does not affect their classification as level 3.

Level 2: Model representation. An accepted model of the parameter behaviour under variation of specific conditions provides valuable information. Such a parameter model can either be based on qualified concepts and data so that it yields reliable values on its own, or it has to be calibrated by measurements. These measurements do not have to be direct measurements of the parameter under consideration but can be carried out under different conditions, as long as they allow extrapolation to the real conditions using the model.

Level 1: Analogy considerations. If no qualified model is available, analogy considerations can provide a means for estimating a parameter value. Such considerations are not based on qualified models but on plausible assumptions, transferring the known behaviour of related parameters to the one under consideration.

Level 0: Plausibility limits. If nothing at all is known about a parameter, at least a plausibility range should be given. There are always lower and upper bounds that cannot be exceeded by reasons everybody accepts. The range should be chosen as small as possible without jeopardising this general acceptance. Moreover, conservativity should be taken into account.

The quality levels given here are not intended to classify data or sets of information according to their uncertainty. It is possible that measured data lead to a high degree of uncertainty, while a model representation or even an analogy consideration results in rather sharp values. The purpose of the scheme is rather to create an order of priority for use of the different sources in the uncertainty quantification process. Direct measurements are more relevant than all other kinds of information. For example, if a model representation yields a sharp value for a parameter, but direct measurements are spread over a wide interval, this is a hint that the model could be faulty or incomplete and we should give more relevance to the measurements.

Often, various sets of information about a parameter value will be available, which may be of different quality level, depending on their origin. While different sets of information of the same quality level may be amalgamated into one data set (see chapter 3.2), data sets with a quality level lower than the highest available quality level may be used to substantiate the knowledge base (see chapter 3.3). Of course, if a plausibility interval is

all that can be given, no supporting information is available, but generally it is recommended to include initially as many different and independent data sets in the assessment as possible.

3.1.2.2 Amalgamation of different sources into one data set

The further procedure depends on the number of sources of the same quality level. If there is only one source, it represents the total information of that level. However, sometimes different sources of information are available that belong to the same quality level and should all be taken into account. In this case one has to check first whether these sets are independent and comparable. Independence means that the different sources do not, explicitly or implicitly, rely on each other or use the same original data. Otherwise they have to be considered as being one source. Comparability means that the different sources really relate to the same (or nearly the same) thing and are based on similar assumptions and preconditions.

If there are more than one independent and comparable sources of information of the same quality level, one has to check whether they confirm each other. If they do, it is an indication for a good reliability of the information and an accordingly low level of uncertainty. In this case, the different data sets can be combined directly into one data set.

If the different data sets do not confirm each other, one should try to judge the reliability of the different sets against each other using expert knowledge. This can be a difficult and time-consuming task, as it may require studies of original literature, assessment of measurement techniques or modelling approaches, assessment of the validity of conditions and assumptions, assessment of the degree of validation and so on. According to the results of this expert judgement one should weight the different data sources when combining the different data sets into one. If, for any reasons, it is not possible to perform a qualified expert judgement, all sets of information should be weighted equally. The uncertainty of a combined set of different non-confirming data sets will always be higher than that of the individual sets.

3.1.2.3 Assessment of information

Even if there are measured data, one should not exclusively rely on them when determining the range of uncertainty, since one does not know whether all possible influences are covered by the experiments, and whether the values, by accident or systematically, show some tendency that is not realistic. Similar considerations apply to lower quality levels. In general, one should attempt to support data at a given quality level by data at lower quality levels. If, for example, the best available data source is a model representation, one should try to support this by some analogy or at least plausibility consideration. However, use of a third level for further supporting is not suggested. It is rather recommended always to use information of the two highest quality levels that are available. Adding the level values uniquely leads to one of the following cases:

5 – A set of measured data supported by models

4 – A set of measured data supported by analogies

3 – A model representation supported by analogies

2 – A model representation supported by plausibility limits

1 – An analogy consideration supported by plausibility limits

0 – A plausibility interval

The theoretical possibility of a set of directly measured data supported by nothing better than plausibility limits (which would also add up to 3) does not need to be considered here because it seems rather unlikely that it could occur. Data that can be directly measured will most probably be supported at least by analogies.

The general procedure for assessing the quality of information is schematically shown in figure 3.1.

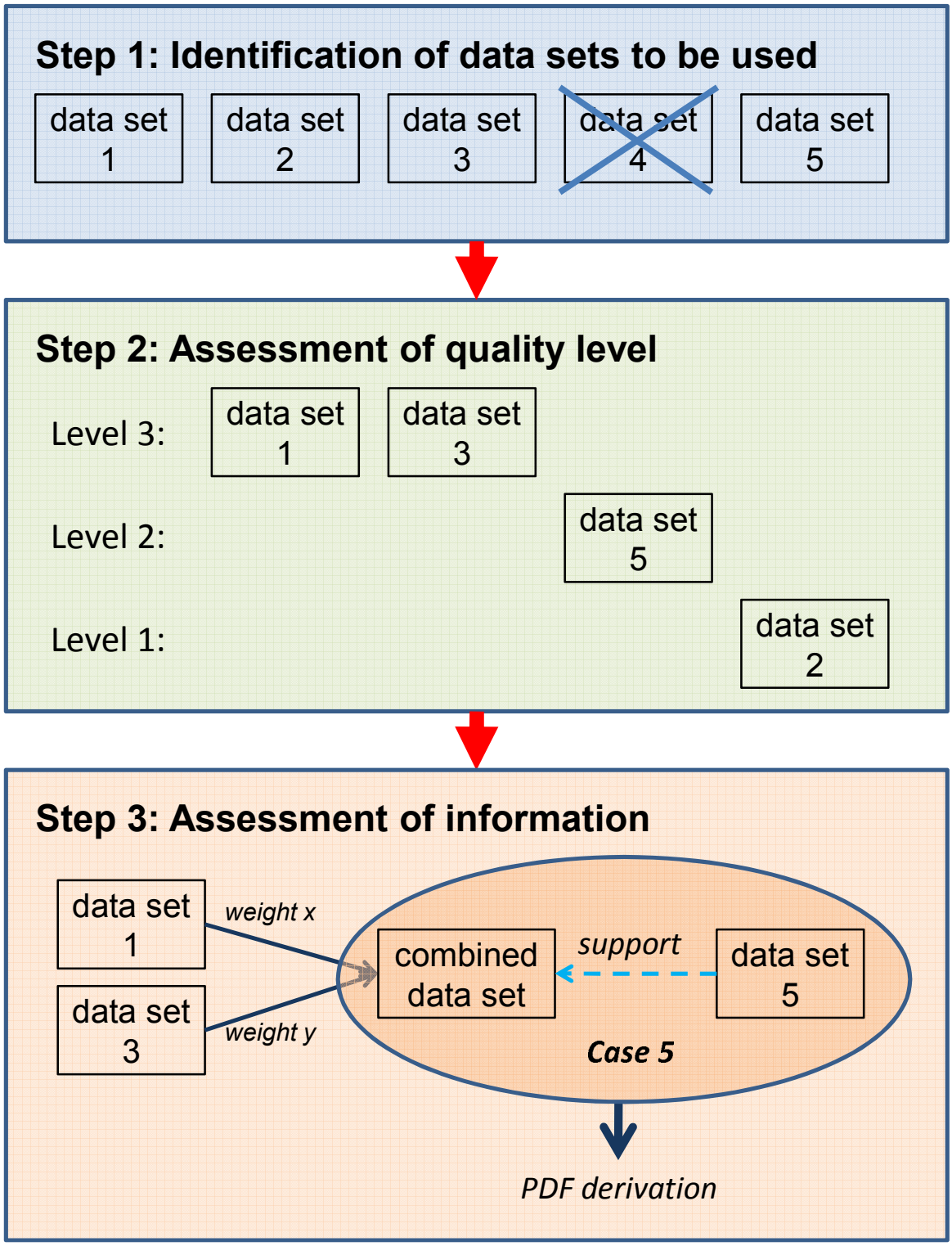

Fig. 3.1 Sketch of general procedure

3.1.3 Assessment of parameter uncertainty

On the basis of the on-hand knowledge, the uncertainty of a parameter is assessed and a PDF shall be derived to represent the parameter uncertainty. This should best be performed in a consistent way. This may become difficult, especially if a data set contains very few values or even only a single one and no information about their degree of uncertainty is available.

3.1.3.1 Consistency

A consistent derivation of a PDF implies that the range and width in the statistical representation of the parameter uncertainty remains constant or decreases when additional information concerning this parameter becomes available at a later stage. The PDF can be considered to be derived in a consistent manner if the following requirement is met:

If the information taken into account in the process of uncertainty determination is increased, the resulting degree of uncertainty should not increase.

In practice, however, consistency of a procedure can never be guaranteed, and proven only with hindsight. If it turns out that newly available data or pieces of information do not fit in a previously defined uncertainty interval, this reveals a misassessment. Each practical procedure for assessment of parameter uncertainty bears the risk of misassessment. This risk should be kept as low as possible without losing too much significance of the PDFs and without allowing too much subjectivity. Therefore, in case of doubt the procedure should favour wider uncertainty ranges and not only one quality level should be considered.

3.1.3.2 Evaluation and determination of PDFs

As soon as the data quality assessment of the available information as described in the previous sections has been performed, a systematic evaluation can be done, which finally leads to a PDF for use in probabilistic analyses. Each of the six cases resulting from the information assessment scheme given above requires its own specific procedure for identifying the most suitable PDF. In the following, for each case a procedure is proposed, which seems most adequate.

Case 0: In this case a plausibility interval is all that is known and not even a rudimentary model or some kind of analogy exists. Therefore, no parts of the interval should be weighted higher than others, and consequently, the PDF must be a uniform distribution between the interval bounds.

Case 1: Some analogies are available, supported by plausibility limits. In this case the PDF has to be transferred from the analogy data or model. First, the analogies should be treated as if they were the actual information about the parameter under consideration, following the procedure described here. The resulting PDF has then to be re-calibrated to make sure that the plausibility limits are not exceeded.

Case 2: In this case a model representation for the parameter under consideration exists. A model, even the roughest one, will always allow the derivation of a PDF. One only has to make sure that no unidentified ideas are taken into account implicitly. All trains of thoughts should either be clearly described and included in the information basis or regarded as subjective and thus as being irrelevant for determining the parameter PDF. For calibration of the PDF only the plausibility limits can be used.

Case 3: This case is very similar to the previous one, as a model representation exists. The PDF has to be derived from the model. Its calibration, however, can be based on analogies instead of simple plausibility. One can try to transfer the model so that it describes, as well as possible, the analogous situation and then re-transfer the PDF to the actual situation. If it turns out that this is impossible, the analogue is not suitable for supporting the PDF determination and one has to get back to case 2.

Case 4: Though it seems to be a comfortable situation to be in possession of directly measured data supported by analogues, this case can become problematic and include considerable subjectivity. Since no model representation is available, the PDF cannot be derived theoretically but has to be derived from the measured data. If only a few values or even a single one are available it is impossible to derive a statistical distribution from them. First, it has to be decided whether the amount of data is sufficient to derive a PDF. If this is the case, the PDF will be derived from the data and compared with the analogue. If there is no strong discrepancy, the PDF is confirmed, otherwise this can be a hint that the uncertainty is higher than the data suggest and one should re-calibrate the PDF accordingly by taking into account transferred information from the analogue. If, however, the directly measured data do not suffice to derive a PDF one has to follow a different approach. Provided that there is enough information from the

analogue to allow a more precise derivation of a PDF, one can transfer this PDF to the actual parameter, calibrating it with the measured data. If even that is not possible, one should perform an expert judgement of the measured data, analysing measurement techniques and assessing possible errors, and take a uniform distribution in an adequate interval. If no detailed background is available to perform a qualified expert judgement, one will have to derive a sufficiently large interval from the analogue. A triangular distribution is probably the best choice in this case.

Case 5: The best situation is that measured data are supported by a model representation. In this case the PDF can be derived from the model and calibrated with the measured data. The only problem that could arise is that the model and the measurements obviously do not fit together. In this case one should perform an expert judgement of both and decide which is more reliable. If a qualified expert judgement is impossible one should generally prefer the measured data. Disregarding the less reliable source of information leads to a lower case, and the PDF determination should be performed accordingly.

3.1.3.3 Determination of a PDF from given data

In some cases no model representations are known and the derivation of the PDF can only be based on some data (case 1 and 4, respectively). If a sufficiently large number of data points is available, the PDF can be read off directly. The other extreme is, however, that there are only very few data points and it is impossible to derive a PDF from them with sufficient significance. In such cases a plausibility interval should be identified and a triangular distribution should be assumed with its peak at the mean of the given data. It is proposed that this approach be followed if the number of data points is less than five.

If the number n of data points is five or more, but not enough for the PDF to be obvious, one should perform a statistical analysis. It is recommended that in such cases only (log-)uniform or (log-)normal distributions be used. First it has to be decided whether the PDF should be defined on a linear or a logarithmic scale. A logarithmic distribution should be used if the values show a clear cumulation at smaller values. This can be tested by calculating the arithmetic and the geometric mean of the values and comparing them with the median. If the median is closer to the geometric mean, a loga-

rithmic distribution should be used. The procedure described in the following should then be applied to the logarithms of the values.

If the given data can be represented sufficiently well by a uniform distribution, it should be preferred, even if a normal distribution would also be possible. Therefore, one should apply a statistical test for the null hypothesis that the data follow a uniform distribution. The interval should be chosen a little wider than actually covered by the data. It is recommended to use the interval $[x_{min} - (x_{max}-x_{min})/(2n-2), x_{max} + (x_{max}-x_{min})/(2n-2)]$. This follows from the requirement that the actual cumulated distribution function (CDF), which is increased by $1/n$ at every data point, is intersected by its theoretical equivalent exactly in the middle of the first as well as of the last step (see figure 3.2). The null hypothesis can be checked using the Kolmogorov-Smirnov-test by determining the maximum absolute deviation of the actual from the theoretical CDF /CON/. This is compared to a critical value that depends on n as well as on the desired level of significance, e. g. 10 % (see table 3.1[2]). If the difference is greater than the critical value the null hypothesis is rejected. Only in this case a second test should be performed with a normal distribution. The parameters of the test distribution are taken directly from the mean and standard deviation of the data set under investigation. Again, the PDF is tested using the Komogorov-Smirnov-test by calculating the maximum difference between the theoretical distribution and the actual data and comparing this with the critical values given in table 3.1. If, however, also the hypothesis of a normal distribution has to be rejected, it is recommended to use a uniform distribution, regardless of its rejection in the first place.

[2] taken from http://www.eridlc.com/onlinetextbook/index.cfm?fuseaction=textbook.appendix&FileName=Table7

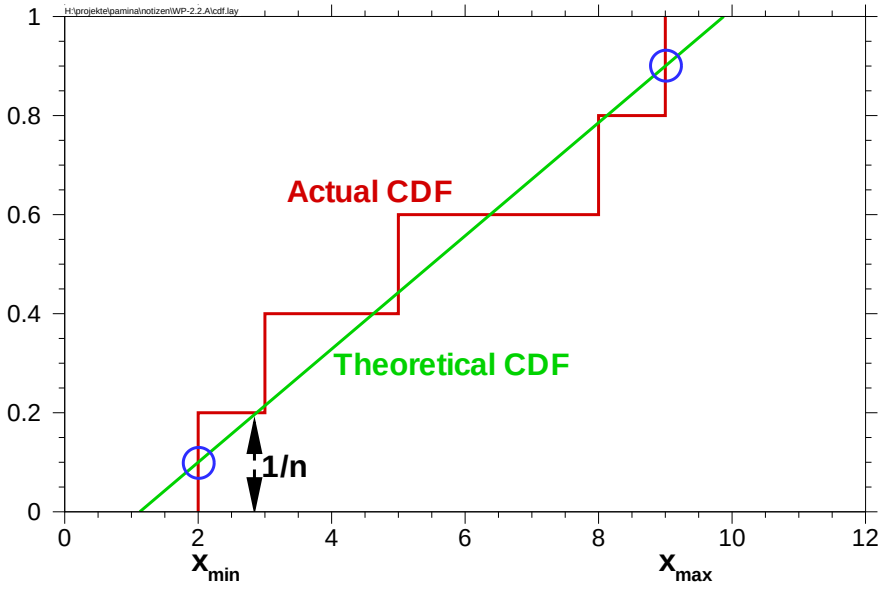

Fig. 3.2 Interval limits for uniform distribution

Tab. 3.1 Critical values for the Kolmogorov-Smirnov-test

	LEVEL OF SIGNIFICANCE				
n	0.2	0.15	0.1	0.05	0.01
1	0.900	0.925	0.950	0.975	0.995
2	0.684	0.726	0.776	0.842	0.929
3	0.565	0.597	0.642	0.708	0.828
4	0.494	0.525	0.564	0.624	0.733
5	0.446	0.474	0.510	0.565	0.669
6	0.410	0.436	0.470	0.521	0.618
7	0.381	0.405	0.438	0.486	0.577
8	0.358	0.381	0.411	0.457	0.543
9	0.339	0.360	0.388	0.432	0.514
10	0.322	0.342	0.368	0.410	0.490
11	0.307	0.326	0.352	0.391	0.468
12	0.295	0.313	0.338	0.375	0.450
13	0.284	0.302	0.325	0.361	0.433
14	0.274	0.292	0.314	0.349	0.418
15	0.266	0.283	0.304	0.338	0.404
16	0.258	0.274	0.295	0.328	0.392
17	0.250	0.266	0.286	0.318	0.381
18	0.244	0.259	0.278	0.309	0.371
19	0.237	0.252	0.272	0.301	0.363
20	0.231	0.246	0.264	0.294	0.356
25	0.210	0.220	0.240	0.270	0.320
30	0.190	0.200	0.220	0.240	0.290
35	0.180	0.190	0.210	0.230	0.270
> 35	1.07 / □ n	1.14 / □ n	1.22 / □ n	1.36 / □ n	1.63 / □ n

3.1.4 Algorithmic description of PDF generation

In the previous sections it was explained how the PDF generation process should be performed. In order to give unique and easy-to-follow instructions for this process, an algorithmic scheme is presented in the following.

Start

Identify the parameter to be considered

Procedure: information analysis

Analyse and categorise all available sets of information (s) about the parameter:

Direct measurements	L(s) = 3
Model representation	L(s) = 2
Analogy consideration	L(s) = 1
Plausibility interval	L(s) = 0

Loop over all levels: = 3, …, 0

N = Number of sets with L(s) = i

If N = 0: Next i

If N = 1: If highest relevant level: L1 = i
If second highest relevant level: L2 = i
Next i

If N > 1: If highest relevant level: L1 = i
If second highest relevant level: L2 = i
Do the sets confirm each other?
No: Are *we able to perform an expert judgement?*
Yes: **Expert judgement** of all sets
Weight the different sets
Combine the sets and regard them as one
Next i

Add the two highest levels: L = L1 + L2

Return

Procedure: Define PDF

If L = 0: PDF = Uniform distribution
Interval limits = plausibility limits
Return

If L = 1: Analysis of analogy: Identify information about a related parameter
Define PDF for related parameter
Re-calibrate PDF for actual parameter using plausibility limits
Return

If L = 2: A: Derive PDF from model
Calibrate PDF using plausibility limits
Return

If L = 3: Derive PDF from model
Transfer model to analogue
Try to calibrate transferred PDF using information from analogue
Is this possible?
No: L = 2
Go to **A**
Yes: Re-transfer calibrated PDF to actual parameter
Return

If L = 4: **B**: *Do the data allow determination of a PDF?*
Yes: **Determine PDF** from the data
C: Transfer PDF to analogue
Is the transferred PDF consistent with the analogue?
No: Re-calibrate PDF
Go to **C**
Return
No: *Does the analogue allow determination of a PDF?*
Yes: **Determine PDF** from analogue
Transfer PDF from the analogue to the actual parameter
Calibrate PDF with measured data
No: *Are we able to perform an expert judgement?*
Yes: **Expert judgement** of measured data
PDF = Uniform distribution in adequate interval
No: Find plausibility limits
PDF = Triangular distribution in plausibility interval
with mean of measured data as maximum
Return

If L = 5: **D**: Derive PDF from model
Is the PDF consistent with the measured data?
Yes: Calibrate PDF using measured data
Return
No: *Are we able to perform an expert judgement of the model?*
Yes: **Expert judgement** of the model
Is the model evidently more reliable than the data?
Yes: Use PDF derived from model
Calibrate PDF using more general data
Return
No: Go to **E**
No: Go to **E**

E: *Can a more general model be given?*
Yes: Use more general model
Go to **D**
No: Find an analogy
L = 4
Go to **B**
Return

End

Procedure: Determine PDF from set of data

n = Number of data values
Is n less than 5?
Yes: No PDF determination possible
Return
No: *Can the PDF directly be seen from the data?*
Yes: Use this PDF
Return
No: A = arithmetic mean of all values
G = geometric mean of all values
M = median of all values
Is M closer to A than to G?
Yes: Linear-scale PDF
No: Logarithmic-scale PDF
Perform a log-transformation of data values
Find smallest and greatest (log-transformed) value: xmin, xmax
Null hypothesis: Uniform distribuion in the interval
[xmin – (xmax-xmin)/(2n-2), xmax + (xmax-xmin)/(2n-2)]
Test null hypothesis with Kolmogorov-Smirnov-Test (10%)
Should null hypothesis be rejected?
No: PDF = (log-) uniform in mentioned interval
Yes: V = variance of all values
Null hypothesis: Normal distribution with σ = sqrt (V)
Test null hypothesis with Kolmogorov-Smirnov-Test (10%)
Should null hypothesis be rejected?
No: PDF = (log-) normal with mentioned parameters
Yes: PDF = uniform in mentioned interval
Return

3.2 Application of different sensitivity analysis methods to a PA model for a repository in rock salt

Probabilistic sensitivity analysis is a widely accepted means for assessing and quantifying the influences of parameter uncertainties to the results of model calculations on the long-term safety of deep underground repositories. A variety of different methods is available for this purpose. In the past, mainly regression and correlation methods and non-parametrical statistical tests were applied. In Germany a number of studies were performed using Spearman's rank correlation coefficients (SPEA), partial rank correlation coefficients (PRCC), standardised rang regression coefficients (SRRC) and the Smirnov test. It was found, however, that these methods are not always adequate to reveal the actual sensitivities of the model under consideration. If, for example, there is a high probability of zero output, as it is typical for repositories in rock salt, the mentioned methods perform rather poorly. Therefore, more sophisticated methods of sensitivity analysis, based on the variance of the model output, have been tested in the investigation described in this paper.

In Germany there is a specific situation concerning final disposal of radioactive waste. It is clear that a repository for spent fuel (SF) and/or high-level waste (HLW) is to be set up in deep underground, but for political reasons, there is yet no preference for a specific repository site or host rock. One candidate host formation, however, is rock salt, as there are large salt structures in the north of Germany and salt has some beneficial properties. Repository systems in rock salt typically show a specific behavioural patterns, which cannot be observed in other host rock formations. For this reason, the investigations performed in the work described here were confined to a rock salt system.

All openings in rock salt formations are subject to convergence. Due to the plastic creep properties of rock salt, which make it behave like an extremely viscous fluid, open voids decrease and are finally closed under the rock pressure. For final disposal of hazardous substances this effect can be favourable or unfavourable. On one hand the convergence leads to permanent watertight enclosure of the waste containers if it can act long enough without being disturbed. On the other hand, if by some reason the substances get in contact with brine before the openings are closed, the convergence will drive the contaminated fluid through and out of the repository structure and accelerate the release to the biosphere. Experiences with abandoned salt production mines

have shown that there is a high risk of brine intrusion prior to the natural closure by convergence. Such mines, however, were not designed to avoid brine intrusion. There are normally lots of interconnections between the openings, which are often excavated in different salt types and possibly close to the edge of the salt dome. An SF/HLW repository, however, will never be established in an existing mine, but set up in a thoroughly selected, homogeneous salt formation and designed to hinder brine movement. Therefore, it is most probable that the wastes are tightly enclosed by salt before they can get in contact with brine and the probability of contaminant release is considered rather low.

The EMOS package was developed and applied by GRS for the numerical analysis of the long-term safety of deep geological repository systems and contains a number of numerical modules for the near field in different host rock formations as well as for the far field and the biosphere. The LOPOS module for repository systems in rock salt yields a zero output if the convergence leads to a tight enclosure of the wastes before they get in contact with brine. For this reason there are a high number of zero- runs in a typical probabilistic set of calculations, which is a situation that can cause strange behaviour of sensitivity analysis methods.

For the investigations performed, a “realistic” generic HLW/SF rock salt repository model was selected as a test case for the different sensitivity methods, since it shows typical important properties of a PA system. Firstly, the distribution of radiation exposure is highly skewed and heavily-tailed which typically spans over several orders of magnitude. Secondly and thirdly, the system of the test case shows non-linear and non-monotonic behaviour. A complete repository setup in rock salt formations is considered in the test case, including the near field, the far field and the biosphere. As model output the annual effective dose to an adult human individual is calculated with the software package EMOS.

Several sensitivity analysis methods were applied to the system, running the model a high number of times. These methods comprise

- correlation and regression based methods,
- non-parametrical statistics,
- variance-based methods,
- graphical methods.

The work presented in the following was partly prepared with collaboration of Ricardo Bolado-Lavin from the EC Joint Research Centre Petten, whose input is gratefully acknowledged.

3.2.1 Modification of the EMOS statistic module for the use of FAST methods

The EMOS statistical framework is not able to perform FAST or EFAST simulations. Therefore a different approach was developed. The samples for the EFAST analyses were generated and analysed with SIMLAB 3 within the MATLAB environment. Since SIMLAB 3 returns the sample data in a different format than required by the EMOS programme, modification of the sample data format is necessary. This affects the format of the spl file where data for each parameter and simulation are stored. The input file *.sud for the probabilistic calculations requires no change. In addition, the EMOS output format (sdo file) need to be modified to read the output data into SIMLAB 3 for the calculation of the indexes. In the following sections, general SIMLAB 3 commands are described; format of the input structure for SIMLAB 3 is briefly explained to generate an EFAST sample; followed by a description of a simple FORTRAN programme with which the sample data are converted into a format compatible with EMOS. The next section presents a description of a FORTRAN programme which task is to convert the output data for certain time steps into a format which can be read by SIMLAB 3. The last section provides a description of how the EFAST method is used to compute the sensitivity indexes from the EMOS data. A more detailed description about commands, instructions and formats used in SIMLAB 3 can be found within the doc files provided for MATLAB and the SIMLAB 2 manual. The appendix lists examples of in- und output data files as well as the two FORTRAN code of the used programmes.

General SIMLAB 3 commands

To initialise the library, each SIMLAB 3 programme shall be started with the command gsaBegin and closed with gsaEnd to clean up and deallocate memory.

Sample generation with SIMLAB 3

After the initialisation with gsaBegin, distribution of the different parameters can be defined. For the investigated test case in clay, only 3 distributions are required which are uniform, log uniform and log normal. The instructions for these distributions look like:

uniform distribution:

```
addFacUnif('Porosityclay2',1,[0.06,0.24,1],'Porosity of the clay in region 2')
```

log uniform distribution:

```
addFacLogUnif('Diffclay3',1,[8.300e-12,8.300e-10,1], 'Diffusion coefficient of the clay in region 3')
```

log normal distribution:

```
addFacLogNorm('flux',10.369184732,0.372562470551105,0.001,0.999, 'flux in far field')
```

The names in the first and second quotation marks present parameter name and note. The note is optional. In the bracket, left and right bounds of the parameter inteval are defined. For the log normal distribution, the numbers in the bracket represent mean (μ) and sigma (σ) value along with the respective quantiles.

After the definition of the distributions, the method needs to be set. The EFAST method can be set with the command “setMethodExtendedFAST(123123,4965)”. The values in the bracket define seed and number of the simulations for a sample, respectively. The sample is produced with the command “sample = createSample”. Generated data can be stored in a sample file (*.sam) defined by SIMLAB 3 with the instruction:

```
saveSampleCfg('path and name of the file.sam')
```

In the appendix, an example is shown for a MATLAB script file to generate a sample for 4 965 simulations and for 5 parameters.

Conversion of the SIMLAB 3 sample data format to EMOS format

The simple FORTRAN programme sam-spl-wesam.e reads values and distribution of the different parameters from the sam file and outputs the data into the spl file. The spl file is the sample file for EMOS. In the appendix, the FORTRAN programme is listed along with examples for a sam and spl file.

Conversion of the EMOS output format to SIMLAB 3 format

With means of the simple FORTRAN programme sdoconv-SD-all.e, output data from the EMOS sdo file (annual radiation exposure) can be extracted for the time steps listed in the sim file (194) for SIMLAB 3 to compute the indexes. The programme further requires the EMOS svs file for reading in number of simulations, time steps and nuclide doses stored in the sdo file. In the sim file, in the first row, there is the path name where the sdo and svs files are found, in the second row, number of time steps for calculation of the indexes is provided followed by the values of the time steps. Every time step requires a new line. sdoconv-SD-all.e simple reads all data in the sdo file and outputs the annual radiation doses to the biosphere along the respective time into the model response data file for SIMLAB 3. Twenty eight different response data files are produced for the 194 time steps due to memory requirement of SIMLAB 3 within the MATLAB environment. The SIMLAB 3 libaries allocate all memory within MATLAB when many simulations and parameters need to be evaluated. In the first 27 model output files for SIMLAB 3, seven time steps for each simulation are stored. In the last file, the remaining time steps (i. e., 5) are saved. In the first 4 lines of the files, number and name of response data (i. e., 1 and Summendosis stands for annual radiation dose), flag for time dependency and number of simulations are provided. An example of a model response data file and a sim file is given in the appendix. The appendix also provides the FORTRAN source code of the sdoconv-SD-all.e programme.

Calculation of the sensitivity indexes within SIMLAB 3

One main and one sub MATLAB script file for an EFAST analysis were used to compute the indexes. In the main script file, a “for loop” is executed 28 times for the model response data in the 28 files. In this loop, file names (model response files, time step file and output data files for the SI1 and SIT indexes) are declared and the sub script file is activated.

In the subscript, for each loop step, the EFAST sample is generated due to technical reasons. The load instruction for the sample file does not at present work. For the current step, the respective model response data file is loaded with the command loadModelOutputFile(path and name of response data file). The time step file is loaded with the MATLAB command load. For the first 27 slb files, a “for loop” is executed 7 times for the 7 time steps to compute the indexes of first and total order (SI1 and SIT). SI1 and SIT are computed for each time step with the commands:

```
getTimeFastFirstValues('annual radiation dose',time)
getTimeFastTotalValues('annual radiation dose',time)
```

Values of the indexes are successively stored in the arrays SI_1 and SI_T. For the last response data file, a “for loop” is executed 5 times with computation of the indexes. When all indexes for the 194 time steps are calculated, values of the indexes are saved in the ASCII output files for the indexes. The appendix lists examples of the two script files.

3.2.2 Test case

A generic performance assessment study for a hypothetic SF/HLW repository in a salt formation has recently been made. On the basis of this study a test system was set up, which was used for testing different methods and techniques for sensitivity analysis. This system shows the typical properties of repositories in rock salt. In the normal evolution scenario there is no release of contaminants. Therefore, a disturbed evolution scenario with shaft seal failure and dam failure was chosen, but even in this case, with the selected parameter distributions, the zero-run probability of the model is about 85 %.

While the majority of simulations with the test model yield very low dose rates, a few ones lead to rather high values. This results in a highly skewed and heavily-tailed distribution of the model output, which spans several orders of magnitude. The system shows non-linear and non-monotonic behaviour.

The generic SF/HLW repository model represents a hypothetical repository for High-Level-Waste (HLW) and Spent Fuel (SF) to be set up in a German rock salt formation. It consists of eight emplacement fields for SF, one for HLW and one for intermediate-level waste (ILW). From the inner transfer drifts boreholes are drilled to a depth of 300 m, including 10 m for a plug for closing the boreholes. Each emplacement drift contains three boreholes. The distance between the central field and the waste sections of the repository is about 450 m. The inner drifts are replaced by one model drift per field. It is assumed that the total amounts of high-level and heat-generating waste that are expected to accumulate in Germany until 2080 are disposed of. The main engineered barriers are the shaft seal, the drift seals, the borehole plugs and the backfill material. A graphical representation of the model structure is given in figure 3.3.

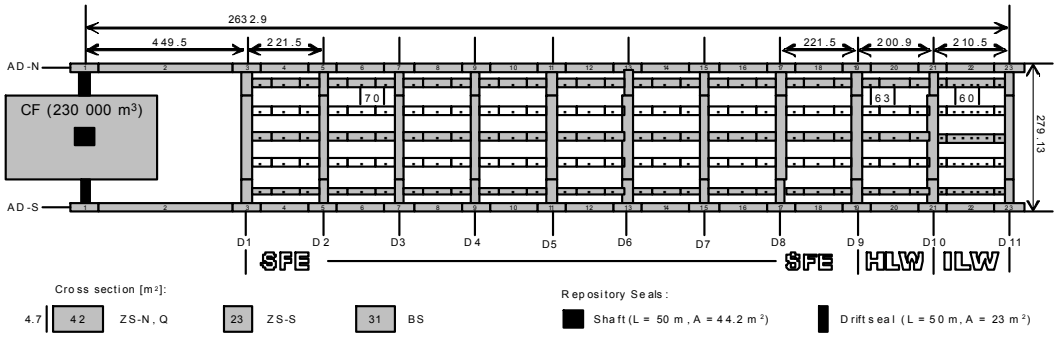

Fig. 3.3 Model Structure for the Generic Repository

Although it is rather improbable, a shaft failure scenario was selected for investigation, in order to demonstrate that the consequences remain low even in such a situation. Six uncertain parameters (4 near field and 2 far field) were considered for the probabilistic investigations. Table 3.2 lists the parameters along with their distribution types and ranges.

Tab. 3.2 Parameter distributions and ranges of the parameters of the test case

Number	Parameter	Distribution	Minimum	Maximum
1	Shaft permeability after failure [m^2]	Log uniform	$1 \cdot 10^{-17}$	$1 \cdot 10^{-14}$
2	Dam permeability [m^2]	Log uniform	$1 \cdot 10^{-17}$	$1 \cdot 10^{-14}$
3	Shaft failure time [yr]	Uniform	25	75
4	Reference convergence rate [1/yr]	Log uniform	$1 \cdot 10^{-3}$	$1 \cdot 10^{-1}$
5	Relative sorption coefficients in the far field	Log uniform	0.1	10
6	Diluting water flow in the aquifer [m^3/yr]	Uniform	$1 \cdot 10^{4}$	$8.6 \cdot 10^{4}$

The sorption coefficients (K_d-values) in the far field are element-specific. Their values are more or less independent of each other, but for the present investigation they are varied together. That means that there is only one random variable, representing a common factor, by which the reference values are multiplied. This factor is varied between 0.1 and 10, where 10 means high sorption and 0.1 low sorption of all elements.

3.2.3 Sensitivity Analysis

The sensitivity analysis was performed using a number of different methods. The following methods were applied:

- Pearson product moment correlation coefficients (PEAR),

- Spearman's rank correlation coefficients (SPEA),
- Partial correlation coefficients (PCC),
- Partial rank correlation Coefficients (PRCC),
- Standardised Regression Coefficients (SRC),
- Standardised Rank Regression Coefficients (SRRC),
- the Smirnov test (SMIR),
- the variance based Extended Fourier Amplitude Sensitivity Test (EFAST).

Apart from these methods, scatterplots, contributions to the sample mean plots (CSM plots) and cobweb plots were utilised as graphical methods to find important parameters.

Four different samples were generated and used for the analysis. EFAST requires a specific sampling scheme, which was applied for two samples with sizes of 3 030 and 6 054. The other two samples were produced using a random sampling scheme. For optimal comparability, the sample sizes were also chosen as 3 030 and 6 054.

3.2.3.1 Analysis of the maximum dose rate

The investigations described in this chapter only consider the peak values of the individual runs, regardless of their times of occurrence. By such an analysis the sensitivity of the maximum model output against variations of the input parameters is investigated.

Input and Output Analysis

Figure 3.4 presents the time-evolution of the calculated dose rate for all simulations using the random samples with 3 030 and 6 054 model runs. The majority of simulations predict zero or very low dose rates, while a few ones lead to rather high values. The result is a highly skewed and heavily-tailed distribution of the calculated maximum values, which spans several orders of magnitude. This is illustrated with a frequency plot of the peak annual doses in figure 3.5. The zero runs are not included in the figure, but it has to be kept in mind that there are 5 136 or 2 579 zero results, respectively.

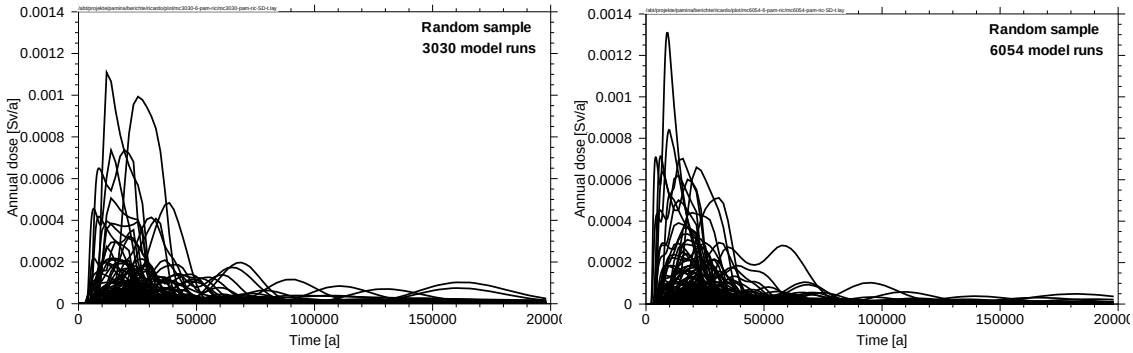

Fig. 3.4 Time evolution of the annual dose rate for all simulations (random samples)

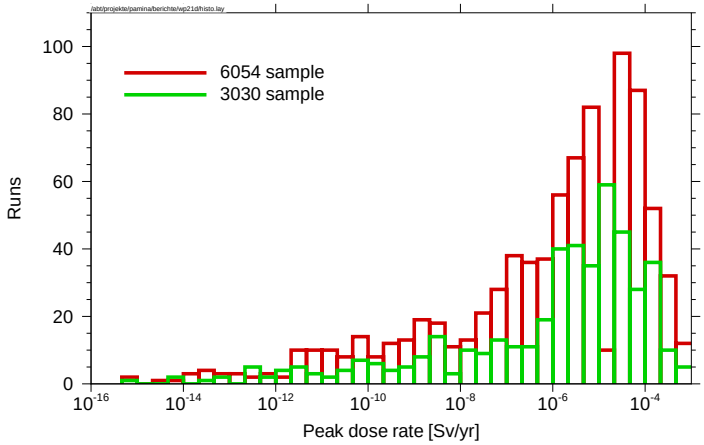

Fig. 3.5 Frequency histogram of the peak dose rates for both EFAST samples

Scatterplots

Figure 3.6 and Figure 3.7 show scatterplots for both random-based sets of model runs. For each parameter the calculated maximum dose rates are depicted versus the corresponding parameter values. Since uniform or log-uniform distributions were used for all parameters, there is a unique, but more or less arbitrarily chosen interval for each of them.

This kind of plots gives a quick visual impression of the sensitivity of the model against the different parameters. Because of the high number of zero-runs only 451 or 918 data points, respectively, can be seen in the figures. The first parameter (shaft permeability after failure) shows a strong accumulation of peak dose rates at the upper end of the range while the values in the lowest decade produce either very low or zero output. The second parameter (dam permeability) shows a similar behaviour, but the data points are distributed over the whole parameter interval. This difference is due to the

uncertainty intervals of the two parameters. This is a good example of how the selection of parameter distributions can influence the results of the sensitivity analysis.

The fourth parameter (reference convergence rate) indicates quite the contrary: accumulation of peak dose rates at the lower end of the range and none at all at the upper end. For the rest of the parameters the peak dose rates are more or less homogeneously distributed all over the range.

Just from the appearance of the parameters in the scatterplots, it can be inferred that the shaft permeability, the reference convergence rate and the dam permeability are important, while the rest are less important since they do not have great impact upon the model results.

In the case of the factor for the sorption coefficients at least the clear tendency can be seen that higher sorption leads to lower maxima, which agrees with the expectation.

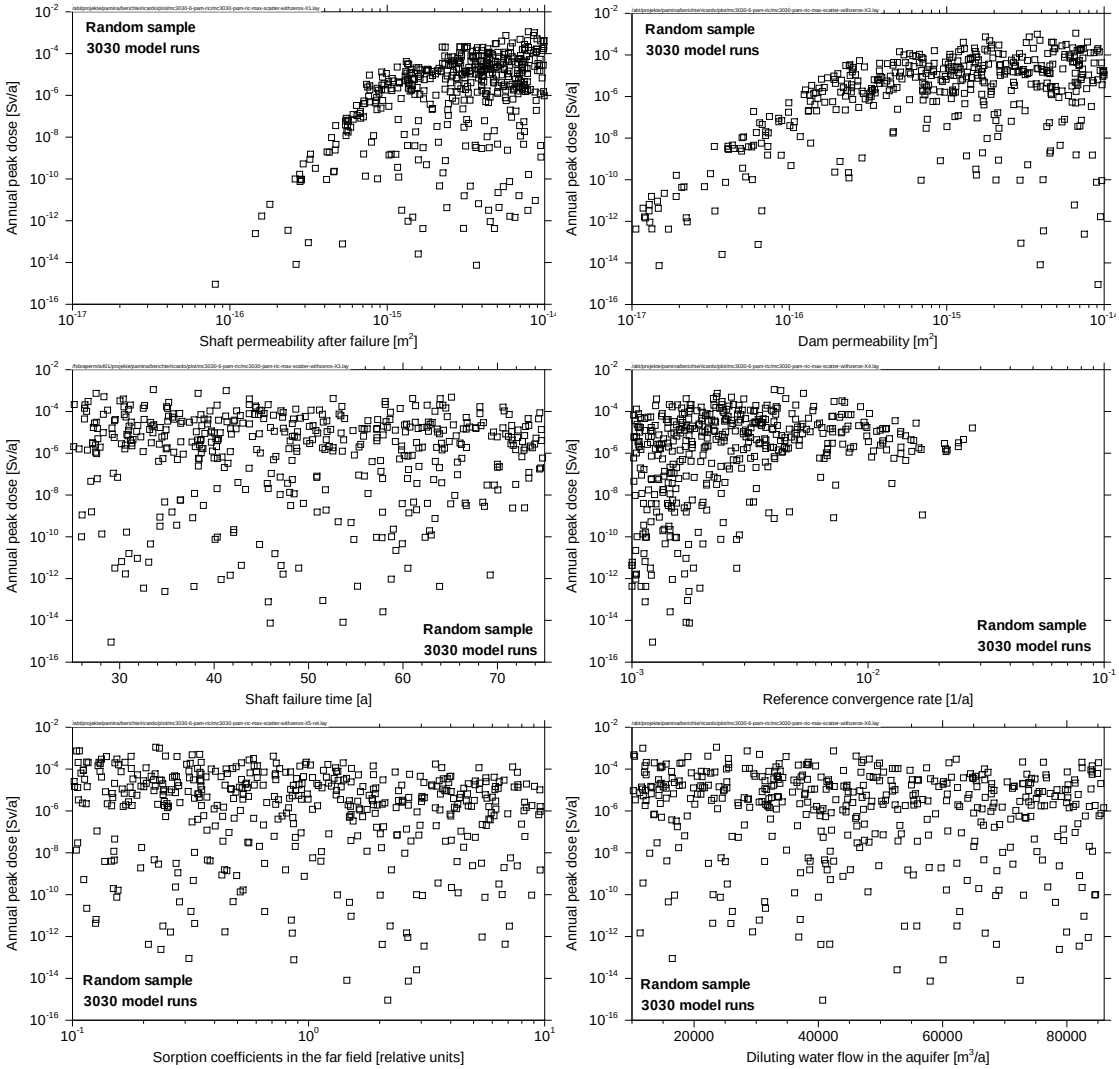

Fig. 3.6 Scatterplots for the 3 030 random sample

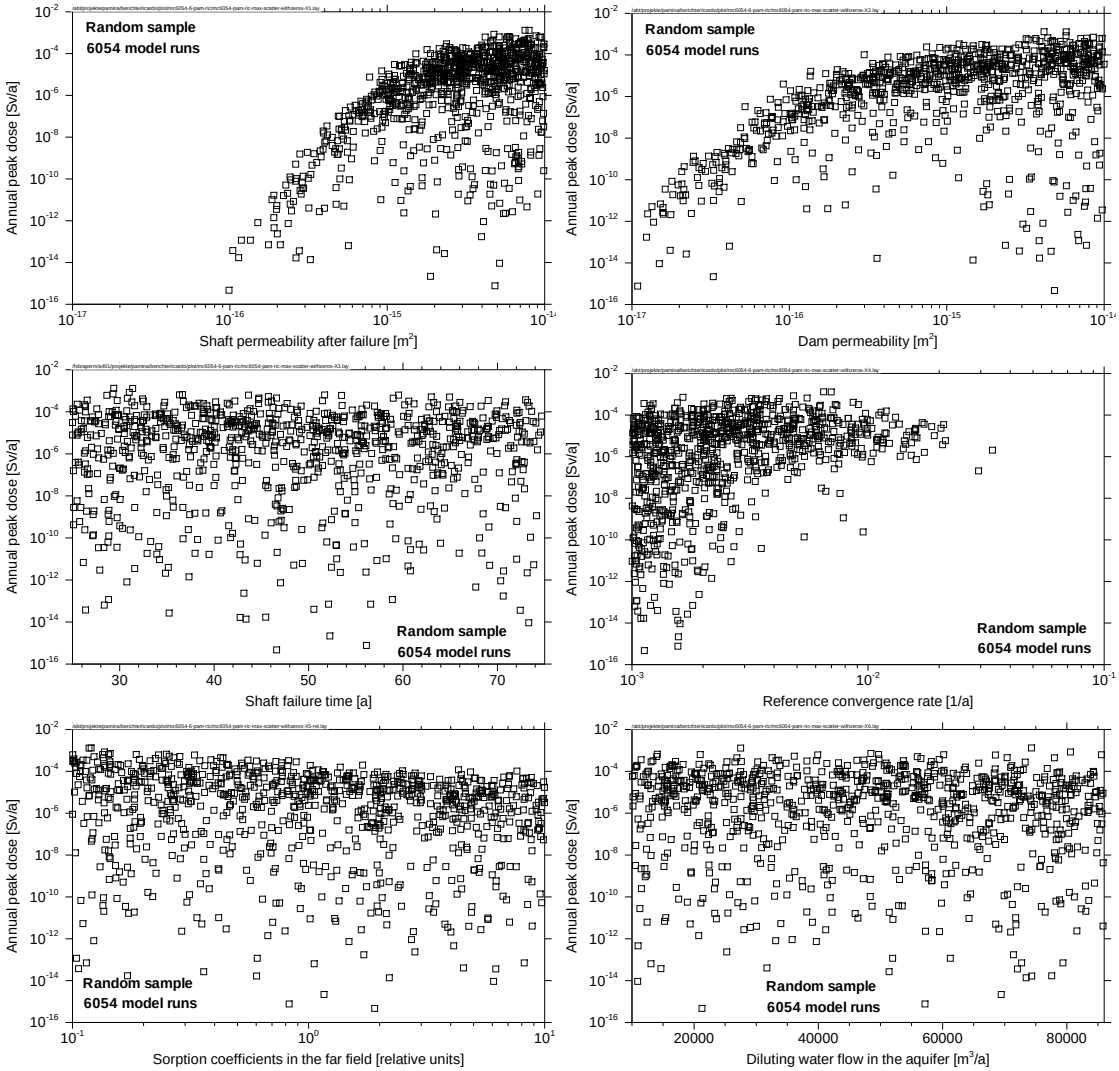

Fig. 3.7 Scatterplots for the 6 054 random sample

CSM plots

Figure 3.8 represents CSM (Contribution to the Sample Mean) plots for all four samples considered. For this kind of plots the *N* model runs are ordered according to the values of the input parameter under consideration. Then the fraction of the sample mean of the peak values is plotted versus the fraction of the sample size. In mathematical terms, the x and y axes in Figure 3.8 correspond to:

$$\text{x-axis: } j/N \quad j = 1,\ldots,N \tag{3.1}$$

$$\text{y-axis: } \frac{1}{\text{mean}(Y)} \sum_{i=1}^{j} \frac{y_i}{N} \; j = 1,\ldots,N \tag{3.2}$$

where N represents the sample size and y_j defines the peak value of the j-th model run in the ordered sample. As a rule of the thumb, important parameters create curves that significantly deviate from confidence bands around the diagonal, while non-important ones generate curves close to the bands of the diagonal. More details about CSM plots can be obtained from /BOL 09/.

A significance band of 25 % is considered in figure 6. For the four samples in this study, the parameter with the most significant deviation from the diagonal is the shaft permeability, followed by the dam permeability and the reference convergence rate. For the two random based samples, also the factor for the sorption coefficients in the far field is identified by the CSM plots in figure 3.8 as an important parameter. This is in line with what could be seen from the scatterplots.

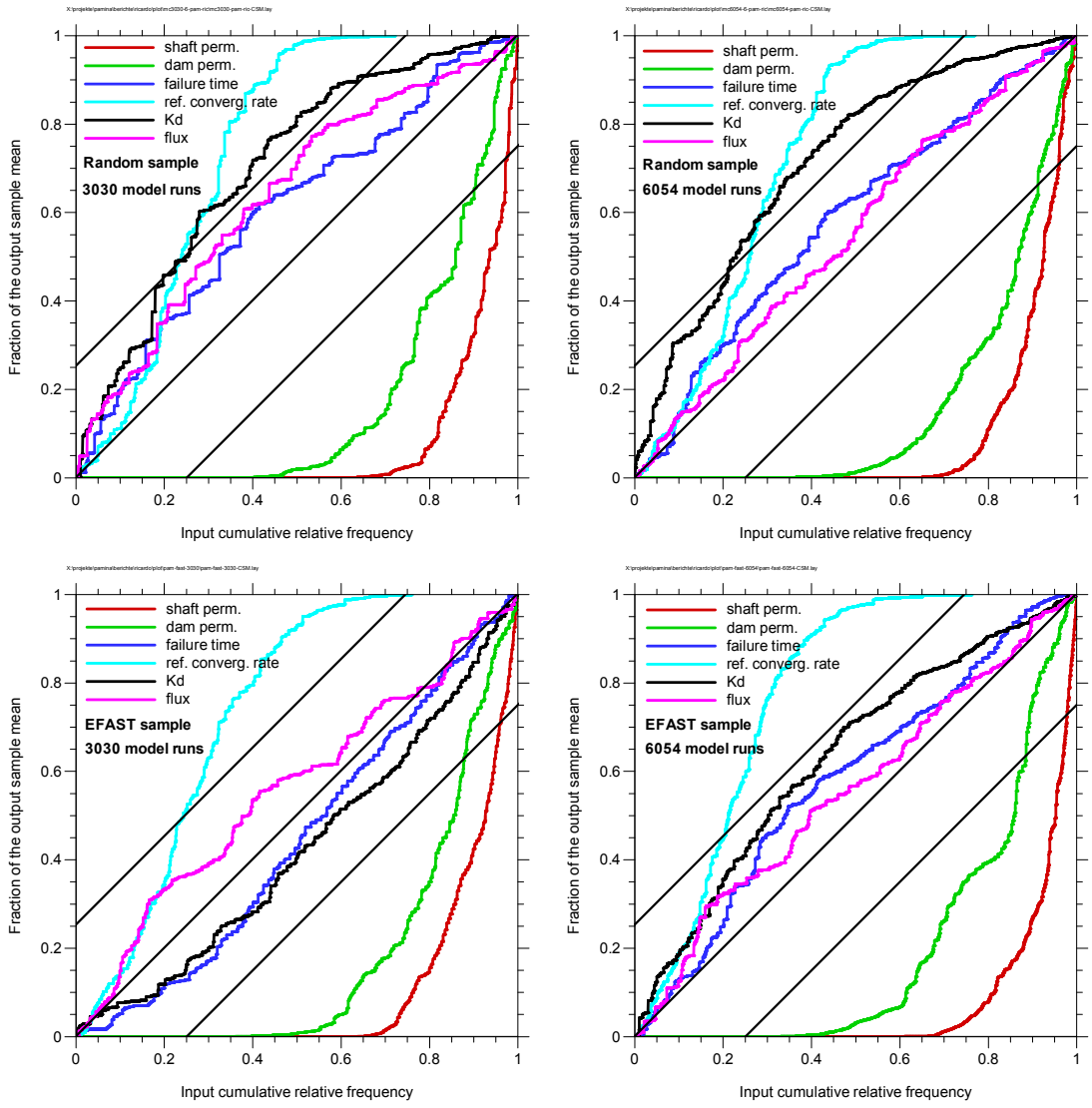

Fig. 3.8 CSM plots for the four samples

For all samples about 70 % of the runs, according to the lowest shaft permeabilities, are responsible for less than 1 % of the mean, since they generate either very low or even zero output. This means that if due to further experimental work, the 30 % upper range of this input parameter could be discarded as a possible range of values, the peak annual dose rate would decrease down to approximately 1 % of the estimate obtained in this study.

In the case of the Dam permeability, the second most important parameter according to this sensitivity measure, its smallest 45 % values contribute less than 1 % to the peak annual dose rate sample mean. The reference convergence rate, on the other hand, shows an inverse behaviour: the lowest convergence rates create high output values, since they allow contact of wastes with brine; the 55 % lowest values are responsible for more than 99 % of the mean.

As regards the sorption factor, in the 6 054 run random sample the 8 % smallest values contribute more than 30 % to the output sample mean while the largest 20 % values contribute less than 5 %. In the 3 030 runs random sample the sorption factor is less important, but still significant. It is, however, a surprising result that the EFAST samples do not seem to clearly reflect the dependency of the maximum on the sorption factor.

The sample size increase has produced two obvious effects on the plots:

- the width of the 99 % band decreases, and
- the lines plotted are smoother, specially the ones corresponding to the four most important input parameters.

Cobweb plots and Smirnov test

The two random samples were analysed using cobweb plots and the Smirnov test. Cobweb plots are a graphical means for showing the importance of the different parameters in one figure. For each run a line is drawn that connects the ranks of all input parameters and the model output value (the maximum dose rate). Figure 3.9 presents the cobweb plots for both random samples. Since the big number of zero-runs is not taken into account, only the highest 15 % of the output ranks appear in the plots. They are predominantly connected to the lower ranks of the reference convergence rate and the higher ranks of the shaft permeability, which shows that these are the most relevant parameters.

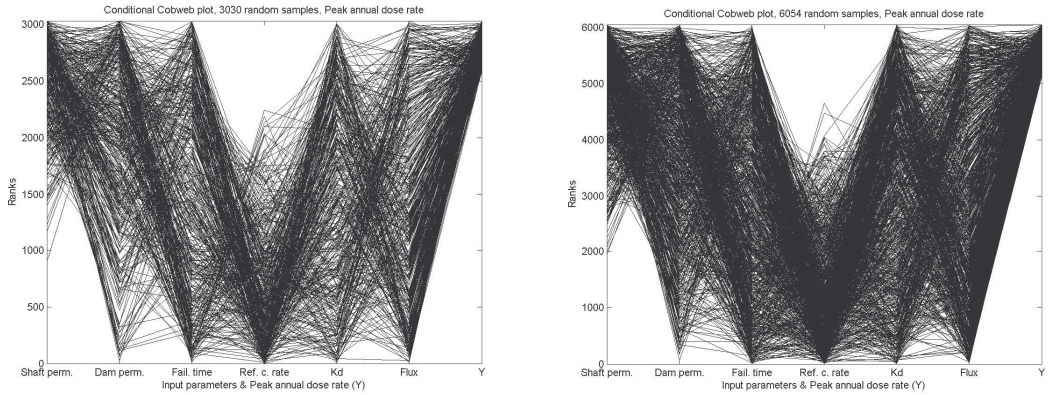

Fig. 3.9 Cobweb plots for the random samples

For a more quantitative ranking the Smirnov test was performed on both sets of calculations. The results are shown in table 3.3. The order of importance calculated by the Smirnov test does not change when passing from 3 030 to 6 054, except for the two parameters identified as least important (sorption factor and flux). It is, however, surprising that the sorption factor is identified as the least or second least important parameter, while it is on rank 4 and clearly significant according to the CSM plots and, unlike the failure time, can also be identified as relevant from the cobweb plots as well as from the scatterplots. This shows that the results of the Smirnov test are not always reliable.

Tab. 3.3 Results of the Smirnov test for the 3 030 and the 6 054 run random samples

	Sub-sample selection criterion: null/non-null Peak annual dose rates	
Input parameter	3 030 run random sample p-value / importance order	6 054 run random sample p-value / importance order
Shaft permeability	1.01E-107 (1)	3.33E-243 (1)
Dam permeability	4.04E-029 (3)	6.03E-047 (3)
Failure time	2.37E-001 (4)	3.62E-003 (4)
Ref. convergence rate	9.27E-088 (2)	1.29E-203 (2)
Sorption factor	4.03E-001 (5)	3.73E-001 (6)
Flux	5.72E-001 (6)	1.37E-001 (5)

3.2.3.2 Time-dependent analysis

In the following the model is analysed for a number of separate points in time, so that the time developments of the different sensitivity measures can be derived. The evaluations were done using the tool SIMLAB 3.

Correlation- and regression- based methods, Smirnov test

Due to technical reasons, no time-dependent evaluation of the two random samples was performed in the exercise described here. EFAST samples are not optimal for evaluation with random-based correlation and regression methods, but nevertheless, such an evaluation can be done. The results presented in the following refer to the EFAST samples exclusively.

The time-dependent evaluation of the two EFAST samples with the random based methods (PEAR, SPEA, PCC, PRCC, SRC, SRRC, Smirnov) indicates that the most important parameter is the shaft permeability since all methods yield the highest coefficients for this parameter at almost all times. The dam permeability and the reference convergence rate are less significant than the shaft permeability, but comparable to each other. From figure 3.10 it can be seen that the rank-based methods (SPEA, PRCC and SRRC) identify the reference convergence rate as the second most important parameter, while for the non-rank-based methods (PEAR, PCC and SRC) yield higher absolute coefficients for the dam permeability. Since the system of the test case is nonlinear, results of the rank-based test may be trusted more than those of the value-based ones.

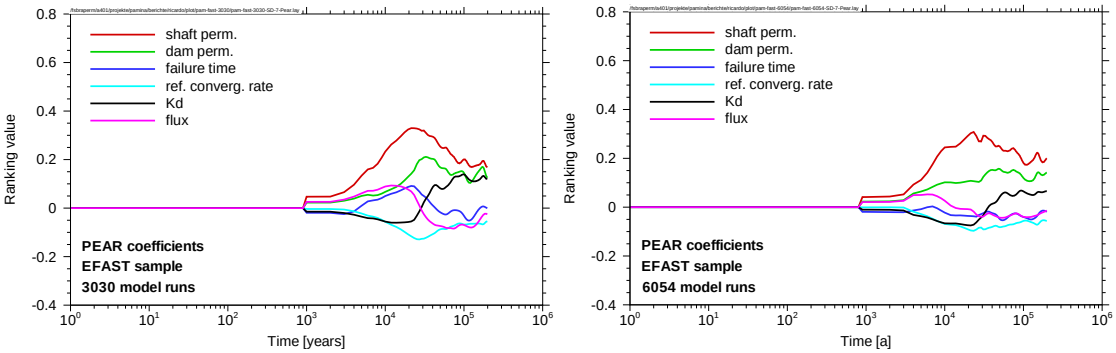
shaft perm.
dam perm.
failure time
ref. converg. rate
Kd
flux
Ranking value
Time [years]
PEAR coefficients
EFAST sample
3030 model runs

shaft perm.
dam perm.
failure time
ref. converg. rate
Kd
flux
Ranking value
Time [a]
PEAR coefficients
EFAST sample
6054 model runs

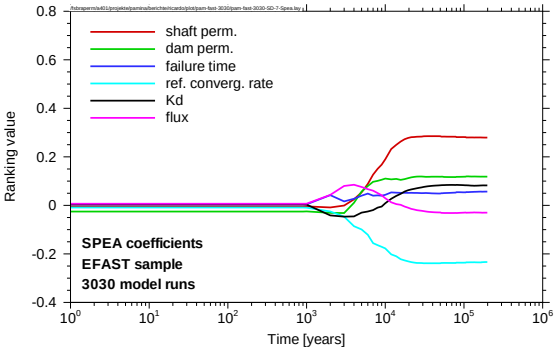
shaft perm.
dam perm.
failure time
ref. converg. rate
Kd
flux
Ranking value
Time [years]
SPEA coefficients
EFAST sample
3030 model runs

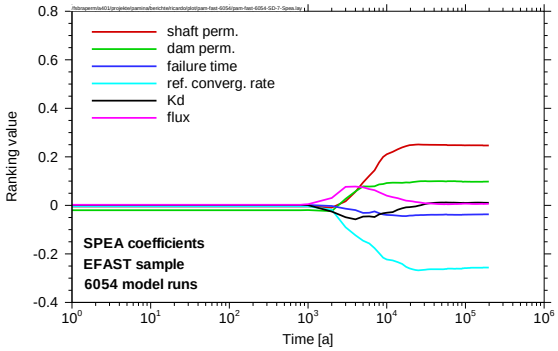
shaft perm.
dam perm.
failure time
ref. converg. rate
Kd
flux
Ranking value
Time [a]
SPEA coefficients
EFAST sample
6054 model runs

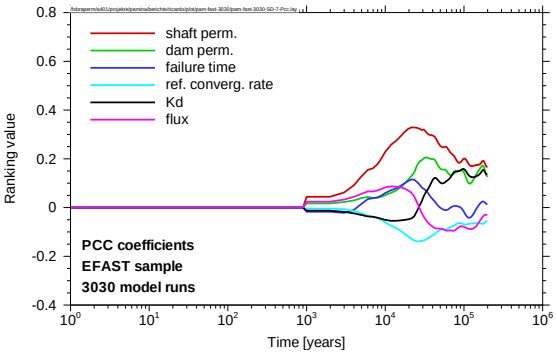
shaft perm.
dam perm.
failure time
ref. converg. rate
Kd
flux
Ranking value
Time [years]
PCC coefficients
EFAST sample
3030 model runs

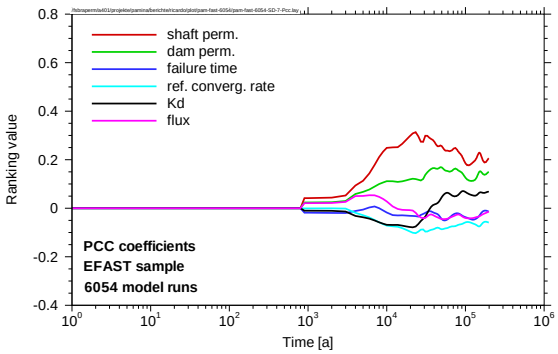
shaft perm.
dam perm.
failure time
ref. converg. rate
Kd
flux
Ranking value
Time [a]
PCC coefficients
EFAST sample
6054 model runs

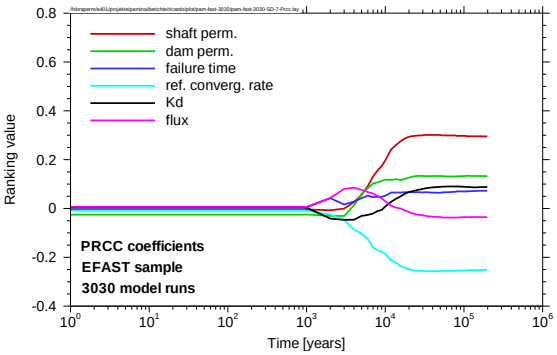
shaft perm.
dam perm.
failure time
ref. converg. rate
Kd
flux
Ranking value
Time [years]
PRCC coefficients
EFAST sample
3030 model runs

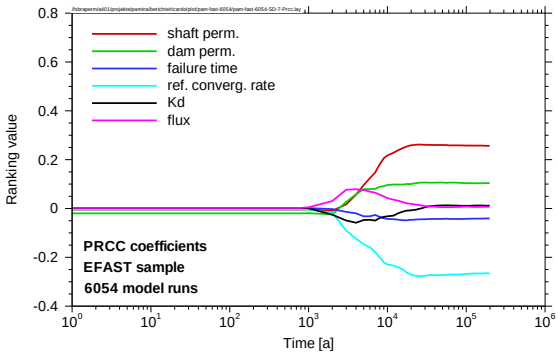
shaft perm.
dam perm.
failure time
ref. converg. rate
Kd
flux
Ranking value
Time [a]
PRCC coefficients
EFAST sample
6054 model runs

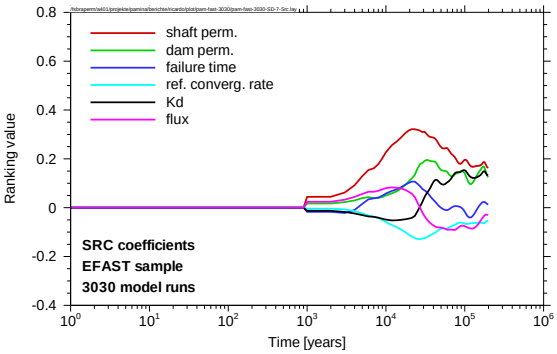
shaft perm.
dam perm.
failure time
ref. converg. rate
Kd
flux
Ranking value
Time [years]
SRC coefficients
EFAST sample
3030 model runs

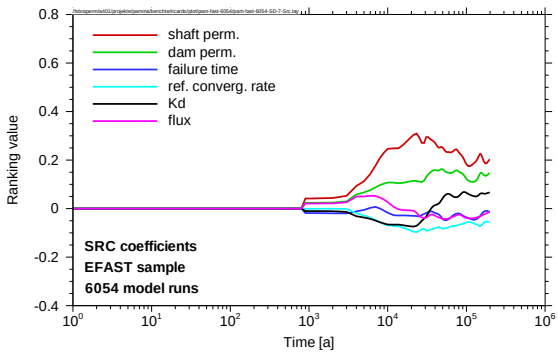
shaft perm.
dam perm.
failure time
ref. converg. rate
Kd
flux
Ranking value
Time [a]
SRC coefficients
EFAST sample
6054 model runs

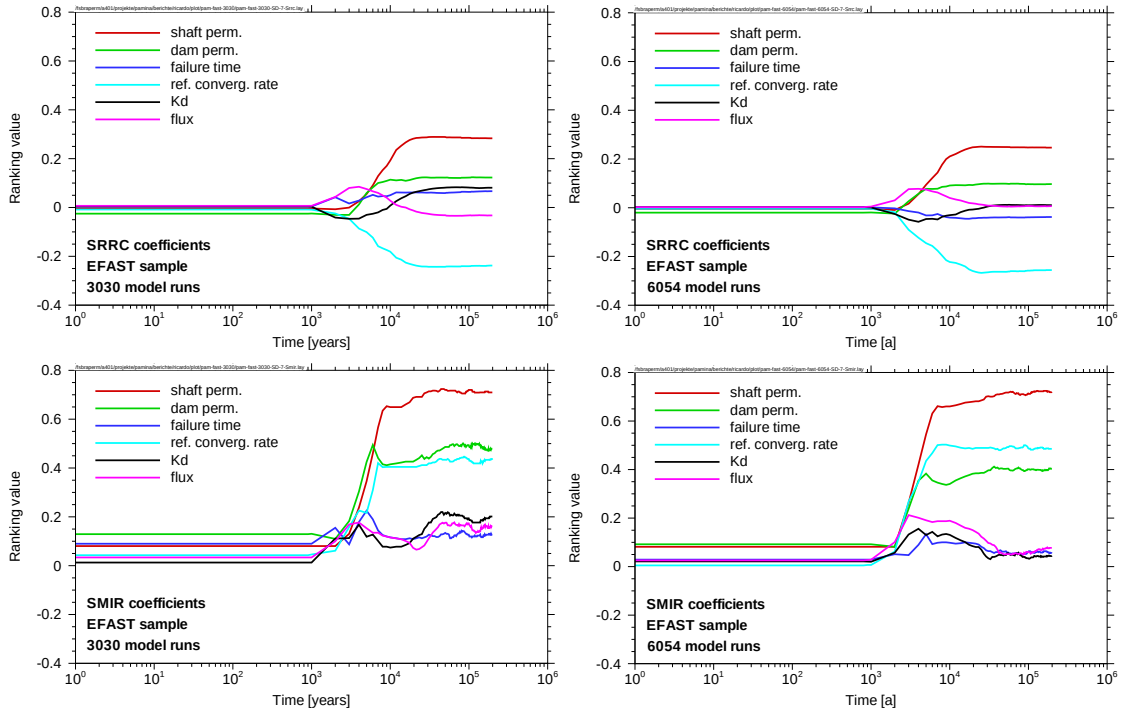

Fig. 3.10 Time-development of the results of various correlation and regression tests of the EFAST samples with 3 030 and 6 054 model runs

The diagrams for the value-based methods (PEAR, PCC and SRC) as well as those for the rank-based methods (SPEA, PRCC, SRRC) look much alike each other. This is due to the close relationship between the methods. Since there are no parameter correlations, PEAR and PCC, as well as SPEA and PRCC, should even theoretically calculate the same results. Since there is no release from the model repository before 1 000 years, all curves start deviating from the zero line at that time.

In general, the curves calculated with the rank-based methods look smoother and allow a more unique parameter ranking at most points in time than those belonging to the value-based evaluations. When comparing the evaluations of the two different samples one sees that the robustness of the methods is not very good. Especially the curves belonging to the less important parameters differ, in part, essentially between both samples. Not even the sign is unique, as can be seen at the curve for the paramteter “failure time”. While for the 3 030 runs sample all regression- or correlation-based evaluations calculate positive values between 4 000 and 60 000 years, they yield slightly negative values for the 6 054 runs sample. In fact, this parameter seems to be of no practical importance for the model results.

The parameter ranking that can be derived from the diagrams for most of the time is much in line with that calculated for the maxima. All methods identify the shaft permeability as the most important parameter at nearly all times. The value-based evaluations, however, show that this dominance begins to decrease after several 10 000 years, while the importance of the dam permeability increases. While the reference convergence rate only reaches relatively low absolute values when assessed with the value-based methods, ist dominance seems nearly as clear as that of the shaft permeability in the rank-base evaluations. The reason for this may be that ist influence to the model is highly non-linear, which means a poor performance of the value-based methods.

The sorption factor shows a specifically interesting behaviour. While all methods agree that it shows a negative influence on the model result (meaning that higher values yield lower model output) the sensitivity measures become positive 10 000 to 20 000 years. This can be explained by the fact that a high sorption means a high delay of release, so that the main peak will appear later. This effect leads to an increased number of high values at late times for high sorption factors.

The Smirnov tests shows for both samples a clear dominance of the shaft permeability and assesses the dam permeability and the reference convergence rate as nearly equally important. The remaining three parameters are identified as unimportant. Although the sorption factor definitely has an influence on the model, this is obviously not identified by the Smirnov test, which was already found out during the sensitivity analysis of the maxima.

Variance-based evaluation

The regression- or correlation-based sensitivity analysis techniques, according to their mathematical nature, are best suitable for models with a close-to-linear behaviour. This, however, is not a typical property of repository models. Many of the effects taken into account are non-linear and their interaction can even increase the nonlinearity. As long as the model behaviour is at least monotonic the rank transformation can improve the significance of the methods, as was shown in the previous section.

A completely different approach to sensitivity analysis of non-linear systems is variance-based analysis. In the study described here some experiments were done with the EFAST method /SAL 97, SAL 00/, which is an extension of FAST (Fourier Ampli-

tude Sensitivity Test), since it seemed promising to yield meaningful results for reasonable computational costs.

The principle of FAST is to calculate the first-order sensitivity indices

$$\frac{\mathrm{Var}_{X_j}[\mathrm{E}(Y|X_j)]}{\mathrm{Var}(Y)} \tag{3.3}$$

by scanning the parameter space with periodic functions using interference-free frequencies and performing a Fourier analysis on the output. A random element can be introduced to the sampling by inserting a random phase shift at some points. It has been shown that this method yields the same sensitivity indices as Sobol's method /SAL 00/ for, at least normally, lower computational costs. The Extended FAST method (EFAST) /SAL 97/ additionally yields the total order sensitivity indices, which describe the influence of a parameter to the output in interaction with all others.

The EFAST method was applied to the model under consideration as a time-dependent evaluation using the two EFAST samples with 3 030 and 6 054 runs, respectively. The results are unsatisfactory as shown in figure 3.11. It is apparent that the shaft permeability is the most important parameter, though it does not reach a sensitivity index of more than 0.15. The other parameters have very low sensitivity indices and show no unique behaviour. The agreement between the two evaluations is poor.

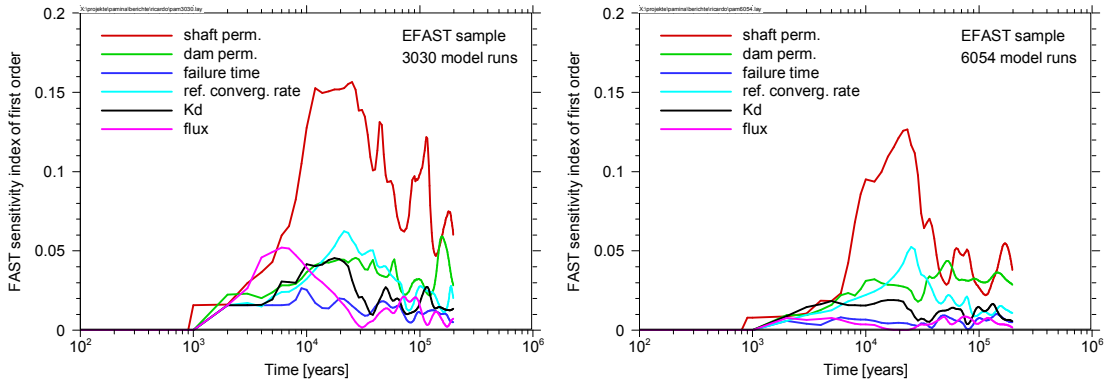

Fig. 3.11 First order EFAST sensitivity index for the two sets

Reasons for the instability of the indices can be

- the highly skewed and heavily tailed distribution of the radiation exposure with many zero-runs and
- an insufficient number of simulations.

Only 430 out of 3 030 or 885 out of 6 054 runs, yield a non-zero output, which means a 15 % probability. Therefore, only these 15 % of the runs can contribute to the calculation of sensitivity indices. Moreover, the periodicity of the model output and with it the Fourier is disturbed by the zero-runs.

There is an additional problem with models like that under consideration. The output of performance assessment calculations typically varies over several orders of magnitude and is best presented on a logarithmical scale. The variance, however, is calculated on a linear scale, which leads to a strong overvaluation of high values. While with the considered model the majority of runs yield zero or very low output values, there are quite a few ones with rather high results. If the variance is evaluated, it is clearly dominated by these few values, which is one reason for the poor robustness of EFAST. This, however, is valid for all kinds of variance-based analysis.

The variance of a sample of data is the mean squared deviance from the mean value. The variance of a set of data values can be decomposed in the individual contributions of subsets. This is shown in figure 10 for the peak values calculated with the two EFAST samples. In the set of 6 054 runs, the 85 % zero-runs are responsible for only a very small fraction of less than 2 % of the variance. On the other hand, the two highest maxima alone make nearly 20 % and the 12 highest maxima more than 50 % of the variance. The set of 3 030 runs shows the same phenomenon, though less pronounced. It becomes obvious from this investigation that the variance of the model output depends on the randomness of the sample and a variance-based analysis will not be very robust, at least if performed with sample sizes of a few thousand. So far it cannot be said which number of simulations would be necessary for the method to produce stable results with the considered model.

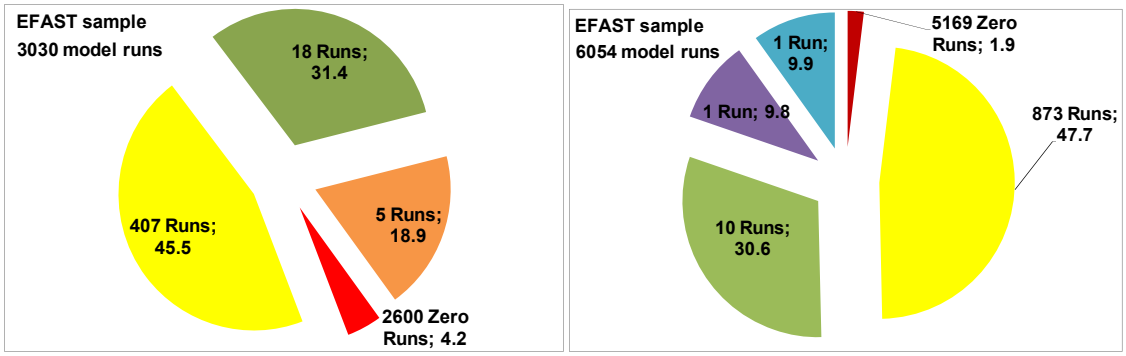

Fig. 3.12 Decomposition of the variance of the model output (peak values)

There is, however, a possibility to increase the robustness and significance of the variance-based evaluations /BEC 08/. In order to mitigate the uneven weighting of the individual runs, a logarithmic transformation could be performed on the model output *y* before applying the EFAST evaluation. This would adapt the evaluation to what is instinctively done when presenting the results on a logarithmic scale. However, instead of solving the problem, such a transformation would turn it into its opposite, because it would give very low values an inadequate weight and even lead to unsolvable problems with exact zero values.

Therefore, the following transformation was done:

$$y^* = \log_2(y/a + 1) \tag{3.4}$$

with some adequate value *a*. In contrast to simply taking the logarithm this transformation does not overvalue extremely small values and allows even zero. It maps 0 to 0, *a* to 1 and big values practically to their logarithm. It does not only solve the occurring mathematical problems but also reflects the specific interests of the evaluator:

When assessing the results of a long-term safety analysis of a repository system one is normally not at all interested in whether the calculated dose rate is 10^{-15} Sv/yr, 10^{-20} Sv/yr, or zero. All such values are equally irrelevant. Higher values that remain some orders of magnitude below the limit should have practically the same weight, even if they differ by a small factor. Only the highest values are really interesting, but they are still best assessed on a logarithmic scale.

The main difficulty is to find a proper value for the transformation parameter *a*. It indicates the transition from “low” to “high” values. One possibility would be to choose some fixed value that is subjectively considered to mark this transition, discriminating

"near-zero" output values from interesting ones. In order to avoid subjectivity, a different approach was followed here by calculating *a* individually for each point in time in such a way that the expectation of the transformed distribution gets equal to 1:

$$\mathrm{E}(y^*) = 1 \tag{3.5}$$

This gives equal statistical weights to "low" and "high" values at each point in time. With this transformation, applied to the set of the peak output values of the 6 054 runs sample, the contribution of the highest value to the total variance reduces from 9.9 % to 0.7 % and that of the zero-output runs increases from 1.9 % to 5 %. Figure 3.13 shows the variance decomposition of the transformed output for both samples.

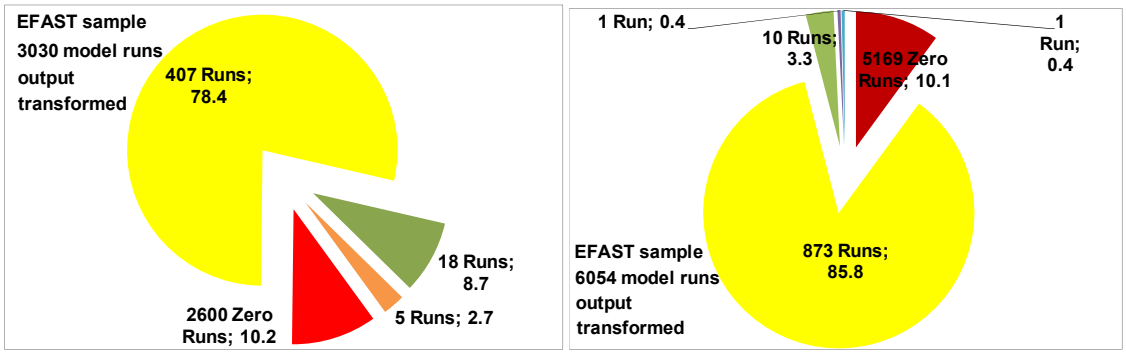

Fig. 3.13 Decomposition of the variance of the transformed model output (peak values)

In comparison with figure 3.12 it becomes obvious that the weighting is much more balanced, since the contributions of the highest values decrease and those of the zero-runs increase. The yellow-coloured part, which represents the vast majority of all non-zero-runs, clearly dominates after the transformation.

In figure 3.14 the time-development of the first order sensitivity indices of the transformed model output, calculated using EFAST, is depicted. In comparison with figure 3.11 the curves look much smoother and allow a more unique ranking of the input parameters. Although there are still differences between the curves of the two evaluations, they are much more similar and the robustness of the method has obviously increased.

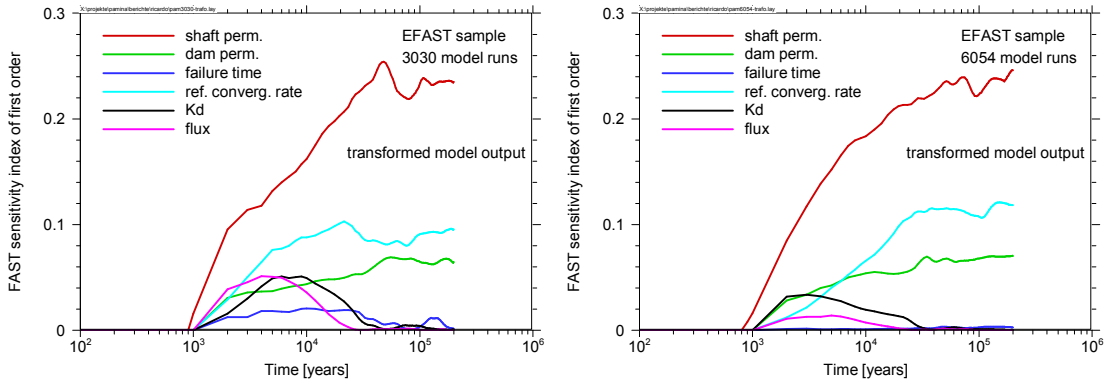

Fig. 3.14 First order EFAST sensitivity index for the two sets (model output transformed)

Figure 3.15 shows the CSM plots of the transformed peak values. The curves are much smoother than those of the untransformed output (see figure 3.8) and allow a more unique statement about the importance of the individual parameters. Especially the plot for the 6 054 runs sample clearly identifies the shaft permeability, the dam permeability and the reference convergence rate as important parameters while the curves for the other parameters hardly deviate from the diagonal. As stated above, this is surprising as far as the sorption factor is concerned, but it is in line with the former results.

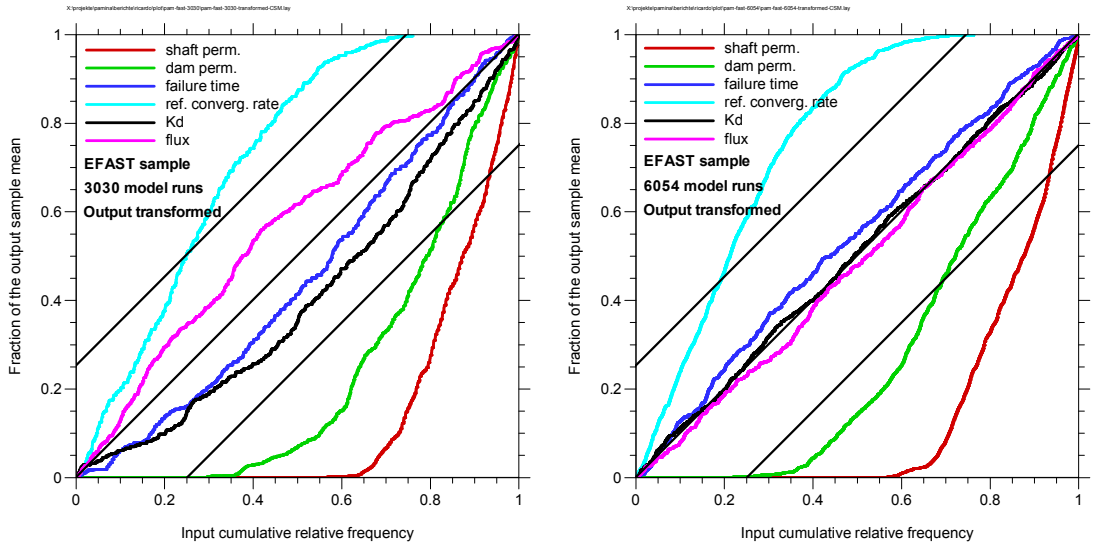

Fig. 3.15 CSM plots of the two EFAST samples (model output transformed)

3.2.4 Summary and Conclusions

A variety of different sensitivity analysis methods were applied to a model system for a generic rock salt HLW/SF repository, which includes a few typical important properties of PA systems in rock salt. The applied methods comprise

- regression and correlation methods on value basis (PEAR, PCC, SRC),
- rank-based regression and correlation methods (SPEA, PRCC, SRRC),
- non-parametrical statistics (Smirnov-Test),
- graphical methods (Scatterplots, CSM plots, cobweb plots),
- variance-based sensitivity analysis (EFAST).

Some of the methods, especially the graphical ones, were only applied to the peak output of the model; others were used to produce time curves of sensitivity indices.

All methods indicate that the most important parameter is the shaft permeability, followed, in varying orders, by the dam permeability and the reference convergence rate. The remaining parameters seem less important.

The graphical methods (scatterplots, CSM plots and cobweb plots) provide a visual impression of the sensitivity of the model against parameter variations. Although no quantitative information can be derived directly from theses graphs, they allow a quick examination of the parameters which ones are important and which ones are less important.

The correlation- and regression-based methods are easy to apply, but yield relatively unclear results concerning the less important parameters. The EFAST method, which requires a higher technical effort, but is, by theory, more adequate to non-linear systems, unfortunately does not resolve this problem.

The reasons for the instability of the results of the different sensitivity tests conducted in this study are:

(i) The highly skewed and heavily-tailed distribution of the model output, including the property of producing exact zero-output in 85 % of the simulations. Due to

this property of the model the evaluation is dominated by very few simulations with high output values.

(ii) An insufficient number of simulations. In view of (i), an extremely high number of model runs would be necessary to achieve robust results.

For the variance based method EFAST, it was shown that an adequate output transformation can improve both the robustness and the significance of the evaluation, which is then in agreement with the ranking results of the rank-based sensitivity tests. In view of the high proportion of zero-runs, which can, by principle, not reflect the variability of the input parameters, the FAST evaluation of the transformed output is surprisingly good. Generally, variance-based sensitivity analysis, if applied and interpreted carefully, seems promising to support the safety case better than regression or correlation methods. Scatterplots, CSM plots and cobweb plots appear to be powerful graphical tools, which can be used rather easy and with any sample.

4 Safety indicators and performance indicators

The robustness of the safety case can be strengthened by the use of multiple lines of evidence leading to complementary also qualitative safety arguments that can compensate for shortcomings in any single argument. One type of evidence and arguments in support of a safety case is the use of safety indicators complementary to dose and risk.

Complementary safety indicators can avoid, to some extent, the uncertainties of doses and risks. In contrast to near-surface and biosphere properties, the possible evolutions of a well-chosen host rock can be predicted with reasonable confidence over much longer time scales, i. e. about one million years into the future. Hence, there is a trend in some recent safety cases towards evaluating safety indicators, in addition to dose and risk, such as radiotoxicity fluxes out of the geosphere, which do not rely on assumptions about human behaviour and can support the safety statement and increase the robustness of the safety case.

Safety indicators provide statements about the overall safety of a repository system. Additionally it can be valuable to investigate the functioning of the repository system and its components on a more technical level by calculating quantities that describe the effectiveness of individual barriers or parts of the system. Such quantities are called performance indicators. Typical performance indicators are radionuclide concentrations and fluxes in or between different parts of the system. They provide a good means for understanding and communicating the functioning of the system and can support the safety case in an illustrative manner.

4.1 Repository in salt

The principal objectives of the work presented in the following was to

- test appropriate safety and performance indicators for repositories in rock,
- determine adequate reference values for the considered safety indicators,
- analyse the robustness of safety indicators and finally,
- identify the potential of the concept of risk and to use it in the context of scenario probabilities and safety indicators.

Section 4.1.1 describes the reference concept, i. e. the underlying assumptions and the relevant parameters, of the repository system and the boundary conditions of the scenario used for the calculation of the applied indicators.

Section 4.1.2 deals with the safety indicators analysed for the scenario presented in section 4.1.1. It describes the derivation of the corresponding reference values of the applied safety indicators for the given repository system. In this report, the most detailed description is provided for the indicator “contribution to power density in groundwater”. It is the only safety indicator that is not used in previous reports on indicators such as [3] or [28]. Additionally, an advanced analysis on safety indicators is provided, which concentrates on the robustness of the indicators. To achieve this, a probabilistic analysis is performed with a number of uncertain parameters varied over adequate ranges. All realisations with a release of radionuclides are used to analyse the robustness of the tested safety indicator. Exemplarily, the effective dose rate is used in this analysis.

The testing of safety indicators does not take into account the probability of the chosen set of parameters. In fact, the results of a repository model in rock salt with plausible parameter combinations very often yield zero emissions of radionuclides. One solution to consider scenario probabilities and these zero emissions is to introduce the concept of risk. Section 4.1.3 deals with this concept. Two different approaches are discussed in this contribution. Eventually, risks indicators are developed by comparing this risk to other risks in everyday life.

Section 4.1.4 describes the performance indicators chosen for the analysis and the compartment structure applied for this analysis and finally, section 4.1.5 gives a summary of the lessons learnt.

4.1.1 Reference concept and scenario information

The reference concept of the GRS contribution is based on a conceptual repository design proposed in /BUH 08a/, a German joint R&D project (BGR, DBE, GRS) for evaluating and assessing safety concepts for high level waste (HLW) repositories in rock salt and for identifying the major needs for future research projects in this field. In this report the most important features are delineated; a description in more detail is provided by /BUH 08/ and /WOL 09/.

The host rock formation is a salt dome with a sedimentary coverage of about 200 m to 300 m. The repository is located in a depth of 870 m below surface (disposal level) in a homogeneous rock salt layer within the salt dome. The repository model consists of an access shaft, a central field (CF) and two access drifts (AD-N and AD-S), which connect the central field with a horizontal network of transfer drifts (fig. 1). The distance between the central field and the waste sections of the repository is about 450 m. From the inner transfer drifts boreholes are drilled to a depth of 300 m (represented by black dots in figure 4.1), 290 m are intended for emplacing the waste canister and 10 m for a plug. In the reference concept crushed salt with an initial porosity of 0.3 is applied for backfilling and for the borehole plug.

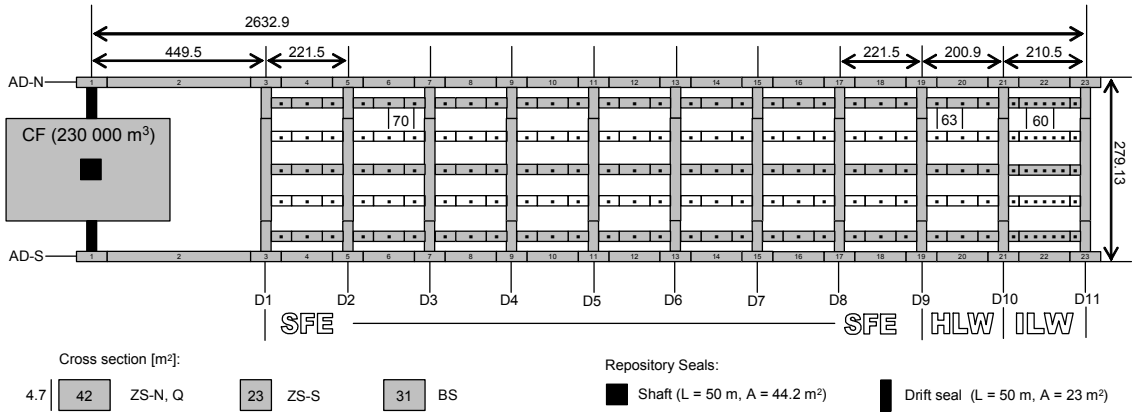

Fig. 4.1 Plane view of the GRS repository concept. Black dots represent the vertical boreholes

The reference concept used is able to emplace the total waste volumes of HLW, which are expected to accumulate in Germany until 2080 [5]. Considered types of waste are spent fuel rods (SF), vitrified waste (HLW) and compacted constituents of spent fuel elements (ILW). The corresponding containers are thin-walled canisters (type BSK 3) for SF with a length of 4.98 m and a radius of 0.22 m, HLW canisters (type CSD-V, length = 1.34 m, radius = 0.22 m) and ILW canisters (type CSD-C, length = 1.35 m, radius = 0.22 m). The chosen geometric configuration of the boreholes guarantees that the maximum temperature near the waste is less than 200 °C in order to avoid chemical or mineralogical changes of the host rock. The minimal distances between the boreholes are about 60 m for HLW and 20 m for ILW. In total, the repository consists of ten major waste sections, eight sections are required for SF (120 boreholes), one section for HLW (15 boreholes), and one section for ILW (35 boreholes). Altogether

– 6 960 (120 × 58) SF canisters,

– 3 225 (15 × 215) HLW canisters,

– 7 455 (35 × 213) ILW canisters,

are emplaced in the conceptual repository used. The inventories of the different waste container types are based on data given in /BUH 08/. The given data and the resulting total amount are listed in table 4.1.

Tab. 4.1a Radionuclide inventory (activation and fission products)

Nuclide	Half life [a]	SF [Bq/can.]	HLW [Bq/can.]	ILW [Bq/can.]	Total [Bq]	Total [mol]
C-14	$5.730 \cdot 10^{3}$	$7.37 \cdot 10^{10}$	-	$1.4 \cdot 10^{10}$	$6.17 \cdot 10^{14}$	$2.67 \cdot 10^{2}$
Cl-36	$3.000 \cdot 10^{5}$	$9.77 \cdot 10^{08}$	-	-	$6.80 \cdot 10^{12}$	$1.54 \cdot 10^{2}$
Co-60	$5.272 \cdot 10^{0}$	$1.63 \cdot 10^{15}$	$3.32 \cdot 10^{13}$	$7.71 \cdot 10^{13}$	$1.21 \cdot 10^{19}$	$4.81 \cdot 10^{3}$
Ni-59	$7.500 \cdot 10^{4}$	$8.14 \cdot 10^{11}$	$7.00 \cdot 10^{07}$	-	$5.66 \cdot 10^{15}$	$3.21 \cdot 10^{4}$
Ni-63	$1.000 \cdot 10^{2}$	$1.16 \cdot 10^{14}$	$9.50 \cdot 10^{09}$	$2.71 \cdot 10^{13}$	$1.01 \cdot 10^{18}$	$7.61 \cdot 10^{3}$
Se-79	$1.100 \cdot 10^{6}$	$2.98 \cdot 10^{10}$	$1.72 \cdot 10^{10}$	$5.51 \cdot 10^{07}$	$2.63 \cdot 10^{14}$	$2.19 \cdot 10^{4}$
Sr-90	$2.864 \cdot 10^{1}$	$5.99 \cdot 10^{15}$	$3.23 \cdot 10^{15}$	$1.40 \cdot 10^{13}$	$5.22 \cdot 10^{19}$	$1.13 \cdot 10^{5}$
Zr-93	$1.500 \cdot 10^{6}$	$1.58 \cdot 10^{11}$	$8.92 \cdot 10^{10}$	$8.60 \cdot 10^{09}$	$1.45 \cdot 10^{15}$	$1.65 \cdot 10^{5}$
Nb-94	$2.000 \cdot 10^{4}$	$1.36 \cdot 10^{11}$	$8.18 \cdot 10^{06}$	-	$9.47 \cdot 10^{14}$	$1.43 \cdot 10^{3}$
Mo-93	$3.500 \cdot 10^{3}$	$6.95 \cdot 10^{09}$	$6.47 \cdot 10^{06}$	-	$4.84 \cdot 10^{13}$	$1.28 \cdot 10^{1}$
Tc-99	$2.100 \cdot 10^{5}$	$1.04 \cdot 10^{12}$	$6.19 \cdot 10^{11}$	$2.31 \cdot 10^{09}$	$9.22 \cdot 10^{15}$	$1.46 \cdot 10^{5}$
Pd-107	$6.500 \cdot 10^{6}$	$8.33 \cdot 10^{09}$	$4.65 \cdot 10^{09}$	-	$7.30 \cdot 10^{13}$	$3.59 \cdot 10^{4}$
Sn-126	$2.345 \cdot 10^{5}$	$4.47 \cdot 10^{10}$	$2.43 \cdot 10^{10}$	$1.51 \cdot 10^{06}$	$3.89 \cdot 10^{14}$	$6.90 \cdot 10^{3}$
I-129	$1.570 \cdot 10^{7}$	$2.44 \cdot 10^{09}$	$1.65 \cdot 10^{04}$	$5.31 \cdot 10^{06}$	$1.70 \cdot 10^{13}$	$2.02 \cdot 10^{4}$
Cs-135	$2.000 \cdot 10^{6}$	$2.45 \cdot 10^{10}$	$1.62 \cdot 10^{10}$	$7.11 \cdot 10^{07}$	$2.23 \cdot 10^{14}$	$3.37 \cdot 10^{4}$
Cs-137	$3.017 \cdot 10^{1}$	$8.60 \cdot 10^{15}$	$4.67 \cdot 10^{15}$	$1.51 \cdot 10^{13}$	$7.50 \cdot 10^{19}$	$1.71 \cdot 10^{5}$
Sm-151	$9.300 \cdot 10^{1}$	$2.00 \cdot 10^{13}$	$1.53 \cdot 10^{13}$	$6.00 \cdot 10^{10}$	$1.89 \cdot 10^{17}$	$1.33 \cdot 10^{3}$

Tab. 4.1b Radionuclide inventory (actinide elements)

Nuclide	Half life [a]	SF [Bq/can.]	HLW [Bq/can.]	ILW [Bq/can.]	Total [Bq]	Total [mol]
						Th-series
Pu-244	$8.000 \cdot 10^{7}$	$6.95 \cdot 10^{04}$	$1.12 \cdot 10^{02}$	-	$4.84 \cdot 10^{08}$	$2.93 \cdot 10^{0}$
Cm-244	$1.810 \cdot 10^{1}$	$3.46 \cdot 10^{14}$	$1.13 \cdot 10^{14}$	$9.51 \cdot 10^{10}$	$2.77 \cdot 10^{18}$	$3.79 \cdot 10^{3}$
Pu-240	$6.563 \cdot 10^{3}$	$3.83 \cdot 10^{13}$	$7.61 \cdot 10^{10}$	$5.20 \cdot 10^{10}$	$2.67 \cdot 10^{17}$	$1.33 \cdot 10^{5}$
U-236	$2.342 \cdot 10^{7}$	$1.91 \cdot 10^{10}$	$6.63 \cdot 10^{07}$	-	$1.33 \cdot 10^{14}$	$2.35 \cdot 10^{5}$
Th-232	$1.41 \cdot 10^{10}$	$2.10 \cdot 10^{00}$	$5.65 \cdot 10^{00}$	-	$3.28 \cdot 10^{04}$	$3.49 \cdot 10^{-2}$
U-232	$6.890 \cdot 10^{1}$	$1.24 \cdot 10^{09}$	$1.11 \cdot 10^{07}$	-	$8.65 \cdot 10^{12}$	$3.76 \cdot 10^{-3}$
						Np-series
Cm-245	$8.500 \cdot 10^{3}$	$2.72 \cdot 10^{10}$	$1.11 \cdot 10^{10}$	-	$2.25 \cdot 10^{14}$	$1.45 \cdot 10^{2}$
Pu-241	$1.435 \cdot 10^{1}$	$9.27 \cdot 10^{15}$	$1.27 \cdot 10^{13}$	$1.00 \cdot 10^{13}$	$6.47 \cdot 10^{19}$	$7.01 \cdot 10^{4}$
Am-241	$4.322 \cdot 10^{2}$	$1.03 \cdot 10^{13}$	$6.20 \cdot 10^{13}$	$3.51 \cdot 10^{10}$	$2.72 \cdot 10^{17}$	$8.89 \cdot 10^{3}$
Np-237	$2.144 \cdot 10^{6}$	$2.63 \cdot 10^{10}$	$1.66 \cdot 10^{10}$	$7.20 \cdot 10^{06}$	$2.37 \cdot 10^{14}$	$3.83 \cdot 10^{4}$
U-233	$1.592 \cdot 10^{5}$	$4.12 \cdot 10^{06}$	$1.83 \cdot 10^{04}$	-	$2.87 \cdot 10^{10}$	$3.46 \cdot 10^{-1}$
Th-229	$7.880 \cdot 10^{3}$	$1.27 \cdot 10^{04}$	$6.63 \cdot 10^{03}$	-	$9.08 \cdot 10^{08}$	$5.41 \cdot 10^{-4}$
						U-series
Cm-246	$4.730 \cdot 10^{3}$	$6.81 \cdot 10^{10}$	$2.27 \cdot 10^{10}$	-	$5.47 \cdot 10^{14}$	$1.96 \cdot 10^{2}$

Nuclide	Half life [a]	SF [Bq/can.]	HLW [Bq/can.]	ILW [Bq/can.]	Total [Bq]	Total [mol]
Pu-242	$3.750 \cdot 10^{5}$	$1.84 \cdot 10^{11}$	$3.08 \cdot 10^{08}$	$2.80 \cdot 10^{08}$	$1.29 \cdot 10^{15}$	$3.64 \cdot 10^{4}$
Am-242	$1.410 \cdot 10^{2}$	$3.06 \cdot 10^{11}$	$1.55 \cdot 10^{11}$	-	$2.63 \cdot 10^{15}$	$2.80 \cdot 10^{1}$
U-238	$4.468 \cdot 10^{9}$	$1.86 \cdot 10^{10}$	$6.67 \cdot 10^{07}$	-	$1.30 \cdot 10^{14}$	$4.37 \cdot 10^{7}$
Pu-238	$8.774 \cdot 10^{1}$	$2.61 \cdot 10^{14}$	$4.28 \cdot 10^{11}$	$4.71 \cdot 10^{11}$	$1.82 \cdot 10^{18}$	$1.21 \cdot 10^{4}$
U-234	$2.455 \cdot 10^{5}$	$4.97 \cdot 10^{10}$	$2.10 \cdot 10^{08}$	-	$3.46 \cdot 10^{14}$	$6.43 \cdot 10^{3}$
Th-230	$7.540 \cdot 10^{4}$	$9.61 \cdot 10^{05}$	$3.17 \cdot 10^{06}$	-	$1.69 \cdot 10^{10}$	$9.63 \cdot 10^{-2}$
Ra-226	$1.600 \cdot 10^{3}$	$1.27 \cdot 10^{03}$	$6.25 \cdot 10^{03}$	-	$2.90 \cdot 10^{07}$	$3.50 \cdot 10^{-6}$
						Ac-series
Am-243	$7.370 \cdot 10^{3}$	$2.13 \cdot 10^{12}$	$1.05 \cdot 10^{12}$	$3.51 \cdot 10^{08}$	$1.82 \cdot 10^{16}$	$1.02 \cdot 10^{4}$
Pu-239	$2.411 \cdot 10^{4}$	$2.10 \cdot 10^{13}$	$4.54 \cdot 10^{10}$	$3.00 \cdot 10^{10}$	$1.47 \cdot 10^{17}$	$2.67 \cdot 10^{5}$
U-235	$7.038 \cdot 10^{8}$	$7.77 \cdot 10^{08}$	$3.51 \cdot 10^{06}$	-	$5.42 \cdot 10^{12}$	$2.88 \cdot 10^{5}$
Pa-231	$3.276 \cdot 10^{4}$	$1.98 \cdot 10^{06}$	$1.22 \cdot 10^{06}$	-	$1.78 \cdot 10^{10}$	$4.40 \cdot 10^{-2}$

The strategy of the safety concept is the isolation of the emplaced waste by the tight and long-term stable salt rock formation. The waste canisters are not assumed to represent a long-term barrier.

The function of the engineered barriers is to reseal the disturbed salt rock formation after the construction of the repository. The main engineered barriers are the shaft seal and the drift seals. The drift seals are located between the central field and the access drifts. All further project relevant general input data related to the modelling of the near field are given in table 4.2.

Tab. 4.2 General data for the modelling of the near field

Parameter	Dimension	Value
Average rock density	kg/m^3	2 300
Average fluid density	kg/m^3	1 200
Depth of repository (= reference level)	m b. s.	870
Rock temperature (reference level)	K	310
Geothermal gradient	K/m	0.03
Rock pressure (reference level)	MPa	18
Hydrostatic pressure (reference level)	MPa	10
Reference convergence rate	1/a	0.01
Permeability of the shaft seal	m^2	10^{-18}
Permeability of the drift seals	m^2	10^{-15}
Lifetime of shaft seal	a	75
Permeability of the shaft seal (after expiration of lifetime)	m^2	10^{-14}
Initial plug porosity	-	0.3
Initial backfilling porosity	-	0.3

For the calculation of the indicators it is assumed that the initial permeability of the shaft seal is only valid for a period of 75 years. After this period the permeability increases by four orders of magnitude. The permeability of the drift seals is set to a con-

stant value of 10^{-15} m^2. This pessimistic parameter combination allows a brine inflow to the emplaced waste. As stated in the introductory section the probability of the scenario is not taken into account for the calculation of the indicators.

The failure of the canisters starts as soon as brine flows into a borehole with emplaced waste. For all canister types a uniformly distributed canister lifetime is assumed in the range between 0 and 10 years. A barrier effect of the canister or the cladding is not taken into account. The release from the waste matrix starts immediately after failure of the canister. Different mobilisation rates are used for the three types of waste. The corresponding mobilisation approaches for SF, HLW and ILW are discussed in /BUH 08/.

The mobilised radionuclides are dissolved in the available water volume of the borehole. The radionuclides may precipitate if they reach their solubility limits within this water volume. Conservative solubility limits (table 4.3) are used for the mobilisation process. Neither temporal change nor spatial differences in chemical conditions are taken into account. Sorption is not considered for the radionuclide transport in the repository.

Tab. 4.3 Solubility limits in the near field [mol/m^3]

Element	Solubility limits [mol/m^3]	Element	Solubility limits [mol/m^3]
C	$1.0 \cdot 10^{1}$	I	$5.0 \cdot 10^{3}$
Cl	$5.0 \cdot 10^{3}$	Cs	$5.0 \cdot 10^{3}$
Co	$5.0 \cdot 10^{3}$	Sm	$1.0 \cdot 10^{-1}$
Ni	$1.0 \cdot 10^{-1}$	Eu	$5.0 \cdot 10^{3}$
Se	$1.0 \cdot 10^{-1}$	Pb	$5.0 \cdot 10^{3}$
Rb	$5.0 \cdot 10^{3}$	Ra	$1.0 \cdot 10^{-3}$
Sr	$1.0 \cdot 10^{0}$	Th	$1.0 \cdot 10^{-3}$
Zr	$1.0 \cdot 10^{-1}$	Pa	$1.0 \cdot 10^{-3}$
Cd	$5.0 \cdot 10^{3}$	U	$1.0 \cdot 10^{-1}$
Nb	$1.0 \cdot 10^{-1}$	Np	$1.0 \cdot 10^{-2}$
Mo	$1.0 \cdot 10^{-1}$	Pu	$1.0 \cdot 10^{-3}$
Tc	$1.0 \cdot 10^{-1}$	Am	$1.0 \cdot 10^{-2}$
Pd	$1.0 \cdot 10^{-1}$	Cm	$1.0 \cdot 10^{-2}$
Sn	$1.0 \cdot 10^{-1}$		

For the further transport in the repository (the drifts and the central field) no solubility limits are applied. For the radionuclide transport outside the repository advection, dispersion and dilution (see table 4.4 for general data on the far field), sorption (table 4.5) and radioactive decay are taken into account. The parameter values for the aquifer are based on investigations of overlying rocks of salt domes in Northern Germany /BUE 85/. The geological formation along the migration pathway is modelled as a homogeneous medium wit a porosity of 0.2 and an average width of 820 m and a thick-

ness of 45 m /CAD 88/. With a pore velocity of about 6.5 m/a, the resulting natural groundwater flow is 48 000 m^3/a (table 4.4).

The application of the biosphere model is in compliance with German regulations /AVV 90/. It is assumed that the contaminated groundwater is used for irrigation, animal watering and drinking water. More information on this calculation, e. g. the applied dose conversion factors are given in section 4.1.2.1.

Tab. 4.4 General data for the modelling of the far field

Parameter	Dimension	Value
Total length (modelled area)	m	9 394
Cross sectional area (modelled area)	m^2	36 900
Natural groundwater flow	m^3/a	48 000
Dispersion length	m	65
Molecular diffusion coefficient	m^2/a	$3 \cdot 10^{-2}$
Porosity	-	0.2
Rock density	kg/m^3	2 500

Tab. 4.5 Sorption coefficients in the far field

Element	Sorption coefficient [m^3/kg]	Element	Sorption coefficient [m^3/kg]
C	$5.0 \cdot 10^{-3}$	Sm	1.0
Cl	0.0	Eu	1.0
Ni	$1.0 \cdot 10^{-2}$	Pb	$4.0 \cdot 10^{-2}$
Se	$3.0 \cdot 10^{-4}$	Po	1.0
Rb	$1.0 \cdot 10^{-3}$	Ra	$9.0 \cdot 10^{-4}$
Sr	$5.0 \cdot 10^{-4}$	Ac	$4.0 \cdot 10^{-2}$
Zr	$1.0 \cdot 10^{-1}$	Th	$3.0 \cdot 10^{-1}$
Nb	$1.0 \cdot 10^{-1}$	Pa	1.0
Mo	$1.0 \cdot 10^{-3}$	U	$2.0 \cdot 10^{-3}$
Tc	$7.0 \cdot 10^{-3}$	Np	$3.0 \cdot 10^{-2}$
Pd	$1.0 \cdot 10^{-2}$	Pu	1.0
Sn	$2.0 \cdot 10^{-1}$	Am	1.0
I	$5.0 \cdot 10^{-4}$	Cm	1.0
Cs	$1.0 \cdot 10^{-3}$		

4.1.2 Safety indicators

One important aspect is the development and testing of complementary safety indicators to dose and risk. These additional indicators are required to strengthen the robustness of the safety case by using multiple lines of evidence and to compensate the shortcomings of single indicators /NEA 04/.

For the contribution to WP 3.4 three additional indicators were identified that could contribute to a higher confidence in the safety statements given by a post-closure safety analysis. These indicators are

- the radiotoxicity concentration in biosphere water,
- the radiotoxicity flux from the geosphere and
- the contribution to the power density in ground water.

The complementary safety indicators “radiotoxicity concentration in biosphere water” and “radiotoxicity flux from the geosphere” are already discussed and applied for a granite formation in the SPIN project /BEC 03/. For rock salt and clay these indicators were intensively discussed in /WOL 09/. In contrast to these indicators the indicator “contribution to the power density in groundwater” is a new proposal suggested by /BAL 07/. Therefore, the main focus in this report is set to this indicator. The other indicators and their corresponding reference values are discussed in less detail here.

The determination of the reference values is based on an approach applied in /WOL 09/. According to this approach the determination is carried out in two steps: The first step is the determination of a natural background value. In a second step a safety margin to this natural background value is applied. That is why the reference value is set to about one third of the natural background value. The general strategy of this procedure is to keep the reference values comparatively low (in a reasonable range) in order to enhance the confidence in the safety statement given by the corresponding safety indicator.

All determined background values refer to the activity (concentration or flux) in the upper groundwater system. This system is the most important system regarding human health for assessing radionuclide releases from a repository in a deep geological formation. Furthermore the most detailed data base exists for this system.

4.1.2.1 Effective dose rate

The effective dose rate to exposed individuals is the main internationally accepted indicator for assessing the safety of a repository system and in many countries the regulatory authorities have established regulatory limits for this indicator. For example, in the German regulation the limit for the effective dose rate is 0.3 mSv/a. This limit was cho-

sen since it represents a small proportion relative to the natural background radiation doses. The average natural background radiation in Germany is in the range of 2 to 3 mSv/a. This radiation originates from cosmic radiation (0.3 to 0.5 mSv/a, depending on altitude), terrestrial radiation (0.4 mSv/a), inhalation (1.2 mSv/a, mainly from inhalation of radon) and ingestion (0.3 mSv/a). Since a release of radionuclides from a repository would mainly cause an exposition by ingestion, it is proposed here to consider only this exposition pathway and to use the average exposition via ingestion as background value.

With the proposed safety margin the suggested reference value for the effective dose rate is **0.1 mSv/a**.

For the conversion of the radionuclide activity in the upper aquifer to the effective dose rate the following exposition pathways are included (the dose conversion factors, table 4.6):

- consumption of contaminated drinking water,
- consumption of fish from contaminated ponds,
- consumption of plants irrigated with contaminated water,
- consumption of milk and meat from cattle, which were watered and fed with contaminated fodder and
- exposure due to habitation on the contaminated land.

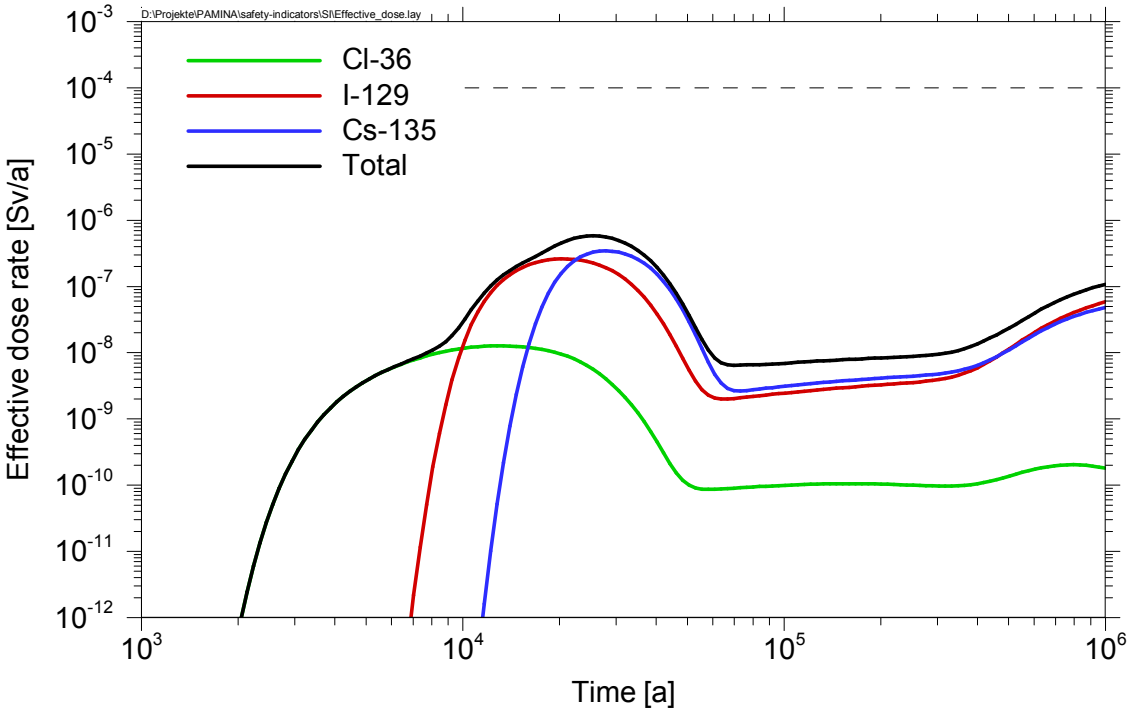

Fig. 4.2 The effective dose rate (the dashed line represents the reference value)

Tab. 4.6 Dose conversion factors for adults [(Sv/a)/(Bq/m^3)]

Nuclide	Dose conversion factor	Nuclide	Dose conversion factor
C-14	$4.6 \cdot 10^{-8}$	Am-241	$8.0 \cdot 10^{-7}$
Cl-36	$3.5 \cdot 10^{-8}$	Np-237	$4.7 \cdot 10^{-6}$
Co-60	$3.9 \cdot 10^{-6}$	U-233	$3.9 \cdot 10^{-6}$
Ni-59	$4.9 \cdot 10^{-9}$	Pa-233	$8.8 \cdot 10^{-9}$
Ni-63	$1.1 \cdot 10^{-9}$	Th-229	$1.7 \cdot 10^{-5}$
Se-79	$3.4 \cdot 10^{-7}$	Ra-225	$1.1 \cdot 10^{-7}$
Sr-90	$1.8 \cdot 10^{-7}$	Ac-225	$3.7 \cdot 10^{-8}$
Zr-93	$3.7 \cdot 10^{-8}$	Pu-242	$9.4 \cdot 10^{-7}$
Nb-94	$3.1 \cdot 10^{-6}$	Am-242	$7.6 \cdot 10^{-7}$
Mo-93	$3.2 \cdot 10^{-7}$	Pu-238	$7.5 \cdot 10^{-7}$
Tc-99	$8.8 \cdot 10^{-9}$	U-238	$7.1 \cdot 10^{-7}$
Sn-126	$1.6 \cdot 10^{-5}$	Th-234	$4.8 \cdot 10^{-9}$
I-129	$5.6 \cdot 10^{-7}$	U-234	$1.4 \cdot 10^{-6}$
Cs-135	$5.7 \cdot 10^{-8}$	Th-230	$3.7 \cdot 10^{-5}$
Cs-137	$9.5 \cdot 10^{-7}$	Ra-226	$3.0 \cdot 10^{-5}$
Sm-151	$3.2 \cdot 10^{-10}$	Pb-210	$2.3 \cdot 10^{-6}$
Cm-244	$3.8 \cdot 10^{-7}$	Po-210	$4.9 \cdot 10^{-6}$
Pu-240	$9.6 \cdot 10^{-7}$	Am-243	$2.0 \cdot 10^{-6}$
U-236	$5.6 \cdot 10^{-7}$	Pu-239	$9.8 \cdot 10^{-7}$
Th-232	$1.1 \cdot 10^{-4}$	U-235	$3.3 \cdot 10^{-6}$
Ra-228	$2.4 \cdot 10^{-6}$	Pa-231	$4.0 \cdot 10^{-5}$
U-232	$5.4 \cdot 10^{-6}$	Ac-227	$1.0 \cdot 10^{-5}$
Th-228	$1.3 \cdot 10^{-6}$	Th-227	$1.9 \cdot 10^{-8}$
Cm-245	$1.4 \cdot 10^{-6}$	Ra-223	$1.1 \cdot 10^{-7}$
Pu-241	$1.8 \cdot 10^{-8}$		

Figure 4.2 illustrates the calculated effective dose rate for the set of parameters described in section 4.1.1. The maximum value of the calculated effective dose rate is $5.8 \cdot 10^{-7}$ Sv/a at 25 000 years. The maximum is dominated by I-129 and Cs-135, at early times by Cl-36. Cl-36 dominates at early times since it is not sorbed at all in the overlying rock (see table 4.5). In general, the radionuclides that contribute essentially to the dose rate are characterised by a high solubility and a weak sorption in the overlying rock.

In this calculation the maximum effective dose rate is about two orders of magnitude lower than the proposed reference value providing a high margin of safety for the given parameter combination.

4.1.2.2 Radiotoxicity concentration in biosphere water

For the derivation of the reference value for the radiotoxicity in biosphere water only radionuclide concentrations in drinking water are evaluated. These values are used since it can be assumed that observed concentrations in drinking water are harmless for human health. Thus characteristic drinking water qualities in Germany provide a safe reference value for the radiotoxicity concentration in biosphere water. Considering characteristic mean values of radionuclide concentrations in drinking water published by the Federal Environment Ministry /BMU 03/ the resulting background value for the radiotoxicity concentration in biosphere water is $7.7 \cdot 10^{-6}$ Sv/m^3 (table 4.7).

Tab. 4.7 Ingestion dose coefficients /ICRP 98/, activity and radiotoxicity concentrations of drinking water in Germany /BMU 03/

Nuclide	Ingestion dose coefficient [Sv/Bq]	Activity concentration [Bq/m^3]	Radiotoxicity concentration [Sv/m^3]
U-238	$4.50 \cdot 10^{-8}$	5.0	$2.25 \cdot 10^{-7}$
U-234	$4.90 \cdot 10^{-8}$	6.0	$2.94 \cdot 10^{-7}$
Ra-226	$2.80 \cdot 10^{-7}$	5.0	$1.40 \cdot 10^{-6}$
Rn-222	$3.50 \cdot 10^{-10}$	5 900	$2.07 \cdot 10^{-6}$
Pb-210	$6.90 \cdot 10^{-7}$	1.5	$1.04 \cdot 10^{-6}$
Po-210	$1.20 \cdot 10^{-6}$	0.5	$6.00 \cdot 10^{-7}$
Th-232	$2.30 \cdot 10^{-7}$	0.1	$2.30 \cdot 10^{-8}$
Ra-228	$6.90 \cdot 10^{-7}$	3.0	$2.07 \cdot 10^{-6}$
Th-228	$7.20 \cdot 10^{-8}$	0.2	$1.44 \cdot 10^{-8}$
U-235	$4.70 \cdot 10^{-8}$	0.3	$1.41 \cdot 10^{-8}$
Total			$7.74 \cdot 10^{-6}$

With the proposed safety margin the suggested reference value for the radiotoxicity concentration in biosphere water is **$2 \cdot 10^{-6}$ Sv/m^3**.

The used ingestion dose coefficients for converting the activity concentrations to radiotoxicity concentrations are given in table 3.3. A plus sign after the radionuclide name indicates that the dose coefficient for this nuclide includes the dose coefficient for all daughter nuclides up to the next one given in the table.

Tab. 4.8 Dose coefficients for ingestion in [Sv/Bq]

Nuclide	Ingestion dose coefficient	Nuclide	Ingestion dose coefficient
C-14	$5.80 \cdot 10^{-10}$	Am-241	$2.00 \cdot 10^{-7}$
Co-60	$3.40 \cdot 10^{-9}$	Np-237	$1.10 \cdot 10^{-7}$
Ni-59	$6.30 \cdot 10^{-11}$	U-233	$5.10 \cdot 10^{-8}$
Ni-63	$1.50 \cdot 10^{-10}$	Pa-233	$8.70 \cdot 10^{-10}$
Se-79	$2.90 \cdot 10^{-9}$	Th-229	$4.90 \cdot 10^{-7}$
Sr-90 +	$3.07 \cdot 10^{-8}$	Ra-225	$9.90 \cdot 10^{-8}$
Zr-93 +	$1.22 \cdot 10^{-9}$	Ac-225 +	$2.43 \cdot 10^{-8}$
Nb-94	$1.70 \cdot 10^{-9}$	Pu-242	$2.40 \cdot 10^{-7}$
Mo-93 +	$3.22 \cdot 10^{-9}$	Am-242m +	$1.90 \cdot 10^{-7}$
Tc-99	$6.40 \cdot 10^{-10}$	Pu-238	$2.30 \cdot 10^{-7}$
Sn-126 +	$5.07 \cdot 10^{-9}$	U-238	$4.50 \cdot 10^{-8}$
I-129	$1.10 \cdot 10^{-7}$	Th-234 +	$3.91 \cdot 10^{-9}$
Cs-135	$2.00 \cdot 10^{-9}$	U-234	$4.90 \cdot 10^{-8}$
Cs-137	$1.30 \cdot 10^{-8}$	Th-230	$2.10 \cdot 10^{-7}$
Sm-151	$9.80 \cdot 10^{-11}$	Ra-226 +	$2.80 \cdot 10^{-7}$
Cm-244	$1.20 \cdot 10^{-7}$	Pb-210 +	$6.91 \cdot 10^{-7}$
Pu-240	$2.50 \cdot 10^{-7}$	Po-210	$1.20 \cdot 10^{-6}$
U-236	$4.70 \cdot 10^{-8}$	Am-243 +	$2.01 \cdot 10^{-7}$
U-232	$3.30 \cdot 10^{-7}$	Pu-239	$2.50 \cdot 10^{-7}$
Th-232	$2.30 \cdot 10^{-7}$	U-235 +	$4.73 \cdot 10^{-8}$
Ra-228 +	$6.90 \cdot 10^{-7}$	Pa-231	$7.10 \cdot 10^{-7}$
Th-228 +	$1.43 \cdot 10^{-7}$	Ac-227	$1.10 \cdot 10^{-6}$
Cm-245	$2.10 \cdot 10^{-7}$	Th-227	$8.80 \cdot 10^{-9}$
Pu-241	$4.80 \cdot 10^{-9}$	Ra-223 +	$1.00 \cdot 10^{-7}$

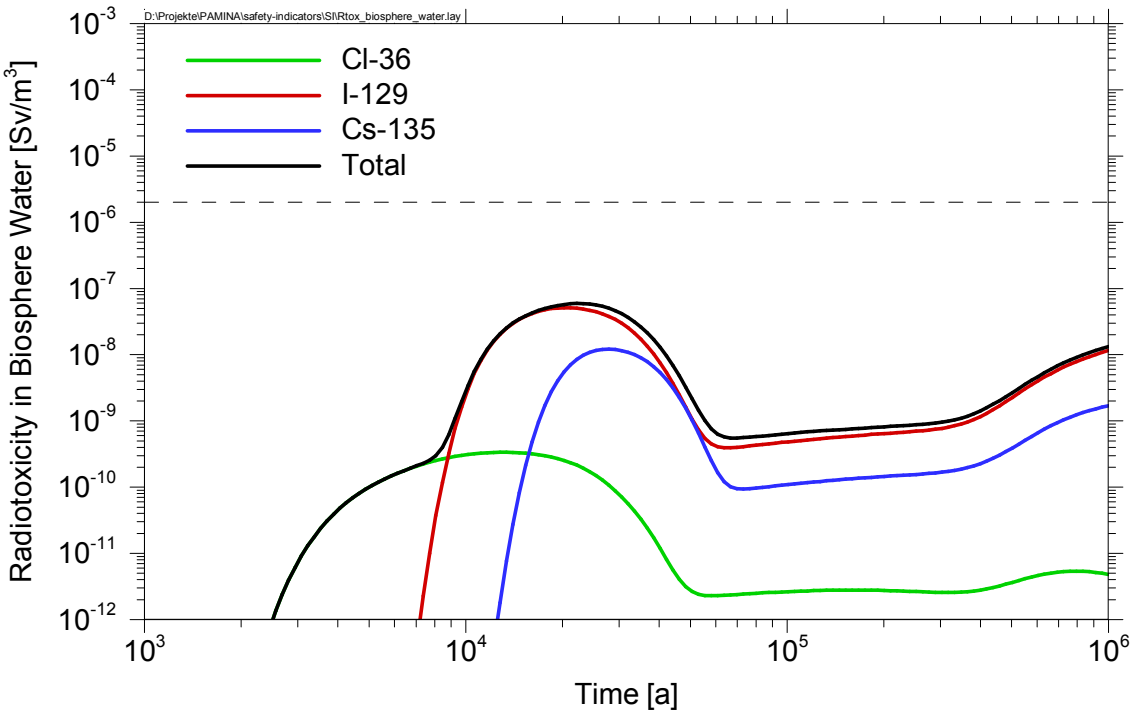

Fig. 4.3 Radiotoxicity concentration in biosphere water (the dashed line represents the reference value)

The calculated radiotoxicity concentration in biosphere water (figure 4.3) shows a similar progression with the same relevant radionuclides as in the case of the calculated effective dose rate. Main difference is the more dominant role of I-129 compared to Cs-135 caused by the corresponding relations of ingestion dose coefficient to dose conversion factor: For I-129 this relation is 0.196, for C-135 it is 0.035 (table 4.6 and 4.8).

The maximum calculated radiotoxicity concentration in biosphere water is $5.9 \cdot 10^{-8}$ Sv/m^3 at 23 000 years and is more than one order of magnitude lower than the proposed reference value.

4.1.2.3 Power density in groundwater

The indicator “contribution to the power density in groundwater” is physically unique and independent of any specific biological species. It is an aggregation over all radionuclides and can be seen as a yardstick for the impact on biota in general. But since the radiological consequences of the radiation can not be assessed by this indicator, it has only a limited relevance for safety. Nevertheless, the information given by this indicator can be very useful as an additional safety argument in a safety case.

Starting point for the calculation of this safety indicator is the calculated activity concentration in the upper aquifer system. Actually, it can be the activity concentration in any subsystem of the repository system, but it has to be adopted to the system used for the determination of the reference value. In /BAL 07/ it was proposed to use the power density in the pore water **and** in the soil matrix in the deeper aquifer system. But so far no reference value has been derived for such a system in rock salt. Measuring the necessary data for the proposed system is quite difficult and out of the scope of the project. Therefore the upper groundwater system was used to compare naturally existing power densities to power densities released from a repository system. The used subsystem is the upper groundwater system **without** considering the power density coming from radionuclides in the soil matrix.

For every considered radionuclide the decay energy, i. e. the total disintegration energy of one individual decay process (unit [MeV]), must be determined (see annex in section 0). The sources for the applied decay energy are /WEA 86/ and /FIR 99/.

The calculation of the power density is carried out with a simple weighting scheme by multiplying the activity concentration of every radionuclide [Bq/m^3] with its decay energy. This operation yields a power density p (power per volume, [MeV/(s·m^3)])

$$p = \sum_{\text{all nuclides}\ n} c_n E_n \tag{4.1}$$

with the activity concentration c_n [Bq/m^3] of radionuclide n in groundwater and the corresponding decay energies E_n.

It is, of course, possible to determine the power density in groundwater contributed by a single radionuclide

$$p_i = c_i \cdot E_i \tag{4.2}$$

In the annex all considered radionuclides and their decay energies are listed. In order to limit the number of radionuclides in the calculations only nuclides with half-lives > 1 a were directly calculated. For the calculation of the power density the decay energies of the short-lived disintegration processes are added to the decay energies of their mother nuclides.

For the activation and fission products the following ‘decay series’ were considered

- Sr-90 → Y-90 → Zr-90 (stable)
- Zr-93 → Nb-93m → Nb-93 (stable)
- Mo-93 → Nb-93m → Nb-93 (stable)
- Sn-126 → Sb-126m (14%) → Sb-126 → Te-126 (stable)
- Sn-126 → Sb-126 (86%) → Te-126 (stable)
- Cs-137 → Ba-137m → Ba-137 (stable)

Determination of a reference value

The background value for the repository system used by GRS is determined for the groundwater in the upper aquifer for the area at Gorleben, since a lot of data from an extensive drilling, exploration and monitoring programme of the Gorleben salt dome are available.

Concentrations for uranium and thorium are available from different wells of the upper aquifer. The concentrations of all other radionuclides are calculated from the concentration of the mother nuclides of the three natural decay chains U-238, U-235 and Th-232. It is assumed that all radionuclides in a decay chain are in secular equilibrium, i. e. the total activity concentration of each radionuclide in the decay chain corresponds to that of the mother nuclide.

The measured concentrations represent the mobile fraction of the total activity concentration. The mobile fraction of each radionuclide is determined by its sorption properties. These are different for the different elements. The total concentration of all radionuclides in a single decay chain is calculated as the product of the concentration of the respective mother nuclide in the groundwater $c_{l,m}$. and the retardation factor of the mother nuclide $R_{f,m}$. The mobile concentration of radionuclide *i* is then derived from

$$c_{l,i} = \frac{c_{l,m} \cdot R_{f,m}}{R_{f,i}} \tag{4.3}$$

with the retardation factor

$$R_f = 1 + \frac{(1-n)}{n} \rho_s K_d \,, \tag{4.4}$$

the porosity n, the rock density ρ_s, and the element specific distribution coefficient K_d. The mother nuclide is denoted by the index m and the respective radionuclide from the same decay chain with index i.

The concentration of each radionuclide in the groundwater is determined by the ratio of the retardation factors of the mother nuclide and the respective radionuclide.

The mean groundwater concentrations for uranium and thorium are derived from data of 14 and 19 samples, respectively, which are available for the near surface aquifer in the Gorleben area. The resulting mean concentrations are 0.72 nmol/l ($1.7 \cdot 10^{-7}$ kg/m^3) for uranium and 1.43 nmol/l ($3.3 \cdot 10^{-7}$ kg/m^3) for thorium. The activity concentration of the three radionuclides in the groundwater is calculated with nuclide-specific activity-to-mass conversion factors taking into account the natural abundance of the uranium isotopes. The resulting average activity concentrations are listed in table 4.9.

Tab. 4.9 Mother isotopes of the three natural decay chains and their average concentration in the groundwater in the near-surface aquifer at Gorleben site

Radionuclide	Half-life [a]	Natural abundance in element [wt.%]	Conversion factor [Bq/kg]	Average conc. [Bq/m^3]
U-238	$4.468 \cdot 10^9$	99.2742	$1.245 \cdot 10^7$	2.12
U-235	$7.038 \cdot 10^8$	0.7204	$8.000 \cdot 10^7$	$9.88 \cdot 10^{-2}$
Th-232	$1.405 \cdot 10^{10}$	100.00	$4.065 \cdot 10^6$	1.35

The R_f-values for each radionuclide are taken from /SUT 98/. For radon no sorption data were used in this approach. Since all radon isotopes are volatile the assumption that radon is in secular equilibrium with its mother nuclides is probably not correct. In spite of its importance for the natural radioactivity it is neglected here. The advantage of this procedure is the provided low reference value. A low reference value enhances the confidence in the safety statement given by the corresponding safety indicator. For the same reason other natural radionuclides, such as K-40, are not considered either.

The total natural power density in groundwater is calculated as the sum of the power densities of all three decay chains. The total natural power density in groundwater is then 78.3 MeV/(s·m^3).

The results show that the highest contribution to the natural radiotoxicity flux stems from the thorium decay chain (table 4.11). The activity concentration of this decay chain is dominated by the two radium isotopes Ra-224 and Ra-228. The reason for these concentrations is the high ratio of the retardation factors (i. e. K_d-values) applied for thorium and radium. The result is quite sensitive to this ratio. The problem is that the determination of K_d-values is very difficult and therefore very uncertain.

In order to base the reference value on a second value a second consideration is used here, in which sorption is neglected. In the second approach a secular equilibrium only for the activity concentrations in the mobile phase is considered. In this case the total power densities of each decay chain can be used to calculate a natural power density in groundwater by multiplication with the observed concentrations for the three mother nuclides. The resulting natural power density in groundwater is 156.4 MeV/(s·m^3). The results for both approaches are summarised in table 4.13. Both approaches give the same order of magnitude for the natural background value. Here, the lower value is chosen.

With the proposed safety margin the suggested reference value for the radiotoxicity flux from the geosphere is **25 MeV/(s·m^3)**.

Tab. 4.10 Calculated activity concentrations and power densities of the uranium series

Nuclide	Decay Energy [MeV]	R_f [-]	Activity conc. [Bq/m^3]	Power density [MeV/(s·m^3)]
U-238	4.270	$2.1 \cdot 10^1$	2.12	9.05
Th-234	0.273	$2.0 \cdot 10^3$	0.022	0.006
Pa-234	2.197	$6.0 \cdot 10^3$	0.007	0.016
U-234	4.856	$2.1 \cdot 10^1$	2.12	10.30
Th-230	4.770	$2.0 \cdot 10^3$	0.022	0.11
Ra-226	4.871	$4.0 \cdot 10^2$	0.111	0.54
Rn-222	(5.590)	n/a		
Po-218	6.115	$1.2 \cdot 10^4$	0.0037	0.00043
Pb-214	1.023	$1.0 \cdot 10^4$	0.0045	0.0046
Bi-214	3.272	$1.7 \cdot 10^4$	0.0026	0.0086
Po-214	7.833	$1.2 \cdot 10^4$	0.0037	0.0029
Pb-210	0.064	$1.0 \cdot 10^4$	0.0045	0.00028
Bi-210	1.163	$1.7 \cdot 10^4$	0.0026	0.00043
Po-210	5.407	$1.2 \cdot 10^4$	0.0037	0.020
Total	39.114		4.43	20.08

Tab. 4.11 Calculated activity concentrations and power densities of the thorium series

Nuclide	Decay Energy [MeV]	R_f [-]	Activity conc. [Bq/m^3]	Power density [MeV/(s·m^3)]
Th-232	4.081	$2.0 \cdot 10^3$	1.35	5.38
Ra-228	0.046	$4.0 \cdot 10^2$	6.68	0.31
Ac-228	2.127	$3.0 \cdot 10^3$	0.89	1.90
Th-228	5.520	$2.0 \cdot 10^3$	1.35	7.39
Ra-224	5.789	$1.0 \cdot 10^1$	6.68	38.69
Rn-220	(6.405)	n/a		
Po-216	6.906	$1.2 \cdot 10^4$	0.22	1.54
Pb-212	0.574	$1.0 \cdot 10^4$	0.27	0.15
Bi-212	2.254	$1.7 \cdot 10^4$	0.16	0.36
Po-212	8.954	$1.2 \cdot 10^4$	0.41	2.00
Total	36.188		17.81	57.72

Tab. 4.12 Calculated activity concentrations and power densities of the actinium series

Nuclide	Decay Energy [MeV]	Rf [-]	Activity conc. [Bq/m^3]	Power density [MeV/(s·m^3)]
U-235	4.679	$2.1 \cdot 10^1$	0.10	0.462
Th-231	0.389	$2.0 \cdot 10^3$	0.0011	0.00040
Pa-231	5.149	$6.0 \cdot 10^3$	0.00035	0.0018
Ac-227	0.045	$3.0 \cdot 10^1$	0.00069	0.000031
Th-227	6.146	$2.0 \cdot 10^3$	0.0010	0.00063
Ra-223	5.979	$4.0 \cdot 10^2$	0.0052	0.031
Rn-219	(6.946)	n/a		
Po-215	7.526	$1.0 \cdot 10^4$	0.00017	0.0013
Pb-211	1.373	$4.0 \cdot 10^2$	0.00021	0.00029
Bi-211	6.750	n/a	0.00012	0.00082
Tl-207	1.423	$1.0 \cdot 10^4$	0.00021	0.00030
Total	39.459		4.54	0.51

Tab. 4.13 Reference values determined by different sorption approaches

Approach	Applied sorption coefficients	Power Density [MeV/(s·m^3)]
1	No sorption	135.3
2	K_d-values by /BUH 08a/	78.3

Calculation of the safety indicator

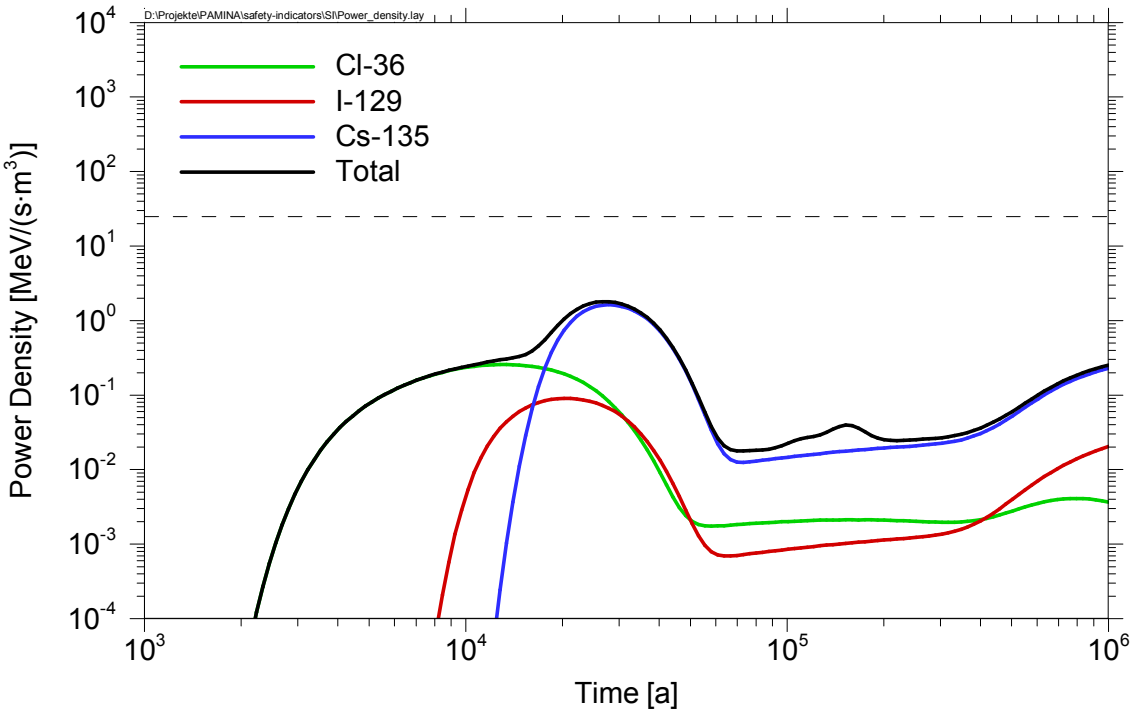

Fig. 4.4 Contribution of the released radionuclides to the power density in groundwater (the dashed line represents the reference value)

Figure 4.4 shows the temporal evolution of the power density caused by radionuclides released from the repository. The dominating radionuclides are Cl-36 at early times (up to 10 000 years) and afterwards Cs-135. A small peak at 150 000 years is caused by Ni-59 and Tc-99. Their relatively high decay energies amplify this peak compared to calculations with ingestion dose coefficients or dose conversion factors. I-129 does not play such an important role due to its relatively low decay energy.

The maximum value of the calculated power density is 1.8 MeV/(s·m^3) at 26 000 years and more than one order of magnitude lower than the proposed reference value.

4.1.2.4 Radiotoxicity flux to/from the geosphere

The derivation of the reference value for the safety indicator radiotoxicity flux from the geosphere is more problematic than the previously described approaches. A reference value for this indicator is usually site-specific since it is based on the natural groundwater flux, which cannot be determined on very large scales. But even on local scales the

determination of a natural groundwater flux in the vicinity of a repository is difficult and implies a lot of uncertainties.

For this WP the reference value is determined for the area at Gorleben, since a lot of data from an extensive drilling, exploration and monitoring programme for the overlying rock of the Gorleben salt dome are available. The basic assumption is that the corresponding natural background value is represented by the product of the radionuclide concentrations and the groundwater flow in the near surface aquifer.

For the natural groundwater flow in the upper aquifer the parameters used in the model for calculating the indicators are applied: The overlying rock formation along the migration pathway is modelled as homogeneous sandy aquifer with an average width of 820 m, a thickness of 45 m, and a porosity of 0.2. With a pore velocity of about 6.5 m/a, the resulting natural groundwater flow amounts to 48 000 m^3/a (see section 4.1.1).

The approach for calculating the activity concentrations described in section 4.1.2 is also used for this indicator. Thus the activity concentrations in the groundwater system are the same as in tables 4.10 to 4.12. For this indicator these concentrations are multiplied with the ingestion dose coefficients in table 4.8.

The resulting total radiotoxicity concentration is $6.8 \cdot 10^{-6}$ Sv/m^3 and the corresponding flux is about 0.3 Sv/a /WOL 09/. With the proposed safety margin the suggested reference value for the radiotoxicity flux from the geosphere is **0.1 Sv/a**.

According to the section heading two indicators are meant here: One for the radiotoxicity flux from the repository to the geosphere and one from the geosphere to the biosphere. The flux from the repository to the geosphere does not take credit of the aquifer system above the salt dome. For a fully consistent use of the term safety indicator, the flux from the repository to the geosphere should be used with a reference value referring to the activity concentration in the deeper aquifer system above the salt dome. But for this investigation it is assumed, that the fluxes/concentrations in the whole aquifer system are constant.

The differences between both indicators show that the aquifer causes a temporal shift of a few thousand years, but the maximum flux is hardly influenced by it (figure 4.5). The maximum calculated radiotoxicity flux from the repository to the geosphere is $5.9 \cdot 10^{-3}$ Sv/m^3 at 9 000 years. This flux is again dominated by I-129, Cs-135, and Cl-36

but also Nb-94 and Mo-93 contribute significantly to the overall radiotoxicity flux. Due to their relatively short half lives the latter two radionuclides only play an important role at early times. The maximum calculated radiotoxicity flux from the geosphere to the biosphere is $2.8 \cdot 10^{-3}$ Sv/m^3 at 22 000 years. This flux is dominated by I-129, Cs-135, and Cl-36 at early times. The overlying rock causes a temporal shift of more than 10 000 years of the maximum radiotoxicity flux. But due to the long half lives of the dominant radionuclides the maximum value is still in same order of magnitude.

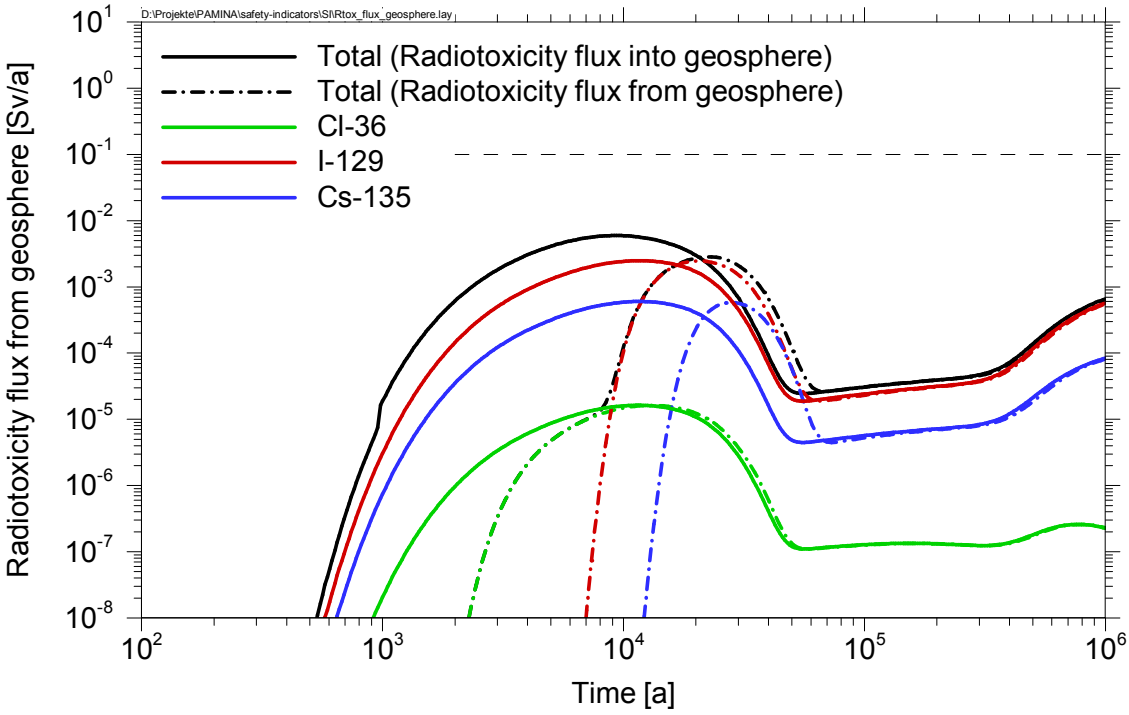

Fig. 4.5 Radiotoxicity flux to/from the geosphere. The horizontal dashed line represents the reference value

4.1.2.5 Normalised safety indicators

Finally, all calculated safety indicators are compared. They are normalised by their corresponding reference value (figure 4.6). In general the temporal evolution of the safety indicators is quite similar. The only exception is radiotoxicity flux from the repository to the geosphere, because this indicator refers to a deeper part of the repository system and is based on fluxes from the repository. Here other radionuclides can play an important role than in the upper groundwater system.

The effective dose rate and the radiotoxicity concentration in biosphere water only differ in the factor each radionuclide is multiplied with (the dose conversion factor in case of the effective dose and the ingestion dose coefficient in case of radiotoxicity). Since only a few radionuclides such as I-129, Cs-135, and Cl-36 dominate the release of radionuclides to the biosphere, the curves' shape is quite similar.

Although the reference values are derived independently, the normalised radiotoxicity concentration in biosphere water and the normalised radiotoxicity flux from the geosphere to the biosphere (blue dash and dot line) are almost the identical: If the radiotoxicity flux from the geosphere is divided by the natural groundwater flow the reference value for the radiotoxicity concentration in the geosphere is $2.1 \cdot 10^{-6}$ Sv/m^3 (0.1 Sv/a divided by 48 000 m^3). The reference value for the radiotoxicity concentration in drinking water is $2.0 \cdot 10^{-6}$ Sv/m^3. Since the natural groundwater flux in the calculation is constant, the resulting indicators give almost the same safety margin to the reference value.

The normalised power density in groundwater differs slightly from this overall scheme since Cl-36, the dominating radionuclide at early times is strongly weighted by the power densities compared with the values of I-129 and Cs-135.

For the given parameter set (section 4.1.1) all indicators remain below their reference value for the calculated period of one million years. The normalised indicators give safety margins between one order of magnitude (radiotoxicity flux into geosphere and power density in upper groundwater) and more than two orders of magnitude (effective dose rate).

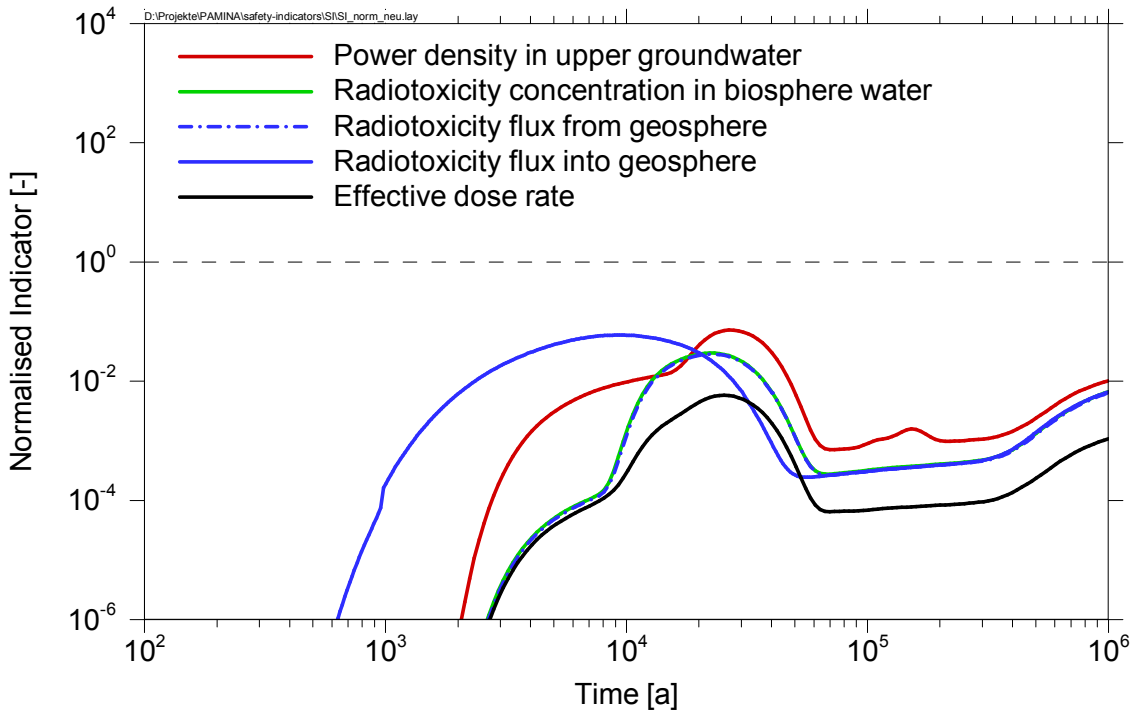

Fig. 4.6 Comparison of safety indicators calculated in WP3.4 (the dashed line represents the reference values)

4.1.2.6 Robustness of safety indicators in case of radionuclide release

As stated in the beginning the calculated indicators are results of a certain set of parameters (section 4.1.1). The chosen parameter values do not state anything about their probability. They were chosen in order to enable a release of radionuclides for the calculation and testing of the discussed indicators.

In general the results of a performance assessment of repository in rock salt differ from the results in other host rock formations. They often have a dual nature regarding the release of radionuclides: A large part of the parameter combinations yield zero emissions and only a few realisations – often with very pessimistic combinations – result in a radionuclide release at all. Some of these releases can be very high and yield expositions in the range of natural background values or regulatory limits.

This behaviour sometimes makes it difficult to describe the results with statistical measures or with sensitivity parameters. Very often only release scenarios are analysed to avoid these problems. But this leads to biased view of the possible radionuclide releases from a repository in rock salt.

Before one possible solution to this problem is introduced in the next chapter by using the concept of risk, this section investigates the robustness of safety indicators only considering realisations with a radionuclide release by applying probabilistic calculations. In this context robustness means the capability of coping well with parameter variations. It does not mean the robustness of the computer code but the robustness of the results.

Tab. 4.14 Parameter variations for the stochastic modelling

Parameter	Distribution	Dimension	Lower Bound	Upper Bound
Permeability of the shaft seal	log uniform	m^2	$5 \cdot 10^{-17}$	$1 \cdot 10^{-14}$
Permeability of the drift seals	log uniform	m^2	$5 \cdot 10^{-17}$	$1 \cdot 10^{-14}$
Lifetime of seals	uniform	a	0	100
Lifetime of waste containers	uniform	a	0	500
Reference convergence rate	log uniform	1/a	$5 \cdot 10^{-3}$	$5 \cdot 10^{-1}$
Solubility limits	log uniform	mol/m^3	element-specific	
Sorption coefficients	log uniform	m^3/kg	element-specific	
Natural groundwater flow	uniform	m^3/a	10^4	10^5

Exemplarily, the robustness of the effective dose rate is analysed with two Monte-Carlo (MC) simulations with different seeds. For these MC-simulations the parameters listed in table 4.14 have been varied. The parameters were chosen since they proved to have significant influence on model results in recent investigations, e. g. /BUH 08/. The lower and upper bound represent still pessimistic assumptions, especially the lower bound of the permeability of the seals.

The number of release realisations in both MC-simulations is 54 and 64, respectively. That means for the given parameter ranges about 1.5 % of the realisations yield a release of radionuclides. To demonstrate the robustness of the effective dose rate figures 3.9 and 3.10 illustrate the results of the realisations with a radionuclide release by

- the realisation with the maximum effective dose rate,
- the realisation with the minimum effective dose rate,
- the time evolution of the maximum in all realisations,
- the time evolution of the minimum in all realisations and
- the mean value of the 54 (64) realisations with a radionuclide release.

Additionally, in both figures the deterministic simulation for the effective dose rate (section 4.1.2.1) is added. Although the parameters of the deterministic run are not all in the boundaries of the probabilistic parameter ranges, the results fit in the overall range of the probabilistic runs.

In figures 4.7 and 4.8 it can be seen that the realisation with the maximum release yields effective dose rates that are about as high as the reference value. The mean value of all release realisations is nearly constant over time at about one order of magnitude lower than the reference value. The progression of the maximum and minimum release realisation reveals the large range the effective dose rate is calculated depending on the selected parameter. The minimum range is about four orders of magnitude, whereas the maximum range is more than six orders of magnitude at 5 000 to 10 000 years. For an assessment of this range a comparison with other indicators and other repositories is necessary. Such a comparison was not planned in this report, but should be carried out in future investigations.

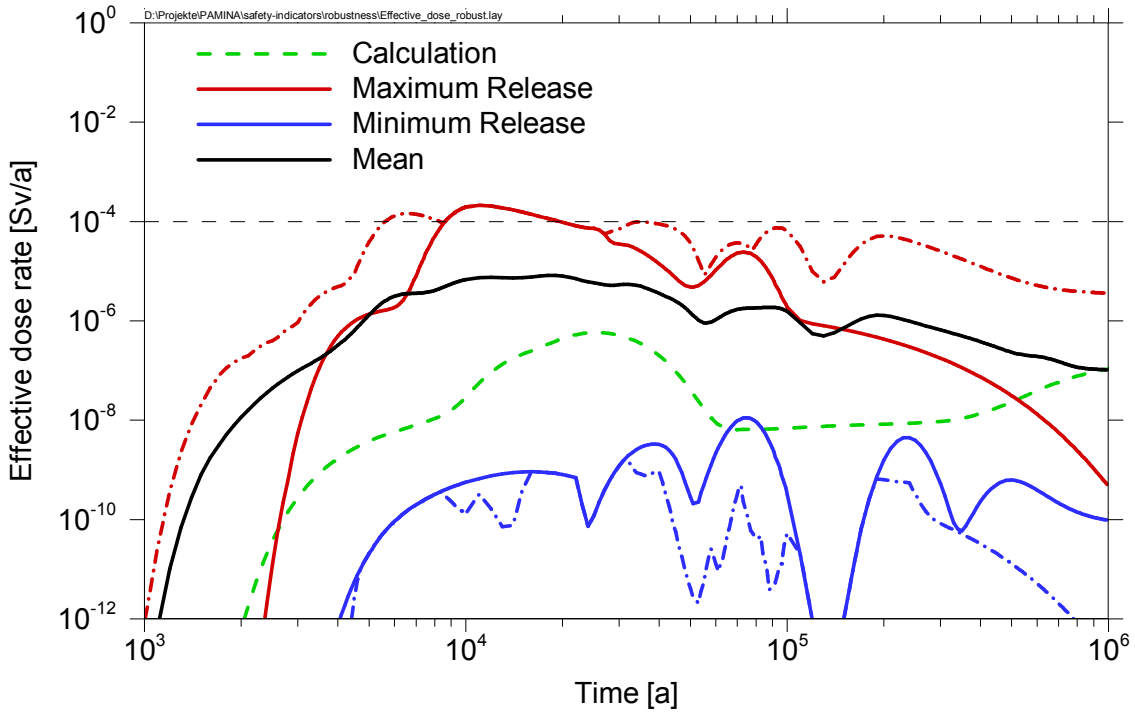

Fig. 4.7 Results of the realisation with a radionuclide release (MC-1) (dash and dot lines represent the maximum (red) and minimum (blue) value at each time step)

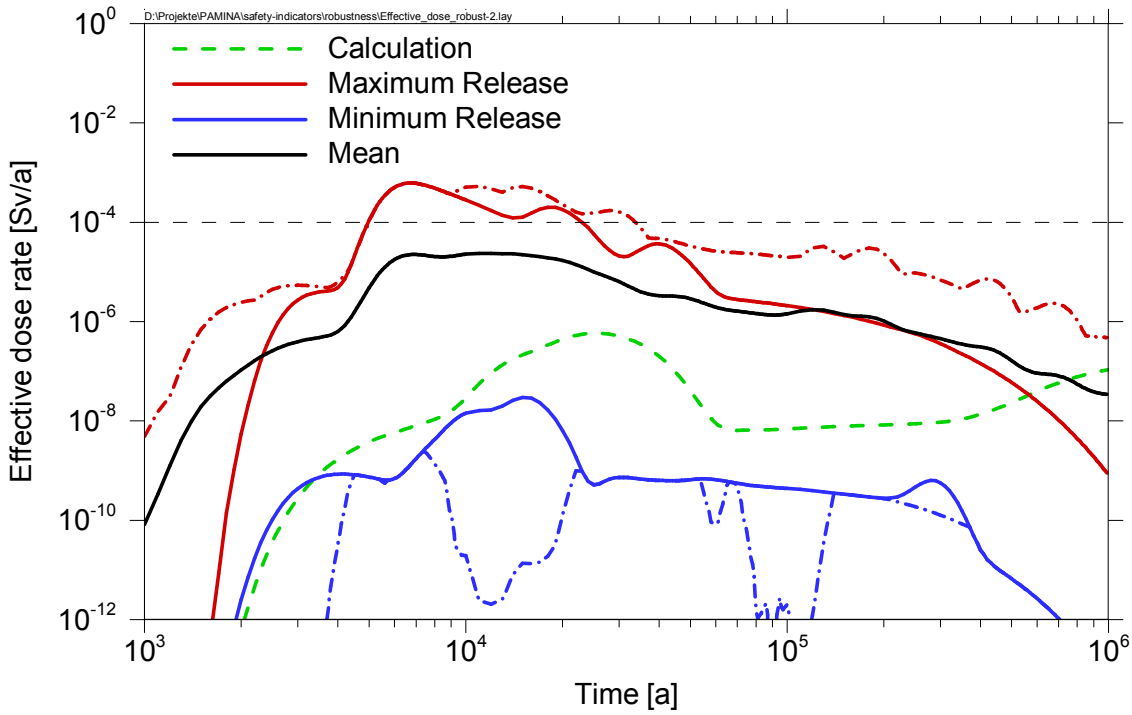

Fig. 4.8 Results of the realisation with a radionuclide release (MC-2) (dash and dot lines represent the maximum (red) and minimum (blue) value at each time step)

4.1.3 Indicators based on risk

The uncertainties associated with the evolution of the disposal system must be appropriately considered. One important tool of managing and communicating these uncertainties is the calculation of the risk emanating from a repository. Risk in general means the probability that a specified undesirable event will occur in a specified period or as a result of a specified situation /HSE 88/. With this general definition, it is obvious, that risk is a possible way taking into account scenario probabilities. Furthermore, the concept of risk will help to calculate single indicators that consider release and zero emission scenarios.

For a quantitative analysis it has to be more clearly defined, what risk means. The general statistical-mathematical formulation defines risk (R) as a combination (the product) of the probability of the occurrence of an adverse event for a defined time frame and a measure of the consequences of this event.

To fulfil the general definition every quantitative description of risk must involve a triple of information: A set of conditions (the scenario S), a probability of the scenario p and

the consequences of the scenario *C* /KAP 81/. The consequence must be a calculable measure, which can itself serve as a safety indicator. Any of the indicators mentioned in the previous chapter could be used, but it seems most sensible to consider the safety aspect “human health” and to calculate the risk on the basis of doses.

The dose risk R_D resulting from a number of possible scenarios S_i with the probabilities p_i can be calculated as

$$R_D = \sum_{S_i} p_i C_i \,, \tag{4.5}$$

where C_i is the dose rate resulting from scenario *i*. Consequently, the dose risk is measured in Sv/yr. The scenario probabilities must add up to 1.

Despite this simple mathematical description of risk, the actual risk originating from a repository is hard to determine. The main problem is to determine the number of scenarios considered to be relevant in the assessment, the conditions of these scenarios and eventually the probabilities of these scenarios.

For the determination of the dose risk over time $R_D(t)$ two approaches are discussed here:

- Deterministic approach: The numbers of scenarios, their conditions as well as their probabilities are defined by expert judgement. For each scenario the consequences are calculated by deterministic model runs. The sum of the weighted scenario consequences yields the dose risk (figure 4.9).
- Stochastic approach: The parameter uncertainties of relevant model parameters are implemented by distribution functions. The outcome of a corresponding Monte-Carlo simulation yields N realisations with probabilities of 1/N each. The sum of the equally weighted realisation results yields the dose risk (figure 4.10).

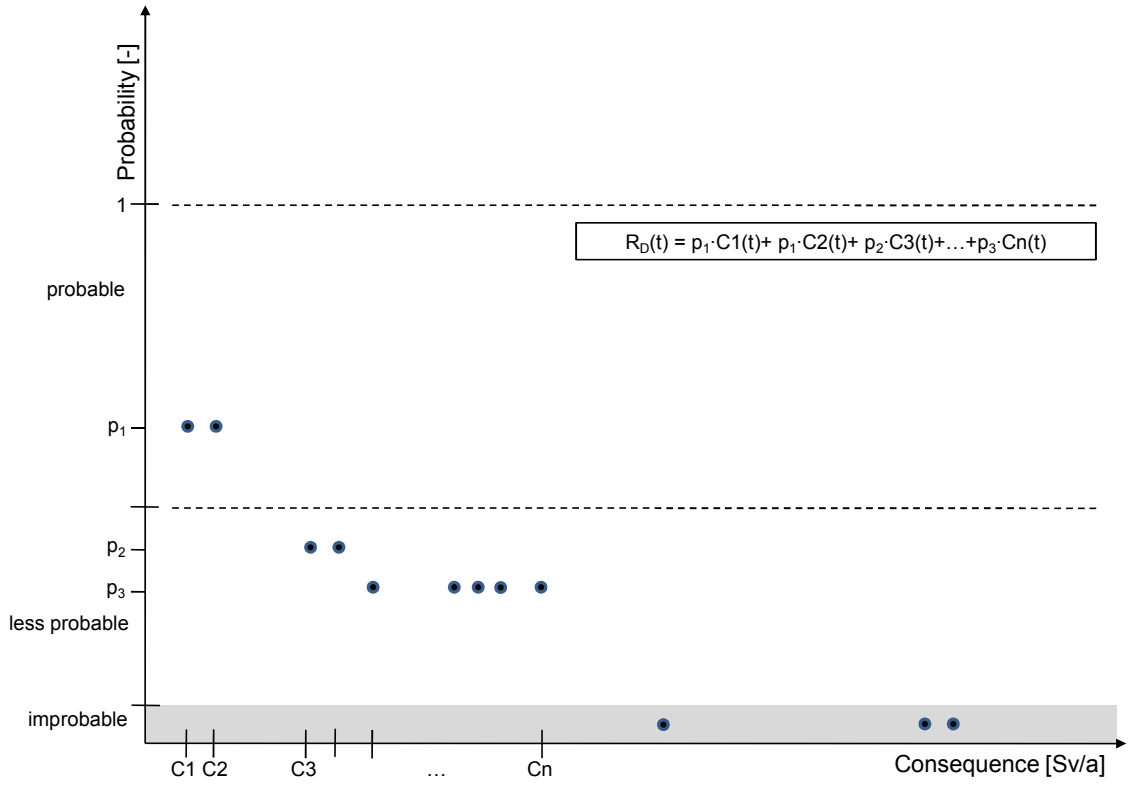

Fig. 4.9 The deterministic approach for the determination of the dose risk

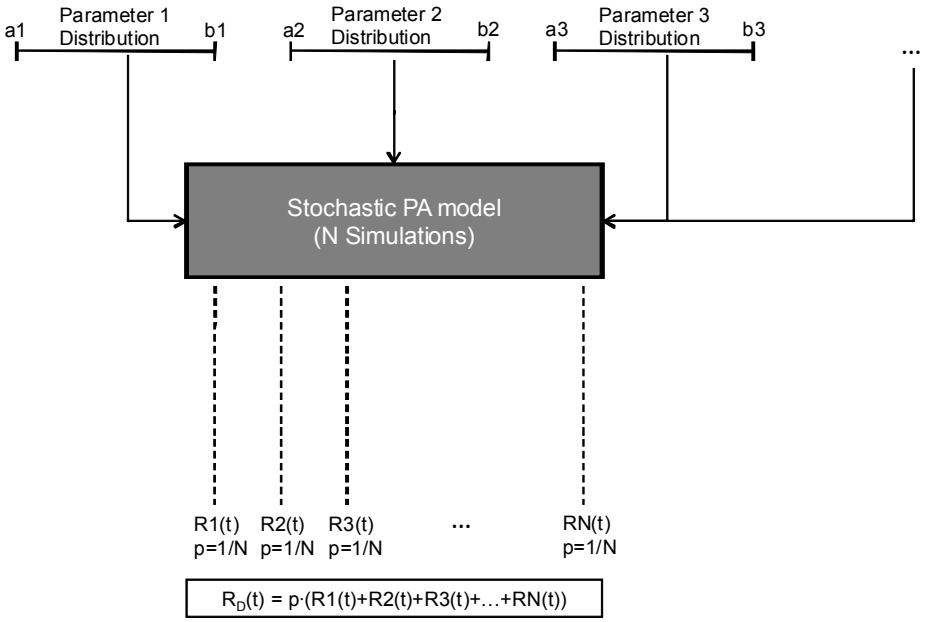

Fig. 4.10 The stochastic approach for the determination of the dose risk

Since the selection of distribution functions for relevant parameters in the second approach cannot be derived in a strictly objective way both methods are based on expert judgement. In general, the use of experts in risk assessments to quantify information is unavoidable /NEA 05/.

In this report the second approach is preferred due to the fact that expert judgement in the first approach is required for the definition of a certain set of scenarios with clearly defined probabilities. If this is done, the calculation of the risk could be carried out by a few deterministic model runs and the first approach could be a good way to communicate the risk emanating from a repository system. But so far it has not been accomplished to quantitatively assess scenario probabilities and it is not clear if this can be carried out in the future. The maximum risk that can result from a set of possible scenarios regardless of their real probabilities can be calculated by assuming a probability of 1 for the most adverse scenario.

For the derivation of parameter distribution functions in the second approach a more informative basis exists, which supports the decisions of the experts. Furthermore, it is much easier to add or reduce uncertainties in the second approach by extending or narrowing parameter distributions than by adding or removing scenarios in the first approach. In total, the second approach is more promising and is therefore carried out in this report.

In order to compare the calculated dose risk with other accepted risks it must be transformed to a more illustrative value that allows assessing the individual risk. For this purpose an indicator based on risk is introduced, which compares the probability of an event and its consequences (e. g. the risk of a certain effective dose R_D) with a risk limit accepted by regulators and/or the society. To compare the consequences with such a measure a quantitative evaluation of the incidence of an adverse effect that is expected in a population as a result of an exposure to these consequences is necessary. For a simple linear dose-response-function without a threshold value this can be done by defining a risk coefficient *r* /FIE 07/:

$$R = rR_D \tag{4.6}$$

The risk of suffering health damage can be much higher than the risk of dying. One could try to quantify the detriment of different adverse health effects, but then one would have to decide how much worse it is to die than to get ill. The probably best way to avoid this problem is to define risk as the risk of getting cancer due to the releases from the repository. This can be coupled with the effective dose. Assuming a linear relationship, risk-per-dose coefficients *r* between about 4 and 7 percent per Sievert have been found, depending on the considered group of people and whether only fatal or all

kinds of cancer are considered. In /ICRP 08/ a value of r = 5.7 percent per Sievert is recommended.

4.1.3.1 Reference values for indicators based on risk

In comparison with risks from other natural or technical sources the calculated risk can be used as a special safety indicator. The derivation of objective risk measures of other technical or natural risks is not trivial and defines an extensive field in science, e. g. /PRO 08/.

It is very important to clearly define the risk measures that are used in the analysis. A lot of comparisons are possible, but is often difficult to get reliable numbers. In this report two well determined technical risks are applied for a comparison with the risk emanating from the repository system:

- the risk of having a fatal accident in road traffic in Germany,
- the risk of dying in a plane crash.

Both risks deal with means of transport humans have to use in everyday life. These risks are necessary technical risks and are generally accepted by the majority. Furthermore, they are relatively easy to determine. But caution is advised about risk measures, if it is not clear how they are defined (e. g. trip-based risks versus distanced-based risks).

The first reference value is derived by dividing the number of road accident fatalities in Germany per year by the total German population (mortality in road traffic in Germany). Both figures are published by the Federal Office of Statistics in Germany /STA 08 and STA 08a/:

- total population in Germany in 2007: 82 217 800
- road accident fatalities in 2007: 4 949

The resulting risk is about **$6 \cdot 10^{-5}$ per year**. This risk definition assumes that the entire German population uses the road transport system. Of course, this risk is not stable. It has been decreasing for the last decades. Here, the reference year is 2007.

The second reference value is the trip-based number of fatalities in world wide air traffic. This number is given in /PRO 08/ with 52 per billion trips. The trip-based number is more useful for air traffic since the distance-based number does not take into account the differences between the risk of taking off or landing and the risk during the remaining flight. Assuming two flights per year for a person the resulting risk is about **$1 \cdot 10^{-7}$ per year**.

Besides these two reference value a third comparison value for the risk emanating from a repository system is mentioned here. It is called the acceptable risk. That is the level of loss a society considers acceptable given existing social, economic, political, cultural, technical and environmental conditions. In environmental and especially in nuclear sciences there is the general agreement, that a risk of **$1 \cdot 10^{-6}$ per year** of suffering a serious health effect is an appropriate level as a regulatory constraint or target, e. g. /IAEA 94/ or /PRO 08/.

4.1.3.2 Calculation of risk

As stated in the introductory section of this chapter only the second approach is applied in this report. For the first approach a rough pessimistic estimation can be made by using one representative pessimistic scenario and set its probability to 1. Provided, that this scenario still holds the dose criterion of 0.3 mSv/a (the German regulatory value), the risk would be $1.71 \cdot 10^{-5}$ per year.

A first step towards calculation of the risk was a test of four Monte-Carlo (MC)-simulations with different seeds and 300 realisations each (figure 4.11). The parameter distributions are the same used in section 4.1.2.6 (table 4.14). The resulting risk curves vary within four orders of magnitude. The numbers of realisations vary either: The first MC-simulation generated eleven realisations with a radionuclide release, whereas in the third simulation only one realisation with a radionuclide release exists. Moreover, the first simulation contains a disastrous parameter combination (the seal permeabilities are both very close to the upper bound and the seal lifetime is very short) yielding high maximum effective dose rates.

Evaluating the results of the first four MC-simulations it is obvious that MC-simulations with more realisations are necessary. Therefore three further MC-simulations were carried out: One with 1 200 realisations and two simulations with 4 000 realisations and

different seeds (the same calculation used in section 4.1.2.6). Additionally the four simulations with 300 realisations were combined (figure 4.12). The highest risk is calculated with the combination of the four simulations with 300 realisations. They are still dominated by the mentioned realisation with the high effective dose rate. Such a high rate is not reached in any other realisation.

The results in figure 4.12 show that the risk emanating from the repository system used in this report remains below $1 \cdot 10^{-7}$ per year. This is the risk of dying in a plane crash and one order of magnitude lower than the acceptable risk.

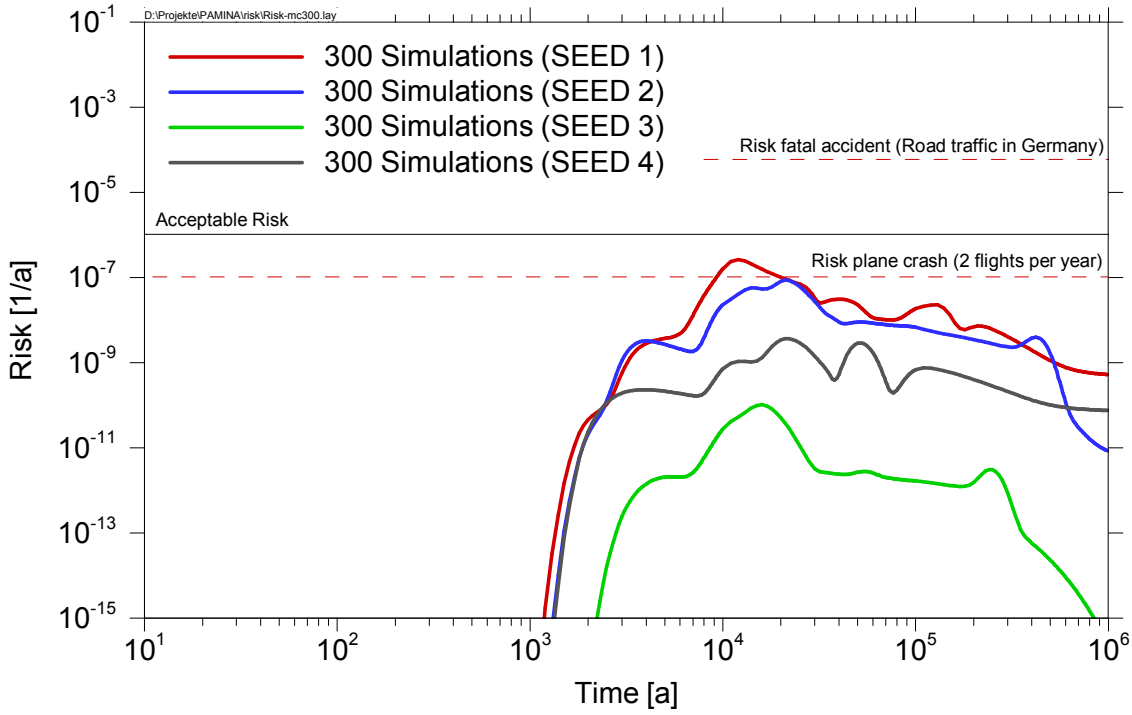

Fig. 4.11 Calculated risks (MC-simulations with 300 realisations)

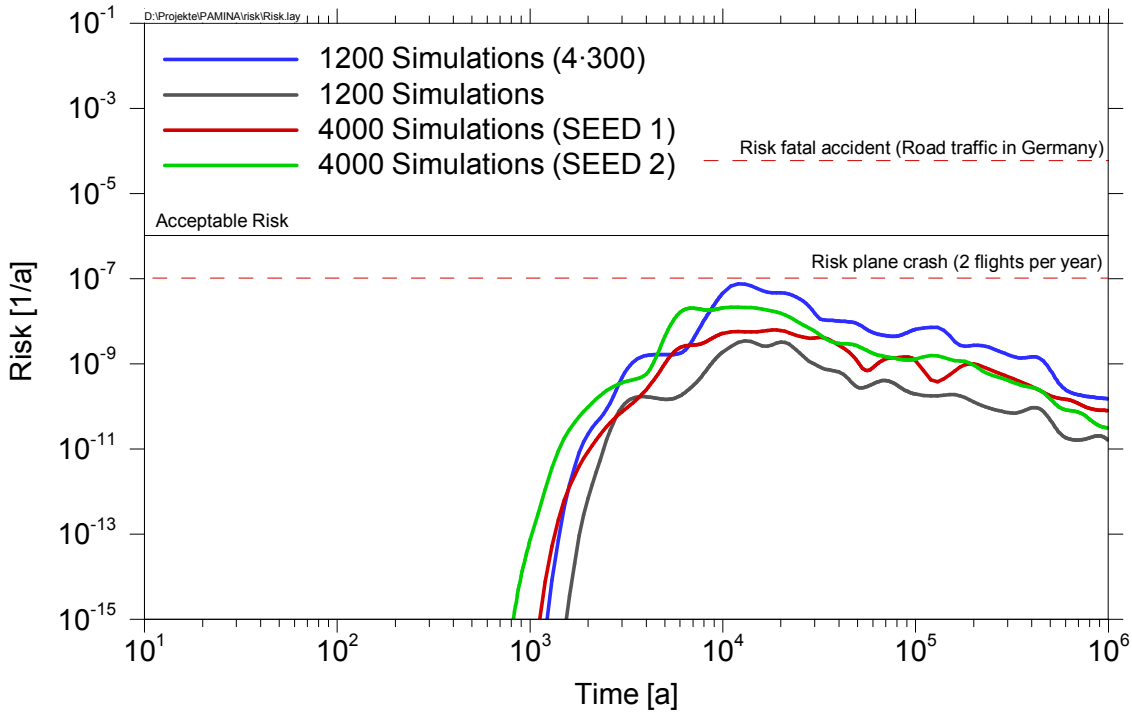

Fig. 4.12 Calculated risks (MC-simulations with 1 200 and 4 000 realisations and the sum of the four simulations in figure 4.11)

4.1.4 Performance indicators

Performance indicators are helpful tools for assessing the effects of subsystems of the repository system (e. g. a geotechnical barrier) to individual radionuclides or groups of radionuclides. The selection of the subsystems or compartments (section 4.1.4.1) mainly depends on the concept. Therefore the following results are strongly related to the presented concept.

Here, three performance indicators were selected and calculated for the repository in rock salt

- the radiotoxicity inventory in different compartments [Sv],
- the radiotoxicity fluxes from compartments [Sv/a] and
- the integrated radiotoxicity fluxes from compartments [Sv].

4.1.4.1 Compartment structure

The general idea of the concept of performance indicators is to look in detail at the transport processes at specifically relevant locations inside the repository system. Comparing the indicators calculated for different locations is often very illustrative for demonstrating the functioning of the system. In view of this purpose, the division into compartments has to be done carefully.

Compartments can represent natural or mined subsystems like the geosphere or the mine building, engineered components like canisters or barriers, or even physically independent phases in specific regions, like the canister water or the precipitate.

The repository concept used comprises emplacement fields for different types of waste in different parts of the mine. This excludes the possibility of a strongly concentric compartment structure. It is more suitable to consider parallel compartments representing, e. g., all boreholes or all emplacement drifts /BEC 08a/. The compartment structure used here is shown in figure 4.13. It contains the following compartments:

- Spent Fuel: The compartment comprises the 120 boreholes with 58 SF canisters in each borehole. The compartment contains the waste forms, the canisters, and the backfill material in the boreholes.
- High Level Waste: The HLW compartment (HLW) includes 15 boreholes with 215 HLW canisters in each borehole. This compartment contains the waste forms of vitrified HLW, the HLW canisters, and the backfill material in the boreholes.
- Intermediate Level Waste: The ILW compartment (ILW) includes 35 boreholes with 213 ILW canisters in each borehole. This compartment contains the waste forms of ILW, the ILW canisters, and the backfill material in the boreholes.

The radiotoxicity in the three waste compartments represents the total mobilised radiotoxicity in the boreholes. The waste compartments are subdivided into two further compartments: the dissolved (mobilised) radiotoxicity and the precipitated (mobilised) radiotoxicity.

- Repository Structure (central field and drifts): This compartment represents all remaining manmade penetrations: the central field, the transfer and the access drifts.

– Overlying Rock: The overlying rock comprises all geological units above the salt dome.

– Total: This compartment includes all compartments given above plus the not mobilised inventory in the waste compartments (SF, HLW and ILW) and the radiotoxicity emitted from the overlying rock to the biosphere. It represents the decay-corrected initial inventory.

The biosphere is not considered as a compartment for the performance indicators.

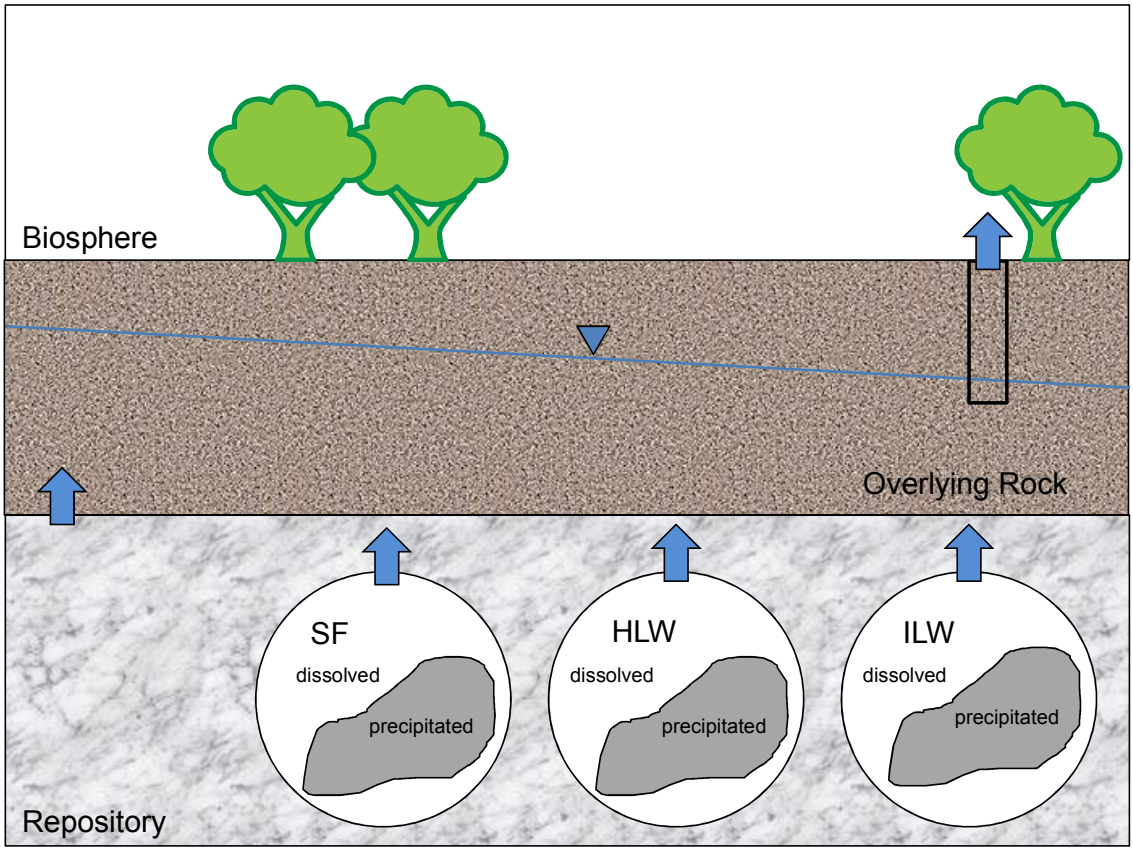

Fig. 4.13 The compartment structure used for the calculation of performance indicators in salt rock

The calculated fluxes for the indicators of sections 4.1.4.3 and 4.1.4.4 are (figure 4.13):

– Flux from SF to repository: The radiotoxicity flux from the SF compartment represents the (time-integrated) radiotoxicity flux from all boreholes of this compartment.

- Flux from HLW to repository: The radiotoxicity flux from the HLW compartment represents the (time-integrated) radiotoxicity flux from all boreholes of this compartment.
- Flux from ILW to repository: The radiotoxicity flux from the ILW compartment represents the (time-integrated) radiotoxicity flux from all boreholes of this compartment.
- Flux from repository to the overlying rock: The (time-integrated) radiotoxicity flux is calculated from the total repository. The interface between the repository within the host rock and the overlying rock is the shaft seal.
- Flux from overlying rock to biosphere: The biosphere receives the release of radionuclides from the upper part of the overlying rock, i. e. the interface between overlying rock and biosphere is the uppermost section of the far field model.

4.1.4.2 Radiotoxicity inventory in different compartments

The radiotoxicity inventories are calculated for the waste compartments (boreholes, red lines in figures), the compartments representing the central field, the access and the transfer drifts (blue lines), and the overlying rock (brown line). Additionally to the calculated inventories in the compartments of the repository the black line represents the decay corrected initial inventory (indicated with 'total' in figure 4.14) and the green line represents the released radiotoxicity into the biosphere.

The radiotoxicity inventory in the waste compartment illustrated in figure 4.14 is the mobilised radiotoxicity inventory. According to section 4.1.4.1 this inventory is divided into a dissolved (dashed orange line) and a precipitated (dotted orange line) fraction. The curves are not plotted for the whole calculation period of one million years due to output limitations of the applied software.

Figure 4.14 illustrates the scenario described in section 4.1.1: After a few years the brine reaches the waste canisters in the first waste compartments (SF). At this time the canister failure and radionuclides mobilisation starts. There is only a release from the SF waste section over the entire time period. The brine does not reach the HLW and ILW section. Due to the very small brine volume at the beginning of the scenario the whole mobilised fraction is precipitated. The inflowing brine volume is increasing and

after about 100 years the borehole is filled with brine and radiotoxicity in the repository compartment occurs (blue line).

When convergence decreases the volumes of cavities and void spaces to a certain value, the convergence stops and diffusion determines the transport of radionuclides through the repository. This leads to an increase of the radiotoxicity inventory in the repository compartments.

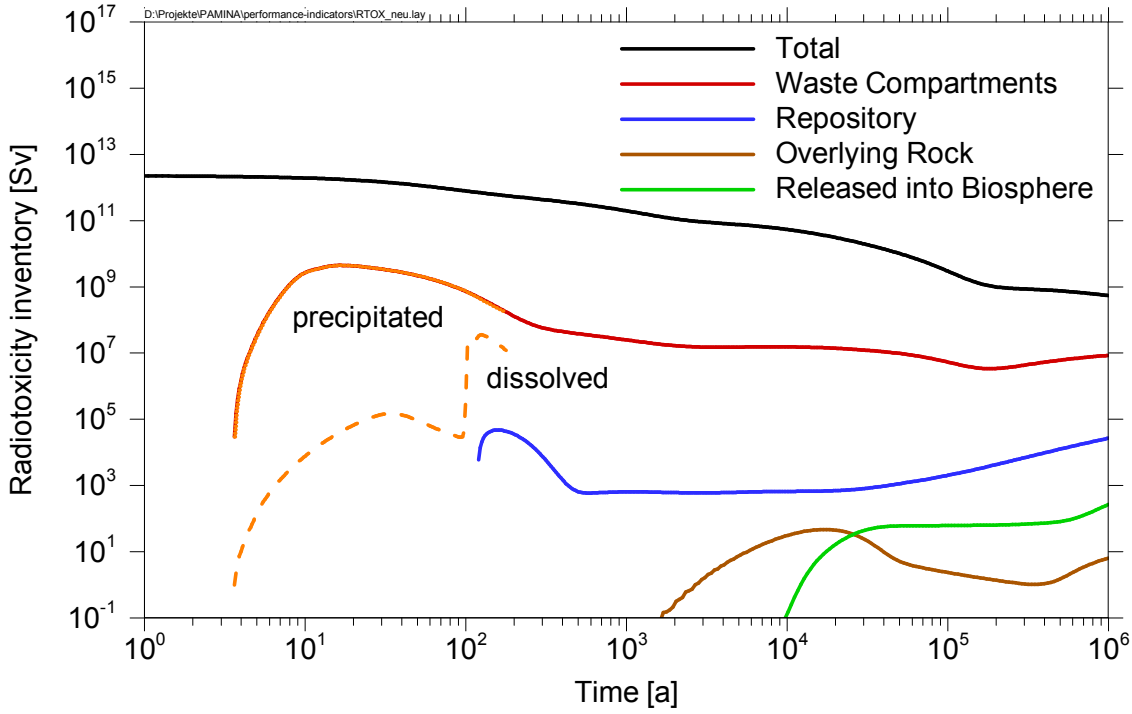

Fig. 4.14 Radiotoxicity inventory in different compartments

After 1 000 years radionuclides are released from the repository to the overlying rock and consequently the radiotoxicity inventory in the overlying rock increases. After 10 000 years the radionuclides reach the biosphere.

4.1.4.3 Radiotoxicity fluxes from compartments

Radiotoxicity fluxes were calculated from the waste compartments (SF, HLW and ILW), from the repository and from the overlying rock (figure 4.13). The radiotoxicity flux from a waste compartment represents the overall flux from the corresponding boreholes in this compartment.

As stated in the last chapter there is only a release from the waste compartment SF. There is no flux from the other waste compartments. The flux from the waste compartment SF starts after about 100 years (red line in figure 4.14). After about 700 years there is the first release from the repository to the geosphere (orange line). The total flux significantly decreases between both compartments. The reduction of the maximum peak of the radiotoxicity flux from the waste package to the flux from the repository is about six orders of magnitude.

The compartment of the overlying rock does not significantly contribute to the reduction of the maximum radiotoxicity flux. This compartment only causes a temporal shift of the release curve (orange and blue lines). The radiotoxicity flux from the repository and from the overlying rock were already used as safety indicators (section 4.1.2.5)

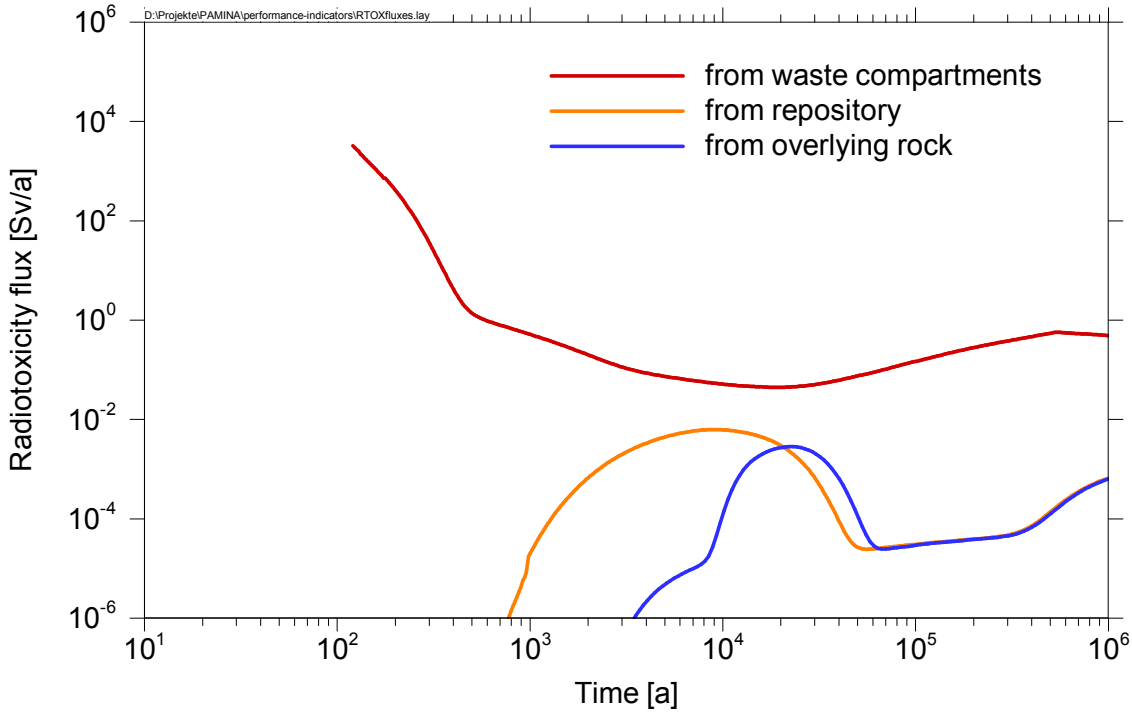

Fig. 4.15 Radiotoxicity fluxes from different compartments for all radionuclides

4.1.4.4 Integrated radiotoxicity fluxes from compartments

One important advantage of this indicator is the possibility to compare the integrated fluxes of the radiotoxicity with the initially emplaced radiotoxicity in the waste compartments in a comprehensive way. Therefore the initially emplaced inventory is added to figure 4.16 as a dashed horizontal line.

The overall initially emplaced radiotoxicity inventory is $2.25 \cdot 10^{12}$ Sv. The total release of all radionuclides within one million years is $5.45 \cdot 10^{5}$ Sv from the waste compartment SF, $3.31 \cdot 10^{2}$ Sv from the repository and $2.75 \cdot 10^{2}$ Sv from the overlying rock. The release from the waste compartment starts after 120 years, after 420 years from the repository and after 1 122 years from the overlying rock.

The total reduction of the radiotoxicity in the whole repository system is about ten orders of magnitude, seven are contributed by the waste sections and three by the repository.

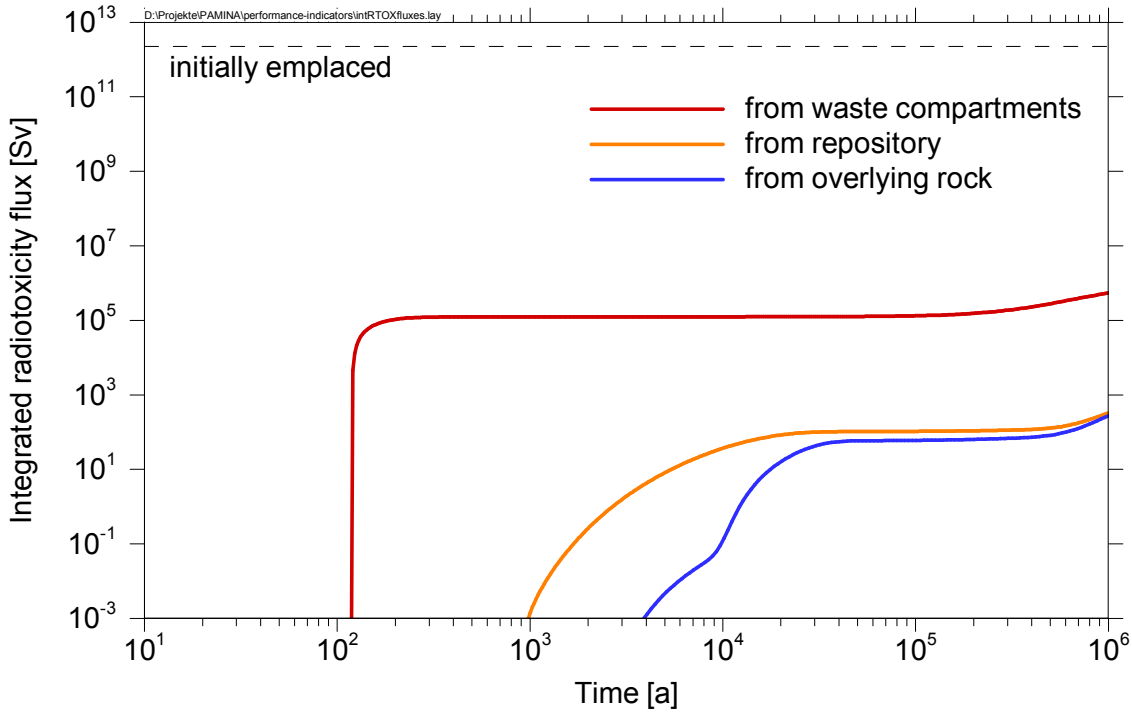

Fig. 4.16 Integrated radiotoxicity fluxes from different compartments for all radionuclides

4.1.5 Summary

In this study, three safety indicators and their corresponding reference values complementary to the effective dose rate were identified and tested for a generic repository in a rock salt formation (salt dome). Due to the independently derived reference values all four safety indicators applied in this report provide four different safety statements (regarding human health, groundwater quality etc.).

The combination of the four indicators and the underlying safety statements gives a strong argument for or against the safety of the repository system. The distinctive uncertainties of every single indicator are thus less important for the overall safety assessment. For the chosen set of parameters all four safety indicators stay significantly below the reference value, the margin of safety is at least one order of magnitude.

The robustness of the safety indicators was analysed exemplarily for the effective dose rate by performing Monte-Carlo simulations. All realisations with a release of radionuclides were analysed. The resulting range of the realisations is about six orders of magnitude. This seems to be a weak robustness. For a deeper analysis of these results a comparison with other indicators and/or other repository systems is necessary. Such a comparison is planned in the future. The aim here was to present a procedure how to present the results of a robustness analysis.

The parameters used in the deterministic calculations are chosen arbitrarily and do not consider the probability of this parameter combination. In order to consider scenario probabilities a risk emanating from the repository was calculated. This is especially helpful for repository concepts in salt, where the expected evolution yields a zero output, but specific scenarios of very low probability can lead to relatively high doses. The expected overall calculated risk originating from a salt repository is then relatively small compared with other technical risks.

Indicators based on risk should be handled with caution, due to the high uncertainty of scenario probabilities. In most cases, these probabilities can only be guessed or roughly estimated, while the resulting risk value may suggest an exact calculation. For this reason a stochastic approach was carried out with clear defined scenario probabilities. But there is still expert judgment necessary to set up the required parameter distributions. Nevertheless, the use of such stochastic-based indicators is an important contribution in providing effective and comprehensive indicators for the safety of a repository system. However, the decisions made by individual humans are only partly based on such numerically expressed indicators /PRO 08/. Risk should be seen as a useful additional concept for the presentation of safety of a repository system.

In general, safety indicators are good means for assessing the level of safety of the total system, but they do not provide information about how the system works and how the level of safety is reached. Such information, however, is of high value for the safety case. For the experts it is essential to understand how the different barriers work to-

gether and where the radionuclides are mainly retained. For communication with licensing authorities as well as with the general public it can be helpful to demonstrate the functioning of the system in an illustrative and understandable way. Such demonstrations can improve the confidence in the performance assessment.

Information of this kind is provided by performance indicators. They are typically concentrations or fluxes of radionuclides in or between specific parts of the repository system, or other descriptive measures that demonstrate specific properties of the system. Performance indicators are very important for the understanding of the modelled processes and they can be used for the optimisation of the repository system and give valuable arguments for increasing the confidence in the safety of a repository system.

Annex: Decay data for the considered radionuclides

Decay energies are given after /FIR 99/ and /WEA 86/.

Tab. 4.15 Decay data (activation and fission products)

Radionuclide	Half-life [a]	Decay Mode	Decay Energy [MeV]	Decay Energy used [MeV]
C-14	$5.730 \cdot 10^{3}$	B-	0.156	0.156
Cl-36	$5.272 \cdot 10^{0}$	B-	0.709	0.709
Ca-41	$1.030 \cdot 10^{5}$	B+	0.421	n.c.
Ni-59	$7.500 \cdot 10^{4}$	B+	1.072	1.072
Ni-63	$1.000 \cdot 10^{2}$	B-	0.065	0.065
Co-60	$5.271 \cdot 10^{0}$	B-	2.824	n.c.
Se-79	$1.100 \cdot 10^{6}$	B-	0.151	0.151
Rb-87	$4.880 \cdot 10^{10}$	B-	0.283	n.c.
Sr-90	$2.864 \cdot 10^{1}$	B-	0.546	2.828
Y-90	$7.312 \cdot 10^{-3}$	B-	2.282	
Zr-93	$1.500 \cdot 10^{6}$	B-	0.091	0.121
Nb-93m	$1.613 \cdot 10^{1}$	Isomeric	0.03	0.030
Nb-94	$2.000 \cdot 10^{4}$	B-	2.04	2.040
Mo-93	$3.500 \cdot 10^{3}$	B+	0.405	0.405
Tc-99	$2.100 \cdot 10^{5}$	B-	0.294	0.294
Pd-107	$6.500 \cdot 10^{6}$	B-	0.033	n.c.
Sn-126	$2.345 \cdot 10^{5}$	B-	0.38	4.05
Sb-126m	$3.641 \cdot 10^{-5}$	Isomeric	0.018	
Sb-126	$3.395 \cdot 10^{-2}$	B-	3.67	
I-129	$1.570 \cdot 10^{7}$	B-	0.194	0.194
Cs-135	$2.000 \cdot 10^{6}$	B-	0.269	0.269
Cs-137	$3.017 \cdot 10^{1}$	B-	1.176	1.838
Ba-137m	$4.943 \cdot 10^{-6}$	Isomeric	0.662	
Sm-151	$9.300 \cdot 10^{1}$	B-	0.077	0.077

Tab. 4.16 Decay data (actinide elements of series 4n)

Radionuclide	Half-life [a]	Decay Mode	Decay Energy [MeV]	Decay Energy used [MeV]
Cm-248	$3.480 \cdot 10^{5}$	A	5.162	n.c.
Pu-244	$8.000 \cdot 10^{7}$	A	4.665	7.253
U-240	$1.608 \cdot 10^{-3}$	B-	0.388	
Np-240	$1.177 \cdot 10^{-4}$	B-	2.2	
Cm-244	$1.810 \cdot 10^{1}$	A	5.902	5.902
Pu-240	$6.563 \cdot 10^{3}$	A	5.255	5.255
U-236	$2.342 \cdot 10^{7}$	A	4.572	4.572
Th-232	$1.405 \cdot 10^{10}$	A	4.081	4.081
Ra-228	$5.750 \cdot 10^{0}$	B-	0.046	2.173
Ac-228	$7.016 \cdot 10^{-4}$	B-	2.127	
U-232	$6.890 \cdot 10^{1}$	A	5.414	5.414
Th-228	$1.913 \cdot 10^{1}$	A	5.52	36.402
Ra-224	$1.002 \cdot 10^{-2}$	A	5.789	
Rn-220	$1.768 \cdot 10^{-6}$	A	6.405	
Po-216	$4.753 \cdot 10^{-9}$	A	6.906	
Pb-212	$1.214 \cdot 10^{-3}$	B-	0.574	
Bi-212	$1.151 \cdot 10^{-4}$	B-	2.254	
Po-212	$9.507 \cdot 10^{-15}$	A	8.954	

Tab. 4.17 Decay data (actinide elements of series 4n+1)

Radionuclide	Half-life [a]	Decay Mode	Decay Energy [MeV]	Decay Energy used [MeV]
Cm-245	$8.500 \cdot 10^{3}$	A	5.623	5.623
Pu-241	$1.435 \cdot 10^{1}$	B-	0.021	0.021
Am-241	$4.322 \cdot 10^{2}$	A	5.638	5.638
Np-237	$2.144 \cdot 10^{6}$	A	4.959	5.531
Pa-233	$7.390 \cdot 10^{-2}$	B-	0.572	
U-233	$1.592 \cdot 10^{5}$	A	4.909	4.909
Th-229	$7.880 \cdot 10^{3}$	A	5.168	35.727
Ra-225	$4.080 \cdot 10^{-2}$	B-	0.357	
Ac-225	$2.740 \cdot 10^{-2}$	A	5.935	
Fr-221	$9.316 \cdot 10^{-6}$	A	6.458	
At-217	$1.023 \cdot 10^{-9}$	A	7.202	
Bi-213	$8.668 \cdot 10^{-5}$	B-	1.426	
Po-213	$1.331 \cdot 10^{-13}$	A	8.537	
Pb-209	$3.710 \cdot 10^{-4}$	B-	0.644	

Tab. 4.18 Decay data (actinide elements of series 4n+2)

Radionuclide	Half-life [a]	Decay Mode	Decay Energy [MeV]	Decay Energy used [MeV]
Cm-246	$4.760 \cdot 10^{3}$	A	5.475	5.475
Pu-242	$3.730 \cdot 10^{5}$	A	4.983	4.983
Am-242m	$1.410 \cdot 10^{2}$	Isomeric	0.048	6.929
Am-242	$1.828 \cdot 10^{-3}$	B-	0.665	
Cm-242	$4.461 \cdot 10^{-1}$	A	6.216	
Pu-238	$8.774 \cdot 10^{1}$	A	5.593	5.593
U-238	$4.468 \cdot 10^{9}$	A	4.27	6.740
Th-234	$6.600 \cdot 10^{-2}$	B-	0.273	
Pa-234	$2.225 \cdot 10^{-6}$	B-	2.197	
U-234	$2.455 \cdot 10^{5}$	A	4.856	4.856
Th-230	$7.538 \cdot 10^{4}$	A	4.77	4.770
Ra-226	$1.600 \cdot 10^{3}$	A	4.871	35.338
Rn-222	$1.047 \cdot 10^{-2}$	A	5.59	
Po-218	$5.799 \cdot 10^{-6}$	A	6.115	
Pb-214	$5.099 \cdot 10^{-5}$	B-	1.023	
Bi-214	$3.784 \cdot 10^{-5}$	B-	3.272	
Po-214	$5.206 \cdot 10^{-12}$	A	7.833	
Pb-210	$2.230 \cdot 10^{1}$	B-	0.064	
Bi-210	$1.732 \cdot 10^{-2}$	B-	1.163	
Po-210	$3.790 \cdot 10^{-1}$	A	5.407	

Tab. 4.19 Decay data (actinide elements of series 4n+3)

Radionuclide	Half-life [a]	Decay Mode	Decay Energy [MeV]	Decay Energy used [MeV]
Cm-247	$1.560 \cdot 10^{7}$	A	5.353	n.c.
Am-243	$7.370 \cdot 10^{3}$	A	5.438	12.329
Np-239	$6.450 \cdot 10^{-3}$	B-	0.722	
Cm-243	$2.910 \cdot 10^{1}$	A	6.169	
Pu-239	$2.411 \cdot 10^{4}$	A	5.244	5.244
U-235	$7.038 \cdot 10^{8}$	A	4.679	5.068
Th-231	$2.911 \cdot 10^{-3}$	B-	0.389	
Pa-231	$3.276 \cdot 10^{4}$	A	5.149	5.149
Ac-227	$2.177 \cdot 10^{1}$	B-	0.045	36.188
Th-227	$5.120 \cdot 10^{-2}$	A	6.146	
Ra-223	$3.130 \cdot 10^{-2}$	A	5.979	
Rn-219	$1.255 \cdot 10^{-7}$	A	6.946	
Po-215	$5.644 \cdot 10^{-11}$	A	7.526	
Pb-211	$6.864 \cdot 10^{-5}$	B-	1.373	
Bi-211	$4.069 \cdot 10^{-6}$	A	6.75	
Tl-207	$9.069 \cdot 10^{-6}$	B-	1.423	

4.2 Repository in clay

In a recent project a first attempt was carried out to test safety and performance indicators for a repository in clay /WOL 09/. The work presented there was lacking from some deficiencies of the used code CLAYPOS to calculate the performance indicators resulting from being neither capable of calculating radionuclide fluxes at the interfaces between different model domains nor the radionuclide inventories in some of those. Therefore, in this project it was planned to improve the computer code CLAYPOS to calculate the additional performance indicators and test the usefulness of the additional information gained.

The work presented in the following is largely based on the work described in /WOL 09/. Deterministic calculations have been performed on a slightly advanced test case compared to the one used in the preceding project. Safety and performance indicators were calculated for the test case and are presented in the following. Besides the deterministic calculations also probabilistic simulations have been performed for two reasons: first, to test whether the principle problems discovered for the use of variance based methods for the test case in salt do also apply for the test case in clay and second, to increase the insight in the clay repository system.

The following section shortly describes the test case used. This is directly based on the model used for the integrated performance assessment calculations performed for a generic repository in the Lower Cretaceous Clay formation in Northern Germany /RUE 07/. The subsequent sections give the results from the deterministic calculations and the probabilistic simulations for the safety indicator dose rate and additional performance indicators.

4.2.1 Test case

The test case represents a generic repository for high level waste in a consolidated clay host rock formation in Northern Germany and is described in more detail in /RUE 07/. The host rock is the Apt, which is part of the Lower Cretaceous Clays and is found in a depth of -250 metres below surface with a thickness of 220 metres. The Apt is overlain by the 200 m thick Alb formation which is also a low permeable, compacted clay formation of similar properties. A cross-section of the geological sequence of formations is shown in figure 4.17. The rock properties and the transport properties of the

radionuclides for both formations as well as the repository layout are described in /RUE 07/. The overburden consists of a sequence of aquifers typical for Northern Germany and the according parameters were taken from /KES 05/.

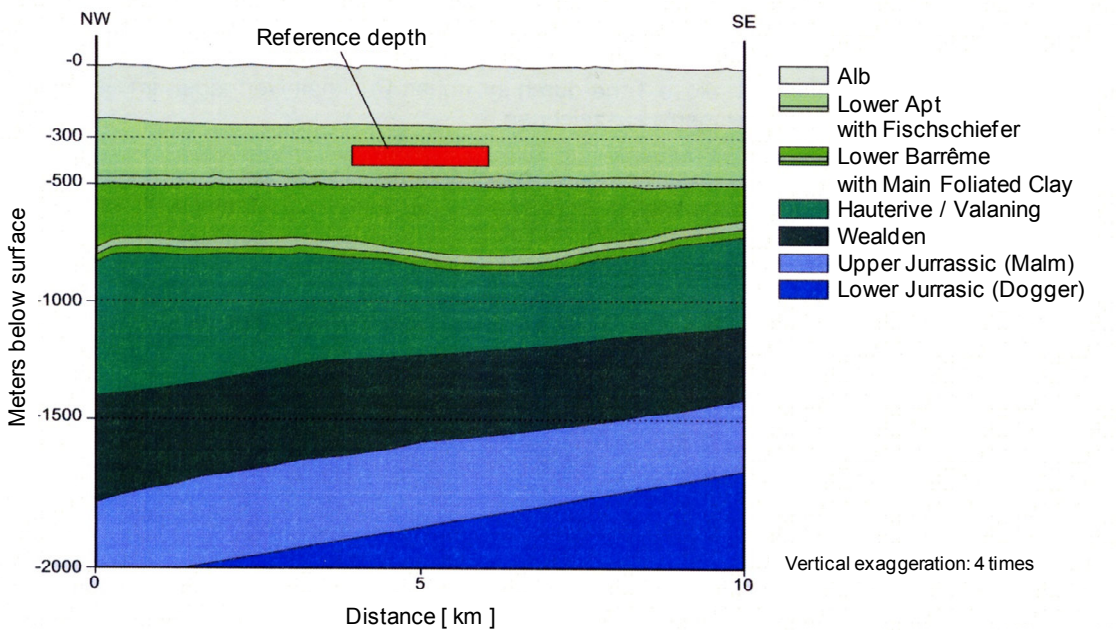

Fig. 4.17 Cross-section of the Lower Cretaceous Clay Formation sequence /PTK 06/

The repository system and the reference scenario for the repository can be described as follows: the containers are stored in vertical boreholes holding five containers each. The cavity around the containers is backfilled with bentonite. It is assumed that before any containers corrode, the bentonite and those parts of the host rock formation that were desaturated during the construction of the repository are re-saturated and all pathways in the bentonite and the excavation-disturbed zone (EDZ) are closed by the swelling process. As soon as the first containers fail, the radionuclides are mobilized and transported. Part of the radionuclides precipitate again in the near-field due to solubility limits. For the reference scenario it is assumed that the mobilized radionuclides are exclusively transported by diffusion through the technical barriers, the host rock itself, and any overlying, similarly impermeable rock strata up to the water-bearing overburden. In all these areas, the radionuclides are retained by sorption. If a contamination of groundwater occurs, the population is exposed to radiation if it uses the groundwater as drinking water or for foodstuff production.

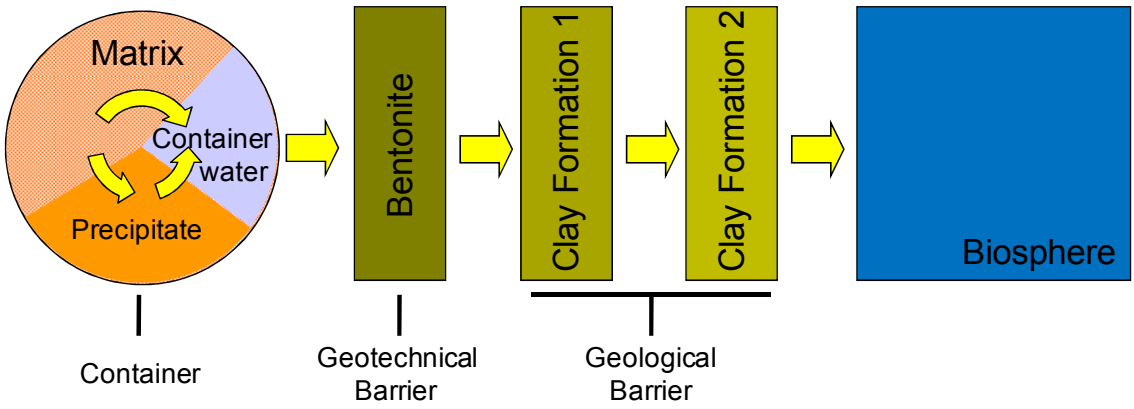

Fig. 4.18 Compartments of the generic repository system in clay

Figure 4.18 shows the different compartments that are distinguished for the calculation of the performance indicators for the repository in a clay formation used here. For the definition of the indicators see /WOL 09/. Different colours represent the different compartments that are used for the calculation of the inventories. The yellow arrows represent those compartment boundaries where radionuclide fluxes are calculated. The different compartments are:

- **Matrix:** This compartment represents the non-mobilised radionuclides in the spent fuel matrix.
- **Precipitate:** This compartment represents those nuclides that were mobilised from the matrix, but are precipitated since solubility limits are reached.
- **Container water:** This compartment represents the mobilised radionuclides from the matrix that are not precipitated. This compartment is used for the calculation of the radionuclide flux from both of the preceding compartments (matrix and precipitate) to the clay formation.
- **Bentonite:** This compartment represents the geotechnical barrier made from bentonite backfill.
- **Clay formation 1 and 2:** These compartments represent both geological barriers, the Lower Cretaceous Apt formation, which is the host rock and the overlying low permeable Alb formation.
- **Biosphere:** This compartment includes all radionuclides which left the host rock formation. This includes not only the biosphere, but also the aquifer.

The retention efficiency of the different geotechnical and geological barriers, the bentonite near-field – host rock – overlying low permeable formations and overburden can be determined by comparing the radionuclide fluxes from each of the listed compartments.

4.2.2 Results from the deterministic simulations

As discussed in /WOL 09/, performance indicators, namely

- the radiotoxicity inventory in different compartments and
- the radiotoxicity fluxes from several compartments,

are helpful to assess the behaviour of different compartments in a repository.

Due to missing features of the module CLAYPOS which was used to perform the integrated safety assessment for the repository in clay it was impossible at that time to calculate some of these indicators. To overcome this deficiency the module CLAYPOS was enhanced within this project and the changes to the module as well as the new results are presented in the following.

4.2.2.1 Enhancements of the CLAYPOS module

In this project some features were added to CLAYPOS to determine additional performance indicators, namely

- the temporal evolution of the radionuclide fluxes from the precipitate and the different parts of the geotechnical and geological clay barrier are calculated and saved,
- the temporal evolution of the radionuclide inventories in the precipitate, the container water and the different parts of the geotechnical and geological clay barrier are calculated and saved.

The module CLAYPOS uses an implicit algorithm to calculate the flux into and from the whole sequence of geotechnical and geological clay barriers at once. Due to the implicit algorithm used by CLAYPOS it is impossible to get the fluxes and concentrations needed for the calculation of the performance indicators in the individual compartments directly. Thus the additional outflows from the different compartments have to be recalculated explicitly out of the final results of the solved equation system. As a conse-

quence of the different treatment, i. e. calculating the overall fluxes with an implicit scheme and the fluxes from compartments with an explicit scheme, the calculated values may match only with an adequate accuracy. In order to prove the correct implementation of the calculation of the additional indicators a simulation with three stable tracers was performed for the aforementioned repository system. The tracers mobilised by rates of 1 Mol/a carry the following properties: The infinitely mobilised T0 is characterised by no solubility limit and no sorption. T1 and T2 were mobilised for 1 000 years and had a high solubility limit, T1 was non-sorbing in contrast to T2 which was sorbing.

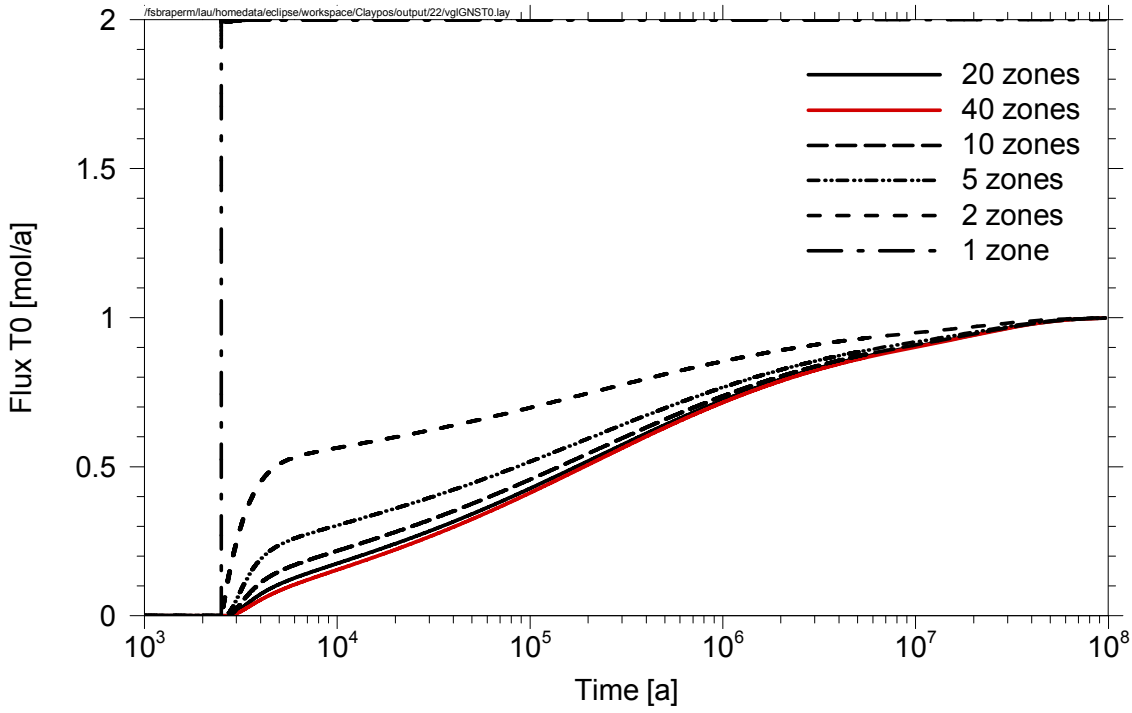

Fig. 4.19 Flux of a stable tracer out of the first clay compartment versus time for a varying degree of discretisation

In the implicit algorithm the number of zones representing the clay barrier has no crucial impact on the results of the calculation of the *overall* fluxes. But for the newly calculated fluxes out of the clay compartments the influence of the numerical zone discretisation is critical due to the used explicit scheme: In figure **4.19** the flux of tracer T0 from the first clay compartment versus time is pictured. The different curves shown are representing a different degree of discretisation: With increasing number of zones the outflow converges to its expected value (cp. figure 4.21). Therefore all following results are obtained with a minimum of 20 zones for each compartment. As far as possible, the additionally calculated performance indicators were compared to results that were available from the implicit algorithm already before.

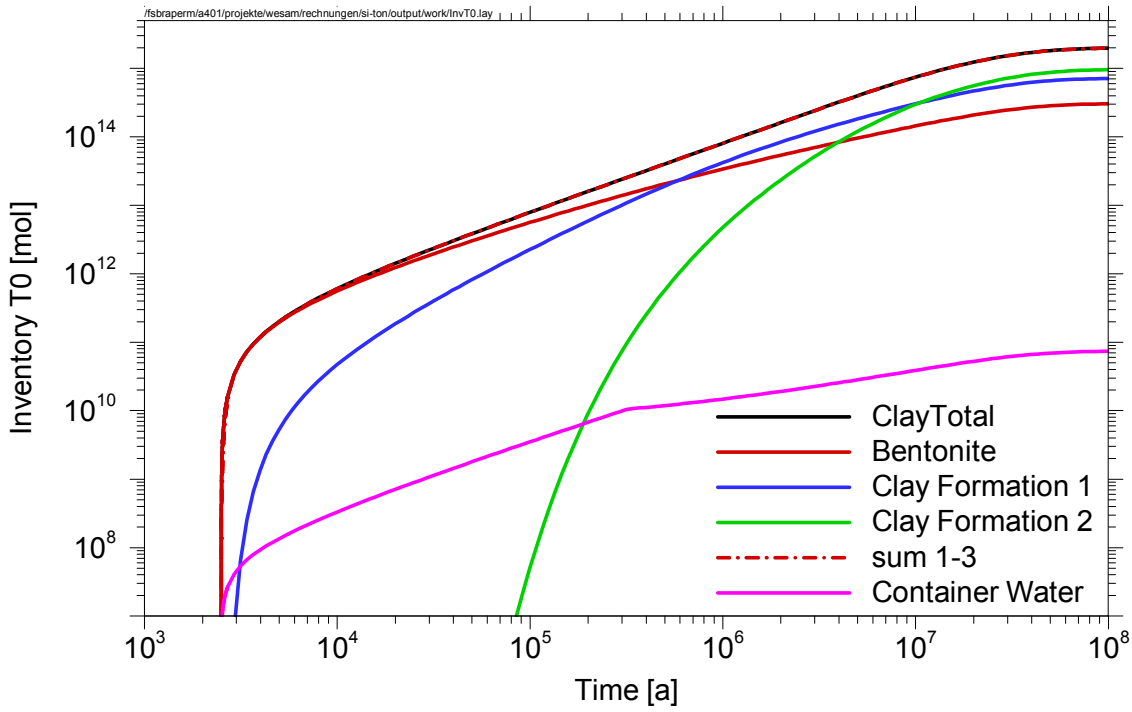

Fig. 4.20 Inventory of non-sorbing tracer T0 without solubility limit versus time for different compartments

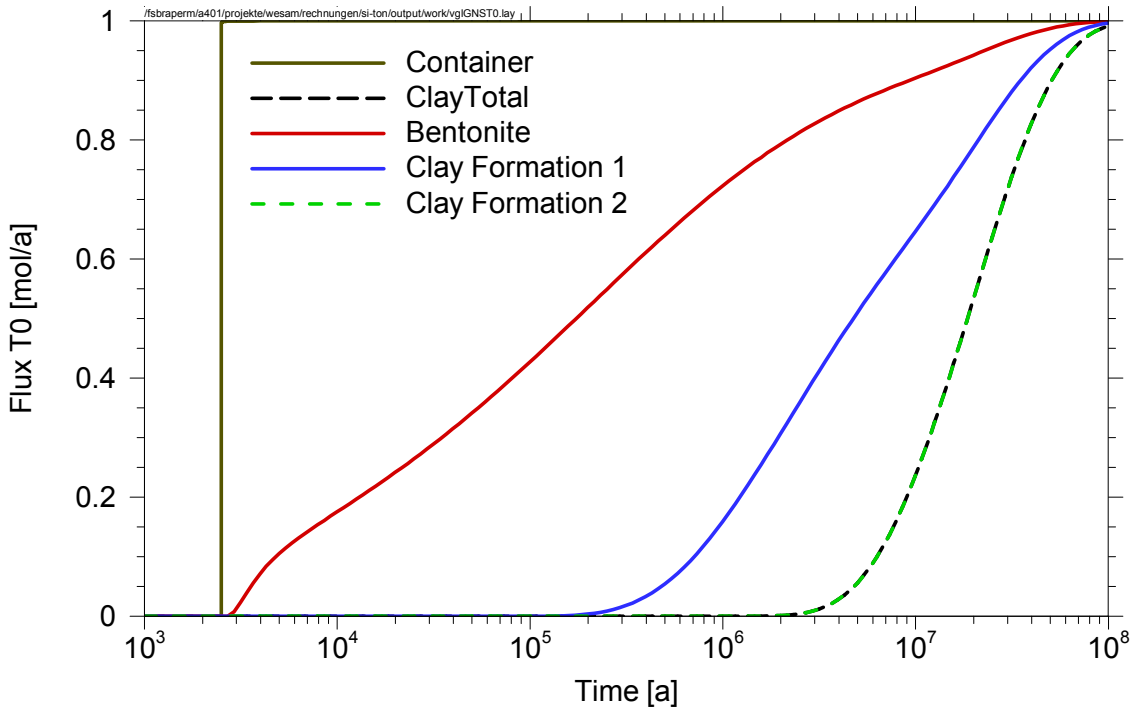

Fig. 4.21 Flux of non-sorbing tracer T0 without solubility limit versus time out of different compartments

The calculated inventories of tracer T0 in the different compartments of the repository system are shown in figure **4.20**: The increasing inventory of T0 in the container water leads to increasing inventories in the succeeding clay compartments. The sum of all three clay compartments agrees well to the known total clay inventory. Due to the infinite mobilisation the inventories converge to a steady state when the loss through the exit is compensated by the gain through the entry.

The flux from the container starts instantaneously after begin of release, while all succeeding compartments get involved one after another in their topological order (cf. figure 4.21). The flux from the second clay formation, i. e. the last clay compartment, is equivalent to the flux out of all clay regions calculated by the implicit algorithm. Due to the specified infinite release from the matrix (resulting from the selected initial inventory in combination with the mobilisation rate) the fluxes of all compartments end up in converging to a steady state.

The finite mobilisation (1 000 years) of tracer T1 is indicated by the early matrix inventory decrease found on left-hand side top in figure **4.22**. The fairly low solubility limit, depicted by the initial constant container water's inventory, causes the main fraction of the released radionuclides to be precipitated. The precipitate is slowly re-dissolved within about $3 \cdot 10^7$ years. After the precipitate is used up, the inventory in the container water is decreasing, too. The constant concentration in the container water as boundary condition can temporarily cause an inventories' steady state in the bentonite already from about $5 \cdot 10^4$ years on, but in all compartments just for a very short period at about $2 \cdot 10^7$ years when all fluxes are the same (cp. figure **4.23**). In the end, the system lacks a driving boundary condition, e. g. the ongoing radionuclide release. Also for this tracer the calculated sum of all three clay compartments matches to the known total clay inventory.

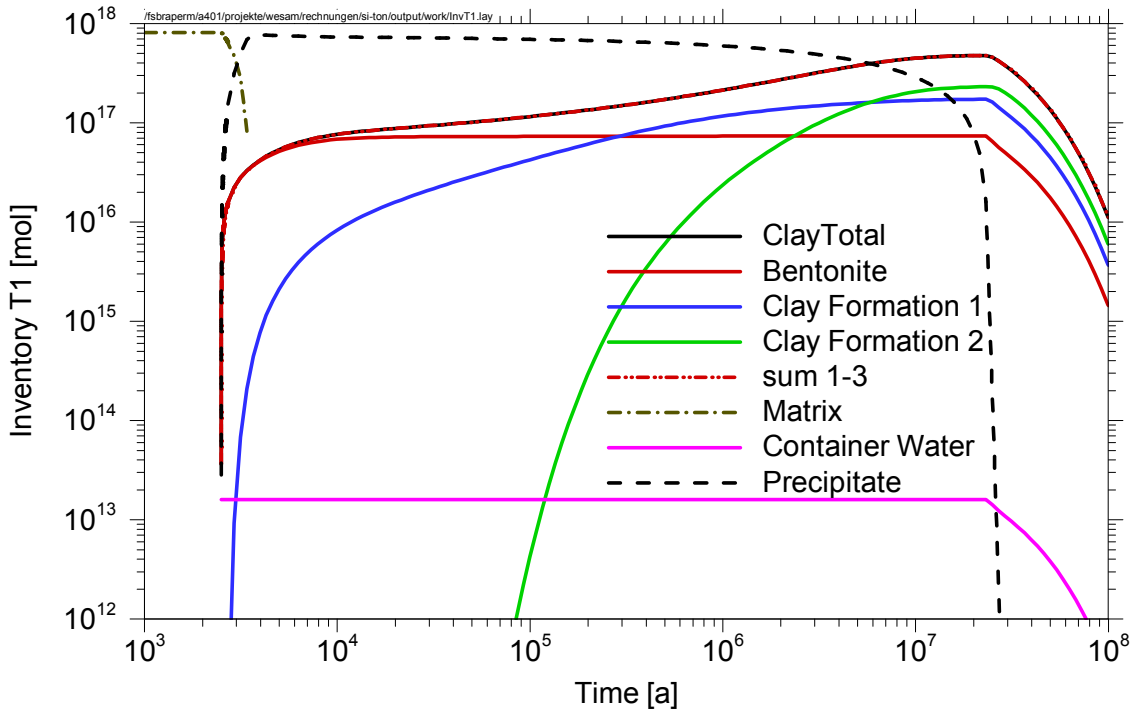

Fig. 4.22 Inventory of non-sorbing tracer T1 with solubility limit versus time for different compartments

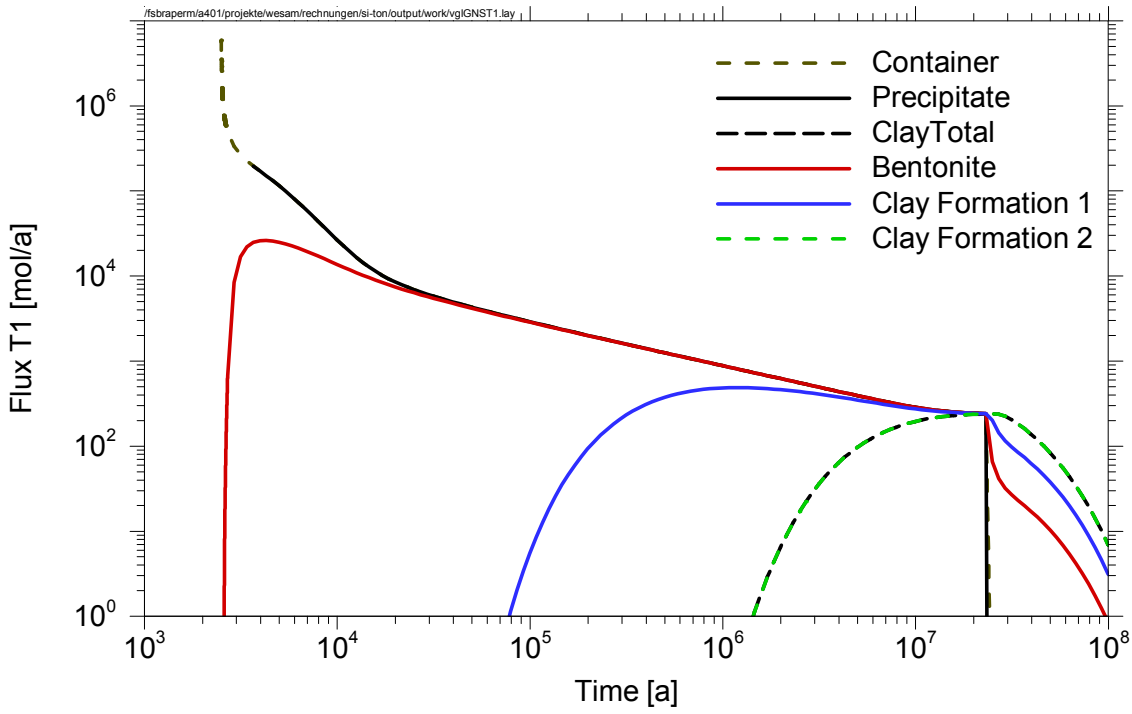

Fig. 4.23 Flux of non-sorbing tracer T1 with solubility limit versus time out of different compartments

The aforementioned steady state of some compartments' inventory meaning that the same amount of nuclides are entering and leaving the compartment is indicated in figure **4.23** by the corresponding values of the respective curves: When the flux out of the precipitate, i. e. into the bentonite, equals to the outflow of the bentonite, i. e. the gain by inflow is compensated by the loss via exit, the bentonite's inventory is temporally constant. Again, the flux from the second clay formation is equivalent to the known final outflow from all clay regions.

As plotted in figure **4.24**, compared to T1 the sorption of tracer T2 in the bentonite shortens the phase while the precipitation inventory keeps the container water concentration on the same level, because the inventory in the pore water of the first clay part, i. e. the bentonite geotechnical barrier, controlling the flux out of the container water is lowered by sorption. The following happens in detail: Due to sorption, the concentration of T2 in the pore water of the bentonite is lower, thus the concentration gradient at the interface to the container water is higher than the one for T1, resulting in a higher flux for T2 than for T1. Therefore, the precipitate is used up already after 10^5 years for T2, in contrast to $2 \cdot 10^7$ years for T1 (cp. figure **4.22**). At about $8 \cdot 10^4$ years the bentonite's inventory has temporarily reached a steady state before its continuous decrease starts. At a very late point in time the inventory of tracer T2 in clay formation 2 starts to increase, also proving the sorbing capability of clay formation 1.

This late involvement of the second clay formation is proven in figure **4.25** by the low flux out of the first clay formation at a very late point in time.

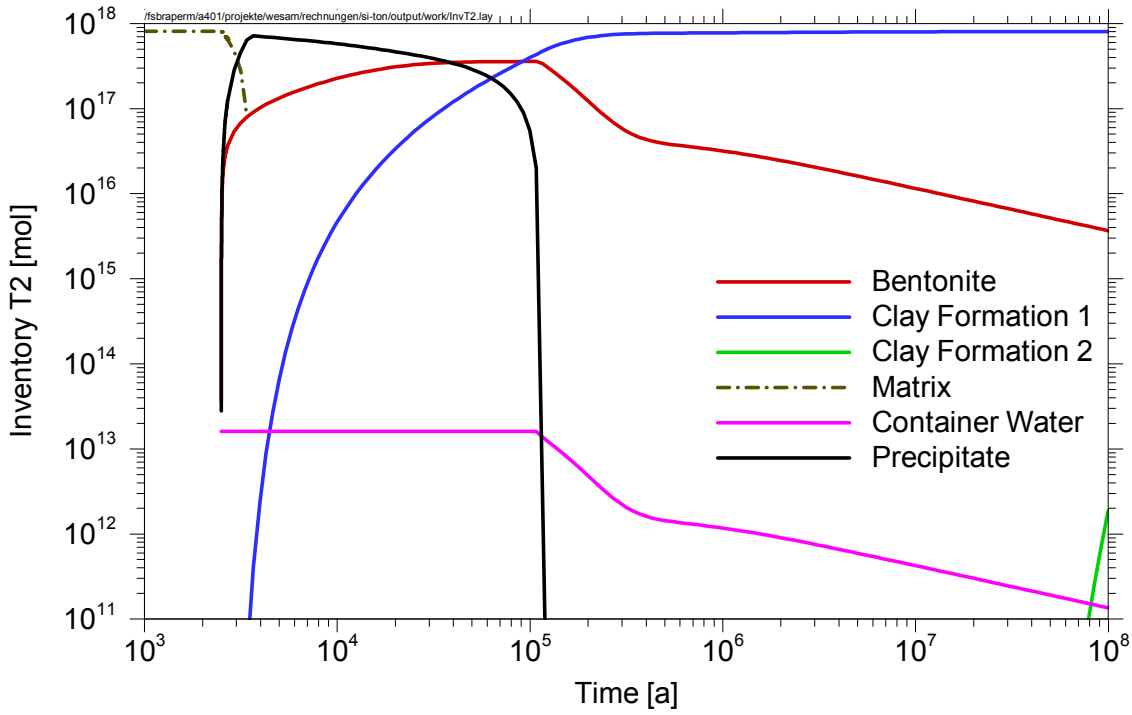

Fig. 4.24 Inventory of sorbing tracer T2 with solubility limit versus time for different compartments

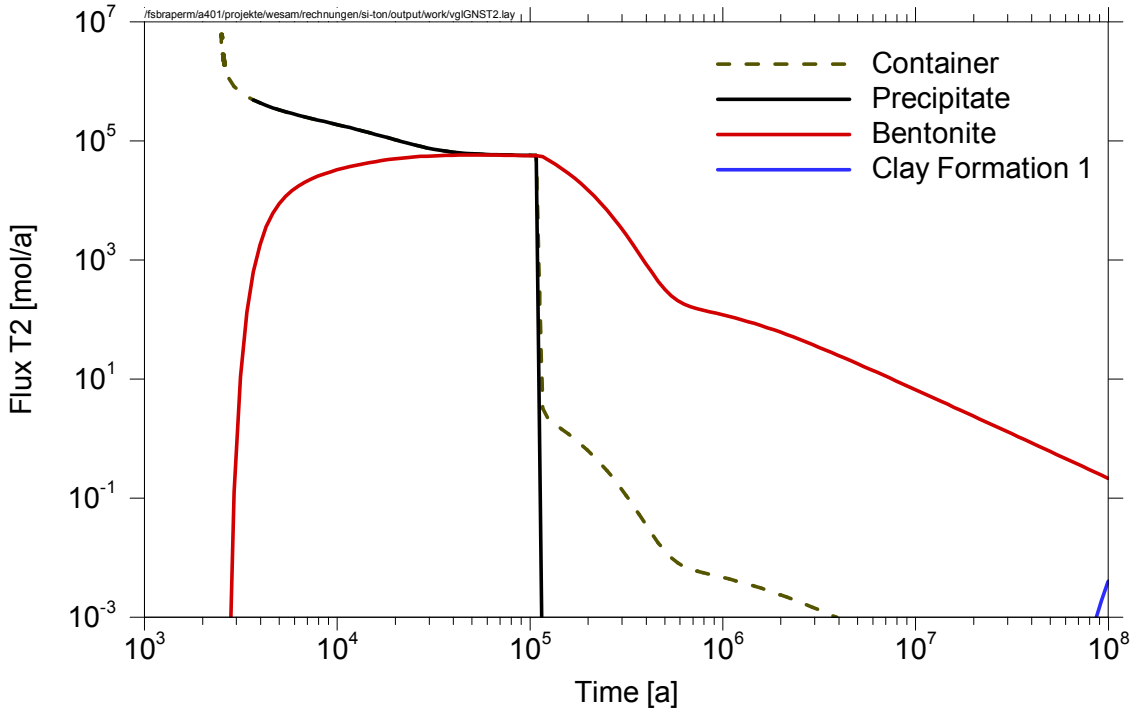

Fig. 4.25 Flux of sorbing tracer T2 with solubility limit out of different compartments

4.2.2.2 Radiotoxicity inventories/fluxes in/from different compartments

Two performance indicators described in /WOL 09/ are calculated for the repository in clay described in chapter 4.2.1; namely

- the radiotoxicity inventory in different compartments and
- the radiotoxicity fluxes from several compartments.

The radiotoxicity performance indicators are presented for the sum of the whole nuclide spectrum as well as for Tc-99, I-129 and Se-79 as exemplifying nuclides. Tc-99 represents a strongly sorbing and solubility limited radionuclide, while I-129 represents a weakly sorbing radionuclide with unlimited solubility. Se-79 is characterised by a solubility limit, but no sorption. All three radionuclides have long half-lives, so radioactive decay plays only a minor role until 10^6 years.

Figures 4.26 to 4.33 show the temporal evolution of the radiotoxicity inventories as well as the respective radiotoxicity fluxes for the sum of all radionuclides, Tc-99, I-129 and Se-79 separately. Each radionuclide has its own properties, thus all radiotoxicity inventories have its characteristic behaviour, but as long as the canisters are intact, all radiotoxicity is located in the waste matrix. At the time of the canister failure after 2 500 years, the radiotoxicity in the precipitate for the sum of all radionuclides shows a sharp peak (fast increase followed by a fast decrease) and rises slowly again later on (cf. figure 4.26). This is an effect of the fast release of radionuclides from the instant release fraction.

During the mobilisation phase from the matrix up to about 10^6 years one fraction of the radionuclides is dissolved in the container water and released into the clay afterwards while another fraction is precipitated due to solubility limits. The individual sorption properties influence the time and fraction of transfer to the successive inventory additionally. It is remarkable that from about 10^6 years on, the main part of the radiotoxicity inventory is retained in the geotechnical barrier; i. e. the radiotoxicity inventory in the bentonite (solid red line) nearly coincides with the total radiotoxicity inventory (dashed black line). Further significant fractions of the total radiotoxicity inventory are kept in the container water or the precipitate up to the end of the simulated test case.

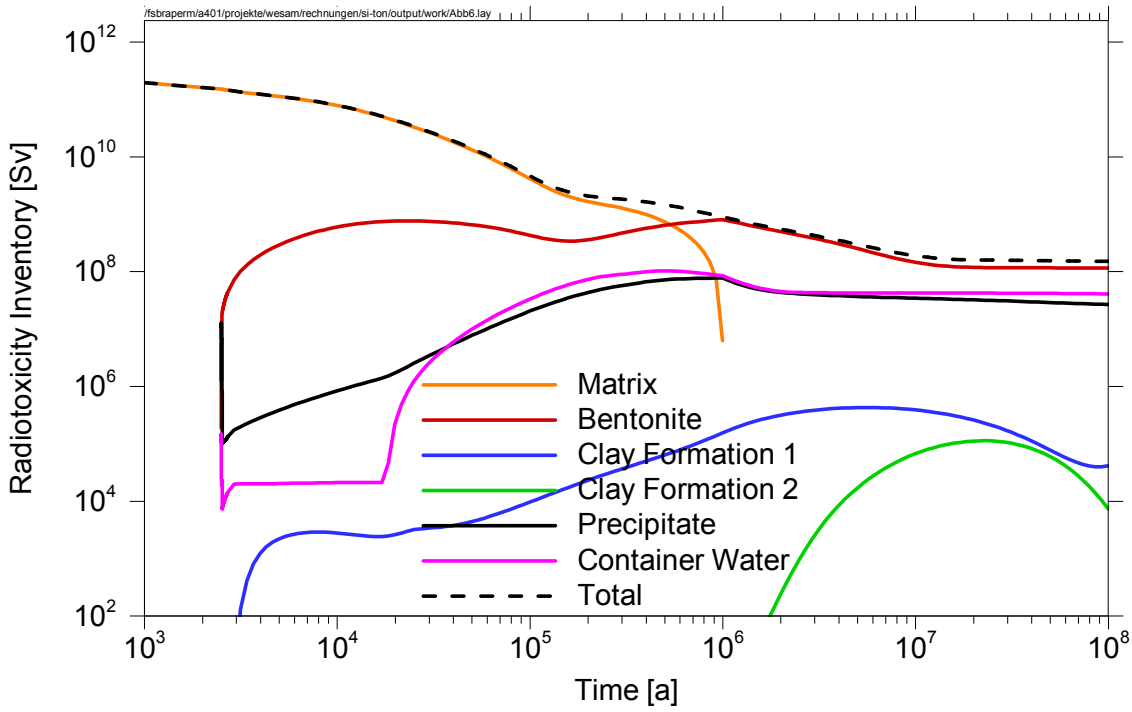

Fig. 4.26 Temporal evolution of radiotoxicity inventory of all radionuclides in different compartments

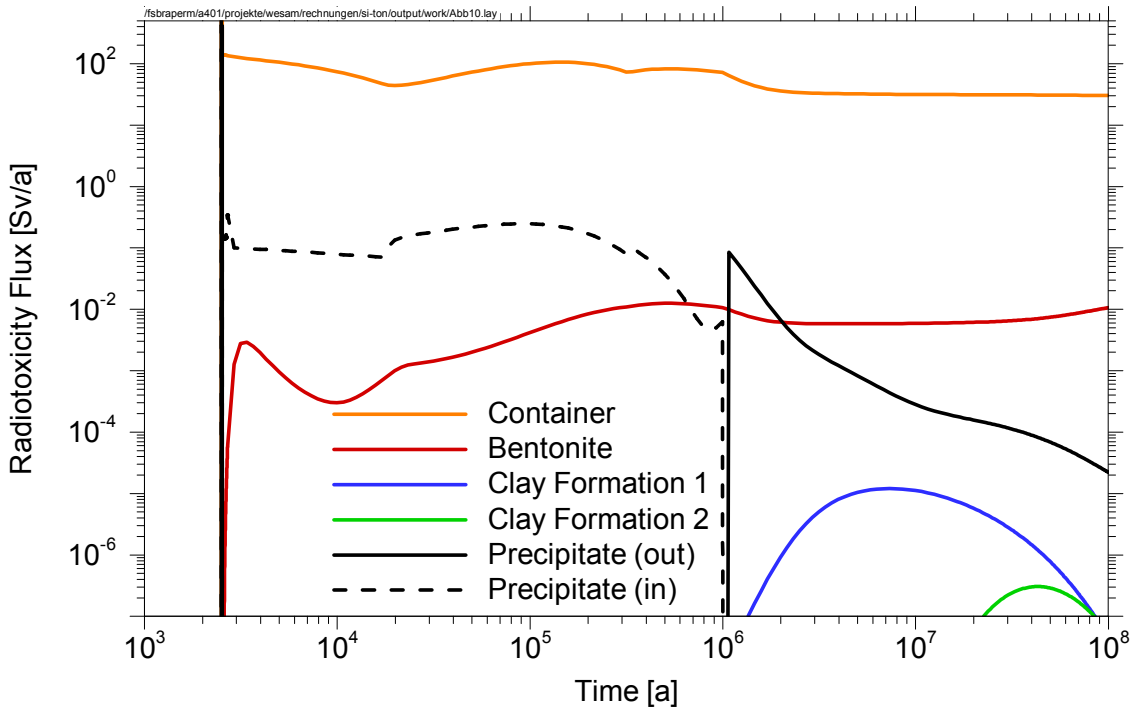

Fig. 4.27 Temporal evolution of radiotoxicity flux from different compartments for all radionuclides

The radiotoxicity flux for all radionuclides (cf. figure 4.27) from the container remains at a high level throughout the whole examined time period of 10^8 years. This is mainly due to a flux of Pb-210, which is constantly produced by its mother nuclides in the Uranium decay series being still present in the precipitate. While all the mother radionuclides have reached their solubility limit, Pb-210 remains below its solubility limit and is released from the container as it is produced at a constant rate in decay equilibrium. Thus the flux out of the bentonite does not decrease at the end of the observed period as all other pictured radionuclides do.

The evolution of precipitate's inventory described before is verified also: The peak of the outflow out of precipitate confirms the one observed for the inventory immediately after container failure. During the mobilisation phase, i. e. up to about 10^6 years, there is an inflow into the precipitate, indicating the accumulation of the radionuclides by the precipitate as well as the increase of its inventory. Afterwards the outflow decreases the precipitate's inventory for the rest of simulation.

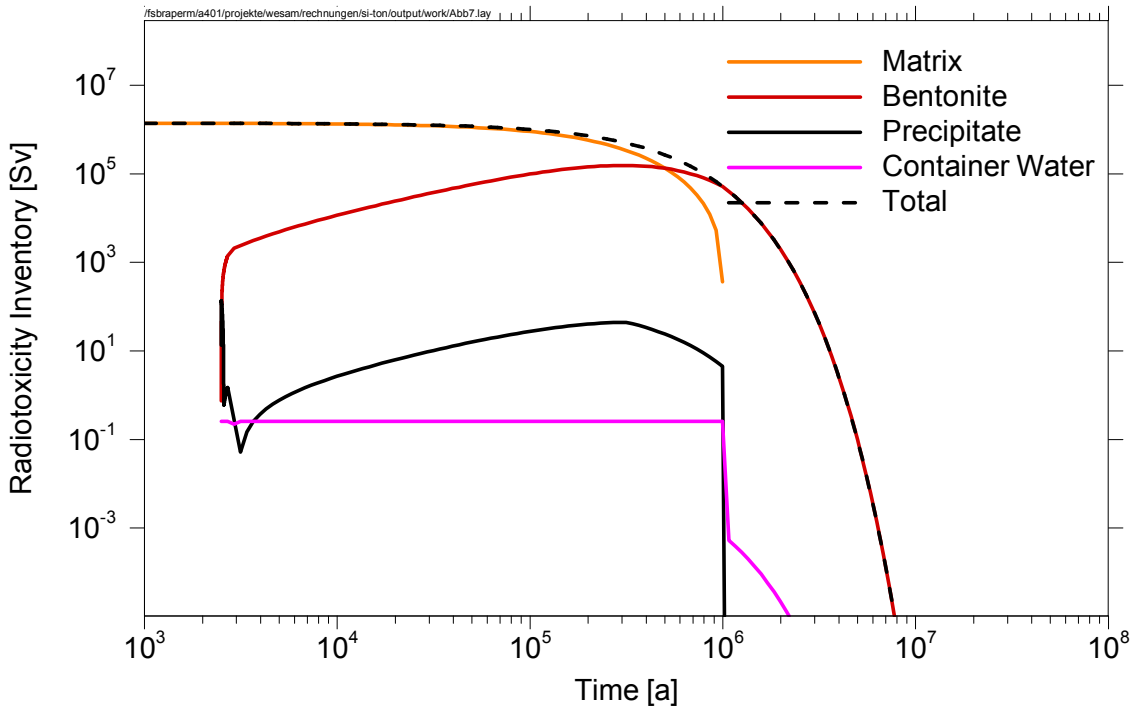

Fig. 4.28 Temporal evolution of radiotoxicity inventory of Tc-99 in different compartments

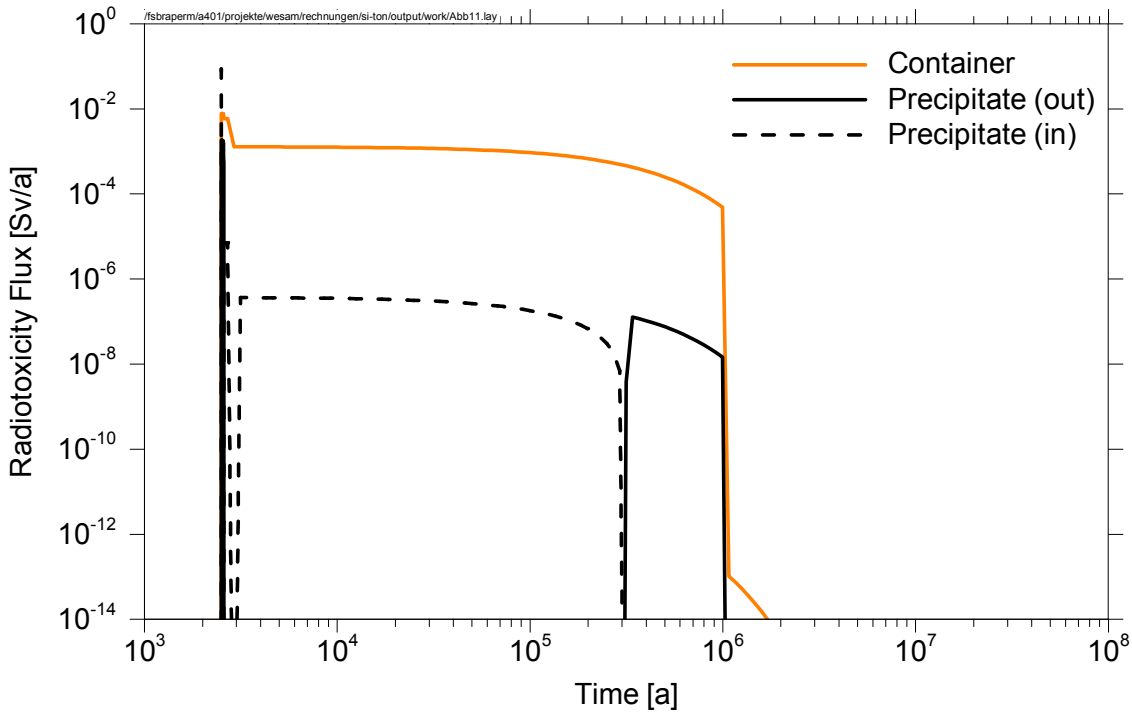

Fig. 4.29 Temporal evolution of radiotoxicity flux from different compartments for Tc-99

Figure 4.28 shows the radiotoxicity inventory of Tc-99 in the different compartments. The constant radiotoxicity in the container water is caused by its solubility limit. The remaining mobilised fraction not dissolved in the container water increases the inventory in the precipitate during the mobilisation phase. The strong sorption of Tc-99 continuously leads to a high concentration gradient between the container water and the bentonite pore water and therefore causes a rather high increase of Tc-99's inventory in the bentonite (cp. figure 4.32). In contrast to all other shown radionuclides, the strongly sorbing Tc-99 is retained completely in the geotechnical bentonite barrier demonstrated by no inventory in the succeeding compartments as well as coinciding curves of bentonite's and total inventory after the end of release out of the container at about 10^6 years.

For Tc-99 one can see in figure 4.29 a slightly increasing flux out of the container for the first hundred years after canister failure resulting from the instant release fraction. This effect is accompanied by the initial inflow into the precipitate and an intermediate outflow off the precipitate at the very beginning (just visible as two narrow peaks). The temporally next inflow into the precipitate is caused by the release from the metal parts and ends after a few hundred years. Finally, the precipitate gets an inflow lasting up to about $3 \cdot 10^5$ years by that fraction released from the matrix, but not dissolved in the container water due to the solubility limit of Tc-99. The aforementioned high concentration gradient on the interface between container water and bentonite pore water due to sorption causes a high radionuclide flux (out of the precipitate and) into the container water to keep its level on the sorption limit.

As pointed out for figure 4.28 the strongly sorbing tracer Tc-99 is more or less completely retained within the geotechnical bentonite barrier, proved by the missing radiotoxicity fluxes out of any clay compartment as shown in figure 4.29.

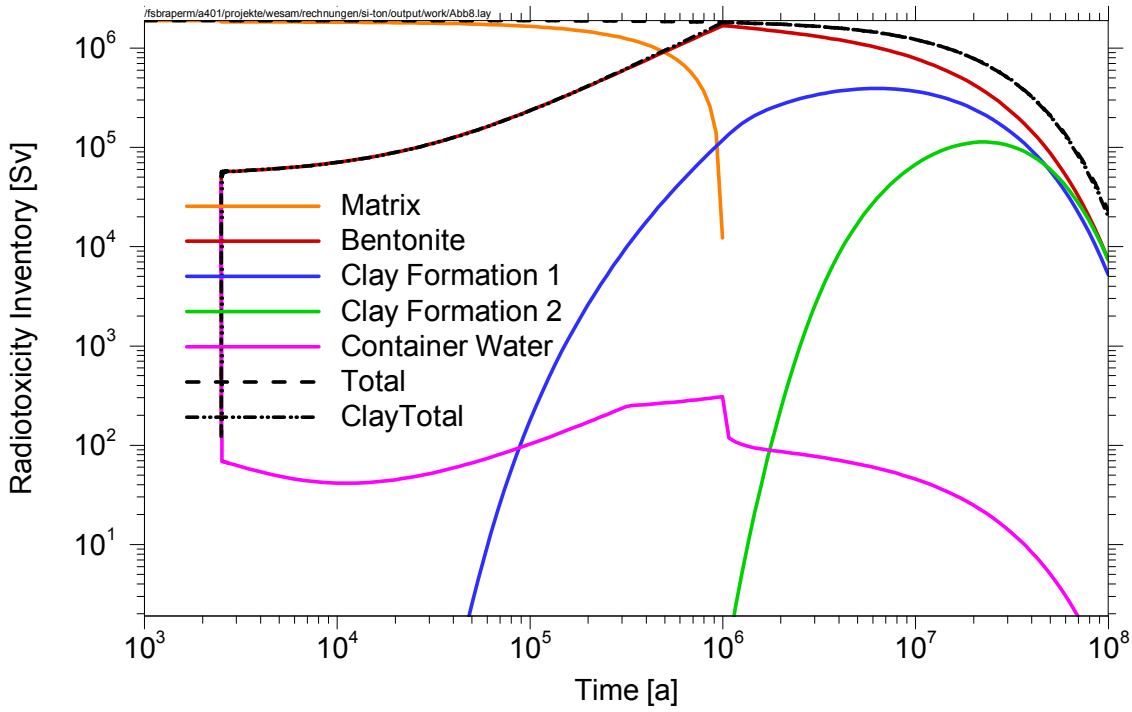

Fig. 4.30 Temporal evolution of radiotoxicity inventory of I-129 in different compartments

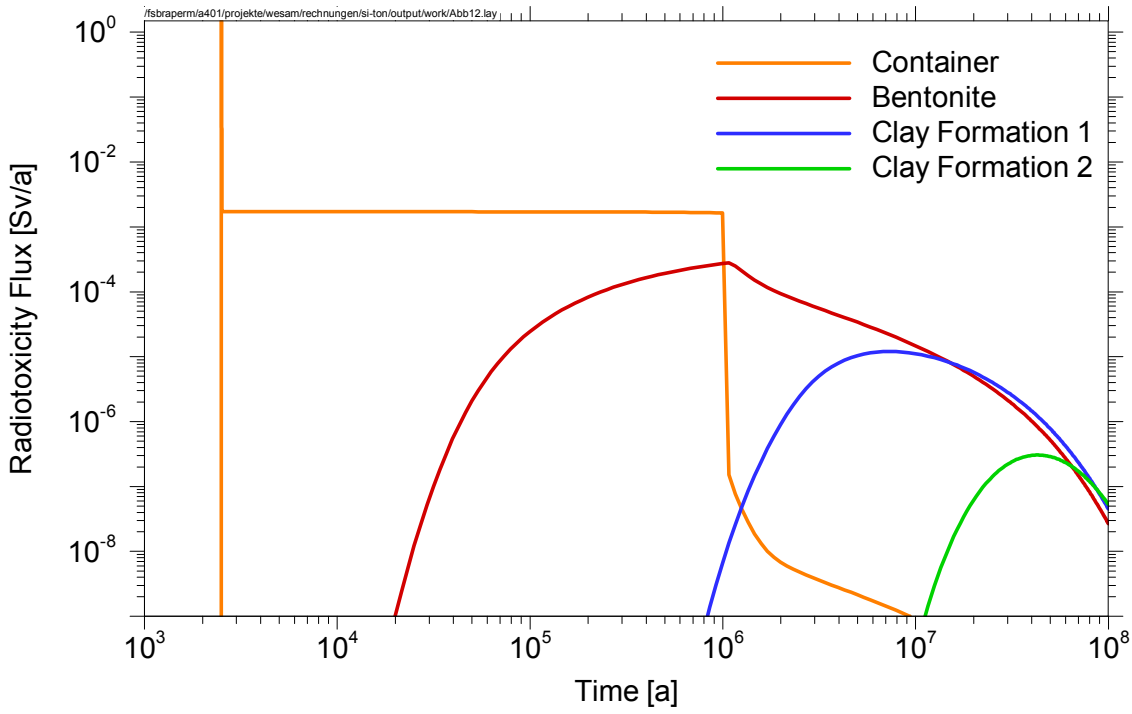

Fig. 4.31 Temporal evolution of radiotoxicity flux from different compartments for I-129

I-129 as non-solubility-limited tracer is completely dissolved in the container water, thus no radiotoxicity inventory in the precipitate occurs (cf. figure 4.30): Directly after failure of the canister, a high concentration in the container water also leads to a high radiotoxicity inventory in the bentonite. The intermediate decrease of the container water's inventory is caused by the ending release from the metal parts, the following increase of its inventory results from the long term dissolution rate of the waste matrix. The radiotoxicity inventory in the container water decreases not before the end of mobilisation. For lack of sorption of I-129 in any compartment, this radionuclide is transferred to all succeeding clay compartments.

At the very beginning, the radiotoxicity flux of I-129 out of the container, as shown in figure 4.31, is determined by the instant release fraction; afterwards by the release from the matrix. After 10^6 years, the radiotoxicity flux of I-129 from the container is controlled by the low concentration difference between the container water and the clay pore water. The decrease of the radiotoxicity inventories and fluxes of I-129 in and from all compartments for very late times is mainly determined by the radioactive decay.

Figure 4.32 exposes the solubility limit of Se-79 immediately after canister failure by the constant container water's inventory, because the concentration of Se-79 in the container water cannot exceed the characteristic limit. The mobilised, but due to the aforementioned solubility limit not dissolved fraction increases the inventory of the precipitate as long as the mobilisation does not come to an end at 10^6 years. In contrast to Tc-99, the transfer of the non-sorbing Se-79 to the succeeding compartments occurs earlier.

As specified in the release characteristics of Se-79 /WOL 09/ no release of the metal fraction occurs in figure 4.33 on the one hand, on the other hand the radiotoxicity flux off the container's inventory is smaller than the one of Tc-99 pictured in figure 4.29. The inflow into the precipitate of Se-79 up to about 10^6 years proves the already given explanation that the mobilised Se-79 is accumulated in the precipitate. Afterwards, the outflow from the precipitate into the container water keeps its concentration level on the sorption limit. This effect ends not before the precipitate is completely used up after 10^7 years. Another remarkable difference to figure 4.29 is the occurrence of the radiotoxicity fluxes out of all existing clay compartments due to the lack of sorption for Se-79 in contrast to Tc-99.

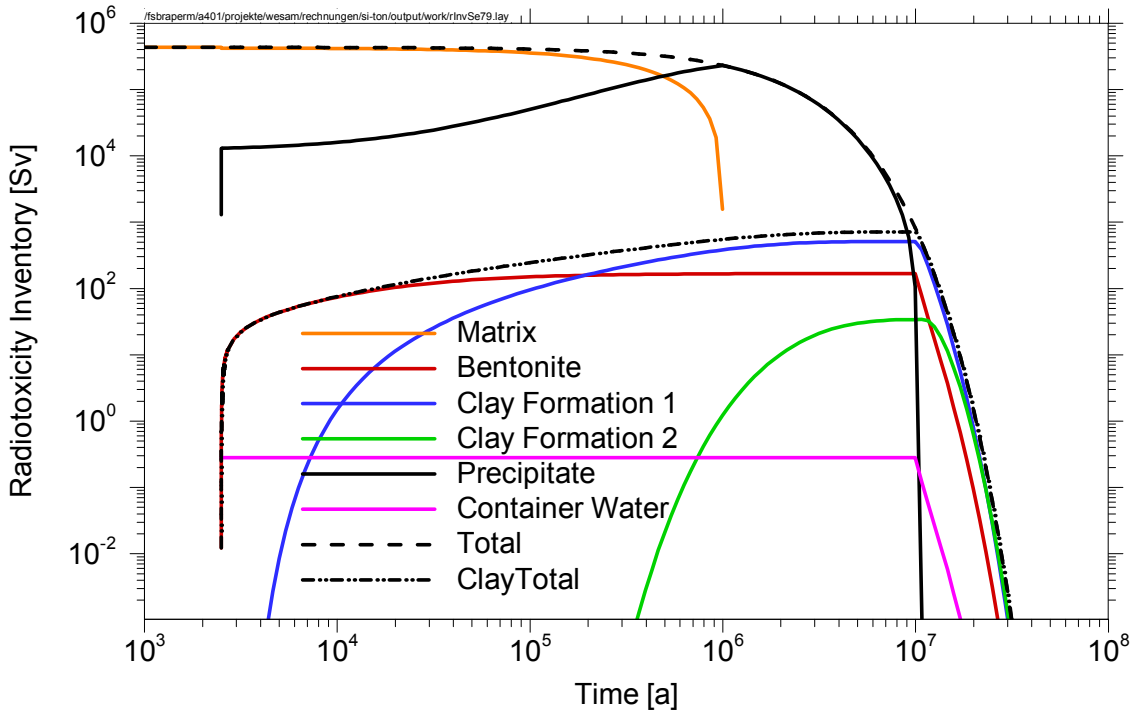

Fig. 4.32 Temporal evolution of radiotoxicity inventory of Se-79 in different compartments

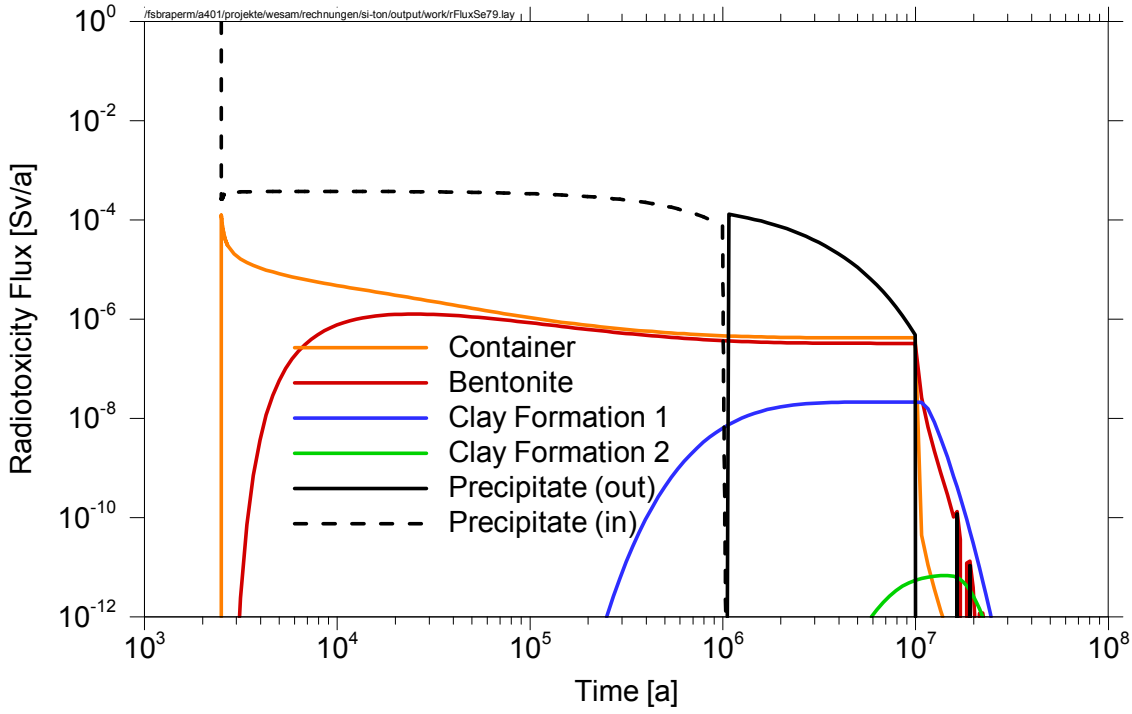

Fig. 4.33 Temporal evolution of radiotoxicity flux from different compartments for Se-79

4.2.3 Results from the probabilistic simulations for the dose as safety indicator

We applied the EFAST method to two Performance Assessment (PA) models for repositories in rock salt. One of these models describes a repository for high-level waste (HLW/SF) and the other one for low- and intermediate-level radioactive waste (LLW/ILW). Both models show typical important properties of a PA model. Firstly, the distribution of the calculated radiation exposure is highly skewed and heavily-tailed and typically spans over several orders of magnitude. Secondly, the systems show non-linear and non-monotonic behaviour. The PA model for the LLW/ILW repository additionally depends on discrete and quasi-discrete parameters.

Major deficiencies of FAST to deal with influential (quasi-) discrete input parameters and with highly skewed and heavily tailed outputs were identified with these two PA models which affected the stability of the sensitivity indexes. Nevertheless, important parameters could be determined for these two PA models (see sections 2.6.3.4 and 3.2). This chapter investigates whether the EFAST method works better for a PA model for a HLW repository in clay that does not include (quasi-) discrete parameters and produces smaller and less scattered peak doses. To verify the EFAST results, CSM (Contribution to the Sample Mean) plots and scatterplots were generated from the annual peak dose and results were compared to the EFAST results. The EFAST results were also compared to results from the rank based methods Spearman's rank correlation coefficients (SPEA), Partial Rank Correlation Coefficients (PRCC), Standardised Rank Regression Coefficients (SRRC) and the Smirnov test (SMIR). Apart from the annual radiation dose, sensitivity indexes were also calculated from radiotoxicity fluxes and inventories (see section 4.2.4).

4.2.3.1 Description of the PA model

The test case represents a generic repository for high level waste in a consolidated clay host rock formation described in section 3.2.2.As model outputs the annual effective dose to an adult human individual is calculated with the software package EMOS. The computer code CLAYPOS is the clay module of the EMOS package for long-term safety analysis calculations for final repository systems. The EFAST samples were generated and analysed using SIMLAB 3.

Ten different samples were generated and used for the analysis. In two of these samples (1 989 and 3 965 simulations), 13 parameters were varied. In the rest of the samples (765, 1 525, 2 485, 4 965, 9 965, 9 965s, 19 965 and 19 995s), only 5 out of the 13 parameters were varied to better study performance and sample size required for the EFAST analysis. The samples 9 965s and 19 965s have the same setup as the samples with 9 965 and 19 965 simulations but were produced with a different seed. The selection of the 5 parameters was based upon previous results with the samples with 13 parameters. Third most important and two less important parameters were chosen from these investigations. **Tab. 4.20** lists the parameters along with their distribution types and ranges. The diffusion coefficients, sorption coefficients (K_d-values), porosities and solubilities in the near field are element-specific (compare section 3.2.2). Abbreviations of the parameters which are used in the figures and tables are also provided in the table.

Tab. 4.20 Parameter distributions and ranges of the parameters of the test case in clay (in the first column, both numbers of the parameters with the samples with 13 and 5 parameters are listed)

No.	Parameter	Abbreviation	Distribution	Minimum	Maximum
1	Container life [yr]		Uniform	1	5 000
2/1	Diffusion coefficient of the bentonite in region 1 [m^2/s]	Diff bentonite 1	Log uniform	$5.556 \cdot 10^{-11}$	$5.556 \cdot 10^{-9}$
3/2	Diffusion coefficient of the clay in region 2 [m^2/s]	Diff clay 2	Log uniform	$8.300 \cdot 10^{-12}$	$8.300 \cdot 10^{-10}$
4/3	Diffusion coefficient of the clay in region 3 [m^2/s]	Diff clay 3	Log uniform	$8.300 \cdot 10^{-12}$	$8.300 \cdot 10^{-10}$
5/4	K_d value of the bentonite in region 1 [m^3/kg]	K_d bentonite 1	Log uniform	4	400
6	K_d value of the clay in region 2 [m^3/kg]	K_d clay 2	Log uniform	2	200
7	K_d value of the clay in region 3 [m^3/kg]	K_d clay 3	Log uniform	2	200
8	Porosity of the bentonite in region 1 [-]	Porosity bentonite 1	Uniform	0.18	0.72
9	Porosity of the clay in region 2 [-]	Porosity clay 2	Uniform	0.06	0.24
10	Porosity of the clay in region 3 [-]	Porosity clay 3	Uniform	0.06	0.24
11	Solubility [mol/m^3]		Log uniform	$3 \cdot 10^{-7}$	$3 \cdot 10^{-5}$
12	K_d value of the aquifer [m^3/kg]	K_d aquifer	Log uniform	$5 \cdot 10^{-4}$	$5 \cdot 10^{-2}$
13/5	Transport velocity in the aquifer [m/yr]	Flow	Log normal	0.271	2.71

4.2.3.2 Analysis of the maximum dose rate

The investigations described in this chapter mainly regard peak values of the each simulation, independent of their times of occurrence (compare section 3.2.3.1).

Input and Output Analysis

Fig. 4.34 presents the time-evolution of the calculated dose rate for all simulations using the EFAST sample with 2 485 model runs. The majority of simulations predict very low dose rates, while a few ones lead to values which are about 10 times higher. As for the HLW salt test case in figure 3.4, the result is a skewed and heavily-tailed distribution of the calculated maximum values, which spans several orders of magnitude. This is illustrated with a frequency plot of the peak annual doses in figure 4.35. The frequency in figure 4.35 is normalised with respect to the number of runs. In comparison with the curves in figure 3.4, the ones in figure 4.34 in clay are rather smooth and less scattered. **Fig. 4.35** demonstrates that the normalised frequencies for the sample with 765 model runs fluctuate most for the different bins of annual peak dose. This may indicate that more than 153 runs per parameter are required for performing a proper analysis for the selected test case. The number of runs per parameter is computed from the number of simulations of the sample (i. e., 765 runs) divided by the number of parameters investigated (i. e., 5).

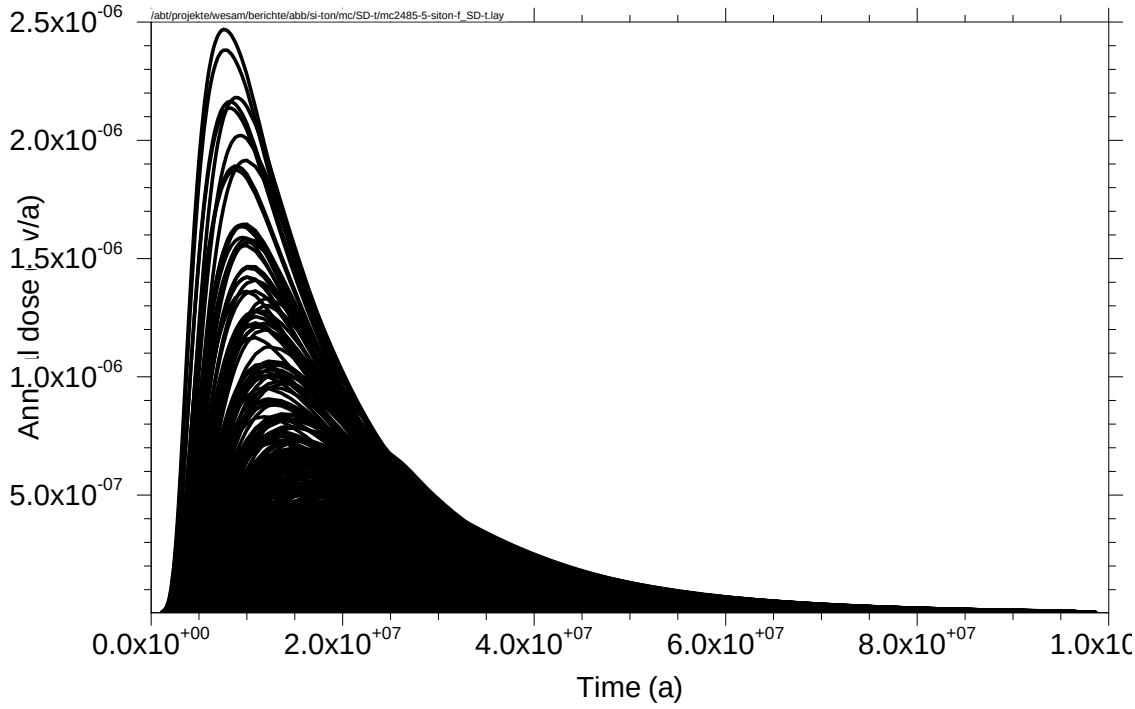

Fig. 4.34 Time evolution of the annual dose rate for the EFAST sample with 2 485 model runs

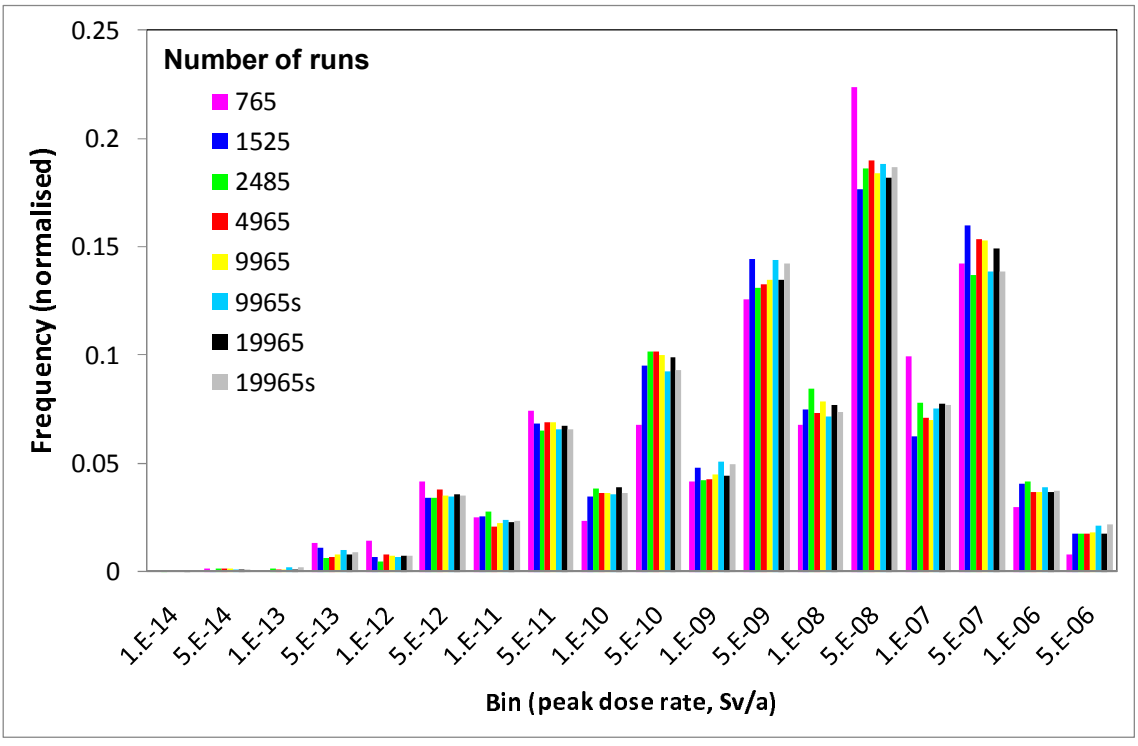

Fig. 4.35 Normalised frequency histogram of the peak dose rates for all EFAST samples with 5 parameters (the y-axis is normalised with respect to the number of runs)

Scatterplots

Figure 4.36 shows scatterplots for the EFAST sample with 4 965 model runs. For each of the 5 parameters, the calculated maximum dose rates are depicted versus the corresponding parameter values.

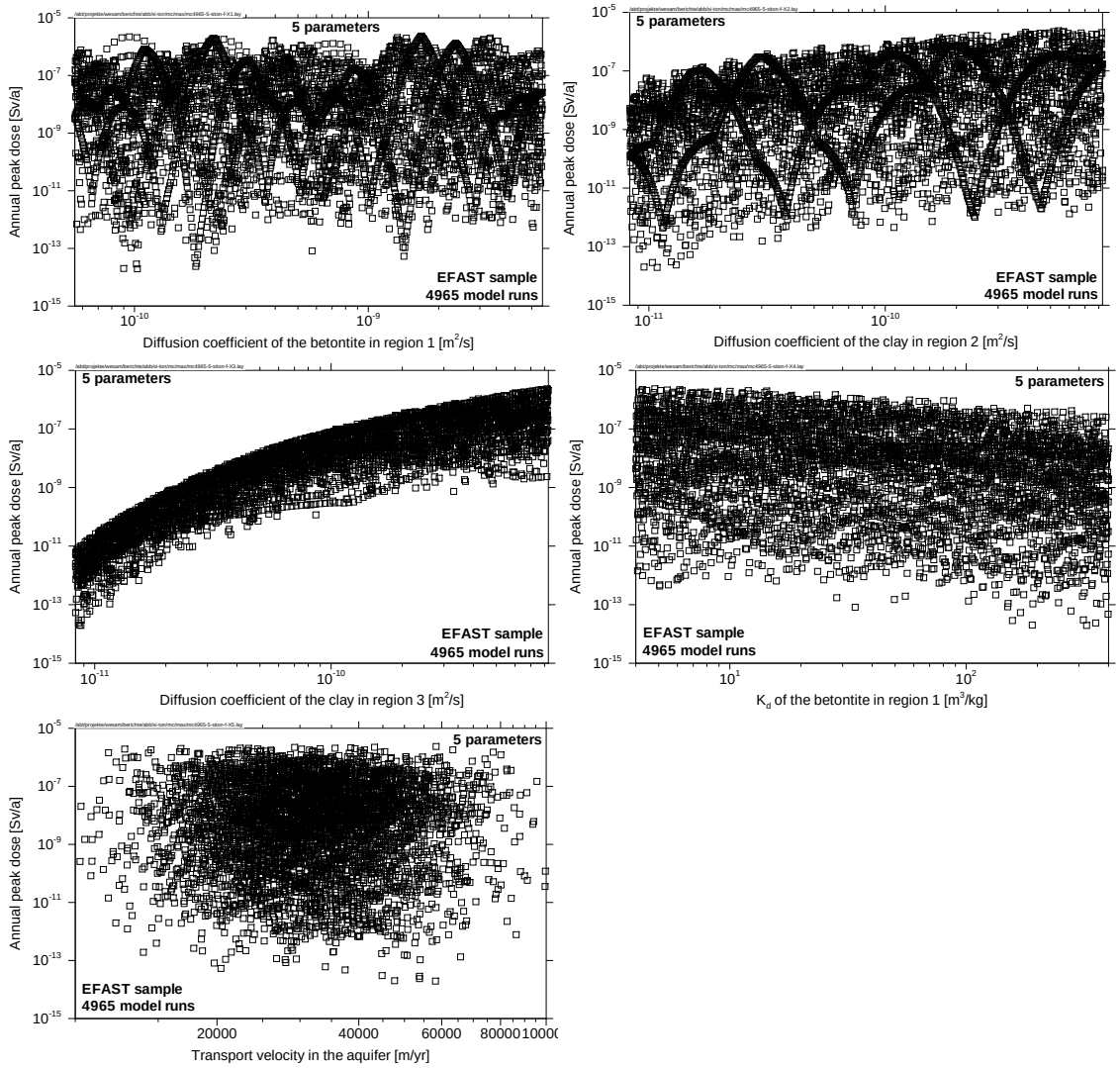

Fig. 4.36 Scatterplots for the 4 965 EFAST sample with 5 parameters

The third parameter (diffusion coefficient of the clay in region 3) shows a diagonal behaviour from the lower end to the upper end of the range. The scatter width of the second and fourth parameters (diffusion coefficient of the clay in region 2 and K_d value of the betontite in region 1) is larger. The diagonal of the fourth parameter goes downward, i. e., they are negatively correlated. The rest of the parameters are distributed more and less homogeneously all over the interval. Due its lognormal distribution, the fifth parameter shows a trend of accumulation of the peak values in the centre. For the

first and second parameter, a periodic development of the values can be recognised in figure 4.36.

Just from the appearance of the parameters in the scatterplots, it can be inferred that the diffusion coefficient of the clay in regions 2 and 3 and the K_d value of the betontite in region 1 are important, while the rest are less important since they do not have a great impact upon the model results.

CSM plots

Figure 4.37 represents CSM (Contribution to the Sample Mean) plots for the samples with 1 989 and 3 965 runs and 13 parameters and with 4 965 runs and 5 parameters. This figure demonstrates that the parameter with the most significant deviation from the diagonal is the diffusion coefficient of the clay in region 3, followed by the parameters diffusion coefficient of the clay in region 2 and K_d value of the betontite in region 1. This is in line with what could be seen from the scatterplots.

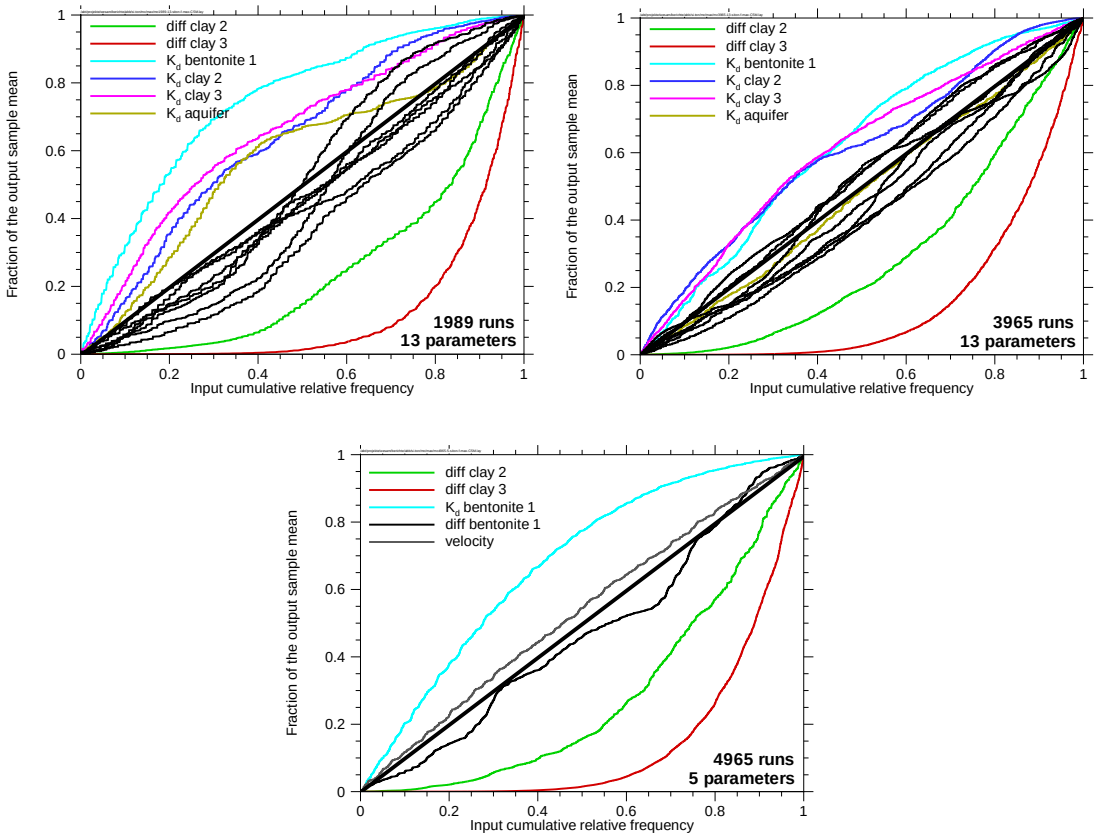

Fig. 4.37 CSM plots for the samples with 1 989 and 3 965 runs and 13 parameters and with 4 965 runs and 5 parameters

Figure 4.38 illustrates CSM plots of each of these 3 parameters in one plot of all 8 samples with 5 parameters. These plots demonstrate that the sample with 765 model runs are not representative, followed by the sample with 1 525 runs but to a less degree. In other words more than 305 simulations per parameter may need to be considered for a proper analysis. An indication of insufficient accuracy of the analysis is also given by the CSM plots of the samples with 1 989 and 3 965 runs and 13 parameters in figure 4.37. Although the development of the curves in figure 4.37 differs, they agree qualitatively. In these samples, 153 and 305 simulations per parameter were considered. The normalised frequency plot, however, indicates that 305 simulations per parameter may already be sufficient as the different bins of peak dose are as stable as the ones of the samples with a higher number of simulations per parameter (figure 4.35). The sample with 305 runs per parameter in figure 4.35 is the one with 1 525 simulations.

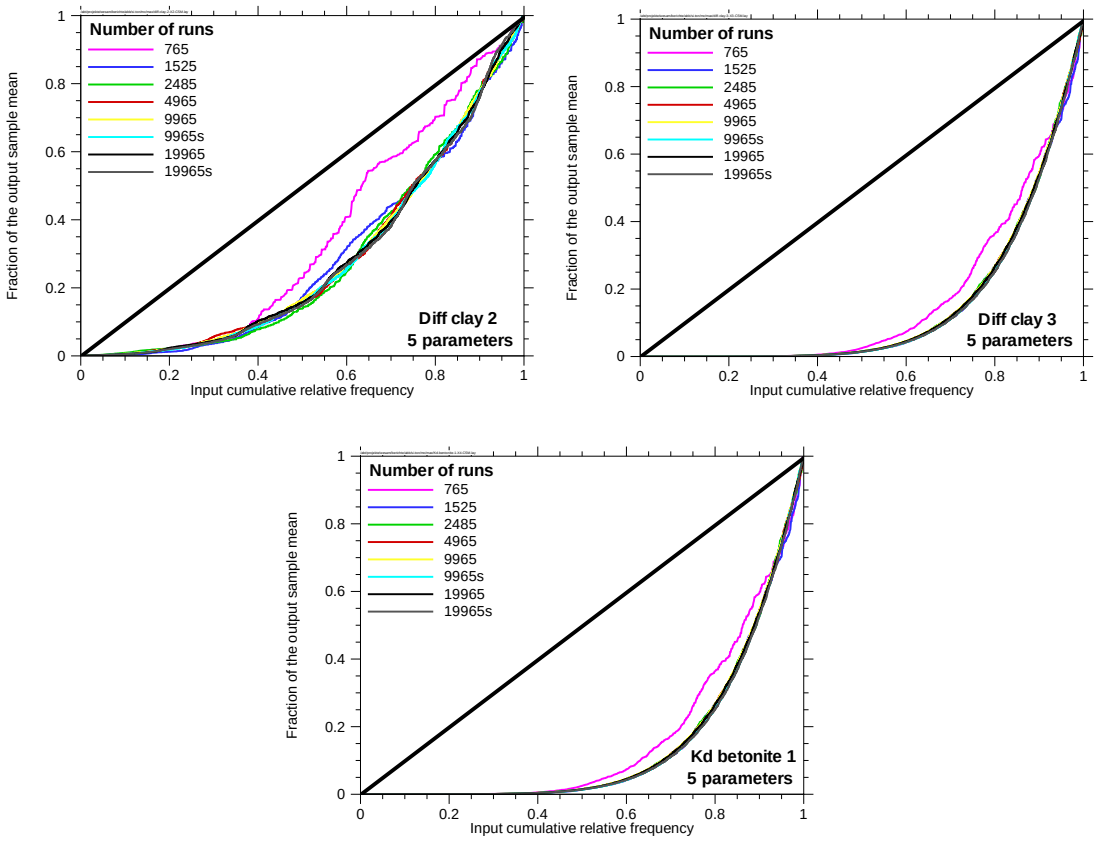

Fig. 4.38 CSM plots of the 3 parameters diffusion coefficient of the clay in regions 2 and 3 and K_d value of the betonite in region 1 in one plot of all 8 samples with 5 parameters

4.2.3.3 Time-dependent analysis

Random based analysis

The EFAST results were also compared to results from the rank based methods Spearman's rank correlation coefficients (SPEA), Partial Rank Correlation Coefficients (PRCC) and Standardised Rank Regression Coefficients (SRRC) as well as the Smirnov test (SMIR). **Tab. 4.21** lists the ranking results of these tests from a random sample with 1 989 simulations at maximum time and at $5 \cdot 10^6$, $1 \cdot 10^7$, $5 \cdot 10^7$ years. As for the EFAST results, the parameter diffusion coefficient of the clay in region 3 is the most important parameter. The next important parameters appear to be the diffusion coefficient of the clay in region 2, the K_d values of the clay in regions 3 and 2 and of the bentonite in region 1. This is not quite in agreement with the EFAST results (see next paragraph).

Tab. 4.21 Ranking results of a random sample with 1 989 simulations for the SPEA, PRCC, SRRC and SMIR tests at maximum time and $5 \cdot 10^6$, $1 \cdot 10^7$, $5 \cdot 10^7$ years

	Parameter	SPEA				PRCC				SRRC				SMIR			
		Maximum	$5 \cdot 10^6$	$1 \cdot 10^7$	$5 \cdot 10^7$	Maximum	$5 \cdot 10^6$	$1 \cdot 10^7$	$5 \cdot 10^7$	Maximum	$5 \cdot 10^6$	$1 \cdot 10^7$	$5 \cdot 10^7$	Maximum	$5 \cdot 10^6$	$1 \cdot 10^7$	$5 \cdot 10^7$
1	Diff clay 3	1	1	1	1	1	1	1	1	1	1	1	1	1	1	1	1
2	Diff clay 2	2	2	2	2	3	2	2	3	3	2	2	3	2	2	2	3
3	K_d clay 3	3	3	3	3	2	4	3	2	2	4	3	2	4	3	3	6
4	K_d clay 2	5	7	4	5	5	5	4	5	5	5	4	5	5	4	4	4
5	K_d bentonite 1	4	10	5	4	4	7	5	4	4	7	5	4	3	9	5	2
6	Porosity clay 3	6	9	9	6	6	8	7	6	6	8	7	6	6	5	6	5
7	Solubility	11	4	6	11	11	3	6	13	11	3	6	13	7	10	7	8
8	Diff bentonite 1	12	6	8	12	8	6	8	8	8	6	8	8	9	8	10	7
9	Porosity clay 2	7	13	10	7	7	9	9	7	7	9	9	7	10	11	9	12
10	Velocity	8	5	7	8	9	13	12	9	9	13	12	9	8	6	8	10
11	Container life	10	8	12	9	10	11	13	10	10	11	13	10	13	7	12	13
12	K_d aquifer	9	12	11	10	12	12	10	11	12	12	10	11	12	12	11	11
13	Porosity bentonite 1	13	11	13	13	13	10	11	12	13	10	11	12	11	13	13	9

EFAST analysis

Figures 4.39 and 4.40 indicate that the diffusion coefficient of the clay in region 3 is the most important parameter, reaching a first order index (SI1) of up to 0.65. The next important parameters (diffusion coefficient of the clay in region 2 and K_d value of the bentonite in region 1) reach SI1 values of up to 0.12. Since there is nearly no release to the biosphere before 10^6 years, the results become significant only for very long time frames.

The SI1 index of the diffusion coefficient of the clay in region 3 starts to increase at about $2 \cdot 10^5$ years and reaches its peak value at 10^8 years. This implies that especially at the end of the simulation time this parameter dominates the system behaviour. At about $1.8 \cdot 10^6$ years, there is a small peak of about 0.2. The SI1 index of the second most important parameter seems to also have two peak values at about the same times as the first important parameter. However, the second peak (value of 0.11) drops at $3 \cdot 10^7$ years. The SI1 index of the third parameter starts later at $3 \cdot 10^6$ years and also seems to reach its peak value at the end of the simulation.

The sensitivity indexes of total order (SIT), which include the effects of parameter interactions yield basically the same ranking of the parameters as the first-order indices (figures 4.41 and 4.42).

Parameter importance may be better determined by the time averaged sensitivity indices. Such indices may be more meaningful for the determination than those of discrete time points. The time averaged sensitivity indices are calculated from the sum of piecewise integrations of the 194 index values divided by the respective time interval. The piecewise integration is computed from an index value at a certain time multiplied by the time difference between this and previous time. Figure 3.12 shows the time averaged SI1 and SIT indices of the samples with 13 parameters and figure 4.44 those of the 5 parameters. The time averaged SI1 indices tell that the diffusion coefficient of the clay in region 3 is about 5 times more important than those of the diffusion coefficient of the clay in region 2 and of the K_d value of the bentonite in region 1. The averaged SI1 indices of the latter two parameters indicate that these have about the same importance. The time averaged SIT indices give the same message with the difference that the time averaged SIT index of the first important parameter is only about 3 times more significant than those of the other two parameters and not 5 times. Apart from this the time average SI1 index of the diffusion coefficient of the clay in region 2 is a little

higher than the ones of the K_d value of the bentonite in region 1. The time averaged SI1 and SIT indices of the samples with 13 parameters indicate that there may be two other less important parameters which are the K_d value of the clay in region 3 and the porosity of the clay in region 3 but the averaged indices are rather small.

The parameter importance of the EFAST analysis (diffusion coefficient of the clay in region 3, diffusion coefficient of the clay in region 2 and K_d value of the bentonite in region 1) is confirmed by the CSM plot and scatterplots. The rank based methods agree with the importance of the parameter diffusion coefficient of the clay in regions 2 and 3.

As already observed by means of the normalised frequency plot and the CSM plots, more than 153 and 305 simulations for each parameter may be required to perform a proper analysis, respectively (figures 4.40, 4.42 and 4.44). This is confirmed by the sensitivity indexes of the two samples with 1 989 and 3 965 simulations and 13 parameters (figures 4.39, 4.41 and 4.43) which imply that there were 153 and 305 simulations per parameter considered. Especially at the beginning of the release, the convergence of the SIT indexes is not as good as that of the SI1 indexes.

The skewness of the distribution can be illustrated with the variance of the peak dose. Already very few runs (up to 1.5 % of the simulations of each set) account to 50 % of the total variance (**Tab. 4.22**).

The convergence of the indexes for the investigated model in this study is better compared to previous EFAST analyses for PA models in rock salt (see chapters 2.6.3.4 and 3.2). The important difference between the salt and clay PA models is that in the former model, the skewed distributions of the annual dose of the different simulations is much higher (factor up to 520, compare figures 3.4 and 4.34) and more scattered than in the latter model. In other words, parameters of the PA model in the clay formation create a more continuous model output with narrower bandwidth. As a result, the variance of the model output is more stable, producing more stable sensitivity indexes.

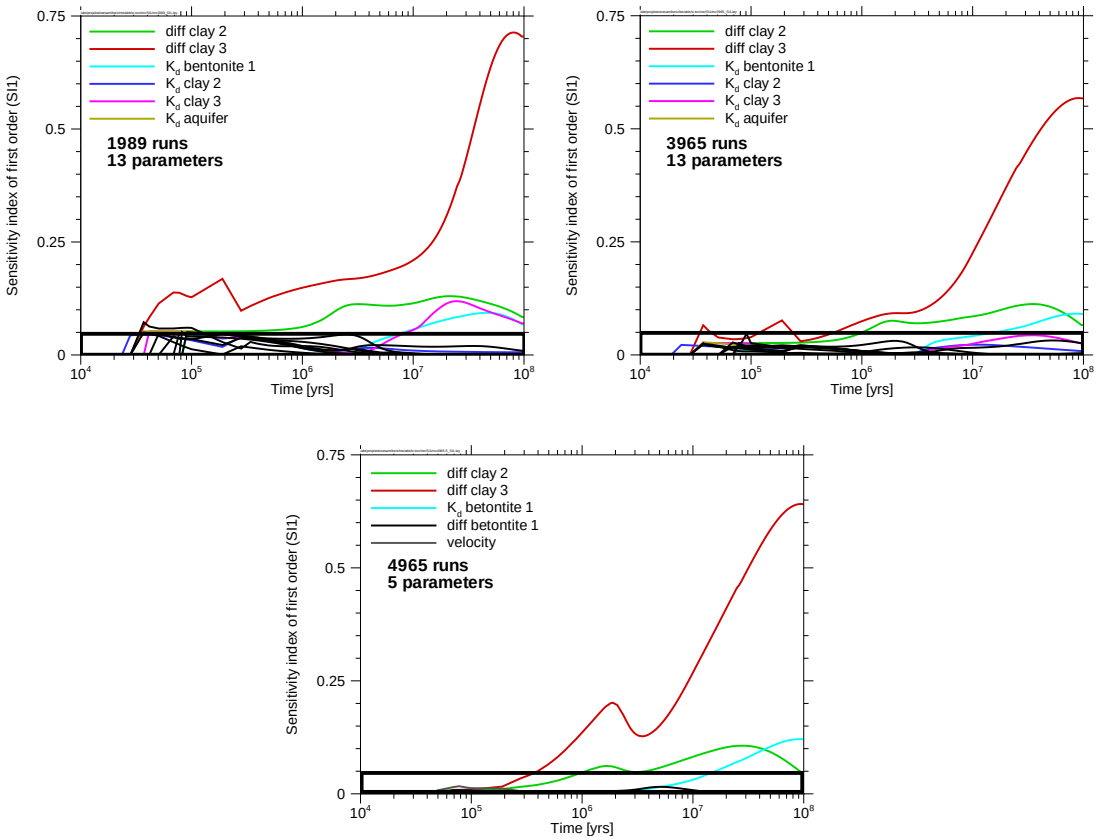

Fig. 4.39 Sensitivity indexes of first order for the samples with 1 989 and 3 965 runs and 13 parameters and with 4 965 runs and 5 parameters

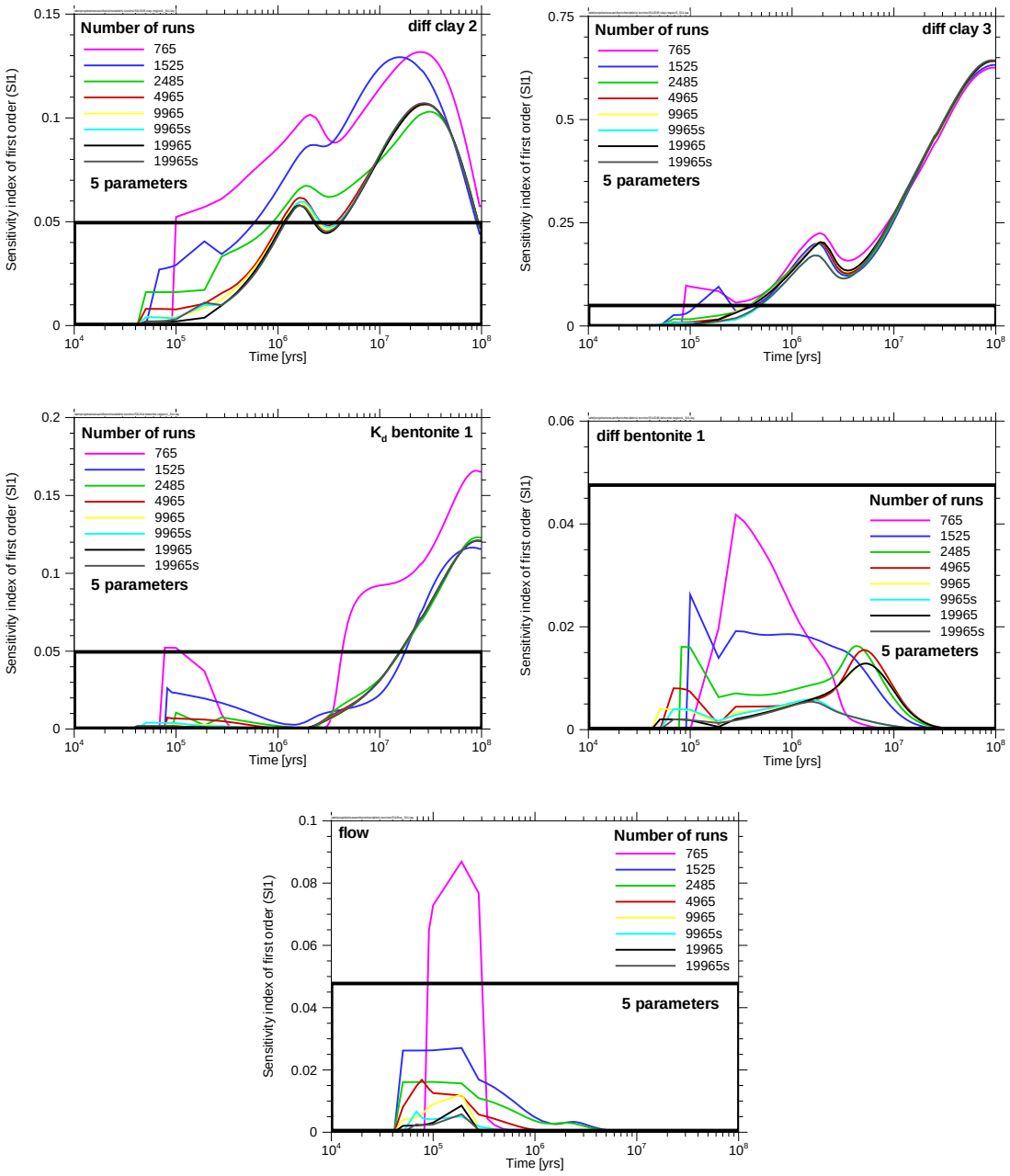

Fig. 4.40 Sensitivity indexes of first order for all 8 samples with 5 parameters

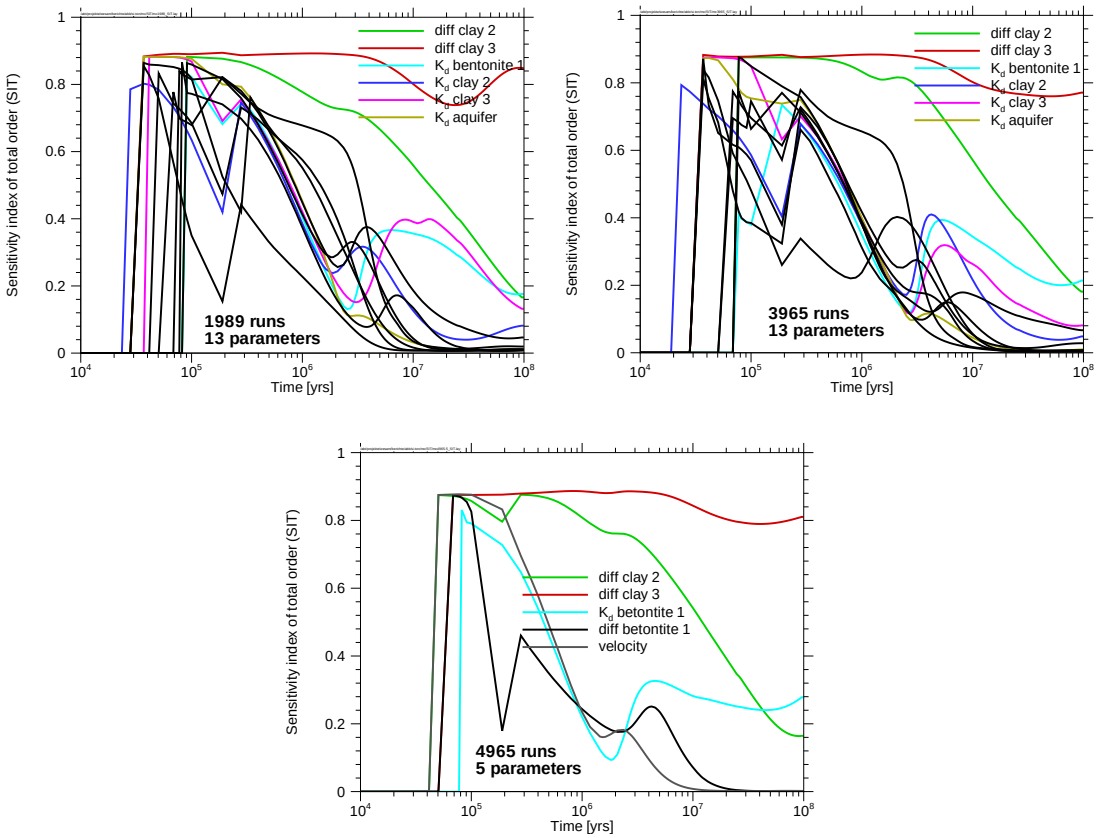

Fig. 4.41 Sensitivity indexes of total order for the samples with 1 989 and 3 965 runs and 13 parameters and with 4 965 runs and 5 parameters

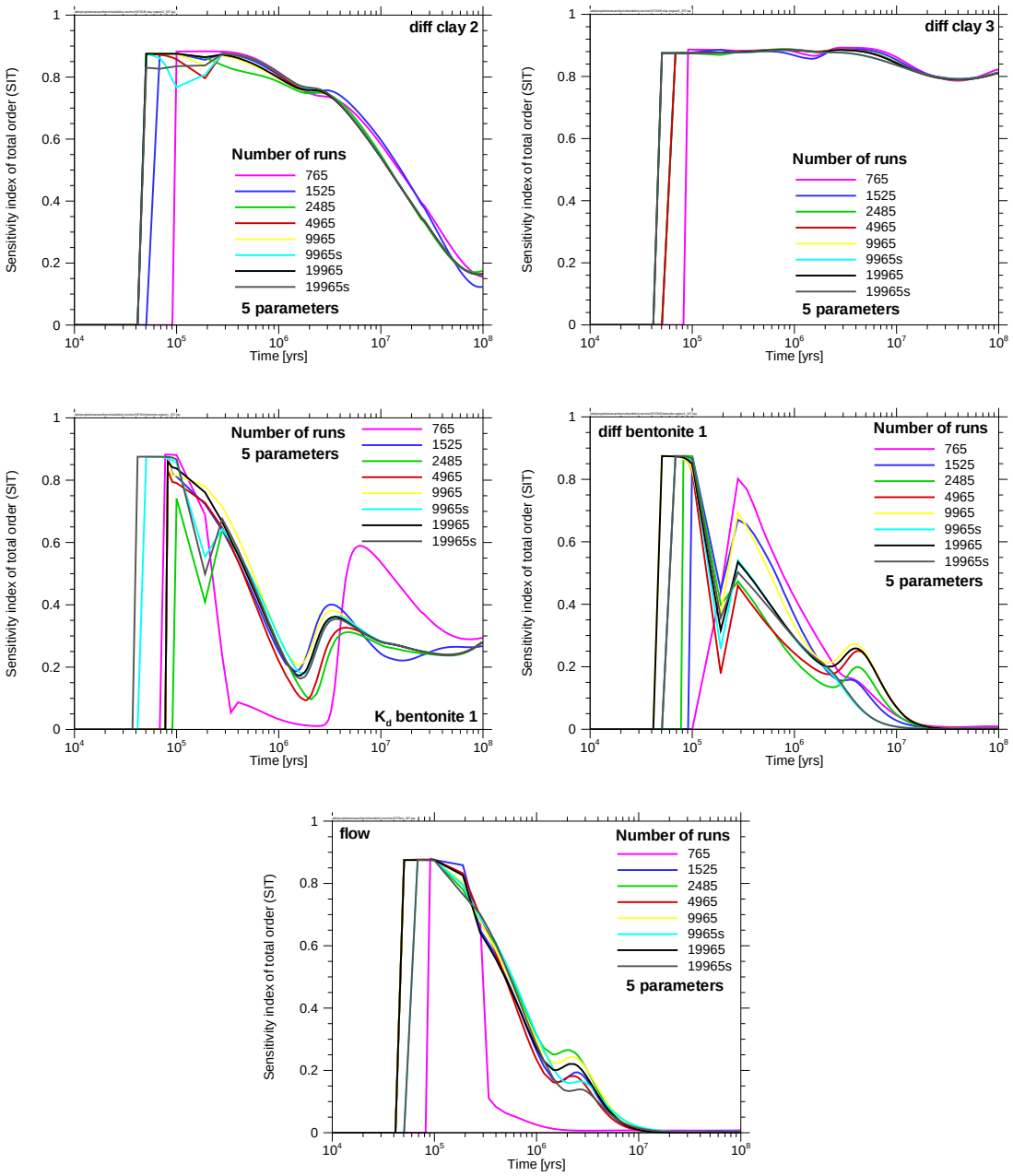

Fig. 4.42 Sensitivity indexes of total order for all 8 samples with 5 parameters

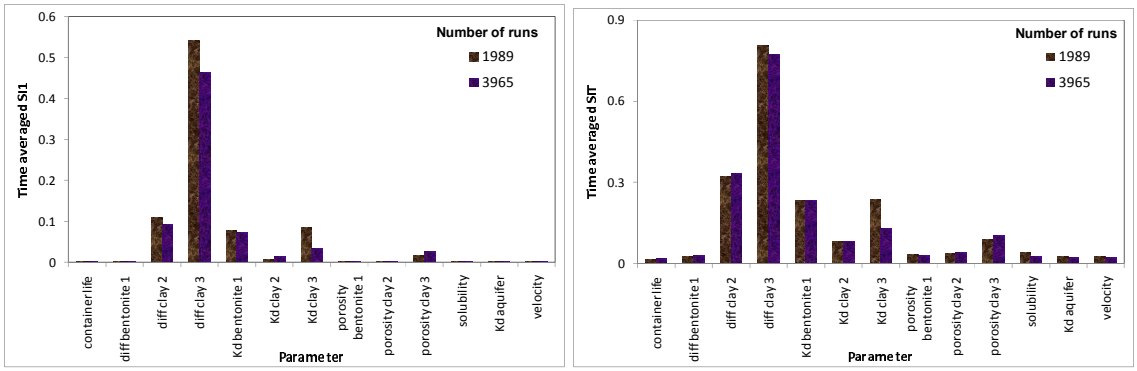

Fig. 4.43 Time averaged SI1 and SIT indices of the samples with 13 parameters

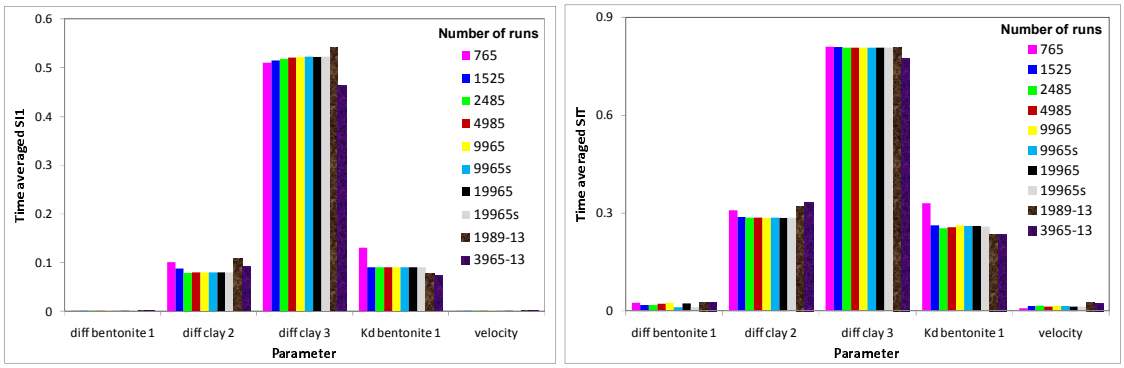

Fig. 4.44 Time averaged SI1 and SIT indices of all samples representing only 5 parameters (abbreviations 1989-13 and 3965-13 refer to the samples with 1 989 and 3 965 runs and 13 parameters)

Tab. 4.22 Fractions of runs which contribute about 50 % to the variance

Sample with 5 parameters	50 % of variance	Number of runs	Fraction of runs
765	50.05	9	1.18
1 525	50.22	18	1.18
2 485	50.23	30	1.21
4 965	50.40	50	1.25
9 965	50.12	124	1.24
9 965s	50.05	152	1.53
19 965	50.05	248	1.24
19 965s	50.06	305	1.53

4.2.3.4 Conclusions

This chapter presented another investigation on whether the EFAST method is suitable for use in long-term safety assessments of geological repositories for radioactive wastes. A generic test case for a HLW repository in a clay formation was selected. This test case includes no (quasi-) discrete parameters and produces a less skewed and

less scattered distribution of the annual dose than the test cases in salt. To verify the EFAST results, they were compared to results from scatterplots, CSM plots and random based methods (SPEA, PRCC and SRRC) as well as the Smirnov test.

As the EFAST results, the scatterplots and the CSM plots suggest that there are three important parameters which are the diffusion coefficient of the clay in regions 2 and 3 and K_d value of the bentonite in region 1. Results of the rank based methods and the Smirnov test also suggest that the diffusion coefficient of the clay in regions 2 and 3 are important. After the ranking of these two parameters it is unclear whether there are other important parameters.

The EFAST sensitivity indices of first order (SI1) demonstrate that there is clearly one most important parameter which is the diffusion coefficient of the clay in region 3. Its magnitude goes up to 0.65 at the end of the simulation time which indicates that the PA model is dominated by this parameter. The SI1 indices of the other two important parameters are by far smaller, i. e., up to 0.12. The time development of the SI1 index of the parameter diffusion coefficient of the clay in region 2 gives the impression that this parameter is the second most important parameter, followed by the K_d value of the bentonite in region 1. However, the time averaged indices suggest that these two parameters are of equal importance. Generally, when assessing the overall importance of the parameters, one can derive clearer messages from the time-averaged indices since these represent all values of the indices and not just of one discrete point in time. The time averaged SI1 indices indicate that the most important parameter is 5 times more significant than the other two parameters. The two important parameters diffusion coefficients of the clay in regions 2 and 3 have a first peak at around $1.8 \cdot 10^6$ years.

The time development of the sensitivity indices of total order (SIT) and the time averaged SIT indices indicate that importance of parameter interactions follow the same ranking of the parameters as of the SI1 indices. The time average SIT indices of the most important parameter are about 3 times higher than those of the other two parameters.

The convergence of the EFAST sensitivity indexes suggests that the distribution of the model output can greatly influence the performance of the EFAST method. In other words, reduced skewness and scatter of the output may ensure convergence of the sensititvity indexes. More than 305 runs for each parameter are required to obtain convergence of the sensitivity indexes. Also the CSM plots suggested that so many runs

are required to perform a proper analysis. The normalised histogram indicates that 305 runs per parameter may already be sufficient. This implies that the EFAST method may not necessarily require more simulations than other methods as long as the model output has a “smooth” behaviour and its distribution is not too much skewed and tailed.

The advantage of the EFAST method over the rank based methods is that they clearly show which parameters are important and which are not. The rank based methods only give a ranking of importance but cannot tell something about the magnitude of importance. In addition, parameter ranking from rank based tests may be different from the ones of the EFAST method. This was indicated by results of the investigated test case. Another important advantage of the EFAST method over the rank based methods is that it can better handle problems which show nonmonotonic and nonlinear behaviour.

The scatterplots and the CSM plots provide a quick insight into which parameters are important. However, they do not give quantitative information like the EFAST method does.

In conclusion, the EFAST results of the investigated PA model in clay seems promising to provide more insight into a safety case than rank based or regression or correlation methods or scatterplots or CSM plots can do.

4.2.4 Results from the probabilistic simulations for radiotoxicity fluxes and inventories as performance indicators

An EFAST analysis was conducted for four radiotoxicity performance indicators (annual radiotoxicity fluxes from the bentonite, clay formations 1 and 2 and inventory in the bentonite). In addition, CSM plots from the peak values were generated for the flux indicators to verify the EFAST results. These four indicators are explained in section 4.2.1. The selection of the four indicators was associated with the objective to investigate potential different parameter importance in the different compartments as well as of the considered indicator itself (annual radiotoxicity flux and inventory).

The model output of the four different indicators was calculated with the software package EMOS and the module CLAYPOS as described in Section 4.2.3 but without the module for the far field (CHETLIN) since this one was not required for the calculation of the indicators. The two parameters for the far field, i. e., the K_d value of the aquifer and transport velocity in the aquifer in **Tab. 4.20**, did not need to be considered in the analysis. Thus, only 11 parameters instead of 13 parameters were varied. The radiotoxicity performance indicators are computed from the sum of the whole nuclide spectrum.

Two EFAST samples (3355 and 5467 runs) for the 11 parameters were generated and analysed with SIMLAB 3 (see section 4.2.3). In these samples, 305 and 497 runs per parameter are regarded. In section 4.2.3, it was shown that for most of the sensitivity indices of the annual radiation dose to the biosphere as well for the normalised histogram and for most of the CSM plots of the annual peak dose to the biosphere, 305 simulations per parameter were sufficient. Therefore, it was worthwhile to investigate whether this will be the case for the CSM plots and sensitivity indices of the additional indicators too.

4.2.4.1 EFAST analysis

Results of the EFAST analysis show that significance of parameters is different for the four indicators. An overview of important parameters for all indicators as well as for the annual radiation dose to the biosphere is provided in **Tab. 4.23**. The ranking of most of the parameters in this table is based upon the time averaged based SI1 indices. The cut off criterion for the parameter ranking in **Tab. 4.23** is about 0.05. It is assumed that

parameters having indices below this value do not have a significant influence upon the system behaviour.

Tab. 4.23 Important parameters of the 4 indicators and of the annual radiation exposure to the biosphere based upon the EFAST SI1 indices

Parameter	Flux from the bentonite	Flux from the clay formation 1	Flux from the clay formation 2	Inventory in the bentonite	Annual radiation exposure to the biosphere (see Section 4.2.3)
Container life	6^v			4^v	
Diff bentonite	1			3	
Diff clay 1	3	$3 / 1^v$	2		2
Diff clay 2		$1 / 2^v$	1		1
K_d bentonite	3	$1 / 2^v$	2	2	2
K_d clay 1		4			
K_d clay 2					
Porosity bentonite	3				
Porosity clay 1					
Porosity clay 2					
Solubility	1			1	

^{v} visual determination

Time averaged sensitivity indices of first order (SI1) of all indicators and samples are demonstrated in **Fig. 4.45** and **Fig. 4.46**. Note that for the parameter container life only seven values for the indices are computed before 10^4 years for the discrete time points 1, 1 000.9, 3 000.7, 5 000.5, 7 000.3 and 9 000.1 years. EFAST sensitivity indices of first order (SI1) for all indicators and samples are showed in **Fig. 4.47**. Solid and dash lines represent samples with 3 355 and 5 467 runs, respectively.

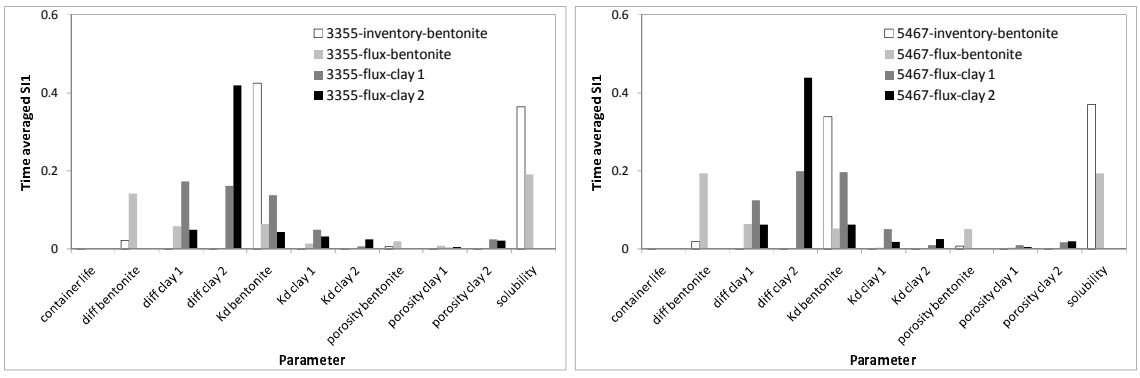

Fig. 4.45 Time averaged sensitivity indices of first order (SI1) of all indicators and samples

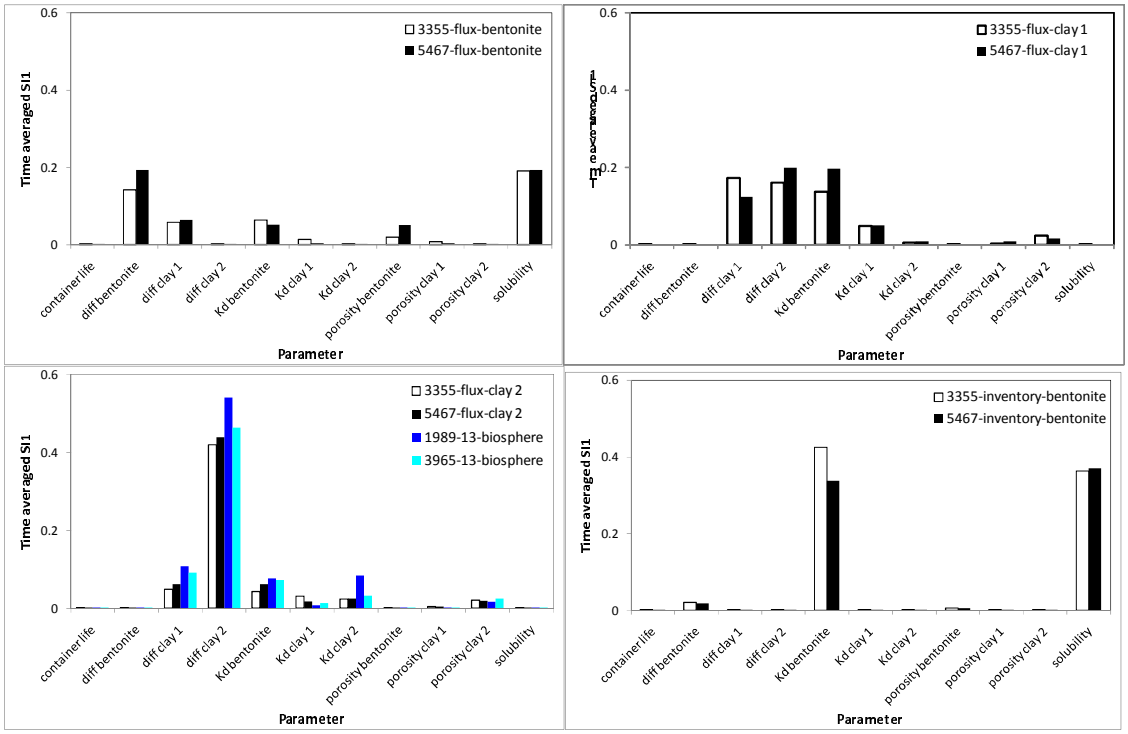

Fig. 4.46 Time averaged SI1 indices of each indicator for both samples (the time averaged SI1 indices for the annual radiation dose rate are presented additionally in the lower left plot)

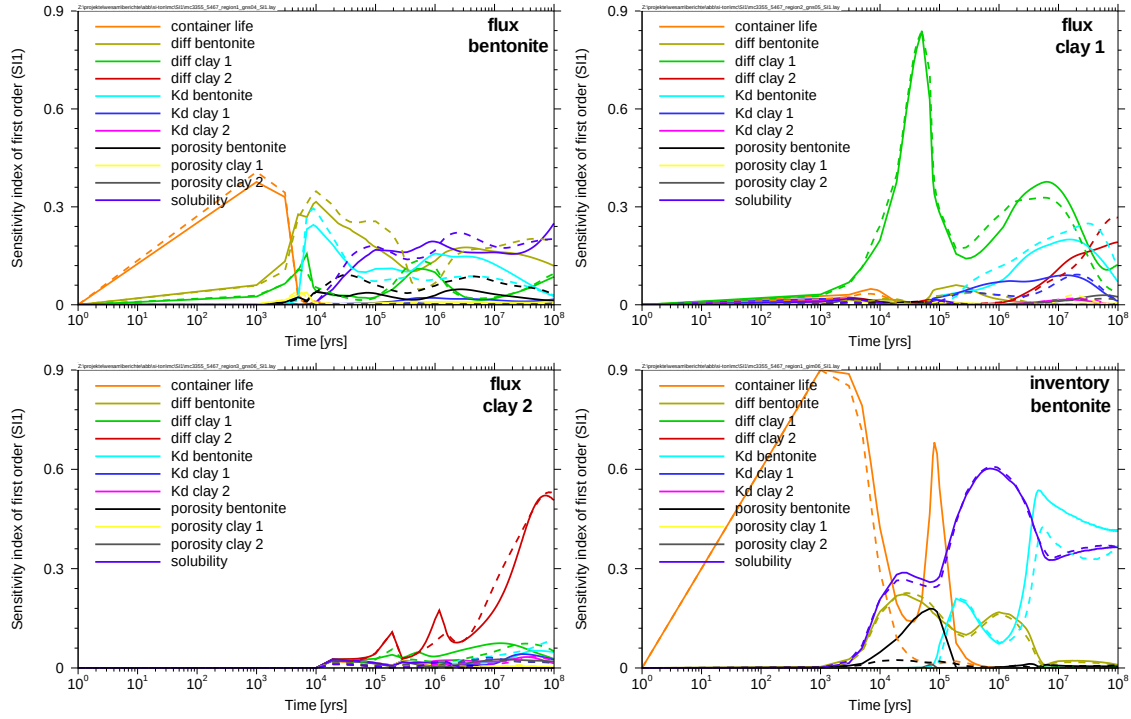

Fig. 4.47 Sensitivity indexes of first order of the 4 indicators (solid and dash lines represent samples with 3355 and 5467 runs, respectively)

Ranks of parameters based upon the time averaged SI1 indices may not necessarily agree with those based upon visual determination. Good examples for differences in the determination of parameter importance are the ranking of the parameters for the flux indicator from the clay formation 1. Through visual inspection of the SI1 indices, the diffusion coefficient of the clay formation 1 is the most important parameter, followed equally by the K_d value of the bentonite and diffusion coefficient of the clay formation 2. The time averaged SI1 indices however give the impression that the diffusion coefficient of the clay formation 2 and the K_d value of the bentonite are equally on the first and second place, closely followed by the diffusion coefficient of the clay formation 1. The difference in ranking is caused by the drop of the SI1 index of the parameter diffusion coefficient of the clay formation 1 and increase of the indices of the parameter-diffusion coefficient of the clay formation 2 and the K_d value of the bentonite after 10^7 years. The importance of the latter two parameters from 10^7 to 10^8 years makes these parameters overall more significant than the diffusion coefficient of the clay formation 1. The question is here whether parameter importance should rather be determined based upon overall importance or based upon certain time frames of the system behaviour. Clearer messages for overall importance may be derived from time averaged indices while for certain time frames, time based inspection of the indices is the way to go (see also section 4.2.3.4). Parameter ranking for the flux indicator from the clay formation 1 based upon visual determination (marked red) is also listed in **Tab. 4.23** as the one based upon the time averaged based SI indices.

Another good example for differences in parameter ranking is the parameter container life of the flux and inventory indicator from/in the bentonite. The importance of this parameter at very early times (until about 10^4 years) is negligible compared to the total time frame of 10^8 years. It is understandable that container life comes into play at early times in the bentonite for the flux and inventory indicator as containers fail, higher doses of radionuclides are released. At times greater than the life times of the containers considered in the probabilistic calculations, when all containers are failed, the parameter container life is not important any more.

For all indicators, most of the important parameters are associated with the diffusion coefficients and K_d values of the respective and adjacent compartment. One of the most important parameter for the flux indicator from the bentonite is the diffusion coefficient of the bentonite. For the radiotoxicity inventory in the bentonite, the K_d value of the bentonite is the second most significant parameter. For the flux indicator from the bentonite, the diffusion coefficient plays apparently a more important role than the K_d

value for the inventory indicator. Equal less importance have the parameters diffusion coefficient from the clay formation 1, K_d value of the bentonite and porosity of the bentonite for the flux indicator from the bentonite.

The flux and inventory indicators from the bentonite have basically the same important parameters except that the less important parameters diffusion coefficient of the clay formation 1 and porosity of the bentonite for the inventory indicator are missing. Another difference is that the ranking of the parameters is different as already indicated above.

One exception to the association of the most important parameters to the diffusion coefficients and K_d values of the respective and adjacent compartment is that one of the important parameters of the radiotoxicity flux indicator from the clay formation 2 is the K_d value of the bentonite. Other exceptions are parameters, which are independent of the compartments such as solubility and container life but appear as important parameters of the indicators in the bentonite. In compartments 2 and 3, the two parameters (container life and solubility) do not play an important role.

The ranking of the three important parameters from the radiotoxicity flux formation 2 agrees with those of the annual radiation exposure to the biosphere. This confirms the result in section 4.2.3 that parameters in the far field (aquifer) do not play a major role on the model output.

It is worthwhile to point out again that for all four indicators, the parameter K_d value of the bentonite is an important parameter. For the inventory indicator from bentonite and for the flux indicator from the clay formation 1, it is more important than for the rest of the indicators.

The number of important parameters describing the transport of radionuclides in the different compartments becomes smaller, i. e., from six to four and in the end to three parameters for the respective radiotoxicity fluxes from the bentonite and the clay formations. This is related to the reduction of radiotoxicity due to sorption in the different compartments and decay of the radionuclides.

The factor of the differences between less and more important parameters based upon the time based SI1 indices is interesting for some indicators. For the three flux indica-

tors, there are factors of 3, 1.6 and 7 times in compartments 1, 2 and 3 respectively. For the inventory indicator from bentonite, there is even a factor of 20 times.

The highest SI1 peaks are reached by the parameters listed in **Tab. 4.24**. The rest of the SI1 peaks is less than 0.4. The second SI1 peak of the parameter container life of the inventory indicator from the bentonite of the sample with 3 355 simulations is probably caused by the insufficient size of the sample. The diffusion coefficient from the clay formation 1 of the flux indicator has two significant peaks at about $4.8 \cdot 10^4$ and $5.5 \cdot 10^6$ years, the K_d value of the bentonite of the inventory indicator at about $2.1 \cdot 10^5$ and $5.7 \cdot 10^6$ years, and the diffusion coefficient of the bentonite of the inventory indicator at $3 \cdot 10^4$ and $1.1 \cdot 10^6$ years.

Tab. 4.24 Significant EFAST SI1 peaks along with the occurring time (based upon the sample with 5467 runs)

No.	Flux from the clay formation 1	Flux from the clay formation 2	Inventory from the bentonite
Container life			0.9, 10^3 yrs
Diff bentonite			
Diff clay 1	0.83, $4.8 \cdot 10^4$ yrs		
Diff clay 2		0.53, $8.4 \cdot 10^7$ yrs	
K_d bentonite			0.43, $5.6 \cdot 10^6$ yrs
K_d clay 1			
K_d clay 2			
Porosity bentonite			
Porosity clay 1			
Porosity clay 2			
Solubility			0.61, $7.9 \cdot 10^5$ yrs

Some differences in the ranking of the sensitivity indexes of total order (SIT) or parameter interactions can be identified for the indicators compared to the first-order indices. For most of the flux indicators of the SIT, there is a clearer ranking of the parameters than it is for the ones of the SI1. In addition, there are up to 2 more important parameters for each indicator. As for the SI1 indices, for all four indicators, the parameter K_d value of the bentonite is an important parameter for interactions. For the inventory indicator from the bentonite and for the flux indicator from the clay formation 1, it is more important than for the rest of the indicators. Tab. **4.25** gives an overview of important parameters of all indicators as well as of the annual radiation dose to the biosphere based upon the SIT indices. As in **Tab. 4.23**, the ranking of most of the parameters in this table is based upon the time averaged based SIT indices except the ones which are marked in red, which are visually determined. The cut off criterion for the parameter

ranks in Tab. **4.25** based upon the time averaged SIT indices is about 0.1. It is assumed that parameter interactions having averaged indices below this value do not have a significant influence upon the system behaviour.

Tab. 4.25 Important parameters of the 4 indicators and of the annual radiation exposure to the biosphere based upon the EFAST SIT indices

Parameter	Flux from the bentonite	Flux from the clay formation 1	Flux from the clay formation 2	Inventory in the bentonite	Annual radiation exposure to the biosphere (see Section 4.2.3)
Container life	7[v]			4[v]	
Diff bentonite	1			3	
Diff clay 1	5	1	2		2
Diff clay 2			1		1
K_d bentonite	3	2	3	2	2
K_d clay 1		3	5		
K_d clay 2	6	4	4		
Porosity bentonite	4			5[v]	
Porosity clay 1		5			
Porosity clay 2			5		
Solubility	2			1	

[v] visual determination

Fig. **4.48** and Fig. **4.49** demonstrate time averaged SIT indices of all indicators and samples. Fig. 4.50 shows EFAST sensitivity indices of total order (SIT) for all indicators and samples. As for the SI1 indices, for each indicator, a plot is represented. Solid and dash lines represent samples with 3 355 and 5 467 runs, respectively.

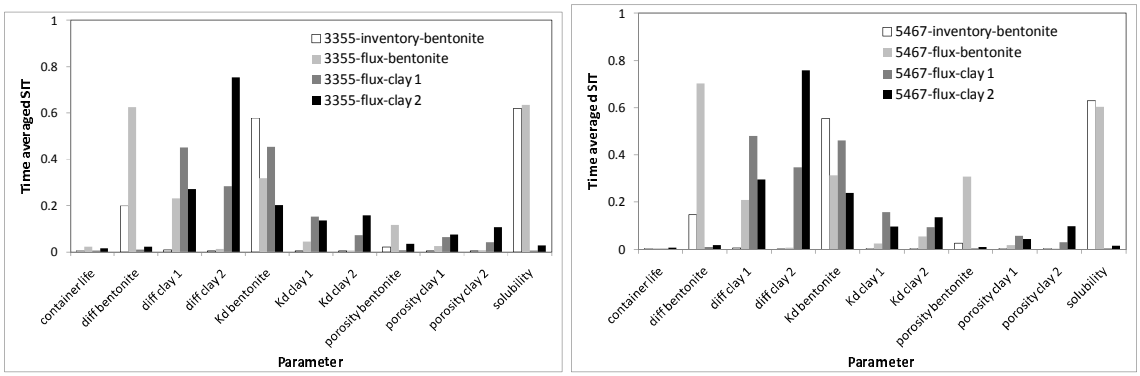

Fig. 4.48 Time averaged SIT indices of all indicators and samples

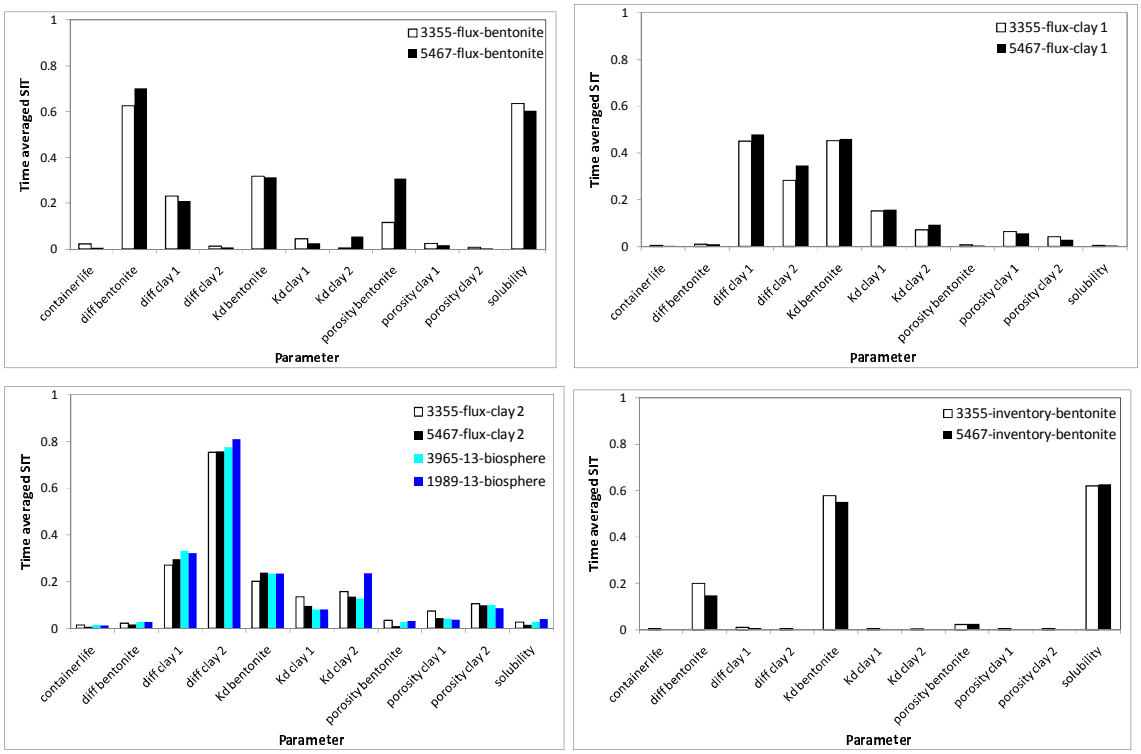

Fig. 4.49 Time averaged SIT indices of each indicator for both samples (for the flux indicator from the clay formation 2, the time averaged SIT indices for the annual radiation dose rate of the two samples are plotted)

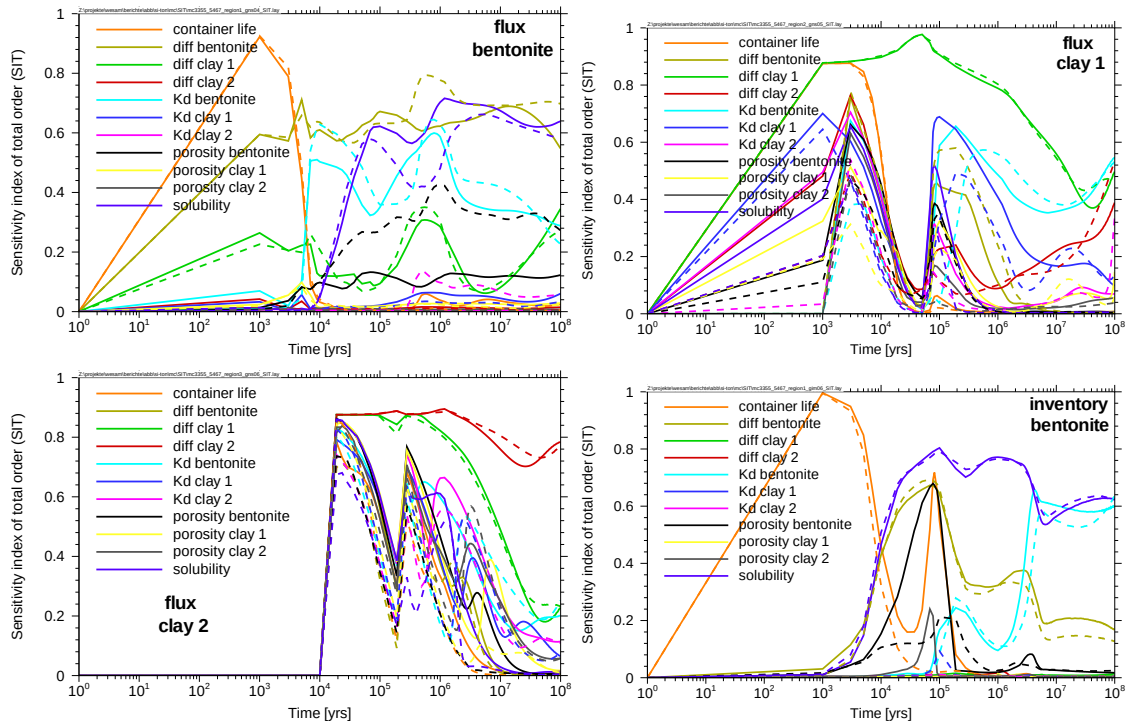

Fig. 4.50 Sensitivity indexes of total order of the 4 indicators (solid and dash lines represent samples with 3 355 and 5 467 runs, respectively)

The differences in factors between less and most important parameters based upon the time based SIT indices are not as big as for the SI1 indices. For the three flux indicators, there are factors of 2, 1.4 and 2.5 times in compartments 1, 2 and 3 respectively. For the inventory indicator from the bentonite, the factor is only 3 times compared to 20 times for the SI1 indices.

Stability of the indices

The sensitivity indices of the two samples in **Fig. 4.45** through **Fig. 4.49** also show how they differ. The greatest differences between the indices of the important parameters between the two samples are listed in **Tab. 4.26** and **Tab. 4.27**. The numbers in these tables are calculated from the ratio of the time averaged indices of the samples with 3 355 and 5 467 simulations.

From the values in Tab. 4.26, it can be said that the biggest instabilities have the SI1 indices of the parameters of the inventory indicator container life and the K_d value of the bentonite, of the flux indicator from the bentonite the container life, the porosity of the bentonite, the diffusion coefficient of the bentonite and the K_d value of the bentonite, of the flux indicator from the clay formation 1, the K_d value of the bentonite, the diffusion coefficients of the clay formations 1 and 2 and of the flux indicator from the clay formation 2 the K_d value of the bentonite and the diffusion coefficient of the clay formation 1.

The biggest instabilities of the SIT indices are listed in Tab. 4.27. These are in particular the important parameters of the bentonite of the inventory indicator container life and the diffusion coefficient, of the flux indicator from the bentonite the K_d value of the clay formation 2, container life and porosity of the bentonite, of the flux indicator from the clay formation 1 the K_d value of the clay formation 2, diffusion coefficient of the clay formation 1 and the porosity of the clay formation 1 and of the flux indicator formation 2 the K_d value of the clay formation 1.

To show how ratios of the time averaged indices for the biosphere look like in comparison, the ratios of the ones of the sample with 2 485 simulations (497 runs per parameter) to the sample with 1 525 simulations with 5 parameters are listed in Tab. 4.28 and Tab. 4.29. In addition, in these tables, all ratios of the other samples to the sample with 1 525 simulations for the biosphere with 5 parameters are provided. The samples with

the greatest instabilities are those with 765 simulations and 5 parameters and with 1 989 simulations and 13 parameters as already observed in section 4.2.3.

Tab. 4.26 List of important parameters with the biggest SI1 instabilities of the samples for the 4 indicators and of the samples with 1 989 and 3 965 simulations for the biosphere (the ratios were made to the respective sample with 305 simulations per parameter)

Flux from the bentonite		**Flux from the clay formation 1**		**Flux from the clay formation 2**	
container life	0.06	K_d bentonite	1.43	K_d bentonite	1.44
porosity bentonite	2.57	diff clay 1	0.72	diff clay 1	1.28
diff bentonite	1.36	diff clay 2	1.23	diff clay 2	1.05
K_d bentonite	0.81	K_d clay 1	1.03		
diff clay 1	1.09				
solubility	1.01				
Inventory in the bentonite					
container life	0.26				
K_d bentonite	0.80				
diff bentonite	0.86				
solubility	1.02				

Tab. 4.27 List of important parameters with the biggest SIT instabilities of the samples for the 4 indicators and of the samples with 1 989 and 3 965 simulations for the biosphere (the ratios were made to the respective sample with 305 simulations per parameter)

Flux from the bentonite		**Flux from the clay formation 1**		**Flux from the clay formation 2**	
K_d clay 2	12.04	K_d clay 2	1.32	K_d clay 1	0.72
container life	0.22	porosity clay 1	0.88	K_d bentonite	1.18
porosity bentonite	2.64	diff clay 1	1.07	K_d clay 2	0.86
diff bentonite	1.12	K_d clay 1	1.04	diff clay 1	1.09
diff clay 1	0.90	K_d bentonite	1.02	porosity clay 2	0.94
solubility	0.95			diff clay 2	1.01
K_d bentonite	0.98				
Inventory in the bentonite					
container life	0.55				
diff bentonite	0.74				
porosity bentonite	1.16				
K_d bentonite	0.96				
solubility	1.01				

Tab. 4.28 List of important parameters with the biggest SI1 instabilities of the samples for the biosphere (the ratios were made to the sample with 305 simulations per parameter or 1 525 simulations)

diff clay 2		diff clay 3		K_d bentonite 1	
1989-13	1.23	3965-13	0.90	765	1.45
765	1.15	1989-13	1.05	3965-13	0.80
2485	**0.90**	9965s	1.02	1989-13	0.86
4965	0.90	19965s	1.02	**2485**	**1.00**
9965	0.90	765	0.99	4965	1.00
9965s	0.90	**2485**	**1.01**	9965	1.00
19965	0.90	4965	1.01	9965s	1.00
19965s	0.90	9965	1.01	19965	1.00
3965-13	1.04	19965	1.01	19965s	1.00

Tab. 4.29 List of important parameters with the biggest SIT instabilities of the samples for the biosphere (the ratios were made to the sample with 305 simulations per parameter or 1 525 simulations)

diff clay 2		diff clay 3		K_d bentonite 1	
3965-13	1.15	3965-13	0.96	765	1.26
1989-13	1.12	765	1.00	3965-13	0.89
765	1.08	1989-13	1.00	1989-13	0.89
2485	**0.99**	9965s	1.00	**2485**	**0.96**
4965	0.99	19965s	1.00	4965	0.98
9965	0.99	**2485**	**1.00**	9965s	0.99
9965s	0.99	4965	1.00	19965	0.99
19965	0.99	9965	1.00	19965s	0.99
19965s	0.99	19965	1.00	9965	1.00

In summary, the convergence of the indices of the sample with 3 355 simulations, i. e., 305 runs per parameter is not as good as of the sample with 1 525 simulations and 5 parameters and as of the samples with 1 989 and 3 965 simulations and 13 parameters for the biosphere. Consequently, for the investigated indicators, more than 305 simulations per parameter are recommended to obtain better convergence of the indices. The reason for the increased instability of the indices is probably due to the increased peak values of the indicators compared to the ones for the biosphere (Fig. 4.51, Fig. 4.52 and Tab. 4.30). Fig. 4.51 shows the maximum values of each simulation of the sample with 5 467 simulations for all four indicators. The peak values of each simulation of the sample with 3 965 simulations for the biosphere are plotted for comparison in this figure as well. The highest peak values have the flux indicator from the bentonite, followed by the ones from the clay formations 1 and 2. The lowest peak values in comparison has the dose rate to the biosphere. In other words, the distribution of the flux and inventory indicators is steeper than the one of the dose rate to the biosphere (Fig.

4.52). Tab. 4.30 summarises the maximum peak values of the samples with 3 355 and 5 467 simulations for all 4 indicators and of the samples with 1 989 and 3 965 simulations for the biosphere. It also provides the factor increase of the flux indicators compared to the sample with 3 965 simulations for the biosphere. The peak increase between the flux indicator from the bentonite and the biosphere is very high, i. e., a factor of up to $5.5 \cdot 10^5$. Between the rest of the indicators and the biosphere, there are only factors up to 268 and 32 for compartments 2 and 3, respectively. This also demonstrates the increasing retention from the compartments and the biosphere.

Another demonstration of the peak values of the different indicators is the normalised frequency histogram. **Fig. 4.53** also clearly shows that the peak values become smaller with increasing compartment and biosphere. Plotted in this figure are peak values of each simulation and indicator of the sample with 5 467 runs and of the sample with 3 965 runs for the biosphere.

It is worthwhile to point out that , as noticed for the biosphere, not only between the sensitivity indices of samples with insufficient and sufficient size are some differences but also between the normalised histogram of the peak radiotoxicity fluxes and inventory. This is demonstrated with the two samples for the four indicators in **Fig. 4.54**.

Although the distribution of the radiotoxicity flux indicator from the bentonite does not visually look as a skewed distribution (**Fig. 4.52**), the percentages of runs which contribute about 50 % to the variance indicates that it is skewed (**Tab. 4.31**). The values in **Tab. 4.31** are calculated from the peak values of each simulation of the different samples. For the flux indicators from compartments 1, 2 and 3, the percentages are below 1.6 %. The flux indicator from the bentonite has the highest percentages for the different samples, followed by the ones from the clay formations 1 and 2. The percentages for the inventory indicator in the bentonite are the highest ones of all indicators and samples (up to 13.7 %). This is probably due to the inaccuracy of model output. Only three scientific digitals are considered in the calculations. The percentages of the samples with 1 989 and 3 965 runs of the biosphere are also listed in Tab. 4.31 for comparison. They are up to a percentage of 1.6.

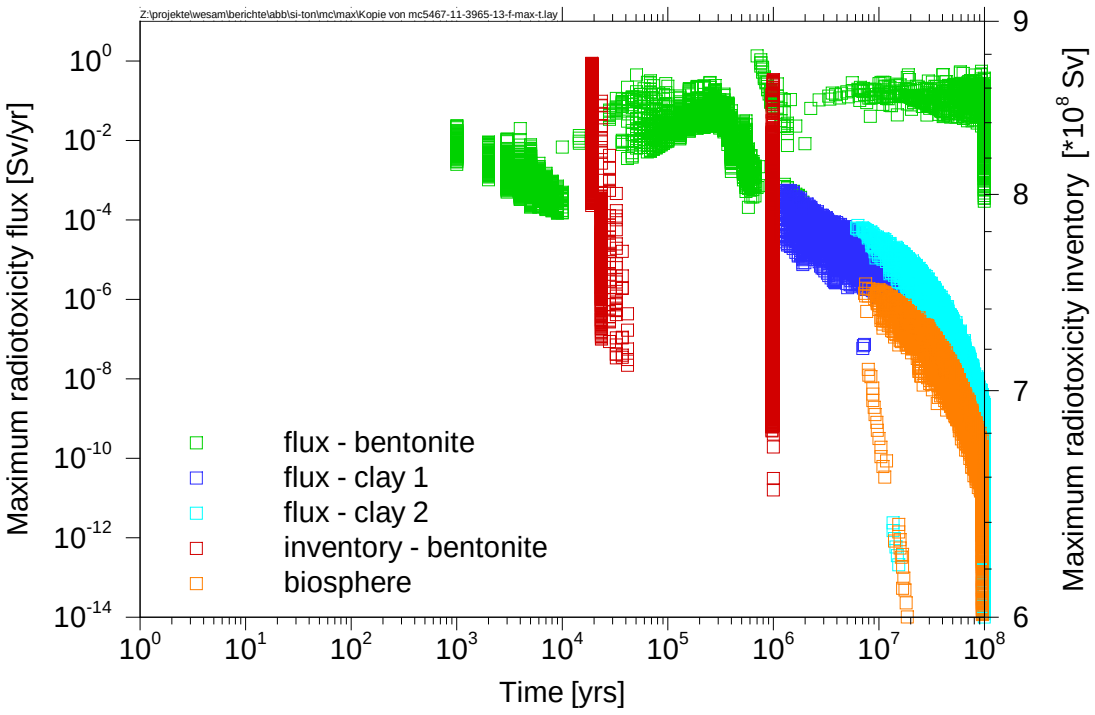

Fig. 4.51 Maximum values of the sample with 5467 simulations for all 4 indicators and of the sample with 3965 simulations for the biosphere

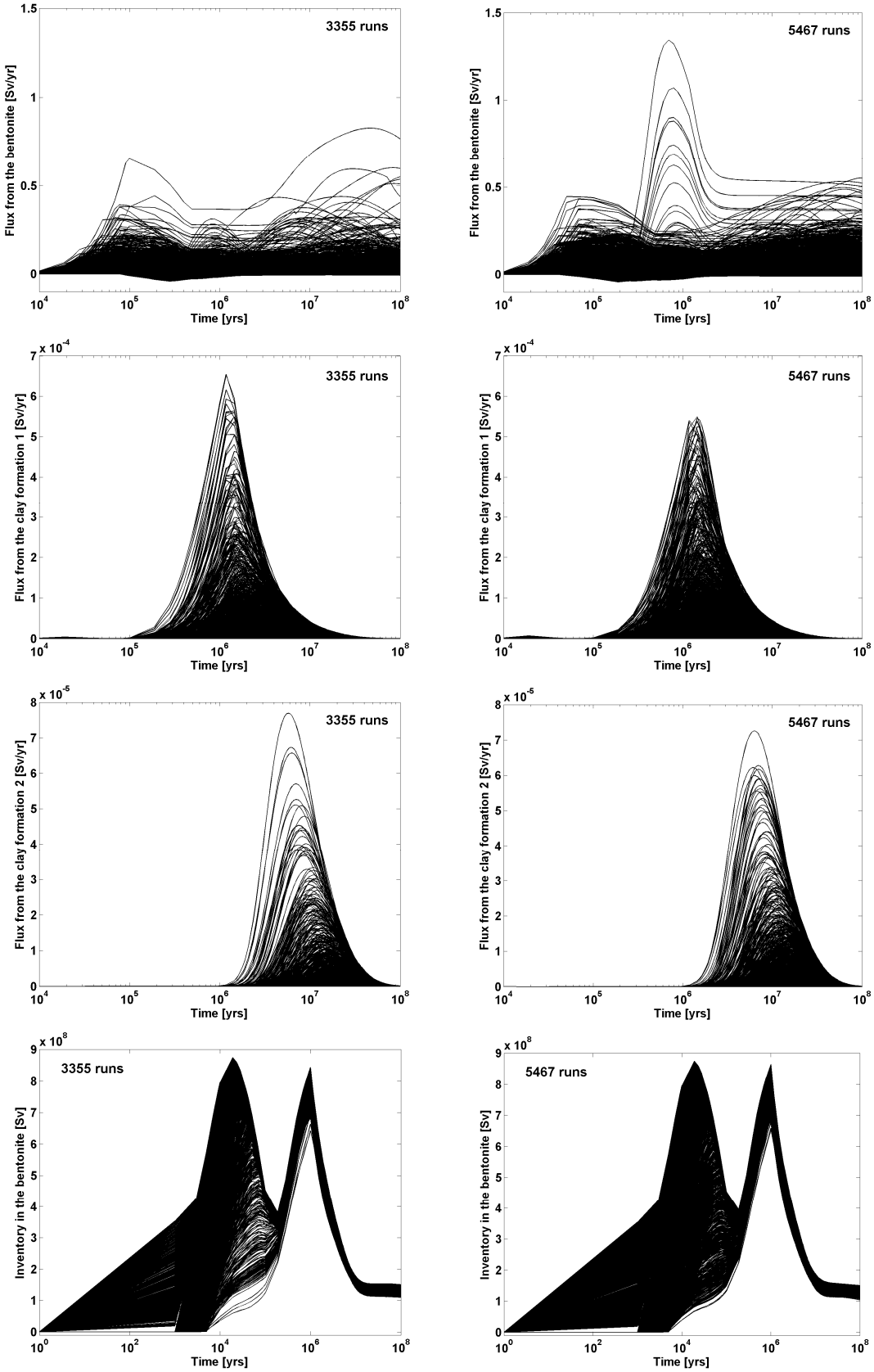

Fig. 4.52 Time evolution of the four indicators for both EFAST samples

Tab. 4.30 Maximum peak values of the samples with 3 355 and 5 467 simulations for all 4 indicators and of the samples with 1 989 and 3 965 simulations for the biosphere

Indicator	3 355/1 989		5 465/3 965	
	Value	Factor to the bio-sphere (sample 3965)	Value	Factor to the biosphere (sample 3965)
Flux from the bentonite [Sv/yr]	8.279×10^{-1}	3.390×10^{5}	1.343×10^{0}	5.5×10^{5}
Flux from the clay for-mation 1 [Sv/yr]	6.545×10^{-4}	268	5.572×10^{-4}	228.2
Flux from the clay for-mation 2 [Sv/yr]	7.693×10^{-5}	31.5	7.256×10^{-5}	29.7
Inventory in the benton-ite [Sv]	8.747×10^{8}		8.746×10^{8}	
Biosphere [Sv/yr]	3.559×10^{-6}		2.442×10^{-6}	

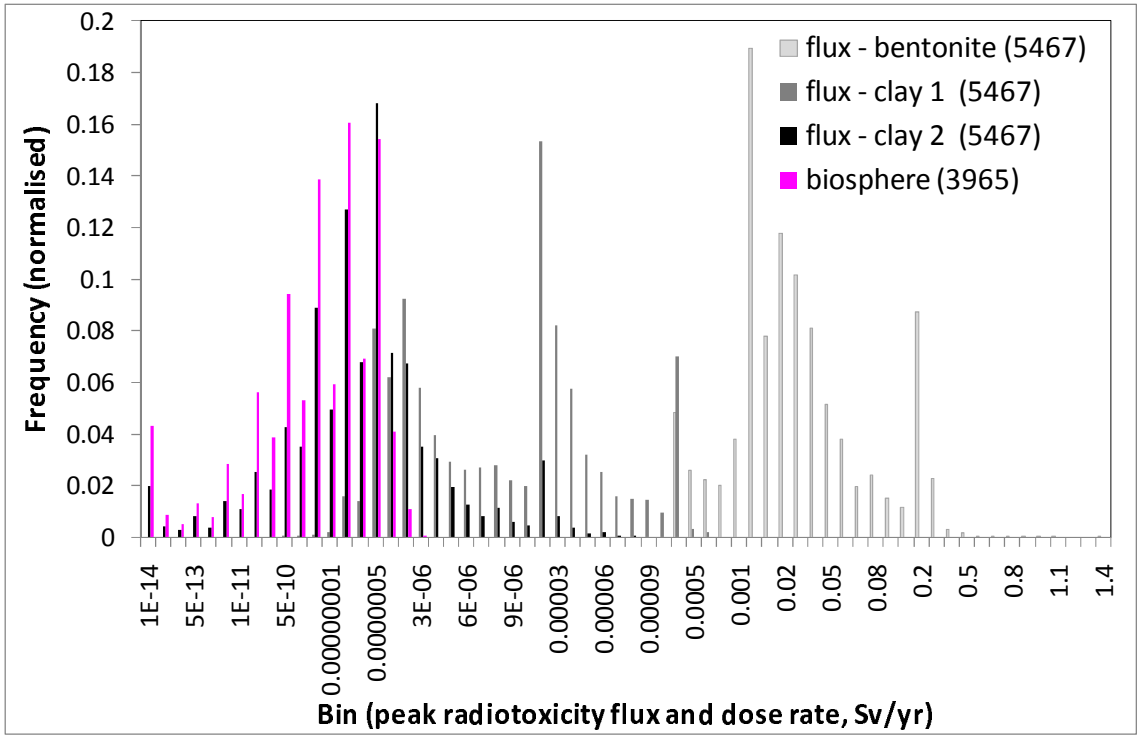

Fig. 4.53 Normalised frequency histogram of the peak radiotoxicity fluxes from compartments 1, 2 and 3 of the sample with 5467 simulations and of the dose rate to the biosphere of the sample with 3965 simulations

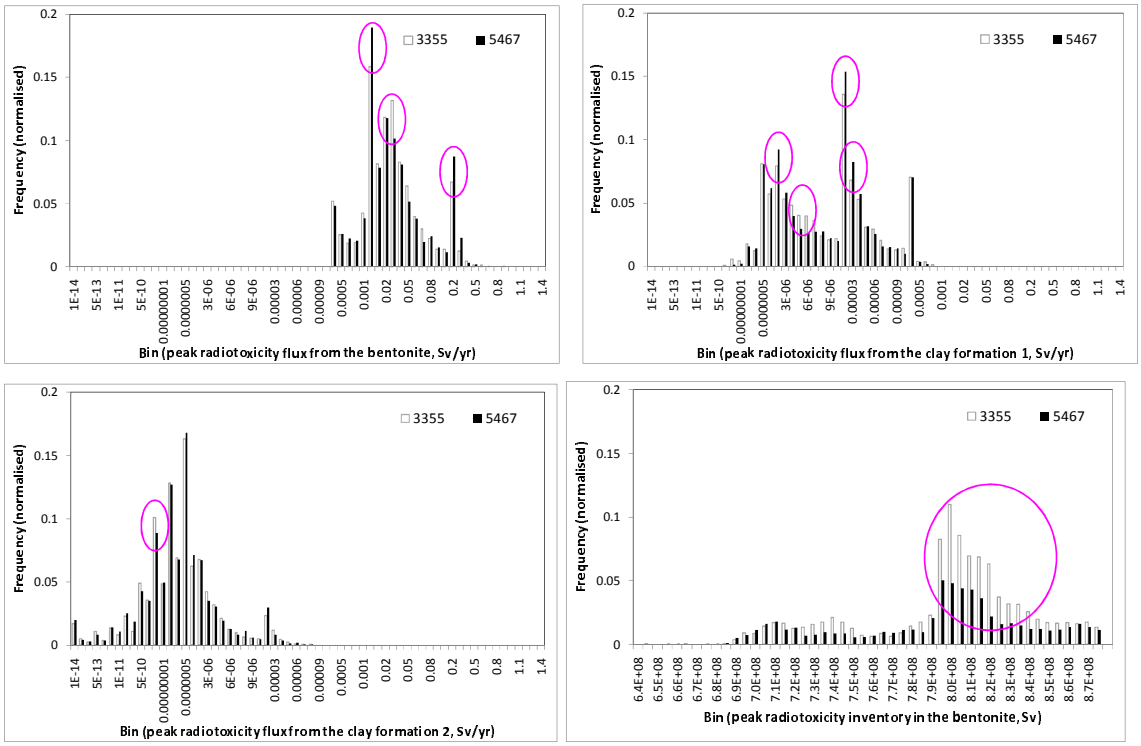

Fig. 4.54 Normalised frequency histogram of the peak radiotoxicity fluxes from compartments 1, 2 and 3 and of the peak radiotoxicity inventory in the bentonite for both samples (the greatest differences are marked)

Tab. 4.31 Percentages of runs which contribute about 50 % to the variance

Indicator	50 % of variance	Number of runs	Percentage of runs
Sample with 3 355 simulations			
Flux from the bentonite	50.27	46	1.37
Flux from the clay formation 1	50.34	38	1.13
Flux from the clay formation 2	50.75	24	0.72
Inventory in the bentonite	50.03	399	11.89
Sample with 5 467 simulations			
Flux from the bentonite	50.14	86	1.57
Flux from the clay formation 1	50.26	71	1.30
Flux from the clay formation 2	50.25	35	0.64
Inventory in the bentonite	50.01	751	13.74
Biosphere			
1 989 simulations	50.35	26	1.31
3 965 simulations	50.26	62	1.56

CSM plots

CSM (Contribution to the Sample Mean) plots generated from the peak values of the three flux indicators for the samples with 3 355 and 5 467 runs are represented in **Fig. 4.55**. Only the most significant parameters, i. e., parameters which most deviate from the 1:1 line are shown in the 3 plots. The most significant parameters shown in **Fig. 4.55** are the same as those from the EFAST analysis in **Tab. 4.23**. No proper CSM plots could be produced for the inventory indicator in the bentonite. This may be associated with the inaccuracy of the peak values and occurence of the peak values in only two time windows over a simulation time of 10^8 years (one from $2 \cdot 10^4$ through $5 \cdot 10^4$ years and the other one at around 10^6 years, **Fig. 4.51**).

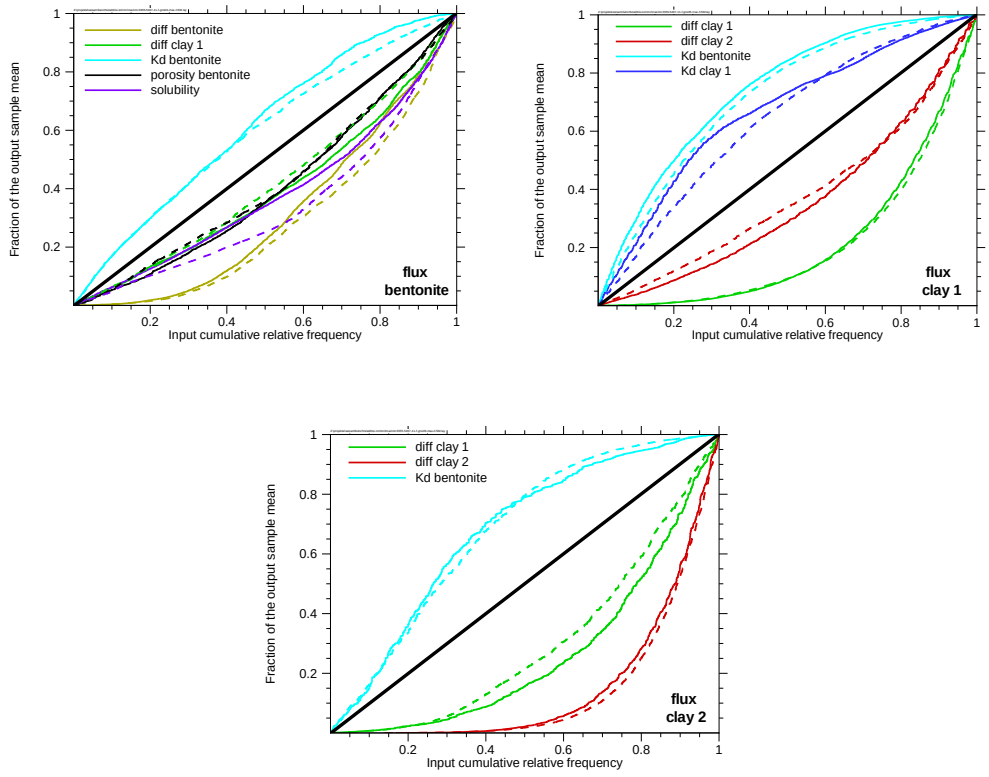

Fig. 4.55 CSM plots of the three flux indicators for both samples

4.2.4.2 Conclusions

EFAST analysis of four different performance indicators (radiotoxicity flux indicators in three different compartments: geotechnical barrier (bentonite) and two geological bariers (clay) and radiotoxicity inventory in the geotechnical barrier) indicated that sig-

nificance of parameters is different for the four indicators. This is caused by (i) the reduction of radiotoxicity due to sorption and decay of the radionuclides and (ii) the importance of the parameters of the respective and the adjacent compartment. In the geotechnical barrier, the most important parameters for the flux indicator are the diffusion coefficient of that barrier and the solubility. For the inventory indicator, the solubility and the K_d value of that barrier are significant. The most important parameters are for the flux indicator from the clay formation 1 the diffusion coefficient of the clay formation 2 and the K_d value of the bentonite and for the second adjacent geological barrier the diffusion coefficient from the clay formation 2. For each indicator, there are between 2 und 4 less important parameters. For the indicators from/in the bentonite, the parameter container life is at early times important. The CSM plots verified the EFAST results of the flux indicators.

Results from the EFAST analysis and CSM plot as well as the normalised frequency histogram indicated that, for the investigated indicators, more than 305 simulations per parameter are recommended for a proper analysis. The reason for the increased instability of the indexes is probably the increased peak values of the indicators compared to the ones of the biosphere.

4.3 Presentation of Safety Indicators and Performance Indicators

This chapter addresses the subject of presenting safety and performance indicators in illustrative figures, so that the intended messages are best conveyed. Since the purposes of safety indictors and performance indicators are fundamentally different, the principles that should be followed differ for both types of indicators. One should never mix up safety and performance indicators in presentation. Therefore, they are treated separately in the following. All considered safety indicators and most performance indicators are time-dependent quantities.

4.3.1 Safety Indicators

When safety indicator results are presented it is essential that the applicable reference values become clearly visible. Generally, there are two possibilities to present time-dependent safety indicators:

- Presentation of the absolute values of the calculated output. In this case, the reference value should be marked as a line in order to demonstrate the safety margin at each point in time.
- Presentation of the dimensionless normalised value, which is calculated by dividing the output by the reference value. In this case, the reference line is 1 via definition.

Which of the two kinds of presentation is to be preferred depends on the concrete situation. If the time-development of an indicator is to be demonstrated in the context of its physical meaning, the absolute value will be more illustrative. If this, however, is of minor importance or several indicators are to be compared with each other, the normalised representation is the better choice.

Since PA results typically span several orders of magnitude and develop over very long times with decreasing speed, time-dependent safety indicators will normally be presented best on a double-logarithmic scale. A problem with this kind of presentation, however, is that it needs getting used to and is sometimes not understood by the general public.

As an example, figure **4.56** shows the time development curves of the five safety indicators that were calculated for the salt model concept, normalised to their reference values. This kind of presentation gives a good overview of the different safety indicators and the safety statements given by them. It can be clearly seen that the power density in the upper groundwater and the raditoxicity flux into the geosphere yield nearly the same safety margin of about one order of magnitude, although they reach their maxima at different times. The radiotoxicity concentration in biosphere water and the radiotoxicity flux from the geosphere to the biosphere yield a slightly larger safety margin[3], and interestingly, the effective dose rate yields the largest safety margin of all considered indicators. This is another argument that it does not suffice to consider only the effective dose rate, because other indicators might lead to stronger safety requirements.

[3] Although the reference values are derived independently, the normalised radiotoxicity concentration in biosphere water and the normalised radiotoxicity flux from the geosphere to the biosphere (blue dash and dot line) are almost the identical: If the radiotoxicity flux from the geosphere is divided by the natural groundwater flow the reference value for the radiotoxicity concentration in the geosphere is $2.1 \cdot 10^{-6}$ Sv/m^3 (0.1 Sv/a divided by 48 000 m^3). The reference value for the radiotoxicity concentration in drinking water is $2.0 \cdot 10^{6}$ Sv/m^3. Since the natural groundwater flux in the calculation is constant, the resulting indicators give almost the same safety margin to the reference value.

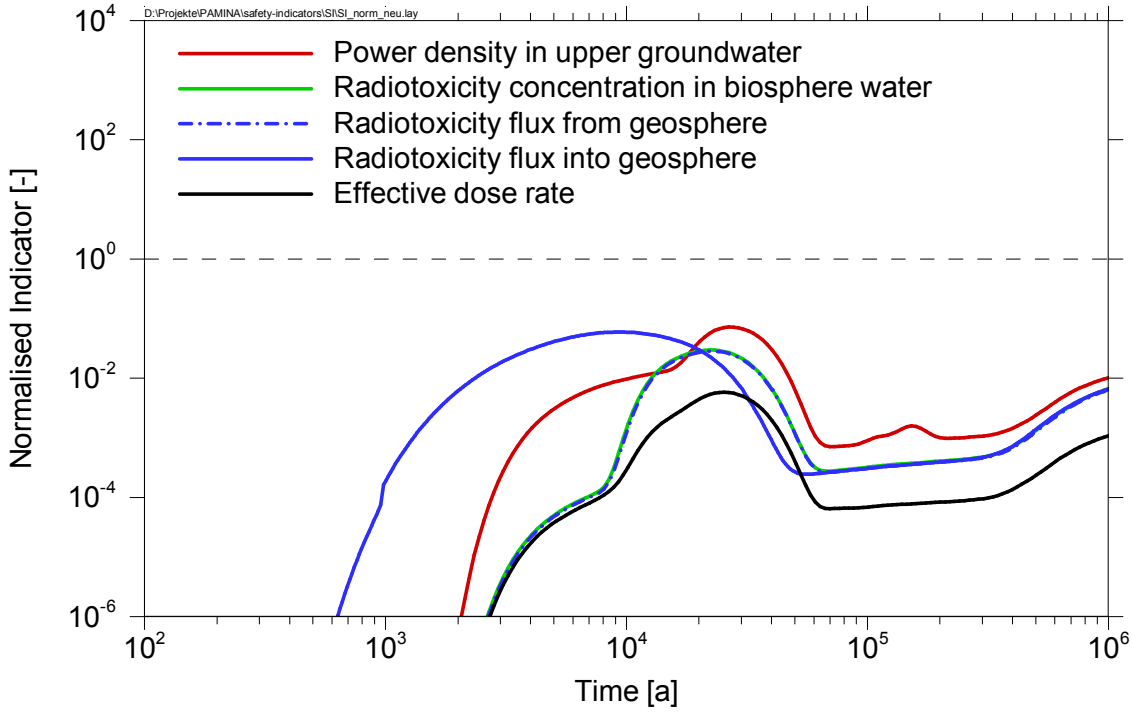

Fig. 4.56 Presentation of several normalised safety indicators in one figure

In general the temporal evolution of the safety indicators is quite similar. The only exception is radiotoxicity flux from the repository to the geosphere, because this indicator refers to a deeper part of the repository system and is based on fluxes from the repository. Here other radionuclides play an important role than in the upper groundwater system.

As long as deterministic results are to be presented it is advisable to show the total time development of the safety indicators. This allows quick identification of the most important time periods as well as the time of the maximum and it gives an impression of the time-development of the system. For probabilistic investigations, however, other aspects are important. In this case one is normally more interested in seeing the most essential results of all runs in one well-arranged figure. Although, in specific cases, it can indeed be helpful to show the time curves of all simulations, even hundreds or thousands, in one figure, so that a few ones, which deviate from the normal behaviour or significantly exceed the others, can easily be identified, one will normally prefer a more integrative presentation. There are two principally different possibilities for showing the results of a probabilistic set of time-dependent calculations together, which have their specific advantages each:

– reducing each individual calculation result to a single data point and presenting all the data points in a scatter diagram,

– calculating statistical measures from all calculation results and presenting them over time.

Normally, the most meaningful point of the time curve of a safety indicator is the maximum, as it shows the time and value of the highest detrimental consequence. Therefore, a scatter diagram of the times and values of the maxima of a probabilistic set of runs provides very useful information. The reference value should also be presented. Then it can be easily seen how close the highest maxima get to the reference value and how many of them are in a critical range. The information provided by such diagrams can even be increased by colour-coding the dots according to specific properties. Figure **4.57** shows an example of a dose rate maximum scatter plot, where the dots are coloured according to the radionuclides that have the highest relevance at the time of the maximum. The figure is taken from the safety case for the ERAM LLW repository /WOJ 09/. It clearly shows that there is a gap of about one order of magnitude between the highest maxima and the reference value. Moreover, it shows that Sn-126 is the dominant radionuclide, particularly in the medium times, whereas at late times Ra-226 (as a daughter product of U-238) becomes more important. At early times, C-14 is responsible for many maxima, and one single maximum is due to Tc-99.

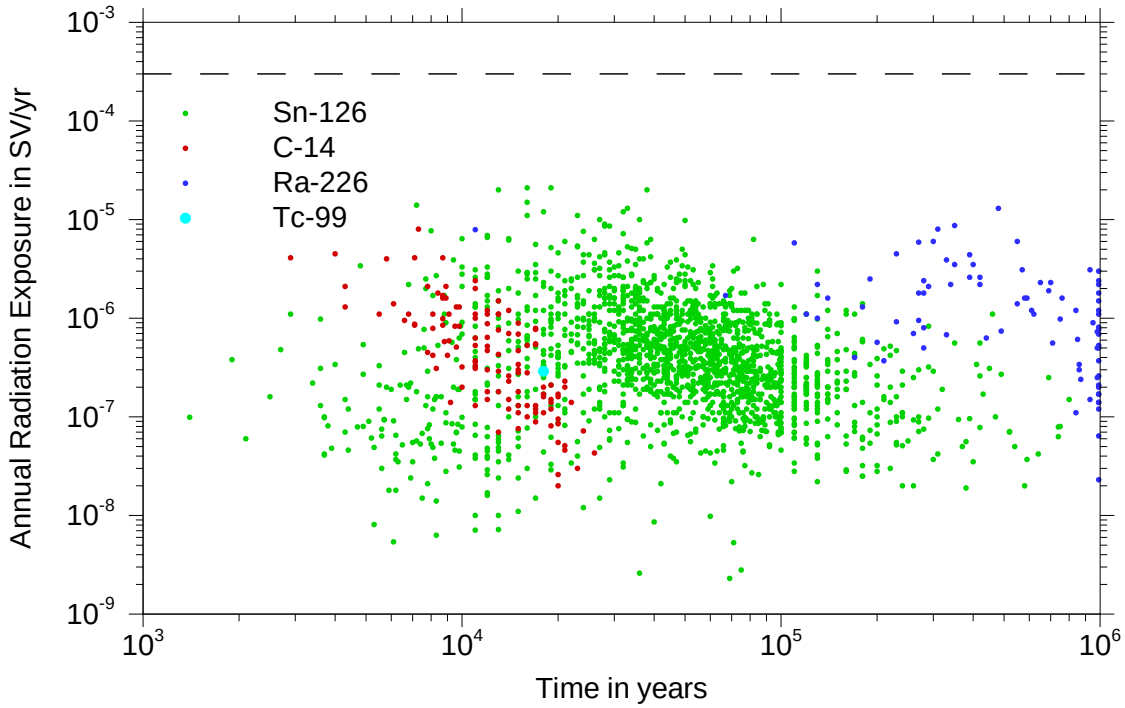

Fig. 4.57 Colour-coded scatter plot of maximum values

If the time of the maximum is of less interest, another possibility to present the maxima of a probabilistic set of calculations is the Complementary Cumulated Distribution Function (CCDF) plot. This kind of plot is better adequate for comparing different (normalised) safety indicators than a scatter plot as it provides one curve per indicator.

A completely different method of presenting probabilistic results is plotting statistical measures like the mean or quantiles versus time. If, for example, the time curves of the maximum, the 95 %- quantile and the median are presented together with a reference line, one can see how close to the reference value the calculated indicator gets, and how probable this is. Also, several normalised indicators can be presented in one figure. Since this kind of figures needs some understanding of statistics, however, it is less adequate for conversation with the general public.

4.4 Performance Indicators

Since performance indicators, unlike safety indicators, are normally designed specifically to illustrate the functioning of a certain system, general recommendations for presentation are hard to give. Normally, it does neither make sense to compare different performance indicators with each other in one figure, nor is there a reference value. Therefore, normalisation is of no use and the indicators should be presented as absolute values. Nevertheless, it can be helpful, in certain cases, to present a comparison line together with the indicator that represents a typical value or a technical threshold.

Performance indicators are used for two different purposes:

- improving the general understanding of the system functioning and triggering optimisation measures,
- demonstrating the performance of barriers or subsystems.

Depending on what is actually to be shown, the optimal presentation of performance indicators can vary. For the first case it is primarily important to show the movements of radionuclides, for example. The curves should be meaningful for the expert who is closely familiar with the model, but need not provide information to others. If, however, the second aspect is of importance, one should choose a kind of presentation that conveys a clear message that is immediately understood at least by the scientific public, for example, by illustrating the retention capabilities of the individual repository compartments. For this purpose, it should be avoided to integrate too much information in

the presentation; each figure should address one specific aspect. As an example, **4.58** shows the time-development of the integrated radiotoxicity flows from the compartments of the salt repository model. Due to the integration all curves are monotonically increasing, but they reach nearly constant values after long times, when the release has come to an end. The differences between these values are characteristic for the retention capabilities of the compartments. If presented together with the initially emplaced inventory, these values show clearly, how much of the inventory is finally retained or decays inside each compartment. One can immediately see that the release from the waste compartments is seven orders of magnitude lower than the emplaced inventory, which means that 99.99999 % of the emplaced radiotoxicity is finally retained in the waste compartments. The release from the repository is three more orders of magnitude lower, while the overlying rock has nearly no retention capability.

There is, however, a drawback of the kind of presentation shown in figure **4.58**. The slight increase of all curves at the end time period is due to Radium-226, which has a high dose ingestion coefficient and is permanently produced from Uranium-238. Although this radionuclide is relatively short-lived and does not actually play a role at late times, it is responsible for an increase of the curves, because the decay is not considered after the integration. The shape of the curves can be misleading in communication to the public and even to experts. Nevertheless, as long as this effect does not dominate, this kind of presentation is very helpful.

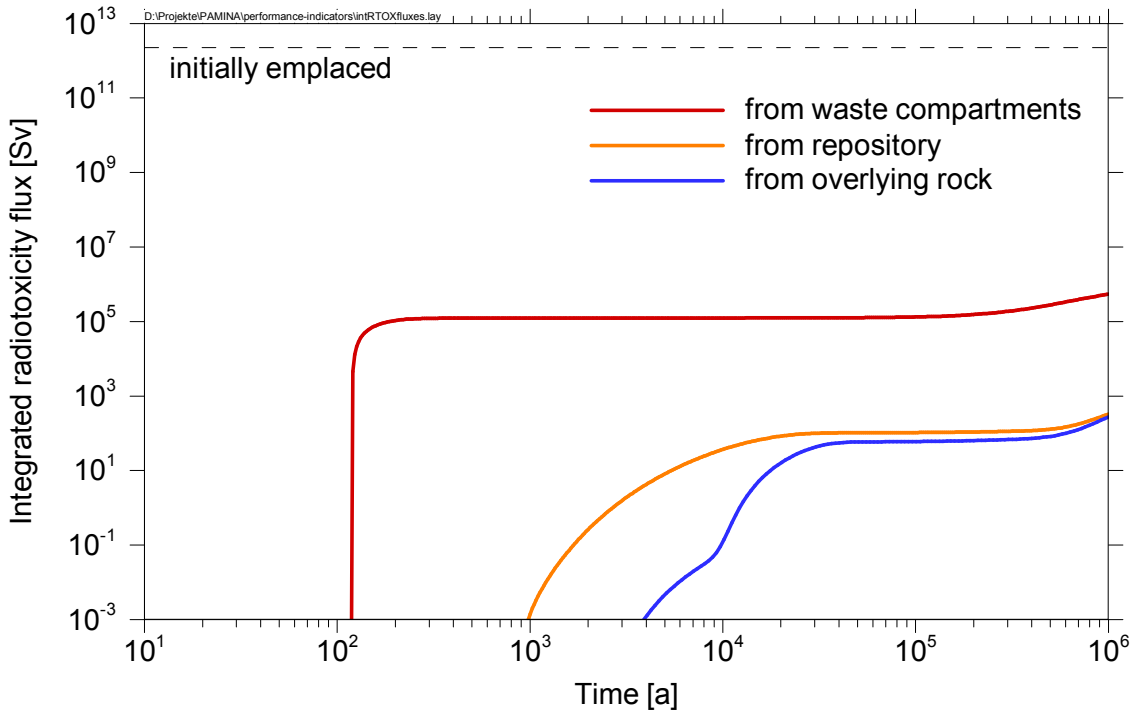

Fig. 4.58 Time-integrated radiotoxicity flows from compartments

Time-independent performance indicators should also be presented in a way that allows a quick assessment of barrier properties. An example is the presentation of radionuclide transport times through a barrier versus their half-lives. From such a figure one can easily see which radionuclides have to be expected to penetrate the barrier and which do not. A very illustrative example is shown in figure **4.59**. It is taken from the Spanish clay case considered in /BEC 09/. The green and orange regions clearly show which radionuclides are expected to fully decay in the clay formation and which radionuclides will suffer negligible decay in the formation, respectively.

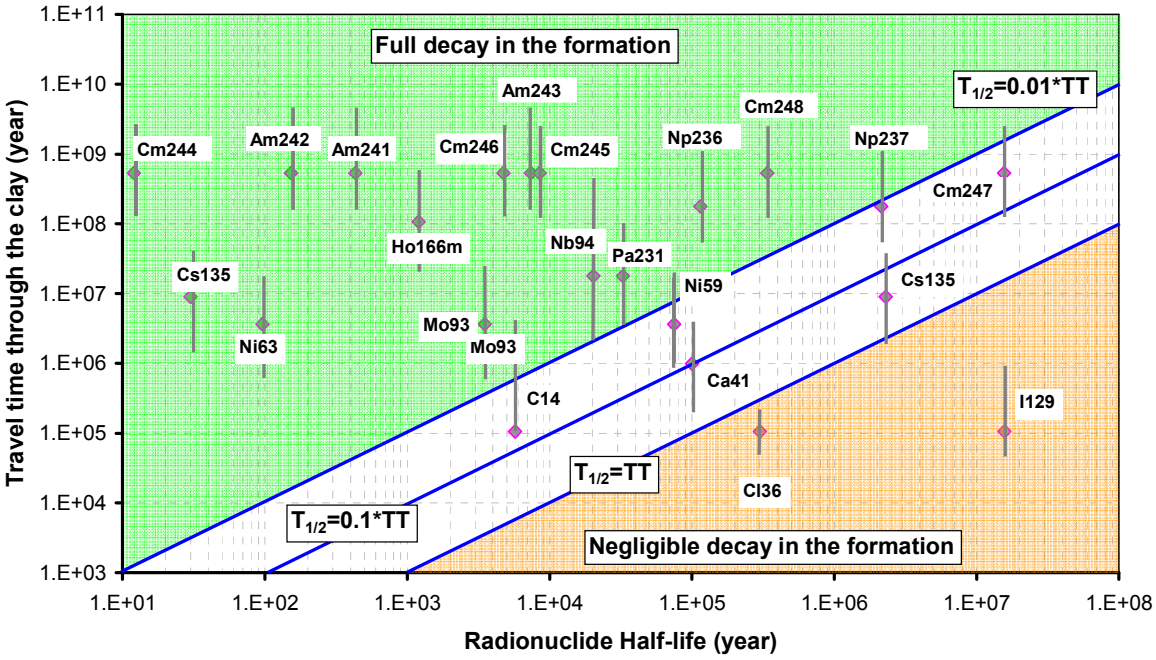

Fig. 4.59 Travel times through the clay formation vs. half-lives in deterministic (diamonds) and probabilistic (bars) calculations

5 Relevance of sophisticated approaches in practical cases

The objectives of the work presented in this chapter are to evaluate whether using more complex and more realistic modelling approaches with the help of actual high-performance tools

- provide an added value in comparison with more simplified approaches used by PA codes, and
- are required to include processes not yet fully accounted for in performance assessment.

The evaluations consist in the comparison between results from fully integrated models and supporting numerical codes with a high level of geometrical accuracy and results from usual compartmental, semi-analytical or simplified models and codes. Through different benchmark exercises on specific processes, the relevance, advantages and limitations inherent to each approach and their associated tools are assessed.

5.1 Testing of the PA approaches for selected near-field processes in a repository in salt

By performing three benchmark exercises, each focussing on specific processes relevant for repository designs in salt rock, the relevance, advantages and limitations inherent to each approach and their associated tools will be assessed. The three processes investigated are the

- convergence of salt,
- intrusion of brine into a backfilled drift and
- radionuclide transport by density driven exchange.

This benchmark is documented in detail in /BUH 09/. Therefore, only the most important results are summarised in the following.

5.1.1 Benchmark on convergence

The disposal of radioactive waste in a salt formation will take place in disposal chambers or disposal boreholes. These chambers and boreholes are connected with the shaft area via drifts and galleries. Since rock salt is a plastic material, it will flow (or creep) towards the area with decreased stress, i. e. towards the excavations. This means that with time the volume of the excavation decreases as long as the stress against the wall of the excavation is less than the lithostatic pressure. This process is referred to as convergence of the rock salt.

In general, the convergence depends on the load capacity of the overlaying salt rock and overburden as well as on the pressure within the cavities and on the resistance of backfill material against compaction. As the pressure inside the cavity may originate from intruded brine or from gas, the expression *fluid pressure* will be used, except if the pressure of liquid or gas is meant in particular.

The transport of contaminants, e. g. radionuclides, is influenced by the convergence in different ways: If intrusion of liquid takes place at late times, the convergence has reduced the pore volume and only a small amount of brine would reach the disposed waste. In addition the flow resistance of backfilled cavities has been increased, so that the intrusion of liquid may be strongly impeded. On the other hand, after the drift and the disposal location are flooded with liquid, the convergence dominates the release of contaminated brine from the repository for the long-term.

During liquid intrusion into a cavity the fluid pressure rises. At the beginning, this pressure corresponds to that of the liquid column in the cavity. If the liquid column extends up to the aquifer, the fluid pressure increases to the hydrostatic pressure corresponding to the depth of the respective cavity in the flooded disposal facility. The fluid pressure reduces the convergence and thus sustains the cavity. If gas is produced and/or stored in the cavity, beside the pressure of liquid also that of gas reduces convergence. Due to flow resistances in the repository the fluid pressure may rise above the hydrostatic value. This so-called hydraulic pressure intensifies the sustaining action of the fluid pressure and thus further reduces convergence.

In a backfilled cavity the progressive compaction of backfill reduces the convergence rate. From experimental investigations it turns out that dry backfill shows quite different compaction behaviour than wet or brine saturated backfill.

A benchmark exercise studying the effect of convergence of rock salt cavities for five different test cases has been performed. It was investigated by this exercise, how reliable the simplifying assumptions and models in PA codes are in predicting convergence processes, if these predictions are compared to more complex process models implemented in rock mechanics codes. Furthermore, it was evaluated whether the more complex and more realistic modelling approaches provide added value and whether they are required to include processes not yet fully accounted for in PA.

The rock mechanics calculations have been performed by DBE-TEC with the FLAC code to get the results for a detailed modelling of the convergence process. The PA code calculations have been done using the LOPOS module.

5.1.1.1 Definition of the test cases

To compare the results from calculations with different models of convergence, as implemented in the EMOS code with those obtained from rock mechanics calculations with FLAC performed by DBE-TEC, several test cases have been established. The benchmark calculations are based on a simplified model of a repository in a salt formation consisting of a cavity as indicated in figure 5.1. The cavity might be a chamber or a gallery, the shaft gives the brine access to the cavity and provides the boundary conditions for the fluid pressure. The shaft has been considered only in the EMOS calculations, where it is modelled as a vertical circular tube backfilled with non-compactable material. Its permeability is selected to achieve a constant fluid pressure, with different values for the test cases. The realization of this fluid pressure is discussed below. To simplify the rock mechanics calculations a homogeneous isotropic rock formation around the cavity is assumed.

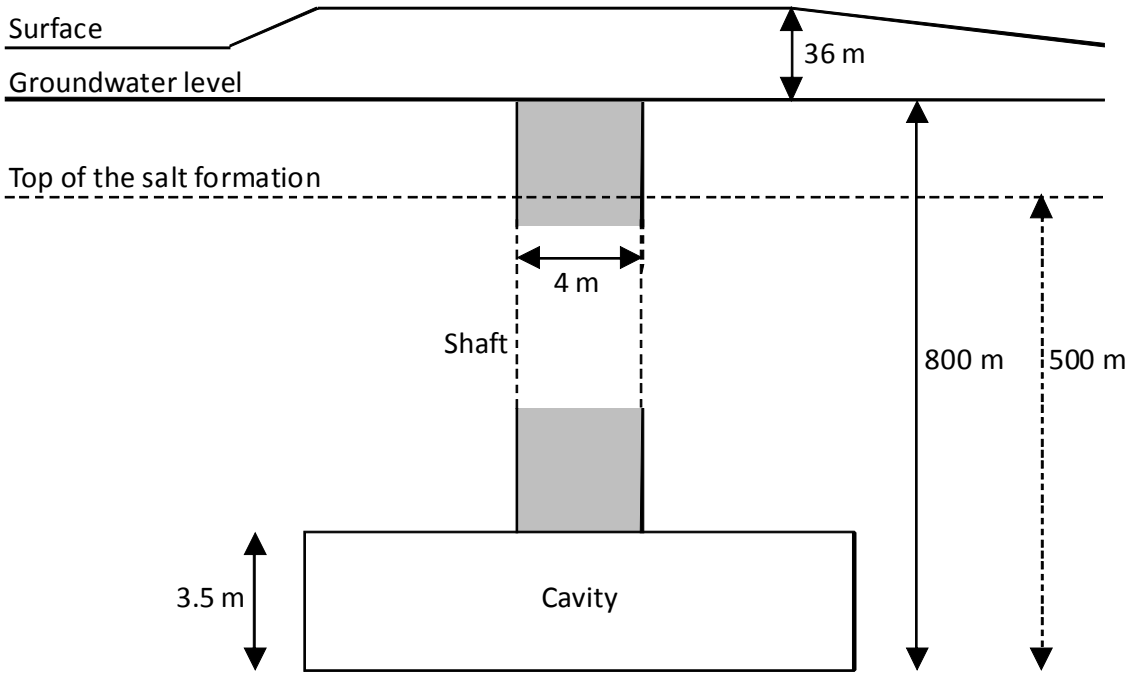

Fig. 5.1 Schematic representation of the repository

The following test cases have been defined:

Case 1: Open cavity with no backfill

- 1a: no brine, atmospheric pressure
- 1b: with constant fluid pressure, brine up to the top of the salt formation
- 1c: with constant fluid pressure, brine up to the surface
- 1d: with time dependent fluid pressure, brine up to the surface

Case 2: Backfilled cavity completely filled with crushed salt, atmospheric pressure

- 2a: dry crushed salt
- 2b: wet crushed salt

Case 3: Backfilled cavity completely filled with crushed salt

- 3a: with constant fluid pressure, brine up to the top of the salt formation
- 3b: with constant fluid pressure, brine up to the surface
- 3c: with time dependent fluid pressure, brine up to the surface

Case 4: Cavity with a layer of uncompactable material at the bottom

- 4a: no backfill in the residual volume, no brine, atmospheric pressure
- 4b: residual volume backfilled with crushed salt, no brine, atmospheric pressure

Case 5: Cavity filled with crushed salt around a steel container lying on the floor

- 5a: no brine, atmospheric pressure
- 5b: with constant fluid pressure, brine up to the top of the salt formation
- 5c: with constant fluid pressure, brine up to the surface
- 5d: with time dependent fluid pressure, brine up to the surface

The results of the rock mechanics calculations of test cases 1a, 2a and 2b are used for the calibration of the convergence models implemented in EMOS. In the EMOS module LOPOS these are case 1a, to find the parameter values of the explicit time dependence of the convergence rate and the asymptotic value of the convergence rate, i. e. the stationary value at late times. Cases 2a and 2b are expected to give the specific backfill parameters of the convergence model of EMOS.

The fluid pressure dependence of the convergence is investigated under different boundary conditions. As a first variant, atmospheric pressure is applied. In the second variant, a hydrostatic pressure of brine is applied, where the repository is filled with brine up to the top of the salt formation. The third variant assumes a hydrostatic pressure from brine filled up to the surface.

To simplify the benchmark calculations and to find a systematic behaviour of the pressure dependence, the test case models are adjusted in such a way that the fluid pressure remains constant during the convergence process except in test cases 1d, 3c, and 5d. The time dependent fluid pressures applied in test cases 1d, 3c, and 5d are calculated with the EMOS codes and then act as boundary conditions in the rock mechanics calculations.

In test cases 4a and 4b a layer of concrete is assumed, whose elastic behaviour is considered. In test cases 5a to 5d a steel container is assumed whose elastic behaviour is also considered.

The input data for all test casers is documented in /BUH 09/. In the following, the results for the convergence rate, the volume decrease, and – for backfilled cavities – the porosity evolution are given as functions of time. In addition, the convergence rates as functions of porosity are plotted for the backfilled cavities.

5.1.1.2 Results

The LOPOS model of convergence is applied to test cases, for which results of rock mechanics calculations are given by DBE-TEC. The reference convergence rate K_{ref} in many cases can be directly obtained from the rock mechanics calculations by extrapolating the respective results to very large times.

Test cases 1a, 1b, and 1c

The comparison of the convergence rates, calculated with different but constant values of the fluid pressure, with those of the rock mechanics calculations is presented in figure 5.2, while figure 5.3 shows the time evolution of the volume of the cavity. The best match of the results is achieved with K_0 = 80 [a^{-1}] and K_{ref} = $2.5 \cdot 10^{-3}$ [a^{-1}]. With these parameter values it is found that for all the three constant-pressure boundaries the convergence rates as well as the volumes match really well.

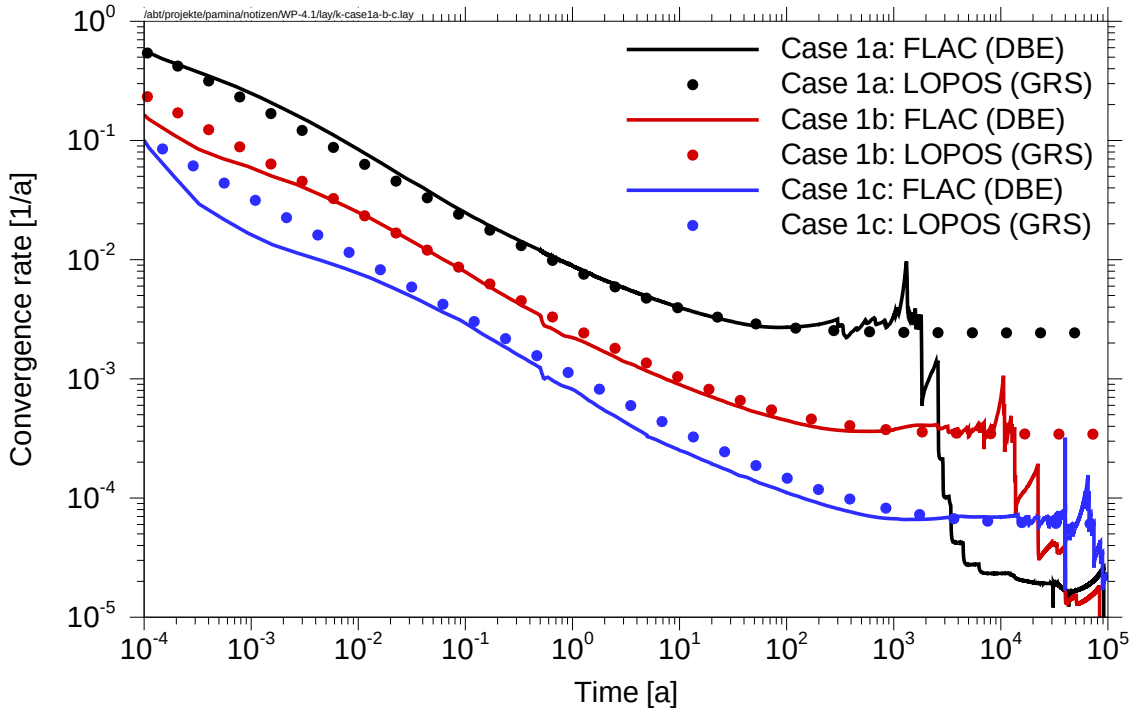

Fig. 5.2 Comparison of convergence rates: Cases 1a, 1b, 1c

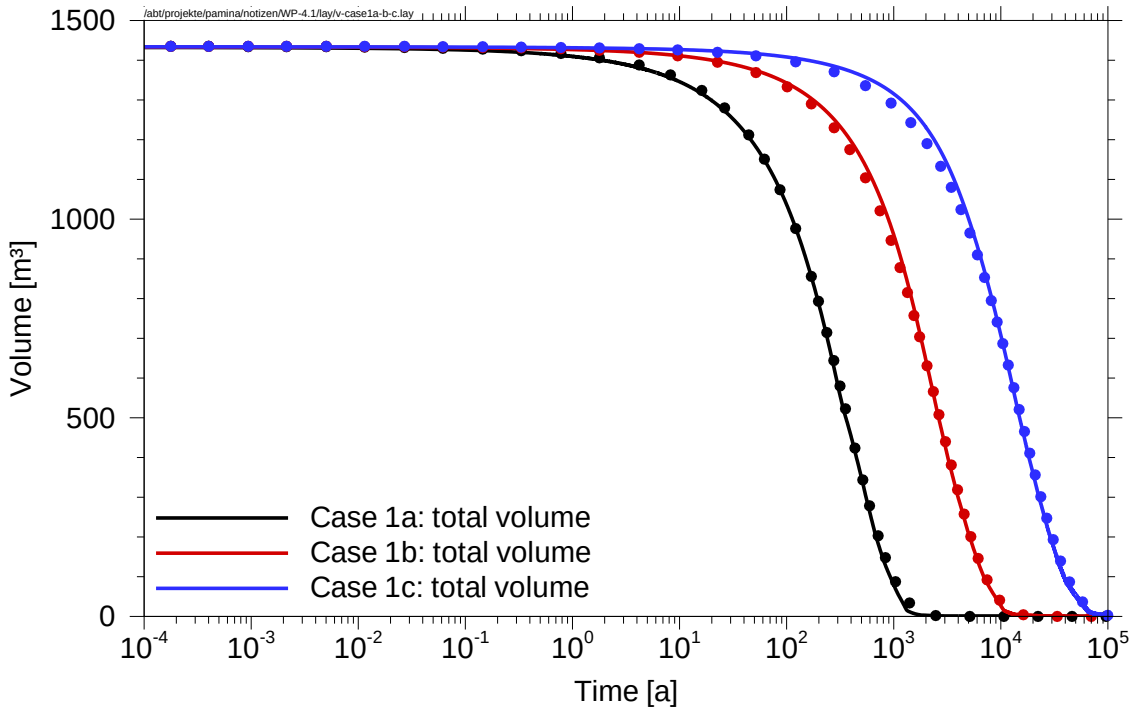

Fig. 5.3 Comparison of time evolution of volumes: Cases 1a, 1b, 1c

Results of test case 1d

In figure 5.4, the convergence rates obtained with the LOPOS model are compared for some test cases. For case 1a atmospheric and for case 1c a constant hydrostatic pressure is applied, which corresponds to a completely brine-filled repository and a negligible flow resistance of the cavity, the shaft segment and its sealing. In case 1d the cavity and the shaft are continuously flooded over a time span of 50 a. During this period the fluid pressure in the cavity increases, until it reaches the hydrostatic pressure of the completely filled repository. Additionally, the shaft sealing permeability is reduced to 10^{-16} m^2, which after 50 a yields a hydraulic pressure increase in the cavity above the hydrostatic value, which is driven by the convergence, when brine is squeezed out of the cavity through the high flow resistance of the shaft sealing.

At the beginning, the convergence rate equals that of case 1a (air filled cavity). With increasing fluid pressure the convergence rate is reduced. After increase of the fluid pressure above the hydrostatic value, the convergence rate is reduced below that of case 1c (completely filled repository). While the fluid pressure decreases to the hydrostatic value, the convergence rate curve approaches that of case 1c. The case 1d time evolution of the cavity's volume is shown in fig. 5.5. At the beginning it follows that of case 1a and later it approaches that of case 1c, as to be expected.

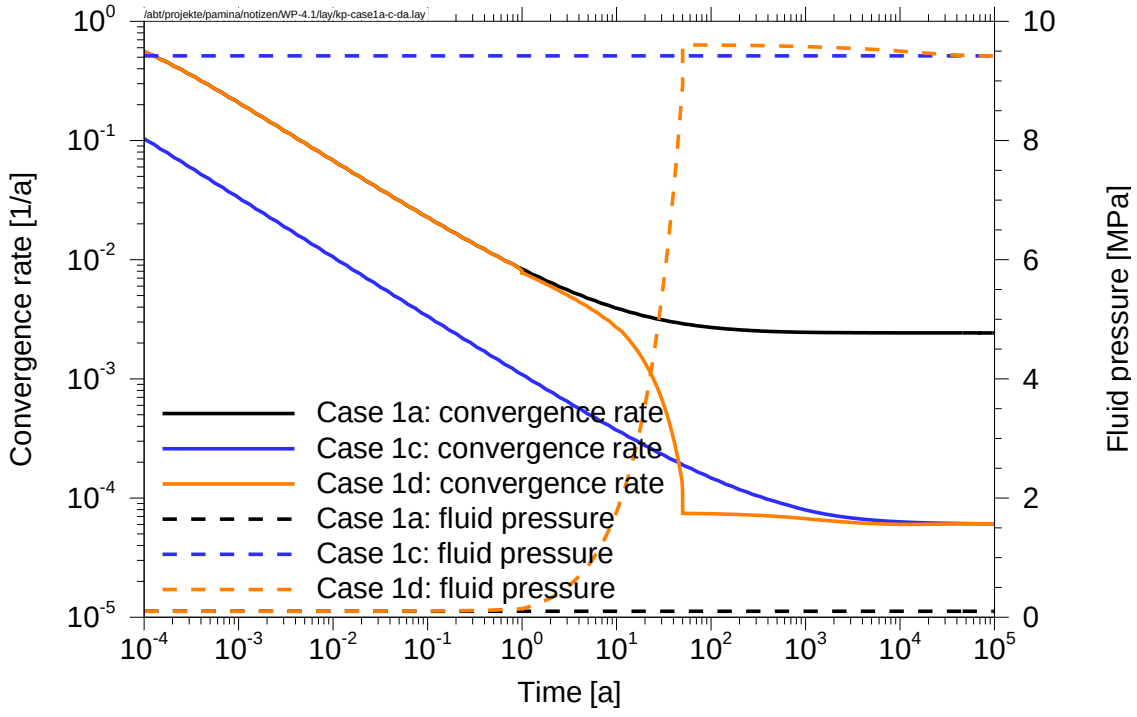

Fig. 5.4 Convergence rate and fluid pressure of cavity in test cases 1a, c and d

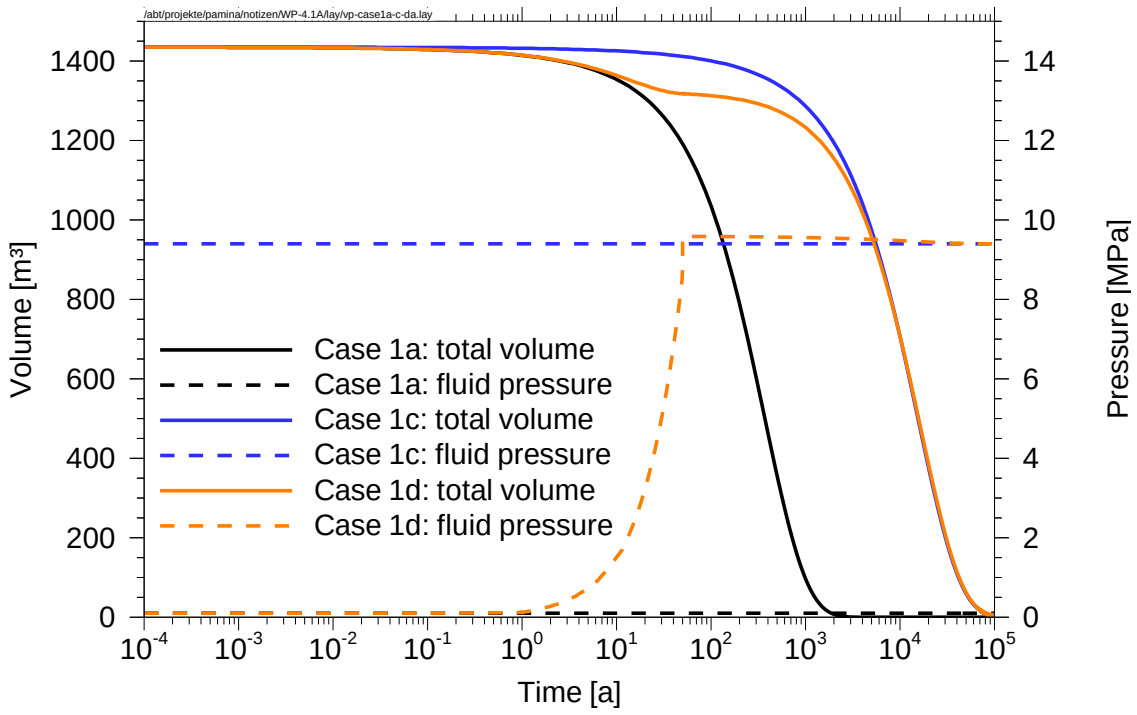

Fig. 5.5 Volumes and fluid pressure of cavity in test cases 1a, c and d

Figure 5.6 shows the result of the rock mechanics calculation and that of the LOPOS calculation for case 1d. Here, a clear difference between the results can be observed at very early times. However, in the rock mechanics calculation the convergence rate is calculated from the cross section reduction of the cavity by numerical differentiation. In LOPOS the convergence rate is calculated analytical formulas. The consequences of the different convergence rates at early times are negligible as can be seen in figure 5.7, where the time evolutions of the volumes are compared.

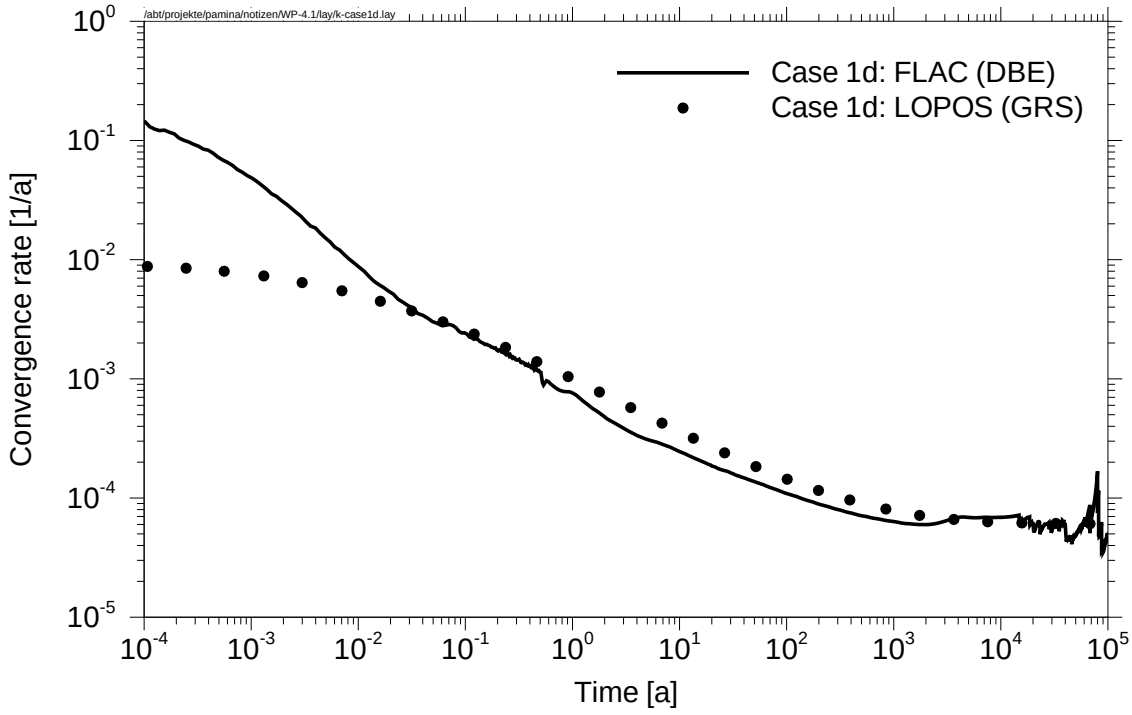

Fig. 5.6 Comparison of convergence rates: Case 1d

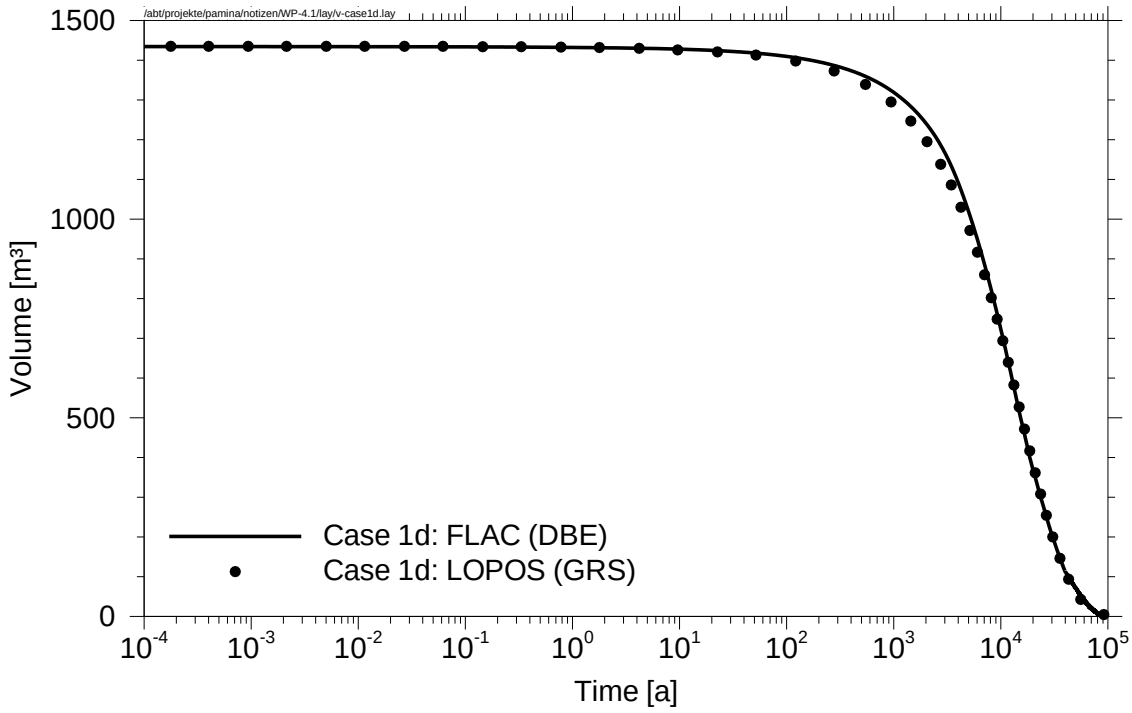

Fig. 5.7 Comparison of time evolution of volumes: Case 1d

Results of test cases 2a and 2b

Figure 5.8 shows the results of the convergence rate calculations of cases 2a and 2b. The LOPOS results are obtained by fitting only the parameter g_2, which is assumed to be responsible for the difference in the convergence rate results for dry and wet backfill. A parameter value of $g_2 = 10^2$ gives a good match with results from the rock mechanics calculations for dry backfill. For wet backfill g_2 is increased to $g_2 = 10^4$, giving also a good match.

Figure 5.9 shows the time evolution of the cavity's volume. The coincidence with results from the rock mechanics calculation is really well.

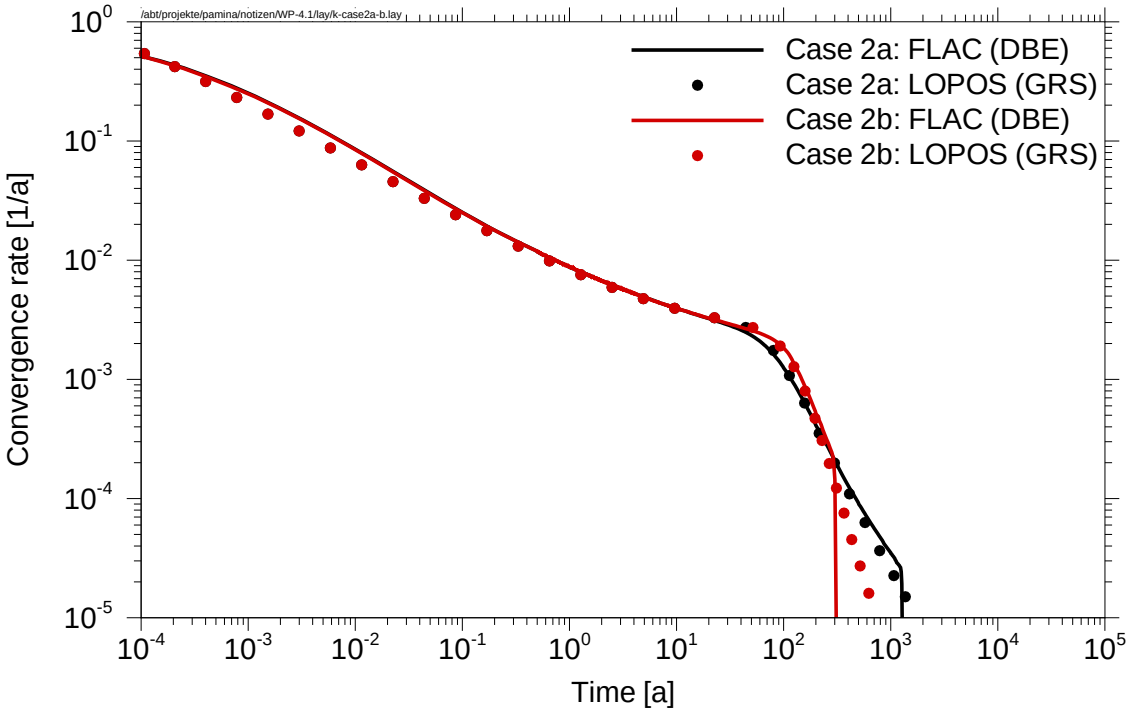

Fig. 5.8 Comparison of convergence rates: Cases 2a and 2b

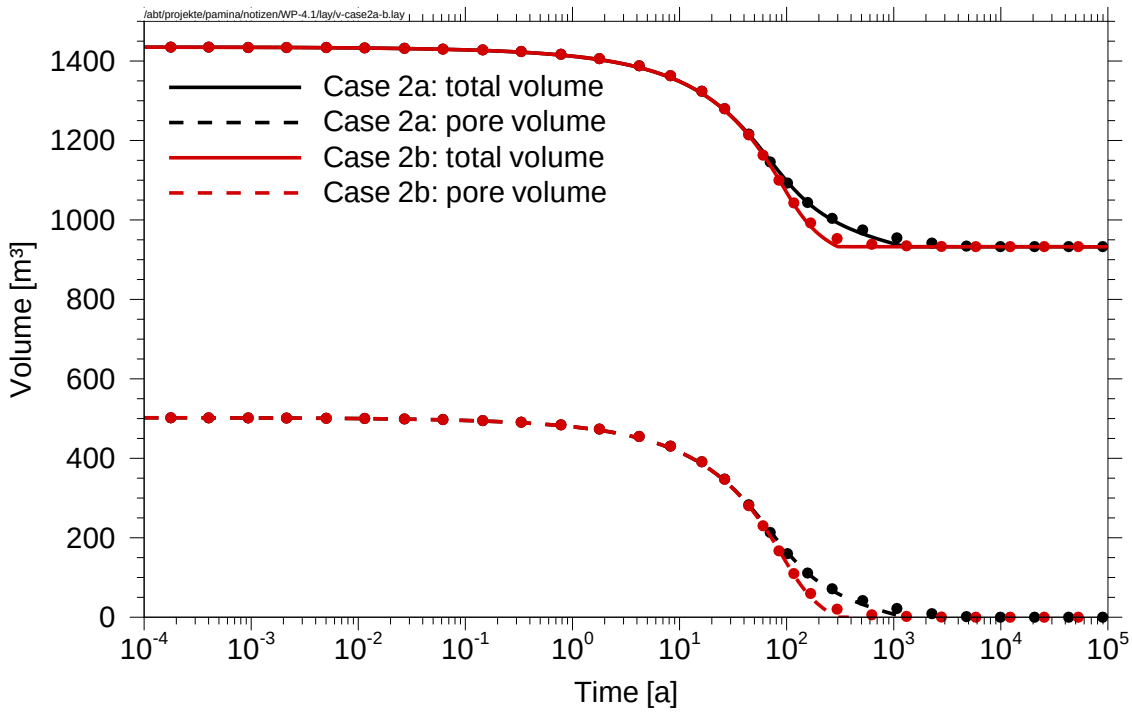

Fig. 5.9 Comparison of time evolution of volumes: Cases 2a and 2b

Results of test cases 3a to 3c

Figure 5.10 shows the results of the convergence rate calculations of cases 3a and 3b. Here, the same constant fluid pressures as in cases 1b and 1c are taken as boundary conditions. The parameter value g_2 for wet backfill is used. No additional parameter fits are necessary to get the results given in the curves. Figure 5.11 shows the time evolution of the cavity's volume. The coincidence with results obtained from the corresponding rock mechanics calculations is really well.

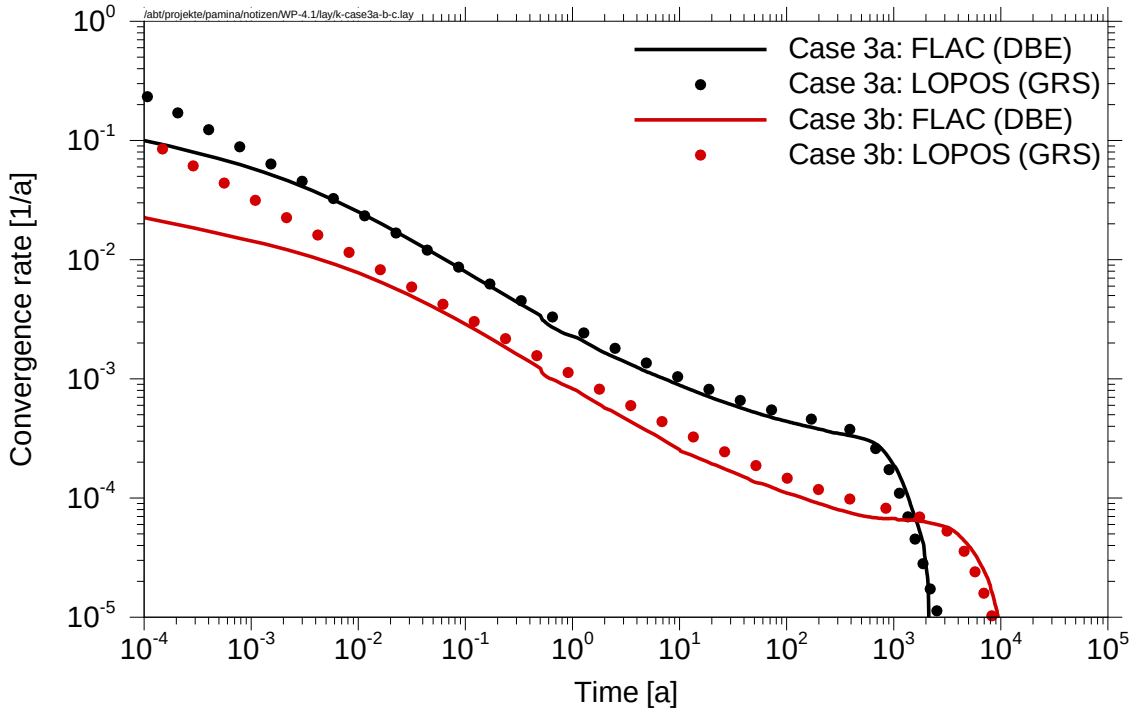

Fig. 5.10 Comparison of convergence rates: Cases 3a and 3b

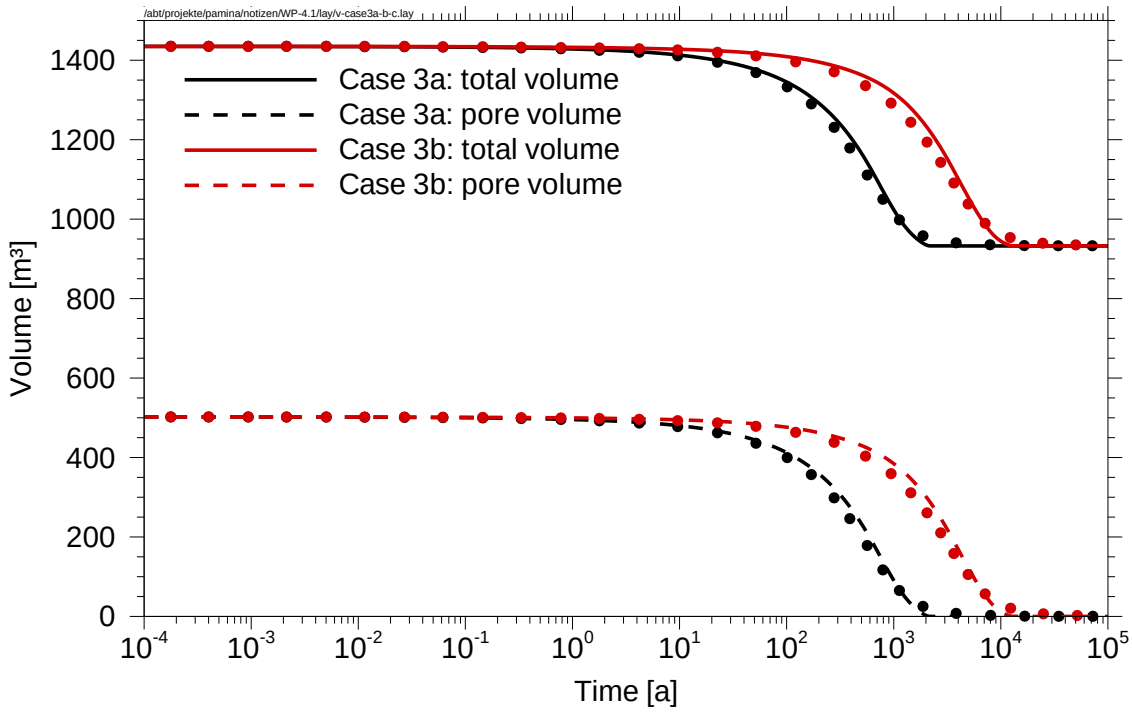

Fig. 5.11 Comparison of time evolution of volumes: Cases 3a and 3b

Results of test case 3c

In case 3c the fluid pressure is raised as in case 1d. Here, the LOPOS model yields the same hydraulic pressure in the cavity, since the backfill of that cavity has almost no influence on the flow resistance of the repository as a whole. This effect can be explained by the segment structure, where the rather flat cavity is located perpendicular to the shaft segment. The results given in the following figures are obtained with no additional parameter fitting.

Figures 5.12 and 5.13 show the results of the LOPOS calculations. Convergence rates and volumes resulting for case 2b (air filled cavity and wet backfill), case 3b (completely filled repository) and case 3c (progressive fill-up of the repository) are compared. The convergence rate of case 3c shows the influence of the increased pressure. At the beginning it follows that curve of 2b, after 50 a the over pressure in the repository reduces the convergence rate below that of case 3b, but at late times it approaches that of case 3b. Figure 5.13 shows the corresponding time evolution of the cavity's volumes.

Figures 5.14 and 5.15 show the results of the rock mechanics calculation compared with those of the LOPOS calculation. Again, there are some differences between the results for the convergence rates. The same explanation as for case 1d holds. Figure 5.15 shows the time evolution of the total and the pore volume of the cavity. Although the convergence rates differ, the volumes match rather well.

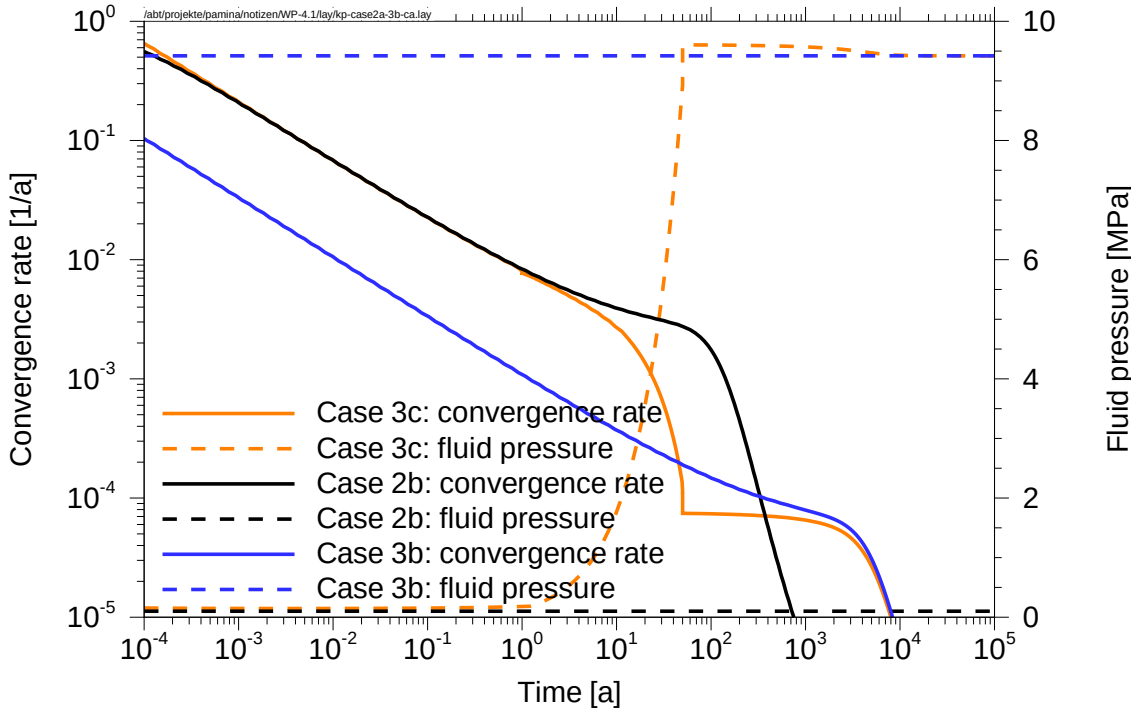

Fig. 5.12 Convergence rate and fluid pressure of cavity in test cases 2a, 3b and c

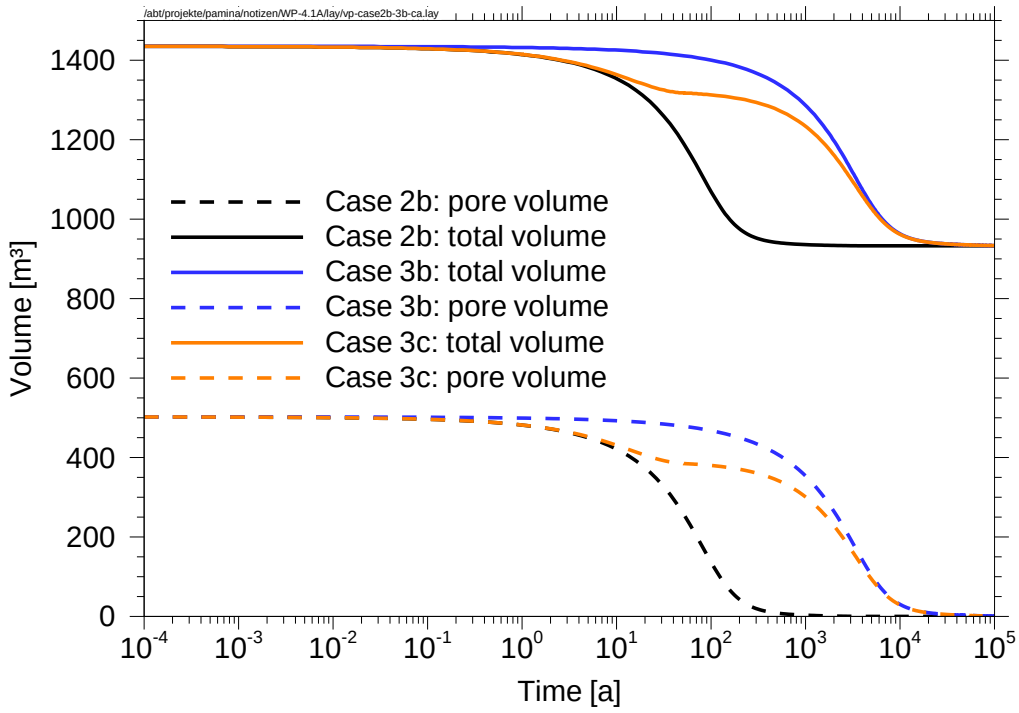

Fig. 5.13 Volumes of cavity in test cases 2b, 3b and c

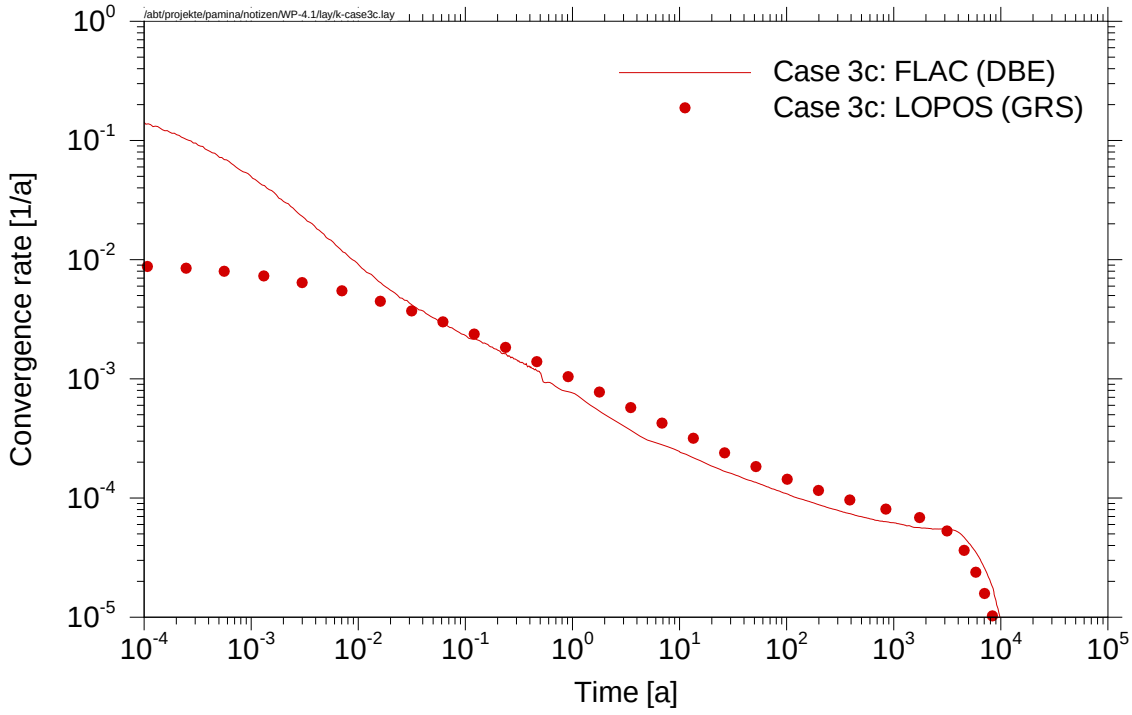

Fig. 5.14 Comparison of convergence rates: Case 3c

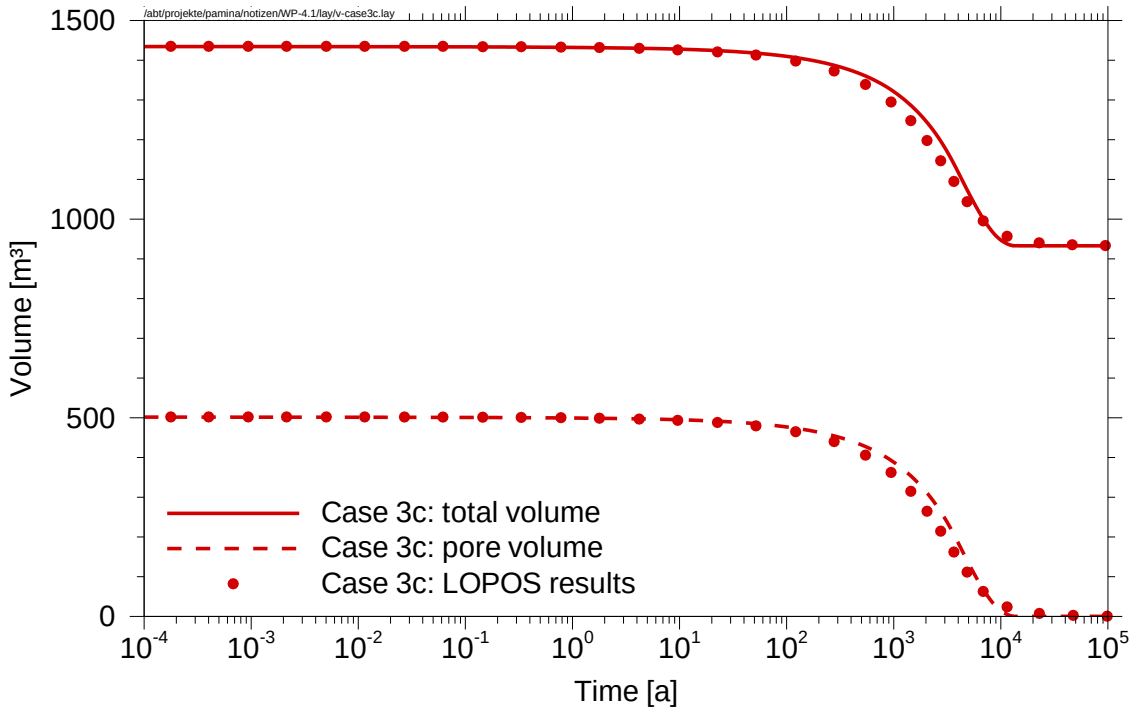

Fig. 5.15 Comparison of time evolution of volumes: Case 3c

Results of test cases 4a and 4b

In cases 4a and 4b a layer of incompactable material is assumed to be placed at the bottom of the cavity. In case 4a the remaining volume is not backfilled, in case 4b the remaining volume is filled with dry backfill. In these cases the volume which is influenced by convergence is reduced to that of the empty or the backfilled part of the cavity, respectively. The volume filled with incompactable material does not change during convergence of the cavity.

Figure 5.16 shows the results for the convergence rate, which is the same as in the corresponding case 1a (cavity without backfill) and almost the same as in case 2a (cavity with dry backfill), respectively. Only for late times the smaller volume of compactable backfill reduces the convergence rate. Figure 5.17 shows the results for the time evolution of the cavity's volume. The results are obtained with no additional parameter fits. The coincidence with results from the rock mechanics calculations is really well.

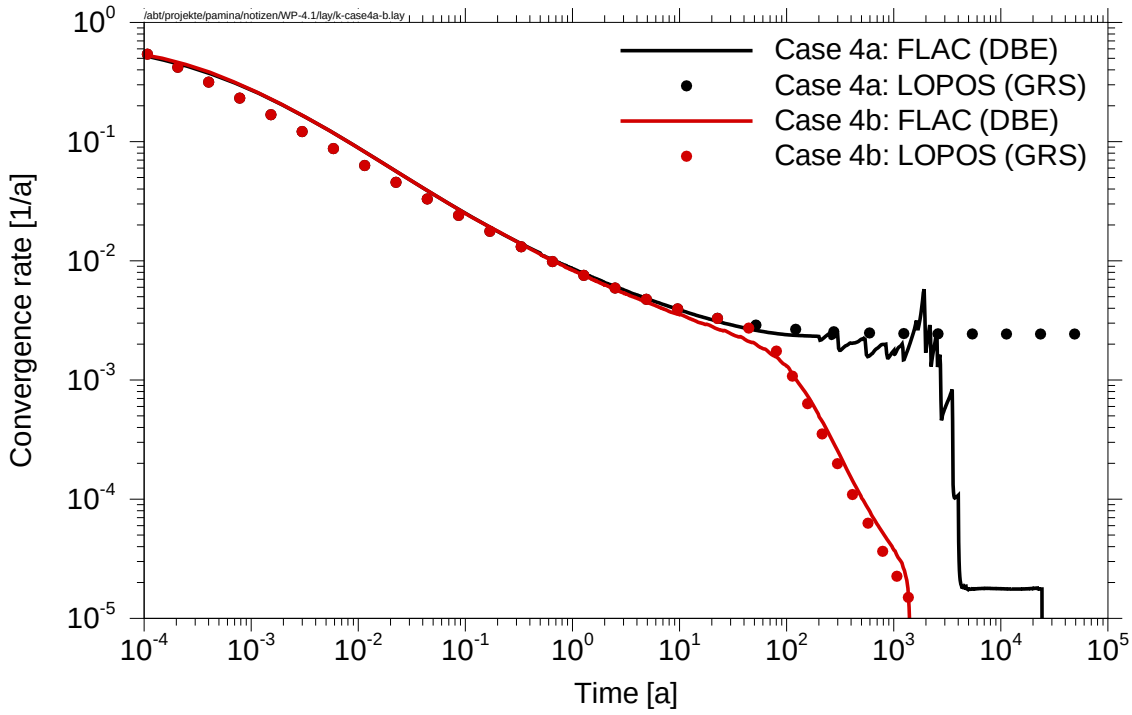

Fig. 5.16 Comparison of convergence rates: Cases 4a and 4b

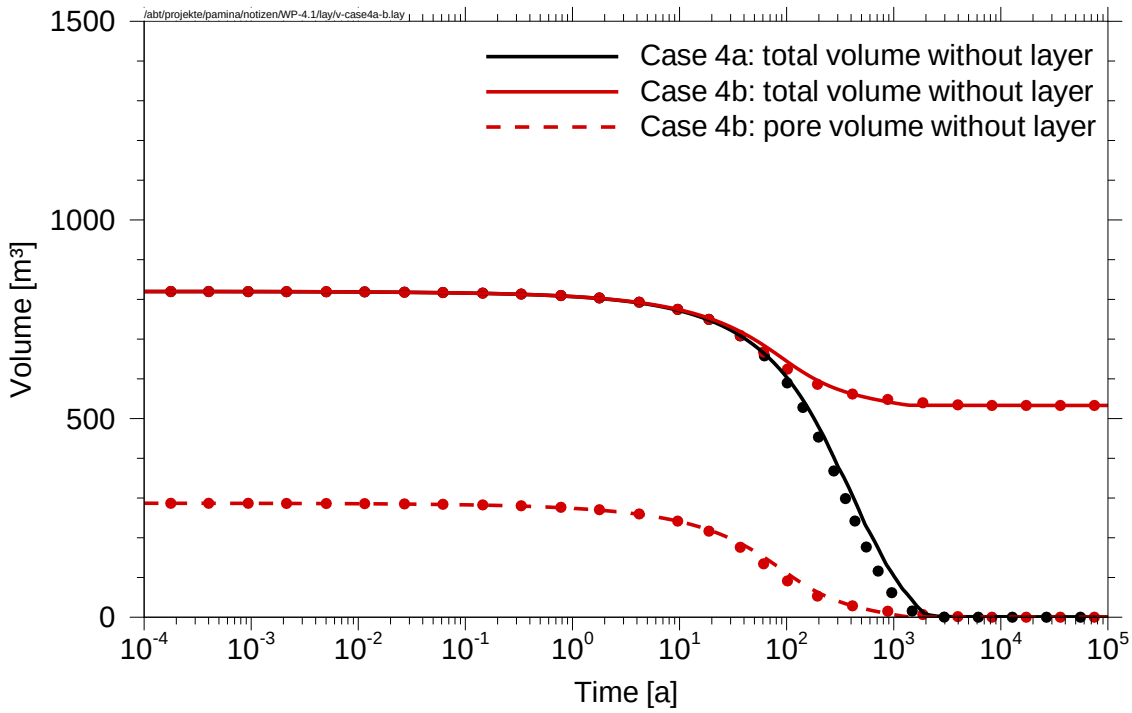

Fig. 5.17 Comparison of time evolution of volumes: Cases 4a and 4b

Results of test cases 5a to 5c

In cases 5a, 5b, and 5c it is assumed that a steel container is place on the floor of the cavity. Different hydrostatic fluid pressures are present in the cavity as given in cases 1a, 1b, and 1c. Figure 5.18 shows the convergence rates. The results are almost the same as obtained for cases 2a, 3a and 3b, respectively, except for late times where the smaller volume of compactable backfill reduces the convergence rate. Figure 5.19 shows results for the time evolution of the cavity's volume. Comparison with the corresponding results from rock mechanics calculation shows a really good match.

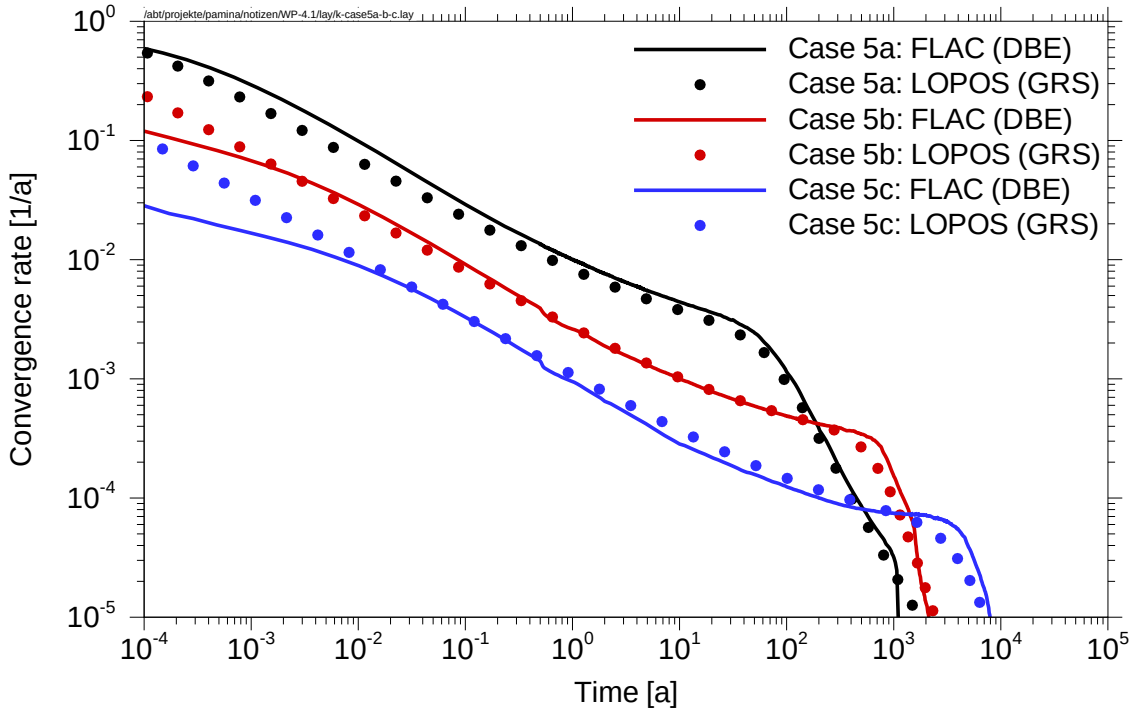

Fig. 5.18 Comparison of convergence rates: Cases 5a, 5b, 5c

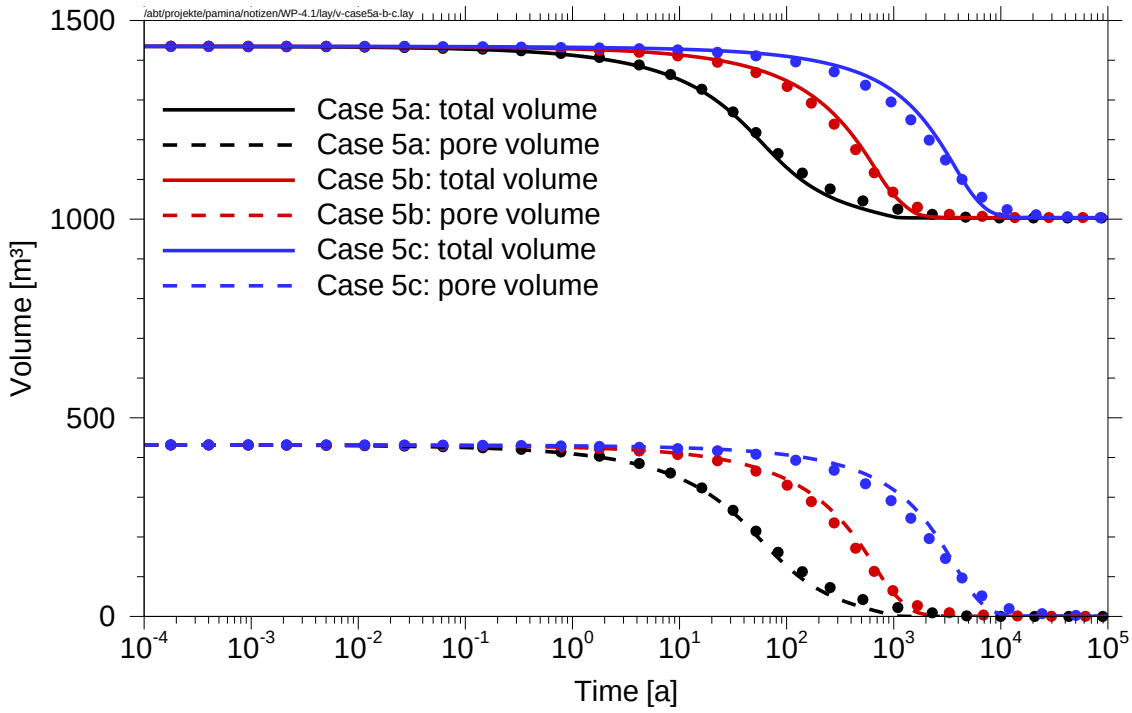

Fig. 5.19 Comparison of time evolution of volumes: Cases 5a, 5b, 5c

Result of test case 5d

In case 5d the fluid pressure is raised as in case 1d. Additionally, compared to case 3c, the steel container is place at the bottom of the cavity, reducing the backfill volume which can be compacted. Again the LOPOS model yields the same hydraulic pressure in the cavity, since the backfill of that cavity has almost no influence on the flow resistance of the repository as a whole. The results given in the figures are obtained with no additional parameter fitting.

In Figures 5.20 and 5.21 the results of the LOPOS calculations for cases 5a, 5c and 5d are compared. The convergence rate of case 5d shows the influence of the increased pressure. At the beginning it follows that of case 5a. Again, after 50 a, the convergence rate decreases below that of case 5c, due to the hydraulic over pressure. At late times it approaches the case-5c curve. Figure 5.21 shows the corresponding results for the time evolution of the cavity's volumes.

Figures 5.22 and 5.23 show the results of the rock mechanics calculation compared with those of the LOPOS calculation. Again, there are some differences between the results for the convergence rate. The same explanation as for case 1d holds. Figure 5.23 shows the time evolution of the total and the pore volume of the cavity. Although the convergence rates differ, the volumes match really well.

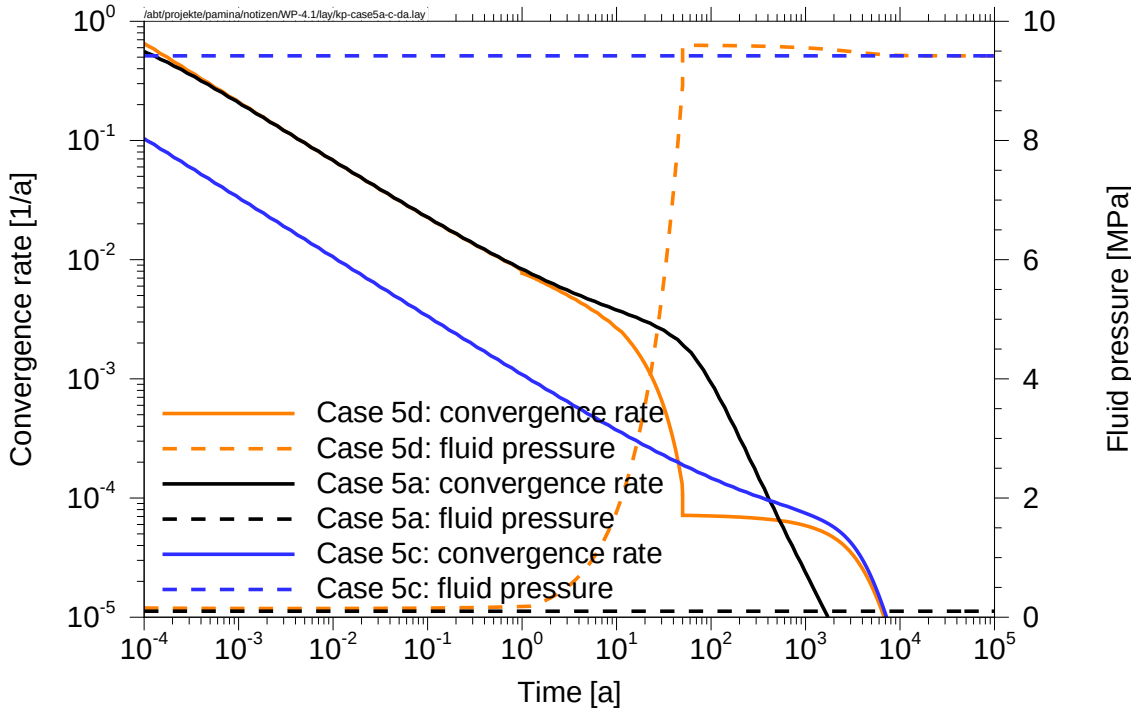

Fig. 5.20 Convergence rate and fluid pressure of cavity in cases 5a, 5c and 5d

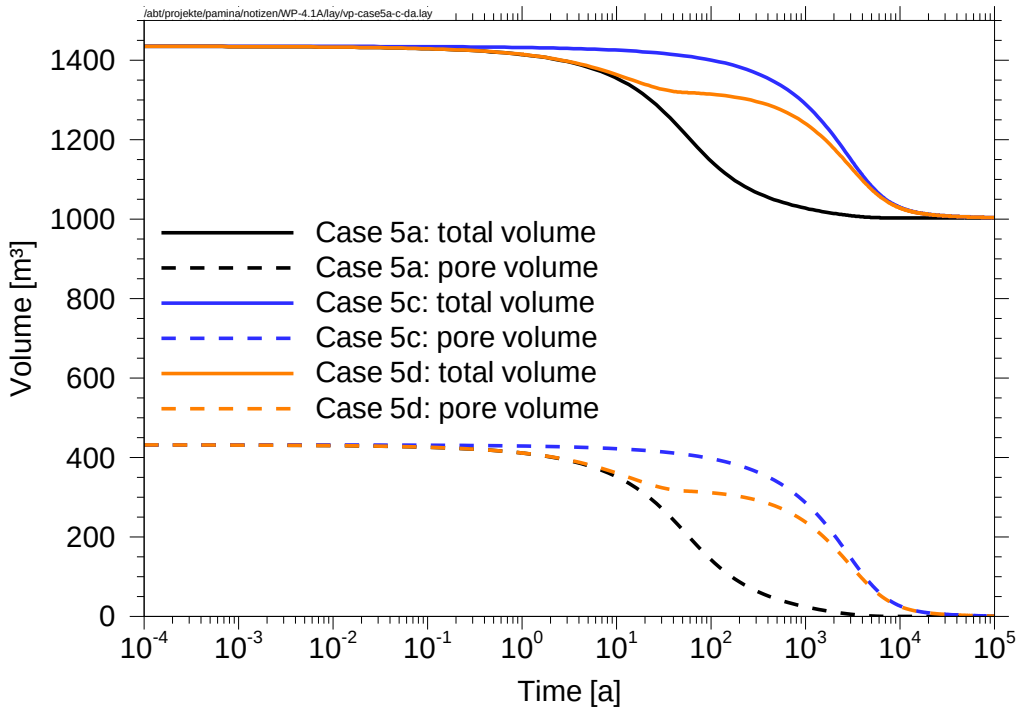

Fig. 5.21 Volumes of cavity in test cases 5a, 5c and 5d

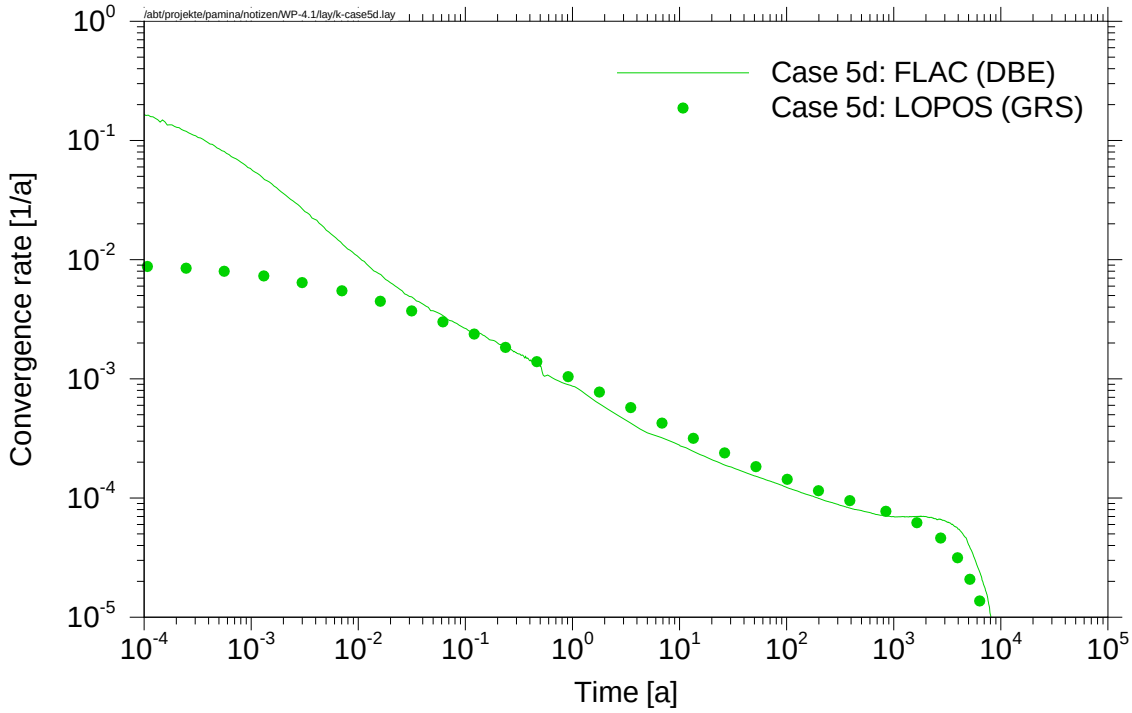

Fig. 5.22 Comparison of convergence rates: Case 5d

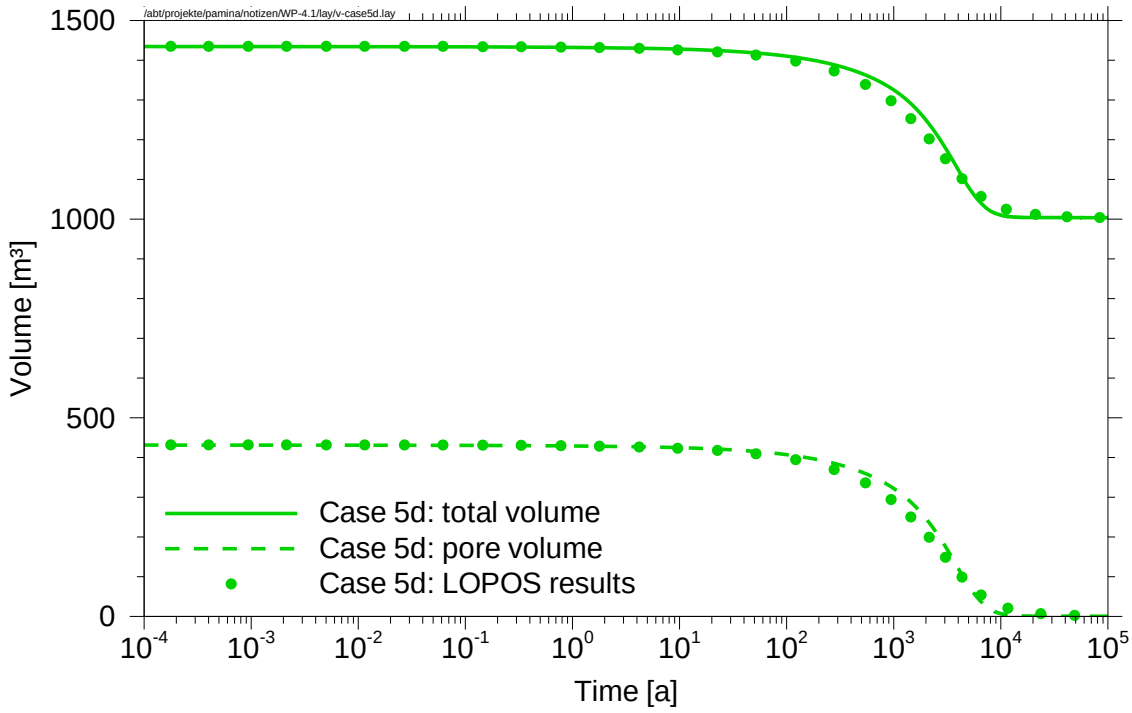

Fig. 5.23 Comparison of time evolution of volumes: Case 5d

5.1.1.3 Conclusions

In the preceding chapter, the results of benchmark tests are described for the process-level code FLAC and the PA code LOPOS. The results from the PA codes and the rock mechanic code are compared to validate the applicability of the models implemented in the PA code.

Convergence of open excavations at various fluid pressures

Two different boundary conditions have been investigated in this benchmark which are first constant and second variable fluid pressure boundary condition. In both cases the parameterisation of the EMOS model has been achieved by fitting the results of the EMOS calculation to those of the FLAC code for the first case of each set of cases for the respective boundary condition. The parameters than have been used to model the other cases within each set. With these parameter values it is found that for all the three constant-pressure boundaries and the variable pressure boundaries, the convergence rates as well as the volumes match really well the results from the FLAC code.

It is also recognised that the convergence of the host rock is strongly affected by the impact, geometry and properties of the large scale in homogeneities in the overall rock salt formation. This means that the values for the model parameters for the convergence model for a real site have cannot be derived from the comparison to the rock mechanic code, but have to be determined in-situ at the location of interest.

Convergence of backfilled excavations at various fluid pressures

Only one additional parameter was used to model the different benchmark cases for backfilled excavations, which is chosen accordingly for dry and wet backfill. No additional parameter fits are necessary compared to the benchmarks for open excavations to achieve the results given. The coincidence with results obtained from the corresponding rock mechanics calculations is really well. While there are some differences between the results for the convergence rates, this does only slightly affect the match between the results for the calculated volumes from the EMOS and the FLAC model. Since the volume is the essential parameter for the radionuclide transport calculation, this small discrepancy in the convergence rates is of no impact on the PA calculations.

Convergence of excavations that contain non-compactable objects

The results for test cases accounting for non-compactable objects by the LOPOS model were obtained without any additional parameter fitting. The non-compactable objects were either introduced by a reduced volume of the cavity or by the use of waste containers. The results are very similar compared to those of the benchmarks with only compactable backfill, since the non-compactable objects only affect the convergence for late times when the smaller volume of compactable backfill is notable. Additionally, this yields the same hydraulic pressure in the cavity, since the backfill of that cavity has almost no influence on the flow resistance of the repository as a whole. The coincidence with results from the rock mechanics calculations is really well.

Generally spoken, the results from the PA code LOPOS matches considerably well to those of the rock mechanics code FLAC. The good correlation between the PA and the process-level code yields to the overall conclusion that no additional development of the PA codes currently has to be envisaged to enhance the modelling of the convergence process.

5.1.2 Benchmark on brine intrusion into a backfilled drift

In a normal evolution of a repository design in rock salt, no transport medium is present in the repository in a salt formation. In case of the analysis of altered evolution scenario, brine intrusion may occur from either outside of the salt formation or from undetected brine inclusions in the neighbourhood of the repository. In both cases, intruding brine may successively fills up the residual voids within the backfilled drifts, chambers or boreholes of the repository, eventually get in contact with the disposed waste Contaminated brine may then be pressed out of the salt formation by convergence of the salt rock or other processes like gas generation. Thus, the process of brine intrusion, where brine percolates through an unsaturated backfill (e. g. crushed salt), is an important safety relevant process, which has to be implemented with sufficient accuracy in a PA code

In the present performance assessment (PA) codes used to model brine intrusion into backfilled drifts, the flow resistance of these drifts is assumed as independent of the gas or brine saturation of the backfill. The permeability only varies as a result of the changing porosity, but not as a function of the gas saturation. Some simplified model,

based on a single (fitted) parameter, may be included in the PA codes to account for instance for the settling of crushed salt when becoming wet or the dissolution of backfill by contact with unsaturated brine. To test the relevance of unsaturated flow processes in case of brine intrusion into a backfilled gallery, a benchmark is performed in which two different models were used: a numerical 3D programme (HYDRUS2D/3D) /SIM 06/ and the PA code LOPOS /BUH 99/.

HYDRUS software package is able to simulate two- and three-dimensional variably-saturated water flow and the transport of heat and solutes, including sequential first-order decay reactions. The HYDRUS program numerically solves the Richards equation for saturated-unsaturated water flow and convection-dispersion type equations for heat and solute transport. The water flow part of the model considers prescribed head and flux boundaries, boundaries controlled by atmospheric conditions, free drainage boundary conditions, as well as a simplified representation of nodal drains. First or third type boundary conditions can be implemented in both the solute and heat transport parts of the model. The governing flow and transport equations are solved numerically using Galerkin-type linear finite element schemes.

5.1.2.1 Test case

The model comprises a backfilled drift (grey) of length L with an adjacent fully-saturated shaft at the left, and an empty chamber at the right (figure **5.24**). The drift is initially dry. The chamber acts as a sink for the outflow from the drift. The initial state of the backfilled region is characterised by the porosity ϕ_s, the permeability k and the residual water/brine saturation ϕ_r. The interface with the disposal chamber may be completely permeable, allowing water to drain freely at atmospheric pressure.

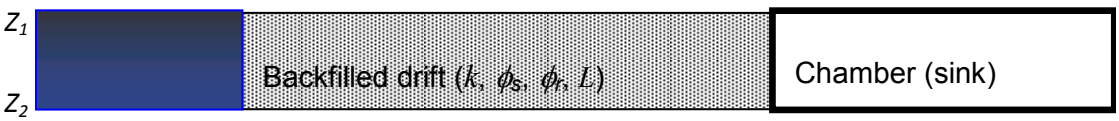

Fig. 5.24 The conceptual model of the test case

Two data sets were considered in the following calculations, which describe water movement through an initially dry low and, respectively, high permeable backfilled drift. The variation of the permeability k with porosity ϕ_s is specific to crushed salt backfills

and it is given by $k = 2.540 \cdot 10^{-10} \cdot \phi_s^{4.175}$ /BUH 99/. The saturated hydraulic conductivity K_s depends on permeability k, water density ρ and viscosity μ and is given by

$$K_s = \frac{\rho g k}{\mu} \tag{5.1}$$

The soil water retention, $\phi(h)$, and unsaturated hydraulic conductivity, $K(h)$, functions are given by Mualem-van Genuchten model /SIM 06/. The van Genuchten parameters ϕ_r, ϕ_S, α, n and l are given in table 5.1. The calculations have been performed with a permeable boundary to the right.

Tab. 5.1 Input data for the two models case 1 (high permeability drift) and case 2 (low permeability drift).

Parameter	Variant 1	Variant 2
Depth of the drift [m]	800	
Length L, and height H of the drift [m]	L = 50 m, H = 5 m	
Viscosity [Pa·s]	0.0017	
Density [kg/m^3]	1 200	
Van Genuchten parameters		
Residual water content ϕ_r [-]	0.001	
Coefficient α [-]	0.2	
Exponent n [-]	3.7	
Pore connectivity parameter l [-]	0.5	
Permeability [m^2]	10^{-14}	10^{-18}
Saturated soil water content ϕ_S [-]	0.088	0.0097
Hydraulic conductivity K_s [m/s]	$6.92 \cdot 10^{-8}$	$6.92 \cdot 10^{-12}$

The relationship between the water content θ [-], and the suction pressure (pressure head), h [m], for variant 1 and 2, usually called soil-water retention curves, are displayed in figure 5.25. This curve is a characteristic for different types of soils (materials). Soil suction, expressed as negative pressure values (as p_{atm} = 0) can change from zero, when water content

$$\theta = \frac{volume\ of\ water}{total\ volume\ of\ soil} \tag{5.2}$$

approaches to porosity n, to 100 m when the material is very dry. When the soil is not saturated, water flows downward by gravity flow through interconnected pores that are filled with water and, to a lesser extent, as a film flowing along particle surfaces in pores incompletely filled with water. The behaviour at low water contents (residual

moisture) reflects the fact that soil never completely looses all of its water. At the lower limit of the moisture content, water coats the solid soil matrix. When the liquid coating becomes too thick to be held by surface tension, a droplet will pull away and be drawn away by gravity. With increasing water content, more pores fill, and the rate of water movement increases. As the soil approaches to saturation, hydraulic conductivity, and consequently the rate of water movement, increases. Low permeability soils have lower hydraulic conductivity and fill slower then high conductivity materials. Darcy law is valid for unsaturated flow, although the unsaturated hydraulic conductivity varies with the water content.

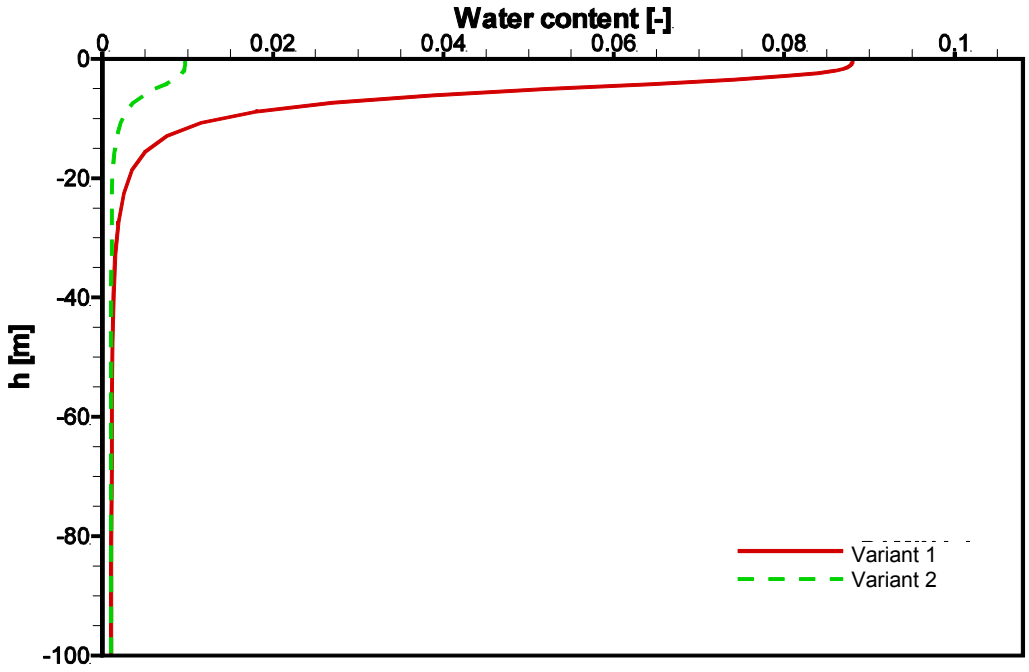

Fig. 5.25 Water-soil retention curve for variant 1 (high permeability) and 2 (low permeability)

5.1.2.2 Results

HYDRUS calculations

The backfilled drift is modelled as a 50 m long and 5 m high, 2-dimensional porous media. The top of the drift is located 800 m below the earth surface. The flow domain of 250 m^2 was discretized in 3 092 triangular elements and 1 657 nodes, corresponding to a distance of 0.5 m between two adjacent nodes.

The initial pressure head distribution is depth-dependent, and it mimics a dry environment, close to the residual moisture content (0.001). Thus, the values of the pressure head imposed on the top of the drift and corresponding to an initial moisture content of 0.0012, are -18.7 m for variant 2 and -47.5 m for variant 1, respectively.

The top and the bottom of the drift are assumed impermeable. At the left, the drift is in contact with a water reservoir under hydrostatic equilibrium. The boundary condition to describe such a situation is given as depth varying pressure head, between z_1 = -800 m and z_2 = -805 m. At the right, at x = L, a seepage face is assumed, through which water leaves the saturated part of the flow domain. The length of the seepage face is not known a priori. The code assumes that:

- the pressure is uniformly equal to zero along the seepage face,
- water leaving the saturated zone along the seepage face is immediately removed by no matter which removal mechanism.

The temporal evolution of the average outflow rates for both variants is shown in figures 5.3 and 5.4, respectively. Water breakthrough appears at 22.78 days (variant 1) and 61.2 years (variant 2), respectively.

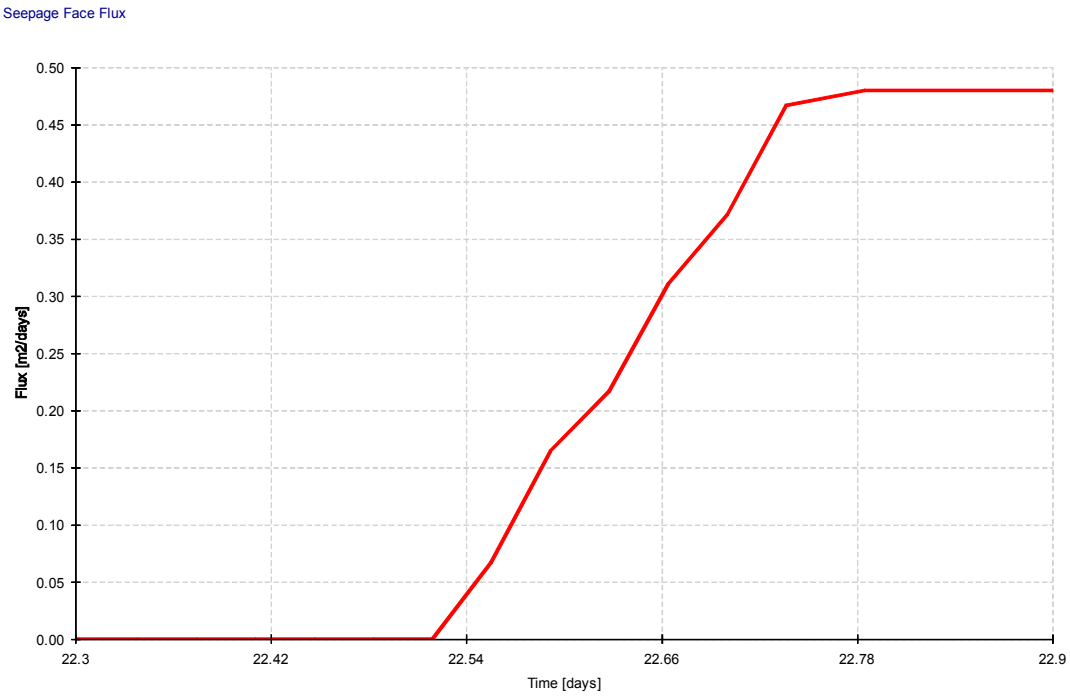

Fig. 5.26 Variant 1 - Average right boundary water flux (outflow)

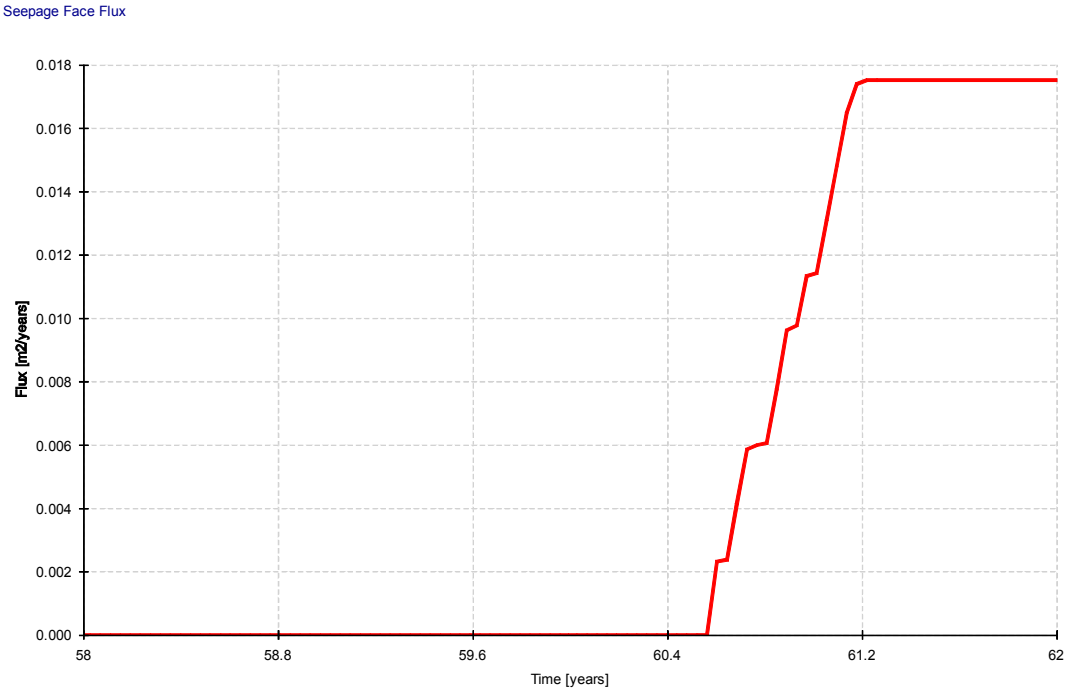

Fig. 5.27 Variant 2 - Average right boundary water flux (outflow)

The moisture front through the backfill is rather sharp for both cases, as shown in figures 5.28 and 5.29. The pressure head remains at the initial value until the moisture front arrives, then it reaches the zero pressure head and it becomes active (i. e., water flows through it).

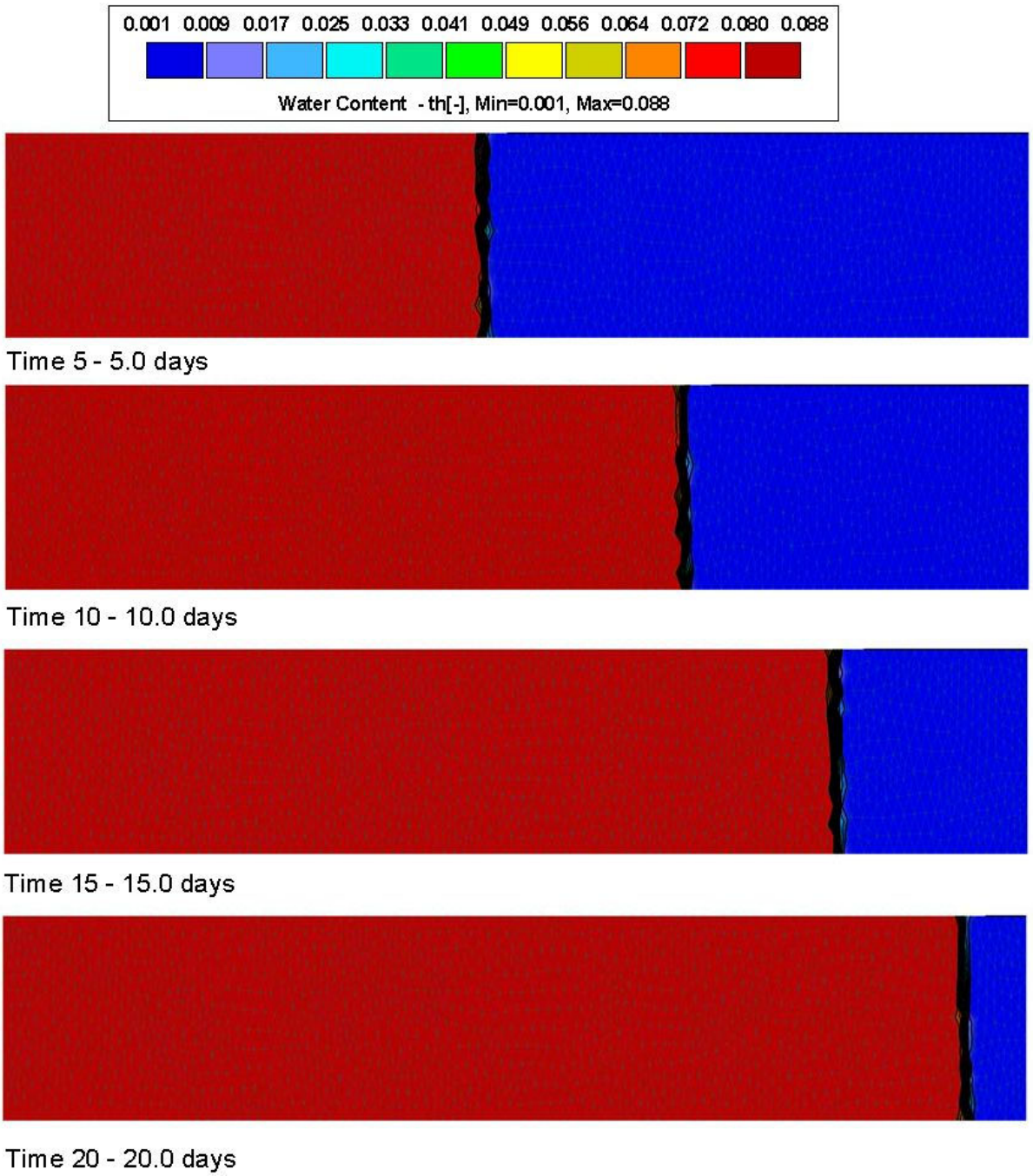

Fig. 5.28 Advance of the moisture front in the high permeable backfilled gallery (variant 1)

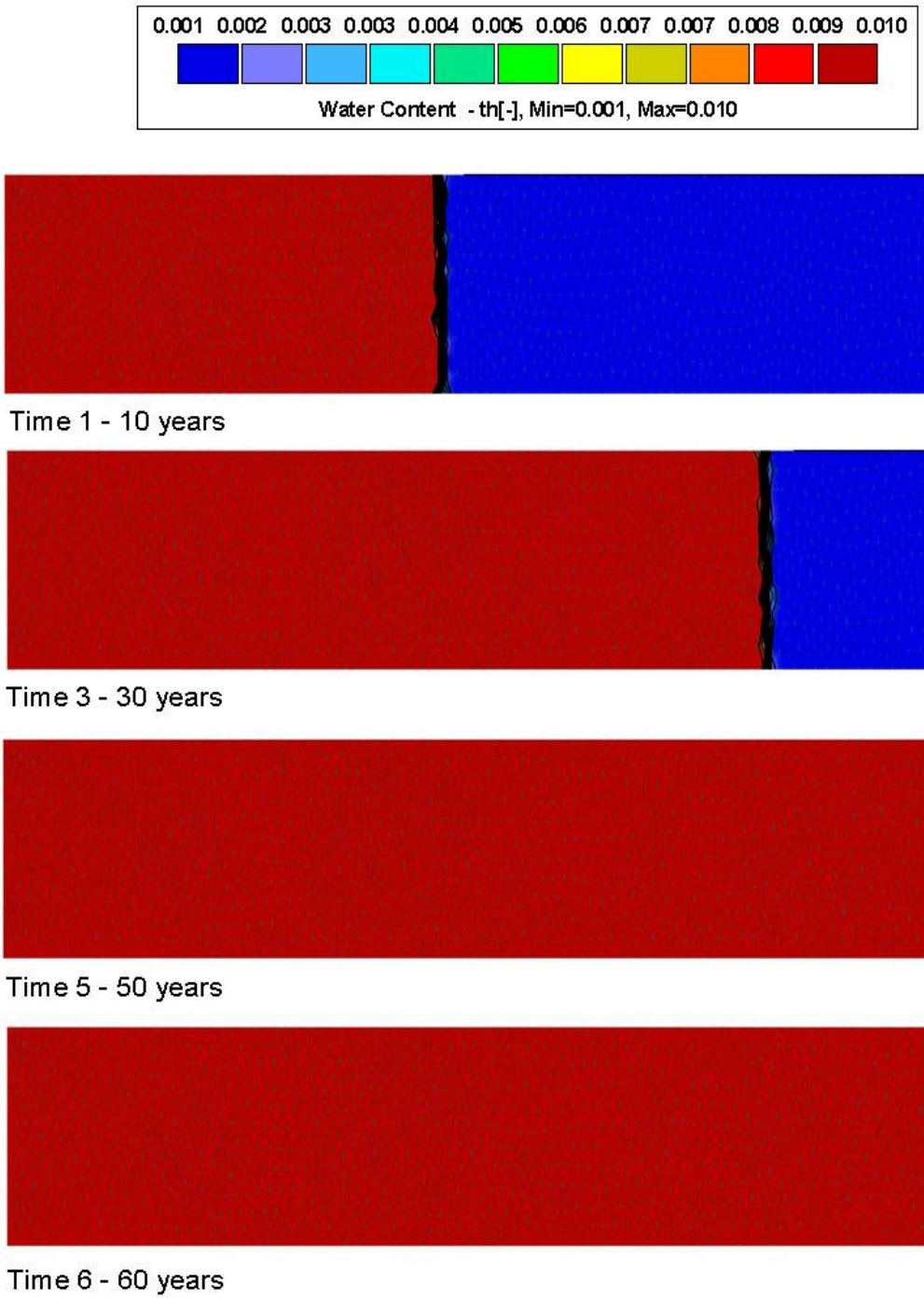

Fig. 5.29 Advance of the moisture front in the low permeable backfilled gallery (variant 2)

The right boundary is considered a seepage face in the modelling, through which water leaves the saturated part of the flow domain. As a consequence, the breakthrough times in different locations of the right boundary are influenced by the rise of the height of the saturated front. Water leaves the flow domain sooner in the lower parts of the boundary. As the moisture content increases to saturation, the height of the seepage

face increases. The breakthrough times for points located closer to the upper boundary are delayed compared to those which are closer to the bottom. For the low permeability case, the domain attains saturation at t = 60.7 years (22.54 days, for variant 1) at the bottom, respectively at t = 61.2 years (22.84 days for variant 1) at the top. The pressure head increases gradually in the same time interval to 0, until full saturation is attained. The effect of the different water contents between high and low porosity cases can be seen from the evolution of the pressure heads. The moisture content at the top is lower then at the bottom, due to gravity which pulls down the water droplets. Consequently, suction is lower at the top, compared to the bottom.

Calculations with the PA code LOPOS

The system modelled for the Test Case is a sequence of three segments: a water reservoir (saturated shaft), a dry backfilled drift and an empty gallery, acting as water sink.

For modelling of the test case with LOPOS code, a horizontal segment structure, with rectangular cross-section has been created, as shown in 5.30. The segment model HIQQN3 has been assigned to the water reservoir, which is also the contact point to the geosphere. The backfilled gallery and the sink were described by the model HKSQNN.

Fig. 5.30 Segment structure and associated segment models used with LOPOS

The HIQQN3 segment model is modelling the constant water inflow/outflow rates in a horizontal segment. Segment model HKSQNN describes water (and contaminant) movement through a horizontal gallery with non-compactable backfill. The gallery is modelled as a geometrical volume with high pore volume to allow water inflow over long time (“source”). Inflow into the gallery stops after complete flooding. During flooding, water pressure rises with increase in the water level. When the segment is completely flooded, water pressure reaches hydrostatic pressure.

In order to assess the effect of spatial discretisation on the results; the drift segment has been discretized either into 50 parts (in the following called blocks), each one 1 m long, or into one segment.

Temporal evolution of the water level, height of the water table, outflow rates and pressures from the gallery for the modelling variant with one block are shown in figures 5.31 and 5.32. The height of the water level rises during the fill-up phase from zero to the height of the segment, while the water content approaches saturation (cf. figure 5.31). As shown in figure 5.32, the outflow starts with first drops of water in the gallery. When the segment is completely flooded, the pressure rises to hydrostatic and the flow rate out of the gallery reaches a plateau. The water pore volume and pressure in the drift increase gradually to saturation, respectively hydrostatic pressure.

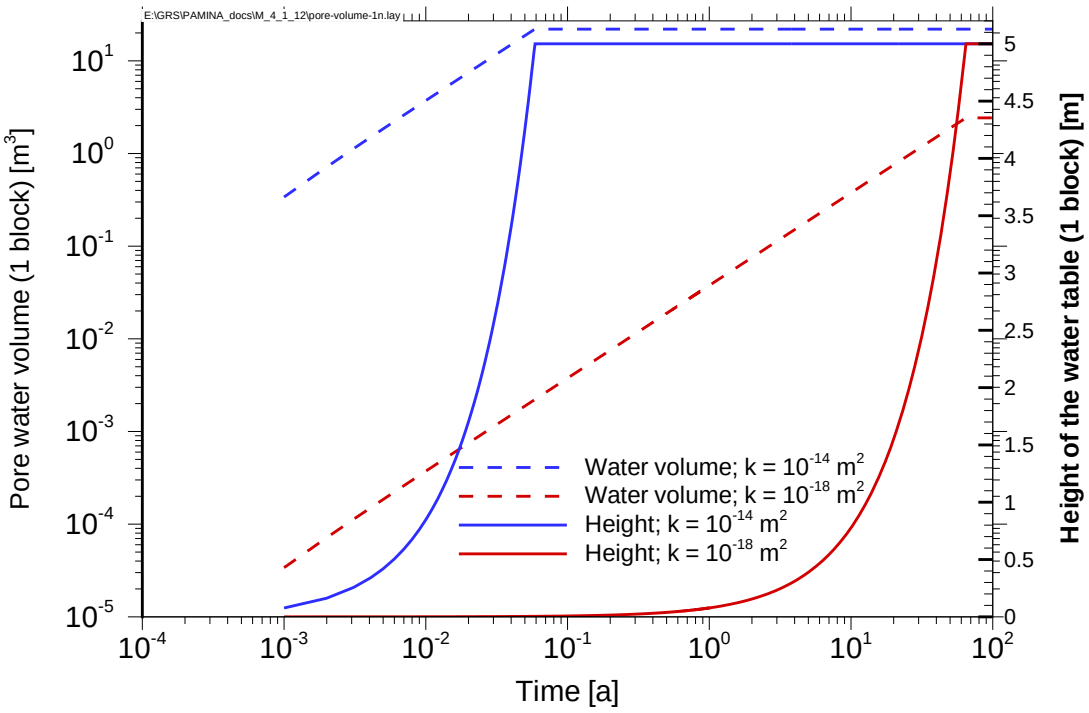

Fig. 5.31 LOPOS model (1 block) – Temporal evolution of the pore water volume and of the height of the water table in the gallery

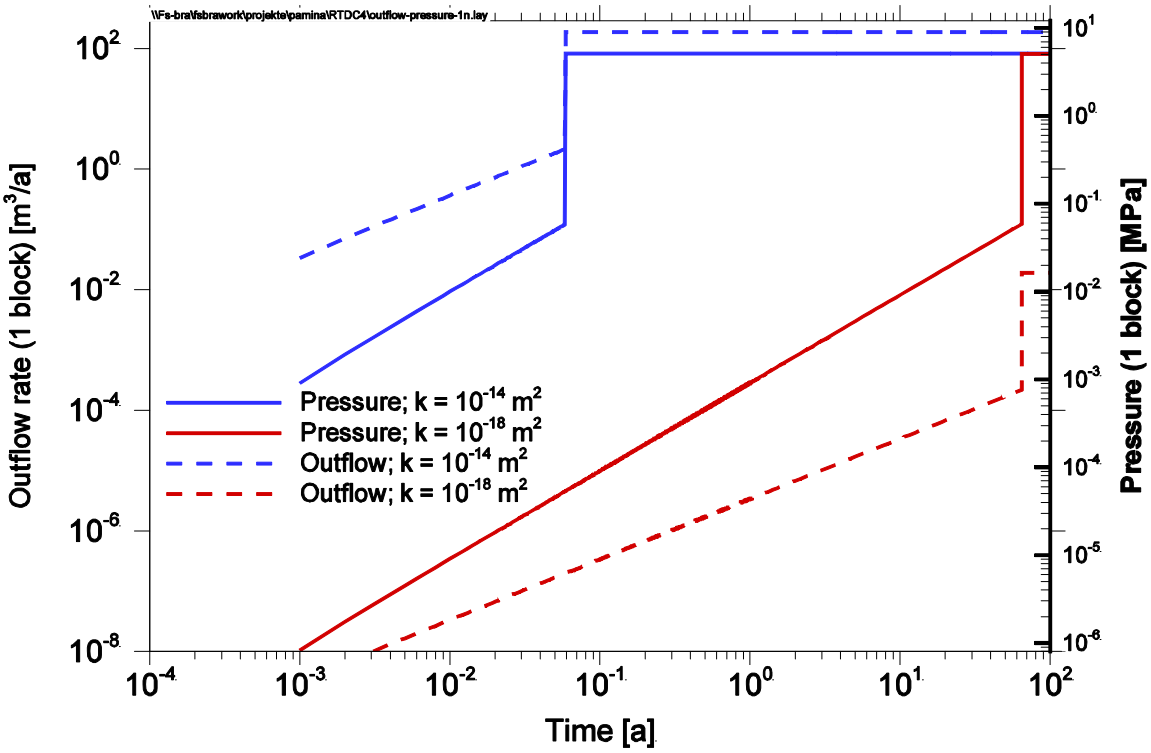

Fig 5.32 LOPOS model (1 block) – Temporal evolution of the outflow from the gallery and of the pressure

The times when fully-developed flow starts for both discretisations are shown in table 5.2. For the high conductivity case (variant 1), where the two codes show very good agreement, discretisation offers a result which is closer to the one obtained with a specialized code. The discretisation introduces a delay in the flow calculation with one time step for each block. Flow through unsaturated domain is slower then saturated flow, which is implemented with LOPOS code, and with appropriate choose of the time steps the discrepancy between the two approaches could be handled. The situation is the other way around when flow through a low permeable domain is to be modelled. In this case, a coarser discretisation seems more favourable, as the results from variant 1 point out.

Tab. 5.2 Times when fully-developed outflow start (times of attaining the plateau), and the corresponding outflow rates averaged over the height of the drift

Case	Discretisa-tion	Time (Relative difference %)	Average outflow rate [m^3/a]
LOPOS variant 1	1 block	21.535 d (95.6 – 94)	186.7
	50 blocks	22.63 d (100.5 – 99.1)	186.8
HYDRUS variant 1 bottom – top		22.52 d – 22.84 d	175.164
LOPOS variant 2	1 block	64.72 a (106.2 – 105.7)	0.01885
	50 blocks	65.62 a (108.1 – 107.2)	0.01885
HYDRUS variant 2 bottom – top		60.7 a – 61.2 a	0.017525

The water inflow and outflow rates are shown in figure 5.33 for variant 1, and figure 5.34 for variant 2, respectively. The initial time steps are different between LOPOS and HYDRUS. LOPOS starts with $\Delta t = 10^{-3}$ years, while HYDRUS has an initial Δt of around 10^{-8} years. Consequently, in the figures the onset of the inflow is set to $t_0 = 10^{-3}$ years. At early times of up to 10^{-2} a, the water inflow rates are slightly overestimated with the 50-blocks model, and strongly underestimated with the 1-block model (by comparison to HYDRUS calculations) (cf. figures 5.33 and 5.34). Afterwards, the inflow obtained with the 1-block model is higher then HYDRUS water inflow, while the 50-blocks model inflow rate is similar to HYDRUS. The time of reaching steady-state is nevertheless the same, no matter of the discretisation scheme used. For low permeability domain, the inflow rates obtained with the discretized model show a step-like behaviour. This is an effect of the pressure increase in each block at the time of complete filling.

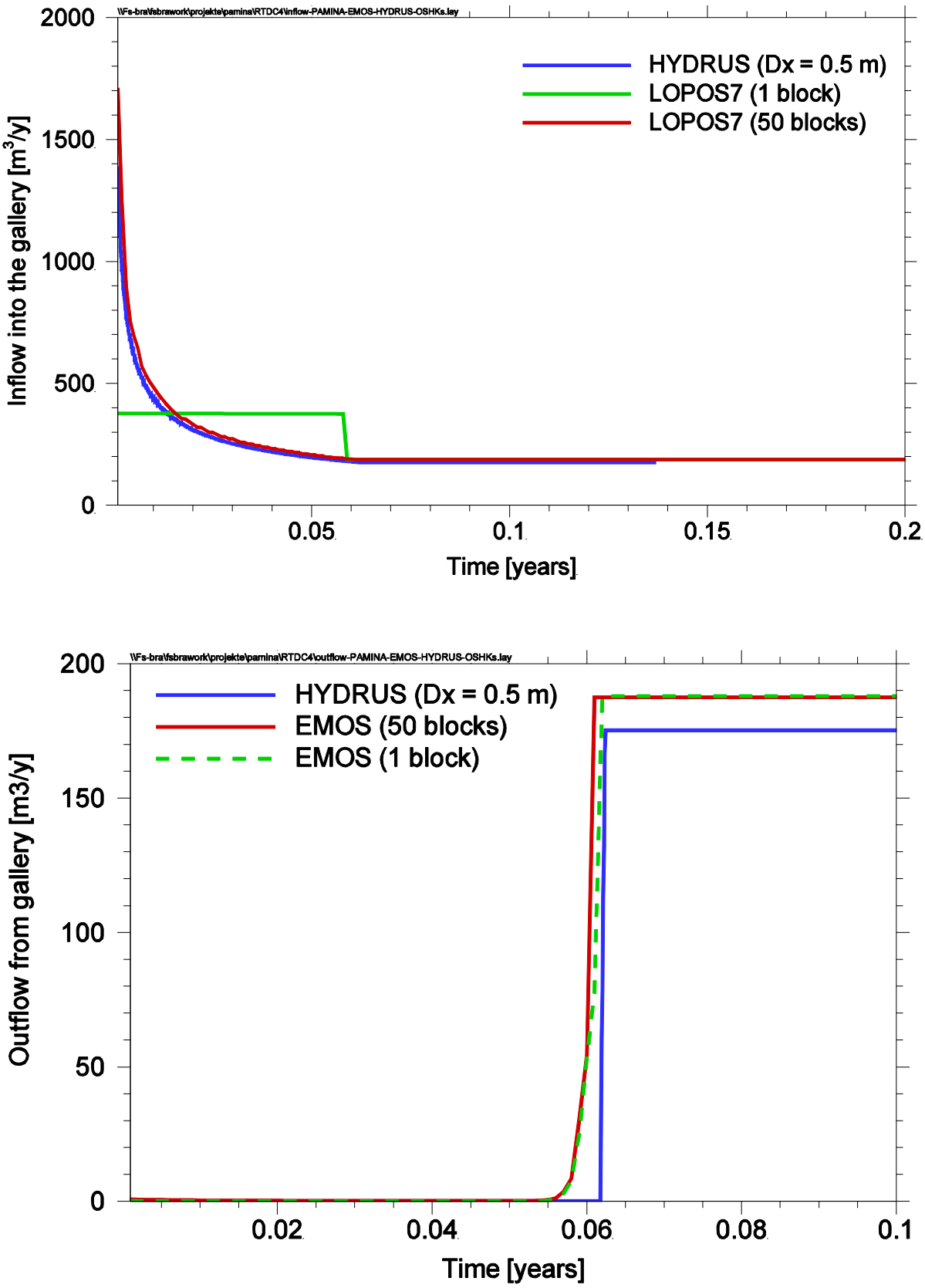

Fig. 5.33 Inflow and outflow into/out of a high permeable backfilled drift (variant 1)

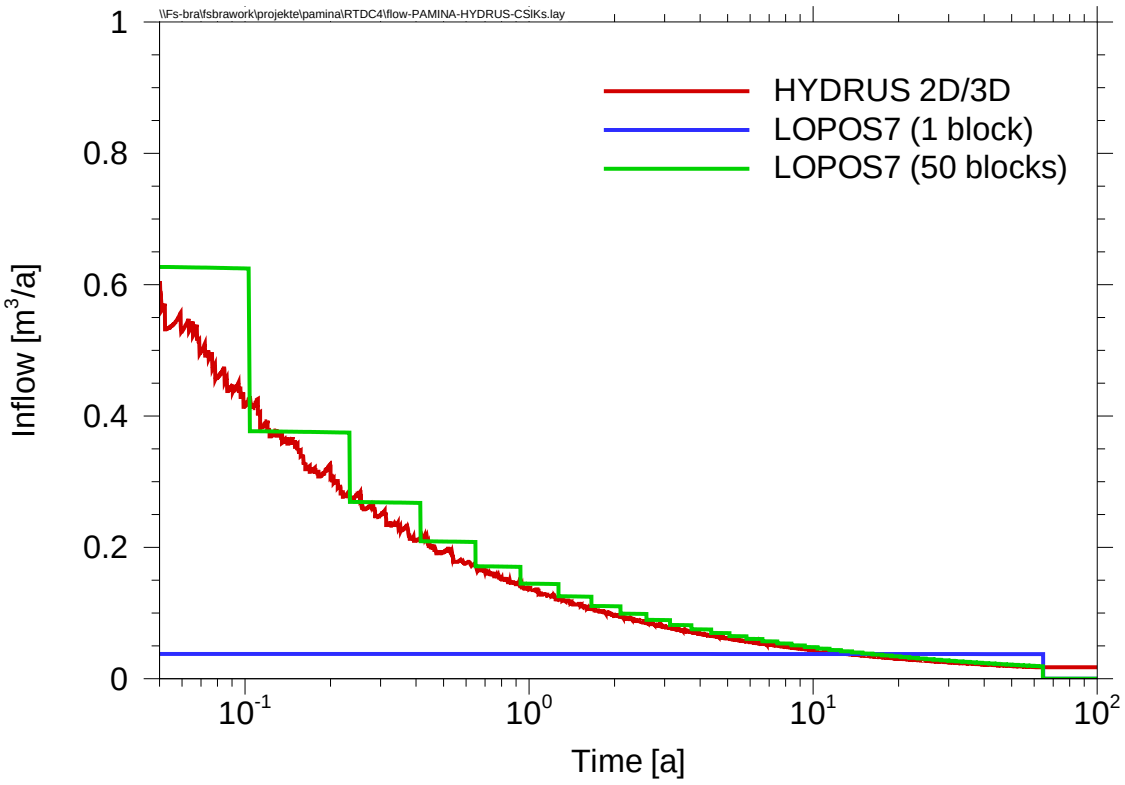

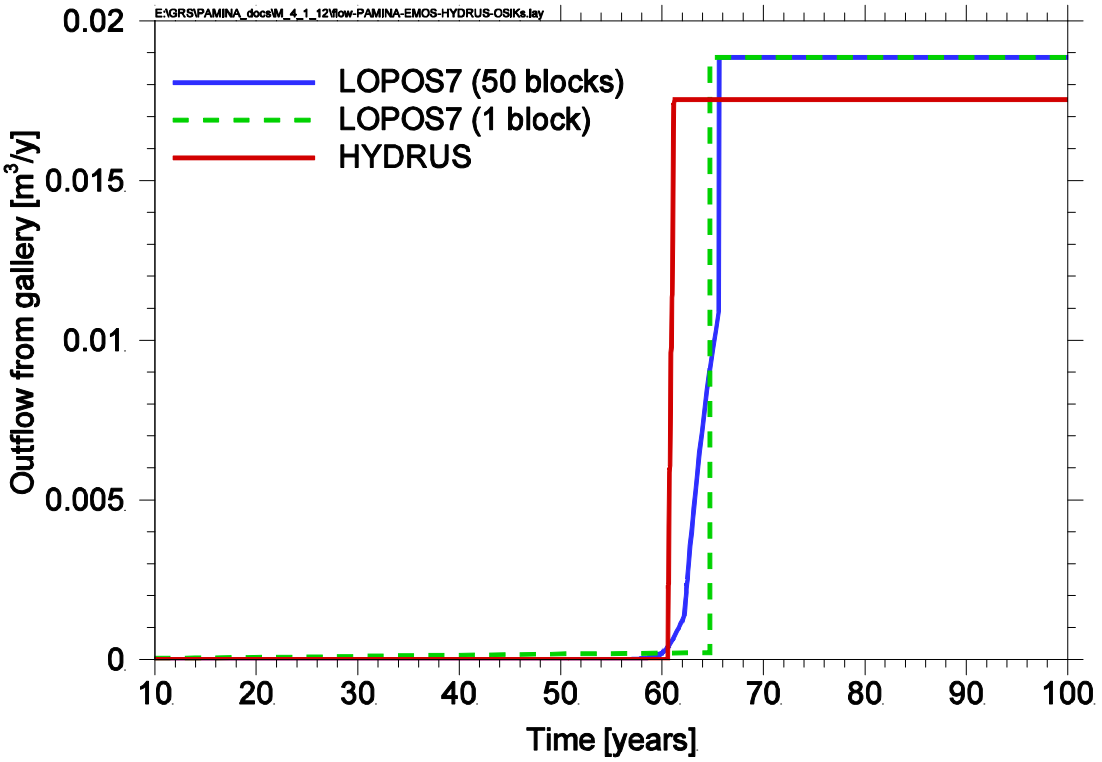

Fig. 5.34 Inflow and outflow into/out of a low permeable backfilled drift (variant 2)

The outflow rates obtained with LOPOS are higher then the HYDRUS results with about 7.6 % in the low permeability case, and 6.6 % for the high permeability case re-

spectively. LOPOS simulations show earlier breakthrough times (about 0.055 years) then HYDRUS results (approx. 0.06 years), at very low rates. That is a consequence of the modelling approach in LOPOS that allows water to flow out of the drift even if this is not completely filled (saturated). The outflow rates increase with several orders in magnitude at the time of the complete filling of the gallery. Enhancement of the outflow rate takes place earlier for highly permeable case, and later for the low permeability case, compared to HYDRUS simulations. Such behaviour indicates an overestimation of the domain conductibility for the high permeability case, while for the low permeability case, the conductive characteristics are underestimated.

Cumulated inflow and outflow rates obtained with LOPOS, for high and low permeability cases are shown in figures 5.35, and, respectively in 5.36. For the high permeability case, compared to HYDRUS results, the amount of water entering into the modelled domain at t = 50 days is 7 % higher for the non-discretized model, and 11 % when discretisation is involved. The corresponding cumulated outflows are with 13 %, respectively 11 % above the HYDRUS results. When the permeability is low, the cumulated inflow (at t = 100 years) obtained with LOPOS is 10 % higher then HYDRUS results, no matter the discretisation used. The cumulated outflow drops below HYDRUS results with 2 %.

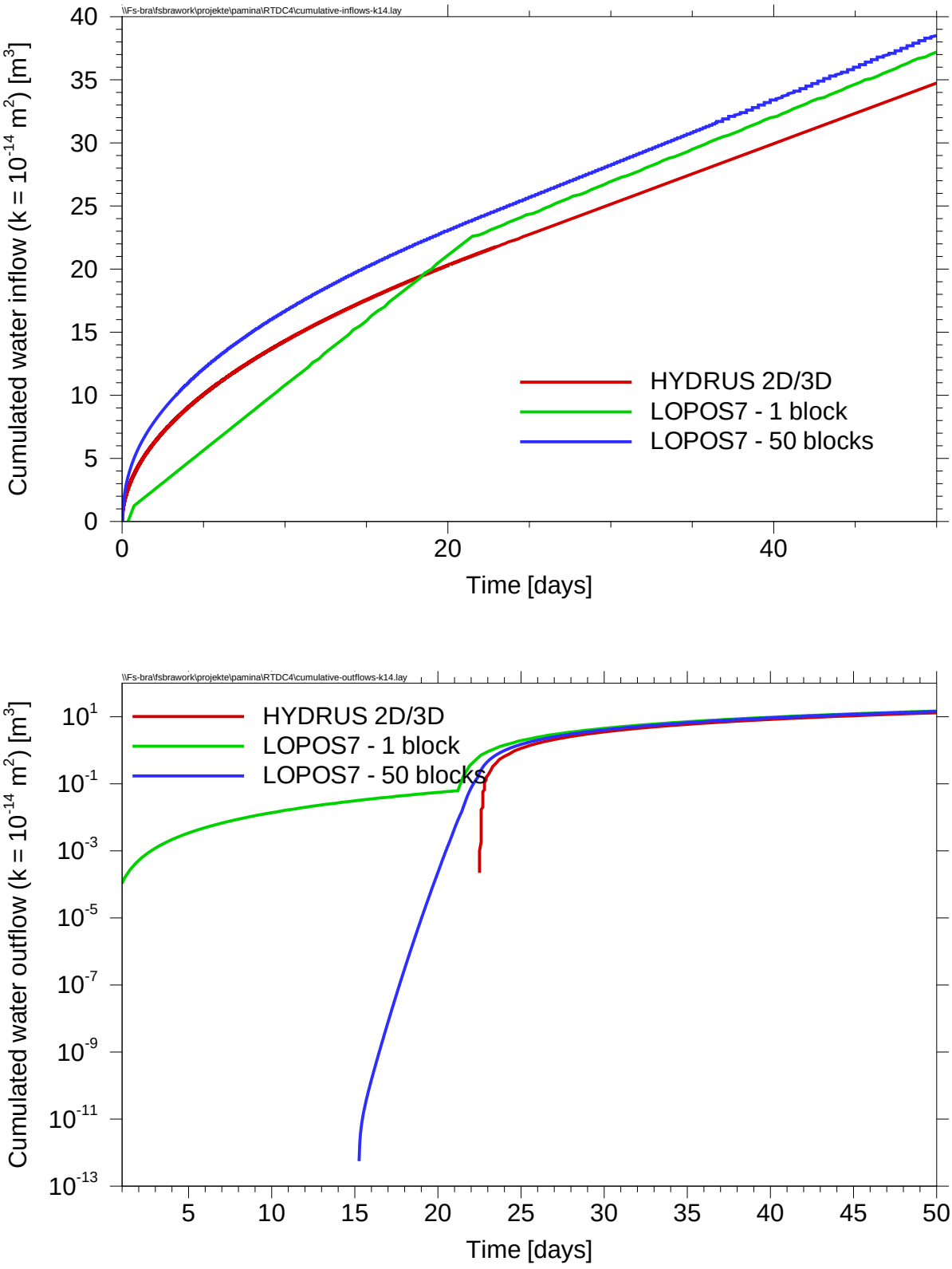

Fig. 5.35 Cumulated water inflow and outflow rates for the high permeability case (LOPOS vs. HYDRUS)

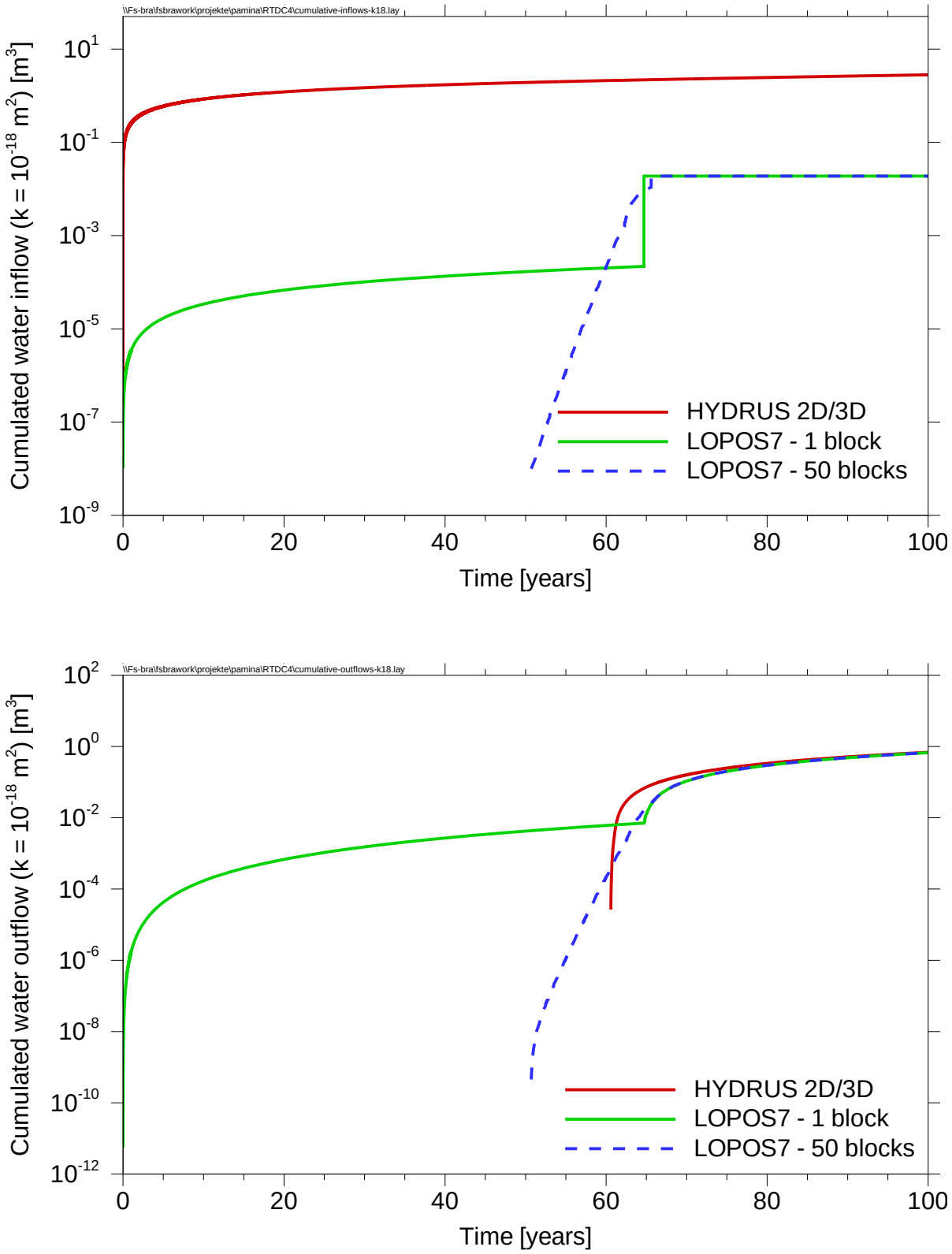

Fig. 5.36 Cumulated water inflow and outflow rates for the low permeability case (LOPOS vs. HYDRUS)

Preliminary calculations with LOPOS have been performed considering an initially wet gallery, to take into account the residual water content (θ_r = 0.001). For the low permeability case, the results were not very different compared to the case when the residual water content was not taken into account. For the high permeability situation though, significant differences were obtained, especially for the discretized model. The differences might be caused by the fact that, while with HYDRUS model the residual water volume is not free water. With LOPOS the residual water content is considered as free, available to flow water. As a result, outflow starts earlier then in the dry gallery, with a much higher rate (three to five orders in magnitude) as shown in figure 5.37. The residual water volume flows out before the onset of the water inflow from the inner neighbouring block. Then, as more water flows into the block, the pressure starts to rise, and the outflow is re-established. The difference between the early outflows for the two discretisation schemes is of about two orders in magnitude.

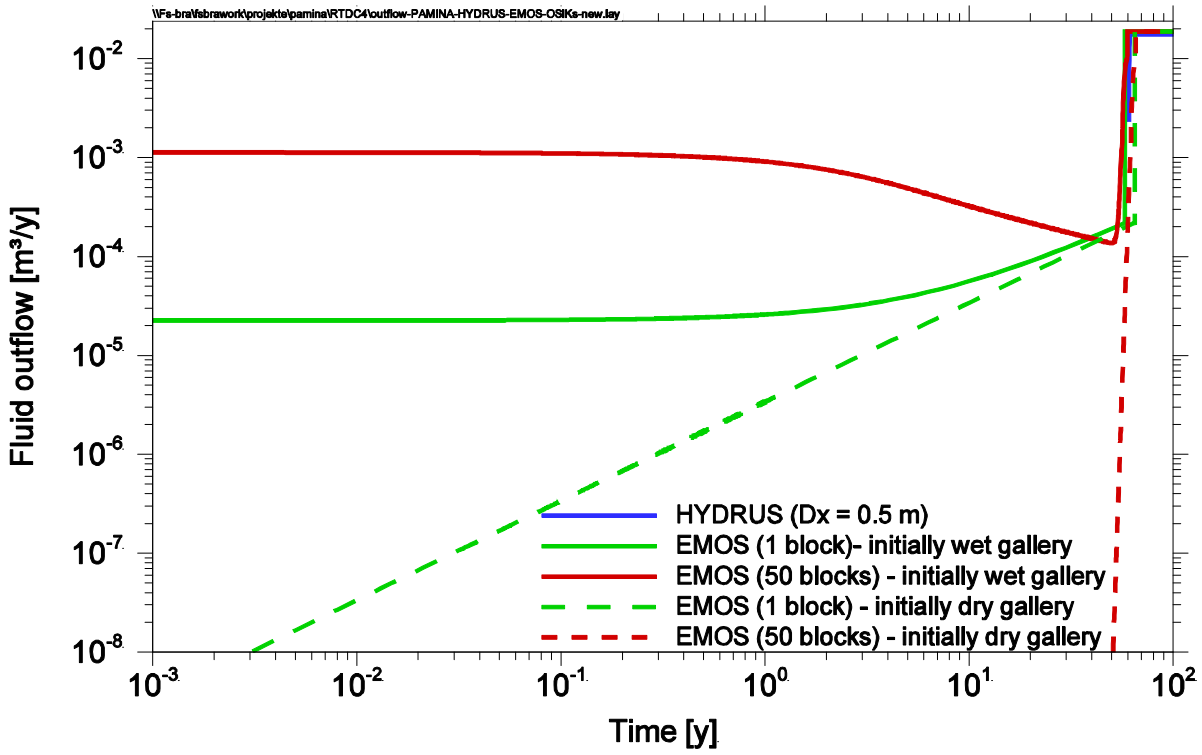

Fig. 5.37 Simulation of the residual water content in the gallery

5.1.2.3 Conclusions

There is a good agreement between the results obtained for the test case with HYDRUS and LOPOS codes. A slight discrepancy can be observed in the inflow rate calculations. At very early times – up to 10^{-2} years, LOPOS results (for the discretized

variant) are slightly higher compared to HYDRUS, of around 30 % for variant 2, and 23 % for variant 1, respectively. After that time, the discrepancies are strongly reduced, to only 6 – 7%. The difference is due the size of the initial constant time steps used in LOPOS (100 time steps of 0.001 years), and it is reduced when the code is adjusting the time mesh size. Since LOPOS is dedicated for calculations of saturated water and contaminant transport, it is using the hydraulic conductivity (i. e., the inverse resistance) of the saturated domain. As a result, the flow calculated with LOPOS is faster. The difference in the inflow rates calculated with LOPOS and HYDRUS is diminishing in time, due to the increase of the water content and, consequently of the hydraulic conductivity of the simulated domain. Nevertheless, both codes show very good agreement regarding the times of complete filling of the drift.

The agreement between the two codes is good for the outflow rates (6 to 7 % higher outflow rates obtained with the PA code LOPOS), despite the fact that LOPOS code cannot simulate accurately the residual water content. For this reason, this feature was not captured with the models used for the calculations. Nevertheless, if the modelled environment has very low residual water content, such as rock salt, the differences in the results are negligible. Both codes simulate breakthrough of water through the saturated height of the right boundary (i. e., water can flow out of the domain through the seepage face).

The discretisation has an important effect on the results, and this is more obvious in the inflow rates. The calculated outflow rates are influenced by discretisation: for the high permeability domain a finer discretisation offers more accurate results (compared with HYDRUS outcome).

In conclusion, LOPOS PA code complies with the expectancy when compared with a process-level code for processes developing within relatively short timeframes (up to tens of years).

5.1.3 Benchmark on convective flow

One aspect that is important in a repository in salt is that after backfilling of the drifts, boreholes, and chambers the remaining void volume will decrease over time due to the convergence process of the surrounding rock salt. In a normal evolution, in general, all open volumes will close and compactable material, such as salt grit, will be com-

pressed and become impermeable at a certain point in time. This provides for the long-term isolation of the waste from our environment, since no medium is present that could mobilize and transport radionuclides from the waste forms to the geosphere.

An important altered evolution scenario that has to be considered in the performance assessment of a repository in rock salt assumes the intrusion of brine into the repository and the subsequent corrosion of waste packages and the leaching of radionuclides into the brine. Because of the creep of the rock salt and the associated convergence of the brine filled volumes, the brine carrying the radionuclides will gradually be squeezed out of the salt formation and pressed into the overburden.

Because the creep of rock salt under hydrostatic conditions is relatively slow, other transport processes for the contamination in the brine can be relevant. One of these processes is the density gradient driven exchange of fluids in adjacent open volumes that are connected by e. g. a gallery. In case, for example, the density of brine in heated sections of the facility (due to heat generating waste) is decreased due to thermal expansion, a density difference may arise between brine in the heated section and in a non-heated section. Density differences may also arise from the chemical interaction between brine and the materials that may be used to immobilize the waste, such as cement. Such density differences may lead to convective, density-driven exchange flows that have the potential to carry radionuclides throughout the different sections of a repository. In some cases the density-driven exchange flows can be more effective than advective transport of contamination.

For this study it has been assumed that the brine density decreases as a result of the reaction with the waste. The resulting density difference between the two considered volumes that can be connected by a gallery or a shaft can be a driving force for a free convective flow. This situation is schematically depicted in figure 5.38.

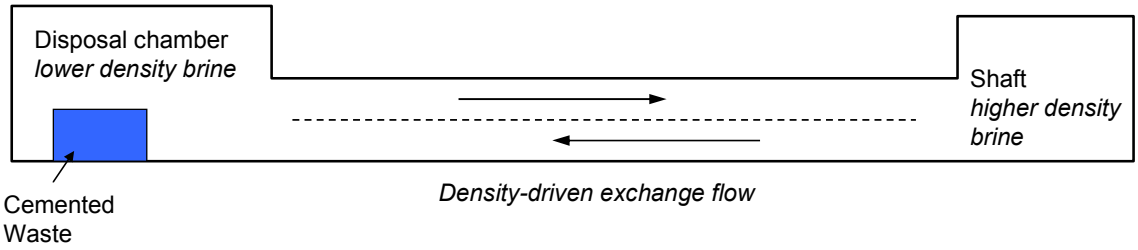

Fig. 5.38 Density-driven exchange flow of brine through a gallery

In figure 5.38 the dashed line in the gallery represents the interface between lighter and heavier brine. The lower density brine flows counter-currently on top of the higher density brine. This flow pattern, where two fluid layers are flowing more or less horizontally on top of each other, is named a ‘stratified flow’. Because of the density difference between the two brine layers, vertical flows are suppressed in the vicinity of the interface between the high- and low-density brine. The buoyancy will prevent brine moving from one ‘stratum’ to the other.

This benchmark exercise aims to compare the results from the PA code REPOS /BUH 99/ and the process-level code d^3f/r^3t /FEI 99 and FEI 04/ to validate the applicability of the models for density-driven exchange flows that are implemented in the PA code. This benchmark was also carried out by NRG using a semi-analytical simulation for the PA model and PORFLOW for the process-level code. The overall comparison is presented in detail in /BUH 09/.

5.1.3.1 Test case

The test case comprises a backfilled gallery (grey) with an adjacent disposal chamber at its left side (green), and a volume modeling a shaft on the right (blue).

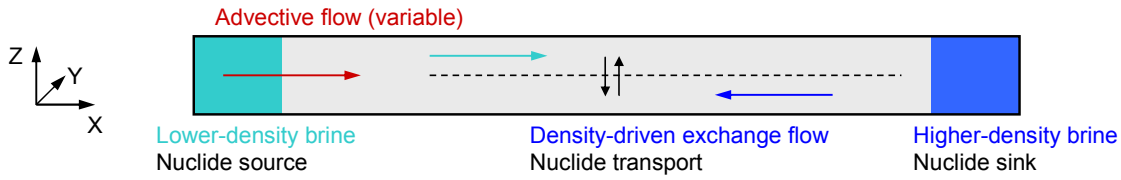

Fig. 5.39 Test case for investigating the radionuclide transport by density-driven exchange

The disposal chamber on the left side has the following characteristics:

- The density of the converted brine is constant and at the **lower** value (1 274 kg/m^3)
- The disposal chamber releases 3 different nuclides with distinct values of the effective diffusion coefficient but otherwise have the same and constant properties. The concentration C_i of the nuclides is set at a constant value of 100 Bq/m^3.

- The disposal chamber acts as a source of low-density brine so that, in addition to the density-driven exchange flow, different values of an advective flow from left to right are established (see also below).

The back-filled gallery is characterised by constant values of the porosity *n*, the permeability *k* and complete brine saturation, as given in table 5.3. It is assumed that the nuclides do not adsorb on the salt grit backfill.

The shaft on the right side has the following characteristics (see also table 5.3):

- The density of the fresh brine is constant and at the **higher** value (1 300 kg/m^3).
- The shaft is a sink volume for both the advective flow and the 3 different nuclides that are released in the waste chamber.

Based on the parameter values in the following table 5.3 the value of the density-driven exchange flow in the absence of an addiiotnal advective flow is estimated as $Q_{exchange,0}$ = $2{,}19 \cdot 10^{-7}$ m^3/s (6,93 m^3/yr). In the benchmark exercise the values of the advective flow rate have been imposed as a source of brine in the disposal chamber, taking into account that $Q_{advective} = n \cdot Q_{exchange,0}$, with n = 1,2,3,4. By imposing these discrete values of the advective flow rate of brine, additional to the density-driven exchange flow, it can be established when the density-driven exchange flow is counteracted by the advective flow, and how the transport of nuclides with different values of the diffusion coefficient is affected.

Tab. 5.3 Overview of model parameters

Section	Symbol	Value	Comments
			Brine
Dynamic viscosity	μ	$1{,}5\cdot10^{-3}$ Pa s	
Density - Higher value (" fresh" brine - Lower value ("converted" brine) Density difference	 ρ $\Delta\rho$	 1 300 kg/m^3 1 274 kg/m^3 26 kg/m^3 (2%)	
			Gallery
Length	L	30 m	
Width	W	4 m	
Height	H	4 m	
Diffusion coefficient of nuclide *1*	D_1	$3{,}0\cdot10^{-10}$ m^2/s	0,00947 m^2/y
Diffusion coefficient of nuclide *2*	D_2	$3{,}0\cdot10^{-9}$ m^2/s	0,0947 m^2/y
Diffusion coefficient of nuclide *3*	D_3	$3{,}0\cdot10^{-8}$ m^2/s	0,947 m^2/y
Partition coefficient of nuclides	k_D	0.0 m^3/s	No adsorption
			Backfill material (Salt grit)
Porosity	n	0,35	Constant value
Permeability[1]	k	$4{,}84\cdot10^{-12}$ m^2	
Density	ρ_{salt}	2 200 kg/m^3	
Disposal Chamber			
Constant lower density value of brine	ρ	1 274 kg/m^3	
Constant concentrations of nuclides *1, 2, 3*	C_1, C_2, C_3	100 Bq/m^3	
Imposed advective flow rates			Source
$Q_{advective} = 0 \cdot Q_{exchange}$		0,0 m^3/s	0,0 m^3/yr
$Q_{advective} = 1 \cdot Q_{exchange}$		$2{,}19\cdot10^{-7}$ m^3/s	6,93 m^3/yr
$Q_{advective} = 2 \cdot Q_{exchange}$		$4{,}39\cdot10^{-7}$ m^3/s	13,9 m^3/yr
$Q_{advective} = 3 \cdot Q_{exchange}$		$6{,}58\cdot10^{-7}$ m^3/s	20,8 m^3/yr
$Q_{advective} = 4 \cdot Q_{exchange}$		$8{,}78\cdot10^{-7}$ m^3/s	27,7 m^3/yr
			Shaft
Constant higher density value of brine	ρ	1 300 kg/m^3	
Constant concentrations of nuclides	C_1, C_2, C_3	0.0 Bq/m^3	Sink
Sink for the advective flow rates, imposed in the "Disposal Chamber"			

[1] Calculated with the relation $3.90\cdot10^{-10}\cdot n^{4.18}$

5.1.3.2 Results

Modelling with d³f/r³t

The steady state density profiles and velocity fields inside the gallery resulting from the d³f-simulations are shown in figure 5.40. The lower density brine flows, in case of n = 1 to 4 additionally driven by advection on the left hand boundary, from the left to the right at the top of the domain, while the higher density brine inflows from the right hand

boundary at the bottom. With growing inflow velocity of the lower density brine, the interface to higher density brine moves more and more to the right, while the mixing zone becomes smaller.

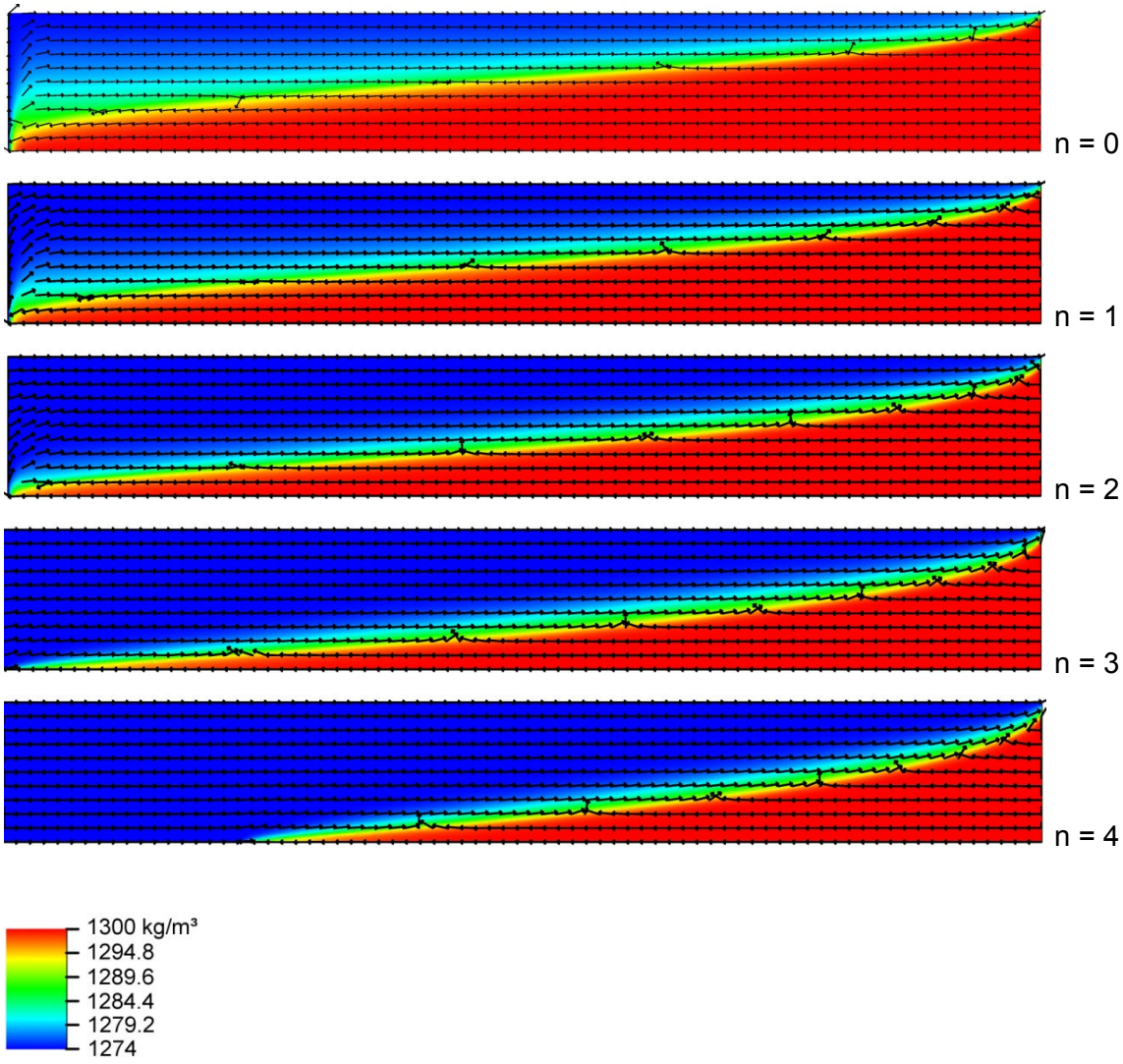

Fig. 5.40 Steady state density profiles and velocity fields as results of d³f-simulations for the different cases of inflow

The velocity profiles in the centre of the gallery (x = 15 m) are depicted in figure 5.41. The Darcy velocity is about 1.01 m/y at the top of the gallery, and 0.77 m/y at the bottom.

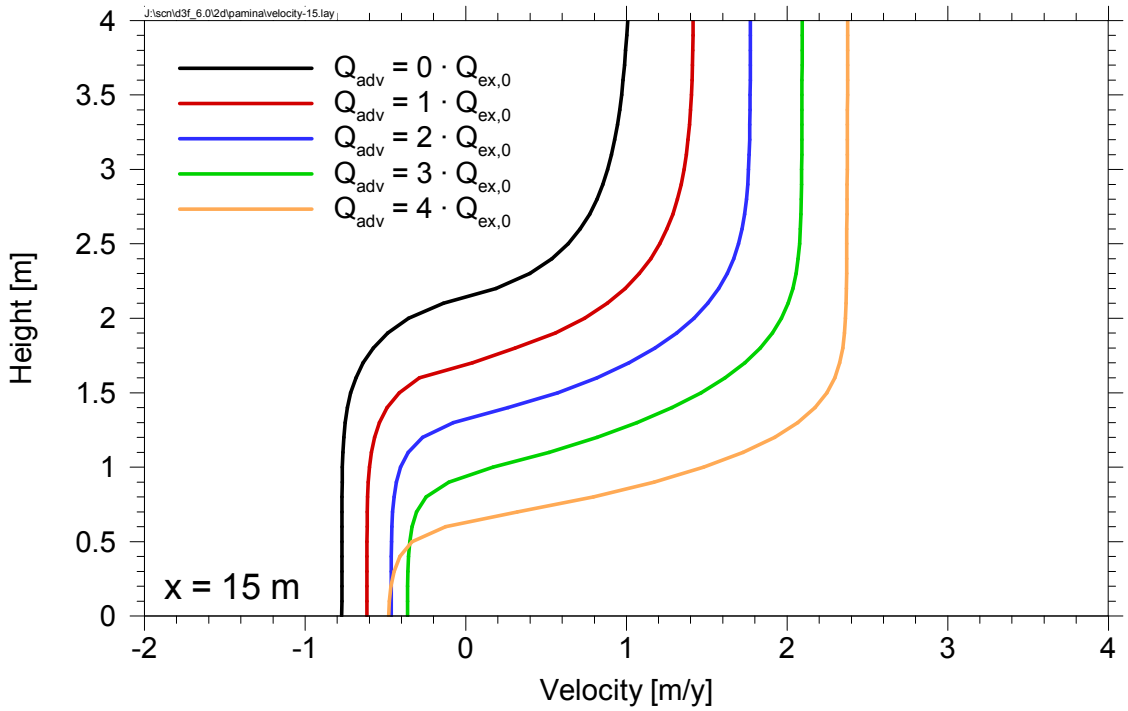

Fig. 5.41 Relative values of Darcy velocity in the centre over the height of the gallery at the steady-state

The nuclide concentrations in the gallery for two cases are depicted in figure 5.42 and 5.43. In case of non advective flow and lower diffusion coefficients the r³t-results show a large transition zone. In case of $Q_{advective} = 4 \cdot Q_{exchange,0}$ this effect diminishes. One reason of this difference is at least the larger diffusion zone in the density driven flow model, as already seen in figure 5.40. Dispersion effects are also to rule out as a reason because dispersivity is scaled by velocity in the equations, and therefore one would expect a larger effect if $Q_{advective} = 4 \cdot Q_{exchange,0}$.

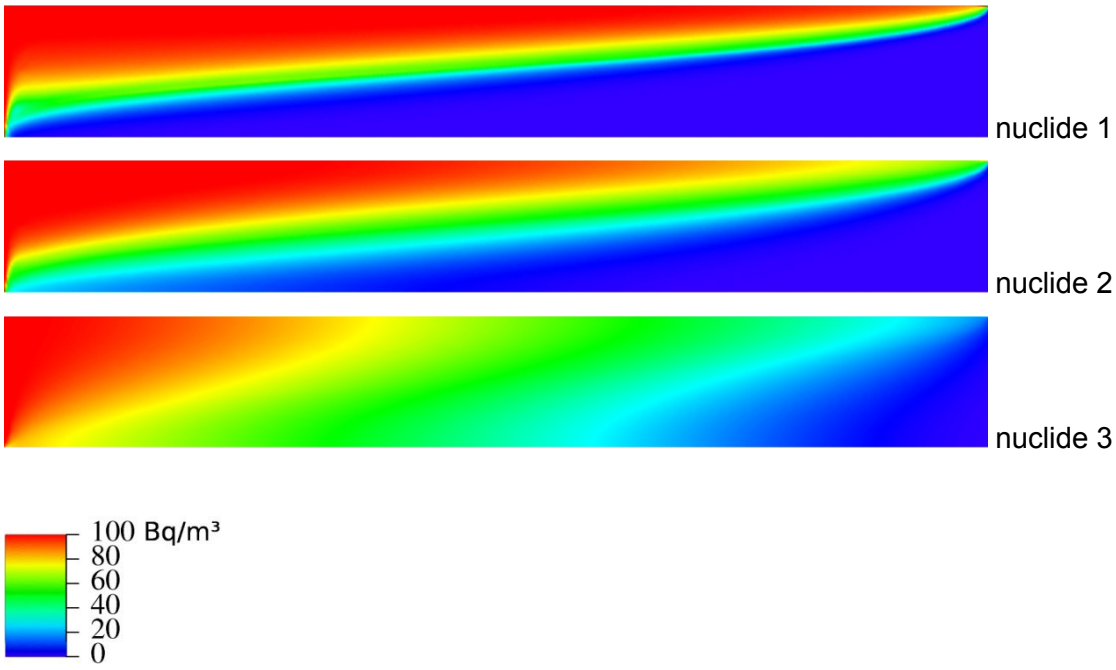

Fig. 5.42 Nuclide concentration in the gallery for non-advective flow

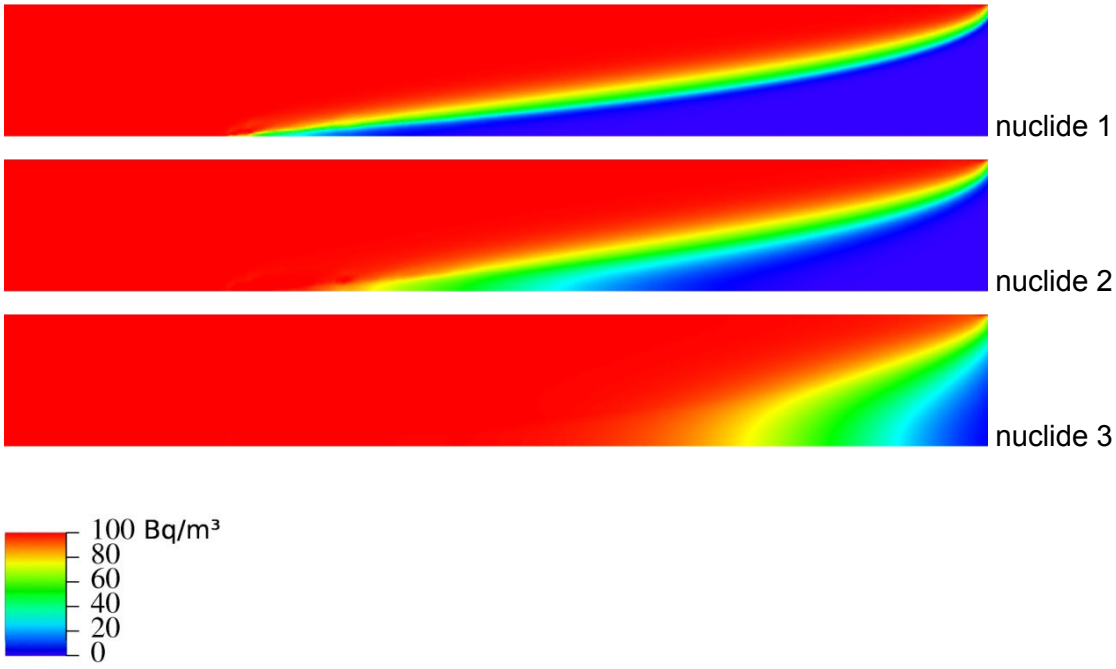

Fig. 5.43 Nuclide concentration in the gallery for the case $Q_{advective} = 4 \cdot Q_{exchange,0}$

Figure 5.44 shows the activity flux through the right hand boundary for the different inflow velocities. Here, the red curve, representing the largest diffusion coefficient, is in all cases the curve of least slope.

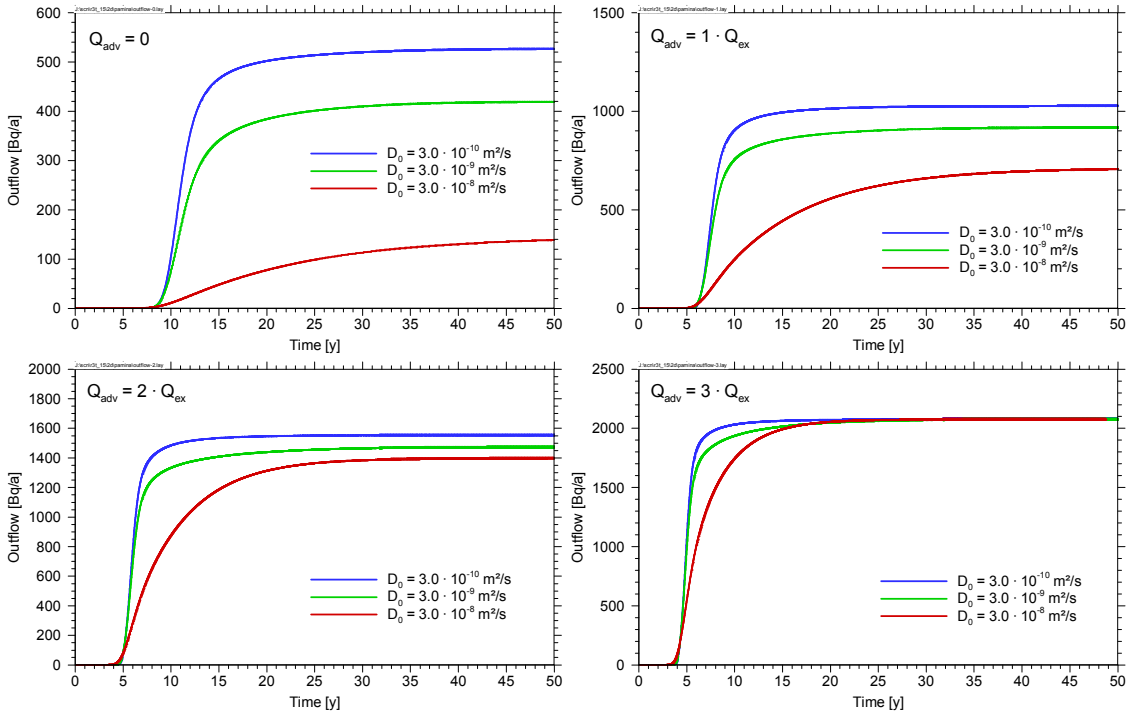

Fig. 5.44 Activity flux at the exit of the gallery for the nuclides 1 to 3 for different advective flow rates

Modelling with REPOS

The specifications of the benchmark exercise envisage modelling of the exchange processes involved in water flow and contaminant transport through a backfilled drift, subjected to density variations. The model used for simulation of the benchmark exercise with REPOS code consists of three parts: the source-term, the drift, and the contact to geosphere. The source term is described through a flooded large cavity undergoing convergence, in which dissolved contaminants are spread homogeneously in the pore water. The source term provides the constant concentration on the left boundary of the drift, and inputs the advective water flow into the drift. The density-gradient was implemented via an equivalent temperature gradient.

Figure 5.45 shows the activity fluxes from the drift on a linear scale. It can be seen that for the no-flow case (k = 0) the activity flux increases with the diffusion coefficient of the nuclide while it is the other way round for all cases taking advection into account. This result for the no-flow case clearly contradicts the results found from d^3f/r^3t simulations, where it is found also for the no-flux case that the activity flux increases the slower, the higher the diffusion coefficient of the nuclide. This is due to radionuclides that are transported by diffusion from low density brine in the upper layer of the drift into the

higher density brine in the lower part of the drift. Consequently, the transport direction of those radionuclide is changed into the opposite direction.

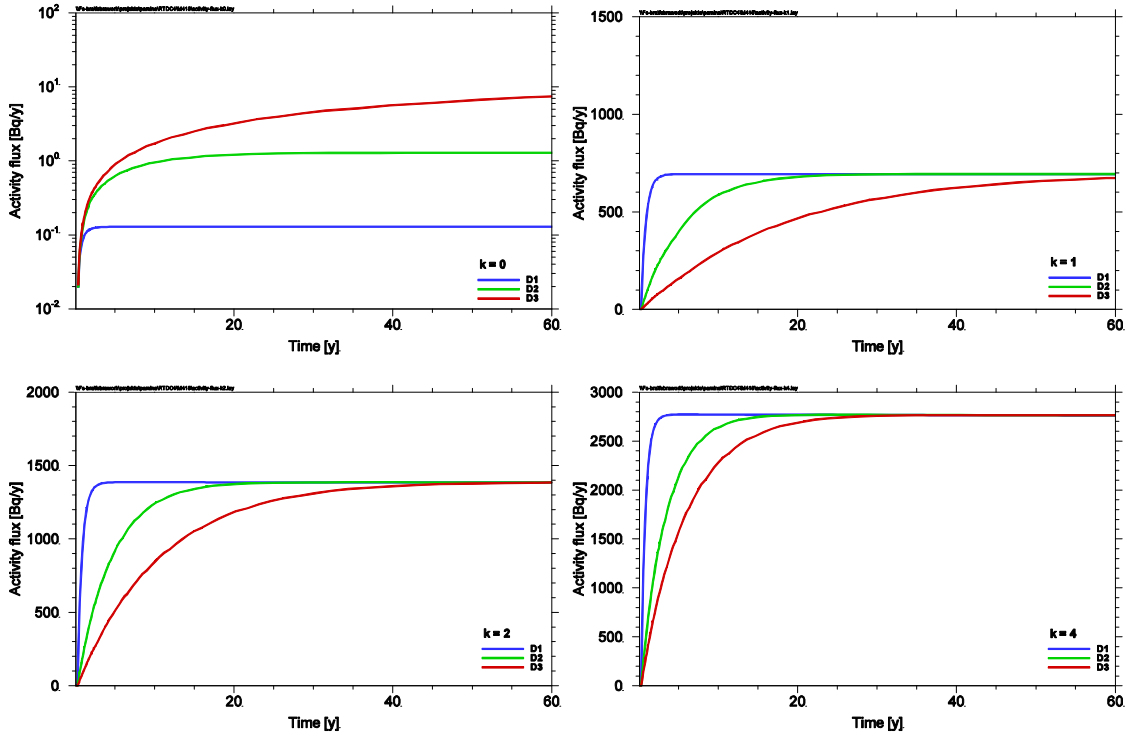

Fig. 5.45 Outflow activity fluxes [Bq/years] for the drift for k = 0, 1, 2 and 3

5.1.3.3 Conclusions

2D simulations have been performed with the program package d^3f/r^3t. As presented in /BUH 09/, these show a good agreement with the results from the PORFLOW code with respect to the density and radionuclide distributions calculated from both programs. However, there are some differences in the details which are most probably due to the different ways of the implementation of the boundary conditions.

The results from the d^3f/r^3t models were compared to simulations performed with the PA code REPOS. With regard to capabilities of REPOS code to represent convective transport processes it has to be concluded that the REPOS code cannot represent the convective driven transport of radionuclides in a sufficient way. This is in particular obvious for the test cases without an additional advective component of the flow. In this case, the activity flux released from the drift increases with the diffusion coefficient. This contradicts the results found from the d^3f/r^3t simulations, where it is found also for the no-flux case that the activity flux increases the slower the higher the diffusion coef-

ficient of the nuclide. As stated above, this behavior is due to the vertical transport of radionuclides between the two layers of different density which is not considered in the 1D PA code.

An alternative implementation of the convective flow representation in the PA code should be found in a future project. One possibility might be a semi-analytical representation described by NRG in /BUH 09/, which shows a reasonable good agreement with the process-level simulations.

5.2 Relevance of the complexity of modelling for the far field of a repository in salt

In the work described in the following, the use of more complex far-field codes in PA was examined. Two generic test cases were defined, both giving a very highly simplified representation of the situation found in the overburden above a real salt dome in Germany. For given radionuclide release rates from the near field, transport calculations were performed for both test cases, once with the PA code CHET /KUE 96/ and once with the more complex d^3f/r^3t /FEI 99 and FEI 04/ codes. As result of these calculations, the time dependent concentrations were compared at different positions in the model to study whether the use of the more complex codes results in a reduction of conservatism and/or a better representation of the actual transport or not. The results are described in detail in /RUE 09/ and are therefore only summarised in the following.

5.2.1 Test case

Both test cases used are abstractions of the hydrogeology situation above the salt dome in Gorleben in Northern Germany. The hydrogeological situation in this area was intensively investigated by a large research programme and the results are described in /KLI 05/. Figure 5.46 shows a cross section from North to South through the uppermost 450 m of the overburden above the salt dome Gorleben.

A highly simplified cross section was proposed in /KLI 05/, which was used as a basis for the construction of a model by /FLU 09/ that was used again as geometry for the simplified test case in the following.

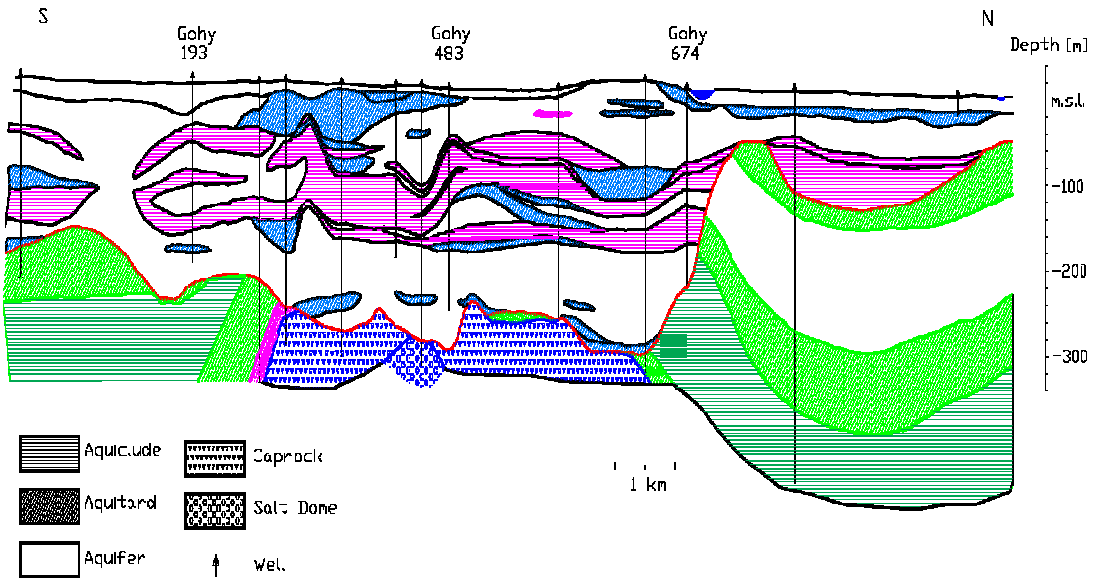

Fig. 5.46 Geological cross section above the Gorleben salt dome in Northern Germany /SCH 95/

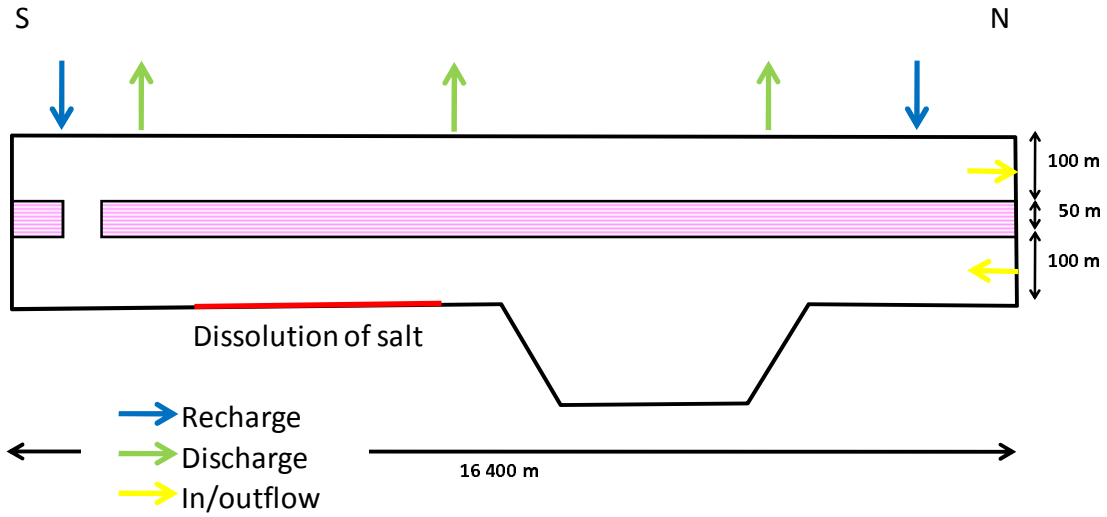

Fig. 5.47 Model representation of the cross section shown in figure 5.46

The model used is shown in figure 5.47. The length of the model is 16.4 km and the height is 400 m. The overburden is divided in three horizontal layers; two aquifers on the top and on the bottom are horizontally separated by an aquiclude. Permeability values are $1 \cdot 10^{-12}$ $m^2 \cdot s^{-1}$ for the aquifer (sand) and $1 \cdot 10^{-16}$ $m^2 \cdot s^{-1}$ for the aquitard (clay). For model 1 regarded in the performed calculations, the aquitard has one gap, through which water can be exchanged between both aquifers at a position of 1 000 to 1 500 m. The model 2 used accounts for an additional leakage at a position of 12 250 to 12 750 m. The lower aquifer is dominated by saline water, while the upper aquifer is dominated by fresh water. The salt stems from the dissolution of salt from the top of the salt dome. The dissolution of salt is simulated in the model by using a constant concen-

tration equal to salt saturation as boundary condition at the position of 3 000 to 7 000 m, i. e. the position of the salt dome.

Water inflow occurs from the North in the lower aquifer and the inflow velocity at the boundary is set to 0.2 $m \cdot a^{-1}$ in model 1 while it is set to 2 $m \cdot a^{-1}$ in model 2. Groundwater recharge in the higher situated regions of the model in the South and in the North and amounts to 160 $mm \cdot a^{-1}$. Outflow is allowed at the Northern boundary of the upper aquifer of model 1. All other boundaries are closed. The two differences in the boundary conditions of model 1 and 2 were chosen to achieve realistic sweet/saltwater distributions in the steady state flow field.

The radionuclides are released into the aquifer directly above the salt dome at a horizontal position of the model of 4 500 m. The data for the radionuclide fluxes from the near-field are taken from /KES 05/ for a very unlikely disturbed evolution scenario of a repository in salt. The data for K_d-values of the radionuclides in the overburden is taken from /SUT 98/ and is listed in table 5.5 while the values of the other transport parameters are listed in table 5.4.

Tab. 5.4 Parameters of the model

Parameter		Value
Geometry of the model		
Length	[m]	16 400
Height	[m]	400
Depth of sink	[m]	150
Thickness of lower aquifer	[m]	100
Thickness of aquitard	[m]	50
Thickness of upper aquifer	[m]	100
Leakage in aquitard at position	[m]	1 000 - 1 500
Additional leakage in model 2	[m]	12 250 - 12 750
Hydrogeological parameters		
Permeability of aquifer (sand)	[$m^2 \cdot s^{-1}$]	$1 \cdot 10^{-12}$
Permeability of aquitard (clay)	[$m^2 \cdot s^{-1}$]	$1 \cdot 10^{-16}$
Porosity		0.1
Longitudinal dispersivity	[m]	10
Horizontal dispersivity	[m]	1
Diffusion coefficient	[$m^2 \cdot s^{-1}$]	$1 \cdot 10^{-9}$
Boundary conditions		
Inflow in lower aquifer (model1)	[$mm \cdot a^{-1}$]	200
Inflow in lower aquifer (model2)	[$mm \cdot a^{-1}$]	2 000
Recharge	[$mm \cdot a^{-1}$]	160

Tab. 5.5 Kd-values for the radionuclides in the far-field /SUT 98/

Element	Sand	Clay	Element	Sand	Clay
C	$2{,}0 \cdot 10^{-4}$	0,002	Cs	0,07	0,4
Cl	$1{,}0 \cdot 10^{-4}$	$1{,}0 \cdot 10^{-4}$	Ra	0,04	0,3
Ni	0,02	0,3	Th	0,2	2,0
Se	0,001	0,001	Pa	0,6	60,0
Zr	0,04	0,1	U	0,002	0,08
Mo	0,001	0,001	Np	0,01	0,3
Tc	0,001	0,006	Pu	0,1	3,0
Sn	0,04	0,1	Am	0,1	20,0
I	0,002	0,002	Cm	0,1	20,0

5.2.2 Results

5.2.2.1 Ground water flow model

As first step, a simulation of the density driven flow with the code d^3f has been performed for both models to determine the steady state flow field of water in the aquifers. The resulting flow fields are shown in figure 5.48 for model 1 and figure 5.49 for model 2 along with the salt concentration in the system. The arrows indicate the flow direction of the water while the colour coding denotes the salt concentration given in relative units compared to saturation.

For the following simulations, these flow fields were used on the one hand as direct input parameter for the transport calculations with the detailed transport code r^3t and in a second step to determine mean ground water velocities for the simulation with the integrated one-dimensional code CHET for the preferential transport paths identified in the transport simulations with r^3t.

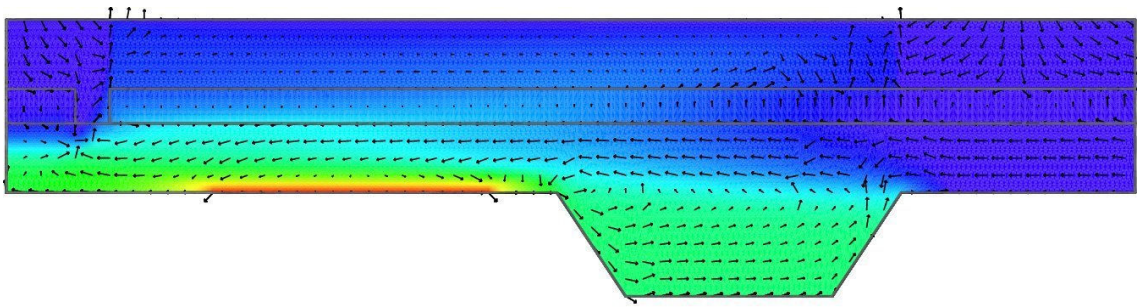

Fig. 5.48 Steady-state flow field for model 1 (the colour scale denotes the salt concentration relative to saturation while the arrows denote the flow field)

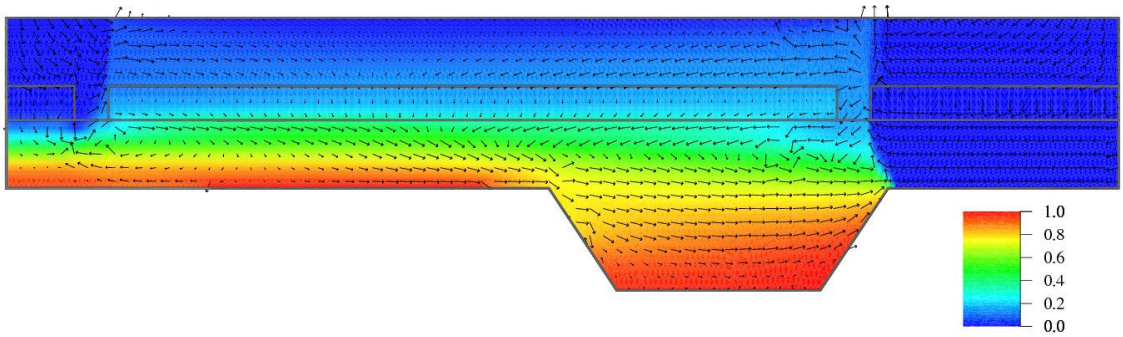

Fig. 5.49 Steady-state flow field for model 2 (the colour scale denotes the salt concentration relative to saturation while the arrows denote the flow field)

5.2.2.2 2D transport model

The radionuclide transport was modelled with the transport code r^3t using the flow field determined in the density driven flow simulations performed before. The radionuclides were released into the model at a horizontal position of 4 500 m at the bottom of the model. The transport calculation was performed for selected fission and activation products as well as for the Uranium decay series.

The results of the transport calculations with r^3t are presented for exemplary radionuclides in terms of cross sections of the concentration distributions of the radionuclides. The figures show the concentrations in Becquerel per cubic metre of water, colour coded on a logarithmic scale ranging from 10^{-15} to 1 Bq/m^3. Note that the numbers given on the colour bar give the according exponent. The concentration distribution is shown for four different points in time demonstrating the propagation of the radionuclide plume.

The further procedure is as follows: The 2D concentration distributions are used to find the position or positions of maximum concentration at the top of the model – i. e. the maxima of potential radiation exposure of the population if the groundwater is used for drinking or other purposes. Those positions are used as observation points for the comparison with the simplified 1D model in terms of curves of radionuclide concentration versus time at these positions. The preferential flow paths from the release point to the observation point is determined visually from the 2D concentration distributions.

Model 1

The results of the transport calculations for model 1 are plotted for C-14. For C-14, the concentration is completely vanishing for times later than 500 000 years due to radioactive decay. Therefore, no concentrations are plotted for late times. It can be clearly seen from most of the pictures – e. g. in figure 5.50 showing the plume of C-14 for a point in time of 10 000 years – that there are two distinct preferential flow paths for the radionuclides in the overburden. The first flow path is from the point of the radionuclide release in direct vertical direction through the lower aquifer, the clay aquitard and the upper aquifer. The second flow path is first directed southwards in horizontal direction in the lower aquifer towards the gap in the clay aquitard and than through the gap into the upper aquifer and to the surface.

The radionuclides are transported in different fractions on the two pathways - depending on their adsorption behaviour. While a high fraction of a low sorbing radionuclide like C-14 is directly transported upwards on pathway 1, the highly sorbing radionuclides like have only a very limited ability to be transported through the clay layer, but get sorbed within.

Figure 5.51 shows the concentration of different radionuclides at the top of the model plotted versus the distance from the left model boundary to find the positions of maximum concentration. The different line styles denote different points in time. All radionuclides show two distinct concentration maxima, one at about 1 600 m and another at about 4 000 m. The position of the two maxima only slightly changes with time. Therefore, these two positions are used in the following as observation points for the comparison between the 2D and the 1D simulation. The radionuclide concentration of different radionuclides at the two observation points at 1 600 m and 4 000 m as calculated by the 2D model from r^3t are shown in figure 5.52.

For all plotted radionuclides, the concentration at the position of 1 600 m, i. e. the radionuclides which were transported on pathway 2, reach a higher maximum concentration and also at an earlier point in time compared to the maximum concentration of the same radionuclide at the position of 4 000 m. However, while the difference of the maximum value between both positions is several orders of magnitude for C-14, the difference is only small for Cl-36. For Uranium and Thorium, the concentration given for the position at 4 000 m is not reached by vertical transport on pathway 1, but by transport on pathway 2 and a subsequent distribution of the radionuclides in the upper aquifer.

Although the maximum concentration value for Cl-36 is higher resulting from radionuclides transported on pathway 2, Cl-36 show periods in time at about 200 000 a, where the concentration at the position of 4 000 m is higher than the one at position 1 600 m. This shows that for Cl-36 both pathways could potentially contribute about the same part to the radiation exposure of the population by Cl-36 if water is used from the upper aquifer. However, the transport on pathway 1 is somewhat slower, even for the low-sorbing Cl-36.

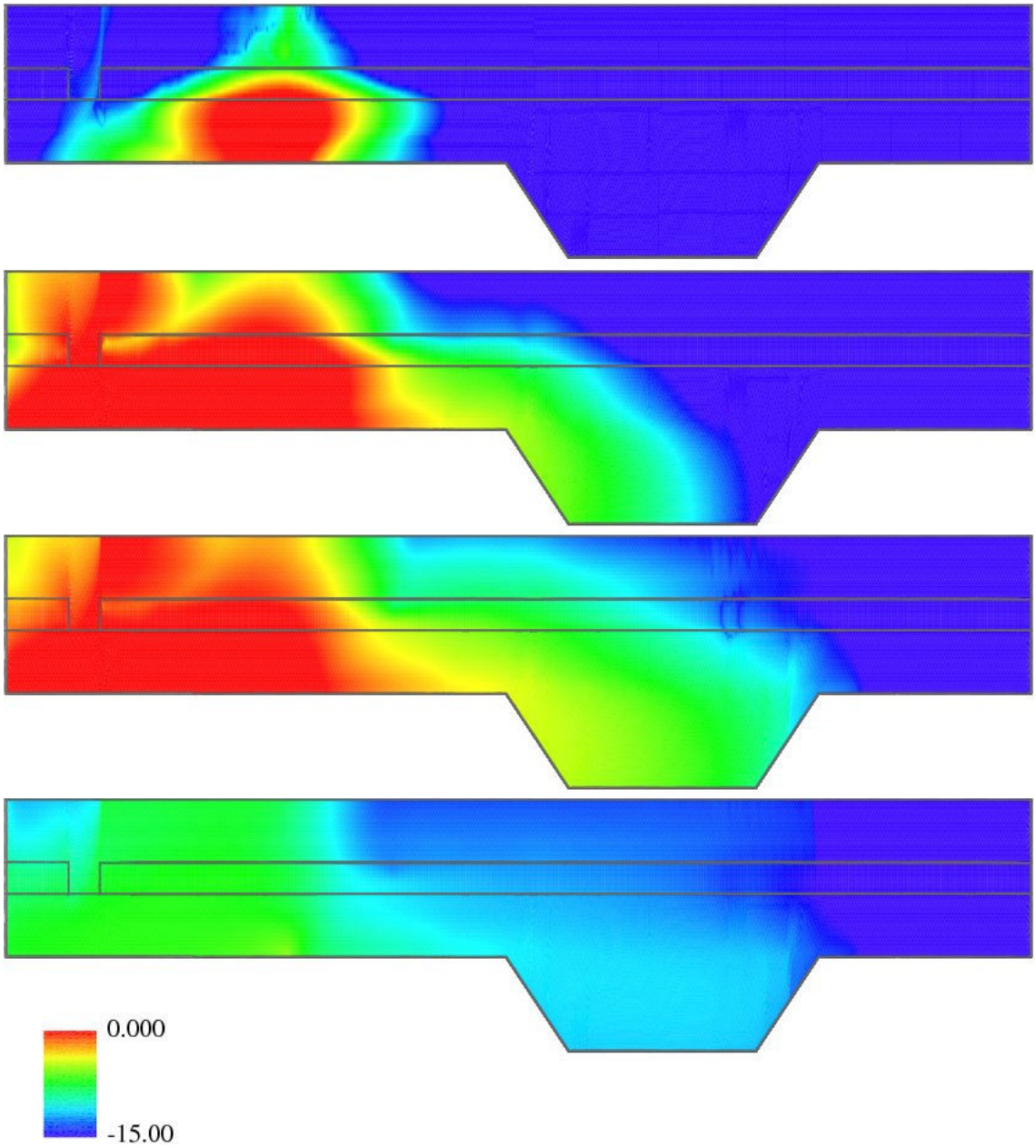

Fig. 5.50 Cross section of the C-14-concentration after 10 000, 50 000, 100 000 and 250 000 years in $Bq \cdot m^{-3}$ (the numbers of the scale are given as common logarithm)

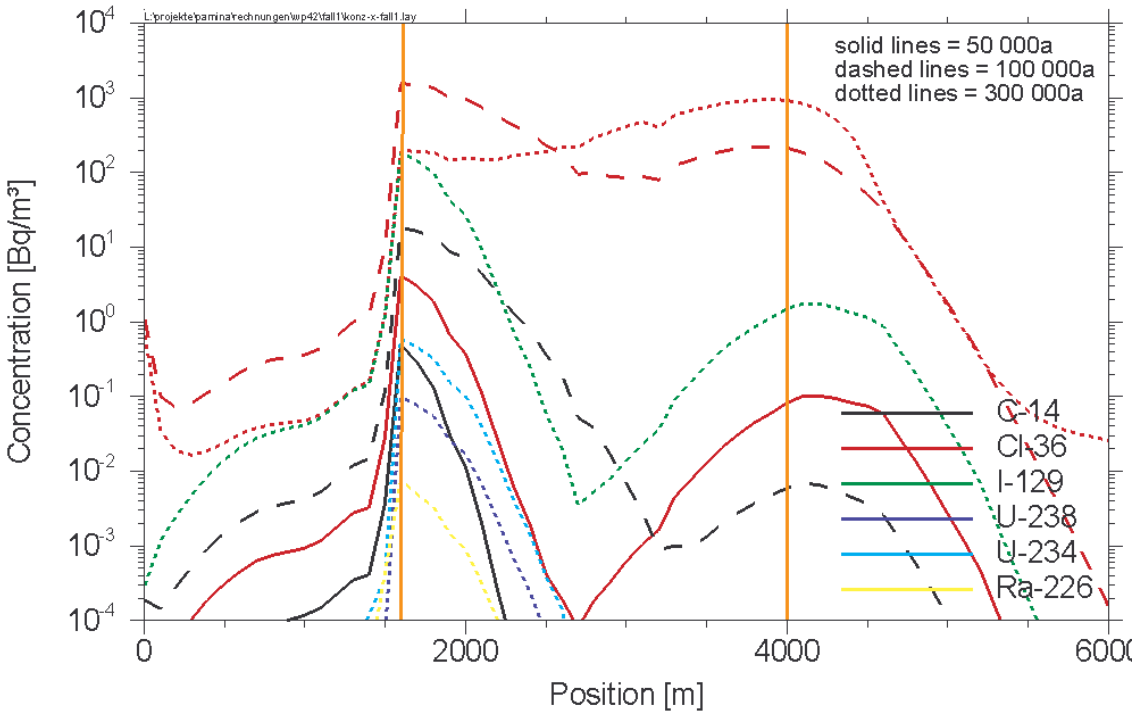

Fig. 5.51 Concentration of different radionuclides at the top of the model versus position

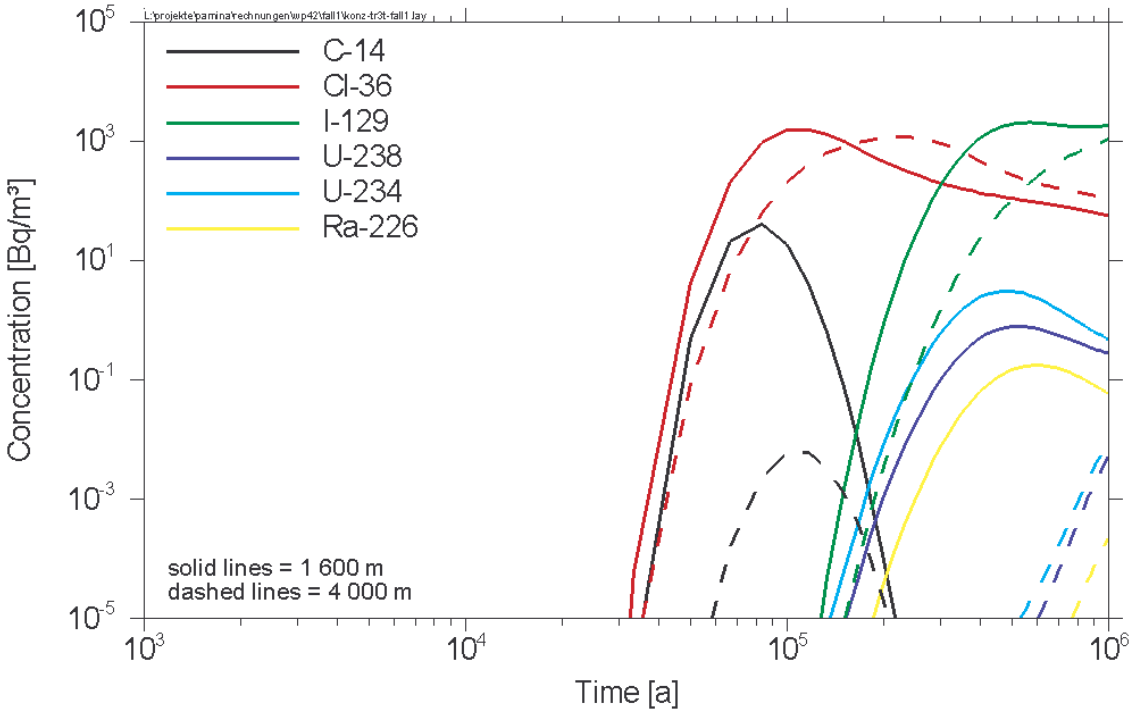

Fig. 5.52 Concentration of different radionuclides at position of 1 600 m (solid lines) and 4 000 m (dashed lines) at the top of the model

Model 2

The results of the transport calculations for model 2 are exemplarily plotted for I-129 in figure 5.53 for times from 10 000 to 300 000 years. Like for the model 1, there are two distinct preferential flow paths for the radionuclides in the overburden. The first flow path is from the radionuclide source in direct vertical direction through the lower aquifer, the clay aquitard and the upper aquifer. The second flow path is first northwards in horizontal direction in the lower aquifer, through the sink and than through the gap into the upper aquifer and to the surface. For some radionuclides also a third transport pathway is relevant. The third transport pathway is southwards in the lower aquifer and through the gap at 1 600 m into the upper aquifer.

Figure 5.54 shows the concentration of different radionuclides at the top of the model plotted versus the distance from the left model boundary to find the positions of maximum concentration. The different line styles denote different points. All radionuclides show two distinct concentration maxima, one at about 5 000 m and another at about 12 650 m, representing the pathways 1 and 2 as described above. Pathway 3 only plays a very minor role and is therefore not regarded further. The positions of the maxima of the first two pathways only slightly change with time. Therefore, these two positions are used in the following as observation points for the comparison between the 2D and the 1D simulation. The radionuclide concentration of different radionuclides at the two observation points at 5 000 m and 12 650 m as calculated by the 2D model from r^3t are shown in figure 5.55.

For all plotted radionuclides, the concentration at the position of 12 650 m, i. e. the radionuclides which were transported on pathway 2, reach a somewhat higher maximum concentration, but the differences are very small for most of the radionuclides. Also the maximum values are reached at similar times through both pathways. So none of the two pathways can be clearly identified to be a preferential pathway for the radionuclides.

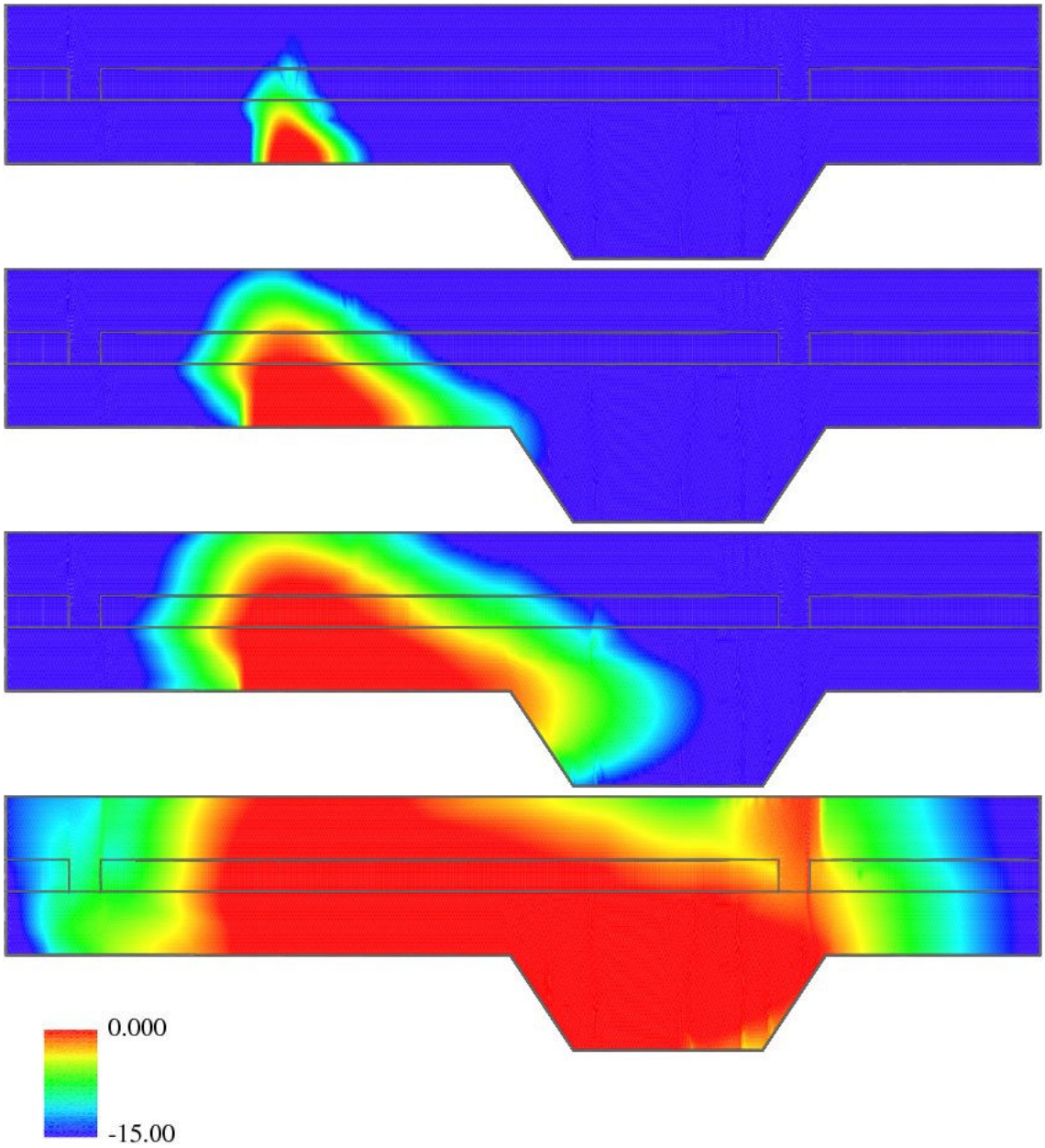

Fig. 5.53 Cross section of the I-129-concentration after 10 000, 50 000, 100 000, 300 000 years in Bq/m^3 (the numbers of the scale are given as common logarithm)

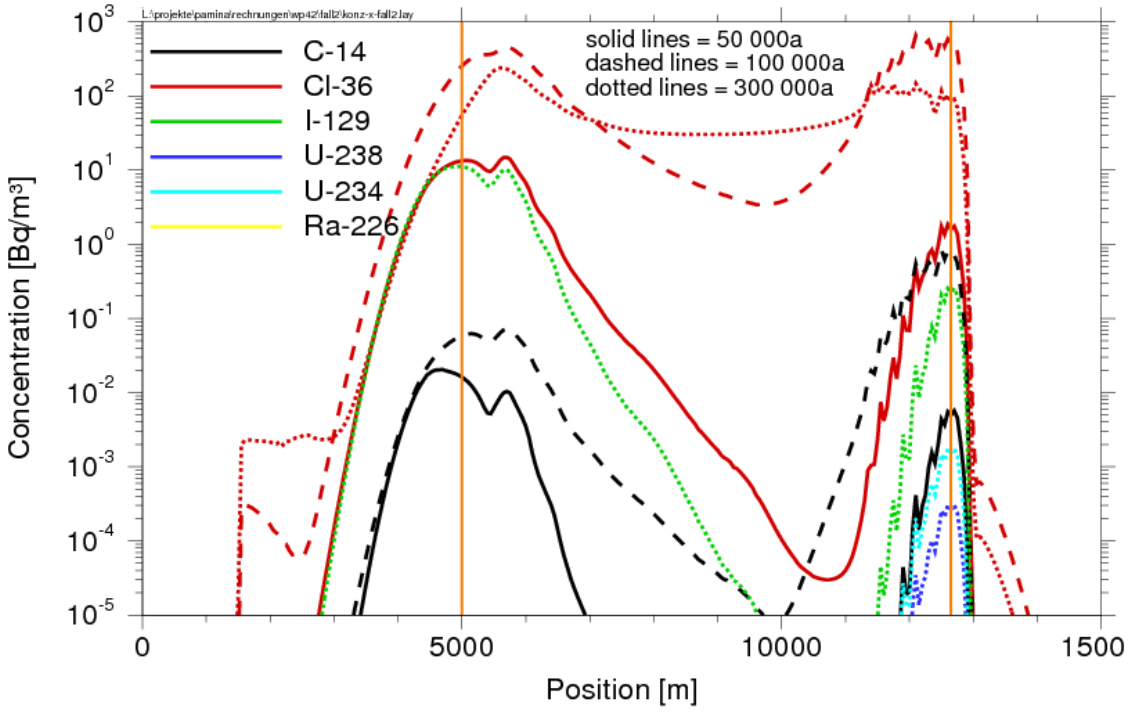

Fig. 5.54 Concentration of different radionuclides at the top of the model versus position

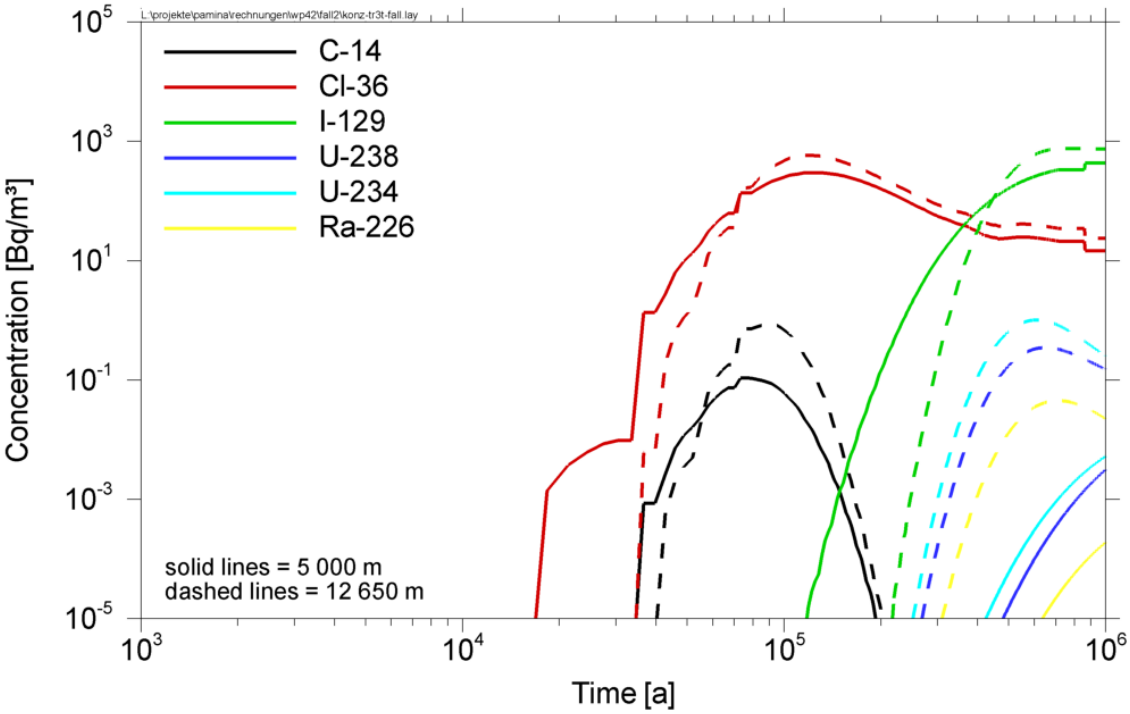

Fig. 5.55 Concentration of different radionuclides at position of 5 000 m (solid lines) and 12 650 m (dashed lines) at the top of the model

5.2.2.3 Abstraction to 1D-model

The transport on the different transport pathways identified for each of the two models above were modelled additionally with the 1D-PA-model CHET. Each of the transport pathways was divided into several modelling blocks or compartments representing either the different materials or the groundwater movement directions. The groundwater velocities needed as input parameter for the one dimensional model were derived for each compartment by averaging the ground water velocities determined in the 2D calculation with the program d^3f (figure 5.47) along the pathways. For the other transport and retention parameters, the same data as for the r^3t simulations was used. While the K_d-values are listed in table 5.5 above, the transport parameters are listed individually for each model below.

The temporal evolution of the radionuclide concentrations determined at the end of each 1D transport pathway were compared to the respective radionuclide concentrations determined for the observation points in the 2D model plotted in figures 5.52 and 5.55 above.

Model 1

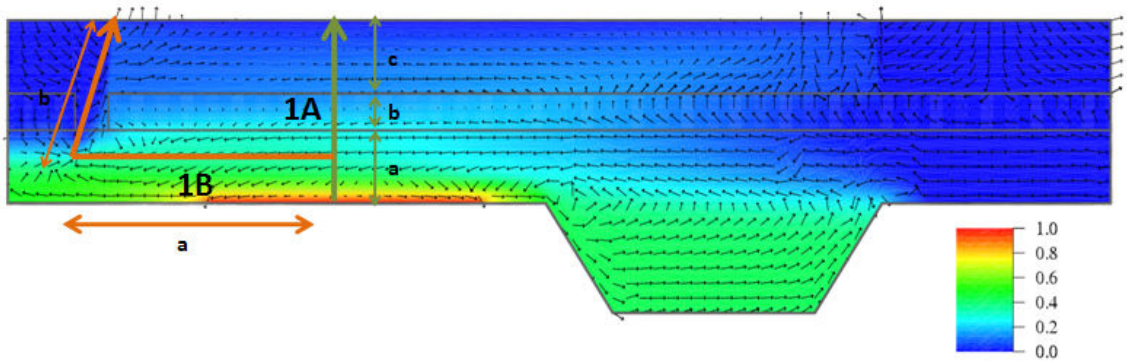

Fig. 5.56 Definition and subdivision of the transport pathways of model 1

Pathway A of model 1 has been divided into three sub-compartments a, b and c; the lower and upper aquifer (1Aa and 1Ac) and the aquiclude (1Ab) in between. Averaging was performed for each of the compartments individually, but it was critical for all compartments of pathway 1A due to very low or even downward directed vertical groundwater velocities. The assumed resulting groundwater velocity for all three compartments of $1 \cdot 10^{-4} m \cdot a^{-1}$ is close to expected travel velocities resulting from diffusion.

Pathway B has been divided into two sub-compartments (a and b). The first compartment (1Ba) represents the horizontal flow in the lower aquifer from the position of the radionuclide release at about 4 500 m to the position of the gap in the aquiclude at about 1 300 m. The second compartment (1Bb) comprises the vertical flow from the lower to the upper aquifer.

Tab. 5.6 Parameters for the 1D transport model CHET for the two transport pathways considered for model 1

Transport pathway 1A		
Number of compartments		3
Compartment 1Aa and 1Ac		
Material		Sand
Pathway length	[m]	100
Porosity		0.3
Cross section	[m^2]	1 000
Mean darcy velocity	[$m \cdot a^{-1}$]	$1 \cdot 10^{-4}$
Compartment 1Ab		
Material		Clay
Pathway length	[m]	50
Porosity		0.1
Cross section	[m^2]	1 000
Mean groundwater velocity	[$m \cdot a^{-1}$]	$1 \cdot 10^{-4}$
Transport pathway 1B		
Number of compartments		2
Compartment 1Ba		
Material		Sand
Pathway length	[m]	3 500
Porosity		0.3
Cross section	[m^2]	100
Mean groundwater velocity	[$m \cdot a^{-1}$]	$3.6 \cdot 10^{-2}$
Compartment 1Bb		
Material		Sand
Pathway length	[m]	200
Porosity		0.3
Cross section	[m^2]	200
Mean groundwater velocity	[$m \cdot a^{-1}$]	$3.15 \cdot 10^{-1}$

For the first compartment (1Ba) the horizontal flow velocity has been determined for 19 positions in x-direction at three different depth levels of the lower aquifer (175 m, 200 m and 225 m depth). The spatial variability of the groundwater velocity values is rather low and is about a factor of three between the highest and the lowest value. The average velocity determined from the mean of those 57 values is $3.6 \cdot 10^{-2}$ $m \cdot a^{-1}$. For the second compartment (1Bb), the vertical velocity has been determined for three different positions in x-direction and 20 different depth levels resulting in an average velocity de-

termined from the mean of 60 values of 0.315 $m \cdot a^{-1}$. The geometric and transport parameters used for the two pathways in model 1 are summarised in table 5.6.

The resulting concentrations calculated in the CHET simulations are plotted in figure 5.57 for pathway 1A and in figure 5.58 for pathway 1B along with the results from r^3t presented before. The comparison results in the following observations:

- For both pathways regarded in model 1, the concentrations calculated with the CHET model are higher compared to the ones obtained by r^3t. This is true for all radionuclides shown and the difference in concentration is at least one to two orders of magnitude.
- The maximum concentrations are reached earlier in the simulations with the CHET model compared to the ones with the r^3t model. Especially for radionuclides with small half life like C-14 this difference in the travel time also results in an additional difference in the maximum concentration.
- The shape of the curves, i. e. the increase of the concentration with time for pathway A is much steeper in the results from the CHET simulation than in the results from r^3t. This is due to the fact that the vertical dispersion regarded in the 2D simulation is not included in a 1D simulation. This effect is especially visible for very slow or diffusion dominated transport – as in pathway A – since diffusive transport has no clear transport direction, but the transport velocity in direction of the pathway regarded is the same than perpendicular to it. The same difference would apply to the 2D simulation if compared to a full 3D one.
- If the curves of the radionuclides from the uranium decay chain (U-238, U-234 and Ra-226) are compared to each other for the transport on pathway B, it can be seen that the curves showing the CHET results plot farer from each other than the ones from r^3t. This indicates that the decay chain is not in radioactive equilibrium in the CHET simulation and therefore the Ra-226 concentration is underestimated. The reason for this is the high increase in the transport velocity towards the end of the transport pathway in the CHET model, and the resulting lack of time to reach the equilibrium.

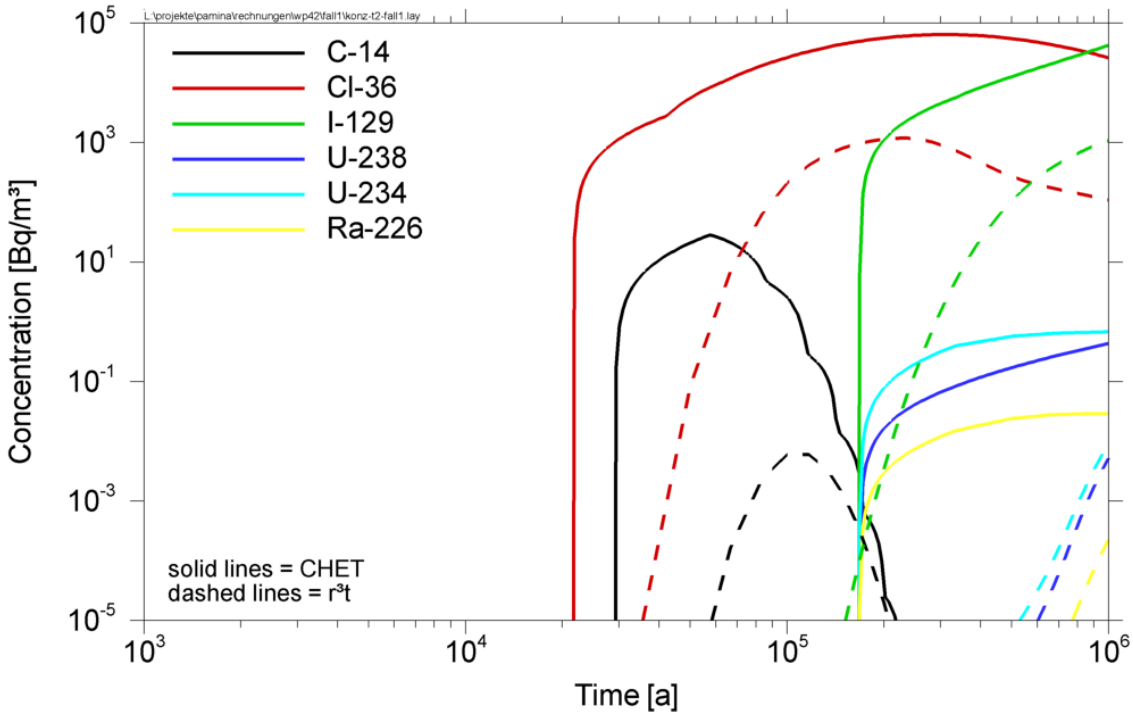

Fig. 5.57: Concentration versus time of different radionuclides at the position of 4 000 m (pathway 1A) calculated with r^3t (dashed lines) and CHET (solid lines)

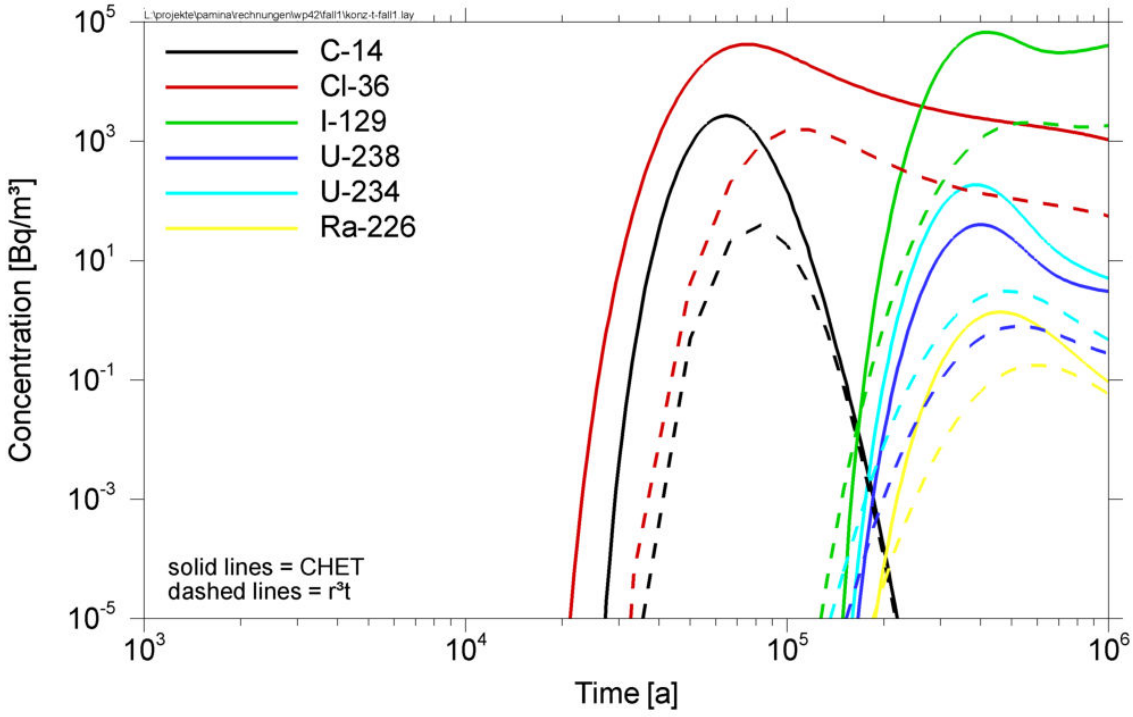

Fig. 5.58 Concentration versus time of different radionuclides at the position of 1 600 m (pathway 1B) calculated with r^3t (dashed lines) and with CHET (solid lines)

Model 2

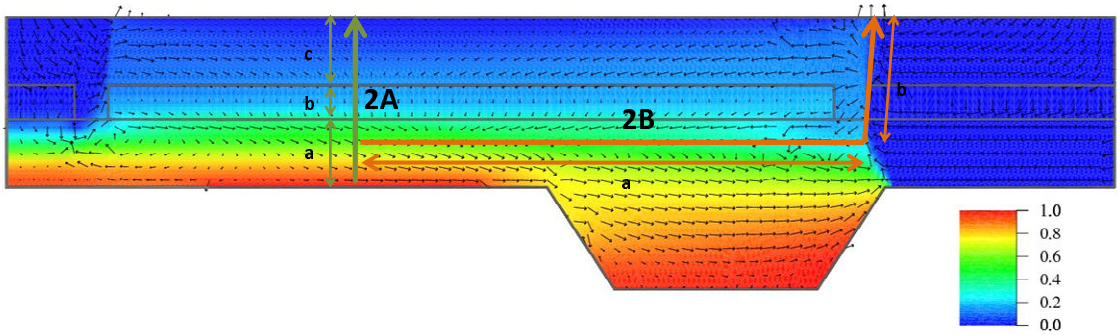

Fig. 5.59 Definition and subdivision of the transport pathways of model 2

Pathway A of model 2 has been handled in the same way as for model 1. It has been divided into three sub-compartments a, b and c; the lower and upper aquifer (2Aa and 2Ac) and the aquiclude (2Ab) in between. Averaging was performed for each of the compartments individually, but it was critical for all compartments. Therefore, the same resulting groundwater velocity for all three compartments of $1 \cdot 10^{-4} m \cdot a^{-1}$ was chosen as for model 1. Pathway B has been divided into two sub-compartments (a and b). The first compartment (1Ba) represents the horizontal flow in the lower aquifer from the position of the radionuclide release at about 4 500 m to the position of the gap in the aquiclude at about 12 650 m. The second compartment (1Bb) comprises the vertical flow from the lower to the upper aquifer.

For the first compartment (2Ba), the horizontal flow velocity has been determined for 774 positions in x-direction at three different depth levels of the lower aquifer (175 m, 200 m and 225 m depth). The spatial variability of the groundwater velocity values is much higher than in the first model. In particular, there are areas where the flow velocity is negative, i. e. the local flow direction is in the opposite direction than the main flow direction. Those negative numbers were not included in the averaging. The average velocity determined is $2.1 \cdot 10^{-2}$ $m \cdot a^{-1}$. The maximum flow velocity is about a factor of 6 higher than the average. For the second compartment (2Bb), the vertical velocity has been determined for one position in x-direction and 40 different depth levels resulting in an average velocity of 2.74 $m \cdot a^{-1}$. The geometric and transport parameters used for the two pathways in model 2 are summarised in table 5.7.

Tab. 5.7 Parameters for the 1D transport model CHET for the two transport pathways considered for model 2

Transport pathway 2A		
Number of compartments		3
Compartment 2Aa and 2Ac		
Material		Sand
Pathway length	[m]	100
Porosity		0.3
Cross section	[m^2]	1 000
Mean darcy velocity	[$m \cdot a^{-1}$]	$1 \cdot 10^{-4}$
Compartment 2Ab		
Material		Clay
Pathway length	[m]	50
Porosity		0.1
Cross section	[m^2]	1 000
Mean groundwater velocity	[$m \cdot a^{-1}$]	$1 \cdot 10^{-4}$
Transport pathway 2B		
Number of compartments		2
Compartment 2Ba		
Material		Sand
Pathway length	[m]	7 740
Porosity		0.3
Cross section	[m^2]	100
Mean groundwater velocity	[$m \cdot a^{-1}$]	$2.1 \cdot 10^{-2}$
Compartment 2Bb		
Material		Sand
Pathway length	[m]	100
Porosity		0.3
Cross section	[m^2]	100
Mean groundwater velocity	[$m \cdot a^{-1}$]	2.74

The resulting concentrations calculated in the CHET simulations are plotted in figure 5.60 for pathway 2A and in figure 5.61 for pathway 2B along with the results from r^3t. The comparison results in the following observations:

- For pathway 2A, the concentrations calculated with the CHET model are higher compared to the ones obtained by r^3t. This is true for all radionuclides shown and the difference in concentration is at least one to two orders of magnitude.
- As for model 1, the shape of the curves for very slow or diffusion controlled transport in pathway 2A is much steeper in the results from the CHET simulation than in the results from r^3t due to neglecting of vertical dispersion in the 1D model.
- For pathway 2 B, the concentrations calculated with the performance assessment model CHET are lower and occur to later times than the concentrations calculated with r^3t. Therefore, for this transport pathway the calculations with CHET are not

conservative. The reason for this is the very inhomogeneous distribution of the transport velocities, resulting in too slow mean transport velocities received from the averaging. The transport velocity in x-direction of model 2 is plotted in figure 5.62. Red colours denote flow in positive (right) direction while blue colours denote flow in negative (left) direction. It can be seen that the flow in the lower aquifer above the sink results from two competing processes, first the convective flow from left to right (red plume) transporting the radionuclides and second, the advective inflow from the right boundary (blue plume).

The radionuclide transport in the lower aquifer is dominated by the high transport velocity from left to right in the lower part of the lower aquifer (i. e. the centre of the red plume), while the averaging over the whole thickness of the lower aquifer results in clearly underestimated transport velocities for the radionuclides.

If the calculation with the code CHET is repeated using the maximum transport velocity observed in the lower aquifer from left to right – which is 5.8 times higher than the average value – a result is obtained that again leads to conservative concentrations and travel times for the CHET calculation as plotted in figure 5.63.

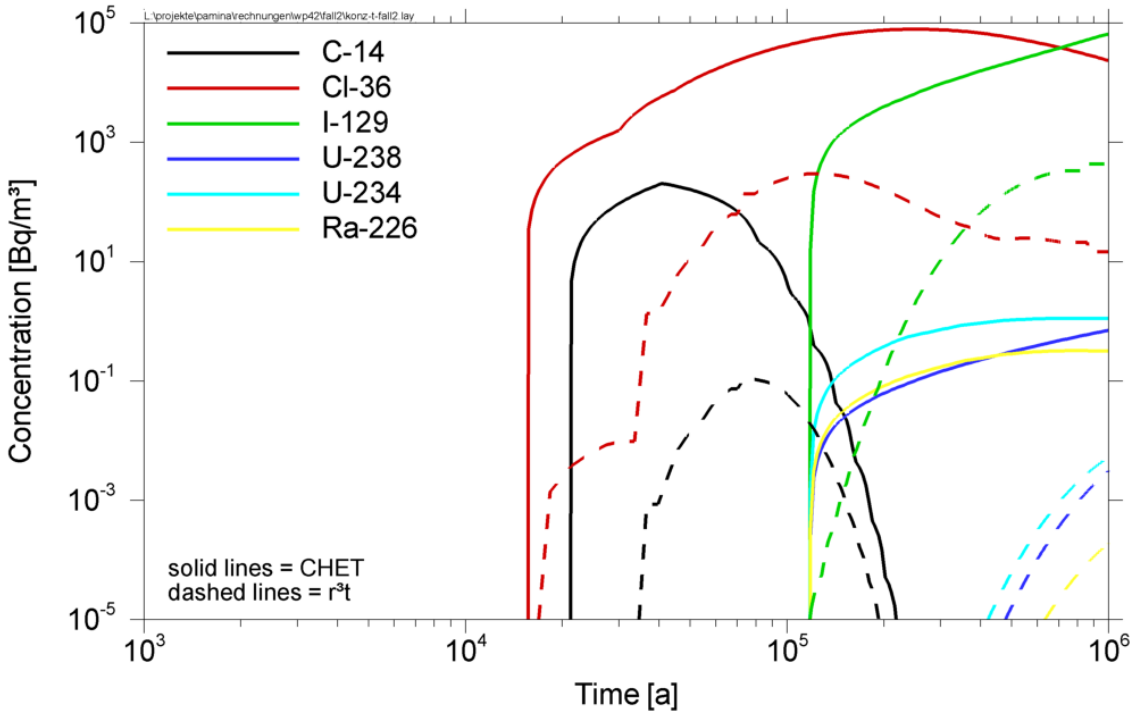

Fig. 5.60 Concentration versus time of different radionuclides at the position of 4 500 m (pathway 2A) calculated with r^3t (dashed lines) and CHET (solid lines) for model

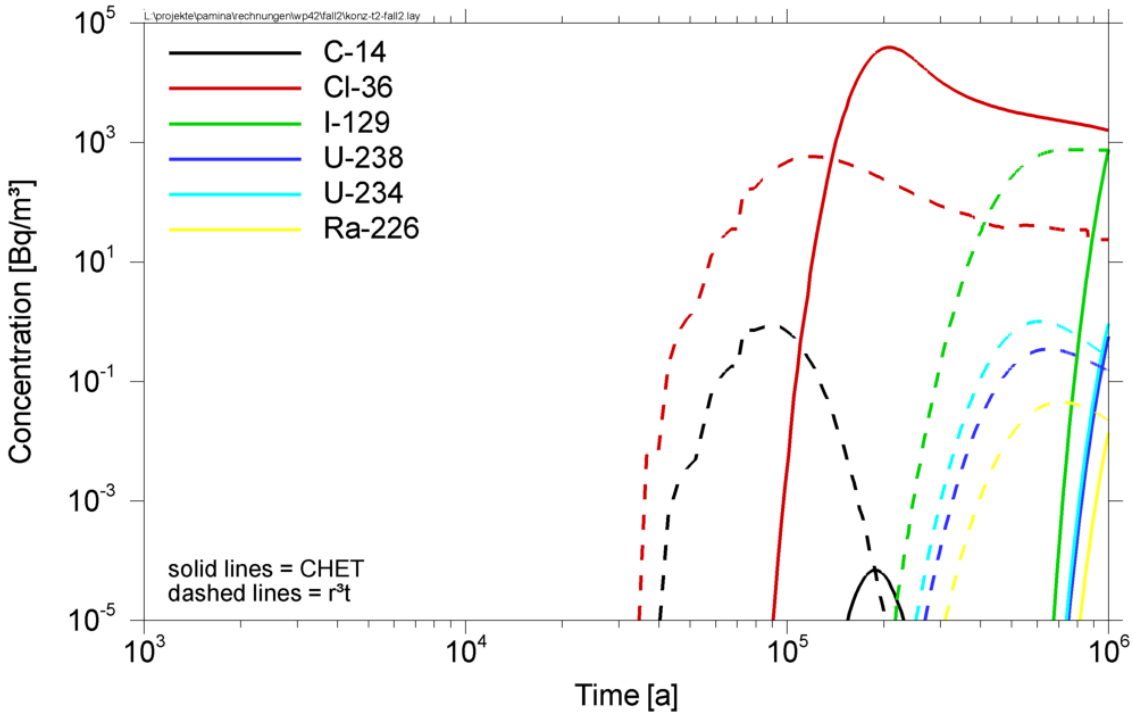

Fig. 5.61 Concentraton versus time of different radionuclides at the position of 12 650 m (pathway 2B) calculated with r^3t (dashed lines) and with CHET (solid lines)

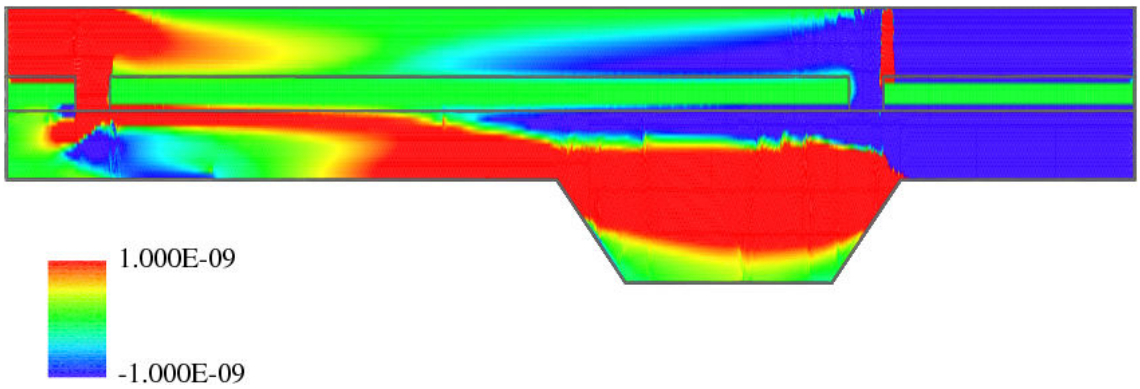

Fig. 5.62 Horizontal component of the flow velocity in model 2 given in [$m \cdot s^{-1}$] (red colours denote flow in positive (right) direction while blue colours denote flow in negative (left) direction)

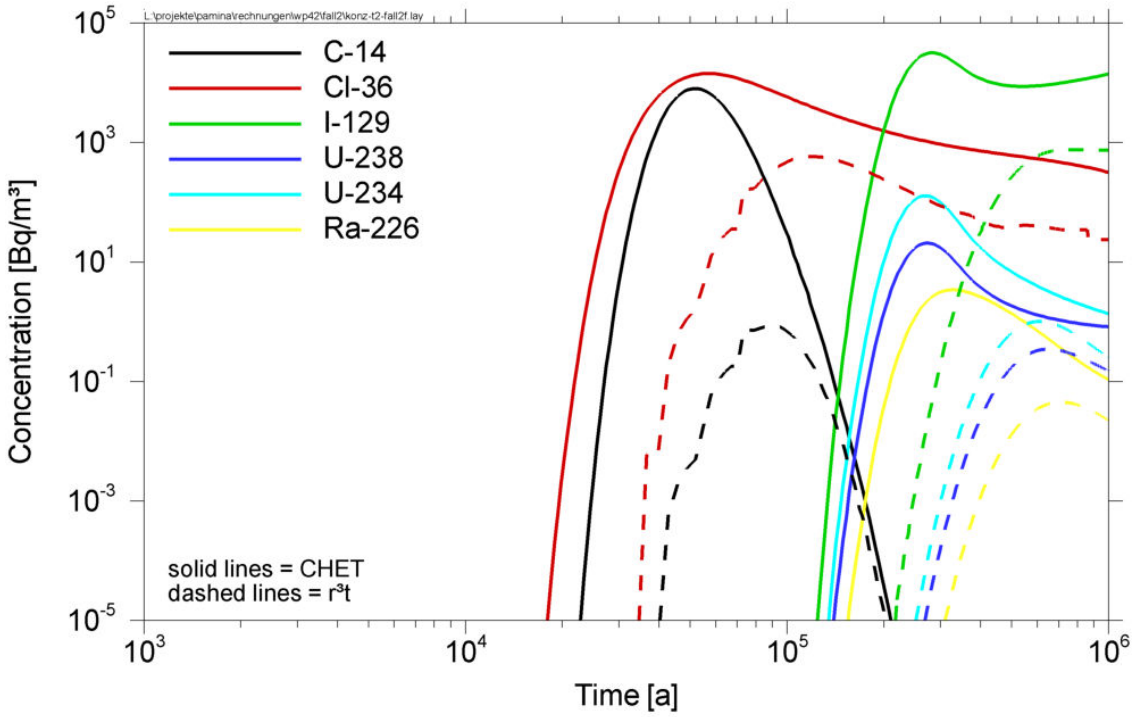

Fig. 5.63 Concentraton versus time of different radionuclides at the position of 12 650 m (pathway 2B) calculated with r^3t (dashed lines) and with high flow velocity used in CHET (solid lines)

5.2.3 Conclusions

In the work presented we examined the use of more complex far-field codes in PA. As result of these calculations, the time dependent concentrations from a PA code and a process-level code were compared at different positions in the model to study whether the use of the more complex codes results in a reduction of conservatism and/or a better representation of the actual transport or not.

On the one hand, with regard to processor time needed for the calculations, the use of the simplified code in PA is inevitable if multiple or even a high number of simulations have to be performed. The time for one simulation ranges from days to several weeks for the complex code r^3t versus only minutes for the PA code CHET. However, on the other hand, the simplification of the model brings along several peculiarities that have to be considered. The results are shortly outlined in the following five bullets:

- The radionuclide distribution calculated with the 2D code r^3t shows that different radionuclides can be transported on different transport pathways depending on

their transport properties. This implies that the transport cannot be depicted by a single 1D model in these cases.

- The fraction of the radionuclides transported on one or the other of the different pathways differs from nuclide to nuclide.
- The missing dispersion to the second dimension results in an overestimation of the concentrations in the 1D model versus the 2D model. This effect is increasing with decreasing flow velocity and is most significant for diffusion dominated transport. The same deviation is expected between the 2D simulation and one using a 3D geometry.
- The heterogeneity of the transport velocities in the real situation and the need for averaging the velocities for the abstraction to 1D may result in large uncertainties on how to determine the correct transport velocity in the abstracted model. The deviation resulting from the averaging can lead to too high transport velocities and therefore an overestimation of the radionuclide concentrations in the aquifer water as observed in model 1, but also in too low transport velocities and resulting underestimations of the radionuclide concentrations as observed in model 2. The latter case is critical for safety assessment.
- A fast transport at the end of the transport pathway in a 1D model can result in an underestimation of the concentration of daughter radionuclides produced from the decay chains during the transport due to lacking residence time to equilibrate the decay chain.

Especially the first one and the last to points have to be considered in PA calculations since they can lead to an underestimation of the radiological consequences what absolutely has to be avoided. The last point is quite common in PA radionuclide transport modelling and can be easily accounted for by considering an additional transport time in the 1D model that gives time to achieve the radioactive equilibrium in the decay chains.

The problem how to calculate average transport velocities for the abstracted model is more serious and a common solution is hard to recommend. One solution is to use the maximum transport velocity occurring in the real situation (i. e. the complex model). However, this approach in most cases might lead to a high conservatism in the model. Since the trend in latest safety assessments in European countries is towards neglecting a barrier function of the far-field anyway, this limitation might not be too harmful.

In cases where the far-field is regarded as barrier in the safety assessment and the hydrogeology shows a very complex flow field, a two-stage approach is needed. In a first step the more complex code and model is used to calculate the concentration distributions and consequences for a reference case. In the second step the results from the complex code are used to qualify the abstracted transport model and to show that the abstracted model does not underestimate the result. Subsequently, the abstracted model can be used for additional PA calculations like variants or probabilistic assessments.

In cases where radionuclides are transported on different pathways resulting in contamination of the surface water at different locations, the maximum radiation exposure cannot be correctly determined with a simple one dimensional model. However, this problem can be easily overcome by using a "multi 1D model", i. e. to model the different pathways independently with the 1D model and combine the results afterwards.

5.3 Coupling of the transport code r^{3}t with the geochemical code Phreeqc

The transport code r^{3}t, used by the GRS to model radionuclide transport in porous media in the far field /FEI 04/ does only consider isothermal sorption models to describe the interaction of the solutes with the porous media. In some cases – especially for spatial or temporal variable chemical conditions – this may not be sufficient to describe the transport processes properly. To overcome this limitation, it was started to develop a coupling between the transport code r^{3}t and the geochemical code Phreeqc /PAR 99/ as part of a preceding project /RUE 07/. In the coupled code, Phreeqc performs the task to calculate the chemical interaction processes between the solution and the surface, namely the ion exchange and surface complexation, while r^{3}t is calculating the transport process. Since the development could not be finalised in the preceding process, this task was continued in this project.

The technical work for implementing the interface between r^{3}t and Phreeqc was finally achieved within this project and a few test cases are presented in the following to show the interface between r^{3}t and Phreeqc to be functional. This test is done by comparing the results of simulations by the coupled version of r^{3}t with results achieved by the standalone version of Phreeqc using its built-in transport modelling capabilities. Since these capabilities are restricted to 1D transport the test case show the same limitations. A more advanced 2D test case has to be conducted in the future.

5.3.1 Phreeqc standard example 11

The first case is the example number 11 given in the Phreeqc manual /PAR 99/ and is used here, to test the modelling of the ion exchange process in combination with advection and dispersive transport.

The test case depicts the intrusion of a calcium-chloride solution into a soil column initially filled with a sodium-potassium solution. The soil contains a cation exchanger supplying exchange sites for Sodium, Potassium, Calcium and Nitrate. The transport through the column is considered to happen either by advection only, or by advection and disperison. The column is continuously flushed from the entry with calcium-chloride solution that reacts with the exchanger up to equilibrium state at all times. The temporal evolution of the concentrations of different solutes at the end of the column is shown in figure 5.64. The abscissa denotes the number of times the column is completely flushed by the intruding solution (i. e. pore volume exchanges in the column) and is directly proportional to the transport time.

Chloride as a conservative solute should arrive at the end of the column at about one pore volume exchange, i. e. the complete column has been flushed once. In the simulation, this happens more or less exact if only advection is considered as transport process (figure 5.64, upper graph). If dispersion is considered additionally (figure 5.64, lower graph), the Chloride concentration curve shows a tailing due to the dispersion effect, with some Chloride arriving earlier and some arriving later than with advection only, but in the mean, the arrival of the Chloride at the end of the column is still after one pore volume exchange. The concentration curves of the other elements plotted show the same tailing effect due to dispersion.

The Sodium initially present in the column exchanges with the incoming calcium and is eluted as long as the exchanger contains sodium. Because potassium exchanges more strongly than sodium, potassium is released after sodium. Finally, when all of the potassium has been released, the concentration of calcium increases to a steady-state value equal to the concentration in the infilling solution /PAR 99/. The curves plotted in figure 5.64 show a good agreement between the simulations performed with the standalone version of Phreeqc and the coupled version of r^3t with Phreeqc.

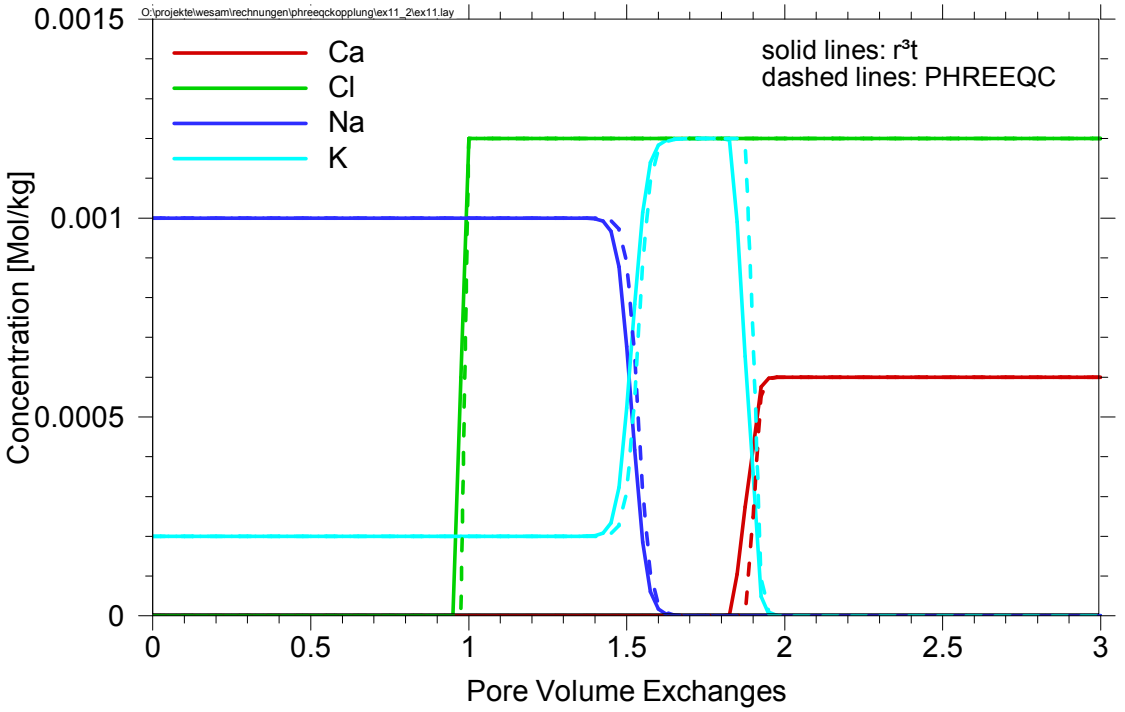

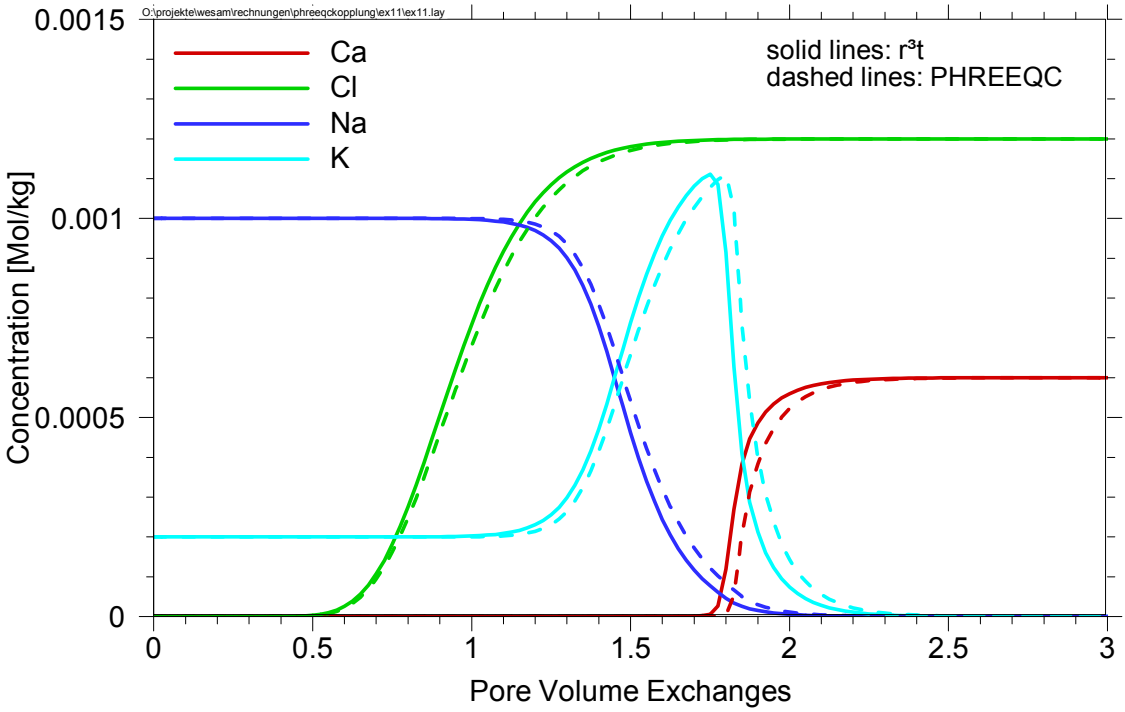

Fig. 5.64 Solute concentration versus time at the end of the reaction column with advection only (upper figure) and advection and dispersion (lower figure)

To be able to compare the coupled version of r^3t with the standalone version of Phreeqc, the results shown in figure 5.64 with r^3t were calculated by using the same

spatial resolution as in Phreeqc. To achieve this goal, a quasi 1D regular grid file was used in the r^{3}t simulation, dividing the column in 40 slices of the same thickness. This grid is shown in the upper part of figure 5.66. This is however an untypical condition for a r^{3}t simulation since this program usually uses irregular triangular grids.

The coupled version of r^{3}t with Phreeqc is calling the geochemical reaction routines of Phreeqc once for every time step for each of the grid elements. Therefore it might be possible that the grid shape and its resolution have an influence on the calculated result. This was tested by repeating the preceding simulation using internally generated irregular grids with two different resolutions. The resulting grids with 3 840 and 15 360 elements are shown in the lower two pictures of figure 5.66. Although it can be seen in this figure that there reaction front is not as plane as in the 1D case and that there is a slight fingering visible, the actual shape of the curves is only minimal affected as can be seen in figure 5.65 which show the comparison between the results of the simulations with the regular 1D-grid and the high resolved irregular grid.

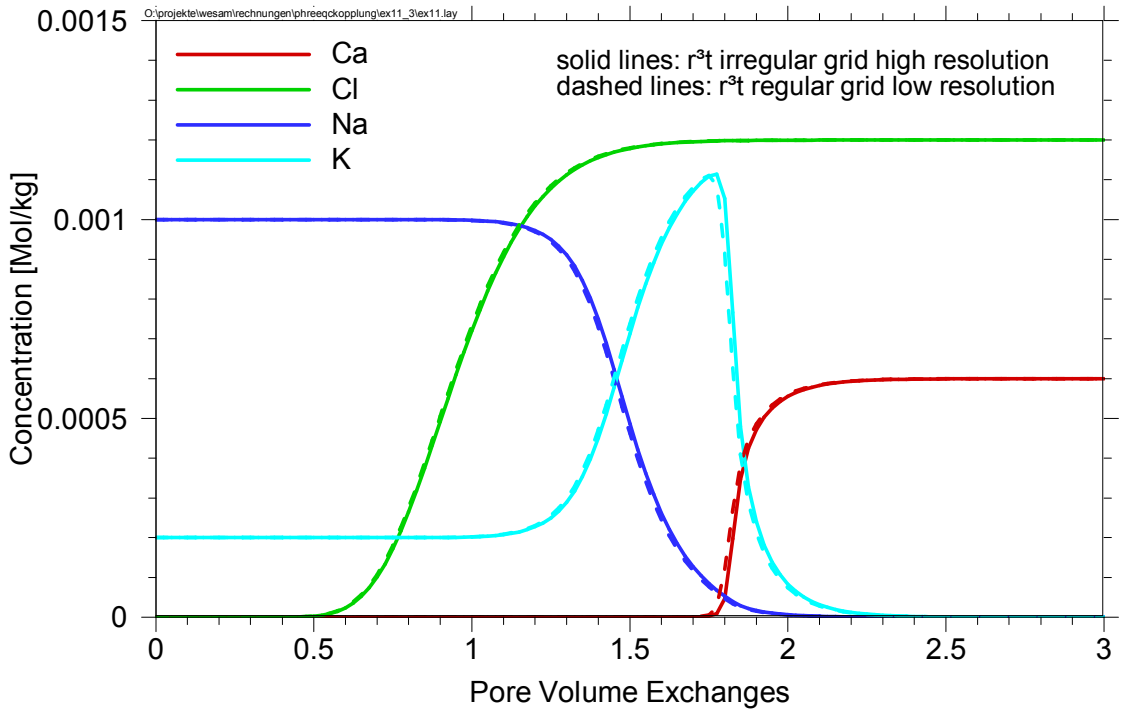

Fig. 5.65 Solute concentration versus time at the end of the reaction column using different grids in r^{3}t

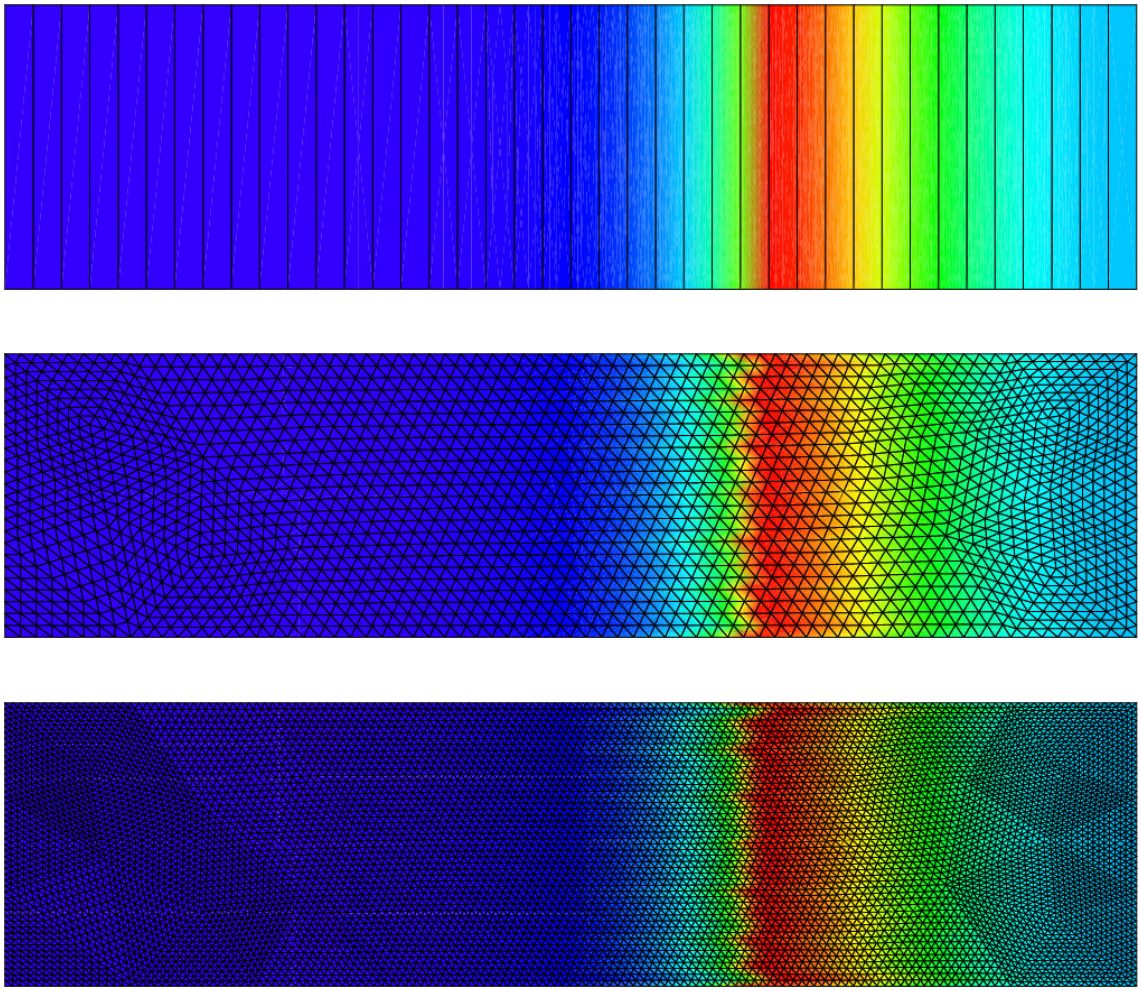

Fig. 5.66 Different grids used in the r^{3}t simulation: regular, low resolution grid (upper figure) and irregular high resolution grids (lower two figures)

5.3.2 Salt water intrusion into a Ca-HCO3-water column

This test case depicts the intrusion of high saline sea water into a water column filled with Ca-HCO_3-water. The solution in the column is in equilibrium with the mineral surface at each time step. Figure 5.67 shows the profile of the Chloride concentration in the column after a certain amount of time for transport. The transport is considered by diffusion only. The composition of the solution at the left hand side of the column is kept constant over time. The profile develops from diffusion of solutes into the column and potentially from reaction in the column.

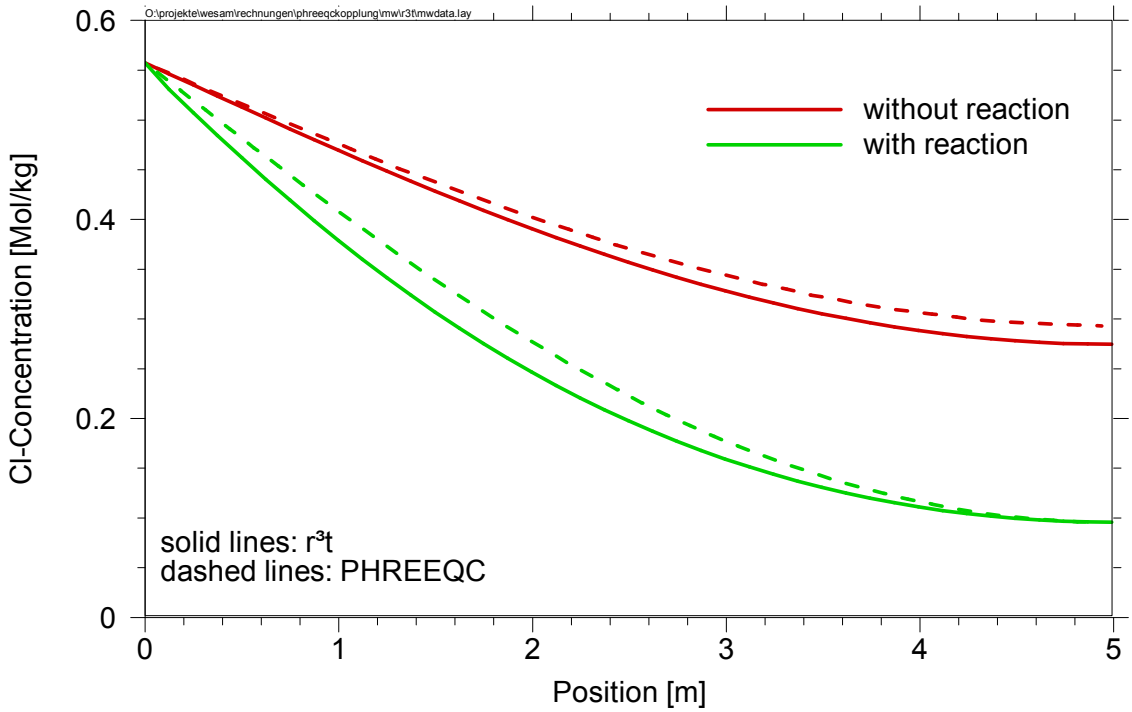

Fig. 5.67 Profile of Chloride concentration with and without consideration of the surface complexation reaction

There exists a slight difference between the results calculated by the standalone Phreeqc program and by the coupled r^3t version. Part of this difference is due to the different implementation of the diffusion process in both programs as can be seen from the difference of the curves not taking any reaction into account. Some additional deviation is obviously induced by the coupling between r^3t and Phreeqc. However, the agreement between the standalone version of Phreeqc and the coupled version of r^3t with Phreeqc is considered as satisfying for this test case.

5.3.3 Conclusion

The selected test cases have shown that the coupling of r^3t with Phreeqc is working and is able to account for ion exchange as well as surface complication processes. The results between the coupled version of r^3t with Phreeqc and the standalone version of Phreeqc for both of the test cases were found to acceptably agree to each other. As noted before, these results will have to be confirmed for a more complex test case in the future.

6 References

/AKE 02/ Arbeitskreis Auswahlverfahren Endlagerstandorte (AkEnd): Auswahlverfahren für Endlagerstandorte – Empfehlungen des AkEnd, Bonn, 2002.

/ATG 85/ Atomgesetz: Gesetz über die friedliche Verwendung der Kernenergie und den Schutz gegen ihre Gefahren (Atomgesetz - AtG) vom 23. Dezember 1959, Neufassung vom 15. Juli 1985 (BGBl. I, S. 1565).

/AVV 90/ Allgemeine Verwaltungsvorschrift zu §45 Strahlenschutzverordnung: Ermittlung der Strahlenexposition durch die Ableitung radioaktiver Stoffe aus kerntechnischen Anlagen oder Einrichtungen (21. Februar 1990). Erschienen im Bundesanzeiger, 42. Jg. Nummer 64a (1990).

/BAL 07/ Baltes, B., Röhlig, K.J., Kindt, A.: Sicherheitsanforderungen an die Endlagerung hochradioaktiver Abfälle in tiefen geologischen Formationen – Entwurf der GRS, Gesellschaft für Anlagen- und Reaktorsicherheit (GRS) mbH, GRS-A-3358, Köln, 2007.

/BEC 03/ Becker, D.-A. et al.: Testing of Safety and Performance Indicators (SPIN). EUR 19965, Brussels 2003.

/BEC 08/ D.-A. Becker and S. M. Spiessl: Variance-Based Sensitivity Analysis for the Long-Term Safety of an Underground Radioactive Waste Repository in Rock Salt, PSAM9 Hong Kong 2008.

/BEC 08a/ Becker, D.-A.; Wolf, J.: General concepts of supporting the safety case by means of safety and performance Indicators. PAMINA Deliverable 3.4.1, Braunschweig, 2008.
http://www.ip-pamina.eu/downloads/pamina3.4.1.pdf

/BEC 09/ Becker, D.A., Cormenzana, J.L., Delos, A., Duro, L., Grupa, J., Hart, J., Landa, J., Marivout, J., Orzechowski, J., Schröder, T.J., Vokal, A., Weber, J., Weetjens, E., Wolf, J.: Safety indicators and performance indicators. PAMINA – Performance Assessment Methodologies in Application to guide the development of the safety case. Deliverable D-N: 3.4.2, 2009.
http://www.ip-pamina.eu/downloads/pamina3.4.2.pdf

/BfS 02/ BfS: Novellierung der AVV zu § 47 Strahlenschutzverordnung. Stand 11.11.2002.

/BfS 05/ Bundesamt für Strahlenschutz: Konzeptionelle und sicherheitstechnische Fragen der Endlagerung radioaktiver Abfälle. Wirtsgesteine im Vergleich. Synthesebericht des Bundesamts für Strahlenschutz. Salzgitter, 2005.

/BGR 07/ BGR: Langzeitsicherheitsanalyse für ein HAW-Endlager im Salz – Geologisches Referenzmodell für ein HAW-Endlagerstandort im Salz. – Technischer Bericht, 11614/05, Beitrag für das Projekt ISIBEL, BGR, Hannover 2007.

/BMI 83/ Bundesministerium des Innern: Sicherheitskriterien für die Endlagerung radioaktiver Abfälle in einem Bergwerk,– RdSchr. D. BMI v. 20.4.1983 – RS – AGK 3 – 515 790/2 –, GMBI 1983.

/BMU 03/ Bundesministerium für Umwelt, Naturschutz und Radioaktivität: Umweltradioaktivität und Strahlenbelastung. Jahresbericht 2002, Bonn, 2003.

/BMU 08/ BMU: Safety Requirements Governing the Final Disposal of Heat-Generating Radioactive Waste – Draft; 29 July 2008.

/BMU 01/ BMU: Bekanntmachung der Dosiskoeffizienten zur Berechnung der Strahlen-exposition. Bundesministerium für Umwelt, Naturschutz und Reaktorsicherheit, RSII1-11413/28, Bonn, 2001.

/BOL 09/ Bolado, R., Castaing, W. & Tarantola, S. 2009. Contribution to the sample mean plot for graphical and numerical sensitivity analysis. Reliability Engineering & System Safety 94: 1041-1049.

/BUE 85/ Bütow, E.; Brühl, G.; Gülker, M.; Heredia, L.; Lütkemeier-Hosseinipour, S.; Naff, R.; Struck, S.: PSE-Abschlussbericht, Fachband 18 - Modellrechnungen zur Ausbreitung von Radionukliden im Deckgebirge. Projektleitung HMI, Berlin, 1985.

/BUH 04/ D. Buhmann, D.-A. Becker et al., Aktualisierung sicherheitsanalytischer Rechenprogramme für Teilsysteme eines Endlagers, GRS-200, 2004, Braunschweig, Germany.

/BUH 08/ Buhmann, D.; Mönig, J.; Wolf, J.: Untersuchungen zur Ermittlung und Bewertung von Freisetzungsszenarien. Gesellschaft für Anlagen- und Reaktorsicherheit (GRS) mbH, GRS-233, Braunschweig, 2008.

/BUH 08a/ Buhmann, D.; Mönig, J.; Wolf, J.; Heusermann, S.; Keller, S.; Weber, J. R.; Bollingerfehr, W.; Filbert, W.; Kreienmeyer, M.; Krone, J.; Tholen, M.: Überprüfung und Bewertung des Instrumentariums für eine sicherheitliche Bewertung von Endlagern für HAW – ISIBEL. Gemeinsamer Bericht von DBE TECHNOLOGY GmbH, BGR und GRS. DBE TECHNOLOGY GmbH Peine, 2008.

/BUH 09/ Buhmann, D.; Grupa, J.; Hart, J.; Hirsekorn, R.-P.; Ionescu, A.; Lerch, C.; Rübel, A.; Schneider, A.; Schröder, T.J. (2009): Report on the benchmarks on rock salt. PAMINA Deliverable D4.1.1.
http://www.ip-pamina.eu/downloads/pamina4.1.1.pdf

/BUH 91/ Buhmann, D.; Nies, A.; Storck, R.: Analyse der Langzeitsicherheit von Endlagerkonzepten für wärmeerzeugende radioaktive Abfälle. GSF-Bericht 27/91. GSF - Forschungszentrum für Umwelt und Gesundheit GmbH, Braunschweig 1991.

/BUH 99/ Buhmann, D.: Das Programmpaket EMOS. Ein Instrumentarium zur Analyse der Langzeitsicherheit von Endlagern. Gesellschaft für Anlagen- und Reaktorsicherheit (GRS) mbH, GRS-159, Braunschweig 1999.

/CAD 88/ Cadelli, N.; Cottone, G., Orlowski, S.; Bertozzi, G.; Girardi, F.; Saltelli, A.: PAGIS: Performance Assessment of Geological Isolation Systems for Radioactive Waste – Summary Report. EUR Report 11775 EN, Luxemburg, 1988.

/COL 05/ Colenco: Untersuchungen der menschlichen Einwirkungen auf ein Endlager für radioaktive Abfälle und der damit verbundenen Auswirkungen auf die Führung des Nachweises der Langzeitsicherheit. Colenco Bericht 3184/11, 2005.

/CON 99/ Conover, W.: J., Practical Nonparametric Statistics. Wiley-VCH, 1999.

/DBE 08/ DBE, BGR, GRS: FEP-Katalog für einen HAW-Standort im Wirtsgestein Salz - Version 01. Gemeinsamer Bericht von DBE Technology, BGR und GRS, Peine, Hannover, Braunschweig, 2008.

/DIN 02/ DIN EN 1990, Eurocode: Basis of structural design, October 2002.

/DIN 08/ DIN EN 1997-1, Eurocode 7: Geotechnical design - part 1: general rules; German version EN 1997-1:2004, October 2008.

/FEI 04/ Fein, E.: Software Package r3t. Model for Transport and Retention in Porous Media. Final report. Gesellschaft für Anlagen- und Reaktorsicherheit (GRS) mbH, GRS-192, Braunschweig März 2004.

/FEI 99/ Fein, E.; Schneider, A.: d3f - Ein Programmpaket zur Modellierung von Dichteströmungen. Gesellschaft für Anlagen- und Reaktorsicherheit (GRS) mbH, GRS-139, Braunschweig, Dezember 1999.

/FIE 07/ Fjeld, R.A.; Eisenberg, N.A.; Comton, K.L.: Quantitative Environmental Risk Analysis for Human Health. - John Wiley & Sons Inc., Hoboken, New Jersey, 2007.

/FIR 99/ Firestone. R.B.: Table of Isotopes - Volume I + II. Eighth edition. John Wiley and Sons. Inc.. New York. 1999.

/FLU 09/ Flügge, J.: Radionuclide Transport in the Overburden of a Salt Dome – The Impact of Extreme Climate States, Dissertation, Technische Universität Carolo-Wilhelmina zu Braunschweig, 2009.

/GAB 08/ Gabriel, S.: Anforderungen an eine sichere Endlagerung. Eröffnungsrede zum Endlagersymposium. Berlin, 30. Oktober 2008.

/GOM 97/ Gomit, J.M.; Hirsekorn, R.P.; Martens, K.-H.; Prij, J.: Evaluation of elements responsible for the effective engaged dose rates associated with the final storage of radioactive waste: Everest project. EUR 17449/3b EN. Luxembourg 1997.

/HSE 88/ Health & Safety Executive: The tolerability of risk from nuclear power stations. HSE, London, 1988.

/IAEA 03/ IAEA: Radioactive Waste Management Glossary. 2003 Edition. Vienna 2003.

/IAEA 06/ International Atomic Energy Agency: Geological Disposal of Radioactive Waste, Safety Requirements No. WS-R-4, IAEA, Vienna, 2006.

/IAEA 94/ International Atomic Energy Agency: Safety indicators in different time frames for the safety assessment of underground radioactive waste repositories. IAEA-TECDOC-767, Vienna 1994.

/ICRP 08/ International Commission on Radiological Protection: Recommendations of the ICRP. - Annals of the ICRP, ICRP 103, Pergamon Press. Oxford, 2008.

/ICRP 98/ International Commission On Radiological Protection: Radiation Protection Recommendations as Applied to the Disposal of Long-lived Solid Radioactive Waste, ICRP Publication 81, Annals of the ICRP, 28, 1998.

/KAP 81/ Kaplan, S.; Garrick, B.J.: On the quantitative definition of risk. Risk Analysis 1(1), pp. 11-27, 1981.

/KES 05/ Keesmann S., Noseck U., Buhmann D., Fein E., Schneider A., 2005: „Modellrechnungen zur Langzeitsicherheit von Endlagern in Salz- und Granitformationen“, Gesellschaft für Anlagen- und Reaktorsicherheit (GRS) mbH, GRS-206.

/KLI 05/ Klinge, H.; Boehme, J.; Grissemann, C.; Houben, G.; Ludwig, R.R.; Rübel, A.; Schelkes, K.; Schildknecht, F.; Suckow, A. (2007): Standortbeschreibung Gorleben: Die Hydrogeologie des Deckgebirges des Salzstocks Gorleben. Geologisches Jahrbuch, Reihe C, Band 71, E.Schweizerbart'sche Verlagsbuchhandlung, Stuttgart.

/KOE 07/ Köthe, A.; Hoffmann, N.; Krull, P.; Zirngast, M.; Zwirner, P.: Standortbeschreibung Gorleben Teil 2: Die Geologie des Deck- und Nebengebirges des Salzstockes Gorleben. - Geol.Jb., Reihe C, Heft 72, 201 S., Hannover, 2007.

/KUE 96/ Kühle, T.; Zude, F.; Lührmann, L.: Das eindimensionale Transportprogramm CHET1 unter Berücksichtigung der Sorption nach dem Kd-Konzept. Gesellschaft für Anlagen- und Reaktorsicherheit (GRS) mbH, GRS-124, Braunschweig 1996.

/NAG 02/ NAGRA: Auswertung von Langzeitsicherheitsanalysen hinsichtlich Kriterien für die Auswahl von Endlagerstandorten. – Schlussbericht NPB-01-31, Arbeitsgemeinschaft NAGRA-Colenco-GRS im Auftrag des BfS, Wettingen, 2002.

/NEA 00/ NEA: Features, Events and Processes (FEPs) for Geologic Dosposal of Radioactive Waste. An International Database. Vers. 1.2. OECD/NEA Publ., Radioactive Waste Management, Paris, 2000.

/NEA 01/ NEA: Scenario Development Methods and Practice. – OECD/NEA, Paris, France, 2001.

/NEA 04/ NEA: Post-closure Safety Case for Geological Repositories. Nature and Purpose, NEA No. 3679, OECD, Paris, 2004.

/NEA 05/ Nuclear Energy Agency – Organisation for Economic Co-operation and Development: Management of Uncertainty in Safety Case and the Role of Risk. - Workshop Proceedings, Stockholm, Sweden, 2-4 February 2004, NEA No. 5302, Nuclear Energy Agency, Paris 2005.

/NEA 95/ NEA: Future Human Actions at Disposal Sites, Safety Assessment of Radioactive Waste Repositories. NEA/OECD, Paris 1995.

/NOS 07/ Noseck U.; Brewitz, W.; Müller-Lyda, I.: To what extent can natural analogues contribute to the safety case for a repository in rock salt? In: Safety Cases for the Deep Disposal of Radioactive Waste - Where do we stand? OECD/NEA. Symposium Proceedings, Paris, France 23. - 25. January 2007.

/NOS 08/ Noseck, U. et al.: Scientific basis for the assessment of the long-term safety of repositories. Gesellschaft für Anlagen- und Reaktorsicherheit (GRS) mbH, GRS-237, Braunschweig, 2008.

/NOS 05/ Noseck, U.; Becker, D.; Rübel, A.; Meyer, Th.; Mauke, R.; Wollrath, J.: Treatment of drift seal disposal in the long-term safety assessment for a repository in a salt formation. In: Engineered Barrier Systems (EBS) in the Context of the Entire Safety Case. OECD/NEA. Workshop Proceedings, La Coruna, 24. -26. August 2005.

/NOS 09/ Noseck, U.; Fahrenholz, C.; Flügge, J.; Fein, E.; Pröhl, G.; Schneider, A.: Impact of Climate change on far-field and biosphere processes for a HLW repository in rock salt. Gesellschaft für Anlagen- und Reaktorsicherheit (GRS) mbH, GRS-241, Braunschweig 2009.

/PAM 06/ Marivoet, J.; Beuth, T.; Alonso, J.; Becker, D.-A.: Task reports for the first group of topics: Safety Functions, Definition and Assessment of Scenarios, Uncertainty Management and Uncertainty Analysis, Safety Indicators and Performance/Function Indicators. PAMINA Report D1.1.1, 2006. http://www.ip-pamina.eu/downloads/pamina1.1.1.pdf.

/PAM 07/ Galson, D.A. and Khursheed, A.: The Treatment of Uncertainty in Performance Assessment and Safety Case Development: State-of-the Art Overview. PAMINA Report M1.2.1, 2007. http://www.ip-pamina.eu/downloads/pamina.m1.2.1.pdf.

/PAM 09/ Capouet, M.; Griffault, L.; Cormenzana, J.L.; Becker, D.-A.: Task reports for the second group of topics: Safety strategy, Analysis of the evolution of the repository system, Modelling strategy, Sensitivity analysis. PAMINA Report D1.1.2, 2009.
http://www.ip-pamina.eu/downloads/pamina1.1.2.pdf.

/PAM 10/ Task reports for the third group of topics: Biosphere, Human Intrusion, Criteria for input and data selection. PAMINA Report D1.1.3, 2010. To be published.

/PAR 99/ Parkhurst, D.L.; Appelo, C.A.J.: User's guide to PHREEQC (Version2) - A computer program for speciation, batch reaction, one-dimensional transport, and inverse geochemical calculations. Water-Resources Investigations Report 99-4259, U.S. Geological Survey, Denver, 1999.

/PRO 08/ Proske, D.: Catalogue of Risks – Natural, Technical, Social and Health Risks. Springer-Verlag, Berlin, 2008.

/PRO 02/ Pröhl, G.; Gering, F.: Dosiskonversionsfaktoren zur Berechnung der Strahlenexposition in der Nachbetriebsphase von Endlagern nach dem Entwurf der Allgemeinen Verwaltungsvorschriften zu §47 Strahlenschutzverordnung in Anlehnung an die Vorgehensweise im Rahmen des Planfeststellungsverfahrens des geplanten Endlagers Konrad. GSF-Forschungszentrum für Umwelt und Gesundheit, Institut für Strahlenschutz. Neuherberg, 2002.

/PTK 06/ PTKA-WTE: Untertägige Entsorgung. Siebtes Statusgespräch zu FuE-Vorhaben auf dem Gebiet der Entsorgung gefährlicher Abfälle in tiefen geologischen Formationen. Forschungszentrum Karlsruhe, Wissenschaftliche Berichte FZKA-PTE Nr. 9, Karlsruhe, 2006.

/RUE 07/ Rübel A., Becker D.-A., Fein E., 2007: Radionuclide transport modelling to assess the safety of repositories in clays, Gesellschaft für Anlagen und Reaktorsicherheit (GRS) mbH, GRS 228.

/RUE 09/ Rübel, A. (2009): PA approaches based on different geometric complexity of modelling for the far field of a repository in salt. PAMINA Deliverable D4.2.1. (http://www.ip-pamina.eu/downloads/pamina4.2.1.pdf)

/SAL 00/ A. Saltelli, K. Chan and E. M. Scott, Sensitivity Analysis, Wiley, 2000, Chichester UK.

/SAL 97/ A. Saltelli, S. Tarantola and K. P. S. Chan, Sensitivity Analysis of Model Output, An Improvement of the FAST Method, EUR 17338EN, 1997, Luxembourg.

/SCH 95/ Schelkes, K.: Modelluntersuchungen zur Bewegung des Grundwassers bei vom Salzgehalt abhängiger Wasserdichte - Fallstudien und Modellvalidierung im Hinblick auf die Langzeitsicherheit von Endlagern für radioaktive Abfälle -. Abschlußbericht zum Forschungsvorhaben 02 E 8301. Bundesanstalt für Geowissenschaften und Rohstoffe, Hannover 1995.

/SIM 06/ Šimůnek, J.; van Genuchten, M. Th.; Šejna, M.: The HYDRUS Software Package for Simulating the Two- and Three-Dimensional Movement of Water, Heat, and Multiple Solutes in Variably-Saturated Media, Technical Manual, March 2006.

/SIM/ Simlab 2.2 Reference Manual, JRC Ispra, Italy.

/STA 08/ Statistisches Bundesamt: Unfallgeschehen im Straßenverkehr 2007. - Statistisches Bundesamt, Wiesbaden, 2008.

/STA 08a/ Statistisches Bundesamt: Statistisches Jahrbuch 2008. - Statistisches Bundesamt, Wiesbaden, 2008.

/STO 04/ Storck, R.; Becker, D.; Rübel, A.; Hirsekorn, P.; Preuss, J.; Wollrath, J.: The Safety Case for the Morsleben Repository. in DISTEC 2004. Disposal Technologies and Concepts. International Conference on Radioactive Waste Disposal, 26.-28. April 2004. Conference Proceedings 2004.

/STO 88/ Storck, R.; Aschenbach,J.; Hirsekorn, R.-P.; Nies, A.; Stelte, N.: Performance Assessment of Geological Isolation Systems for Radioactive Waste (PAGIS): Disposal in Salt Formations. EUR 11778 EN, GSF-Bericht 23/88. Commission of the European Communities, Gesellschaft für Strahlen- und Umweltforschung mbH München, Brussels-Luxembourg 1988.

/SUT 98/ Suter, D.; Biehler, D.; Blaser, P.; Hollmann, A.: Derivation of a Sorption Data Set for the Gorleben Overburden. Proc. DisTec '98 International Conference on Radioactive Waste Disposal, S. 581-584, Hamburg, September 9-11, 1998.

/UVP 90/ Verordnung über die Umweltverträglichkeitsprüfung bergbaulicher Vorhaben (UVP-V Bergbau) vom 13.07.1990 in der derzeit gültigen Fassung.

/WEA 86/ Weast. C.W.: CRC Handbook of Chemistry and Physics. 67th edition. CRC Press. Inc.. Boca Raton. Florida. 1986.

/WOL 09/ Wolf, J.; Becker, D.-A.; Rübel, A.; Noseck, U.: Safety and performance indicators for repositories in salt and clay formations. Gesellschaft für Anlagen- und Reaktorsicherheit (GRS) mbH, GRS-240, Braunschweig, 2009.

/WOJ 09/ Wollrath, J.; Preuss, J.; Becker, D.A.; Mönig, J.: Numerical Assessment oft he long-term safety oft he Morsleben repository for low- and intermediate-level radioactive waste. Proceedings of the 12th ICEM 2009.

A Annex: Example files for the use of the FAST method in EMOS

Example of a MATLAB script file for generating a EFAST sample

```
%
% EFAST sample generation for the WESAM case (clay rock)
% 4965 simulations - 5 parameters
%

% Initialise SIMLAB 3 library within the MATLAB environment
    gsaBegin

% Define distribution for the parameters
     addFacLogUnif('Diffbentonite1',1,[5.556e-11,5.556e-
09,1],'Diffusion coefficient of the bentonite in region 1')
     addFacLogUnif('Diffclay2',1,[8.300e-12,8.300e-10,1],'Diffusion
coefficient of the clay in region 2')
     addFacLogUnif('Diffclay3',1,[8.300e-12,8.300e-10,1],'Diffusion
coefficient of the clay in region 3')
     addFacLogUnif('Kdbentonite1',1,[4.0,400.0,1],'Kd  value  of  the
bentonite in region 1')
     add-
FacLogNorm('flux',10.3616329184732,0.372562470551105,0.001,0.999,'flux
in the far field')

% Create EFast sample for the WESAM case (clay)
     setMethodExtendedFast(123123,4965)
     sample = createSample

% Save sample file
    saveSampleCfg('D:\Simlab\matlab\test-sabine\wesam\si-
ton\mc4965\mc4965-5-siton-f.sam')

% Clean up and deallocate memory
    gsaEnd;
```

FORTRAN programme sam-spl-wesam

```
       PROGRAM SAM_SPL
C*****************************************************************
*
C      GENERATION OF THE EMOS SPL FILE FROM THE SIMLAB 3 SAMPLE FILE
SAM
C*****************************************************************
*
      PARAMETER (LEND=12)
      CHARACTER*11 DIST(LEND)
      CHARACTER*13 VTEILUNG(100)
      CHARACTER*100 SAMPFAD, SPLPFAD
      CHARACTER*80  ZEILE1
      CHARACTER*52 VNAME
      INTEGER  NSPIEL,  NVAR,  I,  J,  K1,  DUMMY,  DUMMY1,  DUMMY2,
ANZAHL(100)
      REAL*8 X(30000,100), XMIN(100), XMAX(100),COR(100), RDUMMY1,
     &       RDUMMY2, XDISCRETE(100,10)
```

```
      DATA DIST(1)/'Normal'/,DIST(2)/'LogNormal'/,DIST(3)/'Uniform'/,
     &     DIST(4)/'LogUniform'/,DIST(5)/'Weibull'/,
     &     DIST(6)/'Constant'/,DIST(7)/'Exponential'/,
     &     DIST(8)/'Gamma'/,DIST(9)/'Beta'/,
     &     DIST(10)/'Triangular'/,DIST(11)/'Relation'/,
     &     DIST(12)/'Discrete'/

C     OPEN THE SAM FILE

      WRITE (*,*) '.SAM-FILE:'
      READ (*,'(A80)') SAMPFAD
      OPEN (15,FILE=SAMPFAD,STATUS='OLD',ERR=7000)

C     OPEN THE SPL FILE

      K1 = 1
      DO WHILE (SAMPFAD(K1:K1) .NE. '.')
         K1 = K1 + 1
      ENDDO
      SPLPFAD = SAMPFAD(1:K1)//'spl'

      OPEN (16,FILE=SPLPFAD,STATUS='UNKNOWN',ERR=7000)

      write(*,*) SAMPFAD, SPLPFAD

C     READ NUMBER OF SIMULATIONS AND VARIABLES FROM THE SAM FILE
      READ (15,*) DUMMY
      READ (15,*) NSPIEL
      READ (15,*) NVAR
      READ (15,*) DUMMY

      write(*,*) NSPIEL, NVAR

C     WRITE NUMBER OF PARAMETERS IN THE SPL FILE
      WRITE (16,292) NVAR                    ! NUMBER OF INDEPENDENT
PARAMETERS


C     READ PARAMETER VALUES FOR EACH SIMULATION FROM THE SAM FILE
      DO 100 I=1,NSPIEL
              READ (15,*) (X(I,J),J=1,NVAR)
  100 CONTINUE

      READ (15,*) DUMMY
      READ (15,*) DUMMY

      DO 200 I=1,NVAR
         READ (15,*) (COR(J),J=1,NVAR)
  200 CONTINUE

       DO 300 I=1,NVAR
                  READ (15,*) (COR(J),J=1,4)
  300  CONTINUE

C READ DUMMY LINES
      READ (15,'(A80)') ZEILE1
      READ (15,*) RDUMMY1,RDUMMY2
      READ(15,'(A80)') ZEILE1
      READ(15,'(A80)') ZEILE1
      READ(15,'(A80)') ZEILE1
```

```
C INITIALISE ARRAYS FOR THE DISTRIBUTIONS AND PARAMETES
      DO I = 1, NVAR
         VTEILUNG(I)='    '
      ENDDO
 VNAME='                                                    '

C     READ NAMES OF THE PARAMETERS AND OF THE DIFFERENT TYPES OF THE
DISTRIBUTIONS
C     AS WELL AS LOWER AND UPPER LIMITS OF THE PARAMETERS FROM THE SAM
FILE
       DO 400 I=1,NVAR
                  READ (15,'(A13)') VTEILUNG(I)
         READ (15,'(A80)') ZEILE1
 READ (15,'(A50)') VNAME
       WRITE (16,293) I, VNAME
 IF (VTEILUNG(I)(1:7).EQ.DIST(3).OR.VTEILUNG(I)(1:10).EQ.DIST(4)) THEN
             READ (15,*) DUMMY1, DUMMY2                        !Uniform,
LogUniform
     READ (15,*) XMIN(I), XMAX(I), DUMMY
         ELSEIF (VTEILUNG(I)(1:6).EQ.DIST(1)) THEN
     READ (15,*) DUMMY, UM, SIGMA, RDUMMY1, RDUMMY2 !Normal
     XMIN(I) = UM-3.0902*SIGMA
     XMAX(I) = UM+3.0902*SIGMA
 ELSEIF (VTEILUNG(I)(1:9).EQ.DIST(2)) THEN
     READ (15,*) DUMMY, UM, SIGMA, RDUMMY1, RDUMMY2 !LogNormal
     XMIN(I) = EXP(UM-3.0902*SIGMA)
     XMAX(I) = EXP(UM+3.0902*SIGMA)
         ELSEIF (VTEILUNG(I)(1:10).EQ.DIST(10)) THEN
     READ (15,*) DUMMY, XMIN(I), RDUMMY1, XMAX(I)  !Triangular
         ELSEIF (VTEILUNG(I)(1:10).EQ.DIST(12)) THEN       !Discrete
     READ (15,*) DUMMY, ANZAHL(I)
     DO 3 J = 1, ANZAHL(I)
        READ (15,*) XDISCRETE(I,J), RDUMMY1, RDUMMY2
    3        CONTINUE
 ENDIF
 READ (15,*)
  400   CONTINUE

C     WRITE NAMES OF THE PARAMETERS AND OF THE DIFFERENT TYPES OF THE
DISTRIBUTIONS
C     AS WELL AS LOWER AND UPPER LIMITS OF THE PARAMETERS IN THE SPL
FILE

        DO 600 J = 1, NVAR
           IF (VTEILUNG(J)(1:7).EQ.DIST(3)) WRITE (16,297) XMIN(J),
     & XMAX(J), '4'    !Uniform
           IF (VTEILUNG(J)(1:10).EQ.DIST(4)) WRITE (16,297) XMIN(J),
     & XMAX(J), '5'    !LogUniform
   IF (VTEILUNG(J)(1:6).EQ.DIST(1)) WRITE (16,297) XMIN(J),
     & XMAX(J), '2'    !Normal
   IF (VTEILUNG(J)(1:9).EQ.DIST(2)) WRITE (16,297) XMIN(J),
     & XMAX(J), '3'    !LogNormal
   IF (VTEILUNG(J)(1:10).EQ.DIST(10)) WRITE (16,297) XMIN(J),
     & XMAX(J), '8'    !Triangular
   IF (VTEILUNG(J)(1:10).EQ.DIST(12)) WRITE (16,297)
     & XDISCRETE(J,2),XDISCRETE(J,ANZAHL(J)), '12'   !Discrete
  600   CONTINUE
C
C     WRITE PARAMETER VALUES OF THE SIMULATIONS IN THE SPL FILE
```

```
         DO 700 I=1,NSPIEL
           IF (NVAR .GT. 7) THEN
              WRITE (16,291) I,(X(I,J),J=1,7)
      K = 7
      DO WHILE (K.NE.NVAR)
                 IF (NVAR .LE. (K+7)) THEN
                    WRITE (16,296)    (X(I,J),J=K+1,NVAR)
   K=NVAR
ELSE
   WRITE (16,296)    (X(I,J),J=K+1,K+7)
   K=K+7
ENDIF
    ENDDO
  ELSE
              WRITE (16,291) I,(X(I,J),J=1,NVAR)
           ENDIF
 700   CONTINUE

 291   FORMAT (I5,5X,7(1PE10.3))
 292   FORMAT (I5)
 293   FORMAT (1X,'VARIABLE ',I4,': ',A50)
 296   FORMAT (10X,7(1PE10.3))
 297   FORMAT (2(E15.3),3X,A2)


       CLOSE (15)
       CLOSE (16)

      STOP

7000 WRITE (*,*) 'ERROR WHILE OPENING A FILE'
      STOP

      END
```

Example of a sim file

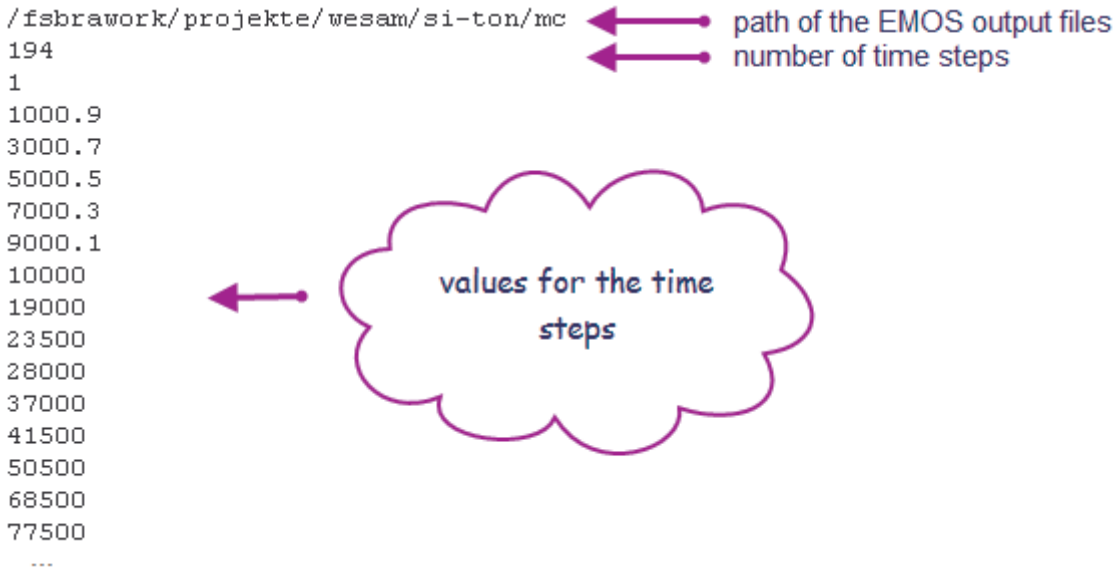

Example of a SIMLAB 3 sample file (*.sam)

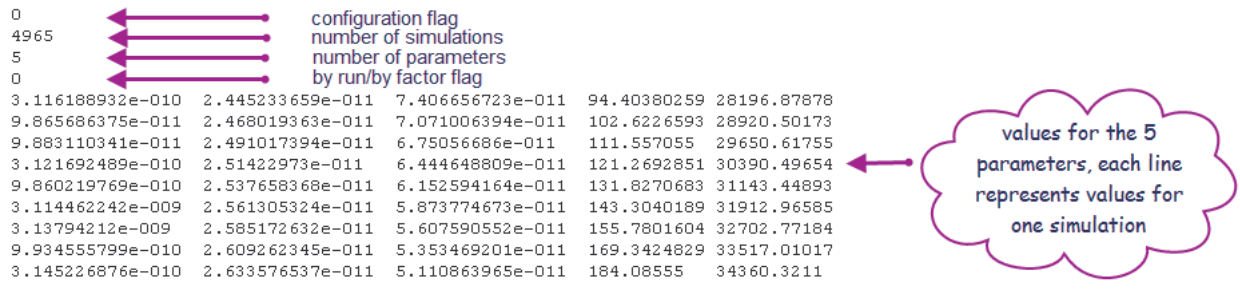

Example of a EMOS sample file (*. spl)

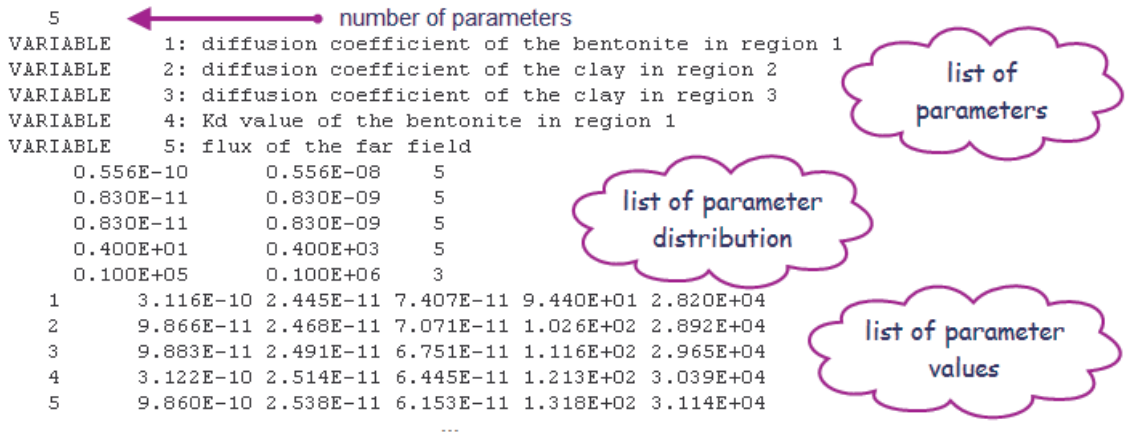

FORTRAN programme sdoconv-SD-all

```
      PROGRAM SDOCONV
C**********************************************************************
***
C      PROGRAMME FOR EXTRACTING OUTPUT DATA FROM THE EMOS SDO FILE
C      (ANNUAL RADIATION EXPOSURE) FOR THE 194 TIME STEPS LISTED IN THE
C        SIM FILE AND OUTPUTING THE DATA INTO 28 MODEL RESPONSE DATA
FILES
C      THE EMOS SVS FILE IS REQUIRED
C**********************************************************************
***

       CHARACTER*100 PFAD, RLNAME, SDONAME, SVSNAME, SLBFILE(28)
       CHARACTER*8   CKENN
       CHARACTER*2   no
       INTEGER K1, K2, NNUKLID, LASTN, DUMMY2, NZEIT, NSPIEL, NZ,
      &         IRUN1, IRUN, II, IJ, IK, IN, NAUS,
      &         IOUT,IAUS,IOUTF
       REAL *8 ZEIT(1000), DOSIS(100), TAUS(200)
       LOGICAL*1 AUSG(1000)


C OPEN SIM FILE
       WRITE(*,*) 'NAME OF THE SIM FILE FOR THE EFAST ANALYSIS:'
```

```
      READ(*,'(A80)') RLNAME
      OPEN (10,FILE=RLNAME,STATUS='OLD',ERR=7000)

C READ DATA FROM SIM FILE
      READ(10,'(A80)') PFAD
      READ(10,'(I3)') NAUS
      DO II = 1, NAUS
 READ(10,*) TAUS(II)
         IF (II .GT. 1 .AND. TAUS(II) .LE. TAUS(II-1)) THEN
            GOTO 100
         ENDIF
      ENDDO

C WRITE TIME STEPS ON SCREEN
      WRITE (*,*) 'TIME STEPS: '
      WRITE (*,*) (TAUS(II), II=1, NAUS)
      write (*,*) PFAD

C DECLARE NAME OF THE SDO, SVS AND MODEL RESPONSE DATA FILES
      K1 = 1
      DO WHILE (PFAD(K1:K1) .NE. ' ')
         K1 = K1 + 1
      ENDDO

      K2 = 1
      DO WHILE (RLNAME(K2:K2) .NE. '.')
         K2 = K2 + 1
      ENDDO

      IF (PFAD(K1-1:K1-1) .NE. '/') THEN
         PFAD = PFAD(1:K1-1)//'/'
         K1 = K1 + 1
      ENDIF

      IOUT =1

      DO II=1,28

         IF (II.GE.10) THEN
             write (no,'(I2)') II
         ELSE
             write (no,'(I1)') II
         ENDIF


         SLBFILE(II)=
     &      PFAD(1:K1-1)//RLNAME(1:K2-1)//'_SD_7_'//no
 write (*,*) SLBFILE(II)
      ENDDO

      SDONAME = PFAD(1:K1-1)//RLNAME(1:K2-1)//'.sdo'
      SVSNAME = PFAD(1:K1-1)//RLNAME(1:K2-1)//'.svs'

C     READ NUMBER OF SIMULATIONS, TIME STEPS AND NUCLIDES FROM THE SVS
FILE

      OPEN (11,FILE=SVSNAME,STATUS='OLD',ERR=7003)
      READ (11,'(A8)') CKENN
      DO WHILE (CKENN .NE. '%%NUKLID')
         READ (11,'(A8)',END=7010) CKENN
      ENDDO
```

```
      READ (11,'(I10)') NNUKLID
      DO WHILE (CKENN .NE. '%%DIVERS')
         READ (11,'(A8)',END=7010) CKENN
      ENDDO
      READ (11,*)
      READ (11,'(4I10)') LASTN, DUMMY2, NZEIT, NSPIEL
      IF (NZEIT .GT. 1000) THEN
         WRITE (*,*) 'TOO MANY TIME STEPS'
         STOP
      ENDIF
      IF (NNUKLID .LE. LASTN) THEN
         WRITE (*,*) 'DOSIS NOT AVAILABLE'
         STOP
      ENDIF
      CLOSE (11)

C     DETERMINATION OF NUMBER OF LINES IN THE SDO FILE
C     WHICH ARE REQUIRED FOR THE NUCLIDES

      NZ = INT (NNUKLID/8.0 - 0.1) + 1

C     READ TIME STEPS FROM THE SDO FILE

      OPEN (12,FILE=SDONAME,STATUS='OLD',ERR=7000)
      DO II=1, NZEIT
         READ (12, '(I5,3X,1PE12.5)') IRUN1, ZEIT(II)
         IF (II .GE. 2) THEN
            IF (IRUN1 .NE. IRUN) THEN
               WRITE (*,*) 'ERROR OCCURRED WHILE READING TIME STEPS'
               STOP
            ENDIF
         ENDIF
         IRUN = IRUN1
         DO IJ = 1, NZ
            READ (12,*)
         ENDDO
      ENDDO
      CLOSE (12)

C     DETERMINATION OF THE TIME STEPS FOR OUTPUT

      IK = 1
      DO II = 1, NZEIT
         AUSG(II) = .FALSE.
         IF (ZEIT(II) .GE. TAUS(IK)) THEN
            IK = IK + 1
            AUSG(II) = .TRUE.
         ENDIF
         IF (IK .GT. NAUS) GOTO 200
      ENDDO
  200 CONTINUE


C     OPEN THE SDO AND MODEL RESPONSE DATA FILES

      OPEN (12,FILE=SDONAME,STATUS='OLD',ERR=7001)


      DO IOUT=1,28
         OPEN (IOUT+14,FILE=SLBFILE(IOUT),STATUS='UNKNOWN',ERR=7002)
```

```
         WRITE (IOUT+14,*) 1                        ! HEADER FOR THE SLB
FILE
         WRITE (IOUT+14,'(A11)') 'Summendosis'
         WRITE (IOUT+14,'(A10)') 'time = yes'
         WRITE (IOUT+14,*) NSPIEL
      ENDDO

C    READ OUTPUT DATA FROM THE SDO FILE AND WRITE RESPECTIVE DATA INTO
THE MODEL RESPONSE DATA FILES

      IK = 1
      DO WHILE (.TRUE.)
         READ (12,'(I5)',END=1000) IRUN
         DO WHILE (IK .LT. IRUN)
            DO IOUT=1,27
               WRITE (IOUT+14,'(A4,I5.5)') 'RUN ', IK-1
               WRITE (IOUT+14,'(I4.4)') 7
    ENDDO
    WRITE (28+14,'(A4,I5.5)') 'RUN ', IK-1
            WRITE (28+14,'(I4.4)') 5
            DO II = 1, NZEIT
       IF (AUSG(II)) THEN
           DO IOUT=1,28
              WRITE (IOUT+14,'(2(1PE12.5))') ZEIT(II), 0.0
   ENDDO
       ENDIF
            ENDDO
            IK = IK + 1
         ENDDO
         DO IOUT=1,27
             WRITE (IOUT+14,'(A4,I5.5)') 'RUN ', IK-1
             WRITE (IOUT+14,'(I4.4)') 7
 ENDDO
 WRITE (28+14,'(A4,I5.5)') 'RUN ', IK-1
         WRITE (28+14,'(I4.4)') 5
 IOUTF=15
 IAUS=1
         DO II = 1, NZEIT
               IF (II .GT. 1) READ (12,*)
               READ (12,'(8E10.3)') (DOSIS(IN), IN=1,NNUKLID)
         IF (AUSG(II)) THEN
               IF (IAUS.EQ.8) THEN
       IOUTF=IOUTF+1
       IAUS=1
      ENDIF
   WRITE (IOUTF,'(2(1PE12.5))')
     &                   ZEIT(II), DOSIS(LASTN+1)
   IAUS = IAUS+1
                ENDIF
         ENDDO
         IK = IRUN + 1
      ENDDO

 1000 DO IK = IRUN + 1, NSPIEL
         DO IOUT=1,27
            WRITE (IOUT+14,'(A4,I5.5)') 'RUN ', IK-1
            WRITE (IOUT+14,'(I4.4)') 7
 ENDDO
         WRITE (28+14,'(A4,I5.5)') 'RUN ', IK-1
         WRITE (28+14,'(I4.4)') 5
         DO II = 1, NZEIT
```

```
            DO IOUT=1,28
               IF  (AUSG(II))  WRITE  (IOUT+14,'(2(1PE12.5))')  ZEIT(II),
0.0
    ENDDO
         ENDDO
       ENDDO


C CLOSE FILES

       DO IOUT=1,28
          CLOSE (IOUT+14)
       ENDDO

       CLOSE (12)

       STOP

  100 WRITE(*,*) 'ERROR IN SIM FILE'
 7001 write(*,*) 'ERROR IN SDO FILE'
 7002 write(*,*) 'ERROR IN SLB FILE'
 7003 write(*,*) 'ERROR IN SVS FILE'
 7000 WRITE (*,*) 'ERROR WHILE OPENING A FILE'
       STOP
 7010 WRITE (*,*) 'KEYWORD IN SVS FILE NOT FOUND'
       STOP

       END
```

Example of a model response file for SIMLAB 3

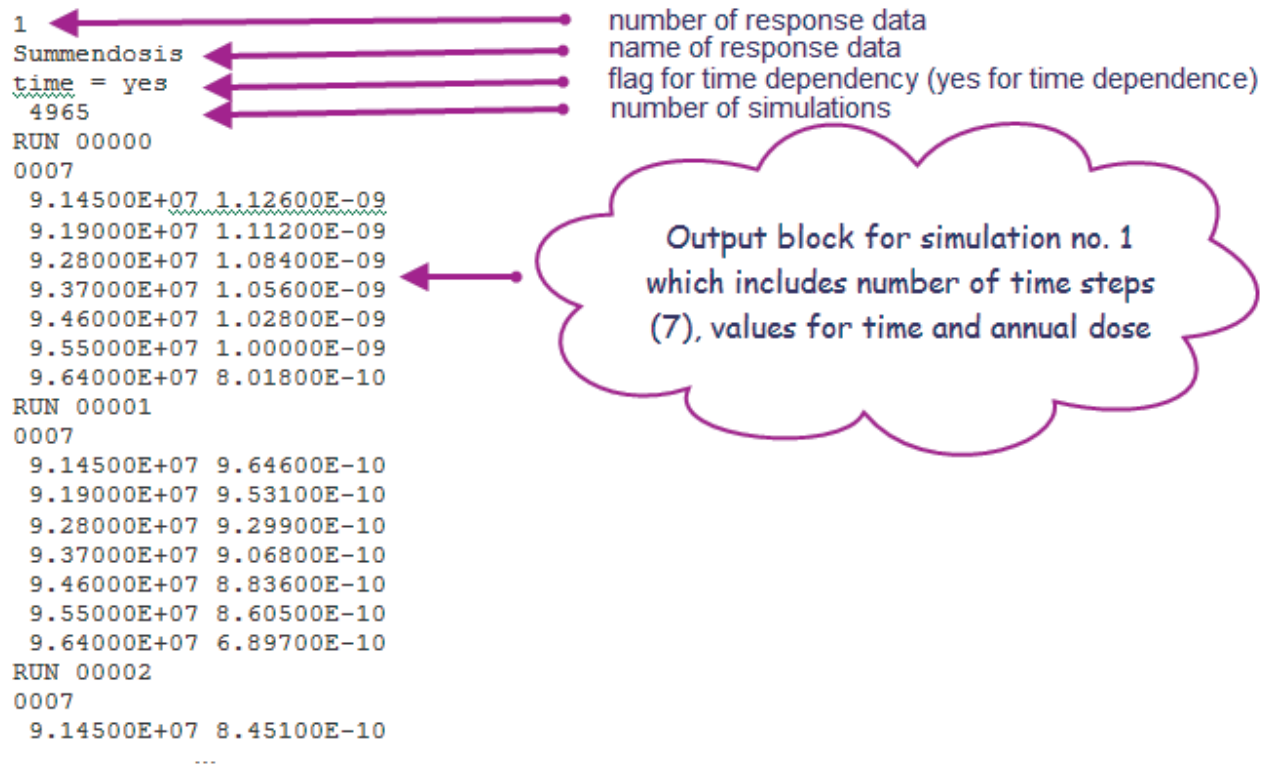

Main MATLAB script file for calculating the EFAST SI1 and SIT sensitivity indexes with SIMLAB 3

```
%
% MAIN MATLAB SCRIPT FILE FOR THE CALCULATION OF THE EFAST SENSITIVITY
INDEXES
% WESAM case (clay rock) for 4965 runs - 5 parameters
%

% FOR LOOP FOR THE 28 MODEL RESPONSE DATA FILES
for j=1:1:28
% DECLARE IN- AND OUTPUT FILES
% Name of the response data files
    filename          =          'D:\Simlab\matlab\test-sabine\wesam\si-
ton\mc4965\mc4965-5-siton-f_SD_7_';
    filename_response = [ filename num2str(j) ]

% Name of the time step file
    filename_time  =  'D:\Simlab\matlab\test-sabine\wesam\si-ton\siton-
f-time.dat';

% Name of the output data files for the SI1 and SIT sensitivity index-
es
    filename_out1 = [ filename 'SI1.out']
    filename_outT = [ filename 'SIT.out']

 % ACTIVIATE SUB MATLAB SCRIPT FILE
     run                          D:\Simlab\matlab\test-sabine\wesam\si-
ton\mc4965\mc4965_5_siton_f_sens;
```

```
 %  CLEAN UP AND DEALLOCATE MATLAB MEMORY SPACE
     clear all;
end;
```

Sub MATLAB script file for calculating the EFAST SI1 and SIT sensitivity indexes with SIMLAB 3

```
%
% SUB MATLAB SCRIPT FILE FOR THE CALCULATION OF THE EFAST SENSITIVITY
INDEXES
% WESAM case (clay rock) for 4965 runs - 5 parameters
%

% Initialise SIMLAB 3 library within the MATLAB environment
     gsaBegin

% Define distribution for the parameters
     addFacLogUnif('Diffbentonite1',1,[5.556e-11,5.556e-
09,1],'Diffusion coefficient of the bentonite in region 1')
     addFacLogUnif('Diffclay2',1,[8.300e-12,8.300e-10,1],'Diffusion
coefficient of the clay in region 2')
     addFacLogUnif('Diffclay3',1,[8.300e-12,8.300e-10,1],'Diffusion
coefficient of the clay in region 3')
     addFacLogUnif('Kdbentonite1',1,[4.0,400.0,1],'Kd  value  of  the
bentonite in region 1')
     add-
FacLogNorm('flux',10.3616329184732,0.372562470551105,0.001,0.999,'flux
in the far field')

% Create EFast sample for the WESAM case (clay)
    setMethodExtendedFast(123123,4965)
    sample = createSample

% Load model output (response) data
    loadModelOutputFile(filename_response)

% Load time steps file
    t = load(filename_time)

% Calculate the EFAST indexes of first and total order (SI1 and SIT)
    u = 7*(j-1);

    if (j < 28)
       for i=1:1:7
               time = t(u+i)

               SAIndex1 = getTimeFastFirstValues('Summendosis',time);
               SAIndexT = getTimeFastTotalValues('Summendosis',time);

               SI_1(i,1) = t(u+i);
               SI_T(i,1) = t(u+i);

               SI_1(i,2:6) = SAIndex1;
               SI_T(i,2:6) = SAIndexT;
      end;
     elseif (j == 28)
           for i=1:1:5
               time = t(u+i)
```

```
                SAIndex1 = getTimeFastFirstValues('Summendosis',time);
                SAIndexT = getTimeFastTotalValues('Summendosis',time);

                SI_1(i,1) = t(u+i);
                SI_T(i,1) = t(u+i);

                SI_1(i,2:6) = SAIndex1;
                SI_T(i,2:6) = SAIndexT;
            end;
    end;

% Output values for the SI1 and SIT indexes into 2 ASCII files
    save (filename_out1, 'SI_1', '-ASCII', '-append');
    save (filename_outT, 'SI_T', '-ASCII', '-append');

% Clean up and deallocate memory
    gsaEnd;
```

List of figures

List of tables

Gesellschaft für Anlagen- und Reaktorsicherheit (GRS) mbH

Schwertnergasse 1
50667 Köln
Telefon +49 221 2068-0
Telefax +49 221 2068-888

Forschungszentrum
85748 Garching b. München
Telefon +49 89 32004-0
Telefax +49 89 32004-300

Kurfürstendamm 200
10719 Berlin
Telefon +49 30 88589-0
Telefax +49 30 88589-111

Theodor-Heuss-Straße 4
38122 Braunschweig
Telefon +49 531 8012-0
Telefax +49 531 8012-200

www.grs.de

ISBN 978-3-939355-34-2